Reliability of polymer adhesive and coating materials for microsystem packaging

Ph.D. thesis

by

Jakob Janting

POEM - Polymer and Engineering Materials Group
Esbjerg Institute of Technology, Aalborg University
Niels Bohrs Vej 8, 6700 Esbjerg, Denmark

Thesis submitted to the Faculties of Engineering, Science and Medicine, Aalborg University, Denmark, for the Degree of Doctor of Philosophy

March 2008

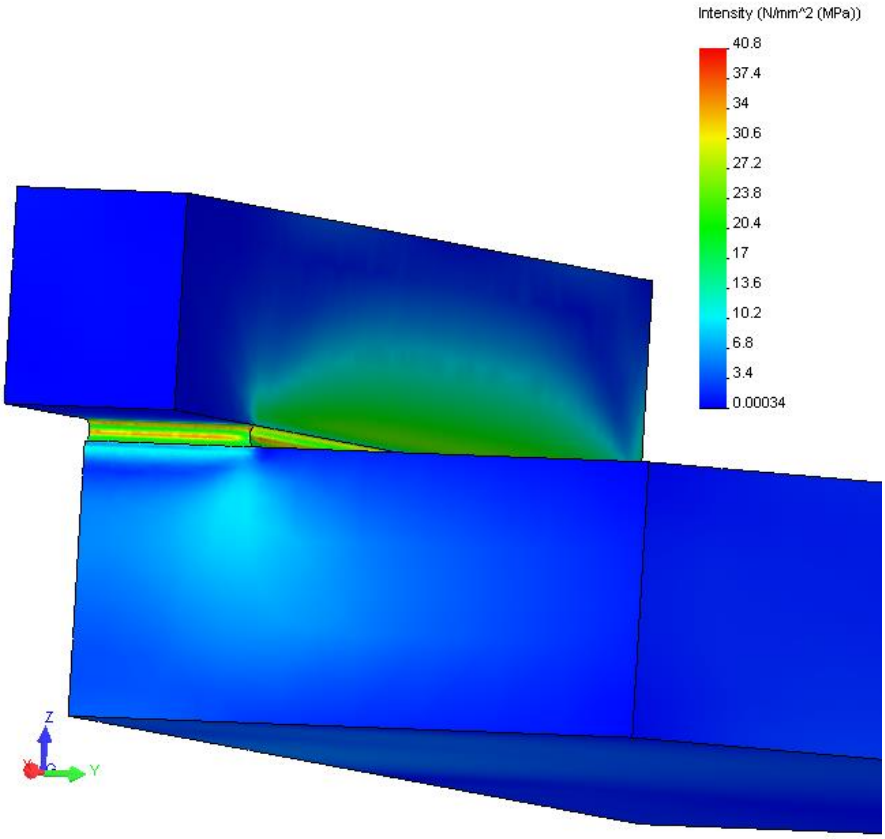

Jakob Janting
Reliability of polymer adhesive and coating materials for microsystem packaging
Ph.D. thesis Esbjerg Institute of Technology, Aalborg University, 2008

ISBN: 978-87-7606-031-2

Published by Esbjerg Institute of Technology, Aalborg University
Niels Bohrs Vej 8
DK-6700 Esbjerg
Denmark
http://470772.g.portal.aau.dk/
Typeset with Microsoft Word 2002

“There is plenty of room at the bottom”

Richard P. Feynman, 1959

Contents

Preface

This thesis is based on research carried out during the past 10 years at Grundfos Sensor Research and at DELTA Danish Electronics, Light & Acoustics. Polymer microsystem packaging materials have been characterized and failure analysis methods have been developed with the aim of gaining higher microsystem reliability. The work has lead to 19 publications in international journals, at conferences or workshops, see the next chapter "Short description of each thesis publication" or chapter 2.5.
In the thesis focus is on the work in relation to how the adhesion of protective polymer adhesives and coatings can be characterized theoretically and practically and optimized regarding intrinsic properties, the surroundings and their interaction. The main conclusion is that the interaction makes a system design approach to development of reliable microsystem packaging mandatory.

The thesis covers a general introduction to reliable microsystem packaging in chapter 1, an abstract in chapter 2 of the compiled work (publications) on two topics within this area which have been studied closer:

1) Polymers and metal / ceramic -polymer composites
2) Failure analysis

and more important topics elaborated on in chapter 3.

The first topic deals with application and chemical / physical protection properties of adhesives, polymer encapsulation and coating materials for microsystems. Emphasis has been on chemical / physical barrier and bond strength characterization. The importance of this work stems from the fact that microsystems due to small size are very sensitive to the often very aggressive surroundings.
Diffusion of water is identified as the most important parameter or physical mechanism influencing microsystem reliability negatively due to corrosion, delamination etc. This topic is therefore treated thoroughly in chapter 3 by mathematical modeling / practical calculations to find diffusivities and methods are given by which water can be kept away from critical areas in microsystems.
This research was carried out as part of the authors work during his employment as a research engineer at Grundfos Sensor Research 1994-1998 and at DELTA Danish Electronics, Light & Acoustics 1998-2005.

The second topic deals with microsystem reliability / failure analysis with focus on one very powerful analytical tool: Scanning Acoustic Microscopy (SAM). New analysis methods for studying thin multilayer structures (cf. delamination detection) and cure degree have been developed and demonstrated.
This research was carried out as part of the authors work during his employment as a research engineer at DELTA Danish Electronics, Light & Acoustics 1998-2005.

Danish preface

Denne afhandling er baseret forskning udført gennem de sidste 10 år ved Grundfos Sensor Forskning og ved DELTA Dansk Elektronik, Lys & Akustik. Polymer mikrosystem packaging materialer er blevet karakteriseret og fejlanalyse metoder udviklet for opnåelse af øget mikrosystem pålidelighed. Arbejdet har ført til 19 publikationer i internationale tidsskrifter, ved konferencer eller workshops, se næste kapitel "Short description of each thesis publication" eller kapitel 2.5.
I afhandlingen er fokuseret på arbejdet i relation til hvorledes adhæsionen af beskyttende polymer lime og belægninger teoretisk og praktisk kan karakteriseres og optimeres med hensyn til indre egenskaber, omgivelserne og deres vekselvirkning. Hovedkonklusionen er at vekselvirkningen gør en systemdesign tilgang til udvikling af pålidelig mikrosystem packaging nødvendig.

Afhandlingen dækker en generel introduktion til pålidelig mikrosystem indkapsling i kapitel 1, en gennemgang i kapitel 2 af det samlede arbejde (publikationer) med to emner indenfor dette område der er blevet undersøgt nærmere:

1) Polymere og metal / keramik -polymer kompositter.
2) Fejlanalyse.

og særligt vigtige delemner der er uddybet i kapitel 3.

Det første emne handler om påføringsegenskaber og kemiske / fysiske beskyttelses-egenskaber af lime og polymere indkapslings og belægningsmaterialer til mikrosystemer. Det primære arbejde er gjort indenfor karakterisering af de kemiske / fysiske barriere og vedhæftningsegenskaber. Vigtigheden af dette arbejde skyldes at mikrosystemer pga. deres lille størrelse er yderst følsomme overfor de ofte meget aggressive omgivelser.
Diffusion af vand identificeres som den vigtigste parameter eller fysiske mekanisme der påvirker mikrosystem pålidelighed negativt pga. korrosion, delaminering etc. Dette emne er derfor behandlet nærmere med matematisk modellering / praktiske beregninger for at finde diffusiviteter og der er angivet metoder til holde vand væk fra kritiske områder i mikrosystemer.
Denne forskning blev udført som en del af forfatterens arbejde under ansættelsen som forskningsingeniør ved Grundfos Sensor Forskning 1994-1998 og ved DELTA Dansk Elektronik, Lys & Akustik 1998-2005.

Det andet emne handler om mikrosystem pålidelighed / fejlanalyse med fokus på et meget nyttigt redskab: Skannet Akustisk Mikroskopi (SAM). Nye analysemetoder til undersøglese af multilagsstrukturer (jf. detektering af vedhæftning) og hærdningsgrad er blevet udviklet og demonstreret.
Denne forskning blev udført som en del af forfatterens arbejde under ansættelsen som forskningsingeniør ved DELTA Dansk Elektronik, Lys & Akustik 1998-2005.

Short description of each thesis publication

Paper 1: *Reliability of industrial packaging for Microsystems.*

This paper is an overview of studies on low cost minimum volume harsh environment microsystem sensor packaging. Focus has been on materials / methods testing and design for differential and absolute pressure sensors. Corrosion, bonding and leakage test results on protective coating (e.g.: Si-Ta-N, and Parylene C) and adhesive (e.g.: Epotek H77 epoxy, and Q3-6611 silicone) materials are presented. Further, new Si-Si bonding and through hole interconnection methods are presented.

Paper 2: *Conformal Coatings for 3D Multichip Microsystem Encapsulation.*

This paper reports on coating materials and methods for 3D low cost and minimum volume protection of microsystems. Especially, the packaging demands to fulfill for a $3 \cdot 3 \cdot 2$ mm^3 silicon based microphone have been addressed. A developed packaging concept involving an insulating / conductive two layer coating is presented together with test results on materials and application methods. The materials have been tested regarding applicability, volume resistivity, tightness, thickness, conformity, and E-field ElectroMagnetic Interference (EMI) shielding to identify the best. The most critical issue of covering the sharp corners and edges of single crystalline Si with the first layer is the main topic of the discussion. It is explained why these places are not easily covered and how this problem can be solved. The paper was presented orally and with poster 1.

Paper 3: *Stacked silicon microphones.*

This paper describes the first complete packaging of stacked silicon microphones of the type also mentioned in paper 2. The packaging influence on microphone performance is reported. The methods used to achieve an applicable, robust, compact and economic packaging concept is reported to be: Anodic bonding / gluing, fluxless solder bump bonding, through hole interconnection, dicing, Stud Ball Bumping (SBB) flip chip interconnection and mounting, underfilling, and protective encapsulation by dip / spray coating.

Paper 4: *Conformal coatings for 3D multichip microsystem encapsulation.*

This paper is an elaboration on paper 2. Especially a more in-depth discussion of the coating distribution at corners and edges of single crystalline silicon is given i.e. it is further accounted for by free energy minimization arguments. It is argued that the wet coating surface tension can be regarded as a driving force away from conformal coverage.

Paper 5: *Chip-size-packaged silicon microphones.*

This paper is an elaboration on the studies of paper 3. Especially a more detailed investigation of the influence of the individual packaging steps on the silicon microphone performance is given. Complete microphones with acceptable performance have been produced. However, reproducibility improvements are necessary for the solder bump bonding, flip-chip, and large microphone membrane handling processes.

Paper 6: *Encapsulation for a three-dimensional microsystem.*

This publication is a patent application extension of the discoveries described in paper 2 and 4. Thus, feasible 3D minimum volume protective coating materials and methods for a broad range of harsh environment microsystems are described. Focus is on the 3D multilayer encapsulation and the sensor access hole structure of the protective coating.

Paper 7: *Simulated SAM A-scans on multilayer MEMS components.*

This paper describes a spreadsheet simulation program which has been developed to analyze Scanning Acoustic Microscopy (SAM) A-scans on thin layered structures better. The simulation is based on calculations of reflection and transmission coefficients and the number *N* of waves received by the transducer at the same time by reflection on the same interfaces in different order. An example of analysis on multilayers in a MEMS absolute pressure sensor component is given. The paper was presented with poster 2.

Paper 8: *Scanning Acoustic Microscopy Study of Flip-Chip Underfill Cure Degree.*

Two procedures to area detect acoustic impedance variation inside materials with SAM are described and demonstrated on isopropanole and epoxy underfill. The advantage of this method as compared to Differential Scanning Calorimetry (DSC) to determine e.g. the cure degree of flip-chip underfill is described. For the 30 μm thick underfill EC 1211 layer between a flip-chip and Printed Circuit Board (PCB) clear differences between cured and uncured material could be detected. The resolution limits are discussed and in the above mentioned case it is found to be around 0.1 MRayl which is most often sufficient. The paper was presented with poster 3.

Paper 9: *Correlation between MEMS Adhesive cure Degree and acoustic Impedance determined with Differential Scanning Calorimetry and Scanning Acoustic Microscopy.*

This paper elaborates on the work described in paper 8, i.e. for the underfill Epotek T7110 between a flip-chip and PCB a rough correlation between SAM determined acoustic impedance and DSC determined reaction degree is established. The paper was presented with poster 4.

Paper 10: *Water Uptake of Polymeric Packaging Materials.*

This paper reports on the importance of keeping away even very small amounts of water from vulnerable MEMS sensor regions by careful selection of materials and designs. Practical measurement and analytical procedures to determine water flux is given. The required water diffusion coefficient and solubility for an underfill epoxy has been determined at 19 °C and 45 °C and from initial measurements it is envisaged that the high diffusion coefficient for the otherwise promising MacroMelt material can be lowered significantly. The paper was presented with poster 5.

Paper 11: *Scanning Acoustic Microscopy Investigation of Adhesive Cure Degree.*

This paper is essentially a short version of paper 8 and was also presented with poster 3.

Paper 12: *FEM Simulation of Influence of Protective Encapsulation on MEMS Pressure Sensor.*

This paper reports on stress analyses made on an absolute MEMS pressure sensor glass frit mounted in a metal bush and capped with epoxy with / without a protective metal coating. The cap serves as a protection towards harsh environments exposure e.g. refrigerants. The stress influence of the cap has been analyzed using Finite Element Modeling (FEM). The main conclusions are that the cap is not altering the sensor sensitivity significantly, that the epoxy leads to much higher vertical displacement when pressure is applied, which might be detrimental, and that the sensor becomes much more temperature sensitive i.e. a temperature change of 15 °C shifts the pressure about 40 bars.

Paper 13: *Simulated SAM A-scans on multilayer MEMS components.*

This paper is essentially a short version of paper 7 and was presented orally and also with poster 2.

Paper 14: *Scanning Acoustic Microscopy for Quality Assurance of MEMS Sensors.*

This paper presents SAM as a failure inspection tool for Quality Assurance (QA) of MEMS sensors. An overview of SAM, detectable failure modes and analytical methods are presented with examples. The paper was presented orally.

Paper 15: *Water Uptake of Polymeric MEMS Packaging Materials.*

This paper is an elaboration of the studies first described in paper 10. It is demonstrated that the effective diffusion coefficient for a MacroMelt molding material can be lowered three orders of magnitude by application of a coating of only 10 μm Parylene C. The paper was presented with poster 6.

Paper 16: *Surface tension driven shaping of adhesive microfluidic channel walls.*

This paper reports on the feasibility of making microfluidic channels by use of close proximity dispensed lines of adhesive between substrates and controlling the shape of the channel walls by control of adhesive and substrate surface tension, adhesive viscosity / thixotropy, line height and distance, and the temperature. From experiments using 4 adhesives, 3 substrates and FEM analysis it is concluded that it is nearly possible to achieve channels with a round cross section, that it is very difficult to dispense close proximity lines, and that the channels tend to have an inner shape like a double trumpet in the flow direction. The paper was presented with poster 7.

Paper 17: *Adhesive Bonding Methods for Polymer microTAS Components.*

An overview of advantages and disadvantages of different bonding techniques for polymer micro Total Analysis Systems (μTAS) components is given. Focus of this work is on adhesive bonding techniques for assembly of micro fluidic channels. A range of approaches including unstructured / structured substrates are proposed and preliminary results are presented. It is so far concluded that spacers are required to avoid voids along or adhesive in the channels. The paper was presented with poster 8.

Paper 18: *Sensor packaging for harsh environments.*

This publication is a comprehensive overview of microsystem sensor packaging for harsh environments. A review of microsystem packaging in general and the challenges faced in this rapidly growing area is given. Following an introduction to first principles of microsystem packaging and technologies, examples of specific sensor packaging solutions are presented.

Paper 19: *Techniques in Scanning Acoustic Microscopy for Enhanced Failure and Material Analysis of Microsystems.*

This publication is a review of SAM analysis with focus on the use for failure analysis and QA of microsystems. SAM is compared with other Non Destructive Analysis (NDA) methods. The basic principles and theory of SAM, detectable failure modes, and methods to get optimal measurements are described and several microsystem analysis examples are given.

1 Microsystem packaging for harsh environments

1.1 Introduction

Microsystems are used in very different sensing applications. Therefore the packaging which comprises electrical interconnection and protective encapsulation involves many different application specific materials and technologies. This chapter reviews the knowledge gathered by the author over the past approx. 15 years in the field of reliable microsystem packaging with focus on sensors placed in harsh environments. It is a modified excerpt of [Paper 18]. Following an introduction to first principles of microsystem packaging and technologies, examples of specific sensor packaging solutions are presented. In general it turns out that a system design approach to microsystem packaging is mandatory

1.2 Overview

The problem of bringing microsystem sensors to the market originates from one important fundamental difference between microelectronics packaging and microsystem sensor packaging which is that in the latter case often very aggressive surroundings has to have access to a sensing part of the naked chip or almost naked chip through a sensor window, fig. 1.

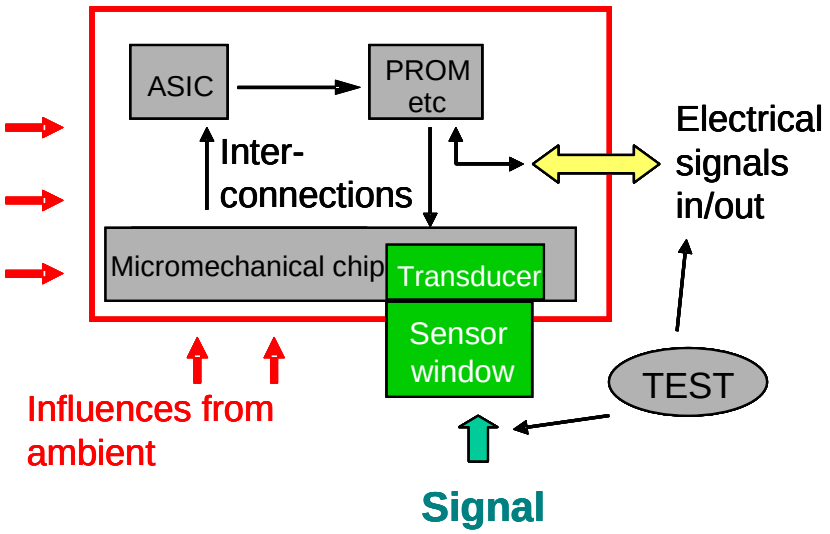

Fig. 1: Typical packaged microsystem sensor.

This implies application specific packaging and test solutions [1-5] which are why microsystem sensor packaging of today and the future is a challenging field. Also due to the often mandatory access hole microsystem failure analysis is considered an area quite different from that of microelectronics. A comprehensive overview of microsystem packaging has been given in [4]. A general overview of microsystem sensor / actuator packaging is given in [5]. Here focus is on the packaging of the sensor chip for harsh environments. About 30 years ago when the first silicon micromechanical sensor and

actuator structures were developed the packaging was not really given any attention by the scientific community. However, during the last 10 years this has changed dramatically. With the appearance of continued miniaturization to NEMS sensors scales are reduced from 1-100 μm to 1-100 nm making packaging issues even more critical. The delay of scientific attention seems not to be repeated for this next generation of sensors where packaging is already having a scientific reputation [6-11]. In the years to come some of the most important packaging activities will be in the areas of Wafer Level Packaging (WLP), System In Package (SIP), lead free electrical interconnect, optical interconnection, and nano-packaging [12-14].
The encapsulation part of the microsystem sensor packaging makes up most of the sensor volume and much of the price. Minimization of the encapsulation volume to keep sensors small requires new materials and processes to achieve sufficient protection, [1, 2]. Since the size reduction means that the surface to volume ratio is increased, surface physical / chemical properties e.g. surface tension become much more dominant than bulk properties. This is for instance seen for fluid in small channels [15, 16] and in unwanted adherence between silicon micromechanical parts (stiction) [17]. It is also used for alignment and self-assembly of microstructures [18].
In some cases the encapsulation accounts for 70% of the total cost of the microsystem sensor [5]. Furthermore, wafer level testing requires specialized equipment, [3].
In many cases bulky and expensive microsensor protective packages have been reduced to thin films and coatings some of which can be applied at silicon wafer level. One example is pressure sensors where steel membranes and oils for pressure transmission have been substituted with coatings [19, 20]. Another example could be a high performance silicon micromechanical microphone for e.g. cell phones or hearing aids [21, 22]. This microphone is placed in the ear where the environment is hot and moist. The microphone has to receive sound as physical stimuli requiring access through a hole in the packaging while at the same time being robust or insensitive towards other physical or chemical stimuli like ElectroMagnetic Interference (EMI) and sweat respectively. To meet these demands special coatings and thin films have been used to protect the device.

1.3 Packaging technologies

Microsystem sensors are miniaturized systems for analysis involving many different disciplines as: Mechanics, fluidics, biology, chemistry, microelectronics, optics, etc. Microsystem sensor packaging comprises (see fig. 1): 1) Die attach, 2) Interconnection between the micromechanical chip and microelectronics, photonics, RF / wireless, 3) In / out interconnection between the system and the outside world, 4) Sensing interconnection (sensor window), 5) Protective encapsulation. These elements are dealt with in the chapters below.
In microsystem sensor manufacturing, the packaging is given more and more attention since it represents a large part of the price and volume. The sensor die is often based on a silicon micromechanical transducer. However, during the last decade a lot of work has also been put into microsensors which are not based on the traditional silicon MicroElectroMechanical Systems (MEMS). They are for instance made of polymers or ceramics [23-33]. Some of the technologies and materials involved in microsystem sensor and microelectronics packaging are the same, however, microsystem sensor packaging is

severely complicated because it is often directly exposed to the surroundings, which are avoided in microelectronics. The consequence is very high demands on the materials and methods used. Especially the protective encapsulation / housing of the component has to be carefully selected keeping in mind that the whole system should be kept small. Very harsh environments are found in e.g. the high market potential automotive and oil / gas industries [34-42]. During a Europractice Workshop on "Packaging Issues and Requirements", September 2000, a survey among the participants was conducted. This survey confirmed that up to 60% or more of the production cost is used on the packaging of microsystems. The survey interestingly showed that the participants found that application specific solutions are nearly always needed. Another conclusion was that the development phase of the product is either in-house or subcontracted to a manufacturer. It is very seldom in collaboration with consultants, institutes, etc. In connection with this, it was said that the search for packaging sources is very difficult and therefore the use is limited. This work has been conducted by the Nordic Microsystems Manufacturing Cluster (NORMIC) consortium.

It should be clear that many aspects of microelectronics packaging can be directly transferred to microsystem sensor packaging, although the sensors have some special requirements to fulfill, e.g. sensor die access holes (see chapter 1.4.1.3.3). Examples of the latter are given in chapter 1.5. Many sensor packaging solutions e.g. adhesive die attach, wirebond interconnection to standard packages originate from microelectronics.

High microelectronics reliability in harsh environment is important for microsystem sensors even when the sensors themselves are non-standard packaged since microelectronics packaging of a more standard kind will most often have to be close to the sensor. Chapter 1.3 therefore mainly deals with a description of microelectronics packaging technologies of relevance for microsystem sensor packaging. Due to the variety of existing and coming microsystem sensors it is not possible to specify a generic package. However, it is attempted to ease production of microsystems by modularization [43-45]. Focus is therefore not on giving a full description of the many existing packages but to give an overview of key packaging components of today and the future which when brought together results in the many complete and existing microsensor packaging solutions and more to come.

1.3.1 Definitions

The purpose of this section is to provide a common understanding of the term packaging with special attention to microsystem sensors. Microsystem, MEMS, and micro machines are the European, American and Japanese terms for the same small sensors and actuators which are typically based on silicon micromechanical structures. Here as in [4] "microsystem" is defined to include microelectronics, photonics, RF / wireless and MEMS. Using this definition the microsystem sensor is not necessarily the MEMS. The focus here is MEMS sensor packaging for harsh environment application.

The word "packaging" covers mounting / assembly of the different parts in a system including electrical, physical, optical, RF / wireless connections and encapsulation. In that way packaging constitutes all the interfacing between the microsystem components (active, passive) and the surroundings: Die attach, mechanical support (substrate, carrier,

encapsulation), interconnection, and protective package (encapsulation) including access to the environment.
Microelectronics packaging is traditionally divided into a 4-level hierarchy which also applies for microsystem packaging [4]:

0 level: Wafer Level Packaging

Wafer Level Packaging (WLP) is packaging before the wafer containing several chips is diced out into single chips. This packaging provides interconnection (plated conductors and / or solder balls) and protection (inorganic, organic, metallic film, encapsulation or sealing) of chip / interconnections.

1st level: Micromechanical chip and / or Integrated Circuit level

Packaging at this level is based either on single or Multi Chip Modules (MCM). The micromechanical chip and / or Integrated Circuit (IC) / Application Specific Integrated Circuit (ASIC) etc. is bonded (e.g. anodic, glued, soldered) to a supporting and interconnecting carrier / substrate / housing which is typically a leadframe, ceramic substrate, silicon substrate, Printed Circuit Board (PCB) or flex print of some sort. The interconnection between components is established by wirebonding, flip-chip soldering / gluing, or conductive adhesive electrical contact to conductors on the carrier. The techniques are also used in 3D packaging by interconnecting stacked chips which saves space [46-49]. For lateral interconnection by the flip-chip method a carrier with interconnecting conductors is needed. Then the component is protected with an encapsulation. The substrate with interconnecting conductors between the components or to the outside world may be part of the encapsulation / housing or vice versa. This is e.g. seen in 3D Mould Interconnect Devices (3D MID) [50]. Encapsulations in direct contact with the components are typically low thermal stress glass / quartz filled epoxies. They are applied by techniques as glob topping and injection molding and combinations thereof. Housings where the components are inside a cavity are typically pre-molded on a leadframe and made of e.g. ceramic, epoxy, Liquid Crystal Polymer (LCP). Lids are then attached by e.g. gluing, soldering, etc.

2nd level: System level or board level

1st level packaging on a MCM including both a micromechanical chip, an ASIC and perhaps more components may result in a complete microsystem or MEMS. However, often more signal processing is required which is certainly the case if the 1st level packaging only comprises the micromechanical chip (single chip module). Then we do only have a MEM component and still not a MEMS. The packaging on this level consists of mounting the 1st level package onto some board (typically FR4 PCB or card) to interconnect active and passive components.

3rd level: Board to board interconnection

High capacity, multi-functionality and / or flexibility needs may require the possibility to interconnect boards like in PCs where several slots for insertion of different cards exist. This is the 3rd level packaging.

1.3.2 Die attach and sealing

Each step in microsystem packaging has a certain direct purpose and influences on the whole system. The first step in microsensor packaging is to attach the chips (Si with a SiO_2 or SiN surface) diced from a wafer to some sort of support (ceramic, plastic, metal, etc.) which also carries the electrical leads to the next level of packaging. Since this is a large area process performed directly on the chip surface, influences on performance can be very large and sometimes detrimental. Most often the chip is glued, soldered, or directly bonded [51, 52]. Except for the adhesion the major concerns are about secondary influences on the chip like stress, thermal management, and barrier properties.

As with the other parameters good adhesion depends on the choice of bonding material / method and the surfaces. Adhesive materials used for die attach are typically epoxies, cyanate ester, urethanes, silicones, and glass frit [4, 53]. To enhance the adhesion with these materials different physical / chemical roughening cleaning, activation and priming methods are used [54-58]. For adhesives adhesion enhancement is often important because the choice of adhesive material has to comply with secondary influences on the die. For instance epoxies usually have a very good adhesion to most materials but introduce high stresses because of high modulus E and Coefficient of Thermal Expansion (CTE). Then a soft silicone might be a better choice although it does not adhere as well. In this way the whole system and all the materials properties have always to be taken into account. O_2 plasma treatment is often used to physically / chemically roughen, clean and activate microsystem surfaces before bonding with adhesives. Especially polymers which are very hydrophobic can have their surface tension much increased with this treatment which in turn often results in better adhesion. Cleaning with solvents and priming with thin layers e.g. silanes, metals, etc., which adhere well to both the microsystem surface and the adhesive, are also used. Using solders most often requires deposition of thin metallic (Cr, Ti, Ni, Au, AuSi) adhesion and diffusion barrier layers. Often fluxless eutectic $Au_{20}Sn_{80}$ is the solder used; however, Sn-Pb is also used. Due to environmental demands lead free solders like $SnAg_{3.9}Cu_{0.6}$ are being developed [59-63]. Cleaning can be performed with the same methods as for adhesives, and adhesion is normally very good.

Stress usually originates from CTE mismatch between materials bonded and the bond material. The quite high CTE for adhesives is accommodated to the surrounding materials by adding ceramic and metallic fillers. For precise positioning of the sensors it is very important that these fillers are very regularly shaped and have a very narrow micron size diameter distribution. Careful handling may also be necessary to avoid fillers with sharp corners scratching through thin protective layers on the die. At the glass transition temperature T_g adhesives change their CTE with a factor up to 4 [4]. They must therefore be carefully selected so that T_g is outside the application temperature range. Very stress sensitive sensor dies are not mounted with solders. To isolate extremely stress sensitive sensors (e.g. some pressure sensors) from mounting stresses some sensors are bonded to glass with a CTE close to that of Si before dicing i.e. as a WLP step. To maintain good electrical contact in flip-chip interconnection the chip is adhesive underfilled to distribute stresses so that they are not only located at the contacts. This also has the secondary effect of holding i.e. bonding the chip to the substrate. Thirdly the underfill adhesive protects (encapsulates) the interconnection sites. Underfill adhesives

are typically highly ceramic filled (up to approx. 90 wt%) and the CTE is matched to the solder ball interconnects.
Sensors do not produce heat which has to be dissipated; however, this might be the case for the adjacent microelectronics which might influence overall microsystem performance. In that case solders are preferably used for the microelectronics die attachment. If adhesives are used they are filled with metal (e.g. Ag) or ceramic (e.g. Al_2O_3) to conduct heat. An important advantage of flip-chip attachment is that heat can be dissipated easily from the upward face of the chip.
In some instances the attachment also functions as barrier towards harsh environment. Flip-chipping is one example where the underfill protects the interconnections. Then the chemical / physical durability of attachment materials is very important. This means that the material should be as stable as possible towards corrosion and diffusion of chemicals and ions. Unlike polymeric adhesives solders are very tight. On the other hand they often corrode faster.

1.3.3 Signal interconnection

The signal interconnections in a microsystem can be electrical or non-electrical (optical, RF / wireless. Ways of creating and carrying the signals e.g. optically is by use of components as Vertical Cavity Surface Emitting Lasers (VCSELs) and optical waveguides as fibers and planar Arrayed Wave Guides (AWG) respectively. Packaging of optical sensors and interconnects requires high positioning precision and clean hermetic environment [64-70]. Here only the electrical interconnections will be discussed in detail.

1.3.3.1 Electrical interconnections

There is a wide variety of electrical connections within a microsystem. They can roughly be divided into internal and external connections, where the internal connections can vary from the connections between the different parts towards connection to a leadframe or the like.
For the internal electrical connections, wirebonding with Au or Al wire is often used. Another option is flip-chip which can be used for chip stacking. Chip stacking can also be accomplished using a combination of wirebonding and flip-chip interconnection. In some cases microsystem sensors are not planar on the surface and thus traditional flip-chip assembly is impossible. In these cases more creative ways of assembly / electrically connecting the parts must be used. Conductive adhesives are also getting more and more widespread in the electronic industry. An interconnection technology which is less used for interconnection of sensors is Tape Automated Bonding (TAB).
The external electrical connections should provide the user of the microsystem with a reasonable way of being connected to the microsystem sensor. In many "standard" microsystem sensor packages leaded or lead-less types of packages are used. With more custom-designed systems wires or some kind of substrate are extended from the inside of the package and thus provides the connection. Here it is not always possible to distinguish between internal and external electrical connections.

1.3.3.1.1 Wirebonding

Wirebonding with both Au and Al wires has been used by the semiconductor industry for many years, where the technique has proven to be very reliable. There are two different bonding techniques used: wedge-wedge and ball-wedge.
Wedge-wedge bonding can be performed using both Au and Al wires. During the bonding process, heat and ultrasound combined with force are forming the metallurgic bond between the wire and the bond pad on the chip and substrate.
The ball-wedge bonding process can only be performed using Au wire. Again, it is the combination of heat, ultrasound and force that is forming the metallurgic bond between the wire and the bond pads. For both bonding processes the metallization on the chip is typically Al, however, Au can also be used. On the substrates the metallization is most often Au. Au is generally preferred for harsh environment applications.

1.3.3.1.2 Flip-chip

Flip-chip mounting is one of the more advanced interconnection techniques used in the semiconductor industry and it is becoming more and more popular mostly because of size and thereby cost reduction. Electrical performance is also better because of the short interconnect distance. Flip-chip can be performed in a number of different ways but in general the idea is to flip the chip upside down so that the interconnection is under the chip [71]. Connection is then made using either solder or Au studs usually placed in an area array under the chip. Flip-chipping can be regarded a combined electrical interconnection and die attachment. However, as already mentioned the interconnect / attachment is too weak to sustain CTE mismatch stresses, and chip underfill with CTE matched with the solder balls or Au studs are used to stress stabilize the interconnection / attachment [4, 72]. In the solder technique solder is deposited by e.g. electroplating onto the chip pads. Then the chip is flipped and soldered to the contact pads on the substrate. In the stud or Stud Ball Bumping (SBB) technique [73-77] the process usually is: Placement of Au wirebond balls or studs on the chip interconnect pads, coining against a flat substrate to ensure same height of the studs, dipping of studs in conductive adhesive, placement on substrate pads, curing of conductive adhesive, underfilling of chip with epoxy, curing of underfill. The advantage of the SBB technique is that no special pad metallization layers like diffusion barriers are needed. Mechanical establishment of contact between Au studs and substrate pads by compression because of underfill shrinkage has also been studied [2].

1.3.3.1.3 Conductive adhesives

A comprehensive overview of conductive adhesives has been given in [78]. Conductive adhesives are typically highly filled epoxies or tapes. Depending on the amount of filler they are either Isotropic Conductive Adhesives (ICA) or Anisotropic Conductive Adhesives (ACA). The filler is Ag, Ni, Cu, or metal (e.g. Au) coated polymer or glass particles with 3 μm -10 μm diameter [79, 80]. Contact resistance is in the mΩ range. Conductive adhesives are very interesting for microsystems for several reasons. Much of the research in the area of conductive adhesives is motivated by their potential as a substitute for solders containing Pb which has become a burden on the environment. According to e.g. the European Union (EU) Pb containing solders will not be allowed in

electronic equipment from July 2006 [61, 62]. Further, conductive adhesives offer combined electrical interconnection and attach, High Density Interconnection (HDI), low temperature processing, good heat conduction, and limited space and alignment requirements [79, 81].
Besides electrical interconnection ICA's are used as high thermal conductivity, low CTE, die attach materials. ACA's are used e.g. for the electrical interconnection of Liquid Crystal Displays (LCD's) and flip-chips without the need for underfill [81, 82]. One important drawback of conductive adhesives is that generally they are not as environmentally stable as e.g. protected wirebond and solder electrical interconnections. Therefore they are less used in sensor packaging for harsh environments.

1.3.3.1.4 Tape Automated Bonding

TAB is less used for microsystem sensor packaging applications. In TAB chips are mounted and interconnected on Cu, Al, steel, or Alloy 42 metallized flexible polymer (polyimide (PI), epoxy-glass, polyester, and Bismaleimide Triazine (BT) resins) tapes before the attachment in a package or on Printed Wiring Board (PWB). The polymer can consist of up to three layers with thickness ranging between 35 μm and 125 μm. The interconnect lines are fabricated by etching the metallization. Free beams of the Cu lines are soldered to both chip and substrate by thermo compression locally on the joints. There is one advantage of TAB compared to wirebonding and that is that TAB has a lower profile, and one disadvantage when compared to flip-chip is that the interconnection is peripheral.

1.3.4 Package components

The package serves as protection of the rest of the system towards the often aggressive environment. Package components can vary in size from a standard ceramic or plastic package with a leadframe, to a thin layer of metal, polymer or a specially designed metal or plastic house. In some microsystem sensors the packaging is more or less integrated in the system (cf. Chip Scale Packaging, (CSP) and System In Package (SIP)). Examples are special metal layers in order to provide protection where the media can be allowed almost directly onto the surface of the system.
The package is what surrounds the chip and interconnection, except usually for the die attach / underfill. Packages or parts thereof are called encapsulations when in direct contact with the chip, and housings when the chip is contained in a cavity i.e. the package is not in direct contact with the chip.

1.3.4.1 Transfer molding

Transfer molding is the most common encapsulation technique in the IC packaging industry. Often the material comes in direct contact with the chip, which means that this type of package can be called an encapsulation. In transfer molding the molten resin, typically silica-filled epoxy, is transferred by pressure from a melting-pot into a mould which is at a temperature above the melting point of the resin. In injection molding, the mould temperature is below the resin melting point. In injection molding the temperature and pressure are e.g. 300 °C and 60 bar respectively. Gentler prototype microsystem sensor encapsulations can be made with thermoplastic materials like the polyamide based Macromelts [2] at temperatures around 150 °C and pressures around 5 bar.

An IC or microsystem interconnected (wirebonding) to a leadframe is placed in the mould and the material is transferred. This kind of encapsulation is typically a Dual Inline Package (DIP) with leads on two sides or Quad Flat Package (QFP) with leads on all four sides. The higher temperature in transfer molding is important for the filling of moulds with high flow length, wall thickness, and to allow for shrinkage compensation. Furthermore, it is very important to avoid bond wire sweeping.
Molding of other substrates than metallic leadframes (Kovar, Alloy 42) with an IC and / or a sensor is also possible. Printed Wiring Boards (PWB) made of ceramic and plastic can also be molded with plastic.

1.3.4.2 Premold

Premold packages are typically made of ceramics, plastics and metals [83]. Ceramics are used for high reliability and high frequency products. The high reliability is due to their hermeticity. In ceramic packages (e.g. CERamic Dual in Line Package, CERDIP and Ceramic Quad Flat Package, Cerquad) the chip or microsystem is mounted in a cavity in a premolded ceramic base with some connections e.g. a leadframe for in / out signals. On top of the base a ceramic lid is typically mounted with different hermetic glass sealings. The lid can also be made of metal, for instance Kovar and soldered with e.g. $Au_{20}Sn_{80}$. In that case the rim and the ceramic base and lid are first plated with metals. Note that the ceramic material is not in direct contact with the chip or microsystem like in traditional IC epoxy encapsulation. Consequently, these types of packages are often termed “housings”. Metal packages are used for microwave multichip modules and hybrid circuits because of their good thermal conduction and electromagnetic shielding. They are typically made of $Cu_{10}W$, $Cu_{15}W$, Silvar™ (Ni-Fe alloy), $Cu_{15}Mo$, Kovar and Alloy 42. Hermetic sealing between base and lid is achieved either by soldering with $Au_{20}Sn_{80}$ or by welding. Hermetic and insulated electrical feedthroughs are achieved with glass or ceramics. Just like the ceramic and metallic packages also plastic houses are made with many different configurations. New high performance (low moisture penetration, low stress and chemical inertness) plastic materials are for instance LCP [50, 84-86]. Packages of all the above mentioned materials can also just consist of molded sheets or foils with plated or screen printed conductors.

1.3.4.3 Glob-top and coatings

To protect wirebond and TAB interconnection against corrosion and / or wire sweep during molding typically epoxies filled with fused silica or quartz is dispensed to cover these areas. In less aggressive environments thin conformal coatings are also used. These are for instance vacuum deposited like Parylene C (poly-para-xylylene) [1, 2, 87] applied by Chemical Vapor Deposition (CVD) and perfluorinated polymers like Teflon AF1600 [1] applied by dip or spray methods. Since all polymers are easily penetrated by moisture it is more important (like for many other packaging materials) that these materials have a low solubility of water and other chemicals, that they are chemically resistant and that they do not take up much volume.

1.3.4.4 Stacked interconnection layers

Newer (around 1990) more compact ways of interconnecting chips as compared to e.g. DIP and QFP are by connecting them to different multilayer interconnection structures

[4, 66, 88-91]. The layers alternate between conductive layers and insulating layers. These packages are more compact than DIP and QFP because the wirebonding to a leadframe is eliminated and because the conducting layers are interconnected vertically inside (flip-chip) or nearly inside (wirebonding) the chip footprint. The substrates are used in two ways: One way is on single chips, the other on multiple chips.
When used on single chips this is just a more compact way of getting the same chips interconnected with the next level of packaging i.e. the chips are connected through the layered structure to the bottom side. The chip is not interconnected directly to the next level of packaging, usually a PWB, because of too fine pad pitch on the chip (typically 100 μm on the chip and 200 μm on the PWB). In that way the layered structure acts as a necessary space transforming interposer. The interconnect points on the bottom are solder balls arranged in an array. This package is called a Ball Grid Array (BGA). They are further subdivided according to different substrates as: plastic (PBGA), tape (TBGA), and ceramic (CBGA). For the flexible TBGA all three conventional interconnection methods are used to interconnect the chip to the interposer. The tape or thin film is typically polyimide, epoxy-glass, polyester, and BT resins. The chip in the rigid PBGA and CBGA packages are interconnected to the substrate by wirebonding and flip-chipping respectively. TAB and wirebond interconnections in TBGA and PBGA are protected by over-molding. The interposer in PBGA packages is FR-4, or BT-epoxy Printed Circuit Boards (PCB). Ceramic interposers in CBGAs are High Temperature Cofired Ceramics (HTCC) and Low Temperature Cofired Ceramics (LTCC) [66, 88-90]. Due to the high sinter temperature of 1550ºC in the HTCC case W, Mo is used as conductors.
When the primary use of the stacked interconnection substrates is to interconnect multiple components on the same substrate these boards are called Multi Chip Modules (MCM). Multi chip packages have also existed before the MCM in form of hybrid circuits. The difference is in the packaging density. A packaged electronic circuit is said to be a MCM when more than half of the substrate area is covered with active devices.
These even more compact packages also come in three types depending on different substrates: Plastic laminate MCM-L, multilayer ceramic MCM-C, and deposited multilayer thin films MCM-D. The plastic laminates are like for the PBGA package often epoxy-glass based PCB-like substrates. More special resins are polyimide, Teflon®, and PEEK. Special fillers are quartz, Kevlar®, and Aramid® [4]. The ceramic substrates are HTCC and LTCC. MCM-D offers the highest packaging density with feature sizes down to around 10 μm. Here deposition often starts out on a silicon wafer. The insulating dielectric layers consist of polyimides deposited by spin coating and CVD SiO_2 and oxynitrides. The conductors are normally Cu, Al, and Au deposited by Physical Vapor Deposition (PVD). Even denser packaging can be achieved if the active / passive component is embedded in the layered structure [66, 88]. Such packages are called System On Package (SOP) or System In Package (SIP).

1.3.4.5 Wafer Level Packaging

WLP or 0-level packaging means packaging before the wafer with chips is diced into separate chips for subsequent packaging. The degree of packaging on wafer level varies. Since this is the only packaging type in which the footprint area of a packaged chip on a board equals that of the unpackaged chip the WLP is considered the ultimate packaging.

The use is already widespread in the field of microsystem sensor packaging [12-15, 17-22, 52, 92-105]. Except for the size reduction which is nearly always beneficial in itself the motivation for WLP originates from huge economic advantages of packaging and test before dicing. One important disadvantage is that also bad dies will be packaged.
Actually many chips are wafer level packaged with a thin inorganic layer of SiO_2, or Si_3N_4 to protect it chemically against corrosion (environment, molding, etc.) and physically against scratches (handling). For more than 30 years IBM has also been bumping chips on wafer level for subsequent single chip packaging (flip-chip) [4]. Flip-chip interconnection and underfilling is also done at wafer level [21]. Interconnection in WLP is almost entirely of the area array type; however, recent studies show that even higher integration can be achieved by using flexible silicon structures. Flexible silicon substrates consist of rigid (thick) regions and thin flexible regions [97, 98]. This interconnect type has many advantages compared to other methods: Complete Wafer Scale Integration (WSI) of microsystem sensors and active circuits is possible, CTE match between components, possibility of 3D folding / stacking of interconnected components, no moisture uptake, can be sealed with glass. Current major types of WLP can be categorized as [4]: Redistribution WLP, encapsulated WLP, and flex / tape WLP. The redistribution type is most commonly used. The Al and Cu rerouting conductors are embedded in Benzocyclobutene (BCB) dielectric. The new contact sites are bumped with solder as on flip-chips and BGAs.
Using wafer level processes underfilling of the area array interconnections is not necessary. Instead interconnections can for instance be embedded in a polymer by combined etch, metallization, and polymer re-deposition. In this way flexible interconnections can be made. In encapsulated WLP the entire wafer is sealed with a glass wafer on one or both sides. The glass can either be glued or anodic bonded [52]. The glass can be lapped down to a thickness of e.g. 100 μm if low profile is needed. For some sensors this “packaging” constitutes part of the sensor bulk structure and functionality to such a degree that it becomes increasingly difficult to define packaging in the traditional sense. This situation is very close to complete WSI or System On Chip (SOC) where all functionalities, mechanical as well as electrical, RF, etc. are integrated inside a single chip. In tape / flex WLP a sheet of tape e.g. wsCSP™ is mounted on and interconnected to the wafer. WLP by molding whole wafers is also a subject to current research [4].

1.3.4.6 System integration

The trend towards system integration i.e. WSI is seen on all packaging levels by features getting smaller and by components brought closer to each other, etc. Overall packaging efficiency is increasing and more and more packages fulfill the Chip Scale Package (CSP) criteria that the package footprint area is maximum 20% larger than that of the naked die. This is for instance the case for CBGA, MCM-D, and WLP packages. Packaging efficiency is defined as the ratio of the naked chip footprint area to the area of the system board / substrate on which it is mounted. Packaging efficiencies for some of the mentioned packages are [4]: DIPs around 10%, BGAs at maximum 50%, MCM up to 80%, SOP up to 90%, WLP close to or at 100%. SOP, WSI (WLP or SOC) are packaging areas of intensive research.

1.3.5 Sensor die – environment interconnection

The drivers for direct, close proximity, partly or no access to sensing elements can be divided up as the economic (minimal size, number of processes), the physical (sensing principle, sensitivity, protection), and the chemical (sensing principle, sensitivity, protection). What is the primary driver depends on the specific sensing situation.
Micro sensors like motion (accelerometers) and optical sensors do not require access in any form (direct, close proximity, partly) to the environment. Chemical (fluidic, gas) sensors may need direct access and others at least partly access through membranes / filters. The surroundings can have direct access (gas) or by use of a thin protective film barrier / interposer close proximity access (aggressive gasses, liquids) to pressure sensors. Close proximity access to the sensing area is often not needed for sensing purposes but because of a cost reduction need. The drive to make the microsystem sensor packaging less expensive is very high since it accounts for up to 70% of the total sensor manufacturing cost [5]. The main reason for this high cost is mainly the many processes performed on single dies more or less separately. To avoid this, the packaging has to approach the chip size by going to the wafer level (WLP, SOC). This in turn has the consequence that the packaging has to be very small and extremely durable to withstand the often very harsh environments sufficiently. Many bulky pressure sensors for harsh environment applications are e.g. packaged with steel membranes and silicone oils as pressure transmitting interface to the sensor element instead of close proximity access through a hole in the outer package to a thin film on the sensing area [19, 102-104]. The huge economic advantage of the thin film is that it can be applied at wafer level. Furthermore, in many applications it is also important that sensors are small even after packaging.
The physical / chemical access hole to the system can be provided in many ways depending on the sensing situation. One type of access is a simple hole (premold package, glob-top / underfill interconnect protection, lid with hole) into the heart of the microsystem sensor. Transfer molding with die access holes can be made with special gentle ways of avoiding mould material on the sensing area [106]. In this case the access is an integral part of the encapsulation. Other examples are optical wires [65-69] for e.g. optical sensors, snouts for microphones [21], micro hoses / tubes, O-rings, etc. for micro liquid handling systems which are mounted / interconnected to the sensor as seen for instance in many Micro Total Analysis Systems (μTAS) [67, 107].

1.4 Packaging strategy

When starting the development of a new microsystem sensor from the elements mentioned above, it is very important to think holistically in terms of system design and of what the system is expected to experience / endure during the projected lifetime i.e. the common design for reliability but also packaging. Examples of different MEMS packaging strategies and designs are given in [17]. All the knowledge (MEM sensor die designers, microelectronics circuit designers, materials scientists, etc.) has to be collected for best performance [108, 109]. Every step in the fabrication of microsystems has a certain purpose but also great influence on what can be done next and in this way often a large influence on final performance. Therefore solutions on each step cannot be freely chosen. It might be as simple as to remember to start fabrication temperatures at the high end. Very costly and well designed MEMS sensors have been fabricated, however, they

were never produced because the packaging was not taken into consideration and it turned out they were impossible to package [110, 111]. Another example of the importance of overall design is that some materials problems cannot be solved directly because of limited intrinsic properties. However, by combined materials design the problems can often be solved. Tightness of protective materials is for instance very important in microsystem sensor packaging for harsh environments. Polymers are attractive for many reasons except for their tightness. Actually no material is hermetic (completely tight), but by properly designed combinations of materials / phases sufficient tightness might be reached [2]. This is very important to remember for microsystem sensor packaging.

1.4.1 Reliability

Reliability issues are far more complex for microsystem sensors than for microelectronics. Common electronics reliability is e.g. reviewed in [112-115]. The reliability of sensors is complicated because they are closely exposed to harsh environments and contain moving parts [17]. Further required service life longer than 10 years is common. For some pressure sensors protected with specially designed thin films for harsh environment applications this means that the allowed corrosion of the film is below one atomic layer per day [103]. Special care in the packaging component materials and process choices for microsystem sensors have already been mentioned in chapter 1.3.

1.4.1.1 Failure modes

The microsystem sensor failures can roughly be divided in two categories: inherent and environmental. Inherent microsystem sensor failures can already occur before the final product service life, but can also be induced / affected by the environment. These failures are specific for microsystem sensors because they occur due to the very nature of the sensor. One inherent failure is where closely separated surfaces come into contact and adhere to each other. This is called stiction [17]. Another example is where the silicon micromechanical parts break during wafer dicing. It could be argued that the latter is actually an environmental failure; however, it has not occurred in the final product environment.

Environmentally induced failures are due to: humidity, thermal cycling, vibration, shock, pressure variations, radiation, etc. separately and in combinations. Combinations usually accelerate failures. The failures may be inevitable due to materials limited intrinsic properties and in that case materials and designs can only be chosen to maximize the time delay to failure. This is for instance the case for hermetic packages for sensors because no package is entirely tight. Here the Mean Time Before Failure (MTBF) may be increased by e.g. designs involving getters [17, 116, 117] and multilayers as already mentioned. In other cases failure is observed because the exposure to these conditions changes the materials properties. T_g for polymers (e.g. epoxy for die attach, molding, etc.) is for instance lowered when water is absorbed [118]. Then essentially we have a new material and perhaps T_g is now in the application temperature range which in turn means that (above T_g) high stresses are developed due to higher polymer volume and CTE. This can have detrimental consequences for the measurement and may lead to delamination [115]. These failures are also seen for ICs in microelectronics, however to a much lesser extent. Because of this sharing of problems some solutions from microelectronics can be used

for the sensor packaging [17]. However, many sensors need application specific solutions as already mentioned in chapter 1.2. Humidity failures are linked to the ingress or out gassing of chemicals from environment and package materials respectively, and loss of package hermeticity. These failures are very important for sensors because they initiate many other failures. They are less important for microelectronics. The consequence of these failures may be seen as e.g. damping of moving parts, corrosion, stress, delamination, etc. When combined with other environmental factors like thermal cycling, vibration, shock, pressure variations, then ingress, out gassing, loss of hermeticity and consequent damping of moving parts, corrosion, stress, delamination, etc. are highly accelerated [119]. Damping of moving parts which can also be induced by other means (e.g. stress) is a failure mode which is not observed at all in microelectronics. Thermal cycling induces solder joint and package failures (e.g. popcorning) in microelectronics but is less important in microsystem sensors except when combined with humid environments as mentioned earlier. Vibration, shock, and pressure variations may result in failures observed as mechanical fatigue, breakage and delamination. The latter will be highly accelerated if also moisture is present. In addition the stresses from vibration, shock, and pressure variations will often accelerate corrosion in humid environment. Polymer packaging materials may also be very susceptible towards radiation and embrittle in e.g. sunlight. This may also be accelerated by other environmental factors. The embrittling may result in e.g. increased stress levels which have impact on sensor performance.

1.4.1.2 Failure analysis

Failure analysis of microsystems is a scientific discipline in itself. When designing for reliability it is mandatory to analyse what the sensor will experience during production and the rest of its lifetime in use. Then from resulting specifications simulations on the whole sensor performance and accelerated testing can be performed. Simulation and statistics can help making fabrication process and design improvements to minimize e.g. unwanted stresses [4, 120-123] influencing sensor measurement. Stresses are one of the major causes for microsystem sensor drift and failure. One way of improving stress simulations and therefore gain better prediction of potential failure sites is by use of actual measured CTE values instead of not very representative (due to differences in processing, etc.) tabulated values. At best the CTE values are measured with the new OMISTRAIN® [124] equipment where nm movements during temperature cycling of whole component surfaces are mapped. The measurements also give direct information on stress levels. Then combined functional / environmental test with in situ electrical measurement can be performed at wafer level on unpackaged, partly packaged or fully packaged sensors with testing equipment also developed recently [3]. Alternatively, it may be done on separate sensors. Then OMISTRAIN® measurements and subsequent simulations may be repeated. Both types of equipment can be used for both microelectronics and microsystem sensors. Among more common instrumental tools to analyse / locate failures are Scanning Electron Microscopy (SEM), Scanning Acoustic Microscopy (SAM) [125], X-rays, electrical probe stations, Focussed Ion Beams (FIB) equipment [126], etc. They are used to detect physical / chemical failures like delamination, cracks bubbles, corrosion and electrical circuit failures.

1.4.1.3 Microsystem materials selection

General overviews of materials for microsystems can be found in [4, 23, 127]. Careful selection of materials is as indicated in previous sections very important for the overall sensor performance and reliability. Sensor performance (access holes, electrical, sensitivity) and minimal size (preferably WLP processing and small hidden pervasive sensors [47, 128]) drive the demand for packaging with high protective capability and applicability without affecting sensor performance negatively. In cases where low cost and small package size is not mandatory materials and design can be chosen more freely and extremely robust sensors can be fabricated.
In table 1 an overview of selected microsystem packaging materials and methods is given.

Table 1: Selected microsystem packaging materials. Italic: Important in microsystem sensor packaging for harsh environments.

Primary purpose, (process and other characteristics)	**Use and materials**
Die attach by:	
Gluing (hard to *compliant* attach, *acceptable electrical* / thermal *conductance, and CTE with fillers)*.	*Mounting on substrates and inside packages.* Adhesives: *Epoxy, cyano esters*, urethane, *silicone*, *filled with* e.g. Ag, *fused silica, quartz.*
Anodic and frit bonding (Silicon CTE matched attach, and sealing).	*Glass, glass frits, silicon (wafer level sealing, stress isolation).*
Electrical conduction by:	
Wirebond (flexibility / compliancy).	*Interconnect between pads on top of die and substrate*. *Au*, Al .
Flip-chip (compact).	*Microelectronics assembly near sensor die (e.g. ASICs).* Sensor die flip-chip interconnect to substrate. *SnPb soldering*, solder materials without Pb, e.g. $SnAg_{3.9}Cu_{0.6}$ or . *Au bumps dipped in Ag filled adhesives (Stud Ball Bumping SBB process)*
Conductive adhesive (low temperature processing, compact, attach*, HDI*, good heat conduction*)*.	*Au, Ag,* Ni, Cu.
TAB (compact).	SnPb soldering, solder materials without Pb, e.g. $SnAg_{3.9}Cu_{0.6}$.
Interconnect on substrate / package by:	
Under Bump Metallization (UBM). (adhesion and diffusion barrier).	*Solder ball interconnect, e.g. ASIC flip-chip* Sensor die flip-chip. Al, Cu,

	Ti, W, TiW, Cu, Mo, Ni, Pt, Pd, Cr.
Pastes (*conductors*, resistors, etc.).	*Hybrid circuits.* *Ag/Pd*, Ru_2O_3 *in matrix of glass, organic fillers and solvents.*
Conductors (high conductance).	Low temperature processed substrates *Au*, Al, Cu.
Leadframes (conductance, high temperature sealing).	*DIP.* *Cu, $Ni_{42}Fe$ (Alloy 42), $Ni_{29}Fe_{53}Co_{17}$ (Kovar™) W, Mo (molded packages).*
Package for protection and chip / interconnection support by:	
Deposition of thin films at wafer and higher levels.	*Physical (mechanical, EMI screening) and chemical protection.* SiO_2, Si_3N_4, *a-CrTa, a-TaO, a-SiC, Cr, Ti, a- Ni.*
Molding / premolding (support, barrier, low stress).	*DIP*, QFP: *Polymers: Heat and UV processed phenolic-epoxy filled with quartz, LCP* MCMs, and hybrid circuits with good thermal dissipation and electromagnetic shielding. Metals: $Cu_{10}W$, $Cu_{15}W$, Silvar™ (Ag-Ni-Fe alloy), $Cu_{15}Mo$, Kovar™ and Alloy 42 plated with Au, Ag, Cu. *Ceramics: Al_2O_3.*
Getters (trapping of unwanted chemicals and particles, use of cheaper packages).	*Inside or as part (ceramic) of hermetic (liquids, gasses) packages.* *Silicone - zeolite composites: STAYDRY™ GA2000-2.* *Metals: Zr-Al-Fe, Ti, Th, Pd, Pt.* *Metal-oxides: PdO.* *Zeolites.* *NanoGetter™.* *Al_2O_3 (e.g. CERDIP).* *Silicon rich oxides.*
Glob-top (barrier, mechanical protection).	*Protection toward liquids, gasses, light.* *Avoidance of wire sweep in molding.* *Adhesives: Anhydride-epoxy e.g. filled with ceramics, carbon.*
Underfill (mechanical protection).	*Microelectronics flip-chip.* Sensor flip-chip *Adhesives:* Anhydride-epoxy, *Cyanate ester e.g. filled with ceramics.*

Coatings (barriers, wear protection).	Microelectronics components / boards, *sensors* protection against *liquids, gasses, light.* Polymers: Solder masks, *Parylene C, Nova HT, Teflon AF, adhesive type* (epoxy, urethane, *cyano esters,* acrylates, silicone) *Polymer-metal composites: e.g. UV curable acrylates with flakes of Cu plated with Ag.*
Lid mounting (tight, low stress lid attachment).	*Lid: Plastics, ceramics, glass, metal.* *Sealing: Adhesives, glass or assembly by anodic* bonding, welding.
Stacked substrate layers (dense, durable low stress interconnection).	Dense MCM packaging of microelectronics and *microsystem sensors.* *Hybrids: Al_2O_3.* *MCMs:* HTCC*, LTCC*, epoxy filled with glass, Kevlar® and Aramid®, *polyimide* (PI), *bismaleimide triazine (BT)*, *Polytetrafluoroethylene (PTFE or Teflon®), Polyether ether ketone (PEEK).*

Some of those which are generally considered most important in microsystem sensor packaging for harsh environment are indicated. Due to the diversity of sensors it is important to stress that whether each material is relevant or not depends on the specific application. These materials and methods have been selected from physical / chemical properties such as high chemical / physical barrier and durability properties, high CTE match capability, low cost processing, etc. which are also important in microelectronics, but are considered even more important for reliable packaging of microsystem sensors.
The major problem to be solved in sensor packaging for harsh environments is to get sufficient access to the sensing area while still providing adequate chip protection. Materials are chosen for different main purposes: Attachment, heat dissipation, conductance (interconnection), insulation, support (boards), protection, and combinations thereof.
However, the materials purposes are all more or less interrelated with each other and the purpose of the final component cf. system design. Table 1 also reflects that generally degrees of freedom in selecting materials for some materials primary purpose is more or less reduced due to some other demands.

1.4.1.3.1 Electrical interconnection materials

Often compromises which severely complicate the packaging have to be made. One simple example is that the demand for a hermetic package which has a low CTE and high physical / chemical durability may require that it is made of ceramic sintered at 1550ºC, i.e. only conductors, e.g. leadframes of W, Mo, with high melting point at the cost of electrical conductance can be used. In that way, the relative importance of purposes / properties (conductance vs. melting temperature, etc.) have been altered because of higher purposes, hermeticity, low CTE, durability, etc. Melting temperatures for these metals are T_m(W) = 3422ºC, T_m(Mo) = 2623, and both have a low CTE of 4.5 ppm which

is very close to that of Si and many sealing glasses like borosilicates. Generally, more corrosion stable metals like Au instead of Al in wirebonding and Cu, Ni in conductive adhesive is used where required by the environment. For microsystem sensors in harsh environment flip-chip interconnection is very attractive from the materials point of view due to small amount of interconnect solder / bump material prone to chemical attach. This explains why Sn-Pb solders can still be used in many applications although they are not very corrosion stable.

1.4.1.3.2 Highly protective die attach, underfill and package materials

Most often the basic innermost microsystem materials (Si, GaAs) and to some extent also the interconnection materials are chosen for their electrical properties without regarding their other properties, which have influence on the reliability.

Therefore one of the most important purposes of die attach, underfill and package materials is to protect the sensor / IC and other packaging materials (wirebonds, etc.) both by constituting a physical (mechanical, temperature) robust interface to the surroundings and by keeping away chemicals, particles, and radiation detrimental for the sensor performance due to their change of materials properties.

The chemicals protected against can be both liquids and gasses. Amongst liquids water and its ionic content are the most common problems. The critical ions are usually Na^+, K^+, and Cl^- coming from salt in sweat, sea water, or it is born from the packaging materials. The ions may diffuse around both in the packaging materials and semiconductors and in this way destroy the electrical functionality directly or they may participate in electrolytic corrosion [129]. The water can also corrode the materials directly (hydrolysis) [4] and indirectly by reactions with corrosive end products. The latter occurs e.g. when too much P is in P doped (to lower melt temperature) glass used as a dielectric layer. Water react with P to give H_3PO_4 acid which further corrodes the surrounding materials [130]. Just the presence of water is most often critical, especially for polymers. The polymers swell, modulus E, CTE, T_g and strength are lowered, etc. The resulting failure modes are e.g. delamination, cracks, popcorning, etc. The presence of water can also induce stiction in silicon micromechanical sensors [17].

The gas chemicals are typically H_2O, H_2, NH_3, SO_2, H_2S, etc. originating from the harsh environment surroundings and out gassed from the packaging materials themselves, e.g. from plated metals and polymers (epoxy). They can all affect microsystem sensors performance severely for instance by corrosion and damping (resonators).

Particles from the surroundings and from component processing can be critical because they can interfere with subsequent processing, short circuit, and block the movement of parts in microsystem sensors. Therefore the processing has to take place in a clean room environment all the way to the final component and appropriate cleaning methods have to be employed.

Electromagnetic radiation can cause the electronics (e.g. amplifiers) and sensors (e.g. capacitive MEMS microphones) to malfunction. To achieve ElectroMagnetic Compatibility (EMC) ElectroMagnetic Interference (EMI) is commonly shielded with the use of metal packages (houses) / grids, metal filled polymers [1], glob-top filled with C, and by deposition of magnetic thin films.

Mechanical robustness is provided first by protecting chips so that they can withstand further handling and processing by applying thin protective films, see table 1. Molded

packages and substrates provide mechanical protection towards the surroundings. Here it is important to note the materials differences in E and toughness.
Generally, heat dissipation from microsystem sensors is not an important issue. However, in special cases as micro hotplate gas sensors where temperatures as high as 500 °C are reached it can be an important issue [131]. A bigger problem is to find packaging solutions which can meet the many high temperature applications within e.g. the automotive and oil / gas industry [34-42].
Ingress of water from the surroundings is often considered to be the biggest problem to solve in microsystem packaging [132-143]. Only 0.1 nL water may be critical due to direct corrosion of narrow Al conductors on chips [133]. No material is actually completely tight towards water. However, their decreasing tightness can be ranked as: Metals, glasses, LCP, Parylene, fluorocarbons, epoxies, silicones. A package is defined as hermetic if the He leak rate is below 10^{-8} cm^3s^{-1} [4]. Qualifying leak testing is usually done in accordance with the military standard MIL-STD-883. However, since the diffusivities of He and water in any material differ a lot testing directly with water is often mandatory. Polymers are attractive because of easy and cheap processing. An extensive overview of polymer permeability data is given in [144]. Water uptake (solubility S) and diffusion constants can be determined in accordance the standard SEMI G66-96 [2, 118, 145-146]. This is done by using the short times approximation of (1):

$$\frac{M_t}{M_E} = 1 - \frac{8}{\pi^2} \sum_{n=0}^{\infty} \frac{\exp\left\{-(2n+1)^2 \pi^2 \frac{Dt}{L^2}\right\}}{(2n+1)^2} \tag{1}$$

where M_t is the weight gain of a thin slab of material after exposure for a period of time t, M_E is the weight gain at equilibrium i.e. after saturation, D is the diffusion constant, and L is the slab thickness [147]. M_E is a power function of the humidity H:

$$M_E = KH^{\alpha} \tag{2}$$

where K and α are temperature dependent constants [4]. The short time approximation of (1) is:

$$\frac{M_t}{M_E} = 4\sqrt{\frac{D}{\pi}}\frac{\sqrt{t}}{L} \tag{3}$$

and given M_E, D can be found from the short times slope h in a plot of M_t/M_E as a function of $t^{1/2}/L$ as:

$$D = \frac{\pi h^2}{16} \tag{4}$$

It is then important to note that the flux F of water will be determined by:

$$F = \frac{DS}{L} = PS \tag{5}$$

where P is the permeability, i.e. that how much is actually passing critical areas is not only determined by D but also by S [2]. It is also very important to realize that for encapsulations S determines how much water is actually in contact with the critical areas. This means that even though a material may have a high D for water (e.g. silicone) they might be a good choice anyway in some application due to low S. The worst case occurs for instance in pressure sensors where a pressure gradient may cause a continuous flux across critical areas. Another critical situation is when the material has taken up a lot of water at high temperature and the temperature then suddenly falls to a temperature where S (determined from M_E) is significantly lower. Then the material literally begins to sweat. This may cause high stresses followed by delamination, cracks, etc. This is one of the reasons why good adhesion at interfaces is so important. Slower mechanisms are creation of weak boundary layers with high water content and hydrated metal oxides and finally delamination. Interfaces are generally very prone to failure due to stress concentration.

The materials used for die attach, underfill, and packages are: polymers, ceramics, glasses, metals, organic / inorganic / metallic thin films and coatings, and getters, see table 1.

Polymers are used more and more in microsystems, especially microelectronics because they are becoming higher grade concerning Na^+, Cl^-, K^+. Nowadays the content of these ions is usually only a few ppm for electronic grade polymers. Further, thin film protection (oxides, nitrides) has also made chips sufficiently mechanically / chemically robust for transfer molding [4]. Generally, the polymers chemical resistance against solvents can be evaluated using the Hansen Solubility Parameters (HSP) [148]. A common polymer mould compound is phenolic epoxy. Better performing polymer packages for microsystem sensors can e.g. be made of LCP [85, 86] or cyano ester adhesive [4, 149]. Both these polymers are highly chemically resistant and water tight. Actually LCP is the tightest polymer known. Also cyano ester adhesive is a very good water barrier in that it actually captures (get) the water by reaction without degradation [4]. They are both very chemically resistant and both come filled with very low CTEs.

Epoxy based polymers are normally used for die attach because of their good adhesion and durability. They are also quite tight compared to many polymers e.g. silicone. Highly filled with quartz the CTE can come as low as 11 ppm. This is not possible with silicones which are also less chemically durable especially toward solvents. However, they are used in sensor applications where completely stress free assembly or encapsulation (silicone gel) is needed. Water flux through silicones can be as low as for epoxies due to low S. Very low stress sensor attach and encapsulation can also be approached by use of UV curable epoxies. This is due to room temperature curing, step curing, and quartz filling [84].

Anhydride epoxies are commonly used for underfill and glob-top base materials, but will not be good enough in the many sensor application where water comes close because these systems give polyester linkages which are prone to hydrolysis [4]. Here cyano ester based adhesive is more promising.

Epoxy is also used for PCBs (FR4) and layered substrates (MCM-L) with different fillers, see table 1. This is also the case for PI, BT, PTFE, and PEEK all of which are very

interesting candidates for microsystem sensor packaging because of low permeability and / or chemical durability.
Ceramic substrates and house packages are typically Al_2O_3, HTCC, and LTCC which are very water tight partly due to their dense structure and because of water getter properties. It is also very tight towards other substances. Besides CTE is very low, chemical durability high, and *E* is high. These materials are very attractive to microsystem sensor packaging [66, 88-90].
Glasses are basically SiO_2. Differently doped (e.g. with P) glasses can have low melting temperatures making them usable for ceramic and metal package sealing (lid and electrical feed-through in metal packages) and actually also for die attach e.g. silver-filled for thermal conductance. In humid environment it is important that the glass contains no alkalis like Na^+ because they can be released by water corrosion and destroy the microelectronic circuit.
Metal packages are usually chosen to have good thermal conductivity and low CTE. Examples are shown in table 1 [83]. The metal packages are used as houses for hybrids and MCMs. Together with glass-sealed lids and electrical feed-throughs these packages are hermetic. Metal lids are also soldered or welded. Moisture is often a serious problem when using metallic packages because metals are generally hydrophilic [4, 150]. Good adhesion of e.g. adhesives is very often correlated with surface energies / tensions [151]. To achieve good adhesive bonding good spreading is usually a prerequisite. This can be achieved by ensuring a low surface tension of the adhesive compared to that of the substrate. Moisture on metals has the effect of lowering the surface tension [152] and therefore often the adhesion strength.
Organic conformal coatings are often urethane based [4]. They are used mostly for circuit board protection. They have very good protective properties regarding humidity, corrosive environment, and toughness. They can be as protective as hermetically sealed packages. They cure both by heat and UV light. Other organic conformal coatings of greater interest for microsystem sensor protection are the parylenes (poly-para-xylylene) and Teflon AF [1]. This is primarily because they cover bond wires and single crystalline silicon edges and corners highly conformal in layers thinner than 10 μm and because of their high chemical durability. Parylene C is also very tight (comparable to LCP) and is therefore used as barrier [20]. Also of interest for MEMS sensors is thin conformal coatings of polymer-metal composites for EMI shielding [1].
Inorganic / metallic thin (around 1 μm) films are of particular interest for compact chemical and EMI protection [19-22, 102-104]. Some coatings are amorphous to avoid chemical attack and fast diffusion otherwise observed at crystallite boundaries, see table 1.
Getters are materials that traps unwanted chemicals e.g. H_2O moisture, H_2, NH_3, SO_2, H_2S either by adsorption or reaction [17, 116, 117]. Silicon gas compatibility guidelines are described in the SEMI F79-0703 standard. Getters are used inside packages because it is well known that no material can keep out the mentioned chemicals sufficiently for the periods of interest. They consist of sticky polymer capturing particles typically from the processing and metal and metal oxides, see table 1. The unwanted gases flow may also be diverted by phase barriers as e.g. air. For moisture this can be very effective since *D* in e.g. epoxy is around 5×10^{-13} m^2s^{-1}, and in air it is around 2×10^{-5} m^2s^{-1} at room temperature. As depicted in section 1.4.1.3 high durability packaging can be achieved

with high durability packages and smaller demands on sensor performance. However, the performance of the above mentioned hermetic ceramic package (section 1.4.1.3.1) may e.g. also be achieved in a cheaper way by use of a less tight polymer package with one or more getters inside and Cu as conductor. This is one way of achieving Reliability WithOut Hermeticity RWOH. Alternatively very high performance concerning tightness and the often ultimate goal to keep chemicals and particles away from the critical sensor parts may be achieved by use of the ceramic package including getters inside.

1.4.1.3.3 Sensor die – environment interconnection materials

In many cases the access hole is part of the package and consequently made of that material. However, often some guide of the media to be sensed on, has to be fixed to the microsystem sensor. For that small commercial or specifically manufactured fittings (plastic, glass, etc.) are used together with adhesives like epoxy and silicone [1, 20, 21, 29, 67, 107]. The fixation has to be completely microsystem sensor compatible regarding the same parameters as the rest of the packaging, i.e. minimum stress, high adhesion, no corrosion, etc.

1.5 Specific applications

Below specific microsystem sensor packaging examples are given. They are grouped according to whether they can be considered standard packaging, modified standard packaging, or custom designed packaging. Pressure sensors and accelerometers represent the largest markets. To cover all these types of packages and sensors the examples comprise 3 pressure sensors, 2 accelerometers, and 1 microphone. They are commented regarding application (environment), and how the packaging has been solved concerning electrical interconnection, sensor die – environment interconnection, and protective package. Many examples can be found in the literature e.g. from other areas like biotechnology and telecommunication [153, 154].

1.5.1 Standard packaging

This kind of packaging involves conventional packaging technologies from microelectronics. An example is the ADXL202 dual axis accelerometer from analog devices, fig. 2. This is a house type ceramic DIP. The accelerometer is mounted in a ceramic package cavity and interconnected with Al-wirebonds to the leadframe. No access hole / window is needed for such a sensor. A lid is hermetically sealed to the package cavity.

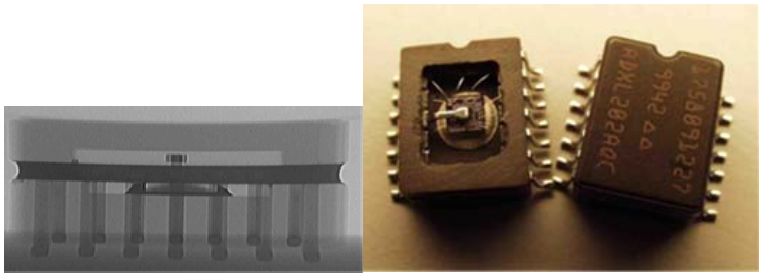

Fig. 2: Left: X-ray photo of dual axis accelerometer. The aluminium wirebonds cannot be seen on an X-ray photo. Right: Grinding the ceramic away opens the package.

1.5.2 Modified standard packaging

These packages are based on materials and shaping of the package that to a varying degree differs from what is seen in the microelectronics industry in order to meet the requirements of the specific microsystem sensor. One example is the SP13 tire pressure sensor from SensoNor, see fig. 3. This is an absolute pressure sensor in a plastic DIP. It

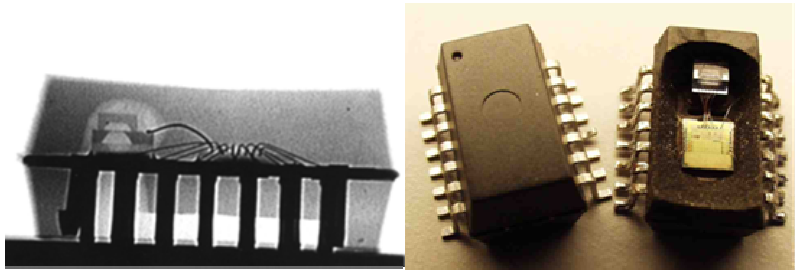

Fig. 3: Left: X-ray photo of absolute pressure sensor. Right: Etching with dry HNO_3 exposes the sensor and the chip.

should be noted that in this case a glob-top has been placed around the sensor stack in order to minimize the thermal stress and wire sweep from the injection molding encapsulation. Gold wirebondings are used as electrical connections from both the sensor to the ASIC and from the system to the leadframe which provides the external connection. Note also that the packaging differs from microelectronics packages as it includes glass bonded at wafer level (cf. WLP) on both sides providing minimum stress on the silicon sensor die in the middle, reference pressure cavity on the top side, and part of the pressure access hole / channel to the sensor die. The rest of the hole to the sensor die is in the leadframe and plastic mould material. Another example is the SLP004D pressure sensor from SensorTechnics, see fig. 4. It can be used for measuring differential

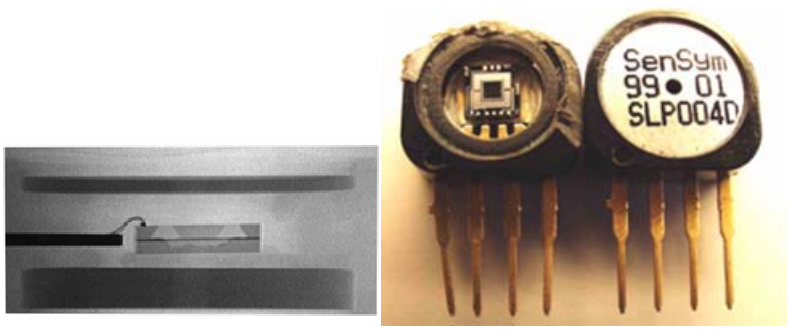

Fig. 4: Left: X-ray photo showing wirebonds, sensor unit and the two aluminium plates. Right: The sensor is exposed for inspection by removing one aluminium plate.

or absolute pressure. This sensor is wirebonded to a leadframe which provides the external connections resulting in a Single Inline Package (SIP). A hole in each Al plate provides physical connection. The hole gives direct access to the chip surface i.e. the component is relatively vulnerable to pollution. The package is a plastic house with Al plates on both front and back.
A third example is the SA20 airbag accelerometer from SensoNor, see fig. 5. The internal

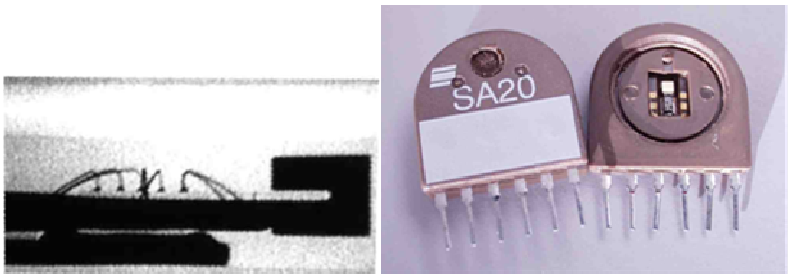

Fig. 5: Left: X-ray photo showing the seismic mass (right) and the wirebonds. Right: Grinding exposes the die.

electrical connections are made using gold wirebonding, and the external connections are provided via the pins, in this case a SIP. The house is a welded polyphenylene sulfide (PPS) plastic housing. This is a thermoplastic material with excellent thermal, mechanical and chemical resistance. The sensor does not need a physical connection to the outside, since it measures only the movement of a seismic mass via a piezo resistive bridge. The cavity in the house is filled with silicone oil for the purpose of dynamic damping.

1.5.3 Custom designed packaging

In more complex packages even the interconnections are of a more advanced type. The development of the bare silicon MEM die, is not the main area of work, however, the entire system including the sensor, the interconnection and the package have to be planned together, because they can have multiple functions and constrain each other severely. At this point there is very little to be said about standard packaging. With the

example in fig. 6 and fig. 7 which is a 3 mm · 3 mm · 2 mm microphone (dummy) for e.g. hearing aids, mobile phones, focus is only on the demands for a protecting encapsulation material that practically takes up no space [1]. Other minimum packaging volume

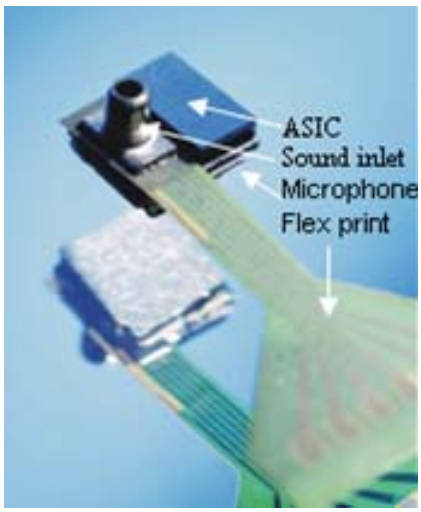

Fig. 6: A dummy sample of a silicon micromechanical microphone before encapsulation.

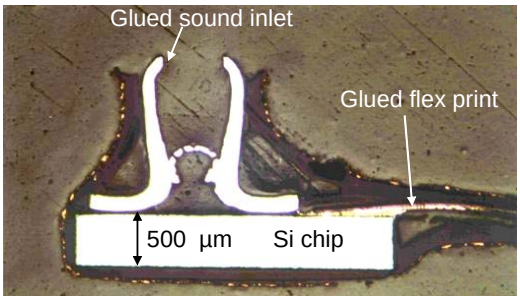

Fig. 7: Cross section showing the built-up of the test structure. Two protective encapsulation layers are needed. A conductive top layer for EMI (Electro Magnetic Interference) shielding and an insulating layer beneath to avoid short circuiting anywhere on the microphone. The first layer has been applied by dipping, the second by spraying. Note that it has been possible to cover the sharp corners of the silicon. Here the insulating layer has a thickness of approx. 50 µm. The thickness of the conducting layer is around 25 µm everywhere.

methods used have been chip stacking involving: anodic bonding, sealing with fluxless solder bump bonding, and through-hole microphone / ASIC interconnection, together with flip-chip interconnection (ASIC, flex print) and mounting (sound inlet) [21, 22].Even though they are often the simplest microsystems, pressure sensors are usually placed in very rough environments. As mentioned earlier, keeping the microsystem small and cheap means high demands on the packaging materials and methods. An example is the Grundfos differential pressure sensor, see fig. 8.

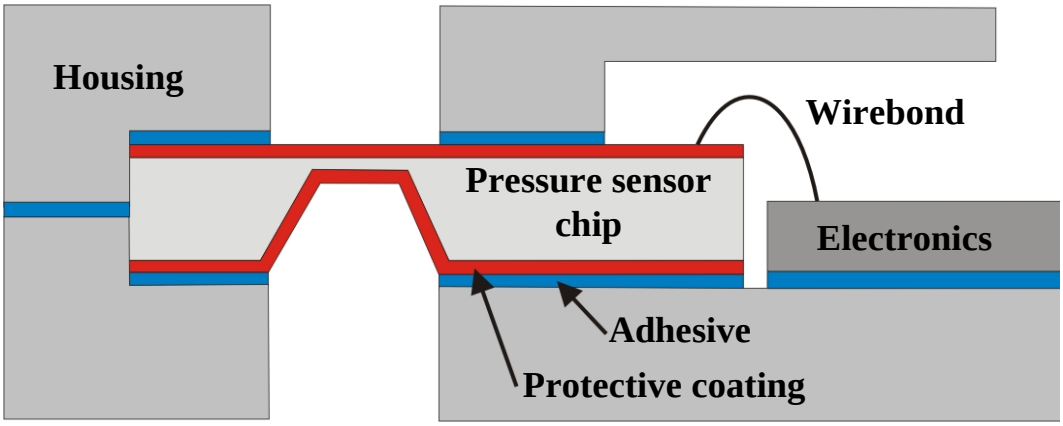

Fig. 8: Cross-sectional drawing of a differential pressure sensor. The sensor chip is protected with a coating on both sides and mounted in a housing using adhesive. Through the access holes in the housing and contact with the coating the media gets in close proximity to the pressure sensor chip.

Here the sensor has to be able to withstand direct exposure to water under pressure at 125 °C via the holes in the housing for at least 10 years. To solve this problem focus has been on:

1) Materials with high corrosion stability. Especially the thin protective film has to be very corrosion stable. For a sufficiently thin film, which should be able to last for 10 years, no more than one atomic layer may be corroded per day [19, 20, 102-104].

2) Tight and low stress mounting / sealing of die in housing. The tightness depends entirely on the adhesives / O-rings bulk and interface tightness to house / film on the die. The tightness is important since the very corrosion sensitive microelectronics is placed close to the water. The allowed leak rate to ensure low enough corrosion has been estimated to $2.5 \cdot 10^{-2}$ mm^3/year/bar [20]. Stress is important because it may couple into the pressure sensing membrane area and thereby disturb the measurement [109, 120]. The stress depends on both adhesives / O-ring and the house materials CTE. The adhesives / O-rings CTE might change significantly over time.

1.6 Glossary

ACA Anisotropic Conductive Adhesive. Adhesive where the amount of electrically conductive filler is adjusted for conduction in only one direction perpendicular to the substrate.

Anodic bonding A joining method where e.g. silicon and borosilicate glass can be bonded making use of heat at around 400 ºC and high voltage.

ASIC Application Specific Integrated Circuit.

BCB Benzocyclobutene. A polymer used in microsystem packaging as dielectric material in layered electrical interconnection.

BGA Ball Grid Array. A package where a chip is interconnected to the next level of packaging using a space transforming interposer. An area array of solder balls on the interposer is typically used for interconnection to the next level of packaging.

BT Bismaleimide Triazine. Polymer used as dielectric material in PCB and layered electrical interconnect substrates.

CBGA Ceramic Ball Grid Array. A BGA where the interposer is HTCC or LTCC.

CSP Chip Scale Packaging. A package where the footprint area is maximum 20% larger than that of the naked die.

CTE Coefficient of Thermal Expansion. Indicates how much a material expands as a function of temperature. The symbol is typically μm/m°C.

CVD Chemical Vapor Deposition. A vacuum deposition process where chemical reactions take place both in the gas and on the substrates. Used e.g. to deposit parylene (poly-para-xylylene) as protective coating.

DIP Dual Inline Package. A package with leads on two parallel sides.

EMC ElectroMagnetic Compatibility. Refers to the situation where an electronic component is constructed / protected so that EMI is not a problem.

EMI ElectroMagnetic Interference. Disturbance of electronics by electromagnetic radiation.

FIB Focused Ion Beams. In electronics FIB is used for failure analysis where e.g. conductors are cut or repaired.

Flip-chip An electrical interconnection method where a chip is turned upside down (flipped) to connect contact points typically in an array area on the chip and chip carrier.

Getter In microsystems a material that traps or keep away unwanted chemicals and particles by being reactive or sticky.

HDI High Density Interconnect. Refers to electrical interconnection with a very low pitch.

HSP Hansen Solubility Parameters. Parameters that helps predicting the chemical durability of polymers towards solvents.

HTCC High Temperature Cofired Ceramic. Electrical interconnect substrates consisting of alternating layers of conductors and ceramic as dielectric material. The soft and compliant ceramic layers are co fired / hardened at high temperature (1550 ºC).

IC Integrated Circuit.

ICA Isotropic Conductive Adhesive. Electrical conductive adhesive with a high filler content resulting in isotropic conduction.

LCD Liquid Crystal Display. Flat displays based on liquid crystals which change orientation when a voltage is applied across them.

LCP Liquid Crystal Polymer. Thermoplastic polymers with unique structural, physical and chemical properties. Consists of linked rigid and flexible monomers. Rigid molecule segments align in the liquid state during flow and this alignment is maintained when cooling to the solid state. An example of a LCP is Vectra A-950.

0 level packaging See WLP.

1st level packaging Packaging at the micromechanical chip and / or IC level. It comprises chip (micromechanical, IC, ASIC, etc.) mounting (anodic bonding, gluing, soldering) on some support (carrier, housing, substrate e.g. with interconnecting conductors) and interconnection (wirebond, flip-chip soldering / gluing, conductive adhesive).

2nd level packaging Packaging at system level or board level. Packaging on this level consists of mounting the 1st level package onto some board (typically FR4 PCB or card) to interconnect active and passive components.

3rd level packaging Packaging at the board to board interconnection level like in PCs where several slots for insertion of different cards exist.

LTCC Low Temperature Cofired Ceramic. Stacked electrical interconnection layers like HTCC, only the ceramic layers are co fired at low temperatures.

MCM Multi Chip Module. A packaged electronic circuit is a MCM when more than half of the substrate area is covered with active devices. The substrate is typically a layered interconnect substrate like HTCC or LTCC.

MEMS MicroElectroMechanical System. Miniaturized sensors and actuators with micrometer size features. Sensing and actuating is electromechanical. The MEMS comprises a MicroElectroMechanical (MEM) component and some low level packaging e.g. interconnection to a substrate, an ASIC, etc. Normally the MEM is a single crystalline silicon micromechanical structure fabricated by etching methods.

Microsystem MEMS together with microelectronics, photonics, RF / wireless packaged to the 2nd and 3rd level.

Microsystem sensor Miniaturized sensor with micrometer size features for analysis involving disciplines as: Mechanics, fluidics, biology, chemistry, microelectronics, optics, etc.

µTAS Micro Total Analysis Systems. Systems with micrometer size features comprising all necessary components for complete analysis.

MID Mould Interconnect Device. Molded polymer supporting and interconnecting carrier where the interconnecting conductors are applied e.g. by chemical / galvanic metallization or by hot embossing.

MTBF Mean Time Before Failure.

NEMS NanoElectroMechanical Systems. Electromechanical sensors or actuators with nanometer size features.

Packaging The interfacing between active / passive microsystem components and the surroundings: Attachment, support (substrate, carrier, encapsulation), signal interconnection between components and environment (electrical, optical, chemical / physical, access for sensing / actuation), and protection (encapsulation, housing).

PBGA Plastic Ball Grid Array. A BGA type where the interposer is made of some kind of plastic which is most often FR-4 or BT-epoxy PCB.

PCB Printed Circuit Board. Typically a FR4 board made of epoxy-glass with printed conductors for electrical interconnection.

Popcorning Cracks and delaminations in house and encapsulation type packages because of sudden heating of entrapped moisture in the materials. The sudden heating is e.g. due to wave soldering.

PWB Printed Wiring Board. Boards with conducting lines for interconnection e.g. FR4.

QFP Quad Flat Package. A package with leads on all four sides.

RWOH Reliability WithOut Hermeticity.

SAM Scanning Acoustic Microscopy. SAM is a Non Destructive Testing (NDT) method for micro inspection which functions like a sonar, though using much higher frequencies, MHz – GHz. Pulses of ultrasound is transmitted through a liquid medium, typically water, to the component and its interior where it is reflected and transmitted at interfaces between materials due to their differences in acoustic impedance *Z*. It is used in microsystem failure analysis for detection of e.g. cracks, bubbles, delamination in packages.

SBB Stud Ball Bumps. Bumps which can be used for electrical interconnection in the flip chip process by first dipping them in conductive adhesive.

SEM Scanning Electron Microscopy. A kind of microscope for surface inspection using electrons instead of light giving much higher magnification.

SIP 1) Single Inline Package. A package with leads on one side. 2) System In Package. Packaging where the components are more or less integrated or encapsulated in the packaging i.e. in layered interconnect substrates. Another word for SIP is System On Package (SOP).

SOC System On Chip. SOC is the ultimate integration level accomplished when a whole functional system is integrated in one monolithic chip.

SOP System On Package. See SIP.

Stiction The unwanted natural adherence between surfaces of MEMS structures that come very close.

TAB Tape Automated Bonding. A low profile chip electrical interconnection method using soldering by thermo-compression of free conductors e.g. Cu on the tape to both chip and some package or PWB.

TBGA Tape Ball Grid Array. BGA where the interposer is made of some kind of polymer tape. The tape is typically polyimide, epoxy-glass.

WLP Wafer Level Packaging. Packaging at the wafer level i.e. before dicing of the wafer into separate components. WLP is also called 0 level packaging.

WSI Wafer Scale Integration. The act of moving the packaging processes to the wafer level.

1.7 References

1. Jakob Janting, Jens Branebjerg, Pirmin Rombach, Sensors and Actuators A 92 (2001), pp. 229-234.

2. Jakob Janting, Proceedings of Micro System Technologies (MST) conference, München, October 7-8, (2003), pp. 520-522.

3. Søren Pihl Rybro, Proceedings of Micro System Technologies (MST) conference, München, October 7-8, (2003), pp. 451-455.

4. Rao R Tummala, McGraw-Hill, (2001), ISBN 0-07-137169-9.

5. Marc Madou, CRC Press (1997), ISBN: 0-8493-9451-1.

6. Y. C. Lee, Babak Amir Parviz, J. Albert Chiou, and Shaochen Chen, IEEE Transactions on Advanced Packaging, Vol. 26, No. 3, August, (2003), pp. 217-226.

7. Matthias Werner, Hans-Jörg Fect and Richard W. Siegel, MSTNEWS, No. 3, (1999), pp. 4-6.

8. Matthias Werner, Thomas Köhler and Werner Grünwald, MSTNEWS, No. 3, June, (2001), pp. 4-8.

9. Ken Snowdon, Calum McNeil and Jeremy Lakey, MSTNEWS, No. 3, June, (2001), pp. 9-10.

10. T. I. Kamins and R. Stanley Williams, MSTNEWS, No. 3, June, (2001), pp. 34-36.

11. Volker Türck and Dieter Bimberg, MSTNEWS, No. 3, (1999), pp. 17-19.

12. R. Tummala, Components, Packaging, and Manufacturing Technology (CPMT) Society Newsletter, Vol. 25, No. 4, (ISSN 1077-2999), December, (2002), pp. 1-2.

13. Mats Robertsson, Proceedings of The IMAPS Nordic Annual Conference, ISBN: 951-98002-6-3, Helsingør, Denmark, (2004), pp. 2-24.

14. Bharat Bhushan, Editor, Springer-Verlag, Berlin, Heidelberg, New York, ISBN: 3-540-01218-4, (2004).

15. Achim Wixforth, Jürgen Scriba and Christoph Gauer, MSTNEWS, No. 5, (2002), pp. 42-43.

16. Kwang-Seok Yun, Il-Joo Cho, Jong-Ik Bu, Chang-Jin (CJ) Kim, and Euisik Yoon, Journal of Microelectromechanical Systems, Vol. 11, No. 5, October, (2002), pp. 454-461.

17. K. Gilleo, proc. IMAPS 2000, Boston, USA, September, (2000), pp. 598-604.

18. Richard R. A. Syms, Eric M. Yeatman, Victor M. Bright, and George M. Whitesides, Journal of Microelectromechanical Systems, Vol. 12, No. 4, August, (2003), pp. 387-417.

19. Karsten Dyrbye, Tina Romedahl Brown, Gert Friis Eriksen, J. Micromech. Microeng., Vol. 6, (1996), pp. 187-192.

20. R. de Reus, C. Christensen, S. Weichel, S. Bouwstra, J. Janting, G. Friis Eriksen, K. Dyrbye, T. Romedahl Brown, J. P. Krog, O. Søndergaard Jensen, and P. Gravesen, Microelectronics Reliability, Vol. 38, (1998), pp. 1251-1260.

21. M. Müllenborn, P. Rombach, U. Klein, K. Rasmissen, J. F. Kuhmann, M. Heschel, M Amskov Gravad, J. Janting, J. Branebjerg, A. C. Hoogerwerf, S. Bouwstra, Sensors and Actuators A 92, (2001), pp. 23 – 29.

22. Christian Wang, Proceedings of Workshop on MEMS Sensor Packaging, ISBN: 87-89935-46-2, Danish Technical University (DTU), Lyngby, Denmark, March 20th and 21th, (2003).

23. Materials Science of Microelectromechanical Systems (MEMS) Devices, Vol. 546 in the MRS Symposium Proceeding Series, Boston, Massachusetts, U.S.A, (1998), Edited by Arthur H. Heuer and S. Joshua Jacobs.

24. Yvette Kaminorz, MSTNEWS, Special issue, August, (2003), pp. 4-6.

25. M. Calleja, J. Tamayo, A. Johansson, P. Rasmussen, L. M. Lechuga, and A. Boisen, Sensor Lett. Vol. 1, No 1, (2003).

26. J. Thaysen, A. D. Yalçinkaya, R. K. Vestergaard, S. Jensen, M. W. Mortensen, P. Vettiger and A. Menon, Proceedings of MEMS 2002, Las Vegas, January, (2002), pp. 320-323.

27. Mark Denninger, Claus Narholm-Hansen and Jacques Jonsmann, Proceedings of Workshop on MEMS Sensor Packaging, ISBN: 87-89935-46-2, Danish Technical University (DTU), Lyngby, Denmark, March 20th and 21th, (2003).

28. F. J. Blanco, M. Agirregabiria, J. Garcia, J. Berganzo, M. Tijero, M. T. Arroyo, J. M. Ruano, I. Aramburu and Kepa Mayora, J. Micromech., Microeng., Vol. 14, January, (2004), pp. 1047-1056.

29. Jakob Janting, Elisabeth K. Storm, Oliver Geschke, Proceedings of μTAS, 8th International Conference on Miniaturised Systems for Chemistry and Life Sciences, Malmö, Sweden, 26-30 September, (2004), pp. 378-380.

30. Peter Friis, Elisabeth K. Storm, Karsten Hoppe, and Jakob Janting, Proceedings of μTAS, 8th International Conference on Miniaturised Systems for Chemistry and Life Sciences, Malmö, Sweden, 26-30 September, (2004), pp. 354-356.

31. I-B. Kang, M. Manda, A. Hariz, N. D. Samaan, M. R. Haskard, Proc. MICRO 1997, pp. 129-133, Melbourne, Australia.

32. Y.C. Su, L. Lin, IEEE MEMS-2001 Conference, Interlaken, Switzerland, January 21-25, (2001), pp. 50-53.

33. Dr. G. Krötz, MST News 21/97, (1997).

34. Colin Johnston, MSTNEWS, No. 4, September, (2001), pp. 4-5.

35. Eberhard Kaulfersch, Jürgen Auersperg, Bernd Michel and Andreas Schubert, MSTNEWS, No. 4, September, (2001), pp. 8-9.

36. K. Gottfried, M. Vogel. R. Hoffmann, C. Kauffmann, St. Guenther and F. Dieckmann, MSTNEWS, No. 4, September, (2001), pp. 10-11.

37. Emanuele Pace and Mara Bruzzi, MSTNEWS, No. 4, September, (2001), pp. 12-13.

38. Ovidiu Vermesan, Ralph W. Bernstein and Geir Uri Jensen, MSTNEWS, No. 4, September, (2001), pp. 14-15.

39. Riccardo Groppo, Wolfgang Wondrak, Guenter Lugert and Thomas Riepl, MSTNEWS, No. 4, September, (2001), pp. 16.

40. U. Kaufmann, J. Hauβelt and H. Moritz, MSTNEWS, No. 4, September, (2001), pp. 35-38.

41. Martin Nese and Frode Meringdal, MSTNEWS, No. 4, September, (2001), pp. 35-40.

42. Patrick McCluskey and LiangYu Chen, MSTNEWS, No. 4, September, (2001), pp. 41-42.

43. Volker Grosser, Matthias Schuenemann, Herbert Reichl, Helmut Kergel, MSTNEWS, No. 1, February, (2000), pp. 4-8.

44. Jeroen M. Wissink, MSTNEWS, No. 1, February, (2000), pp. 20-22.

45. Marcel F. Dierselhuis and Gerben W. A. Kolkman, MSTNEWS, No. 1, February, (2000), pp. 16-17.

46. Vern Solberg, Proceedings of The IMAPS Nordic Annual Conference, ISBN: 951-98002-6-3, Helsingør, Denmark, (2004), pp. 42-48.

47. E. Jan Vardaman, Linda Matthew, Proceedings of The IMAPS Nordic Annual Conference, ISBN: 951-98002-6-3, Helsingør, Denmark, (2004), pp. 26-29.

48. G. Kelly, J. Alderman, C. Lyden, J. Barrett and A. Morrissey, Microsystem packaging in 3D, Proceeding of SPIE 3224, Vol. 142, (1997).

49. V. K. Varadan and V. V. Varadan, Proc. SPIE Vol. 2722, (1996), pp. 156-164.

50. Ulrike Scholz, Wolfgang Eberhardt, Ulrich Keβler, Heinz Kück, Proceedings of Micro System Technologies (MST) conference, München, October 7-8, (2003), pp. 172-179.

51. Leo G. Feinstein, in Electronic Materials Handbook, ASM International, Vol. 1: Packaging, ISBN: 0-87170-285-1, (1989), pp. 213-223.

52. Elmar Cullmann, Proceedings of Workshop on MEMS Sensor Packaging, ISBN: 87-89935-46-2, Danish Technical University (DTU), Lyngby, Denmark, March 20th and 21th, (2003).

53. Charles H. Small, EDN July 21, (1988), pp. 74-82.

54. Barbara Kanegsberg, Edward Kanegsberg, Editors, CRC Press, Boca Raton, London, New York, Washington , D.C. ISBN: 0-8493-1655-3, (2001).

55. P. Amirfeiz, A. Weinert, and S. Bengtsson, Proceedings of Eurosensors XIV, The 14th European Conference on Solid-State Transducers, pp. 427-430, August 27-30, (2000), Copenhagen, Denmark.

56. Liyu (Steve) Yang, Joseph B. Bernstein, and Kai Choong Leong, IEEE transactions on electronics packaging manufacturing, Vol. 25, No. 2, pp. 91-99, April, (2002).

57. Shijian Luo, and C. P. Wong, IEEE Transactions on components and packaging technologies, Vol. 24, No. 1, March, (2001), pp. 43-49.

58. Shijian Luo and C. P. Wong, IEEE Transactions on components and packaging technologies, Vol. 24, No. 1, March, (2001), pp. 38-42.

59. Al Hawes and Tom Adams, Electronic Production, April, (2001).

60. Zhuqing Zhang and C. P. Wong, IEEE Transactions on Electronics Packaging Manufacturing, Vol. 25, No. 2, April, (2002), pp. 113-119.

61. J. Stary, I. Szendiuch, Proceedings of The IMAPS Nordic Annual Conference, ISBN: 951-98002-6-3, Helsingør, Denmark, (2004), pp. 49-55.

62. Hirokazu Tanaka, Akihiko Saito, Toshiro Nagayama, Hiromi Umeda, Proceedings of The IMAPS Nordic Annual Conference, ISBN: 951-98002-6-3, Helsingør, Denmark, (2004), pp. 56-67.

63. Minna Arra, David Geiger, Dongkai Shangguan, Jonas Sjöberg, Proceedings of The IMAPS Nordic Annual Conference, ISBN: 951-98002-6-3, Helsingør, Denmark, (2004), pp. 68-73.

64. F. Caloz, D. Ernst, P. Rossini, L. Gherardi, L. Grassi, J. Arnaud, Microelectronics Reliability, Vol. 42, pp. 1323-1328, (2002).

65. Guenter Schiebel, Proceedings of The IMAPS Nordic Annual Conference, ISBN: 951-98002-6-3, Helsingør, Denmark, (2004), pp. 216-225.

66. Jaakko Lenkkeri, Tuomo Jaakola, Kari Kautio, Markku Lahti, Proceedings of The IMAPS Nordic Annual Conference, ISBN: 951-98002-6-3, Helsingør, Denmark, (2004), pp. 108-114.

67. Oliver Geschke, Henning Klank, Pieter Telleman, Wiley-VCH Verlag GmbH & Co. KGaA, Weinheim, ISBN: 3-527-30733-8, (2004).

68. Jochen Kuhmann, Lior Shiv, Gordon Elger, Andreas Hase, Matthias Heschel, Proceedings of Workshop on MEMS Sensor Packaging, ISBN: 87-89935-46-2, Danish Technical University (DTU), Lyngby, Denmark, March 20th and 21th, (2003).

69. Magnus Olson, Proceedings of Workshop on MEMS Sensor Packaging, ISBN: 87-89935-46-2, Danish Technical University (DTU), Lyngby, Denmark, March 20th and 21th, (2003).

70. Kim P. Hansen and Hans Ole Nielsen, DOPS-NYT 1, ISSN: 0901-4632, (2001), pp. 20.

71. Torben Hillingsøe Lisby, Proceedings of Workshop on MEMS Sensor Packaging, ISBN: 87-89935-46-2, Danish Technical University (DTU), Lyngby, Denmark, March 20th and 21th, (2003).

72. P. Fine, B. Cobb, and L. Nguyen, IEEE Transactions on Components and Packaging Technologies, Vol. 23, No. 3, September, (2000), pp. 420-427.

73. R. Aschenbrenner, A. Ostmann, G. Motulla, K. Becker, E. Zakel and H. Reichl, IZM Proceedings, Vol. 2, (1996), pp. 258-269.

74. Masahiro Ono, Yoshihiro Tomura, Yoshihiro Bessho, Tsukasa Shiraishi, Kazuo Eda and Toru Ishida, Proceedings IEMT/IMS, Japan, (1997).

75. Richard Estes, Frank Kulesza, Proceedings of workshop on smart card technologies and applications, Berlin, Germany, November 18-20, (1996), pp. 315-323.

76. Bela Rösner, Johan Liu and Zonghe Lai, Proceedings of the 46th Electronic Components and Technology Conference (ECTC), May 28-31, Florida, USA, (1996), pp. 578-581.

77. Alan M. Lyons, G. W. Kammlott, Y-H. Wong, and G. Adams, Proceedings of International Conference on Flex Circuits, Flexcon'95, Sunnyvale, California, USA, (1995), pp. 1-8.

78. Conductive Adhesives for Electronics Packaging, Edited by J. Liu, Electrochemical Publications Ltd., London, U.K, 1999.

79. H. Kristiansen, T. O. Grønlund and Johan Liu, Proceedings of The IMAPS Nordic Annual Conference, ISBN: 951-98002-6-3, Helsingør, Denmark, (2004), pp. 86-91.

80. Liquang Cao, Yanli Wang, Guoliang Chen and Johan Liu, Proceedings of The IMAPS Nordic Annual Conference, ISBN: 951-98002-6-3, Helsingør, Denmark, (2004), pp. 92-97.

81. Itsuo Watanabe, N. Nakazawa, Tohru Fujinawa, Motohiro Arifuku, Masaki Fujii, Yasushi Gotoh, Proceedings of The IMAPS Nordic Annual Conference, ISBN: 951-98002-6-3, Helsingør, Denmark, (2004), pp. 74-79.

82. Petri Savolainen, IIkka Saarinen, Proceedings of The IMAPS Nordic Annual Conference, ISBN: 951-98002-6-3, Helsingør, Denmark, (2004), pp. 98-103.

83. R. D. Gerke, in Publication 99-1, Jet Propulsion Laboratory, Pasadena, California, January, (1999).

84. K. K. Baikerikar, A. B. Scranton, Polymer 42, (2001), pp. 431-441.

85. Xuefeng Wang, Jonathan Engel and Chang Liu, J. Micromech. Microeng. Vol. 13, (2003), pp. 628-633.

86. Liu (Caroline) Chen, Midhat Crnic, Zonghe Lai, and Johan Liu, IEEE Transactions on electronics packaging manufacturing, Vol. 25, No. 4, October, (2002).

87. Jiali Wu, Randy T. Pike, C. P. Wong, Namsoo P. Kim, and Minas H. Tanielian, IEEE Tansactions on Advanced Packaging, Vol. 23, No. 4, November, (2000).

88. Jaakko Lenkkeri and Tuomo Jaakola, Proceedings of Workshop on MEMS Sensor Packaging, ISBN: 87-89935-46-2, Danish Technical University (DTU), Lyngby, Denmark, March 20th and 21th, (2003).

89. H. Kopola, J. Lenkkeri, K. kautio, A. Torkkeli, O. Rusanen, and T. Jaakola, Proc. of MICRO/MEMS 2001, Adelaide, Australia, December, (2001).

90. Torsten Thelemann, Heiko Thust, Michael Hintz, Microelectronics International, 19/3, (2002), pp. 19-23.

91. S. Manjula, V. Sundararaman, S. K. Sitaraman, C. P. Wong, J. Wu, and R. T. Pike, Proceedings of International Symposium on Advanced Packaging Materials. Processes, Properties and Interfaces, 14-17 March, (1999).

92. Harrie Tilmans, Myriam Van de Peer and Eric Beyne, MSTNEWS, No. 1, February, (2000), pp. 9-11.

93. Heiko Krassow and F. Campabadal, MSTNEWS, No. 1, February, (2000), pp. 12-13.

94. Stéphane Renard and Vincent Gaff, MSTNEWS, No. 1, February, (2000), pp. 18-19.

95. Sonbol Massoud-Ansari, Yafan Zhang, Srinivas Tadigadapa and Nader Najafi, MSTNEWS, No. 3, (1999), pp. 8-9.

96. Frank Niklaus, Peter Enoksson, Edvard Kälvesten and Göran Stemme, 13th IEEE Int. Conference on MicroElectroMechanical Sytems (MEMS'00) Miyazaci, Japan, January 23-27, (2000), pp. 247-252.

97. T. Lisby, S. A. Nikles, K. Najafi, O. Hansen, S. Bouwstra, J. A. Branebjerg, Journal of Microelectromechanical Systems, Vol. 13, Issue 3, June, (2004), pp. 452-464.

98. Torben Hillingsøe Lisby, Proceedings of Workshop on MEMS Sensor Packaging, ISBN: 87-89935-46-2, Danish Technical University (DTU), Lyngby, Denmark, March 20th and 21th, (2003).

99. Pirmin Rombach, Matthias Müllenborn, Kurt Rasmissen, Christian Wang, Eddie H. Pedersen, Jörg Rehder, Thor Viken, Proceedings of Workshop on MEMS Sensor Packaging, ISBN: 87-89935-46-2, Danish Technical University (DTU), Lyngby, Denmark, March 20th and 21th, (2003).

100. Frank Niklaus, Proceedings of Workshop on MEMS Sensor Packaging, ISBN: 87-89935-46-2, Danish Technical University (DTU), Lyngby, Denmark, March 20th and 21th, (2003).

101. Karsten Dyrbye, Proceedings of Workshop on MEMS Sensor Packaging, ISBN: 87-89935-46-2, Danish Technical University (DTU), Lyngby, Denmark, March 20th and 21th, (2003).

102. Gert F. Eriksen and Karsten Dyrbye, J. Micromech. Microeng., Vol. 6, (1996), pp. 55-57.

103. Carsten Christensen, Roger de Reus, Per E. Andersen and Gert Friis Eriksen, Proceedings of Workshop on MEMS Sensor Packaging, ISBN: 87-89935-46-2, Danish Technical University (DTU), Lyngby, Denmark, March 20th and 21th, (2003).

104. Nicholas Pedersen, Per E. Andersen, Proceedings of Second IEEE International Conference on Sensors, Vol. 1, Toronto, Canada, October 22-24, (2003), pp. 320-325.

105. Heikki Kuisma, Proceedings of Workshop on MEMS Sensor Packaging, ISBN: 87-89935-46-2, Danish Technical University (DTU), Lyngby, Denmark, March 20th and 21th, (2003).

106. Torsten Eggers, H. Dobrinski, I, van Dommelen, O. Lüdtke, A. Nebeling, J. Raben, D. Wüllner, Proceedings of Workshop on MEMS Sensor Packaging, ISBN: 87-89935-46-2, Danish Technical University (DTU), Lyngby, Denmark, March 20th and 21th, (2003).

107. Ashish V. Pattekar and Mayuresh V. Kothare, J. Micromech., Microeng., Vol 13, (2003), pp. 337-345.

108. Way Kuo, V. Rajendra Prasad, IEEE transactions on reliability, Vol. 49, No. 2, June, (2000).

109. Simon Tage Jespersen, MSc Eng. Thesis, ISBN: 87-89935-68-3, Research Center MIC, Technical University of Denmark, 10th September, (2003).

110. David Forman, Smaal Times (10/03), Vol. 3, No. 6, pp. 16.

111. Erik Jung, Maik Wiemer, Volker Grosser, Karlheinz Bock, Jürgen Wolf, OnBoard Technology, October, (2002), pp. 36-39.

112. Finn Jensen, John Wiley & Sons Ltd, ISBN: 0-471-95296-6, (1995).

113. V. Lakshminarayanan, Test & Measurement Europe, Issue, Vol. 8, No. 4, August-September, (2000), pp. 21.

114. William L. Schultz and Sheldon Gottesfeld, Report, The Harris Semiconductor Corporation, 1994, Download at: http://uk.builder.com.

115. P. Liu, L. Cheng, and Y.-W. Zhang, Interface IEEE Transactions on advanced packaging, Vol. 26, No. 1, February, (2003), pp. 1-9.

116. M. Moraja, M. Amiotti, G. Longoni, Proceedings of Micro System Technologies (MST) conference, München, October 7-8, (2003), pp. 195-201.

117. Thierry Corman, Vacuum-Sealed and Gas-Filled Micromachined Devices, PhD thesis, ISBN: 91-7170-482-5, KTH, Stockholm, (1999).

118. R. D. Adams, J. Comyn and W. C. Wake, Chapman & Hall, ISBN: 0-412-70920-1, (1997).

119. L. T. Nguyen, S. A. Gee, M. R. Johnson, H. E. Grimm, H. Berardi, and R. L. Walberg, IEEE Transactions on Components, Packaging, and Manufacturing Technology, Part A, Vol. 18, Issue 1, pp. 210-217, March, (1995).

120. C. Pedersen, S. T. Jespersen, K. W. Jacobsen, J. P. Krog, C. Christensen, E. V. Thomsen, Proceedings of Eurosensors XVII – 17th European Conference on Solid-State Transducers, Guimarães, Portugal, September 21-24, (2003), pp. 418-421.

121. Zhimin Mo, Helge Kristiansen, Morten Eliassen, Proceedings of Workshop on MEMS Sensor Packaging, ISBN: 87-89935-46-2, Danish Technical University (DTU), Lyngby, Denmark, March 20th and 21th, (2003).

122. Qingshan Yao, Jens Branebjerg, Jakob Janting, Proceedings of Workshop on MEMS Sensor Packaging, ISBN: 87-89935-46-2, Danish Technical University (DTU), Lyngby, Denmark, March 20th and 21th, (2003).

123. Douglas C. Montgomery, John Wiley & Sins, Inc., New York, Chichester, Weinheim, Brisbane, Toronto, Singapore, ISBN: 0-471-31649-0, (2001).

124. Liam Kehoe, Vincent Guènebaut, Pat Lynch, Maura O'Sullivan, Pat Kelly, European Semiconductor, October, (2003), pp. 2-4.

125. Jakob Janting, Dirch Hjorth Petersen, Christoffer Greisen, Microelectronics Reliability, Vol. 42, (2002), pp. 1811-1814.

126. Stefan Lipp and Trevor Dingle, MSTNEWS, No. 3, (1999), pp. 20-21.

127. M. G. Pecht & R. Agarwal, CRC Press, ISBN 0-8493-9625-5, (1999).

128. J. Johansson, M. Völker, J. Eliasson, Å. Östmark, P. Lindgren, J. Delsing, Proceedings of The IMAPS Nordic Annual Conference, ISBN: 951-98002-6-3, Helsingør, Denmark, (2004), pp. 265-271.

129. H. Koelmans, IEEE-IRPS Proceedings, (1974), pp. 168-171.

130. W. M. Paulsson and R. W. Kirk, 12th Annual Proc. Rel. Phys., (1974), pp. 172-179.

131. Don L. DeVoe, IEEE Transactions on Components and Packaging Technologies, Vol. 25, No. 4, December, (2003), pp. 576-583.

132. Helmut Eckhardt, Jerome J. Cuomo, C. Richard Guarnieri, Vinay Sakhrani, H. Troy Nagle, and Stefan Ufer, Advancing Microelectronics, November/December, (2002), pp. 10-11.

133. D. Stroehle, 15th Annual Proceedings, Reliability Physiscs Symposium, (1977), pp. 101-106.

134. Malcolm L. White, Proceedings of the IEEE, Vol. 57, No. 9, pp. 1610-1615, September, (1969).

135. Harry A. Schaft, ARPA/NBS Workshop II, Hermeticity testing for integrated circuits, (1974).

136. A. DerMarderosian, V. Ginot, 16th Ann. Proc., Rel. Phys. Symp., April, (1978), pp. 179-183.

137. Michal Tencer, 44th Proceedings of Electronic Components and Technology Conference, (1994).

138. J. Gordon Davy, IEEE Transactions on parts, hybrids, and packaging, Vol. PHP-11, No. 3, September, (1975).

139. A. Christou, Electronic Packaging and Production, April, (1979).

140. Diane Feliciano-Welpe, Metals Handbook, ASM International, Vol. 1: Packaging, (1993).

141. Robert W. Thomas, IEEE Transactions on parts, hybrids, and packaging, Vol. PHP-12, No. 3, September, (1976).

142. Marjorie Byrnes, Jerry L. Carter, Jerry E. Sergent, Dennis King, Solid State Technology, August, (1984).

143. S. A. Tison, Vacuum, Vol. 44, No. 11/12, (1993), pp. 1171-1175.

144. Liesl K. Massey, Plastics Design Library, William Andrew Publishing, ISBN: 1-884207-97-9, (2003).

145. Chi-Hung Shen and George S. Springer, J. Composite materials, Vol. 10, January, (1976), pp. 2-20.

146. Ken Oota, Hiroshi Iida, and Masumi Saka, IEEE Transactions on components and packaging technologies, Vol. 25, No. 1, March, (2002), pp. 164-168.

147. J. Crank, Oxford University Press, Oxford, (1975).

148. Charles M. Hansen, CRC Press, ISBN: 0-8493-1525-5, (2000).

149. Irving Y. Chien, My N. Nguyen, Solid State Technology, November, (1994), pp. 87-88.

150. W. E. Swartz, Jr., J. H. Linn, J. M. Ammons, M. Kovac, and K. Wilson, Proc. Reliability Physics Symposium, (1983), pp. 52-59.

151. J. R. Huntsberger, Journal of Adhesion, Vol. 12, Issue 1, (1981), pp. 3-12.

152. M. K. Bernett, Journal of Colloid and Interface Science, Vol. 28, Issue 2, (1968), pp. 243-249.

153. Thomas Baal, MSTNEWS, No. 1, February, (2004), pp. 5-8.

154. Marlene Bourne, Ayman el-Fatatry and Patric Salomon, MSTNEWS, No. 4, September, (2003), pp. 5-8.

2 Abstract of compiled work

This abstract is a compilation of selected materials characterisation studies and methods. Roughly, it is divided in chapters 2.1, 2.2 dealing with materials characterisation with focus on stability / reliability of more or less complete microsystems and chapter 2.3 dealing with micrometer scale materials characterisation with emphasis on analysis method development. The abstract reviews the main findings with reference to published papers and supplementary reading for further theoretical and experimental details. The papers are listed in chronological order.

Note, that in the thesis context focus is on the work in the obvious relation to how the adhesion of protective polymer adhesives and coatings can be characterized theoretically and practically and optimized regarding intrinsic properties, the surroundings and their interaction. The main conclusion is that the interaction makes a system design approach to development of reliable microsystem packaging mandatory.

Microsystems, Micro Electro Mechanical Systems (MEMS), and micro machines are the European, American, and Japanese terms for the same small sensors and actuators which are typically based on silicon micromechanical structures. A "microsystem" is defined to include microelectronics, photonics, RF / wireless and MEMS. They are μm scale miniaturised systems for analysis involving many different disciplines as e.g. mechanics, fluidics, biology, chemistry, microelectronics, optics [Paper 18].

The first silicon micromechanical sensors and actuators were developed about 30 years ago. Development of silicon micromechanical sensors and actuators in Denmark started in 1990 by the establishment of the Microelectronics Centre. Due to the strong collaboration with the industry it was realized around 1994, that to achieve useful products research was needed in the area of packaging, which covers mounting / assembly of the different parts in a system including electrical, physical, optical, RF / wireless connections and encapsulation [Papers 1-19]. Today several institutes and companies are involved in micro / nano –system development in Denmark.

2.1 Microsystem materials

It should be emphasized that microsystems is a huge interdisciplinary scientific field and that it is outside the scope of this thesis to give a complete overview of all possible microsystem materials and characterization methods. For that the reader is referred to general books / reviews on materials for electronics and microsystems, see e.g. references 4, 23, 127 in [Paper 18] and a broad range of material science books. Supplementary and introductory books and papers are referred throughout the thesis. However, for specific reviews on packaging design, materials and characterization methods for high microsystem reliability the reader may also refer to [Papers 1, 18].

2.2 Materials studied in this thesis

This abstract gives an overview of characterized materials and descriptions of material characterizations with one important tool. The chapters are divided accordingly into the two topics: 1) Polymers, metal / ceramic –polymer composites, 2) Failure analysis.

2.2.1 Adhesive, encapsulation, and coating materials, papers 1-6, 8-12, 14-19, posters 1-8

Polymers are gaining more and more attention because of their physical / chemical properties and easy, low cost industrial processing [1-8]. Some polymers are even found to be intrinsically conducting or semi conducting and therefore constitute active elements (e.g. conductors, diodes which can be light emitting, transistors) of electronics [6-8].
Adhesives and / or encapsulation materials constitute very important materials or elements of microsystem packaging. This is clear from the complete review of microsystem packaging with focus on packaging of sensors for use in harsh environments given in [Paper 18]. Among other things papers 1, 3, 5, 8-19 all deal with different aspects of adhesives. They have been characterized concerning: Bond strength dependency on media exposure and surface treatment (durability), water leakage dependency on media exposure and surface treatment, cure degree, homogeneity, water uptake, stress, surface tension and related use as construction material.

Paper 1 presents test results on Epotek H77 epoxy from Epoxy Technology and Q3-6611 silicone from Dow Corning as adhesive bonding / encapsulation / barrier materials for a CrTa protectively coated 5 mm · 7.5 mm · 0.35 mm silicon micromechanical differential pressure sensor chip in titanium housing, see fig. 1 in [Paper 1]. The sensor should be able to withstand 120 °C and pH 11 water at 6 bar for at least 10 years. The two different classes of adhesives were chosen for comparison of their very different general advantages and disadvantages. Other adhesive materials were also tested. Epoxies bond very well to most substrates; they are hard and very durable both chemically and physically. Silicones do not bond as well; they are soft and relatively durable. From this it was expected that due to the hardness and mismatch in Thermal Coefficient of Expansion (TCE) between adhesive and chip / housing Epotek H77 would introduce a more pronounced sensor off-set change on cooling down from the 150 °C curing temperature. This was confirmed by experiments although Epotek H77 is filled with Al_2O_3 µm size flakes lowering its TCE, and most unpleasantly the off-set change is time dependent due to ageing which would have to be accounted for electronically in the final product. Also the epoxy exhibit significant hardness changes as function of temperature as shown in the bend experiments described in [Paper 1], which in itself influences the offset severely. The epoxy was also expected to be more water tight due to a denser molecular structure. This was confirmed by experiments using chips glued over a hole in titanium flanges mounted on a vacuum system equipped with a mass spectrometer; see fig. 11 in [Paper 1]. A chamber with a stirrer and temperature control was screw mounted and o-ring sealed to the top of the flange and filled with alkaline (to resemble domestic heating water) D_2O instead of H_2O to enhance leakage detection sensitivity a factor of 100-1000. Further the higher bond strength of Epotek H77 was confirmed in burst off experiments where chips had been mounted on titanium pieces with holes, through which pressure was applied, see fig. 10b in [Paper 1]. Except for the offset influence, Epotek H77 was the only adhesive considered to perform well enough, but only for a limited temperature range concerning water tightness, see fig. 11 in [Paper 1]. It was therefore attempted to improve the performance of especially Q3-6611 by increasing bond strength and leakage. Although Q3-6611 is self priming in the sense that it contains low molecular weight siloxanes, bond strength could be increased by titanium cleaning and additional silane

(octamethyltrisiloxane) priming procedures see fig. 10a in [Paper 1], and for the best procedure it was higher than the cohesive strength of the adhesive. The general silane formula is R_nSiX_{4-n} where R is an organic group which bonds well to the adhesive and X is typically involved in the reaction with an inorganic substrate. Later it was also shown that by anodizing the titanium it was possible to grow a columnar oxide (approx. 100 nm high) on the titanium which resulted in a 10 times lower leakage rate through Q3-6611 bondings. This is still not good enough but indicates that water transport along the interfaces plays an important role. Experiments to separate bulk adhesive and interface water transport by varying adhesive thickness was planned but never carried out. Often corrosion of Al bondwires, see fig. 1 in [Paper 1] was observed. By introducing a venting slit at the adhesive arrow in fig. 1 in [Paper 1] this corrosion disappeared completely. The explanation for this is that the slit vent opens up a fast escape route through air before the electronics is reached i.e. the diffusion constant for H_2O in air at RT is around $2.5 \cdot 10^{-5}$ m^2s^{-1}, in silicone and epoxy it ranges from around 10^{-10} m^2s^{-1} to 10^{-14} m^2s^{-1}. This combination of materials properties with geometrical design is just one example of the importance of holistic thinking or system design as also highlighted in the chapter on "Packaging strategy" in [Paper 18]. However, due to the instability of the adhesives, a more stable EPDM o-ring solution which had been tested alongside these experiments was finally chosen.

Microphones are widespread in our every day life. Collectively papers 2-6, 18, and poster 1 describe the complete microsystem packaging developed for a small 3 mm · 3 mm · 2 mm microphone comprising the silicon micromechanical sensor, electrical interconnection between microphone and Application Specific Integrated Circuit (ASIC), electrical interconnection between ASIC and surroundings (loudspeaker, current supply), and protective encapsulation. The microphone is developed for use in e.g. hearing aids where it should be small enough to be invisible in the ear channel, high performance mobile phones / headsets etc.

Papers 3, 5, and 18 focus on a description of the involved packaging steps. Four of these involve adhesive. Interconnection between ASIC and microphone is established through the SBB technique wherein coined Au wire bond balls on the ASIC are dipped in conductive adhesive (typically Ag filled epoxy), the ASIC is placed on the microphone interconnection pads, adhesive is cured, the mounted ASIC is underfilled (low CTE filled epoxy) and the underfiller cured to establish mechanical and thereby electrical contact stability. The same procedure is used for the interconnection through a flex print to the surroundings. The encapsulation part of the packaging is described in more detail later.

Important microsystems reliability issues are materials stability, reproducibility, and uniformity [Paper 18] and easy means of monitoring.
Together papers 8, 9, 11, 14, 19, and posters 2, 3, 4 present acoustic microscopy as an analytical tool to determine changes and / or differences in materials mechanical properties. It is thus shown how adhesive (EC1211 epoxy from Emerson and Cuming, Epotek T7110 from Epoxy Technology) cure degree [Papers 8, 9, 11, 14, 19], [Posters 3, 4] and uneven adhesive (flip-chip underfill) filler distribution [Papers 14, 19], [Poster 4] inside components can be monitored non-destructively in 2D due to changes / differences

in acoustic impedance $Z \approx (\rho E)^{1/2}$. The acoustic impedance resolution is found to be around 0.1 MRayl [Papers 8, 11]. Further cure degree as given by Z determined from SAM is correlated with reaction degree determined by DSC [Papers 9, 19]. DSC in general is described in [1, 2]. Determination of adhesive cure degree was motivated by a need to monitor whether an adhesive used to establish electrical contact by shrinkage between wire bond bumps on a chip and interconnection pads on a flex-print was fully cured after assembly in a fast flip-chip machine, see fig. 1 in [Paper 8]. Electrical interconnection in this way would have some advantages over e.g. traditional wirebonding which is less compact, durable etc. [Papers 8, 9, 11, 14, 19]. However, these interconnections turned out not to be sufficiently reliable (stable) in the application (the differential and absolute pressure sensors described in [Paper 1] figs. 1 and 3) environmental temperature / humidity tests. Determination of flip-chip underfill filler distribution was motivated by a wish to wafer level underfill (cf. Wafer Level Packaging (WLP), see [Paper 18]) the ASIC component of the silicon micromechanical microphone described in [Papers 2-6]. When underfilling over that long distances careful control of process parameters is mandatory, see fig. 14 in [Paper 14]. Uniform distribution of underfill turned out to be possible at certain temperatures. SAM was chosen as the monitoring tool for two main reasons. This technique for monitoring is much faster than e.g. DSC which requires samples from inside the components and which is therefore tedious and destructive and SAM, as opposed to X-absorption, provides high contrast in adhesives even when materials variations are due to minor variation in atomic mass. Comprehensive reviews of SAM with focus on use for microsystem analysis are given in [Papers 14, 19].

In many packaging cases materials are doing more than one job. This is also the case for adhesives [Paper 18]. In the above mentioned flip-chip interconnection cases the adhesive is doing the combined job of attachment and encapsulation protection of the electrical interconnection sites.
Protective microsystem encapsulations cover the microsystem or parts thereof in 3D and are in direct contact with these, otherwise they are called substrates or housings. Further, no matter the material, microsystem protective encapsulations are termed coatings if the thickness is below 250 μm, otherwise the protection is called a molding [Papers 2, 4, 6, 18].

The work on water uptake of polymeric packaging materials was motivated by the fact that no material is actually completely water tight, and that polymer materials belong to the low end concerning water tightness while still being widely used in microsystems where even minute amounts of water (less than 10^{-4} μL) may be critical concerning corrosion [Papers 10, 15, 18], [Posters 5, 6], [4, 5]. Epoxy (Epotek U300-1) attach / mould, polyamide (MacroMelt 6970 from Henkel) mould and poly(p-xylylene) (Parylene C from ParaTech) coating materials were tested as water barrier encapsulations. The flux of water into these materials was determined from sorption curve fits using appropriate diffusion equations. The sorption was measured by weighing the water uptake of immersed coated / uncoated 5 cm · 5 cm · 0.1 cm samples at certain time intervals. The samples were made in Teflon® moulds for easy removal. For Epotek U300-1 the temperature dependent flux was determined. It was found to be too high for

the above mentioned differential pressure sensor application where its primary use was to establish electrical contact by shrinkage compression in a flip-chip and curing process. So, perhaps the reason for bad electrical contact reliability observed earlier was found here to be the water saturation which reaches the contact points after a very short time. The MacroMelt molding material was studied because of its low temperature, pressure processing and soft stress compliant properties which make it generally attractive as encapsulation material for fragile / sensitive silicon micromechanical structures. Here the specific intended use was as a harsh environment absolute pressure sensor encapsulation material in direct contact with the sensor membrane, see fig. 2 in [Paper 15] and [Poster 6]. It was demonstrated that the unbeneficial high diffusion coefficient for a MacroMelt molding material can be effectively lowered three orders of magnitude by application of a coating of only 10 μm Parylene C, which is again an example of the importance of system design as stressed in [Paper 18]. In total this encapsulation is then useful. Connected to that it was found that generally it is of major importance to chose materials with a low water saturation level, especially when in direct contact with critical component parts, because the water will reach these regions anyway within a short time in polymers, and to chose materials / geometries that divert fluxes of water away from the critical component parts (cf. the slit in the differential pressure sensor house mentioned earlier).

Stress is very important to avoid or isolate from sensitive areas in microsystem packaging because the performance may otherwise be severely jeopardized [Papers 1, 12, 18], [9-14]. Stress is typically analyzed theoretically by FEM. One example is given on the thesis front cover where a 50 μm thick high CTE, modulus epoxy adhesive is used for mounting of a silicon beam on a Al_2O_3 snapstrate, and where thermal stresses is shown to concentrate in the adhesive edges when cooling down from the cure temperature. Not only may the stress impair performance immediately, it may also be time dependent due to ageing or natural fast variations in the surroundings, e.g. temperature, humidity, radiation etc. [Papers 1, 18]. Soft adhesive, encapsulation and coating materials are often preferred due to their mechanical compliancy, but have other shortcomings like implied open structure and consequent bad barrier properties as exemplified more than once earlier (Q3-6611 silicone, Macromelt which is a soft modified polyamide).

Paper 12 presents a stress influence analysis of such a protective encapsulation consisting of a cap (Epotek H77 epoxy) with / without coating (e.g. amorphous electroless Ni) on the performance of the high pressure absolute pressure sensor in fig. 3 in [Paper 1]. The protected sensor configuration is shown in fig. 1, [Paper 12]. The low CTE sensor is low CTE glass frit mounted in a low CTE metal bush. The stress analysis was made by FEM. The main conclusions are that the high CTE cap is not altering the sensor sensitivity significantly, that the epoxy leads to much higher vertical displacement when pressure is applied, which might be detrimental, and that the sensor becomes much more temperature sensitive i.e. a temperature change of 15 °C shifts the pressure about 40 bars. These findings make the encapsulation useful for a limited range of applications. More broadly applicable encapsulations comprise highly durable coatings.

Microsystems based on polymers become as already mentioned more and more dominant due to low fabrication cost. One area of use is liquid handling in μTAS, i.e. as base material for microfluidic channels. Besides being e.g. good combined mounting / barrier materials adhesives also play an important role as construction / assembly materials. Although polymers are generally difficult to bond with adhesives due to low surface tension, bond strength can often be enhanced especially with O_2 plasma pre-treatment which by the introduction of –OH groups in the surface usually increases the polar surface tension component and thereby the overall surface tension significantly. However, the effect most often decays significantly within few hours. The surface tension of the adhesives can also be tuned (lowered) for better wetting by mixing e.g. with small amounts of silane (cf. Q3-6611). The number of chemical / physical adhesive / substrate tuning possibilities is virtually endless [Paper 18], [15-18].

This is the reason why papers 16, 17 and posters 7, 8 explore with theory and experiments how control of adhesive and substrate parameters (surface tension, viscosity / thixotropy, structure, height and distance, temperature) makes easy / fast fabrication of polymeric microfluidic channels with controlled shape and without adhesive in the channel feasible. Control of channel shape is important for proper control of the flow.
From experiments using four adhesives, three substrates and FEM analysis it is concluded that it is nearly possible to achieve channels with a round cross section, that it is very difficult to dispense close proximity lines especially with low surface tension and viscosity adhesive materials, and that the channels tend to have an inner shape like a double trumpet in the flow direction [Paper 16], [Poster 7]. Further it is concluded that in assembly of channels, structured polymer substrates / spacers are required to avoid voids along or adhesive in the channels [Paper 17], [Poster 8]. The studies had no aim at specific applications.

With papers 2, 4, 6, and poster 1 focus is again on the previously mentioned microphone and coating protective encapsulation. Paper 2 and 4 describe the main demands and solutions which have been expanded to include all possible and relevant microsystems in a patent application [Paper 6].
In short the coating demands are: > 50 dB E-field EMI damping to avoid noise from e.g. mobile phones when used in hearing aids, $>10^{12}$ Ωcm electrical insulation not to short circuit the electrical conductors, thickness below 200 μm to keep the system small, microsystem compatibility not to introduce stress, corrosion etc., physical and chemical durability to further protect the microphone. It was found that the only feasible coating would be one consisting of two layers where the bottom one in direct contact with the system to be protected should be insulating and the top coating conductive (cf. system design again by materials properties combination), see fig. 1 in [Paper 4]. Materials and methods were tested and characterized as described thoroughly in [Paper 4]. The tests included volume resistivity, tightness, thickness and conformity, E-field EMI shielding, and applicability by the gentle techniques dipping, spraying, plating. The most difficult task to solve was the conformal pinhole free coverage of sharp single crystalline silicon corners and edges with the bottom layer. This problem was solved with a low surface tension and viscosity solution of Teflon® AF. In fact all tested materials were low surface

tension and viscosity materials to be gently applicable. The first bottom layer was applied by dip coating, the top layers by spraying or plating. The top layer was intrinsically conductive polymers, metal filled polymers, or plated metal. Alternating insulative-conductive multilayers were also tested. A Three layer combinations of Teflon® AF, Cho-Shield 2052 (metal filled acrylate polymer), Leitsilber 200 (silver seed layer used for subsequent plating) turned out to perform best concerning E-field EMI damping (70-90 dB) in a standard test (NT ELEC 030) developed by DELTA.

2.3 Failure analysis

Failure analysis is important in the development for reliability or QA of microsystems. A thorough treatment of these issues in a larger context is given in [Papers 18, 19].

2.3.1 Scanning Acoustic Microscopy, papers 7-9, 11, 13, 14, 18, 19, posters 2-4

SAM is an excellent tool to detect mechanical variations in materials e.g. cracks, bubbles, delaminations and uniformity. A comprehensive review on SAM in general and for analysis of microsystems with practical examples is given in [Paper 19].
Different established techniques have been explored and new developed theoretically and experimentally to deal with A-scan interpretation and small distances between layers (cf. delamination) [Papers 7, 13, 14], [Poster 2], adhesive cure degree analysis [Papers 8, 9, 11, 14, 19], [Posters 3, 4] and uniformity [Papers 8, 14, 19]. The techniques are all described in detail in the mentioned papers. In the evaluation of the adherence of microsystem adhesives and coatings all these three topics are important.

2.4 References

1. Ulf W. Gedde, Polymer Physics, Chapman & Hall London, 1995, ISBN 0 412 59020 4.

2. http://www.pslc.ws/mactest/level5.htm

3. Ulrich Eisele, Introduction to Polymer Physics, Springer-Verlag Berlin Heidelberg, 1990, ISBN 3-540-50777-9.

4. J. Comyn, Polymer permeability, Chapman & Hall, 1985, ISBN 0 412 53820 2.

5. R. D. Adams, J. Comyn and W. C. Wake, Structural Adhesive Joints in Engineering, Second edition, Chapman & Hall, 1997, ISBN 0 412 70920 1.

6. Science and Applications of Conducting Polymers, Proceedings of the 6th Europhysics Industrial Workshop held in Lofthus, Norway, May 1990, Edited by W. R. Salaneck, D. T. Clark, E. J. Samuelsen, Adam Hilgar, 1991, ISBN 0-7503-0049-3.

7. Bjørn Winther-Jensen, Towards Micro-patterning of Conducting Polymers, - Polymerisation routes and characterization of selected conjugated polymer systems, Ph.D. Thesis, Technical University of Denmark, Dept. of Chemical Engineering, 2004, ISBN 87-91435-13-7.

8. Organic light-emitting devices, A survey, Edited by Joseph Shinar, Springer-Verlag, 2004, ISBN 0-387-95343-4.

9. R. D. Adams and V. Mallick, The Effect of Temperature on the Strength of Adhesively-Bonded Composite-Aluminium Joints, J. Adhesion, Vol. 43, 1993, pp. 17-33.

10. J. M. Hu, M. Pect and A. Dasgupta, Design of Reliable Die Attach, The International Journal of Microcircuits and Electronic Packaging, Vol. 16, No. 1, First Quarter 1993, (ISSN 1063-1674), pp. 1-21.

11. Y. Weitsman, Stresses in Adhesive Joints Due To Moisture and Temperature, J. Composite Materials, Vol. 11, Oct. 1977, pp. 378-394.

12. Guo-Quan Lu, Gary B. Kromann, Boris Mogilevsky, and Tapan K. Gupta, Evaluation of die-attach adhesives by curvature measurements, Proceedings of I-Therm III, InterSociety Conference on Thermal Phenomena in Electronic Systems, 5-8 Feb 1992, pp. 155-158.

13. J. Arnold, Low Stress Aerobic Urethanes; Lower Costs for Microelectronic Encapsulation, SME Adhesives 1995, EE95-263, September 1995.

14. http://www.specialchem4adhesives.com/resources/articles/article.aspx?id=943#a

15. Handbook of Adhesion, Edited by D. E. Packham, Longman Scientific & Technical, 1992, ISBN 0-470-21870-3.

16. Adhesion Aspects of Polymeric Coatings, Edited by K. L. Mittal, Plenum Press, New York, 1983, ISBN 0-306-41250-0.

17. Polymer Surface Modification: Relevance to Adhesion, Edited by K. L. Mittal, VSP BV, 1996, ISBN 90-6764-201-0.

18. Contact Angle, Wettability and Adhesion, Volume 2, Editted by K. L. Mittal, VSP BV, 2002, ISBN 90-6764-370-X.

2.5 List of papers

1. R. de Reus, C. Christensen, S. Weichel, S. Bouwstra, J. Janting, G. Friis Eriksen, K. Dyrbye, T. Romedahl Brown, J.P. Krog, O. Søndergård Jensen, P. Gravesen, Reliability of industrial packaging for microsystems, Microelectronics Reliability 38 (1998) 1251-1260.

2. J. Janting, J. Branebjerg, P. Rombach, Conformal Coatings for 3D Multichip Microsystem Encapsulation, in: Proceedings of the 14. European Conference on Solid-State Transducers August 27-30, 2000, Copenhagen, Denmark, pp. 275-278. Paper presented orally and with poster 1.

3. M. Müllenborn, P. Rombach, U. Klein, K. Rasmussen, J.F. Kuhmann, M. Heschel, S. Bouwstra, M. Amskov, J. Janting, A. Hoogerwerf, Stacked Silicon Microphones, in: Proceedings of the 14. European Conference on Solid-State Transducers August 27-30, 2000, Copenhagen, Denmark, pp. 209-212.

4. J. Janting, J. Branebjerg, P. Rombach, Conformal coatings for 3D multichip microsystem encapsulation, Sensors and Actuators A 92 (2001) 229-234.

5. M. Müllenborn, P. Rombach, U. Klein, K. Rasmussen, J.F. Kuhmann, M. Heschel, M. Amskov Gravad, J. Janting, J. Branebjerg, A. Hoogerwerf , S. Bouwstra, Chip-size-packaged silicon microphones, Sensors and Actuators A 92 (2001) 23-29.

6. J. Janting, J. Branebjerg, P. Rombach, Encapsulation for a three-dimensional microsystem, Patent application PCT/DK00/00559.

7. Jakob Janting, Dirch Hjorth Petersen, Christoffer Greisen, Simulated SAM A-scans on multilayer MEMS components, Proceedings of 13th European Symposium on Reliability of Electronic Devices, Failure Physics and Analysis, ESREF 2002, pp. 1811-1814. The paper was presented with poster 2.

8. Jakob Janting, Dirch Hjorth Petersen, Bjarke Schønwandt, Scanning Acoustic Microscopy Study of Flip-Chip Underfill Cure Degree, Proceedings of Materials Week conference, München, Germany, 30. sep. – 2. oct. 2002. The paper was presented with poster 3.

9. Jakob Janting, Uffe Bennov, Anders Black, Correlation between MEMS Adhesive cure Degree and acoustic Impedance determined with Differential Scanning Calorimetry and Scanning Acoustic Microscopy, Proceedings of Workshop on MEMS Sensor Packaging, March 20th and 21th 2003, ISBN87-89935-46-2. The paper was presented with poster 4.

10. Jakob Janting, Elisabeth Kjærside Storm, Water Uptake of Polymeric Packaging Materials, Proceedings of Workshop on MEMS Sensor Packaging, March 20th and 21th 2003, ISBN87-89935-46-2. The paper was presented with poster 5.

11. Jakob Janting, Dirch Hjorth Petersen, Scanning Acoustic Microscopy Investigation of Adhesive Cure Degree, Proceedings of Workshop on MEMS Sensor Packaging, March 20th and 21th 2003, ISBN87-89935-46-2. The paper was presented with poster 3.

12. Qingshan Yao, Jens Branebjerg, Jakob Janting, FEM Simulation of Influence of Protective Encapsulation on MEMS Pressure Sensor, Proceedings of Workshop on MEMS Sensor Packaging, March 20th and 21th 2003, ISBN87-89935-46-2.

13. Jakob Janting, Dirch Hjorth Petersen, Christoffer Greisen, Simulated SAM A-scans on multilayer MEMS components, Proceedings of Workshop on MEMS Sensor Packaging, March 20th and 21th 2003, ISBN87-89935-46-2. The paper was presented orally and with poster 2.

14. Jakob Janting, Scanning Acoustic Microscopy for Quality Assurance of MEMS Sensors, Proceedings of Sensor 2003, 11th International Conference, pp. 255-260, 13-15 May 2003, Nuremberg. The paper was presented orally.

15. Jakob Janting, Elisabeth Kjærside Storm, Water Uptake of Polymeric MEMS Packaging Materials, Proceedings of MicroSystem Technologies (MST) 2003, pp. 520-522, ISBN 3-7723-7020-9. The paper was presented with poster 6.

16. Jakob Janting, Elisabeth K. Storm, and Oliver Geschke, Surface tension driven shaping of adhesive microfluidic channel walls, Proceedings of μTAS, 8th International Conference on Miniaturised Systems for Chemistry and Life Sciences, Malmö, Sweden, 26-30 September, (2004), pp. 378-380. The paper was presented with poster 7.

17. Peter Friis, Elisabeth K. Storm, Karsten Hoppe, and Jakob Janting, Adhesive Bonding Methods for Polymer microTAS Components, Proceedings of μTAS, 8th International Conference on Miniaturised Systems for Chemistry and Life Sciences, Malmö, Sweden, 26-30 September, (2004), pp. 354-356. The paper was presented with poster 8.

18. J. Janting, Sensor packaging for harsh environments, Encyclopedia of Sensors, Vol. 3, pp. 271-288, Edited by C. A. Grimes, E. C. Dickey, and M. V. Pishko, American Scientific Publishers, 2006, ISBN: 1-58883-065-9.

19. J. Janting, Techniques in Scanning Acoustic Microscopy for Enhansed Failure and Material Analysis of Microsystems, MEMS/NEMS Handbook, Techniques and Applications, Vol. 3, pp. 293-309, Edited by Cornelius T. Leondes, Springer, 2006, ISBN: 0-387-24520-0.

2.6 List of posters

1. Jakob Janting, Jens Branebjerg, Conformal coatings for 3D multichip microsystem encapsulation. Paper 2 presentation at the 14. European Conference on Solid-State Transducers August 27-30, 2000, Copenhagen, Denmark. The poster also supports papers 4, 6.

2. J. Janting, D. H. Petersen, C. Greisen, Simulated SAM A-scans on Multilayer MEMS Components. Paper 7 presentation at the 13th European Symposium on Reliability of Electronic Devices, Failure Physics and Analysis, ESREF 2002. The poster also supports paper 13.

3. J. Janting, D. H. Petersen, Scanning Acoustic Microscopy Study of Flip-Chip Underfill Cure Degree. Paper 8 presentation at the Materials Week conference, München, Germany, 30. sep. – 2. oct. 2002. The poster also supports paper 11.

4. Jakob Janting, Uffe Bennov, Anders Black, Correlation between MEMS Adhesive Cure Degree and acoustic Impedance determined with Differential Scanning Calorimetry and Scanning Acoustic Microscopy. Paper 9 presentation at the Workshop on MEMS Sensor Packaging, March 20th and 21th 2003.

5. J. Janting, E. K. Storm, Water Uptake of Polymeric Packaging Materials. Paper 10 presentation at the Workshop on MEMS Sensor Packaging, March 20th and 21th 2003. The poster also supports paper 15.

6. J. Janting, E. K. Storm, Water Uptake of Polymeric Packaging Materials. Paper 15 presentation at MicroSystem Technologies (MST) 2003. The poster also supports paper 10.

7. Jakob Janting, Elisabeth K. Storm and Oliver Geschke, Surface Tension Driven Shaping of Adhesive Microfluidic Channel Walls. Paper 16 presentation at μTAS, 8th International Conference on Miniaturised Systems for Chemistry and Life Sciences, Malmö, Sweden, 26-30 September, (2004).

8. P. Friis, E. K. Storm, K. Hoppe and J. Janting, Adhesive Bonding Method for Polymer μTAS Components. Paper 17 presentation at μTAS, 8th International Conference on Miniaturised Systems for Chemistry and Life Sciences, Malmö, Sweden, 26-30 September, (2004)

3 Discussion of selected topics

As has become clear from the previous chapters the manufacturing of high reliability microsystem packaging demands special materials and methods. A lot of parameters influence the reliability separately and in combination and the characterization sometimes require the development of special equipment and techniques.
Below some of the most important reliability subjects and techniques are explained or discussed deeper than previously in the papers and this thesis.

3.1 Diffusion and stress

Based on the work described in chapter 2 it is the author's opinion that the most important parameter or physical mechanism influencing microsystem packaging reliability is diffusion. Stress is also a very important parameter.

3.1.1 Water diffusion in polymeric packaging materials

As also stated in chapter 1.4.1.3.2 when polymers constitute the only barrier between sensitive microsystem parts and the environments water in-diffusion is generally considered the most severe environmental factor decreasing reliability. This is because water is everywhere, is easily transported in polymers, and generally changes / impairs the microsystem materials cf. delamination (chapter 3.2), corrosion etc. No matter this, because of many other positive properties (e.g. prize, easy processing, stress compliancy etc.) polymers are widely used in microsystems, also as barrier materials. It is then of utmost importance to evaluate what reliability can be expected in each case. Below a thorough discussion of water diffusion in polymers is therefore given with reference to earlier work and chapters in this thesis. In all of what follows, if nothing else is specified, the diffusion is assumed be Fickian and the diffusion coefficient to be constant. It is also assumed that diffusion can be properly described in terms of concentration gradients instead of chemical potential gradients.

3.1.1.1 Solution methods for the diffusion equation

The diffusion equation (1) is a parabolic homogeneous linear partial differential equation:

$$\frac{\partial C}{\partial t} = D\frac{\partial^2 C}{\partial x^2} \tag{1}$$

Three methods of solving the equation exist. These are [1]:

1. The method of reflection and superposition
2. The method of separation of variables
3. The method of the Laplace transform

Usually the solutions are of two types. Either it is a series of error functions or related integrals (method 1) or it is in the form of a trigonometrical series (method 2). When diffusion occurs in a cylinder the trigonometrical series are replaced by series of Bessel functions. The two types of solutions are most suitable / accurate for evaluation at short

time and long time diffusion respectively. The Laplace transform method, which is the most powerful, gives both types of solutions [1].

3.1.1.2 Non-steady state vs. steady state

The delineation between non-steady state and steady state diffusion is generally important because at steady state the rate of water entering critical areas is higher than at the initial stages of in-diffusion. It may be it takes so long time of the product service life for the diffusion to adjust to steady state that the non-steady state can not be ignored considering the flux integrated with respect to time. Also dealing with products like e.g. point of care medical microsystems with very short service life (e.g. minutes) compared to the time it takes to reach steady state diffusion, the non-steady state diffusion can not be ignored. Such microsystem products for short time use are becoming more and more common. However, today for most consumer products, it is demanded that they last for several years and the steady state solutions to the diffusion equation are generally considered most valid.

In judging what kind of solution is most relevant, looking at time of exposure and polymer barrier thickness, it can be used that the solution (e.g. by use of the Laplace method) to the diffusion equation in a semi-infinite medium with boundary conditions:

$$C(x,0) = C_0 \tag{2}$$

$$C(\infty,t) = C_0 \tag{3}$$

$$C(0,t) = C_1 \tag{4}$$

is:

$$C_x = C_1 - (C_1 - C_0)erf\left(\frac{x}{2\sqrt{Dt}}\right) \tag{5}$$

where

$$erf(z) = \frac{2}{\sqrt{\pi}}\int_0^z \exp(-y^2)dy \tag{6}$$

is the error function and where C_0 is the initial concentration throughout the polymer, C_1 is the surface concentration, see fig 1. Values for the *erf* function can be found in mathematical tables. Note that $erf(0) = 0$, $erf(\infty) = 1$ and $erf(0.5) \approx 0.5$. From this we see that for $C_0 = 0$ and $x = \sqrt{Dt}$:

$$C_{x=\sqrt{Dt}} = C_1 - C_1 erf(0.5) \approx C_1 - 0.5C_1 = 0.5C_1 \tag{7}$$

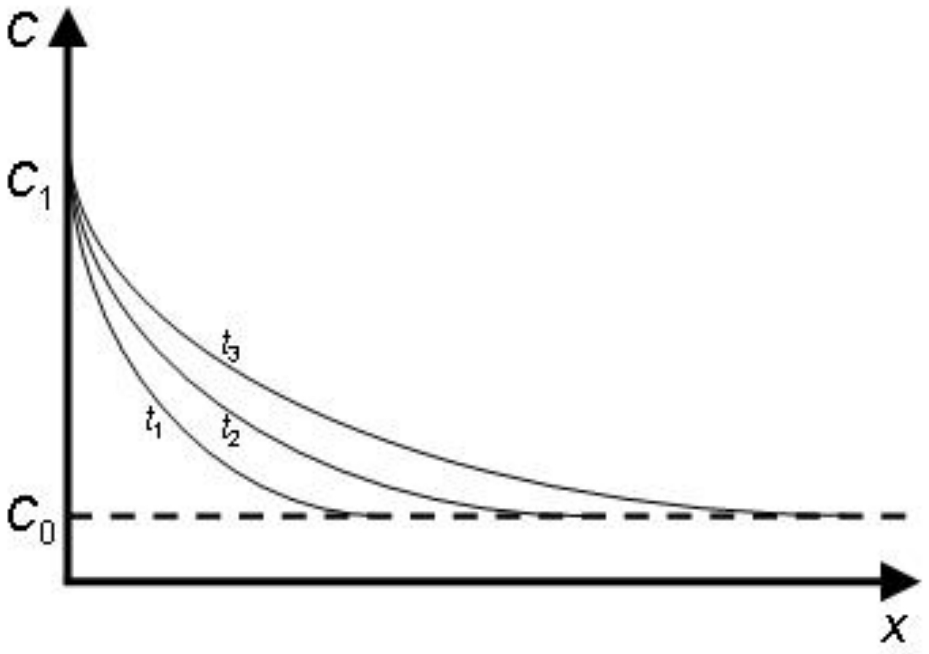

Fig. 1: Diffusion into a semi-infinite medium. The concentration profiles at three different times $t_1 < t_2 < t_3$ are shown.

That is, at the distance $x = \sqrt{Dt}$ the concentration has reached half the surface concentration C_1 or half saturation. It is further noted that iso-concentration depths will have to obey:

$$\frac{x}{\sqrt{Dt}} = k \tag{8}$$

$$\Updownarrow$$

$$x = k\sqrt{Dt} \tag{9}$$

where k is a constant, i.e. that the depths are proportional to $\sqrt{t}$. That is, to e.g. double the penetration depth requires a fourfold increase in time.

We get for the flux J:

$$J = -D\frac{d}{dx}\left(C_1 - C_1 erf\left(\frac{x}{2\sqrt{Dt}}\right)\right) = DC_1\frac{e^{-\frac{x^2}{4Dt}}}{\sqrt{\pi}\sqrt{Dt}} \tag{10}$$

The water uptake in time t can then be calculated by integration of the flux at $x = 0$:

$$M_t = \int_0^t \frac{ADC_1}{\sqrt{\pi}\sqrt{Dt^*}}\,dt^* = \frac{2AC_1}{\sqrt{\pi}}\sqrt{Dt} \tag{11}$$

where A is the sample cross-sectional area perpendicular to the x direction. The water molecules diffuse by a random / stochastic walk process. Therefore their positions along the x axis can be described by a continuous probability density function $p(x)$ and:

$$\sigma_x = \sqrt{\left\langle \left(x - \langle x\rangle\right)^2 \right\rangle} = \sqrt{\langle x^2\rangle - \langle x\rangle^2} = \sqrt{\int \left(x - \langle x\rangle\right)^2 p(x)dx} = \sqrt{\int \left(x - \int xp(x)dx\right)^2 p(x)dx} \tag{12}$$

where σ_x is the x standard deviation which is a measure of the positional spread along x, the kites denote averages and the integrals are taken over the range of x positions.
The probability that a water molecule is at a certain depth x at the time t is given by the amount of molecules at this depth divided by the total amount of in-diffused molecules in time t. By integrating x times the probability of x over all depths we arrive at the average depth of in-diffusion <x> in time t:

$$\langle x\rangle = \int_0^\infty x \frac{AC_1\left(1 - erf\left(\frac{x}{2\sqrt{Dt}}\right)\right)}{\frac{2AC_1}{\sqrt{\pi}}\sqrt{Dt}}dx = \frac{\sqrt{\pi}}{2\sqrt{Dt}}\int_0^\infty x\left(1 - erf\left(\frac{x}{2\sqrt{Dt}}\right)\right)dx$$

$$= \frac{\sqrt{\pi}}{2\sqrt{Dt}}\left[-\frac{1}{2}erf\left(\frac{x}{2\sqrt{Dt}}\right)x^2 + \frac{x^2}{2} - \frac{xe^{-\frac{x^2}{4Dt}}\sqrt{Dt}}{\sqrt{\pi}} + erf\left(\frac{x}{2\sqrt{Dt}}\right)Dt\right]_0^\infty = \frac{\sqrt{\pi}}{2\sqrt{Dt}}Dt$$

$$= \frac{\sqrt{\pi}}{2}\sqrt{Dt} \approx 0.89\sqrt{Dt} \tag{13}$$

$\langle x^2\rangle$ can be calculated using the same procedure:

$$\langle x^2\rangle = \frac{\sqrt{\pi}}{2\sqrt{Dt}}\int_0^\infty x^2\left(1 - erf\left(\frac{x}{2\sqrt{Dt}}\right)\right)dx$$

$$= \frac{\sqrt{\pi}}{2\sqrt{Dt}}\left[-\frac{1}{3}erf\left(\frac{x}{2\sqrt{Dt}}\right)x^3 + \frac{x^3}{3} - e^{-\frac{x^2}{4Dt}}\left(\frac{2x^2\sqrt{Dt}}{3\sqrt{\pi}} + \frac{8(Dt)^{3/2}}{3\sqrt{\pi}}\right)\right]_0^\infty = \frac{\sqrt{\pi}}{2\sqrt{Dt}}\frac{8(Dt)^{3/2}}{3\sqrt{\pi}}$$

$$= \frac{4}{3}Dt \tag{14}$$

This leads to:

$$\sigma_x = \sqrt{\frac{4}{3}Dt + \frac{\pi}{4}Dt} = \sqrt{\frac{4}{3}+\frac{\pi}{4}}\sqrt{Dt} \approx 1.46\sqrt{Dt} \tag{15}$$

The fraction of molecules at distances x between 0 and $\langle x \rangle$ is then:

$$\int_0^{\langle x \rangle} \frac{AC_1\left(1-erf\left(\frac{x}{2\sqrt{Dt}}\right)\right)}{\frac{2AC_1}{\sqrt{\pi}}\sqrt{Dt}}dx = \frac{\sqrt{\pi}}{2\sqrt{Dt}}\left[x - \frac{2\sqrt{Dt}e^{-\frac{x^2}{4Dt}}}{\sqrt{\pi}} - erf\left(\frac{x}{2\sqrt{Dt}}\right)x\right]_0^{\frac{\sqrt{\pi}}{2}\sqrt{Dt}}$$

$$= \frac{\pi}{4} - e^{-\frac{\pi}{16}} - erf\left(\frac{\sqrt{\pi}}{4}\right)\frac{\pi}{4} + 1$$

$$\approx 0.60 \tag{16}$$

The fraction of molecules at distances x between $\langle x \rangle$ and $\langle x \rangle + \sigma_x$ is:

$$\int_{\langle x \rangle}^{\langle x \rangle + \sigma_x} \frac{AC_1\left(1-erf\left(\frac{x}{2\sqrt{Dt}}\right)\right)}{\frac{2AC_1}{\sqrt{\pi}}\sqrt{Dt}}dx = \frac{\sqrt{\pi}}{2\sqrt{Dt}}\left[x - \frac{2\sqrt{Dt}e^{-\frac{x^2}{4Dt}}}{\sqrt{\pi}} - erf\left(\frac{x}{2\sqrt{Dt}}\right)x\right]_{\frac{\sqrt{\pi}}{2}\sqrt{Dt}}^{\left(\frac{\sqrt{\pi}}{2}+\sqrt{\frac{4}{3}+\frac{\pi}{4}}\right)\sqrt{Dt}}$$

$$= \frac{\sqrt{\pi}}{2}\left(\frac{\sqrt{\pi}}{2} + \sqrt{\frac{4}{3}+\frac{\pi}{4}}\right) - e^{-\frac{\frac{\pi}{4}+\frac{4}{3}+\frac{\pi}{4}+\sqrt{\pi}\sqrt{\frac{4}{3}+\frac{\pi}{4}}}{4}} - erf\left(\frac{\sqrt{\pi}}{4} + \sqrt{\frac{1}{3}+\frac{\pi}{16}}\right)\frac{\sqrt{\pi}}{2}\left(\frac{\sqrt{\pi}}{2} + \sqrt{\frac{4}{3}+\frac{\pi}{4}}\right)$$

$$-\frac{\pi}{4} + e^{-\frac{\pi}{16}} + erf\left(\frac{\sqrt{\pi}}{4}\right)\frac{\pi}{4}$$

$$\approx 0.35 \tag{17}$$

So, 95 % of the water molecules are at distances $x \le \langle x \rangle + \sigma_x \approx 2.35\sqrt{Dt}$.
In the symmetric situation (e.g. a very narrow channel containing water) where diffusion takes place in both directions from the y-z plane through $x = 0$ the root mean square of x, is a direct measure for the spread of water molecules because then $\langle x \rangle = 0$ in equation (12), i.e.:

$$\sigma_x = \sqrt{\langle x^2 \rangle} = \frac{2}{\sqrt{3}}\sqrt{Dt} \approx 1.15\sqrt{Dt} \tag{18}$$

In this case the fraction of molecules in the distance interval $\pm\sigma_x$ is:

$$\int_0^{\sigma_x} \frac{AC_1\left(1-erf\left(\frac{x}{2\sqrt{Dt}}\right)\right)}{\frac{2AC_1}{\sqrt{\pi}}\sqrt{Dt}}dx = \frac{\sqrt{\pi}}{2\sqrt{Dt}}\left[x - \frac{2\sqrt{Dt}e^{-\frac{x^2}{4Dt}}}{\sqrt{\pi}} - erf\left(\frac{x}{2\sqrt{Dt}}\right)x\right]_0^{\frac{2}{\sqrt{3}}\sqrt{Dt}}$$

$$= \sqrt{\frac{\pi}{3}} - e^{-\frac{1}{3}} - erf\left(\frac{2}{\sqrt{3}}\right)\sqrt{\frac{\pi}{3}} + 1$$

$$\approx 0.39 \qquad (19)$$

All in all, to judge whether it is appropriate to use a non-steady state model or a steady state model, we can use that in the semi-infinite model the average distance the water molecules have traveled in time t is $\langle x\rangle = \frac{\sqrt{\pi}}{2}\sqrt{Dt}$ with a standard deviation of $\sigma_x = \sqrt{\frac{4}{3}+\frac{\pi}{4}}\sqrt{Dt}$. Further, approximately at the average water distance $\sqrt{Dt}$, the concentration will be half the surface concentration C_1. The standard deviation along x in the symmetric situation with diffusion in both the negative and positive x – direction from the y-z plane through $x = 0$ is determined by $\sigma_x = \frac{2}{\sqrt{3}}\sqrt{Dt}$.

Obviously if $\langle x\rangle$ and σ_x begins to be comparable to a barrier thickness, using the steady state solutions to the diffusion equations should be considered. Below in table 1 some numbers relevant for microsystems are shown for comparison:

		***t* = 24 hrs**		***t* = 30 days**		***t* = 1 year**	
Material	**Typical water diffusivity m^2/s**	$\langle x\rangle$	σ_x	$\langle x\rangle$	σ_x	$\langle x\rangle$	σ_x
Epoxy	10^{-13}	0.082 mm	0.14 mm	0.45 mm	0.74 mm	1.57 mm	2.58 mm
Silicone	10^{-11}	0.82 mm	1.35 mm	4.51 mm	7.41 mm	15.7 mm	25.85 mm
Air	$2.5\cdot10^{-5}$	1.30 m	2.14 m	7.13 m	11.72 m	24.88 m	40.87 m

Table 1: Typical diffusion distances and standard deviations in the semi-infinite model.

The water diffusivity in polymers is several orders of magnitude larger than typical metal atom diffusivities in metals. Given sufficient time the diffusion through a polymer wall, will eventually reach steady state i.e.:

$$\frac{\partial C}{\partial t} = D\frac{\partial^2 C}{\partial x^2} = 0 \tag{20}$$

$$\Updownarrow$$

$$\frac{\partial^2 C}{\partial x^2} = 0 \tag{21}$$

$$\Updownarrow$$

$$\frac{\partial C}{\partial x} = \text{const} \tag{22}$$

With the boundary conditions, see fig. 2:

$$C(x=0) = C_1 \tag{23}$$

$$C(x=L) = C_2 \tag{24}$$

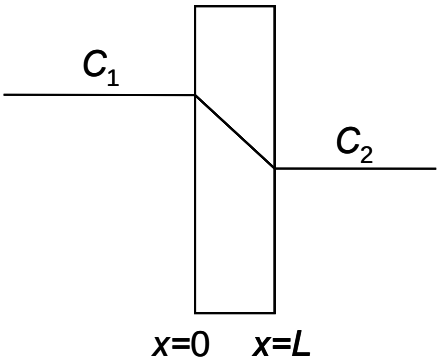

Fig. 2: Steady state diffusion of water through polymer barrier. Water concentrations in the air on each side are C_1 and C_2.

we get:

$$C(x) = C_1 + (C_2 - C_1)\frac{x}{L} \tag{25}$$

From Ficks' first law we then have for the flux J (also sometimes named F):

$$J = -D\frac{\partial C(x)}{\partial x} = -D\frac{C_2 - C_1}{L} \tag{26}$$

In the more realistic case where concentrations are different inside and outside the polymer wall, see fig. 3, it is often assumed that Henrys law applies (requires low

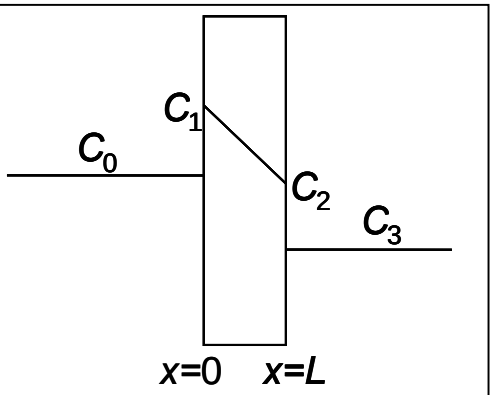

Fig. 3: Steady state diffusion of water through a polymer barrier. Water concentrations in the air on each side are C_0 and C_3. Inside the barrier the corresponding concentrations of water on each side is C_1 and C_2.

concentration inside polymer wall. This condition is most often satisfied for polymers) on both interfaces and hence the Henrys' law partition / distribution coefficient, equilibrium constant or solubility coefficient κ can be introduced to include a description of transfer / partition at / across the interfaces:

$$J = -\frac{D(C_2 - C_1)}{L} = -D\kappa\frac{C_3 - C_0}{L} = -P\frac{C_3 - C_0}{L} \tag{27}$$

where

$$\kappa = \frac{C_1}{C_0} = \frac{C_2}{C_3} \tag{28}$$

and P is the permeability constant [2]. Clearly, the first case in fig. 2 corresponds to $\kappa = 1$. Given the situation of a polymer as depicted in fig. 3, which can contain only small amounts of water, if $C_2 \approx 0$, C_3 is even closer to zero and:

$$J \approx D\kappa\frac{C_0}{L} = P\frac{C_0}{L} \tag{29}$$

This is a quite common situation. A less common definition of the permeability not considering partition at interfaces, and thus only the transport inside the polymer, is used in [Papers 10, 15, 18] and [Posters 5, 6]:

$$J = -\frac{D(C_2 - C_1)}{L} = P(C_1 - C_2) \tag{30}$$

When $C_2 \approx 0$ and C_1 is equal to the water solubility S of the polymer we have:

$$J = PS \tag{31}$$

Looking at equation (29) this correspond to the special situation $\kappa = 1$, i.e. $C_0 = C_1 = S$. More generally the equations should be expressed in terms of activities instead of concentrations.
A number of important factors influencing polymer permeability are given in [3]. For instance no hydrophilic substituents, small substituents, close packaging and absence of polar groups are mentioned as important prerequisites for low water permeability.

It turns out that for polymer barriers like in figs. 2 and 3, a clear time distinction between non-steady state diffusion and steady state diffusion can be found analytically. This can in many specific cases help a lot in making the right choice between a non-steady state and a steady state model. The well known analytical time lag formula (117) giving the time before steady state diffusion sets in is derived in chapter 3.1.1.5.1 below.

3.1.1.3 Water diffusivity in polymers from diffusion into a slab

Determination of the water diffusivity in the used polymeric packaging materials is clearly important to evaluate microsystem reliability. Earlier in chapters 1.4.1.3.2, 2.2.1 and in [Papers 10, 15, 18], [Posters 5, 6] it is mentioned and demonstrated that the diffusivity of water in polymers can be determined by sorption experiments using 5 cm · 5 cm · 0.1 cm slabs of the materials. The slabs should be so thin that on full humidity exposure or water immersion the edge face area and therefore edge water in-diffusion can be ignored. If the surface water concentration is C_1 then the absorbed mass of water at infinite time M_∞ is:

$$M_\infty = \int_0^L AC_1 dx = AC_1 L \tag{32}$$

Then at short time where the water from the two 5 cm · 5 cm faces have not yet met at half the sample thickness $L/2 = 0.05$ cm we have from equations (11) and (32):

$$\frac{M_t}{M_\infty} = \frac{2\frac{2AC_1}{\sqrt{\pi}}\sqrt{Dt}}{AC_1 L} = \frac{4}{\sqrt{\pi}}\frac{1}{L}\sqrt{Dt} \tag{33}$$

where M_t is the mass of water absorbed at time t. Thus, if at short times M_t / M_∞ is plotted against $\sqrt{t}/L$ in the sorption plot, we get a straight line with slope α :

$$\alpha = 4\sqrt{\frac{D}{\pi}} \tag{34}$$

and hence:

$$D = \frac{\pi}{16}\alpha^2 \tag{35}$$

which is the short time expression mentioned in chapter 1.4.1.3.2 and in [Papers 10, 15, 18]. From the previous chapter we can use that at time *t* 95 % of the water is within a distance of $2.35\sqrt{Dt}$ to estimate when the above equations applies i.e. farther away than *L*/2 measured from both faces we require much less than 5 % "overlap" of water in-diffused from the other face:

$$2.35\sqrt{Dt} << \frac{L}{2} \tag{36}$$

$$\Updownarrow$$

$$t << \frac{L^2}{22.09D} \tag{37}$$

From this we get:

$$\frac{M_t}{M_\infty} = \frac{4}{\sqrt{\pi}}\frac{1}{L}\sqrt{Dt} << \frac{4}{\sqrt{\pi}}\frac{1}{L}\frac{L}{4.7} \approx 0.48 \tag{38}$$

So, as long as M_t / M_∞ is well below 0.5 we can use equation (33). However, using this equation requires that M_∞ is known which it most often is not. Then the whole sorption process can just as well be monitored. Having the full sorption curve we can use the short time expression on the first M_t / M_∞ values or the fitted full sorption curve to estimate *D*. The latter requires a solution to the diffusion equation which is valid at all times and which is fitted to the data. This solution is derived below using the Laplace transform technique [3, 4]. It involves the theory of functions of a complex variable in order to carry out a contour integration.

As a start we have the general boundary conditions:

$$C(0, t \geq 0) = C_1 \tag{39}$$

$$C(L, t \geq 0) = C_2 \tag{40}$$

$$C(0 < x < L, 0) = C_0(x) \tag{41}$$

Then the Laplace transform of the diffusion equation is:

$$\int_0^\infty \frac{\partial^2 C}{\partial x^2} e^{-pt} dt = \frac{\partial^2}{\partial x^2} \int_0^\infty C e^{-pt} dt = \frac{\partial^2 \overline{C}}{\partial x^2} \tag{42}$$

$$\int_0^\infty \frac{\partial C}{\partial t} e^{-pt} dt = \left[C e^{-pt} \right]_0^\infty + p \int_0^\infty C e^{-pt} dt = -C_0(x) + p\overline{C} \tag{43}$$

$$\Downarrow$$

$$D \frac{\partial^2 \overline{C}}{\partial x^2} = -C_0(x) + p\overline{C} \tag{44}$$

$$\Updownarrow$$

$$D \frac{\partial^2 \overline{C}}{\partial x^2} - p\overline{C} = -C_0(x) \tag{45}$$

$$\Updownarrow$$

$$\frac{\partial^2 \overline{C}}{\partial x^2} - q^2 \overline{C} = -\frac{C_0(x)}{D} \tag{46}$$

where $\overline{C}$ denotes the Laplace transform of C, p is a number which is sufficiently large to make the integrals converge, and $q^2 = p/D$. Thus, the partial differential diffusion equation has been reduced to an ordinary linear, nonhomogeneous second order differential equation. At the boundaries we have:

$$\underline{\text{x = 0}}: \overline{C} = \int_0^\infty C_1 e^{-pt} dt = C_1 \left[-\frac{e^{-pt}}{p} \right]_0^\infty = \frac{C_1}{p} \tag{47}$$

$$\underline{\text{x = L}}: \overline{C} = \int_0^\infty C_2 e^{-pt} dt = C_2 \left[-\frac{e^{-pt}}{p} \right]_0^\infty = \frac{C_2}{p} \tag{48}$$

The characteristic equation for the Laplace transformed diffusion equation is (variable is m): $m^2 - q^2 = 0 \Leftrightarrow m = \pm q$. This leads to:

$$\overline{C} = k_1 e^{qx} + k_2 e^{-qx} - \frac{e^{qx}}{2q} \int e^{-qx} \frac{C_0(x)}{D} dx + \frac{e^{-qx}}{2q} \int e^{qx} \frac{C_0(x)}{D} dx$$

$$= k_1 e^{qx} + k_2 e^{-qx} + \frac{1}{2qD} \left(e^{-qx} \int e^{qx} C_0(x) dx - e^{qx} \int e^{-qx} C_0(x) dx \right) \tag{49}$$

where k_1 and k_2 are constants.

At x = 0 we have:

$$\overline{C} = k_1 + k_2 + \frac{1}{2qD}\left[e^{-qx}\int e^{qx}C_0(x)dx - e^{qx}\int e^{-qx}C_0(x)dx\right]_{x=0} = \frac{C_1}{p} \tag{50}$$

Defining:

$$C_0^{'}(0) = \frac{p}{2qD}\left[e^{-qx}\int e^{qx}C_0(x)dx - e^{qx}\int e^{-qx}C_0(x)dx\right]_{x=0} \tag{51}$$

We get:

$$\overline{C} = k_1 + k_2 + \frac{C_0^{'}(0)}{p} = \frac{C_1}{p} \tag{52}$$

$$\Updownarrow$$

$$k_2 = \frac{C_1}{p} - \frac{C_0^{'}(0)}{p} - k_1 = \frac{1}{p}\left(C_1 - C_0^{'}(0)\right) - k_1 \tag{53}$$

Then:

$$\begin{aligned}\overline{C} &= k_1 e^{qx} + \left(\frac{1}{p}\left(C_1 - C_0^{'}(0)\right) - k_1\right)e^{-qx} + \frac{C_0^{'}(x)}{p} \\ &= k_1\left(e^{qx} - e^{-qx}\right) + \frac{1}{p}\left(C_0^{'}(x) - C_0^{'}(0)e^{-qx}\right) + \frac{C_1}{p}e^{-qx} \\ &= 2k_1 \sinh qx + \frac{1}{p}\left(C_0^{'}(x) - C_0^{'}(0)e^{-qx}\right) + \frac{C_1}{p}e^{-qx}\end{aligned} \tag{54}$$

At x = L we then have:

$$\overline{C} = 2k_1 \sinh qL + \frac{1}{p}\left(C_0^{'}(L) - C_0^{'}(0)e^{-qL}\right) + \frac{C_1}{p}e^{-qL} = \frac{C_2}{p} \tag{55}$$

$$\Updownarrow$$

$$k_1 = \frac{\frac{C_2}{p} - \frac{C_1}{p}e^{-qL} - \frac{1}{p}\left(C_0^{'}(L) - C_0^{'}(0)e^{-qL}\right)}{2\sinh qL} = \frac{C_2 - C_1 e^{-qL} - C_0^{'}(L) + C_0^{'}(0)e^{-qL}}{2p\sinh qL} \tag{56}$$

Then:

$$\overline{C} = \frac{C_2 - C_1 e^{-qL} - C_0'(L) + C_0'(0)e^{-qL}}{p \sinh qL} \sinh qx + \frac{1}{p}\left(C_0'(x) - C_0'(0)e^{-qx}\right) + \frac{C_1}{p} e^{-qx}$$
$$= \frac{\left\{C_2 - C_1 e^{-qL} - C_0'(L) + C_0'(0)e^{-qL}\right\}\sinh qx + \left\{C_0'(x) - C_0'(0)e^{-qx} + C_1 e^{-qx}\right\}\sinh qL}{p \sinh qL} \quad (57)$$

To find C we now apply the Bromwich integral (inverse Laplace transformation):

$$C = \frac{1}{2\pi i}\int_{\gamma - i\infty}^{\gamma + i\infty} \overline{C} e^{pt} dp = \frac{1}{2\pi i} 2\pi i \sum R\left[\overline{C} e^{pt}\right] = \sum R\left[\overline{C} e^{pt}\right] \quad (58)$$

where γ is a vertical contour in the complex plane chosen so that all singularities of $\overline{C} e^{pt}$ are to the left of it. R denotes residue, i.e. C is given by the sum of residues for $\overline{C} e^{pt}$. On calculating C no branch cut is necessary as it could seem due to the multivalued (double) behavior of the square root term in $\sinh x\sqrt{p/D}$ because $\sinh x\sqrt{p/D}$ appears both in the numerator and the denominator by which discontinuities / sign changes cancel out and $\overline{C}$ becomes a well defined single valued function. First it is noted that $\overline{C} e^{pt}$ has a simple pole for $p = 0$ and:

$$R\left[\overline{C} e^{pt}, p = 0\right] = \lim_{p \to 0} \overline{C} e^{pt}(p - 0) \quad (59)$$

It is also noted that the Final Value Theorem [5-8] states that[1]:

$$\lim_{p \to 0} p\overline{C}(p) = C(t = \infty) \quad (60)$$

which means that $p = 0$ in $\overline{C}$ corresponds to $t = \infty$ in C. At $t = \infty$ the steady state diffusion equation $\frac{d^2 C}{dx^2} = 0$ applies and the solution for $t = \infty$ is immediately found to be given by equation (25) above.

$$\int_0^\infty \frac{dC(t)}{dt} e^{-pt} dt = \left[C(t)e^{-pt}\right]_0^\infty + p\int_0^\infty C(t)e^{-pt} dt = p\overline{C}(p) - C(t = 0) \Rightarrow$$

[1] $\lim_{p \to 0} p\overline{C}(p) - C(t = 0) = \int_0^\infty \frac{dC(t)}{dt} dt = C(t = \infty) - C(t = 0)$

$\Updownarrow$

$\lim_{p \to 0} p\overline{C}(p) = C(t = \infty)$

Proceeding from equation (57) for $\overline{C}$ above note that at $t=\infty$ we know that the initial concentration distribution has leveled out to a constant value C_0 throughout the slab so that we can introduce:

$$C_0^{'} = C_0^{'}(L) = C_0^{'}(0) \tag{61}$$

We then have:

$$C(t=\infty) = R\left[\overline{C}e^{pt}, p=0\right] = \lim_{\mathrm{p}\to 0} p\overline{C}(p)e^{pt} = \lim_{\mathrm{p}\to 0} p\overline{C}(p)\lim_{\mathrm{p}\to 0} e^{pt} = \lim_{\mathrm{p}\to 0} p\overline{C}(p)$$

$$= \lim_{\mathrm{p}\to 0} \frac{\left\{C_2 - C_1 e^{-qL} - C_0^{'}\left(1-e^{-qL}\right)\right\}\sinh qx + \left\{C_0^{'}\left(1-e^{-qL}\right) + C_1 e^{-qx}\right\}\sinh qL}{\sinh qL}$$

$$= \lim_{\mathrm{p}\to 0} \frac{\left\{C_2 - C_1 e^{-qL}\right\}\sinh qx}{\sinh qL} + \lim_{\mathrm{p}\to 0} C_1 e^{-qx} = C_1 + (C_2 - C_1)\lim_{\mathrm{p}\to 0}\frac{\sinh qx}{\sinh qL}$$

$$= C_1 + (C_2 - C_1)\lim_{\mathrm{p}\to 0}\frac{\frac{d}{dp}\sinh qx}{\frac{d}{dp}\sinh qL} = C_1 + (C_2 - C_1)\lim_{\mathrm{p}\to 0}\frac{\frac{1}{2}\sqrt{p}\,\frac{x}{\sqrt{D}}\cosh\left(\frac{x}{\sqrt{D}}\sqrt{p}\right)}{\frac{1}{2}\sqrt{p}\,\frac{L}{\sqrt{D}}\cosh\left(\frac{L}{\sqrt{D}}\sqrt{p}\right)}$$

$$= C_1 + (C_2 - C_1)\frac{x}{L} \tag{62}$$

where L'hospitals' rule was used in line four. The solution is the same as given earlier in equation (25) as it should be.

Further $\overline{C}e^{pt}$ has simple poles for:

$$\sinh qL = 0 \Leftrightarrow -i\sin iqL = 0 \Leftrightarrow iqL = \pm n\pi \Leftrightarrow qL = \pm n\pi i \tag{63}$$

This leads to:

$$q^2 = \frac{p}{D} = -\frac{n^2\pi^2}{L^2} \Leftrightarrow p = -\frac{n^2\pi^2}{L^2}D \tag{64}$$

If we put:

$$\overline{C}e^{pt} = \frac{f(p)}{g(p)} \tag{65}$$

we then have:

$$R\left[\overline{C}e^{pt}, p=-\frac{n^2\pi^2}{L^2}D\right]=\left[\frac{f(p)}{\frac{d}{dp}g(p)}\right]_{p=-\frac{n^2\pi^2}{L^2}D} \tag{66}$$

Here we have:

$$\frac{d}{dp}g(p)=\frac{d}{dp}p\sinh qL=\sinh qL+p\frac{d}{dp}\left(\sinh\left(\frac{L}{\sqrt{D}}\sqrt{p}\right)\right)=\sinh qL+p\frac{1}{2\sqrt{p}}\frac{L}{\sqrt{D}}\cosh qL$$

$$=\sinh qL+\frac{1}{2}qL\cosh qL \tag{67}$$

$$\Downarrow$$

$$\left[\frac{d}{dp}g(p)\right]_{p=-\frac{n^2\pi^2}{L^2}D}=0+\frac{1}{2}n\pi i\cosh n\pi i=\frac{1}{2}n\pi i\cos i^2 n\pi=(-1)^n\frac{1}{2}n\pi i \tag{68}$$

and inserted in equation (58) we get:

$$R\left[\overline{C}e^{pt}, p=-\frac{n^2\pi^2}{L^2}D\right]$$

$$=\frac{\left\{\left[C_2-C_1e^{-n\pi i}-\left(C_0'(L)-C_0'(0)e^{-n\pi i}\right)\right]\sinh\frac{n\pi ix}{L}+\left[\left(C_0'(x)-C_0'(0)e^{-n\pi i\frac{x}{L}}\right)+C_1e^{-n\pi i\frac{x}{L}}\right]\sinh n\pi i\right\}e^{-n^2\pi^2\frac{Dt}{L^2}}}{(-1)^n\frac{1}{2}n\pi i}$$

$$=\frac{\left[C_2-(-1)^nC_1-\left(C_0'(L)-(-1)^nC_0'(0)\right)\right]i\sin\frac{n\pi x}{L}\cdot e^{-n^2\pi^2\frac{Dt}{L^2}}}{(-1)^n\frac{1}{2}n\pi i}$$

$$=\left[\frac{2}{\pi}\frac{(-1)^nC_2-C_1-(-1)^nC_0'(L)+C_0'(0)}{n}\right]\sin\frac{n\pi x}{L}\cdot e^{-n^2\pi^2\frac{Dt}{L^2}} \tag{69}$$

and finally we have the general equation:

$$C=\sum R\left[\overline{C}e^{pt}\right]$$

$$=C_1+(C_2-C_1)\frac{x}{L}+\frac{2}{\pi}\sum_{n=1}^{\infty}\left[\frac{(-1)^nC_2-C_1-(-1)^nC_0'(L)+C_0'(0)}{n}\right]\sin\frac{n\pi x}{L}\cdot e^{-n^2\pi^2\frac{Dt}{L^2}} \tag{70}$$

Below some examples using equation (70) valid for all t starting with different initial concentration distributions are given.

For initial parabolic concentration $C_0(x) = C_0\left(2x^2 - 2Lx + 1\right)$ with surface concentrations $C_0(0) = C_0(L) = C_0$ and minimum $C_0(L/2) = ½C_0$ we get:

$$C_0'(x) = C_0\left(2x^2 - 2Lx + \frac{4}{q^2} + 1\right) \Rightarrow \tag{71}$$

$$C_0'(L) = C_0'(0) = C_0\left(\frac{4}{q^2} + 1\right) \Rightarrow \tag{72}$$

$$\frac{2}{\pi}\sum_{n=1}^{\infty}\frac{-(-1)^n C_0'(L) + C_0'(0)}{n} = \frac{2}{\pi}\sum_{n=1}^{\infty}\frac{-(-1)^n C_0\left(\frac{4}{q^2}+1\right) + C_0\left(\frac{4}{q^2}+1\right)}{n} = \frac{2}{\pi}\sum_{n=1}^{\infty}\frac{\begin{matrix}0 \text{ for } n \text{ even} \\ 2C_0\left(\frac{4}{q^2}+1\right) \text{for n odd}\end{matrix}}{n}$$

$$= \frac{2}{\pi}\sum_{n=0}^{\infty}\frac{2C_0\left(\frac{4}{\left(\frac{(2n+1)\pi i}{L}\right)^2}+1\right)}{2n+1} = \frac{2C_0}{\pi}\sum_{n=0}^{\infty}\frac{2-\frac{8L^2}{(2n+1)^2\pi^2}}{2n+1} = \frac{4C_0}{\pi}\sum_{n=0}^{\infty}\frac{1}{2n+1} - \frac{16L^2C_0}{\pi^3}\sum_{n=0}^{\infty}\frac{1}{(2n+1)^3} \tag{73}$$

This leads to the solution:

$$C = C_1 + (C_2 - C_1)\frac{x}{L} + \frac{2}{\pi}\sum_{n=1}^{\infty}\left[\frac{(-1)^n C_2 - C_1}{n}\right]\sin\frac{n\pi x}{L}e^{-n^2\pi^2\frac{Dt}{L^2}} + \frac{4C_0}{\pi}\sum_{n=0}^{\infty}\frac{1}{2n+1}\sin\frac{(2n+1)\pi x}{L}e^{-(2n+1)^2\pi^2\frac{Dt}{L^2}}$$
$$-\frac{16L^2C_0}{\pi^3}\sum_{n=0}^{\infty}\frac{1}{(2n+1)^3}\sin\frac{(2n+1)\pi x}{L}e^{-(2n+1)^2\pi^2\frac{Dt}{L^2}} \tag{74}$$

For initial concentration $C_0(x) = C_0 x$ we get $C_0'(x) = C_0 x$ and:

$$C = C_1 + (C_2 - C_1)\frac{x}{L} + \frac{2}{\pi}\sum_{n=1}^{\infty}\frac{(-1)^n C_2 - C_1}{n}\sin\frac{n\pi x}{L}e^{-n^2\pi^2\frac{Dt}{L^2}} + \frac{2C_0L}{\pi}\sum_{n=1}^{\infty}\frac{(-1)^{n+1}}{n}\sin\frac{n\pi x}{L}e^{-n^2\pi^2\frac{Dt}{L^2}} \tag{75}$$

For initial concentration $C_0(x) = C_0$ we get $C_0'(x) = C_0$ and:

$$C = C_1 + (C_2 - C_1)\frac{x}{L} + \frac{2}{\pi}\sum_{n=1}^{\infty}\frac{(-1)^n C_2 - C_1}{n}\sin\frac{n\pi x}{L}e^{-n^2\pi^2\frac{Dt}{L^2}} + \frac{4C_0}{\pi}\sum_{n=0}^{\infty}\frac{1}{2n+1}\sin\frac{(2n+1)\pi x}{L}e^{-(2n+1)^2\pi^2\frac{Dt}{L^2}} \tag{76}$$

If $C_1 = C_2$ and $C_0 = 0$ in the last equation we arrive at:

$$C = C_1 + \frac{2}{\pi}\sum_{n=1}^{\infty}\frac{C_1\left((-1)^n - 1\right)}{n}\sin\frac{n\pi x}{L}e^{-n^2\pi^2\frac{Dt}{L^2}} = C_1 + \frac{2C_1}{\pi}\sum_{n=1}^{\infty}\frac{\begin{matrix}0\,\text{for}\,n\,\text{even}\\ -2\,\text{for}\,n\,\text{odd}\end{matrix}}{n}\sin\frac{n\pi x}{L}e^{-n^2\pi^2\frac{Dt}{L^2}}$$

$$= C_1\left(1 - \frac{4}{\pi}\sum_{n=0}^{\infty}\frac{1}{2n+1}\sin\frac{(2n+1)\pi x}{L}e^{-(2n+1)^2\pi^2\frac{Dt}{L^2}}\right) \qquad (77)$$

This is the concentration equation used in chapters 1.4.1.3.2, 2.2.1, [Papers 10, 15, 18], [Posters 5, 6] to find M_t by integration over the entire slab thickness L. Thus, in fig. 4 the concentration profiles at different times through 5 cm · 5 cm · 0.1 cm slabs of the epoxy Epotek U300-1 according to equation (77) is illustrated. To validate equation (77) the corresponding FEM simulated concentration profiles are included in the same graph. The exact C plots were made using Microsoft Excel for $n = 0$ to 14 which is by far enough for the illustration of the exact C, since the contributions to the sum decrease very rapidly with increasing n. As can be seen, there is a good agreement between exact and simulated data.

The simulated concentration profiles obtained from equation (1) are shown separately in the graphical way by the vertical view in fig. 5 below. The simulation represents a corner cut-out of the studied slabs. The simulated data in fig. 4 was taken from the left (colored) vertical edges of the slabs. The used FEM software was COSMOSWorks 2008. The software is developed for thermal diffusion studies. However, the mass diffusion equations are the same. Only, temperature is replaced by concentration and the thermal conductivity constant is replaced with the diffusion constant.

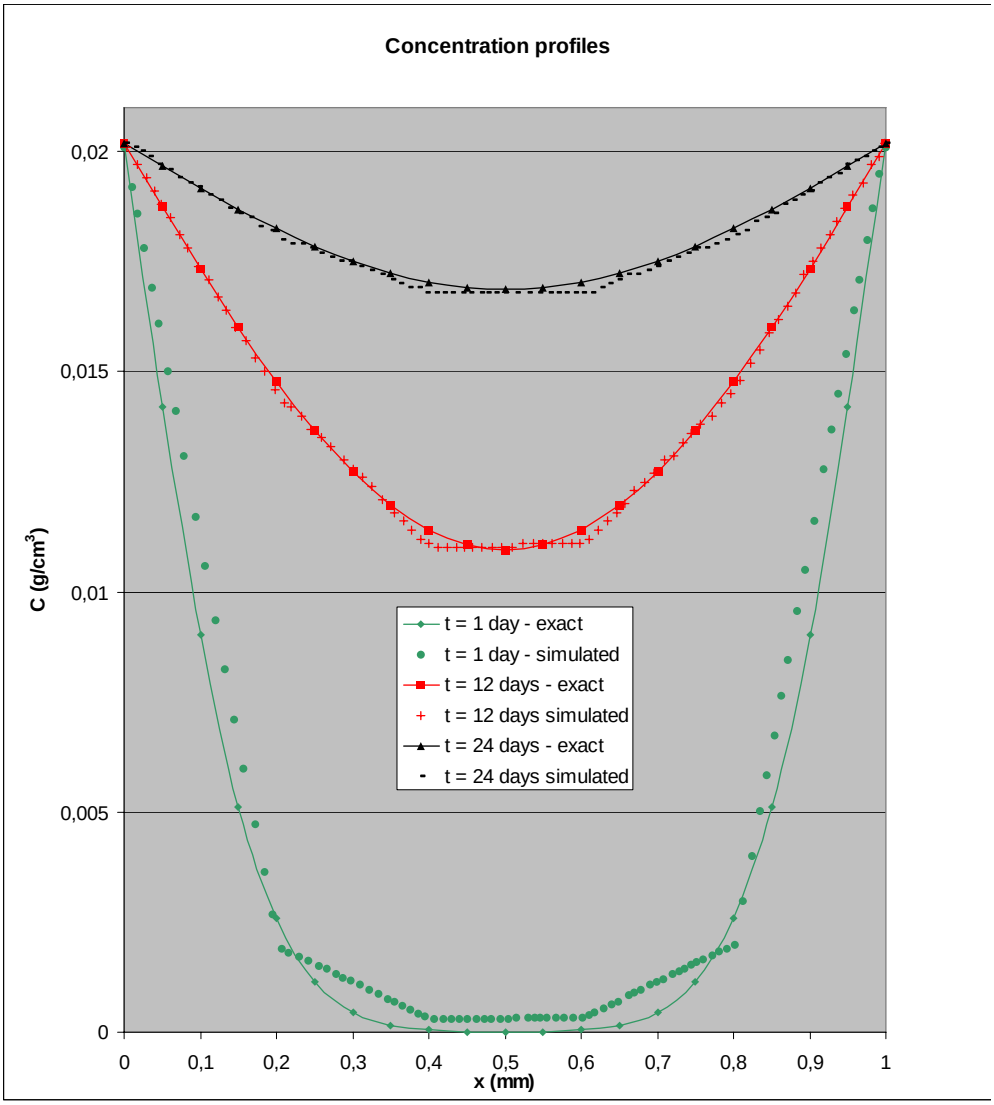

Fig. 4: Exact (equation (77)) and simulated (cf. fig. 5) water concentration profiles for $5\text{cm}\cdot 5\text{cm}\cdot 0.1\text{cm}$ slabs of Epotek U300-1 adhesive at different times. $D = 10^{-13}$ m^2 s^{-1}, $C_1 = 0.0202$ g cm^{-3}. The exact C plots were made using Microsoft Excel for $n = 0$ to 14 which is by far enough for the illustration of the exact C, since the contributions to the sum decrease very rapidly with increasing n. The simulated data were taken from the left vertical edges of the repective simulated views at different times in fig. 5. As can be seen, there is a good agreement between exact and simulated data.

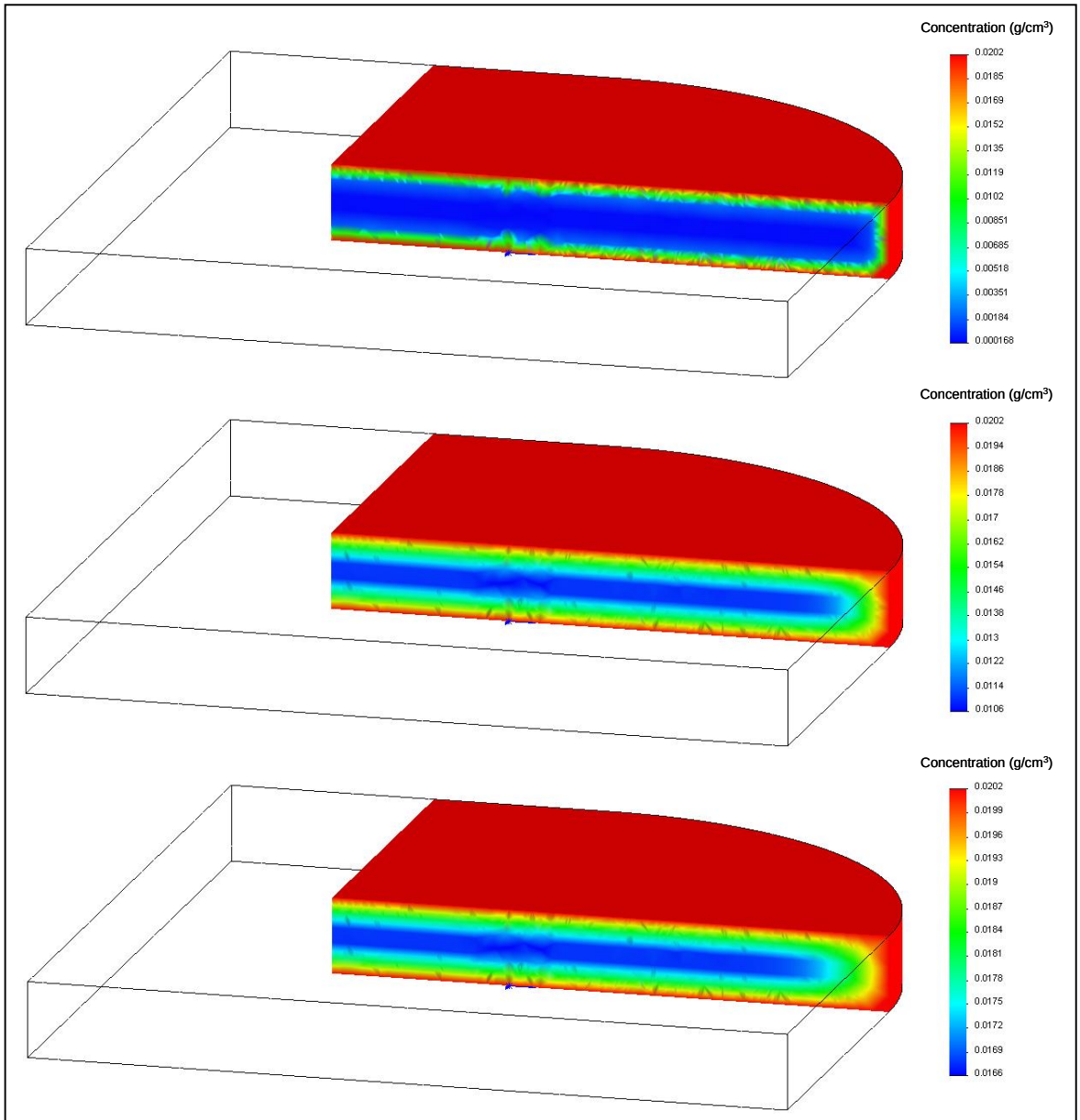

Fig. 5: Graphical representation of FEM simulation concentration data obtained from equation (1) on water diffusion in the epoxy Epotek U300-1. A 1 mm thick slab is shown after different times. Top: concentration profile after 1 day, middle: profile after 12 days, bottom: profile after 24 days. $D = 10^{-13}$ m^2 s^{-1}, $C_1 = 0.0202$ g cm^{-3}.

The integration of equation (77) over the entire slab thickness to find M_t gives:

$$M_t = AC_1 \int_0^L \left(1 - \frac{4}{\pi} \sum_{n=0}^{\infty} \frac{1}{2n+1} \sin \frac{(2n+1)\pi x}{L} e^{-(2n+1)^2 \pi^2 \frac{Dt}{L^2}} \right) dx$$

$$= AC_1 L - \frac{4AC_1}{\pi} \sum_{n=0}^{\infty} \frac{e^{-(2n+1)^2 \pi^2 \frac{Dt}{L^2}}}{2n+1} \int_0^L \sin \frac{(2n+1)\pi x}{L} = AC_1 L - \frac{4AC_1}{\pi} \sum_{n=0}^{\infty} \frac{e^{-(2n+1)^2 \pi^2 \frac{Dt}{L^2}}}{2n+1} \left[-\frac{L \cos\left(\frac{(2n+1)\pi x}{L} \right)}{(2n+1)\pi} \right]_0^L$$

$$= AC_1 L - \frac{4AC_1}{\pi} \sum_{n=0}^{\infty} \frac{e^{-(2n+1)^2 \pi^2 \frac{Dt}{L^2}}}{2n+1} \left(\frac{2L}{(2n+1)\pi} \right) = AC_1 L - \frac{8AC_1 L}{\pi^2} \sum_{n=0}^{\infty} \frac{e^{-(2n+1)^2 \pi^2 \frac{Dt}{L^2}}}{(2n+1)^2} \tag{78}$$

For the sorption plots we then finally have as stated in chapters 1.4.1.3.2, 2.2.1, [Papers 10, 15, 18] and [Posters 5, 6]:

$$\frac{M_t}{M_\infty} = \frac{AC_1 L - \frac{8AC_1 L}{\pi^2} \sum_{n=0}^{\infty} \frac{e^{-(2n+1)^2 \pi^2 \frac{Dt}{L^2}}}{(2n+1)^2}}{AC_1 L} = 1 - \frac{8}{\pi^2} \sum_{n=0}^{\infty} \frac{e^{-(2n+1)^2 \pi^2 \frac{Dt}{L^2}}}{(2n+1)^2} \tag{79}$$

From equations (33) and (79) we know that for small t where $M_t / M_\infty << 0.5$ we have:

$$\frac{M_t}{M_\infty} = 1 - \frac{8}{\pi^2} \sum_{n=0}^{\infty} \frac{e^{-(2n+1)^2 \pi^2 \frac{Dt}{L^2}}}{(2n+1)^2} = \frac{4}{\sqrt{\pi}} \frac{1}{L} \sqrt{Dt} \tag{80}$$

At large t the exponentials for $n > 0$ in the sum (79) decrease very quickly because they depend on $(2n+1)^2$, meaning that these terms can be omitted. We then have the very good approximation for $n = 0$:

$$\frac{M_t}{M_\infty} \approx 1 - \frac{8}{\pi^2} e^{-\pi^2 \frac{Dt}{L^2}} \approx 1 - 0.811 e^{-9.87 \frac{Dt}{L^2}} \tag{81}$$

$$\Updownarrow$$

$$\ln\left(1 - \frac{M_t}{M_\infty} \right) \approx \ln \frac{8}{\pi^2} - \pi^2 \frac{Dt}{L^2} \tag{82}$$

This means that plotting $\ln(1 - M_t / M_\infty)$ against t / L^2 for large t we get a straight line with slope:

$$\beta = -\pi^2 D \tag{83}$$

$$\Updownarrow$$

$$D = -\frac{\beta}{\pi^2} \tag{84}$$

In these studies the sum-function (79) was fitted for all t to the function:

$$\frac{M_t}{M_\infty} \approx G = 1 - ae^{-k\left(\frac{Dt}{L^2}\right)^p} \tag{85}$$

and a good fit ($r^2 = 1.00$) was found for $a = 0.877$, $k = 9.18$, $p = 0.931$, see fig. 6.

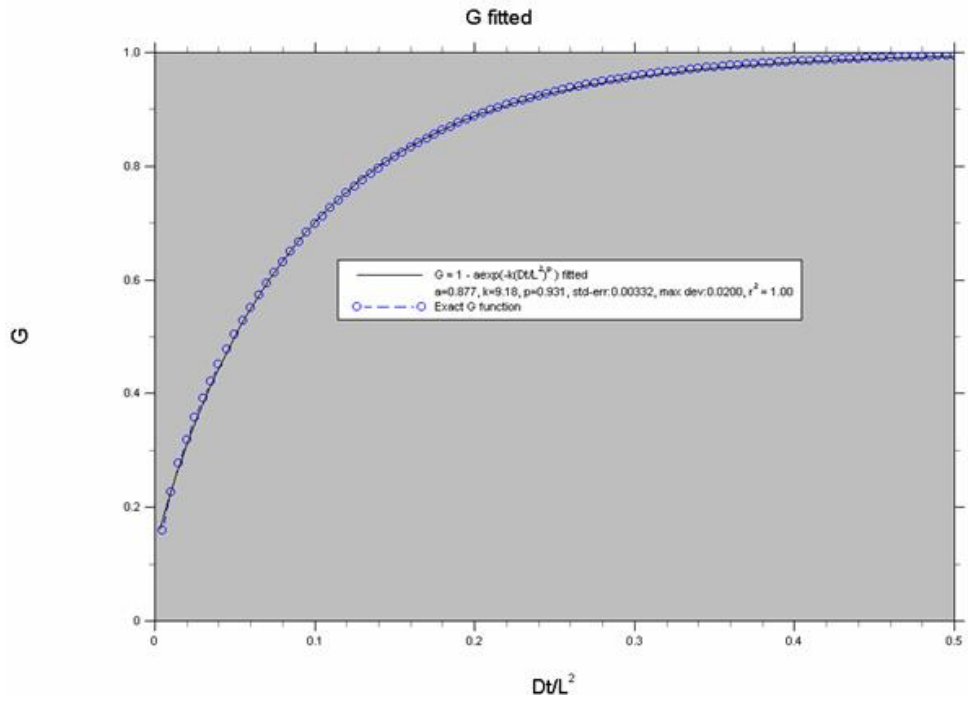

Fig. 6: Fitting of G function to the exact M_t / M_∞ theoretical sorption data. G is then used to find the D's by fitting it to the experimental sorption data.

The D's were then determined by fitting G to all the sorption data.
Naturally $C_1 = C_2$ by the water immersion used here. It is more questionable if C_0 was really zero in these experiments. To use equation (79) this was generally attempted by drying out the slabs in exicator or in chambers with a constant dry N_2 flow for more than a month before immersion. However, this was unfortunately done without following the

weight of the samples meaning that it is still not completely certain that C_0 was really zero in these experiments. This is one reason why the found D's should only be considered good estimates.

If $C_1 = C_2$ and $C_0 > 0$ which is more likely we get:

$$\frac{M_t}{M_\infty} = 1 - \frac{8}{\pi^2}\sum_{n=0}^{\infty}\frac{e^{-(2n+1)^2\pi^2\frac{Dt}{L^2}}}{(2n+1)^2} + \frac{C_0}{C_1}\frac{8}{\pi^2}\sum_{n=0}^{\infty}\frac{e^{-(2n+1)^2\pi^2\frac{Dt}{L^2}}}{(2n+1)^2}$$
$$= 1 - \left(1 - \frac{C_0}{C_1}\right)\frac{8}{\pi^2}\sum_{n=0}^{\infty}\frac{e^{-(2n+1)^2\pi^2\frac{Dt}{L^2}}}{(2n+1)^2} \quad (86)$$

That is, the error in M_t / M_∞ using equation (79) with a non-zero C_0 is given by the last term in equation (86). It has not been attempted to estimate the corresponding errors in the found D's. Note that of cause in this case at $t = 0$:

$$\frac{M_{t=0}}{M_\infty} = 1 - \left(1 - \frac{C_0}{C_1}\right)\frac{8}{\pi^2}\sum_{n=0}^{\infty}\frac{1}{(2n+1)^2} = 1 - \left(1 - \frac{C_0}{C_1}\right)\frac{8}{\pi^2}\frac{\pi^2}{8} = \frac{C_0}{C_1} \quad (87)$$

The fitting function (85) was inspired by how the sum function (79) behaves for large t as described by equation (81). The found constants in the fitting match quite well with those in equation (81) although small t's are included in the fit, indicating that the time interval (small t) with significant deviation from the large t behavior as described by equation (81) is relatively narrow as compared to the total time fitted or even more to the to the total time needed for saturation. Therefore all the sorption data can be fitted to the fit function G for M_t / M_∞ without introducing too much error in the found D's. Nevertheless, if D varies with time, the D found from G corresponds to the large t. The D's for large t in polymers are often smaller than the early D's because of less free volume for diffusion and because water begins to interact with itself through hydrogen bondings [2]. This effect will be most pronounced for relatively hydrophilic polymers.
The pre-exponential $a \neq 1$ in equation (85) results in an overall better fit to the theoretical sorption curve in fig. 6 than omitting it by setting it equal to 1 (otherwise p would of cause get equal to 1 in the fitting procedure). However, note that having $a \neq 1$ is un-physical, because then $M_{t=0} / M_\infty \neq 0$ which is in contradiction to what is known for $C_0 = 0$. Deviations from the data are thus of cause largest at short times. According to another similar study [9] having $a = 1$ results in the following fit function G' to determine D:

$$\frac{M_t}{M_\infty} \approx G' = 1 - e^{-7.3\left(\frac{Dt}{L^2}\right)^{0.75}} \quad (88)$$

This function fits the data better at small t but not as good for large t as can be seen by comparing the constants k and p with those in equation (81) and equation (88). Clearly, both fits are inaccurate at short times since they deviate much (G the most) from the linear dependence on $\sqrt{t}$ as dictated by equation (33). This can be seen by differentiating with respect to $\sigma = \sqrt{t}$:

$$\frac{dG}{d\sigma} = 14.99 \cdot \left(\frac{D}{L^2}\right)^{0.931} e^{-9.18\left(\frac{D}{L^2}\right)^{0.931}\sigma^{1.862}} \sigma^{0.862} \tag{89}$$

$$\frac{dG'}{d\sigma} = 10.95 \cdot \left(\frac{D}{L^2}\right)^{0.75} e^{-7.3\left(\frac{D}{L^2}\right)^{0.75}\sigma^{1.5}} \sqrt{\sigma} \tag{90}$$

That is, instead of a constant slope in the sorption plots at small t equation (89) and (90) have slopes dependent on t and which approaches zero as t approaches zero.
The sorption results reported in this thesis follow the Fickian $\sqrt{t}$ behavior nicely at the early stages of in-diffusion. Fickian behavior is attributed to a rate of diffusion which is much less than the polymer segment mobility [2]. Generally in the early stages of in-diffusion we have [2]:

$$\frac{M_t}{M_\infty} = kt^n \tag{91}$$

where k and n are constants. Different cases of n have been observed. n = ½ is Case I, Fickian diffusion. n = 1 is Case II diffusion. ½ < n < 1 is non-Fickian or anomalous diffusion. Case II diffusion is attributed to fast diffusion compared to other relaxation processes. Non-Fickian diffusion speed is in-between Case I and Case II i.e. the penetrant mobility and polymer segment relaxation is comparable.
In these experiments sorption was performed simply by dipping in DI-water. It should be possible to get the same results by exposing the slabs to a relative humidity (RH) of 100 % since:

$$RH = \frac{p_{H_2O}}{p^*_{H_2O}} 100\% = a^{Vapor}_{H_2O} 100\% \tag{92}$$

where p_{H_2O} is the partial pressure of water in the gas mixture, $p^*_{H_2O}$ is the saturation vapor pressure of water at the temperature of the gas mixture, and $a^{Vapor}_{H_2O}$ is the water vapor activity. At equilibrium we have:

$$\mu^{Liquid}_{H_2O} = \mu^{Vapor}_{H_2O} = \mu^{Polymer}_{H_2O} \tag{93}$$

where $\mu_{H_2O}^{Liquid}$, $\mu_{H_2O}^{Vapor}$, $\mu_{H_2O}^{Polymer}$ denotes the chemical potentials of water in the three phases liquid water, water vapor and water dissolved in the polymer. A 100 % RH means that $a_{H_2O}^{Vapor} = 1$. Then equation (93) states that:

$$a_{H_2O}^{Liquid} = a_{H_2O}^{Vapor} = a_{H_2O}^{Polymer} = 1 \tag{94}$$

which means that exposing the slab to 100 % RH is equal to dipping. The advantage of this exposure is that careful wiping off excess drops of water before weighing the slabs is not necessary. This procedure was also attempted in these experiments but without success due to bad control of the humidity and temperature.
At other p_{H_2O} than $p_{H_2O}^{*}$ the equilibrium amount of water uptake M_{eq} at infinite time is different from M_{∞}. Curves describing the equilibrium water uptake as a function of p_{H_2O} are called sorption isotherms [2, 3]. The power function dependency of M_t / M_{eq} on humidity / activity as reported in chapter 1.4.1.3.2, [Paper 18] and in [9] can be explained by the Flory-Huggins polymer solution theory which applies well to hydrophobic polymers [2] which are used in microsystems. Here we have [10, 11]:

$$\begin{aligned} &\ln a_{H_2O}^{Vapor} = \ln x_{H_2O} + x_{Polymer} + \chi_{WP} x_{Polymer}^2 \\ &= \ln x_{H_2O} + 1 - x_{H_2O} + \chi_{WP}\left(1 - x_{H_2O}\right)^2 \end{aligned} \tag{95}$$

$$\Updownarrow$$

$$a_{H_2O}^{Vapor} = x_{H_2O} e^{1 - x_{H_2O} + \chi_{WP}\left(1 - x_{H_2O}\right)^2} \tag{96}$$

where $x_{H_2O}, x_{Polymer}$ are the volume fractions of water and polymer respectively and χ_{WP} is the water-polymer interaction parameter:

$$\chi_{WP} = \frac{\Delta H_{mix}}{NRT x_{H_2O} x_{Polymer}} \tag{97}$$

where ΔH_{mix} is the polymer-water mixing enthalpy, N is the total number (moles) of lattice sites in the model, R is the universal gas constant, T is the absolute temperature.
That is, x_{H_2O} depends on $a_{H_2O}^{Vapor}$ and is implicitly determined by equation (96). In fig. 7 a power function is fitted to equation (96) for $\chi_{WP} = 2.5$ corresponding to positive (hydrophobic) ΔH_{mix}. A good agreement with power function behavior is found.

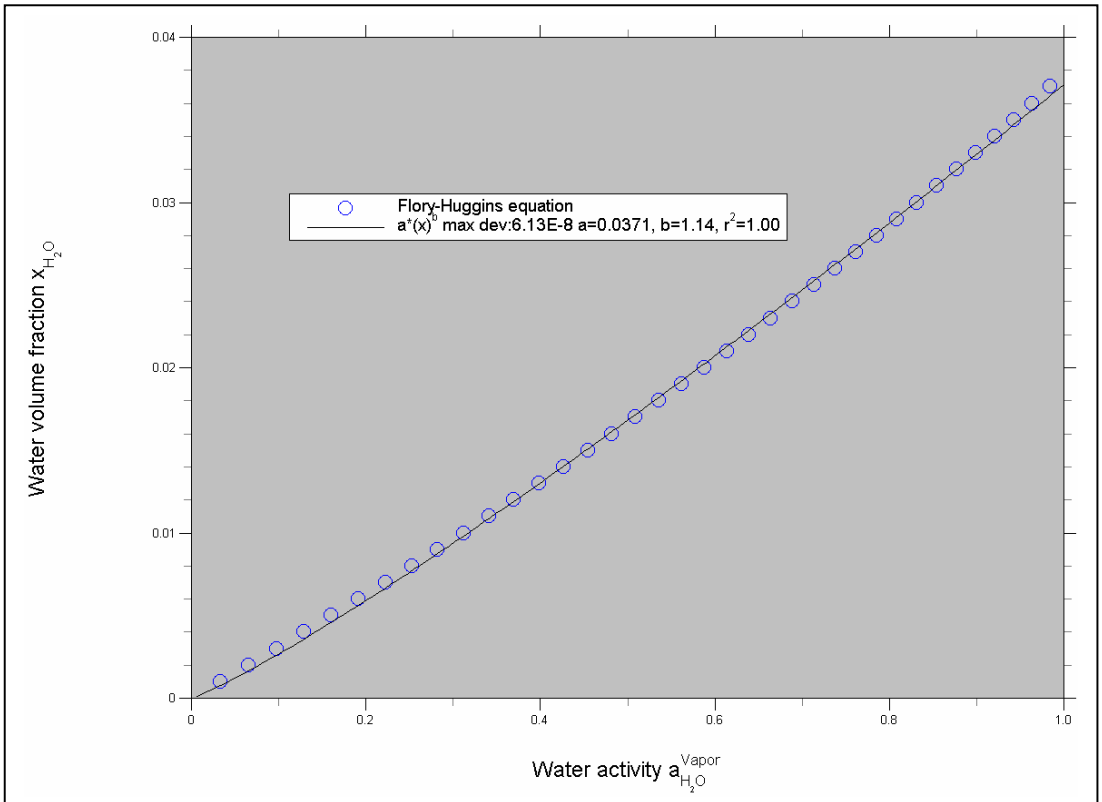

Fig. 7: Fit of power function to data from the Flory-Huggins equation.

3.1.1.4 Bond pad corrosion in cylindrical diffusion

In chapters 1.4.1.3.2, 2.2.1, in [Papers 10, 15, 18], and in [Posters 5, 6] less than 10^{-4} mm^3 water ingress has been mentioned as critical for microsystem reliability. This is because even less than that has been reported critical for failure due to bond pad corrosion. Below this is supported by theoretical considerations on cylindrical diffusion from the inside of round sensing area access holes.

The dimensions of a typical Al bond pad is 100 µm · 100 µm · 1 µm which means that it contains roughly $6 \cdot 10^{14}$ Al atoms. The actual Al atom corrosion amount reported critical for a microsystem [12] is $3 \cdot 10^{14}$ atoms, i.e. one half of a bond pad. Galvanic corrosion in the presence of an applied potential is widespread and can for Al e.g. take place according to [12]:

$$2Al + 6H^+ \rightarrow 2Al^{3+} + 3H_2$$

$$2Al^{3+} + 3H_2O \rightarrow 2Al(OH)_3 + 3H_2$$

That is, corrosion of one Al atom takes three H_2O molecules. This in turn means that at failure approximately 10^{15} H_2O molecules corresponding to the volume of three bond pads are consumed. 10^{-4} mm^3 (or 10^{-4} µL or 0.1 nL) H_2O molecules have the same

volume as approx. 10 bond pads i.e. this is roughly three times more than the critical amount given every H_2O molecule participate in corrosion. The acceptable amount of H_2O molecules with diffusional direction towards an aluminum bond pad has been set to this value based on the arbitrary assumption that for some reasons (electrode passed before reaction takes place due to low reaction rate etc.) only about one third of the H_2O molecules that arrive at an Al electrode protected by a polymer will also get to participate in the corrosion reaction mentioned above. Therefore it should be remembered that in the worst case where every H_2O molecule that arrive at the electrode also react according to the reaction scheme above the limit is actually around $3 \cdot 10^{-5}$ mm^3 H_2O.

In [Papers 10, 15] and [Posters 5, 6] the calculated fluxes were based on the simplifying assumption of square shape sensor access holes, i.e. the projected area at water entrance to some place of concern is constant. In that case, the steady state flux as a function of distance is also constant. Most sensor access holes are round. In that case the flux depends on 1/r where *r* is the distance to the centre, see below. Note that this can actually be used to limit the amount of water that get in contact with sensitive parts of the microsystem. Anyhow, for the small distances involved in microsystems the above square shape access hole is often a good approximation.
For radial diffusion through the wall (a polymer, e.g. adhesive) of a circular sensor access hole the steady state diffusion equation is [1]:

$$\frac{\partial C}{\partial t} = \frac{1}{r}\frac{\partial}{\partial r}\left(rD\frac{\partial C}{\partial r} \right) = 0 \tag{98}$$

$$\Updownarrow$$

$$\frac{d}{dr}\left(r\frac{dC}{dr} \right) = 0 \tag{99}$$

where *r* is the distance from the centre. This equation has the general solution:

$$C = A + B\ln r \tag{100}$$

where *A* and *B* are constants. Solutions at short time are significantly more complicated and involve Bessel functions [1, 4].

Solving equation (100) for *A* and *B* with the boundary conditions (see fig. 8):

$$C(r = a) = C_1 \tag{101}$$

$$C(r = b) = C_2 \tag{102}$$

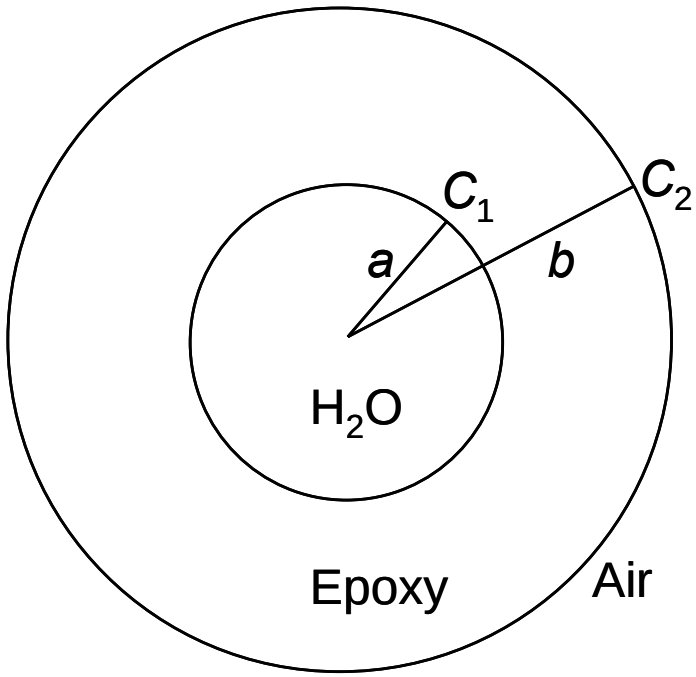

Fig. 8: Illustration of boundary conditions in radial water diffusion from the inside of a sensor access hole.

gives the solution to the diffusion equation as:

$$C = \frac{C_1 \ln\left(\frac{b}{r}\right) + C_2 \ln\left(\frac{r}{a}\right)}{\ln\frac{b}{a}} \tag{103}$$

Then the flux is:

$$J = -D\frac{dC}{dr} = -D\frac{-C_1\frac{1}{r} + C_2\frac{1}{r}}{\ln\frac{b}{a}} = D\frac{C_1 - C_2}{r\ln\frac{b}{a}} \tag{104}$$

From this we see by integration that the amount of water which at steady state diffuses through one unit length of the access hole in time t is [1]:

$$Q_t = \frac{2\pi Dt\left(C_1 - C_2\right)}{\ln\frac{b}{a}} \tag{105}$$

For C_2 = 0 and exposure of a bond pad and / or bump interconnection we have for a typical sensor-adhesive configuration like the one in fig. 9 which correspond well to the one studied for the Compression UnderFill adhesive Epotek U300-1 in [Papers 10, 15] and [Posters 5, 6]:

$$Q_t = \frac{\theta h C_1 D t}{\ln \frac{b}{a}} \tag{106}$$

where h is the bond pad or bump interconnection height. Note that Q_t expresses the amount diffusing through the area $r\theta h$ in time t. For a typical bump we have:

$\theta = 0.025\,\text{rad}\left(\sim 31\,\mu\text{m width at } r = 1.25 \cdot 10^{-3}\,\text{m}\right)$

$h = 31\,\mu\text{m}$

$C_1 = 20.2\,\text{kg m}^{-3}$

$D(19\,^\circ\text{C}) = 10^{-13}\ \text{m}^2\text{s}^{-1}$

$t = 1\,\text{yr} \approx \pi \cdot 10^7\,\text{s}$

$a = 0.5 \cdot 10^{-3}\ \text{m}$

$b = 1.5 \cdot 10^{-3}\,\text{m}$

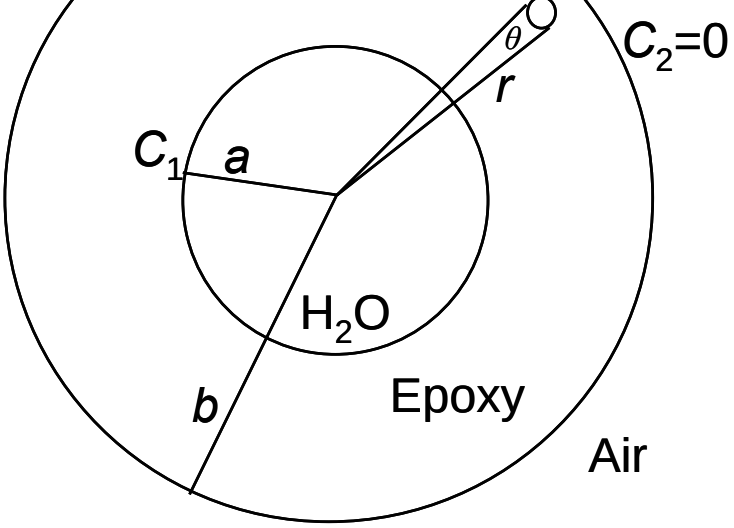

Fig. 9: Illustration of bond pad / bump interconnection water exposure from the inside of a circular access hole in epoxy.

and from this we get:

$$J = 0.046\,\mu\text{L}\,\text{mm}^{-2}\,\text{yr}^{-1}$$
$$= 0.046\frac{\mu\text{L}}{10^4 \cdot 100\,\mu\text{m}^2\,\text{yr}} = 4.6 \cdot 10^{-6}\frac{\mu\text{L}}{100\,\mu\text{m}^2\,\text{yr}} \quad (107)$$
$$\Downarrow$$
$$Q_{t=1\,\text{yr}} = 0.044\,\text{nL} \quad (108)$$

For a typical bond pad we have keeping everything else as above:

$$\theta = 0.0801\,\text{rad}\left(\sim 100\,\mu\text{m width at } r = 1.25 \cdot 10^{-3}\,\text{m}\right)$$
$$h = 1\,\mu\text{m}$$

and from this we get:

$$Q_{t=1\,\text{yr}} = 0.0046\,\text{nL} \quad (109)$$

That is, functional failure due to bond pad corrosion at RT is not likely before 6.5 years have passed. If only one third of the H_2O molecules that arrive at the bond pad participate in corrosion, which is of cause a very uncertain assumption, the bond pad could last for nearly 19.5 years. As shown in [Papers 10, 15] and [Posters 5, 6] elevated temperatures can easily increase the flux two orders of magnitude making the lifetime of the bond pad and thereby the product unacceptable low.

3.1.1.5 Heterogeneous media

Factors other than the polymer properties influence the diffusion of water in polymers. For the most reliable microsystems the interest is in factors that effectively divert or delay water in-diffusion to sensitive regions. Diversion / delay is established though the introduction of phase barriers. Complete diversion of water from sensitive areas is of cause of greatest interest.

3.1.1.5.1 Phase barriers and moisture traps

Diversion of water can in principle take place in two fundamentally different ways. One is by introducing less penetrable structures / materials / phases in the polymer which force the water to follow less critical directions in the polymer. The other is by introducing highly penetrable structures / materials / phases in which the water is transported away fast from critical areas. However, the water arrival at critical areas can also be delayed by enhancing the effective diffusion length or by adsorbance / absorbance by introduction of other materials / structures in the polymers. These kinds of delay phase barriers can e.g. consist of small particles of different kind mixed into the polymer.

Perhaps the most effective diversion method is the second fundamental way by the introduction of air channels. This is due to the large difference in water diffusivity in

polymers and in air, see table 1. If $C_2 > 0$ in the circular case from fig. 9 diffusion into the air phase at $r = b$ is commonly accounted for by an evaporation boundary condition (Newton evaporation) of the form [1, 4]:

$$\frac{dC}{dr} + h(C - C_2) = 0 \tag{110}$$

where $h = \alpha / D$, α is a constant of proportionality and C_2 is the equilibrium concentration just within the surface from which water evaporates. This boundary condition which describe the speed by which the water crosses the interface is physically more realistic than the abrupt inside-outside jumps in concentration where $dC/dx = \infty$. Using this boundary condition and constant concentration C_1 at $r = a$ leads to the following steady state solution to the diffusion equation [1]:

$$C = \frac{C_1\left(1 + hb\ln\left(\frac{b}{r}\right)\right) + hbC_2 \ln\frac{r}{a}}{1 + hb\ln\frac{r}{a}} \tag{111}$$

From this we get the following amount of water that diffuses through one unit length of the access hole in time t [1]:

$$Q_t = 2\pi Dt(C_1 - C_2)\frac{hb}{1 + hb\ln\frac{b}{a}} \tag{112}$$

Introducing less penetrable barriers (particles) on the water path toward the sensitive areas the water flux is lowered and at the same time, the time before steady state diffusion sets in is prolonged. In continuation of the subject of chapter 3.1.1.2 about material-inherent flux delay, equation (76) in chapter 3.1.1.3 can be used to give at very useful information on when steady state diffusion sets in [1]. This transition is generally important because at steady state the flux is higher than at the initial stages of in-diffusion (see below). Given the typical flat wall / barrier condition that both C_0 and C_2 are zero the equation (76) for C is:

$$C = C_1 - C_1\frac{x}{L} - \frac{2C_1}{\pi}\sum_{n=1}^{\infty}\frac{1}{n}\sin\frac{n\pi x}{L}e^{-n^2\pi^2\frac{Dt}{L^2}} \tag{113}$$

Sensitive electronics might be placed at $x = L$ where the flux is:

$$J_{x=L} = -D\left[\frac{dC}{dx}\right]_{x=L} = -D\left[-\frac{C_1}{L} - \frac{2C_1}{L}\sum_{n=1}^{\infty}\cos\frac{n\pi x}{L}e^{-n^2\pi^2\frac{Dt}{L^2}}\right]_{x=L}$$

$$= DC_1\left(\frac{1}{L} + \frac{2}{L}\sum_{n=1}^{\infty}(-1)^n e^{-n^2\pi^2\frac{Dt}{L^2}}\right) \tag{114}$$

From this it is seen that at small t the flux is small as compared to large t where the exponential terms vanish.

Integration from time 0 to some time t gives:

$$M_t = DAC_1\int_0^t\left(\frac{1}{L} + \frac{2}{L}\sum_{n=1}^{\infty}(-1)^n e^{-n^2\pi^2\frac{Dt'}{L^2}}\right)dt' = DAC_1\left[\frac{t'}{L} - \frac{2}{L}\frac{L^2}{\pi^2 D}\sum_{n=1}^{\infty}\frac{(-1)^n}{n^2}e^{-n^2\pi^2\frac{Dt'}{L^2}}\right]_0^t$$

$$= \frac{AC_1Dt}{L} + \frac{2AC_1L}{\pi^2}\sum_{n=1}^{\infty}\frac{(-1)^n}{n^2}\left(1 - e^{-n^2\pi^2\frac{Dt}{L^2}}\right) = \frac{AC_1Dt}{L} + \frac{2AC_1L}{\pi^2}\left(-\frac{\pi^2}{12}\right) - \frac{2AC_1L}{\pi^2}\sum_{n=1}^{\infty}\frac{(-1)^n}{n^2}e^{-n^2\pi^2\frac{Dt}{L^2}}$$

$$= \frac{AC_1Dt}{L} - \frac{AC_1L}{6} - \frac{2AC_1L}{\pi^2}\sum_{n=1}^{\infty}\frac{(-1)^n}{n^2}e^{-n^2\pi^2\frac{Dt}{L^2}} \tag{115}$$

For $t \to \infty$ the exponentials become very small and we get the linear dependency of M_t on t:

$$M_{t\to\infty} = AC_1\left(\frac{Dt}{L} - \frac{L}{6}\right) \tag{116}$$

This line intersects the time axis at:

$$t = \frac{L^2}{6D} \tag{117}$$

which is a good measure of when the diffusion enters steady state behavior having a certain barrier thickness L. C_1 (the solubility) can be found from the M_t axis intersection. For the epoxy in fig. 9 t = 19 days. For the same epoxy transition to steady state at 5 mins. correspond to a thickness of only 13 μm. Most adhesive barriers will be at least around 100 μm thick corresponding to transition to steady state at t = 4.6 hours. So, for point of care microsystems the non-steady state calculations are the most relevant. For other applications with barrier thicknesses of the same order which should last for years, steady state diffusion calculations apply.

The delay action of getters which were mentioned in chapters 1.4.1.1, 1.4.1.3.2 and in [Paper 18] varies a lot and may be chemical or physical in nature.
Water tends to adsorb to porous materials or just finely structured surfaces. This is because structured surfaces may confine vapor to such an extent that condensation is thermodynamically favorable even at relative humidity (RH) lower than 100 %. This phenomenon is called liquid bridging or capillary condensation and is described by the Kelvin equation [13-16] which has not been mentioned earlier in this thesis.
The Kelvin equation can be derived from the theory of thermodynamics by considering the vapor pressure change above a liquid when subjected to a pressure change ΔP [15]. At equilibrium we have for the chemical potentials μ of the two phases liquid (L) and vapor (V):

$$d\mu_L = d\mu_V \tag{118}$$

From the fundamental thermodynamic potentials we have for a closed system:

$$\begin{aligned} G &= H - TS \\ &= U + pV - TS \\ &\Updownarrow \\ dG &= dU + PdV + VdP - TdS - SdT \\ &= TdS - PdV + PdV + VdP - TdS - SdT \\ &= VdP - SdT \end{aligned} \tag{119, 120}$$

At constant temperature T we thus have in molar quantities:

$$d\mu = VdP \tag{121}$$

Using this in equation (118) we get for a pressure change ΔP assuming ideal gas behavior of the vapor:

$$V_L dP_L = \frac{RT}{P_V} dP_V \tag{122}$$

$$\Updownarrow$$

$$RT\int_{p^*}^{p} \frac{1}{p_V} dp_V = V_L \int_{p^*}^{p+\Delta P} dP_L \tag{123}$$

$$\Updownarrow$$

$$\frac{RT}{V_L} \ln \frac{p}{p^*} = p - p^* + \Delta P \approx \Delta P \tag{124}$$

where R is the universal gas constant, p^* is the original vapor pressure without applied pressure, p is the new vapor pressure as a consequence of the applied pressure ΔP. Naturally the pressure inside the liquid is the sum of the applied pressure ΔP and the new

vapor pressure p. As expressed by equation (124) the resulting vapor pressure change is so small that it can be ignored in comparison to ΔP. In case ΔP is the Laplace pressure which originates from the liquid surface tension and curvature [17, 18] we have the Kelvin equation:

$$\Delta P = p_L - p_V = \gamma_{LV} H = \gamma_{LV}\left(\frac{1}{R_1}+\frac{1}{R_2}\right) = \frac{RT}{V_L}\ln\frac{p}{p^*} \tag{125}$$

$$\Updownarrow$$

$$\frac{p}{p^*} = e^{\frac{V_L \gamma_{LV} H}{RT}} = \frac{RH}{100\%} = a_V \tag{126}$$

where p_L is the pressure inside the liquid, p_V is the vapor pressure ($p \approx p^*$) above the liquid, γ_{LV} is the liquid-vapor surface tension, H is the liquid surface mean curvature, R_1 and R_2 are two principal (perpendicular) radii of curvature for the liquid surface, p^* is the vapor pressure above the flat liquid surface, a_V is the activity in the vapor phase. Note, that the radius of curvature is negative for a concave surface and positive for a convex. That is, the vapor pressure above a concave meniscus is less than above a flat $p < p^*$ or convex. Now, the water capture mechanism is that any narrow slit, concave edge etc. will fill up spontaneously to the limit where the surrounding pressure $p_s = p$ because the vapor in the surroundings will seek to lower pressures. The amount captured will of cause also be limited by the extension of the slit, edge etc. and the wetting angle on the surfaces. Edges can easily be integrated in microsystem packaging structures by e.g. introducing a large number of small cavities. Actually such cavities can function in 3 different ways regarding avoidance of water in certain areas: 1) water capillary condensation capture at nm -µm scale at the bottom edges and at µm - mm scale across the cavities, 2) capture of small water puddles condensed elsewhere. Due to gravity the puddles / drops may move from the condensation site when large enough and get captured by the cavities because here surface free energy can be saved [Paper 2, 4]. Clearly for the water to be held effectively in the cavities a wetting angle $\theta < 90°$ is important, 3) water diversion if the bottom wall of the cavities is made very thin so that the captured water can diffuse away through that keeping in mind equations (30) and (117). For liquid bridging in a narrow slit between two identical parallel walls only the one radius of curvature contributes significantly to *H*. It is easily seen that it is:

$$|R| = r = \frac{d_S}{2\cos\theta} \tag{127}$$

where d_S is the distance across the liquid meniscus normal to the walls and θ is the liquid wetting angle on the surfaces. The condition for liquid bridging to occur is that $\mu_L < \mu_V$, which for a concave liquid surface leads to the liquid bridging condition [19]:

$$d_S < \frac{2V_L\gamma_{LV}\cos\theta}{RT\ln\frac{p^*}{p}} = \frac{2V_L(\gamma_{SV}-\gamma_{SL})}{RT\ln\frac{p^*}{p}} \tag{128}$$

where Young's relation $\gamma_{SV} = \gamma_{SL} + \gamma_{LV}\cos\theta$ was used and γ_{SV} and γ_{SL} are the solid-vapor and solid-liquid surface tensions, see chapter 3.2.2. Clearly, this requires $\gamma_{SV} - \gamma_{SL} > 0$ which is to say that $\theta < 90°$.
The geometric situation at an edge is not as straight forward as for the slit, see fig. 10.

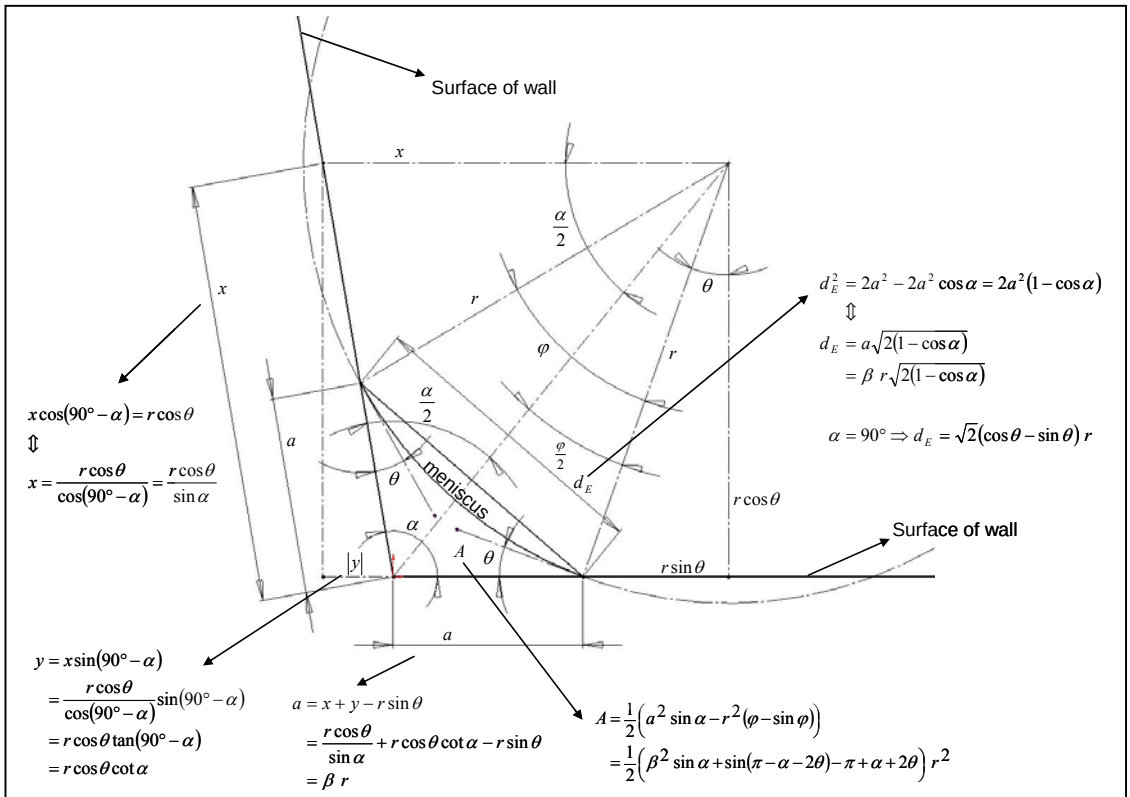

Fig. 10: Cross sectional view of the geometry of liquid condensed at a concave edge. The edge is formed by two walls which meet at an angle α. Note that from the geometry of the wetted triangle at flat meniscus we have the bridging condition $2\theta + \alpha < 180° \Leftrightarrow \theta < 90° - \frac{\alpha}{2}$. This corresponds to $\beta > 0 \Leftrightarrow \theta < \tan^{-1}\left(\cot\alpha + \frac{1}{\sin\alpha}\right)$.

The corresponding condition at an edge on the distance d_E across the meniscus is found to be:

$$d_E < \frac{V_L\gamma_{LV}\beta\sqrt{2(1-\cos\theta)}}{RT\ln\frac{p^*}{p}} \tag{129}$$

where β is a geometric factor defined in fig. 10. At $\alpha = 90°$ this expression simplifies to:

$$d_E < \frac{V_L \gamma_{LV} \sqrt{2}(\cos\theta - \sin\theta)}{RT \ln \frac{p^*}{p}} = \frac{V_L(\gamma_{SV} - \gamma_{SL})\sqrt{2}(1 - \tan\theta)}{RT \ln \frac{p^*}{p}} \tag{130}$$

From the factor $(1 - \tan\theta)$ we see that at $\alpha = 90°$ we have the condition $\theta < 45°$ which is the same as to say $\theta < 90° - \frac{\alpha}{2}$ or that $\theta < \tan^{-1}\left(\cot\alpha + \frac{1}{\sin\alpha}\right)$, see fig. 10.

Generally, it is observed that d_S and d_E decrease as θ increase. d_E also decrease as α increase, see table 2.

α	θ	RH/% above meniscus	r	d_S	a	d_E	Water cross sectional area A at edge/mm^2
45	20	50	0.8 nm	1.50 nm	1.54 nm	1.18 nm	$6.28 \cdot 10^{-13}$
		99	54 nm	101.49 nm	104.04 nm	79.63 nm	$2.86 \cdot 10^{-9}$
		99.999	54μm	101.49 μm	104.04 μm	79.62 μm	$2.86 \cdot 10^{-3}$
		99.9999	0.54 mm	1.01 mm	1.04 mm	0.80 mm	0.29
91	20	50	0.8 nm	1.50 nm	0.47 nm	0.66 nm	$7.60 \cdot 10^{-14}$
		99	54 nm	101.49 nm	31.40 nm	44.79 nm	$3.46 \cdot 10^{-10}$
		99.999	54 μm	101.49 μm	31.40 μm	44.78 μm	$3.46 \cdot 10^{-4}$
		99.9999	0.54 mm	1.01 mm	0.31 mm	0.45 mm	$3.46 \cdot 10^{-2}$
45	40	50	0.8 nm	1.23 nm	0.97 nm	0.74 nm	$2.84 \cdot 10^{-13}$
		99	54 nm	82.73 nm	65.16 nm	49.87 nm	$1.30 \cdot 10^{-9}$
		99.999	54 μm	82.73 μm	65.16 μm	49.87 μm	$1.30 \cdot 10^{-3}$
		99.9999	0.54 mm	0.83 mm	0.65 mm	0.50 mm	0.13
91	40	50	0.8 nm	1.23 nm	0.09 nm	0.13 nm	$3.67 \cdot 10^{-15}$
		99	54 nm	82.73 nm	5.94 nm	8.47 nm	$1.67 \cdot 10^{-11}$
		99.999	54 μm	82.73 μm	5.94 μm	8.47 μm	$1.67 \cdot 10^{-5}$
		99.9999	0.54 mm	0.83 mm	59.40 μm	84.74 μm	$1.67 \cdot 10^{-3}$

Table 2: Influence of cavity wall geometry and humidity on the geometry and the amount of condensed water. The calculations are based on water for which $\frac{V\gamma_{LV}}{RT} = 0.54$ nm. The parameter *a* is important to see if menisci meet at e.g. a cavity bottom.

Note that:

$$\frac{d_E(\alpha = 90°)}{d_S} = \frac{1 - \tan\theta}{\sqrt{2}} < 1 \tag{131}$$

which means that at a certain ambient p for edges like this d_E needs to be smaller than d_S for liquid bridging to take place. This also holds for $\alpha \neq 90°$. The difference increases as α increases, as is also clear from table 2.
The amount of e.g. water which can condense under different α, θ and RH's can be calculated from the total edge length and the cross sectional area A perpendicular to an edge as determined in fig. 10. A for different α, θ and RH's are given in table 2. As can be seen from table 2, the most effective water capture structures are those with low α and θ. Largest amounts are captured at RH very close to 100 %. On the other hand, the smaller the possible difference between the meniscus RH and the surrounding RH the less pronounced / fast the vapor capture effect will be. It should also be noted that for edges at low surrounding RH's condensation might start at higher distances than d_E because of wall surface roughness on the nm or µm scale. This is because at lower RH's the sensitivity toward wall surface roughness on the nm or µm scale is high and then the geometric situation where the walls meet to form an edge may locally look like a slit between two walls with distance d_S.
So, in this way water can to a varying extent be kept away from critical areas and e.g. corrosion and stiction between micro / nano mechanical parts by capillary force action can be avoided.
Concerning stiction, in equilibrium, the external force F necessary to separate e.g. two parallel plates of area A with liquid in between must counterbalance the capillary pressure force F which is often large compared to typical mass and spring forces involved in micro / nanosystems and from equation (127) we get:

$$F = \Delta P A = \frac{\gamma_{LV}}{r} A = \frac{2 A \gamma_{LV} \cos\theta}{d_S} \tag{132}$$

Thus, humidity conditions must influence tribological properties [14, 16].
The presence of water most often results in anodic corrosion. If water can not be avoided cathodes can be protected by sacrificial anode protection or by impressed current cathodic protection (ICCP). Anodic protection is a less common electrical protection using impressed current by which a protective passivation layer is grown on the anode [20].

3.1.1.5.2 Parylene as a water barrier

Parylene C is a very good barrier toward water ingress as the measurements in [Papers 10, 15], [Posters 5, 6] showed. 10 µm Parylene C on top of Macromelt lower the in-diffusion coefficient from $5 \cdot 10^{-11}$ m^2s^{-1} to $5 \cdot 10^{-14}$ m^2s^{-1} i.e. three orders of magnitude. Further by applying 10 µm to e.g. a 0.5 thick Macromelt barrier the corresponding time lag before steady state diffusion sets in is increased approximately from 14 mins. to 9.6 days.
It is furthermore very well suited for microsystem protection because it can be applied in thin completely conformal layers close to room temperature.
From the determined diffusion coefficients for Macromelt and Macromelt coated with Parylene C the diffusion constant for water in Parylene C can be estimated from the

steady state behavior if it is assumed that the water solubility coefficient at the interface between the two materials is equal to 1, see fig. 11. In that case the total concentration

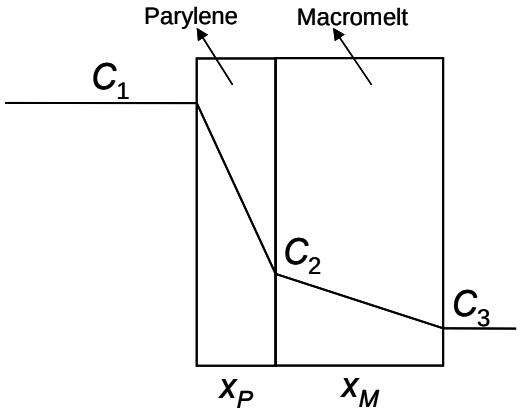

Fig. 11: Illustration of water transport through Macromelt with a coating of Parylene C.

drop across the two layers is equal to the sum of the concentration drops across each layer. Further, the flux through the combined layers is equal to the flux through each layer. That is:

$$C_3 - C_1 = (C_2 - C_1) + (C_3 - C_2) \tag{133}$$

$$\Updownarrow$$

$$-J_{MP}\frac{x_P + x_M}{D_{MP}} = -J_P\frac{x_P}{D_P} - J_M\frac{x_M}{D_M} \tag{134}$$

$$\Updownarrow$$

$$\frac{x_P + x_M}{D_{MP}} = \frac{x_P}{D_P} + \frac{x_M}{D_M} \tag{135}$$

$$\Updownarrow$$

$$D_P = \frac{x_P}{\frac{x_P + x_M}{D_{MP}} - \frac{x_M}{D_M}} \tag{136}$$

where $J_{MP} = J_P = J_M$ are the flux through the combined Macromelt and Parylene layers, the flux through Parylene, and the flux through the Macromelt respectively, x_P, x_M are the thicknesses of the Parylene and Macromelt materials in the flow direction, D_{MP}, D_P, D_M are the effective diffusion constant for the combined Macromelt and Parylene layers, and the diffusion constants for Parylene and Macromelt separately. Equation (136) can of

cause be extended to any number of materials and thicknesses. Here with 0.5 mm Macromelt and 10 µm Parylene on top we have:

$$D_P = \frac{0.01\,\text{mm}}{\frac{0.51\,\text{mm}}{D_{MP}} - \frac{0.5\,\text{mm}}{D_M}} \approx \frac{0.01\,\text{mm}}{0.51\,\text{mm}} D_{MP}$$

$$\approx 10^{-15}\ \text{m}^2\text{s}^{-1} \tag{137}$$

This water diffusivity is the lowest ever encountered for polymers by the author.

Generally the full solutions to the diffusion equation, like equation (79) for the slab given above, are too involved when it comes to laminates. Instead time-lag formulas involving individual layer time-lags are used [21].

3.1.1.6 Leak rate measurements

Leak rates are measured in a number different ways as described in [22]. Often packages constitute housings or enclosures for the electronics. In that situation moisture build-up will follow the equation:

$$C_i = C_a\left(1 - e^{-\frac{AP}{VL}t}\right) \tag{138}$$

where C_i is the internal housing water concentration which is initially zero, C_a is the ambient water concentration, A is the area of a housing wall of thickness L through which the water penetrates, P is the polymer permeability, V is the housing volume [23].
The water leakage through the chip mount adhesives studied in [Paper 1] and further described in chapter 2.2.1 was measured with a setup principally as shown in fig. 12 below.

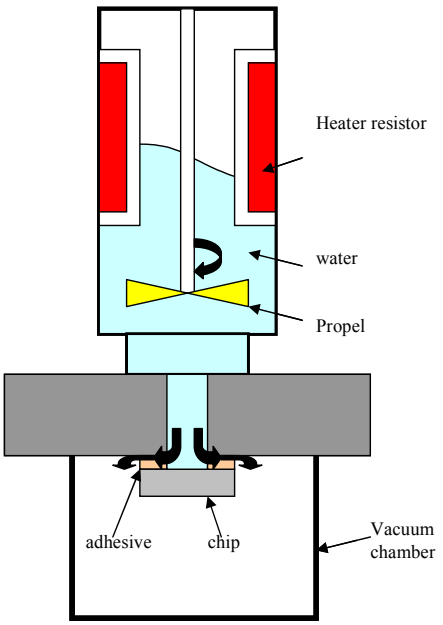

Fig. 12: Schematic illustration of Residual Gas Analysis (RGA) equipment for measurement of water leakage through adhesively bonded chips. RGA was performed with a mass spectrometer connected to the vacuum chamber.

The measuring situation illustrated in fig. 12 corresponds to a real situation where there is 1 bar inside / outside pressure difference on the adhesive. In the real situation water could pass along conductors on its way out or condense on Al bond pads or interconnection wires as illustrated in fig. 8 in chapter 1.5.3 and in [Paper 1].
A detailed drawing of the chip mounting is shown in fig. 13 and the whole setup is shown in fig. 14. To make realistic measurements it was made possible to heat and stir the water. Water was detected with a mass-spectrometer connected to the vacuum chamber, fig. 12.

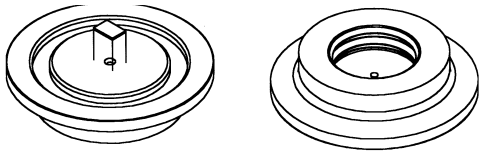

Fig. 13: Sketch of how the chips were mounted on the inside of vacuum flanges (left). The stirrer with heated water was mounted on the other side (right).

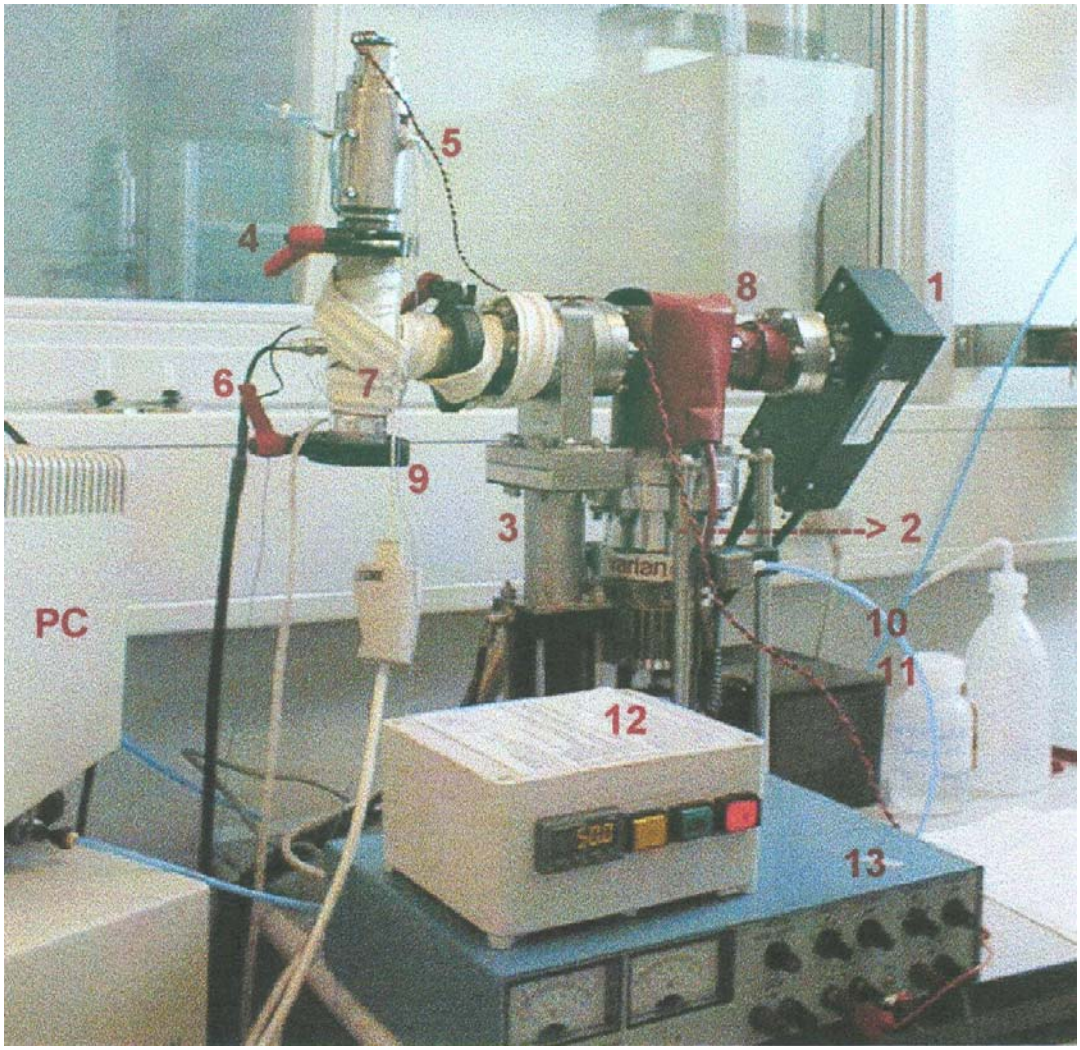

Fig. 14: Equipment for measurement of water leakage through adhesively bonded chips. 1: Mass spectrometer, 2: Turbomolecular pump, 3: Pneumatic safety valve (mass spectrometer W-filament protection), 4: Quick clamp for fixing vacuum flanges with glued chips, 5: Stirrer with temperature control, 6: Wires for cold cathode pressure sonde, 7: Heating belt to enhance evacuation on T-cross, 8: Heating on top of turbomolecular pump, 9: T-cross flange opening to remove things that have accidentally been dropped into the vacuum chamber during sample mounting, 10: N_2 purge, 11: Temperature control for the heating belt (8), 12: Temperature control for stirrer (5), 13: Current supply for control of stirring speed.

To enhance detection sensitivity D_2O instead of ordinary H_2O was used. The volume leak rate Q_{LX} of some gas X (here typically D_2O) is defined [24]:

$$Q_{LX} = S_X P_X \tag{139}$$

where S_X is the pumping speed for the gas X (here it was taken to be 45 Ls^{-1}) and P_X is the partial pressure of the gas X at equilibrium. From the ideal gas law:

$$n_{LX} = \frac{PV}{RT} = \frac{Q_{LX}}{RT} \tag{140}$$

we can then get an expression for the mass leak rate m_{LX} (flux through unit area) of gas X in g yr^{-1}:

$$m_{LX}\left[\frac{g}{year}\right] = \frac{Q_{LX} M_X \pi 10^7 s}{83\, mbar\, L\, mol^{-1}\, K^{-1}\, T} = 3.79 \cdot 10^5 \frac{Q_{LX} M_X mol\, K}{mbar\, L\, T}\left[\frac{g}{year}\right] \tag{141}$$

where M_X is the molar mass of the gas X. Note, that the equipment was not calibrated using a leak rate standard and hence the measured leak rates are at best only used for relative comparison. More detailed leak rate calculations based on RGA can be found in [22].
Assuming that nothing but the water diffusivity change when the temperature is changed it was e.g. possible to determine the steady state activation energies for water diffusion in the silicone DC Q3-661 and in the epoxy Epotek H77 to be 0.4 eV and 0.8 eV respectively from the Arrhenius plots in fig. 11, [Paper 1] using the equation:

$$D(T) = D_0 e^{-\frac{E_A}{k}\left(\frac{1}{T} - \frac{1}{T_0}\right)} \tag{142}$$

in the expression for flux (Ficks first law) where $D(T)$ is the diffusivity at the absolute temperature T, D_0 is a known diffusivity at the absolute temperature T_0, E_A is the water diffusion activation energy, k is Boltzmanns constant. Inserting equation (142) in the expression for the flux (Ficks first law) gives:

$$\begin{aligned} \ln m_{LX} &= \ln(D(T)) + \ln\left(-\frac{dC}{dx}\right) \\ &= -\frac{E_A}{kT} + \ln D_0 + \frac{E_A}{kT_0} + \ln\left(-\frac{dC}{dx}\right) \end{aligned} \tag{143}$$

From this it is seen that in plotting $\ln m_{LX}$ as a function of $1/T$ (Arrhenius plot) at steady state gives a line with slope $\alpha = -E_A / k$, i.e. no matter the constants D_0 and dC/dx the activation energy for water diffusion is:

$$E_A = -\alpha k \tag{144}$$

The activation energy 0.8 eV for water diffusion in Epotek H 77 is quite high compared with other polymers [25]. Part of the explanation is probably that this adhesive is highly filled with Al_2O_3 particles the main purpose of which is to lower the CTE. However, some fluoro polymers exhibit significantly higher activation energies (2 eV) for water diffusion [25]. It should also be mentioned that in these measurements diffusion in the bulk and along the interfaces were not separated. It was planned but never carried out to do that by measurements on adhesive joints with different thicknesses which keep the interface areas constant while more or less adhesive bulk material is exposed. By linear extrapolation of the leak dependency on adhesive thickness to zero thickness it should be possible to find the diffusivity along the interfaces which might be significantly different from that in the bulk adhesive.

3.1.2 Adhesive stress coupling, T_g, DSC and DOE

Stress coupling to sensing areas in the packaging of microsystem sensors is often a problem because it affects offset and sensitivity of measurements, see chapters 1.3.2, 1.4.1.1, 1.4.1.2, 1.5.3, 2.2.1, [Papers 1, 12, 18]. Sensor offset change is most often a direct indication of stress coupling. If the offset remains constant it is less a problem because this can easily be accounted for by calibration. However, if it is time dependent it is a serious problem since this can not as easily be accounted for electronically. A very good example of this is seen in [Paper 1] figs. 12 and 13. Here adhesives for a silicon micromechanical pressure sensor mounting have been studied.
Thermal stresses build up in the Epotek H77 sensor chip adhesive bonding on lowering the temperature from the cure temperature of 150 °C. Later it is clearly observed that as temperature change so does the sensor offset and sensitivity. At temperatures above 70 °C – 80 °C the offset and sensitivity changes are largely reduced, fig. 13 in [Paper 1]. This corresponds well with the change in bend direction of silicon test chips glued with Epotek H77 on Al_2O_3 substrates, fig. 12 in [Paper 1], when heated above the same temperatures. The change in bend direction is attributed to a passage of the adhesive glass transition temperature T_g (absolute), whereupon the adhesive softens. That the adhesive softens at this temperature can be seen from the thermodynamic expression for T_g [11]:

$$T_g = \left[\frac{\Delta\kappa \Delta c_P}{(\Delta\alpha)^2} \right]_{T=T_g} \tag{145}$$

where κ is the compressibility, c_p is the specific heat capacity at constant pressure and α the CTE. The Δ's denotes the change when heating from temperatures below T_g to temperatures above T_g. The thermodynamic quantities can be determined from [11, 26, 27]:

$$\frac{1}{\kappa} = B = -V_0\left[\frac{\partial P}{\partial V}\right]_T = -V_0\left[\frac{\partial\left[-\frac{\partial E}{\partial V}\right]_T}{\partial V}\right]_T = V_0\left[\frac{\partial^2 E}{\partial V^2}\right]_T$$

$$= \frac{\sigma}{\frac{\Delta V}{V_0}} = \frac{\sigma}{\varepsilon_{xx}+\varepsilon_{yy}+\varepsilon_{zz}} = \frac{E}{3(1-2\nu)} \tag{146}$$

$$\alpha = \frac{1}{V_0}\left[\frac{\partial V}{\partial T}\right]_P \tag{147}$$

$$c_P = T\left[\frac{\partial S}{\partial T}\right]_P \tag{148}$$

where B is named: bulk modulus, bulk modulus of elasticity, incompressibility, compression modulus, hydrostatic modulus, modulus of compression, or modulus of volume elasticity [28, 29]. V is the adhesive volume, V_0 is the original volume before compression, T is the absolute temperature, E is Young's modulus or just the elastic modulus (linear), $\sigma = \sigma_{xx} = \sigma_{yy} = \sigma_{zz} = -P$ is the applied uniform normal stress which equals the pressure in magnitude, $\varepsilon_{xx}, \varepsilon_{yy}, \varepsilon_{zz}$ are the normal strains, ν is Poison's ratio, S is entropy.

The ratio of the change in pressure to the fractional volume compression is called the bulk modulus of the material. This can also be expressed as the ratio of hydrostatic pressure to the relative volume change, equation (146). The reciprocal of the bulk modulus is called the compressibility of the substance.
From equation (146) T_g is clearly a transition, when heating, to a state with higher compressibility i.e. a positive $\Delta\kappa$. From the same equation this corresponds to a transition to lower E, which means a softer material. Above T_g the material gets more rubbery like. In turn this means that usually ν increase at the transition which to some small extent compensates the lowering of E in equation (146). As the material softens the stress level is lowered and less stress is coupled to sensitive areas. However increasing the temperature further might rapidly introduce stresses again since at T_g α is also changing rapidly. For Epotek H77 the change is from 33 ppm below T_g to 130 ppm above T_g i.e. a factor of 4. So, above T_g where E is low, increasing temperature may nevertheless introduce high stress because of large differences in CTE between adhesive and surroundings.
Due to these mechanical changes at T_g it is generally recommended to choose adhesives with T_g outside the application temperature interval.
From equation (145) it is also worthwhile noting that adhesives with low T_g are characterized by small changes in κ, c_p and / or large change in α at T_g. This will

typically be soft adhesives like e.g. silicones. Adhesives with high T_g are characterized by large changes in κ, c_p and / or small change in α. This will typically be hard adhesive like e.g. epoxy.
If therefore silicone is chosen it will typically be best if T_g is below the application temperature interval. Though, in this case it is not critical that T_g is below the application temperature interval because the adhesive is soft and is not changing much regarding this property on passage of T_g. If an epoxy is chosen it may be important that T_g is high enough that it is never passed in the application. Otherwise it might soften significantly, loose strength and / or bonding and significant stress coupling changes may be observed. If the adhesive is not getting too soft on heating above T_g, it is sometimes observed that the passage result in higher bond strength. This is due to the fact that thermal stress disappears completely or partly when the adhesive soften and / or the temperature approaches the cure temperature.
In-diffusion of water lowers T_g according to equation (149) [30]:

$$\frac{1}{T_{g,polymer+water}} = \frac{w(\mathrm{p})}{T_g(\mathrm{p})} + \frac{w(\mathrm{w})}{T_g(\mathrm{w})} \tag{149}$$

where $T_{g,polymer+water}$ is the glass transition temperature of the polymer / water composite, $w(\mathrm{p})$ is the weight fraction of polymer, $w(\mathrm{w})$ is the weight fraction of water in the polymer, $T_g(\mathrm{p})$ is the glass transition temperature of the dry polymer, and $T_g(\mathrm{w})$ is the glass transition temperature of water (-134 °C - -138 °C). The lowering can be as high as 20 °C - 30 °C [30]. So, when water in-diffusion is likely, which is most often the case due to air humidity, it is advisable to choose adhesives with T_g at least 30 °C above the highest application temperature.

Stress coupling may also be affected chemically in presence of water by hydrolysis of adhesives. The rate k of hydrolysis is described by a modified Arrhenius equation (150) [30]:

$$k = Ae^{\frac{-(E_H - \nu\sigma)}{RT}} \tag{150}$$

where A and ν are constants, E_H is the activation energy for hydrolysis, σ is the stress (tensile), R is the universal gas constant and T is the absolute temperature. From equation (150) it is clear that with stress present, the activation energy for hydrolysis is lowered and therefore the reaction rate accelerated. In turn, during this hydrolysis the adhesive intrinsic strength and bond strength is lowered and therefore also the stresses.

For heat curing adhesive which are still most widespread in electronics stress coupling can also be lowered by minimizing the thermal or CTE adhesive-substrate mismatch by curing at lower temperatures than that prescribed in the datasheet. It is then of paramount importance for reliable bond performance to achieve full curing by curing for a longer time. How long time is necessary depend the adhesive reaction kinetics which is analyzed

by DSC. For isothermal conditions the time t necessary to reach a reaction degree α can be determined from the kinetic parameters Z, E_A, n found in the DSC kinetic analysis by using equations (151) and (152) [31]:

$$t = \frac{1-(1-\alpha)^{(1-n)}}{Z(1-n)e^{\frac{-E_A}{RT}}} \text{ for } n = 1 \tag{151}$$

$$= \frac{-\ln(1-\alpha)}{Ze^{\frac{-E_A}{RT}}} \text{ for } n \neq 1 \tag{152}$$

where Z is the Arrhenius reaction rate pre-exponential constant, E_A is the reaction activation energy, n is the reaction order, R is the gas constant and T is the absolute temperature.
If the adhesive cure conditions are adiabatic the needed time can be determined from the kinetic parameters Z, E_A, n and the thermodynamic constants C_p and ΔH found in the DSC kinetic analysis by numerical integration of equation (153) [31]:

$$\int_0^{t_f} dt = -\frac{C_p}{\Delta H}\int_{T_0}^{T_f} \frac{dT}{(1-\alpha)^n Ze^{\frac{-E_A}{RT}}} = -\frac{C_p}{\Delta H}\int_{T_0}^{T_f} \frac{dT}{\left(1+\frac{C_p(T-T_0)}{\Delta H}\right)^n Ze^{\frac{-E_A}{RT}}} \tag{153}$$

where C_p is the adhesive heat capacity at constant pressure and ΔH is the adhesive reaction enthalpy.

Since so many parameters influence packaging reliability performance it is obvious to use statistical methods for optimization. The use of Taguchis approach and Design Of Experiment (DOE) approaches [32-35] have found widespread use in many industries. Taguchis approach can be considered a certain way of doing classical DOE. Both methods employ the factorial type of experiment designs and the techniques are basically based on Analysis Of VAriance (ANOVA). Using the methods it is possible to achieve the most information about how certain factors influence a goal with the least experimental effort. Exploring different factors influence on a specified goal is often studied varying each factor believed to be of importance one at the time. This takes excessive time and no information about the factors interdependence / interaction is gained. In DOE statistical techniques several parameters are varied at the same time, less experiments are needed and factor interaction information is provided.

DOE was e.g. used to optimize (lower) the adhesive and mould stress coupling to the sensing area of the absolute pressure sensor described in [Papers 10, 15], [Posters 5, 6]. Classical DOE was preferred because in this approach no pre-assumptions on factor interactions are made. A 2-level 5 factor ¼ resolution III fractional factorial design was used to identify significant sensor assembly process factors and factor interactions influencing stress coupling. To increase accuracy 2 replicates of each experiment was used which requires a total of $2^{5-2} \cdot 2 = 16$ experiments. This should be compared with making the full five factors design of all $2^5 = 32$ possible 2 level experiments with no replicates. Factors, levels and responses are shown in table 3 below.
The stress coupling was measured by monitoring the offset change upon assembly. Factor A (categorical) is the material used for mounting the sensor inside the bolt hole, factor B is the bolt hole diameter, factor C (categorical) is the surface shape of the sensor tip potting material (here Q3-6611 Dow Corning silicone) in the mould/pot (made of Teflon) before placing the sensor in it, factor D is the temperature of the mould/pot material before oven cure, factor E is the initial temperature of the oven when placing the sensor in the oven for mould/pot material cure at 150 °C for 1 hour. The software used for the analysis was Design-Expert6. The analysis showed that all chosen best model terms

Run	Factor A	Factor B	Factor C	Factor D	Factor E	Response
	Adhesive type	Hole Diameter / mm	Form filling	Adhesive pre-heat temperature / °C	Oven start Temperature / °C	Offset Change / mV
1	UV-acrylate	3,5	convex	20	150	-44
2	silicone	7,5	convex	20	20	-15,5
3	silicone	3,5	convex	70	20	-
4	silicone	7,5	convex	20	20	-36,8
5	UV-acrylate	3,5	concave	20	20	-
6	UV-acrylate	3,5	convex	20	150	-5,6
7	UV-acrylate	3,5	concave	20	20	-64,1
8	UV-acrylate	7,5	concave	70	20	-
9	UV-acrylate	7,5	convex	70	150	-100,8
10	silicone	7,5	concave	20	150	-15,8
11	silicone	3,5	concave	70	150	-14,7
12	silicone	3,5	convex	70	20	-42,4
13	silicone	7,5	concave	20	150	-28
14	silicone	3,5	concave	70	150	-
15	UV-acrylate	7,5	convex	70	150	-98,9
16	UV-acrylate	7,5	concave	70	20	-6,2

Table 3: DOE 2-level 5 factor ¼ reslotion III fractional factorial experiments generated by Design-Expert6 for optimising stress coupling in assembly of an absolute pressure sensor. Factor generator: D = AB, E = AC. Factorial effects defining contrast: I = ABD = ACE = BCDE. Due to the replicates the analysis could be carried out although some sensors were destroyed and data was missing.

(factors) are significant meaning that the probability that their response contribution is not just due to noise is higher than 95 %. The best model half normal plot is shown in fig. 15 and the Design-Expert6 annotated ANOVA analysis in blue below.

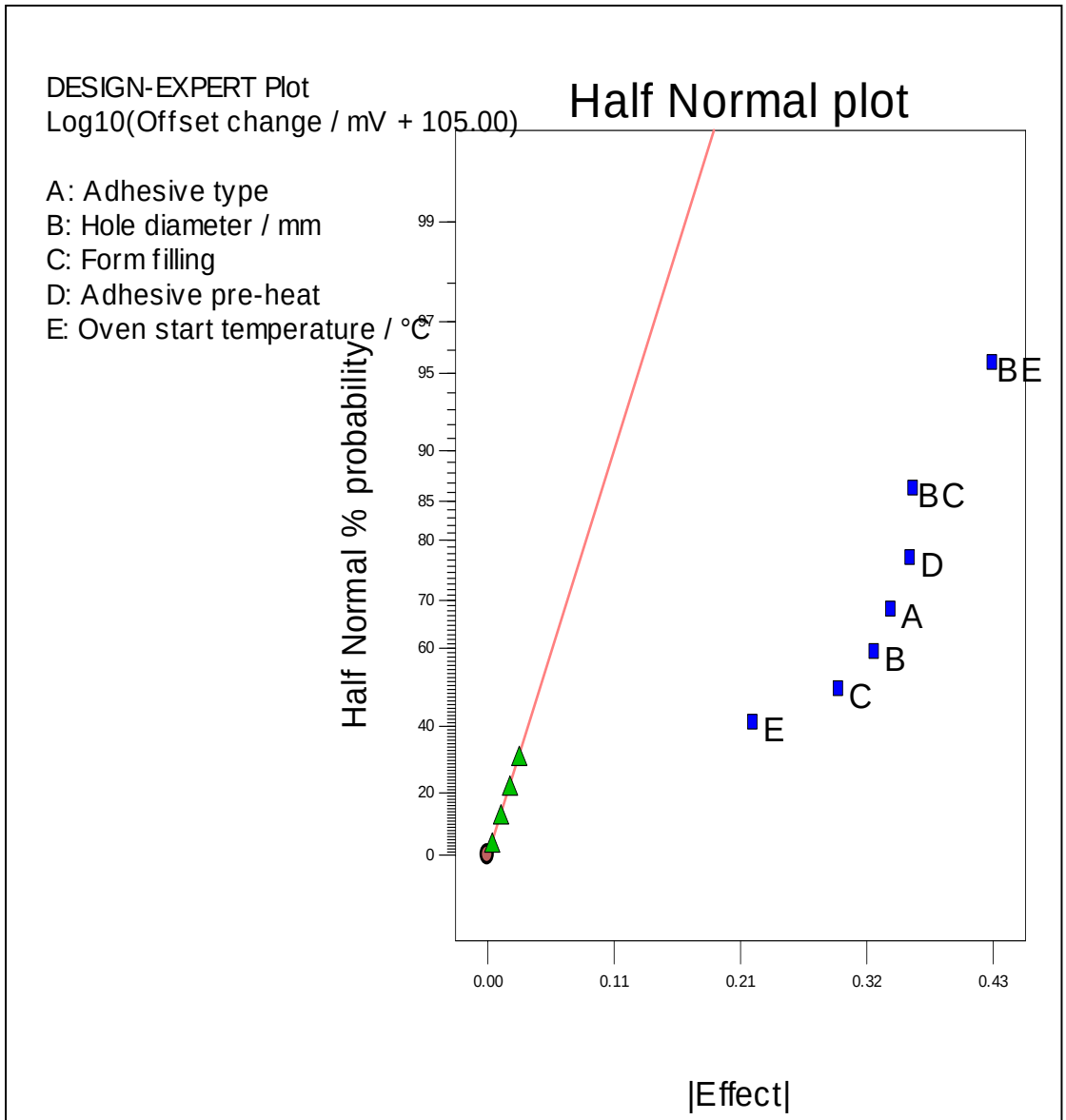

Fig. 15: Half normal plot showing the chosen model of all 1-factors included together with two 2-factor interactions BC and BE. The green triangles represent unused degrees of freedom that are leftover from replicates.

Response:Offset change / mVTransform:Base 10 logConstant: 105

ANOVA for Selected Factorial Model

Analysis of variance table [Partial sum of squares]

Source	Sum of Squares	DF	Mean Square	F Value	Prob > F	
Model	2.39	7	0.34	30.62	0.0026	significant
A	*0.31*	*1*	*0.31*	*27.69*	*0.0062*	
B	*0.093*	*1*	*0.093*	*8.29*	*0.0450*	
C	*0.24*	*1*	*0.24*	*21.35*	*0.0099*	
D	*0.12*	*1*	*0.12*	*11.13*	*0.0290*	
E	*0.11*	*1*	*0.11*	*10.19*	*0.0331*	
BC	*0.34*	*1*	*0.34*	*30.83*	*0.0051*	
BE	*0.48*	*1*	*0.48*	*43.36*	*0.0028*	
Pure Error	0.045	4	0.011			
Cor Total	2.44	11				

The Model F-value of 30.62 implies the model is significant. There is only a 0.26% chance that a "Model F-Value" this large could occur due to noise.

Values of "Prob > F" less than 0.0500 indicate model terms are significant.
In this case A, B, C, D, E, BC, BE are significant model terms.
Values greater than 0.1000 indicate the model terms are not significant.
If there are many insignificant model terms (not counting those required to support hierarchy),
model reduction may improve your model.

Std. Dev.	0.11	R-Squared	0.9817
Mean	1.68	Adj R-Squared	0.9496
C.V.	6.28	Pred R-Squared	N/A
PRESS	N/A	Adeq Precision	14.963

Case(s) with leverage of 1.0000: Pred R-Squared and PRESS statistic not defined

"Adeq Precision" measures the signal to noise ratio. A ratio greater than 4 is desirable. Your ratio of 14.963 indicates an adequate signal. This model can be used to navigate the design space.

Factor	Coefficient Estimate	DF	Standard Error	95% CI Low	95% CI High	VIF
Intercept	1.72	1	0.032	1.63	1.81	
A	-0.17	1	0.032	-0.26	-0.080	1.13
B	-0.093	1	0.032	-0.18	-3.341E-003	1.09
C	-0.15	1	0.032	-0.24	-0.060	1.09
D	-0.11	1	0.032	-0.20	-0.018	1.09
E	-0.10	1	0.032	-0.19	-0.013	1.09
BC	-0.18	1	0.032	-0.27	-0.090	1.12
BE	-0.21	1	0.032	-0.30	-0.12	1.12

Final Equation in Terms of Coded Factors:

Log_{10}(Offset change / mV + 105.00) =

+1.72	
-0.17	* A
-0.093	* B
-0.15	* C
-0.11	* D
-0.10	* E
-0.18	* B * C
-0.21	* B * E

Final Equation in Terms of Actual Factors:

Adhesive type = silicone
Form filling = concave
Log_{10}(Offset change / mV + 105.00) =

+1.36601	
+0.18246	* Hole diameter / mm
-4.31502E-003	* Adhesive pre-heat
+7.42073E-003	* Oven start temperature / °C
-1.63807E-003	* Hole diameter / mm * Oven start temperature / °C

Adhesive type = UV
Form filling = concave
Log_{10}(Offset change / mV + 105.00) =

+1.02567	
+0.18246	* Hole diameter / mm
-4.31502E-003	* Adhesive pre-heat
+7.42073E-003	* Oven start temperature / °C
-1.63807E-003	* Hole diameter / mm * Oven start temperature / °C

Adhesive type = silicone
Form filling = convex
Log_{10}(Offset change / mV + 105.00) =

+2.05479	
+2.88095E-003	* Hole diameter / mm
-4.31502E-003	* Adhesive pre-heat
+7.42073E-003	* Oven start temperature / °C
-1.63807E-003	* Hole diameter / mm * Oven start temperature / °C

Adhesive type = UV
Form filling = convex
Log_{10}(Offset change / mV + 105.00) =

+1.71445	
+2.88095E-003	* Hole diameter / mm

-4.31502E-003 * Adhesive pre-heat
+7.42073E-003 * Oven start temperature / °C
-1.63807E-003 * Hole diameter / mm * Oven start temperature / °C

Diagnostics Case Statistics

Run Order	Actual Value	Predicted Value	Residual	Leverage	Student Residual	Cook's Distance	Outlier t
11	1.96	1.96	0.000	1.000			
7	1.61	1.61	0.000	1.000			
10	1.95	1.92	0.032	0.500	0.428	0.023	0.379
13	1.89	1.92	-0.032	0.500	-0.428	0.023	-0.379
16	1.99	1.99	0.000	1.000			
12	1.80	1.80	0.000	1.000			
6	2.00	1.89	0.11	0.500	1.420	0.252	1.745
1	1.79	1.89	-0.11	0.500	-1.420	0.252	-1.745
2	1.95	1.89	0.059	0.500	0.790	0.078	0.745
4	1.83	1.89	-0.059	0.500	-0.790	0.078	-0.745
15	0.79	0.70	0.081	0.500	1.085	0.147	1.119
9	0.62	0.70	-0.081	0.500	-1.085	0.147	-1.119

Case(s) with leverage of 1.0000: Student Residuals, Cooks Distance & Outlier T undefined.

Proceed to Diagnostic Plots (the next icon in progression). Be sure to look at the:
1) Normal probability plot of the studentized residuals to check for normality of residuals.
2) Studentized residuals versus predicted values to check for constant error.
3) Outlier t versus run order to look for outliers, i.e., influential values.
4) Box-Cox plot for power transformations.

If all the model statistics and diagnostic plots are OK, finish up with the Model Graphs icon.

According to the analysis the model turns out to be quite good. This is also the case looking at the diagnostic plots which are mentioned in the end of the analysis.
However, it should be remembered that this is only a resolution III experiment (worst!), which means that at least one 1-factor is confounded / aliased with at least 1 2-factor interaction term [35]. In fact, in this model the alias structure is as shown in table 4 below:

Model terms / effects	Aliases
A	BD, CE
B	AD, CDE
C	AE, BDE
D	AB, BCE
E	AC, BCD
BC	DE, ABE, ACD
BE	CD, ABC, ADE

Table 4: Alias structure of experiment.

This means that really A = A + BD + CE and so forth. Anyhow, this aliasing makes the model less certain concerning where the offset contributions really come from. Sometimes aliased effects cancel out. This means that even when nothing comes out significantly it is not possible to infer that there are no active effects / factors. The opposite may of cause also happen. However, note that no 2-factor model terms (BC, BE) are aliased with 1-factor terms - hence these two 2-factor effects (or their aliases) are very likely to be present as also evident from the half normal plot.
The main motivation for a resolution III design should therefore be only to pre-screen for any large effects among the tested, not exactly which. Then preferably, a resolution V ½ fractional factorial study should subsequently be performed on the found highly significant factors. This is because in that study, 1 factor contributions are only aliased with 4 factor interactions which are not very likely, and 2 factor interaction contributions are only aliased with 3 factor interaction contributions which are also not very likely (except, though, sometimes in categorical designs like here [35]).

The results can be viewed in a number of different ways. However, unfortunately a resolution V ½ fractional factorial DOE was not employed in this study and the results presented here therefore only serve for illustration of what analysis is possible keeping the aliasing in mind.
To estimate the influence of each factor 1-factor plots depending on the settings of the other parameters can be made. These plots have uncertainty bars included. Given the possible combinations of categorical factors, equations for the offset changes are given in the analysis above. From this it is possible to graph two-factor interactions like in fig. 16. From the graph it is clear (as it is from the half-normal plot) that there is a pronounced interaction between the B and E factors. Concerning packaging optimization by stress coupling minimization it is important to note that the second blue contour line from the right in fig. 16 has been set to zero. This means that all combinations of hole diameters and oven start temperatures on this contour results in a zero BE interaction contribution to the offset change. A part of Design-Expert6 can do more elaborate optimization in accordance with some pre-set constraints. Below (in blue), given the indicated constraints, this has been used to find 28 combinations (solutions) of factor settings resulting in zero offset change i.e. zero stress coupling. One important advantage of having these solutions to choose between is that optimization regarding other parameters can be taken into consideration. For instance, if it is know that one adhesive performs

better than the other regarding other parameters than stress coupling (e.g. bond strength, physical / chemical durability), solutions including this adhesive should of cause be used. Unfortunately none of these combinations were subsequently tested.

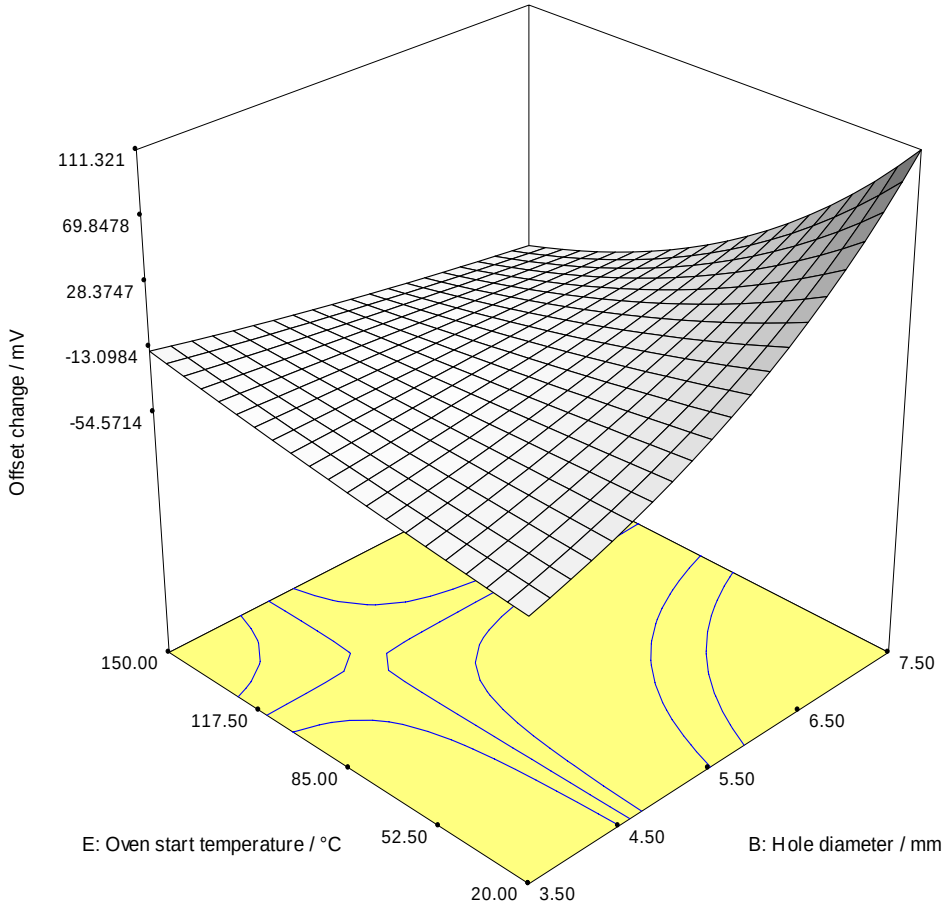

Fig. 16: Response surface for BE interaction. The other factors are here: A: silicone, C: concave filling, D: Adhesive pre-heat 70 °C.

Constraints

Name	Goal	Lower Limit	Upper Limit	Lower Weight	Upper Weight	Importance
A	is in range	silicone	UV	1	1	3
B	is in range	3.5	7.5	1	1	3
C	is in range	concave	convex	1	1	3
D	is in range	20	70	1	1	3
E	is in range	20	150	1	1	3
Offset change	is target = 4.26326E-014	-100	100	1	1	3

Solutions

Number	A	B	C	D	E	Offset change	Desirability
1	silicone	5.71	concave	37.75	115.80	-0.00087	1.000
2	silicone	4.03	concave	37.26	98.57	0.000567273	1.000
3	silicone	4.92	concave	52.04	28.30	0.000427508	1.000
4	silicone	4.40	concave	38.96	95.46	-0.000636056	1.000
5	silicone	6.29	concave	45.39	102.92	9.29658E-006	1.000
6	silicone	5.53	concave	62.12	52.65	0.000170677	1.000
7	silicone	5.11	concave	51.87	56.25	0.000140582	1.000
8	silicone	4.42	concave	37.53	56.71	0.000747305	1.000
9	silicone	5.70	concave	38.08	115.08	0.000842587	1.000
10	silicone	6.57	concave	50.83	97.05	0.000913766	1.000
11	UV	6.73	concave	20.53	40.03	-0.000567896	1.000
12	UV	6.76	concave	35.07	23.79	1.73589E-005	1.000
13	UV	6.42	concave	21.22	27.25	0.000527727	1.000
14	UV	7.13	concave	34.40	36.98	-0.00053569	1.000
15	UV	7.21	concave	41.05	32.50	-0.000534401	1.000
16	UV	7.40	concave	26.50	51.08	0.000317288	1.000
17	UV	6.37	concave	23.20	22.17	0.000379379	1.000
18	UV	7.35	concave	53.00	25.34	0.000772316	1.000
19	UV	6.70	concave	24.14	34.71	-0.000955381	1.000
20	silicone	3.61	convex	51.85	118.77	-0.000574896	1.000
21	silicone	4.25	convex	22.31	109.95	0.000845867	1.000
22	silicone	3.95	convex	27.43	76.99	-0.000205839	1.000
23	silicone	3.62	convex	45.73	102.46	0.000789951	1.000
24	silicone	3.58	convex	51.59	114.42	-0.000891448	1.000
25	silicone	4.11	convex	20.10	59.93	0.000178645	1.000
26	silicone	3.65	convex	40.05	89.32	0.000652352	1.000
27	silicone	3.70	convex	29.78	62.12	0.000261751	1.000
28	silicone	4.13	convex	31.62	138.15	0.000682405	1.000

3.2 Adhesion theories, adhesion promotion, and adhesion in moist environment

At least 6 theories of adhesion exist [30, 36-40]. These are:

- Mechanical interlocking
- Electronic theory
- Theory of boundary layers and interphases
- Adsorption (thermodynamic) theory
- Diffusion theory
- Chemical bonding theory

The theories focus on different dominating mechanisms of adhesion. So, normally to account for the total adhesion strength more than one of the theories is needed. This indicates that there are several ways of improving adhesion strength and that best results are achieved by activating as many adhesion mechanisms as possible at the same time. The two dominating adhesion theories are the Chemical bonding theory and the Adsorption theory. Adhesion by covalent chemical bonding results in the strongest bonds. The bond energies are in the range 63 kJ mol^{-1} – 710 kJ mol^{-1}. Van der Walls adsorption bond energies are in the range 6 kJ mol^{-1} – 65 kJ mol^{-1}. Another important adsorption bond type is the hydrogen bond with energies in the range 10 kJ mol^{-1} – 42 kJ mol^{-1} [39].

3.2.1 The chemical bonding theory

In the Chemical bonding theory the bond strength originates from chemical bonds either directly between adhesive and substrate or through a coupling agent (adhesion promoter) which is typically a silane. The idea of using coupling agents is that they are tailored with functional groups with high chemical bonding (covalent) affinity to both adhesive (R) and substrate (R'), see fig. 17 below. The use of such silanes as coupling agents has been described in [Papers 1, 2, 4, 6, 18]. In [Paper 1] the differences in adhesion strength observed for various substrate treatments are probably partly due to the different amounts of –OH groups introduced at the surfaces.

As has become clear from chapters 1 and 2 despite their weaknesses in humid environment adhesives find widespread use in microsystems. However, probably the only book reference on adhesives uses in electronics is [36].
In [Paper 1] it was clearly seen that adhesive bond strength decreased when the bond line was exposed to water. Below this is explained from a semi-empirical theory and at the same time it is shown that adhesives and surfaces can be chosen so that bond strength does not deteriorate.

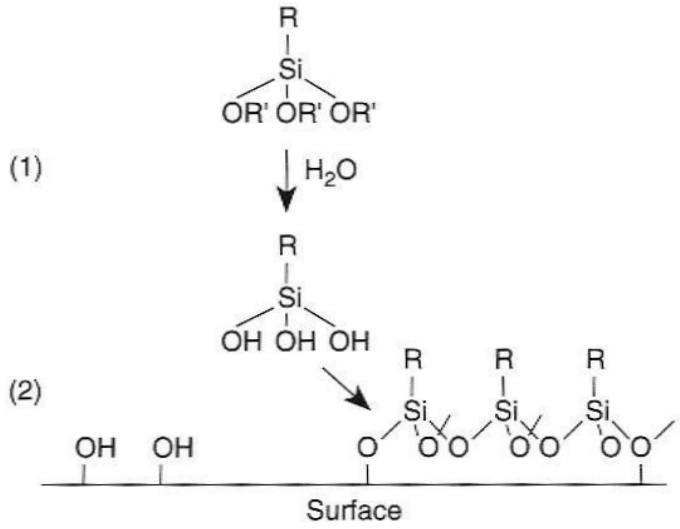

Fig. 17: Bonding mechanism of silane to a substrate with –OH groups at the surface.
Such a surface could typically be metal, glas, polymer, especially after O_2 plasma treatment. The illustrated mechanism of silane bonding to the –OH surface is: (1) hydrolysis to a trisilanol, (2) condensation copolymerization of trisilanol and surface –OH to produce a polysiloxane network covalently bonded to the surface [32]. The adhesive can then react with the R groups.

3.2.2 The adsorption theory

The adhesion theory accounting best for the effect of bond line moisture ingress is the adsorption or thermodynamic theory of adhesion. This is also the most widespread theory of adhesion. In the adsorption theory bonding is formed by molecular attraction forces at short distances. Here, the most famous equation is that of Young describing the adhesive or more generally just liquid wetting angle θ on the substrate [30, 36-38, 40]:

$$\gamma_{SV} = \gamma_{SL} + \gamma_{LV} \cos\theta \tag{154}$$

The angle θ and the solid-vapor γ_{SV}, solid-liquid γ_{SL}, and liquid-vapor γ_{LV} surface tensions are illustrated in fig. 18. At equilibrium these surface tensions are in balance according to Young's equation. Low θ means good wetting and is most often a prerequisite for good adhesion but not a necessity. In that way low θ can be regarded an indicator that good adhesion can be achieved. This is because it means that substrate and adhesive has a high affinity for each other i.e. they get in close contact.

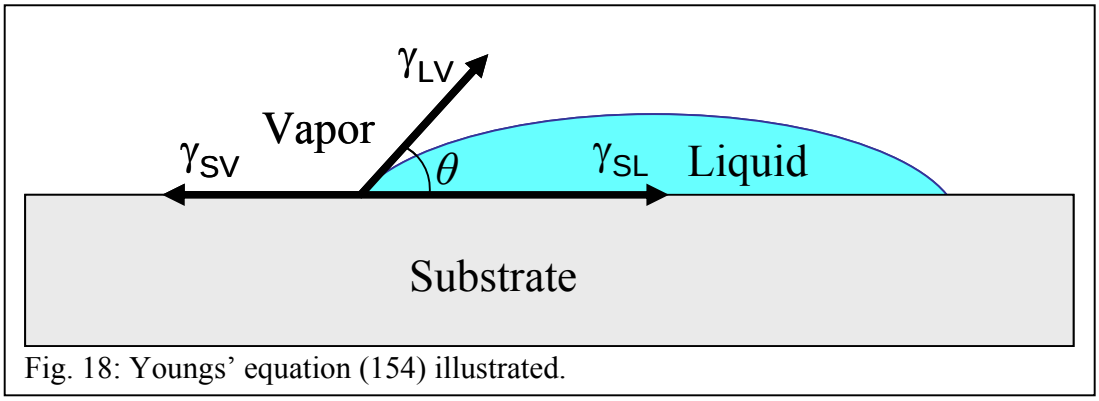

Fig. 18: Youngs' equation (154) illustrated.

The surface tension γ is normally split up into two molecular attraction components representing dispersion (d) and polar (p) forces [30, 37, 38, 40]:

$$\gamma = \gamma^d + \gamma^p \tag{155}$$

Collectively the dispersion component (London's fluctuating dipole-induced dipole interactions), the polar dipole-dipole component (Keesom's interactions), and the polar dipole-induced dipole component (Debye's interactions) of γ is called the Van der Wall's forces. Here the last term γ^p, correspond to all non-dispersion forces including Keesom and Debye interactions as well as hydrogen bonding [37].

The work of adhesion W_A in dry environment is given by the Dupré equation [30, 36-38, 40]:

$$W_A = \gamma_a + \gamma_b - \gamma_{ab} \tag{156}$$

where a is the adhesive and b the substrate. -W_A is equal to the free energy per unit area ΔG_{ab} of new interface formed [40].

3.2.2.1 Adhesion in moist environment

Likewise in humid environments the work of adhesion (A) is given by the Dupré equation as [30, 37, 38, 40]:

$$W_{A,Liq} = \gamma_{aLiq} + \gamma_{bLiq} - \gamma_{ab} \tag{157}$$

where *Liq* denotes some liquid e.g. water *W*, see fig. 19. According to Fowkes [30, 40] the surface tension γ_{SL} between a solid (S) and a liquid (L) can be determined by the semi-empirical equation [30, 40, 41]:

$$\gamma_{SL} = \gamma_{SV} + \gamma_{LV} - 2\sqrt{\gamma_S^d \gamma_L^d} - 2\sqrt{\gamma_S^p \gamma_L^p} \tag{158}$$

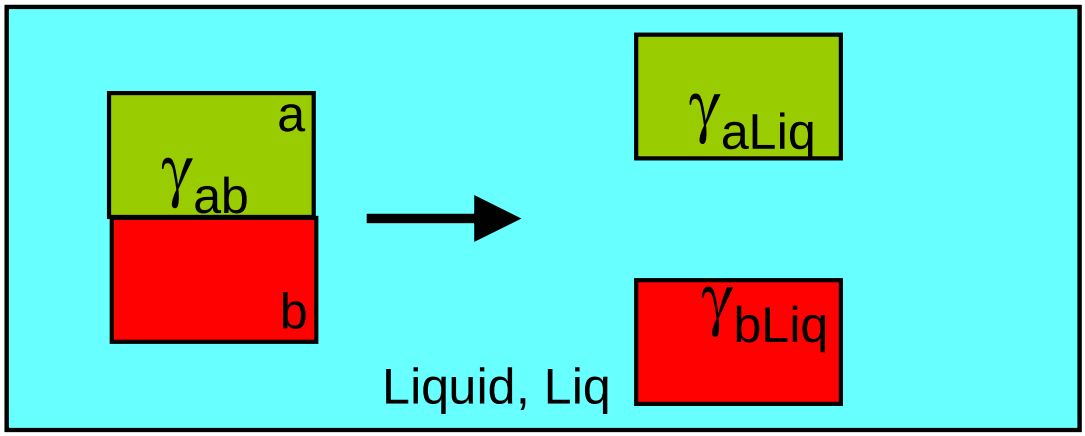

Fig. 19: Illustration of terms in equation (158).

Inserting equation (158) with $s = b$, $L = a$ leading to $\gamma_{SL} = \gamma_{ab}$, $\gamma_{LV} = \gamma_a$, $\gamma_{SV} = \gamma_b$ in equation (156) gives the work of adhesion between a and b W_A in dry environment [30, 37, 38, 40]:

$$W_A = 2\sqrt{\gamma_a^d \gamma_b^d} + 2\sqrt{\gamma_a^p \gamma_b^p} \tag{159}$$

Inserting Young's equation (154) for γ_{SV} in Fowkes' equation (158) (or in Dupre's equation (156)) we get the Young-Dupre equation (161) for the work of adhesion in dry environment [30, 36-38, 40]:

$$\gamma_{ab} = \gamma_{ab} + \gamma_a \cos\theta + \gamma_a - 2\sqrt{\gamma_a^d \gamma_b^d} - 2\sqrt{\gamma_a^p \gamma_b^p} \tag{160}$$

$$\Updownarrow$$

$$W_A = \gamma_a (1 + \cos\theta) \tag{161}$$

$$\Updownarrow$$

$$\frac{\gamma_a (1 + \cos\theta)}{2\sqrt{\gamma_a^d}} = \frac{W_A}{2\sqrt{\gamma_a^d}} = \sqrt{\gamma_b^d} + \sqrt{\gamma_b^p}\sqrt{\frac{\gamma_a^p}{\gamma_a^d}} \tag{162}$$

Equation (161) means that W_A can be determined solely from the liquid / adhesive surface tension and wetting angle with the substrate and that the maximum W_A equals $2\gamma_a$ which is the adhesive cohesion energy (note that for liquids surface tension and surface free energy are numerically the same but have different dimensions, mN/m and mJ/m^2 respectively). This is quite accurate for adhesives on polymer surfaces with non-zero contact angle where no liquid / adhesive is adsorbed on the substrate close to the contact point of the three surface tensions [40]. If the environment is not dry i.e. liquid / adhesive vapor is present and adsorbed on the substrate close to the contact point of the three phases γ_S (or γ_b) is reduced to γ_{SV} (or γ_{bV}), $\gamma_{SV} = \gamma_S - \pi$ where π is called the

spreading pressure. This can be seen by reformulating Dupre's equation (156) in accordance with the presence of vapor [40]:

$$W_A = \gamma_{LV} + \gamma_S - \gamma_{SL} = -\Delta G_{SL} \tag{163}$$

and inserting Young's' equation (154):

$$\begin{aligned} W_A &= \gamma_{LV} + \gamma_S - \gamma_{SV} + \gamma_{LV}\cos\theta \\ &= \gamma_{LV}(1+\cos\theta) + \gamma_S - \gamma_{SV} \\ &= \gamma_{LV}(1+\cos\theta) + \pi \end{aligned} \tag{164}$$

π can be high for high energy surfaces such as metals or oxides [40]. At best $(\theta = 0)$ for adhesives this means that W_A is significantly higher than the cohesive energy of the adhesive.
Equation (162) means that knowing different test liquids / adhesives i.e. γ_a^d, γ_a^p and the wetting angles θ on some substrate *b*, γ_b^d and γ_b^p can be determined from the intercept and slope respectively of the linear plot of $\gamma_a(1+\cos\theta)/2\sqrt{\gamma_a^d}$ against $\sqrt{\gamma_a^p/\gamma_a^d}$.

Inserting equation (158) in equation (157) leads to the following work of adhesion in water:

$$W_{A,W} = \gamma_{aV} + \gamma_{WV} - 2\sqrt{\gamma_a^d\gamma_W^d} - 2\sqrt{\gamma_a^p\gamma_W^p} + \gamma_{bV} + \gamma_{WV} - 2\sqrt{\gamma_b^d\gamma_W^d} - 2\sqrt{\gamma_b^p\gamma_W^p} - \gamma_{aV} - \gamma_{bV} + 2\sqrt{\gamma_a^d\gamma_b^d} + 2\sqrt{\gamma_a^p\gamma_b^p}$$

$$= 2\left[\gamma_{WV} - \sqrt{\gamma_a^d\gamma_W^d} - \sqrt{\gamma_a^p\gamma_W^p} - \sqrt{\gamma_b^d\gamma_W^d} - \sqrt{\gamma_b^p\gamma_W^p} + \sqrt{\gamma_a^d\gamma_b^d} + \sqrt{\gamma_a^p\gamma_b^p}\right]$$

$$= \gamma_{WC} + W_{ab} - W_{aW} - W_{bW} \tag{165}$$

where γ_{WC} is the water cohesion energy, W_{ab} is the work of adhesion in dry environment, W_{aW} is the work of adhesion of adhesive and water in dry environment, W_{bW} is the work of adhesion of substrate and water in dry environment. The negative terms may result in spontaneous separation of adhesive and substrate when the overall $W_{A,W}$ gets negative, which is most often the case. However, by chemically modifying adhesives and substrates surfaces to minimum work of adhesion to water, $W_{A,W}$ can get positive i.e. the adhesive bond is stable in water.
The work of adhesion in dry and wet environment is at maximum when the ratio of the dispersive and polar contributions to the adhesive surface tension is equal to the ratio of the dispersive and polar contributions to the substrate surface tension. This can be seen by differentiating W_A with respect to e.g. γ_a^d and equating to zero:

$$\frac{dW_A\left(\gamma_a^d\right)}{d\gamma_a^d}=\frac{d\left(2\sqrt{\gamma_a^d\gamma_b^d}+2\sqrt{\left(\gamma_a-\gamma_a^d\right)\gamma_b^p}\right)}{d\gamma_a^d}=\frac{\gamma_b^d}{\sqrt{\gamma_a^d\gamma_b^d}}-\sqrt{\frac{\gamma_b^p}{\gamma_a-\gamma_a^d}} \tag{166}$$

$$\frac{dW_A\left(\gamma_a^d\right)}{d\gamma_a^d}=0 \tag{167}$$

$$\Updownarrow$$

$$\frac{\left(\gamma_b^d\right)^2}{\gamma_b^d\gamma_a^d}=\frac{\gamma_b^p}{\gamma_a-\gamma_a^d} \tag{168}$$

$$\Updownarrow$$

$$\frac{\gamma_a^d}{\gamma_a^p}=\frac{\gamma_b^d}{\gamma_b^p} \tag{169}$$

Further, from this the γ_a^d resulting in maximum W_A is found to be:

$$\gamma_a^d=\frac{\gamma_b^d}{\gamma_b^p}\left(\gamma_a-\gamma_a^d\right) \tag{170}$$

$$\Updownarrow$$

$$\gamma_a^d\left(1+\frac{\gamma_b^d}{\gamma_b^p}\right)=\frac{\gamma_b^d}{\gamma_b^p}\gamma_a \tag{171}$$

$$\Updownarrow$$

$$\gamma_a^d=\frac{\frac{\gamma_b^d}{\gamma_b^p}\gamma_a}{1+\frac{\gamma_b^d}{\gamma_b^p}}=\frac{\gamma_b^d\gamma_a}{\gamma_b^d+\gamma_b^p}=\gamma_b^d\frac{\gamma_a}{\gamma_b} \tag{172}$$

Thus, it is suggested that the large difference in adhesive bond strength achieved by substrate surface treatment 1 and 2 in [Paper 1] is also due to different degree of match of substrate and adhesive γ^d, γ^p proportion i.e. highest bond strength is achieved for the best match (treatment 2). 2-propanole merely removes dirt, especially grease whereas soap both removes dirt and introduces less polar –OH groups on the oxidized titanium surface. The –OH groups are also generally easy to bond chemically. Following soap treatment with 2-propanole is a good way of removing H_2O.
With the same argumentation it is also suggested that treatment 2 before use of silane (treatment 4) enhance the match / non-covalent bond strength component of silane to substrate and thereby the overall bond strength of the adhesive to the substrate. The large effect of heat treatment is probably due to removal of H_2O residues from the condensation reaction of trisilanol with surface –OH groups, see fig. 17 above.

Also in [Paper 1], a decrease in bond strength is observed for both the silicone (Q3-6611) and the epoxy (Epotek H77) upon exposure to water. That is, in both cases $W_{A,W}$ is negative (disregarding other bond strength mechanisms e.g. covalent bonding) and the substrate surface would rather have water present than adhesive.
In both cases adhesion strength could probably have been enhanced by better substrate-adhesive proportional match of γ^d, γ^p. However, in these experiments (dry/wet) no matches of this kind were attempted to improve adhesion. Most metals have a very polar oxide surface layer. Therefore, if bonding is purely by adsorption, it is likely that relatively much higher bond strength could have been achieved by chemically introducing polar groups to the adhesives chemistry.
Covalent chemical bonding is generally preferred because it results in the strongest and most durable bonds. In case water is present chemical attack i.e. hydrolysis has to take place to degrade bond strength which takes longer time.

3.3 Conformal coatings and surface tension

According to [Papers 2, 4], the higher the surface tension the higher the driving force away from conformal coating. However, the model used in [Papers 2, 4] to explain how coatings distribute on surfaces (edges, corners) is very simple and should only be considered heuristic. It is viz. only valid on round edges / corners and when surface tension dominates gravity and hydrostatic pressure etc. Although microsystems are small and surface tension normally dominates over bulk properties like gravity and hydrostatic pressure it is an approximation considering coating shape to ignore these properties when surface tension is low.
The shape of liquids on structured surfaces is more accurately described by the Young-Laplace equation [17-19, 42-44]:

$$\Delta P = \gamma \frac{dA}{dV} - \Delta\rho g z = \gamma\left(\frac{1}{R_1} + \frac{1}{R_2}\right) - \Delta\rho g z = \gamma(\kappa_1 + \kappa_2) - \Delta\rho g z = \gamma H - \Delta\rho g z \tag{173}$$

where ΔP and $\Delta\rho$ is the pressure and density drop respectively across the liquid – surrounding atmosphere interface, γ is the liquid surface tension, A is the liquid surface area, V is the liquid volume, $\Delta\rho g z$ is the hydrostatic pressure at vertical liquid surface distance z from the liquid apex, g is the gravity, κ_1 and κ_2 are two principal (perpendicular) liquid suface curvatures at z with corresponding radii R_1 and R_2, $H = \kappa_1 + \kappa_2$ is the mean curvature.
It is thus evident that the degree of conformity of coatings to structured surfaces is determined by the balance between the surface tensions, gravity forces etc. The liquid surface free energy $G = \gamma A$ or A will be at the minimum corresponding to the situation of forces acting on the liquid, i.e. the liquid and substrates surface tension, gravity forces etc. From differential geometry the more free the liquid is the smaller A is and the less H will vary from place to place.
It is also clear that from liquid shape analysis this equation can be used for surface tension determination e.g. by the pendant drop method cf. [Paper 16]. The mean curvature H is defined in the realm of differential geometry and can be determined for

any surface shape directly from the equation for the surface [44, 45] or by fitting procedures [43]. For the pendant drop in fig. 20 we have e.g.:

$$H = \kappa_1 + \kappa_2 = \frac{d\phi}{ds} + \frac{\sin\phi}{x}$$
$$= \frac{f''(x)}{\left(1+f'(x)^2\right)^{\frac{3}{2}}} + \frac{f'(x)}{x\sqrt{1+f'(x)^2}} = \frac{xf''(x)+f'(x)\left(1+f'(x)^2\right)}{x\left(1+f'(x)^2\right)^{\frac{3}{2}}} \tag{174}$$

where f is the function fitted to the contour of the drop at the apex. Note, that due to the rotational symmetry at the apex $H = H_{apex} = \kappa_{1,apex} + \kappa_{2,apex} = 2\kappa_{1,apex} = 2\kappa_{2,apex}$, so that: $\Delta P = \frac{2\gamma}{R_1} = \frac{2\gamma}{R_2}$, which of cause is the same equation as for a spherical drop with radius $R_1 = R_2$.

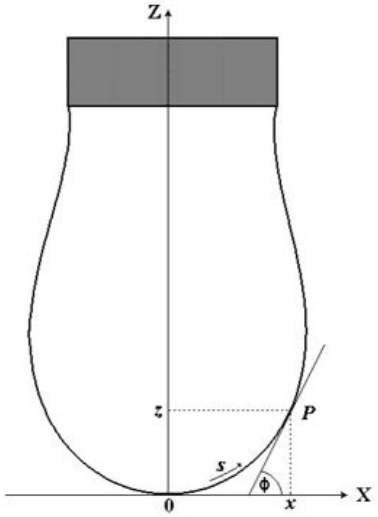

Fig. 20: Sketch of pendant drop showing the parameters in equation (174).

3.4 The reflection coefficient *R* in SAM

As pointed out in [Papers 7-9, 14, 19], [Posters 2, 3] the reflection coefficient R_{12} for longitudinal sound waves traveling in a material 1 with acoustic impedance Z_1 in a direction perpendicular to an interface to a material 2 with acoustic impedance Z_2 is:

$$R_{12} = \frac{Z_2 - Z_1}{Z_1 + Z_2} \tag{175}$$

Here $Z = \rho v$, where ρ is the density of the materials and v is the speed of sound in the materials. The indices denote the respective materials. Then the reflected amplitude with polarity at the interface between the two materials 1 and 2 is:

$$A(R)_{12} = A_0 R_{12} = A_0 \frac{Z_2 - Z_1}{Z_1 + Z_2} \tag{176}$$

In the literature there is some ambiguity as to whether R_{12} is really [46]:

$$R_{12} = \frac{Z_1 - Z_2}{Z_1 + Z_2} \tag{177}$$

This is most probably due to the similar expression for transversal p-waves moving along a taut string which is [47]:

$$R_{12,taut\ string} = \frac{v_2 - v_1}{v_1 + v_2} = \frac{Z_1 - Z_2}{Z_1 + Z_2} \tag{178}$$

where 1 and 2 denote two joined strings, $v = \sqrt{T/\mu}$ is the speed of sound, $Z = \frac{T}{v} = \frac{\mu v^2}{v} = \mu v$ is the acoustic impedance, T is the string tension, μ is the taut string mass per unit length. Likewise contributing to the confusion is the similar expression for transversal light p-waves [47, 48]:

$$R_{12,p,light} = -R_{12,s,light} = \frac{Z_1 - Z_2}{Z_1 + Z_2} \approx \frac{n_2 - n_1}{n_1 + n_2} = \frac{v_1 - v_2}{v_1 + v_2} \tag{179}$$

where $Z = \sqrt{\frac{\mu}{\varepsilon}}[\Omega] \approx \frac{1}{\sqrt{\varepsilon}} = \frac{1}{n}$ is the intrinsic impedance, μ is the permeability, ε is the permittivity, and n is the refractive index.

Below it is shown that equation (175) is the correct reflection coefficient expression to use for longitudinal sound waves.

3.4.1 Acoustics preliminaries

First it is noted that there is an analogy between sound and electricity physical behavior in the sense that the fundamental parameters are governed by equations of the same type. The most fundamental equation from electricity is Ohms law $U = R \cdot I$ which for sound converts into $p = Z \cdot v$ where p is the sound pressure, i.e. p corresponds to U, Z to R and the particle velocity v to I, see more details in fig. 21 below.

Connection of acoustic sizes for even progressive acoustic waves

UdK Berlin
Sengpiel
09.2004
Schall

	ξ	v	a	p	J	E	P_{ac}
Particle displacement ξ	–	$\frac{v}{\omega}$	$\frac{a}{\omega^2}$	$\frac{p}{\omega \cdot Z}$	$\frac{1}{\omega}\sqrt{\frac{J}{Z}}$	$\frac{1}{\omega}\sqrt{\frac{E}{\rho}}$	$\frac{1}{\omega}\sqrt{\frac{P_{ac}}{Z \cdot A}}$
Particle velocity v	$\xi \cdot \omega$	–	$\frac{a}{\omega}$	$\frac{p}{Z}$	$\sqrt{\frac{J}{Z}}$	$\sqrt{\frac{E}{\rho}}$	$\sqrt{\frac{P_{ac}}{Z \cdot A}}$
Particle acceleration a	$\xi \cdot \omega^2$	$v \cdot \omega$	–	$\frac{p \cdot \omega}{Z}$	$\omega\sqrt{\frac{J}{Z}}$	$\omega\sqrt{\frac{E}{\rho}}$	$\omega\sqrt{\frac{P_{ac}}{Z \cdot A}}$
Sound pressure p	$\xi \cdot \omega \cdot Z$	$v \cdot Z$	$\frac{a \cdot Z}{\omega}$	–	$\sqrt{J \cdot Z}$	$c\sqrt{\rho \cdot E}$	$\sqrt{\frac{P_{ac} \cdot Z}{A}}$
Sound intensity $J = P_{ak} / A = p \cdot v$	$\xi^2 \cdot \omega^2 \cdot Z$	$v^2 \cdot Z$	$\frac{a^2 \cdot Z}{\omega^2}$	$\frac{p^2}{Z}$	–	$E \cdot c$	$\frac{P_{ac}}{A}$
Sound energy density E or w	$\xi^2 \cdot \omega^2 \cdot \rho$	$v^2 \cdot \rho$	$\frac{a^2 \cdot \rho}{\omega^2}$	$\frac{p^2}{Z \cdot c}$	$\frac{J}{c}$	–	$\frac{P_{ac}}{c \cdot A}$
Sound power $P_{ac} = J \cdot A$	$\xi^2 \cdot \omega^2 \cdot Z \cdot A$	$v^2 \cdot Z \cdot A$	$\frac{a^2 \cdot Z \cdot A}{\omega^2}$	$\frac{p^2 \cdot A}{Z}$	$J \cdot A$	$E \cdot c \cdot A$	–

White = linear sound field strength and gray = squared sound energy strength.

Acoustic impedance $Z = \rho \cdot c = \frac{p}{v} = \frac{J}{v^2} = \frac{p^2}{J}$ in $\frac{N \cdot s}{m^3}$

Density of air ρ in $\frac{kg}{m^3}$ is 1.204 kg/m³ at 20 °C

Angular frequency $\omega = 2 \cdot \pi \cdot f$

Frequency f in Hz = $\frac{1}{s}$ in air of 20 °C: Z = 413 $\frac{N \cdot s}{m^3}$

Area through a unit area normal to the direction A in m²

Displacement of air particles (excursion amplitude) ξ in m

Particle velocity (velocity amplitude) v in $\frac{m}{s}$

Particle acceleration a in $\frac{m}{s^2}$

Sound pressure (excess pressure) $p = \frac{F}{A}$ in $\frac{N}{m^2}$ = Pa

Sound intensity $J = p \cdot v = \frac{P_{ak}}{A}$ in $\frac{W}{m^2}$

Sound energy density E or $w = \frac{J}{c}$ in $\frac{W \cdot s}{m^3}$

Here is 1 joule J = W · s = N · m

Sound power $P_{ac} = J \cdot A$ in W

Speed of sound c in m/s (at 20 °C is c = 343 m/s)

Because 1 W · s = 1 N · m, the sound energy density is 1 W · s / m³ ≙ 1 N·m / m³ = 1 N / m² and that is the unit of a sound pressure in pascals! To remember: W · s = N · m = J (joule).

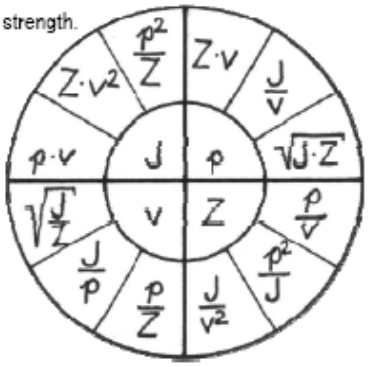

To the comparison: U means here V

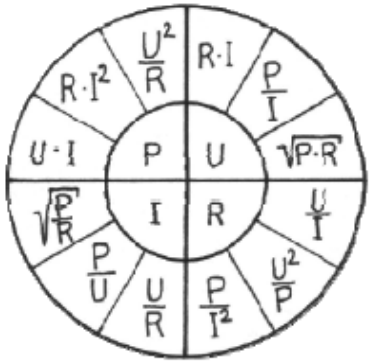

Fig. 21: Connection of acoustic sizes [49].

Secondly it is noted sound propagation is pressure (or density) propagation where the phase velocity is different from the particle velocity. The acoustic wave equation is:

$$\frac{\partial^2 \xi}{\partial x^2} = \frac{1}{v_p^2} \frac{\partial^2 \xi}{\partial t^2} \tag{180}$$

where ξ is the particle displacement in the x direction, v_p is the phase velocity and t the time. The solution to the equation is:

$$\xi = \xi_0 \sin(kx - \omega t) \tag{181}$$

where ξ_0 is the particle displacement amplitude, $k = \frac{2\pi}{\lambda}$ is the wave number, λ is the wavelength, and $\omega = 2\pi f = \frac{2\pi}{T}$ is the angular frequency. Note that $\frac{\omega}{k} = \frac{2\pi\lambda f}{2\pi} = f\lambda = v_p$. The pressure can be written:

$$p = -E \frac{\partial \xi}{\partial x} \tag{182}$$

where E is Young's modulus. Using this, the force needed to compress an area A a distance Δx can be written:

$$F = -A\Delta x \frac{\partial p}{\partial x} = A\Delta x E \frac{\partial^2 \xi}{dx^2} \tag{183}$$

Alternatively this can be written (Newton 2nd law):

$$F = ma = \rho A \Delta x \frac{\partial^2 \xi}{dt^2} \tag{184}$$

where m is the mass of the moved material, and ρ is the materials density. Equating these two equations for F we can write the acoustic wave equation as:

$$\frac{\partial^2 \xi}{dx^2} = \frac{\rho}{E} \frac{\partial^2 \xi}{dt^2} \tag{185}$$

Comparison with the first mentioned acoustic wave equation (180) leads to:

$$v_p = \sqrt{\frac{E}{\rho}} \tag{186}$$

This can be used to show that $v = \frac{p}{Z}$. We get from equation (181) and (182):

$$p = -E\frac{\partial \xi}{\partial x} = -Ek\xi_0 \cos(kx - \omega t) = -\rho v_p^2 k\xi_0 \cos(kx - \omega t) = -Zv_p k\xi_0 \cos(kx - \omega t) \tag{187}$$

The particle velocity is:

$$v = \frac{d\xi}{dt} = -\omega\xi_0 \cos(kx - \omega t) = -v_p k\xi_0 \cos(kx - \omega t) \tag{188}$$

Comparison of equation (187) and (188) gives:

$$v = \frac{p}{Z} \tag{189}$$

3.4.2 Derivation of *R*

The reflection coefficient R_{12} can be derived by demanding energy conservation or wave amplitude and gradient continuity at the interface between the two materials. Below the former method is used. To do that the situation in fig. 22 is considered. From fig. 21 we

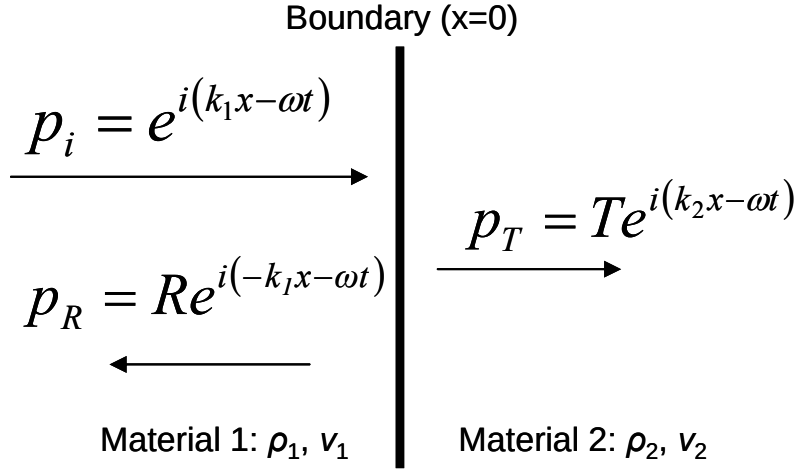

Fig. 22: Sound reflection and transmission at a material boundary. p_i, p_R and p_T denotes the incoming, reflected and transmitted pressure waves. T is the transmission coefficient. Note that $1 + R = T$. Note also that the fraction of energy transmitted across the boundary is $1 - R^2$ and not T^2 as $T^2 \neq 1 - R^2$.

see that the sound intensity is pv. Energy conservation requires that the flux of energy towards the boundary equals the flux of energy away from the boundary. The average incoming energy at time $t = 0$ of one wave cycle / period of duration T corresponding to one wavelength $\lambda = \frac{2\pi}{k}$ is:

$$\langle pv \rangle_i = \langle pv \rangle_R + \langle pv \rangle_T$$

$$= \frac{1}{T}\int_0^T p_1 v_1 \, dt = \frac{1}{T}\int_0^T p_1 \frac{p_1}{\rho_1 v_1} dt = \frac{1}{Z_1 T}\int_0^T p_1^2 \, dt = \frac{k_1}{2\pi Z_1}\int_0^{\frac{2\pi}{k_1}} e^{i2k_1 x} dx \tag{190}$$

Taking only the real part we get:

$$\langle pv \rangle_i = \frac{k_1}{2\pi Z_1}\int_0^{\frac{2\pi}{k_1}} \cos^2(k_1 x) dx = \frac{k_1}{2\pi Z_1}\left[\frac{x}{2} + \frac{\sin(2k_1 x)}{4k_1}\right]_0^{\frac{2\pi}{k_1}} = \frac{1}{2Z_1} \tag{191}$$

Using the same calculation on $\langle pv \rangle_R$ and $\langle pv \rangle_T$ we get:

$$\langle pv \rangle_i = \langle pv \rangle_R + \langle pv \rangle_T \tag{192}$$

$$\Updownarrow$$

$$\frac{1}{2Z_1} = \frac{R^2}{2Z_1} + \frac{T^2}{2Z_2} \tag{193}$$

$$\Updownarrow$$

$$\frac{1}{Z_1} = \frac{R^2}{Z_1} + \frac{(1+R)^2}{Z_2} \tag{194}$$

$$\Updownarrow$$

$$R = \frac{Z_2 - Z_1}{Z_1 + Z_2} \vee R = -1 \qquad q.e.d. \tag{195}$$

3.5 The calculation of *N* in simulated SAM A-scans

The formula in [Paper 7] for the number N of waves received by the SAM transducer at the same time by reflection at the same interfaces in different order is a modified version of the formula for the multinomial coefficients. In what follows the formula is not proved in a strict mathematical sense but justified inductively by:

- Showing the derivation of the multinomial coefficients formula which can be found in standard textbooks on combinatorics [50].

- Showing some of the uses of the formula for the multinomial coefficients in physics [51, 52, 53] including one which can be directly adopted in a limited number of reflection sequence permutation cases [53].
- Giving some examples on how the derived formula for *N* is used.

3.5.1 Combinatorics preliminaries

The well known binomial formula is:

$$(x+y)^n = \sum_{k=0}^{n} \binom{n}{k} x^k y^{n-k} = \sum_{k=0}^{n} \frac{n!}{k!(n-k)!} x^k y^{n-k} \tag{196}$$

where the coefficients are called binomial coefficients. The binomial coefficients are the number of ways *k* elements can be combined from *n* elements. Fore more variables we get the less known multinomial formula:

$$\left(\sum_{i=1}^{r} x_i\right)^n = \sum_{k_1+\ldots+k_r=n} \binom{n}{k_1,\ldots,k_r} x_1^{k_1} x_2^{k_2} \ldots x_r^{k_r} = \sum_{k_1+\ldots+k_r=n} \frac{n!}{\prod_{i=1}^{r} k_i!} x_1^{k_1} x_2^{k_2} \ldots x_r^{k_r} \tag{197}$$

where the coefficients are called multinomial coefficients (M.C.). The M.C. is the number of ways *n* distinct elements can be partitioned / permuted into *r* unordered subsets, the i^{th} set having k_i elements where $k_1 + k_2 + \ldots + k_r = n$. The M.C. are derived by realizing that first we can combine k_1 elements taken from the *n* elements in $\binom{n}{k_1}$ ways. Next, from the rest $n - k_1$ elements we can combine k_2 elements in $\binom{n-k_1}{k_2}$ different ways, and so on. Hence by the product rule from combinatorics we can permute the *n* distinct elements among the *r* subsets in the following number of ways:

$$\begin{aligned}
\text{M.C.} &= C(n;k_1,k_2,\ldots,k_r) = \binom{n}{k_1}\binom{n-k_1}{k_2}\binom{n-k_1-k_2}{k_3}\cdots\binom{k_r}{k_r} \\
&= \frac{n!}{k_1!(n-k_1)!}\frac{(n-k_1)!}{k_2!(n-k_1-k_2)!}\cdots\frac{(k_{r-1}-k_r)!}{k_{r-1}!k_r!}\frac{k_r!}{k_r!0!} \\
&= \frac{n!}{k_1!k_2!\cdots k_r!} \\
&= \frac{n!}{\prod_{i=1}^{r} k_i!} \quad q.e.d.
\end{aligned} \tag{198}$$

3.5.1.1 Physical uses of the multinomial coefficients

The M.C. are used in many calculations in physics. Here three important examples from statistical physics are mentioned:

Example 1:
The number of atomic configurations in a binary alloy $\Omega(A,B)$ consisting of N atoms of which N_A are atom A and N_B are atom B is [51]:

$$\Omega(A,B) = \frac{N!}{N_A!N_B!} \tag{199}$$

From this it can be shown [51] that the entropy S is given by:

$$S = kT \ln \Omega(A,B) \tag{200}$$

where k is Boltzmann's constant and T is the absolute temperature.

Example 2:
The number of ways the same total energy can be distributed among 6 identical but distinguishable particles on the energy levels in fig. 23 is according to Maxwell-Boltzman statistics [52]: Left: $\frac{6!}{5!\,1!} = 6$, middle: $\frac{6!}{3!\,2!\,1!} = 60$, right: $\frac{6!}{2!\,2!\,1!\,1!} = 180$.

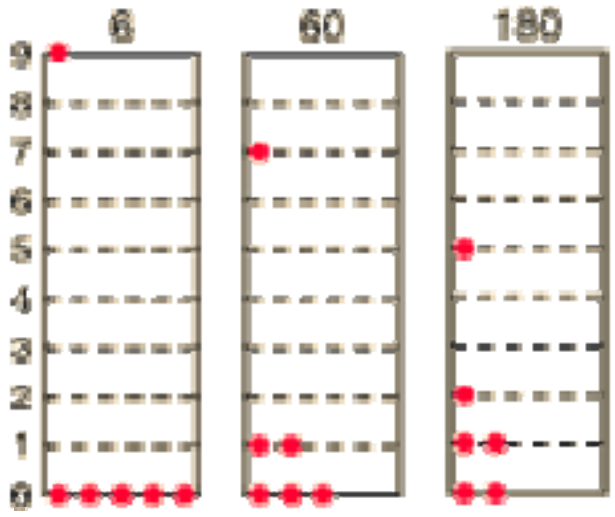

Fig. 23: Three ways of distributing the same total energy between 6 identical but distinguishable particles.

Example 3:
Combining two systems like those in example 2 we have from statistical thermodynamics that the number of states $\Omega(a,b)$ of the AB system in fig. 24 with molecules / particles a_j and b_j, where the systems A and B are in thermal contact is [53]:

$$\Omega(a,b) = \frac{A!}{\prod a_i!}\frac{B!}{\prod b_k!} \tag{201}$$

where A and B are the total numbers of A and B molecules / particles and a_i, b_k are the numbers of A and B molecules at energy levels i and k respectively. Note that the ensemble must satisfy:

$$\sum_i a_i = A \tag{202}$$

$$\sum_i b_i = B = A \tag{203}$$

$$\sum_i \left(a_i E_{A_i} + b_i E_{B_i}\right) = \varepsilon \tag{204}$$

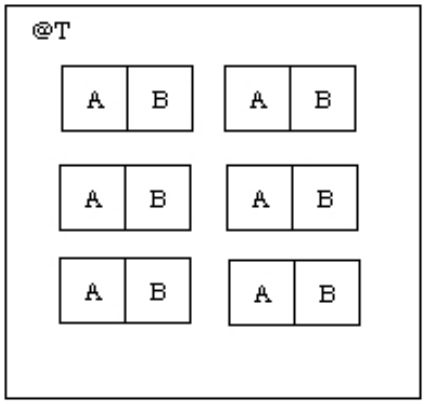

Fig. 24: AB system where A and B parts are in thermal contact. A and B are characterized by N_A, V_A, E_{Ai}, a_i and N_B, V_B, E_{Bi}, b_i, where N denote the numbers of A or B, V the volume of A or B parts, E_{A_i} and E_{B_i} the energies of the i^{th} level for the A and B molecules / particles respectively, a_i and b_i the numbers of A and B molecules respectively at energy level i.

where a_i and b_i are the numbers of A and B molecules respectively at energy level i, E_{A_i} and E_{B_i} the energies of the i^{th} level for the A and B molecules / particles respectively and ε is the total energy of the AB system. Note again that the possible number of states / permutations for the combined system is achieved by using the product rule from combinatorics i.e. it is the product of the possible number of states for the A and B systems separately.

3.5.2 A few illustrating examples on calculating *N*

Clearly equation (201) is very similar to the one found in [Paper 7], for $N(M,V)$ = the number of waves received by the SAM transducer at the same time by reflection at the same interfaces in different order which is:

$$N(M,V) = \frac{(k-a_k)\cdot(k-1-a_{k-1})\cdot\ldots\cdot(1-a_1)}{A_2!\cdot A_3!\cdot A_4!\cdot\ldots\cdot A_n!}\cdot\frac{(k-1-p_1)\cdot(k-2-p_2)\cdot\ldots\cdot(1-p_{k-1})}{P_1!\cdot P_2!\cdot P_3!\cdot\ldots\cdot P_{n-1}!} \tag{205}$$

where:

k = number of reflections up
m_i = number of an up reflecting impedance transition
v_j = number of a down reflecting impedance transition
a_i = number of elements in $V \geq m_i$, $i \in \{1, 2, \ldots, k\}$
p_j = number of elements in $M \leq v_j$, $j \in \{1, 2, \ldots, k\text{-}1\}$
A_n = number of elements in M with value n
P_n = number of elements in V with value n

where M and V are the following orders of reflections up and down respectively:

$$M = \{m_1, m_2, \ldots, m_i, \ldots .. m_k\} \quad m_i \geq m_{i+1}$$
$$V = \{v_1, v_2, \ldots, v_j, \ldots .. v_{k-1}\} \quad v_j \geq v_{j+1}$$

Using equation (201) on the up and down reflection sequence of sound, A is the number of up reflections in the sequence, a_i is the number of up reflections on impedance transition i, B is the number of down reflections in the sequence, b_i is the number of down reflections on impedance transition i. However equation (201) is not generally valid when calculating the number of possible ways reflections on a number of interfaces can be permuted. This is illustrated below.
Given the up and down reflections can be separated by a horizontal line as in the example in fig. 25 equation (201) can be adopted directly to calculate the number N of ways (permutations) we can have the same reflections just in different order. Then A and B are the numbers of up and down reflections respectively and a_i, b_i are the numbers of up and down reflections respectively on the i^{th} interface. In the example we have:

$$N = 3!\cdot 2! = 12 \tag{206}$$

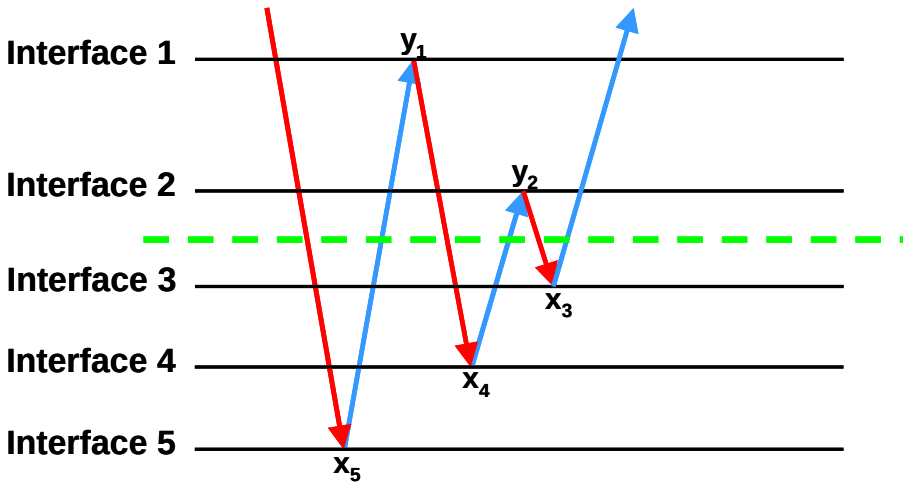

Fig. 25: Reflection sequence example where reflection on each interface only takes place once and where up / down reflections can be separated by a horizontal line (green). Angles are only for illustration. Actually the transducer – interface sound pulse path both up and down is much more vertical.

The reflection permutations are illustrated in fig. 26 below.

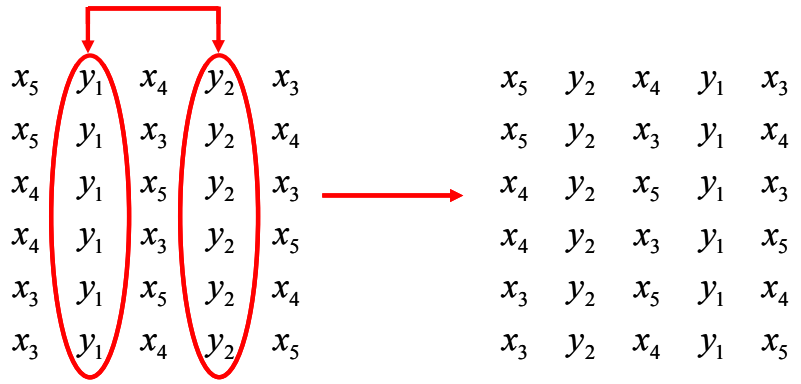

Fig. 26: Illustration of the possible permutations of the reflections in fig. 25 above. x's denote up reflections, y's denote down reflections. There are 3 up reflections i.e. they can be permuted in 3! = 6 different ways. There are 2 down reflections i.e. they can be permuted in 2! = 2 different ways. Combining the possible up / down reflections gives a total of 12 possible permutations. To the left the 6 permutations of the x's are combined with the first permutation of the y's, to the right with the second.

Using equation (205) we get:

$M = \{5, 4, 3\}$, $V = \{2, 1\}$, $k = 3$, $a_i = p_j = 0$, $A_n = P_n = 1$

which also leads to:

$$N(M,V)=3!\cdot 2!=12 \tag{207}$$

Fig. 27 is another reflection sequence case where up / down reflections can be separated by a horizontal line. However, unlike the previous example in this case some reflections take place at the same interfaces. Using equation (201) to calculate the total number N of possible similar permutations we get:

$$N=\frac{3!}{2!}\cdot\frac{2!}{2!}=3 \tag{208}$$

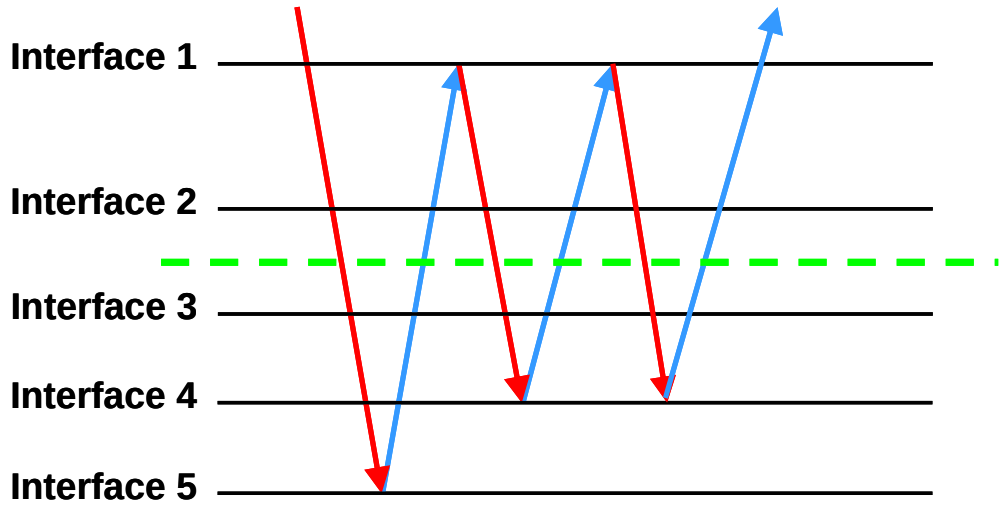

Fig. 27: Illustration of reflection sequence where up / down reflections can be separated by a horizontal line (green) and where there is an interface on which there is more than one (two on interface 4) reflection of one of the types (up).

Using equation (205) with:

$M = \{5, 4, 4\}$, $V = \{1, 1\}$, $k = 3$, $a_i = p_j = 0$, $A_4 = 2$, $A_5 = 1$, $P_1 = 2$

we also get:

$$N(M,V)=\frac{3!}{2!}\cdot\frac{(3-1)!}{2!}=3 \tag{209}$$

In equation (201) there is no restriction on the relative energy levels of the a_i, b_i molecules / particles. However, in some cases when dealing with consecutive reflections

in SAM, the number of allowed up / down reflection permutations equal to (i.e. indistinguishable in SAM because the reflections are on same impedance interfaces) a given up / down reflection sequence is reduced as compared to equation (201) in accordance to what orders of reflections are actually physically possible, which is determined by the relative positions of the reflecting impedance interfaces. That is, when a wave is reflected up at some impedance interface it can not be combined / followed by a reflection down at the same interface or some deeper down interface and vice versa. The needed modification of equation (201) is what is accounted for in the numerator of equation (205). Fig. 28 illustrates such a case in which equation (201) is not valid and where equation (205) has to be used. Here up / down reflections can not be separated by a horizontal line and there is no equal reflections (up/down) on the same interfaces. Note, that on two interfaces (2 and 3 marked with red and green circles) we have both up and down reflections. Using the equation (201) we get the wrong result:

$$N = 4! \cdot 3! = 24 \cdot 6 = 144 \tag{210}$$

Fig. 28: Example of a reflection sequence where up / down reflections can not be separated by a horizontal line. Further it is an example where there no more than one up or down reflection on each involved interface / impedance transition. However, there are two interfaces (interfaces 2 and 3 marked with red and green circles respectively) on which both up and down reflections are observed.

Using equation (205) with:

$M = \{5, 4, 3, 2\}$, $V = \{3, 2, 1\}$, $k = 4$, $a_4 = 2$, $a_3 = 1$, $a_2 = 0$, $a_1 = 0$, $p_1 = 2$, $p_2 = 1$, $p_3 = 0$
A_n=1, $P_n = 1$

we get the correct result which can be confirmed by sketching all possibilities:

$$\begin{aligned} N(M,V) &= (4-2)(4-1-1)(4-2)(4-3)\cdot(4-1-2)(4-2-1)(4-3) \\ &= 2\cdot 2\cdot 2 \cdot 1\cdot 1\cdot 1 \\ &= 8 \end{aligned} \tag{211}$$

The "-2" in the first bracket originates from the fact that up reflection 21 can not be followed by down reflections 24 and 35 for up reflections on interfaces 4 and 5 when the reflection order is permuted. Likewise in the second bracket the second "-1" comes from the fact that up reflection 32 can not be followed by down reflection 35 for up reflection on interface 5 when permuting the reflection order, and so on in the expression (211) above. The equation has also been confirmed by sketching the reflection sequences in cases resulting in much higher $N(M,V)$ numbers. It has not yet been possible to find reflection sequence cases where $N(M,V)$ is not valid.

3.6 Acoustic impedance determination

As mentioned in [Papers 8, 9, 11, 14, 19], [Posters 3, 4] SAM can be used to characterize the interior uniformity of materials concerning acoustic impedance and strain. That is, with reference to fig. 29 the interior acoustic impedance Z_x can be

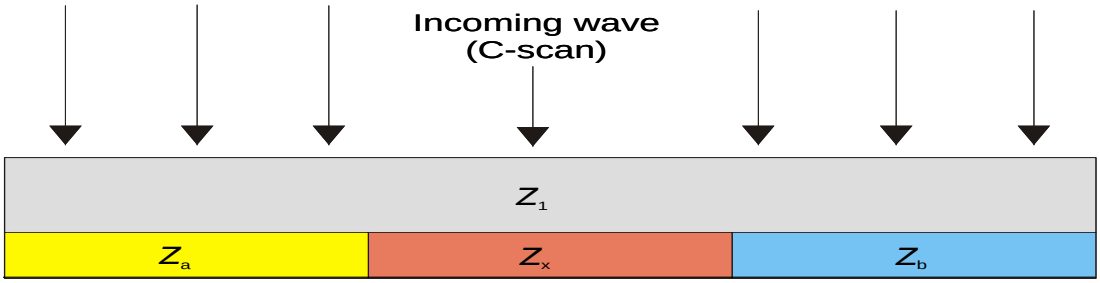

Fig. 29: Illustration of acoustic impedances used in equations (219) and (225) to find unknown acoustic impedance Z_x.

determined from C-scan grey tone values *g* in two ways. Here the equations are derived:

Case 1:
The acoustic impedance Z_1 of the top material is unknown. Two reference acoustic impedances Z_a and Z_b are known. Then the calculation of the unknown Z_x is based on the approximation that R_{12} and therefore *g* varies linearly with Z_2, i.e. that:

$$g(Z_2) = \alpha Z_2 + k \tag{212}$$

where α is the slope of the line and k is a constant. Looking at fig. 30 where $R_{12}(Z_2)$ or just $R(Z_2)$ is plotted for some typical microsystem packaging material Z_1 values the approximation seem to be very good especially for high Z_1 values compared to the Z_2 values. The chosen values of Z_1 and Z_2 in fig. 30 correspond well to adhesives

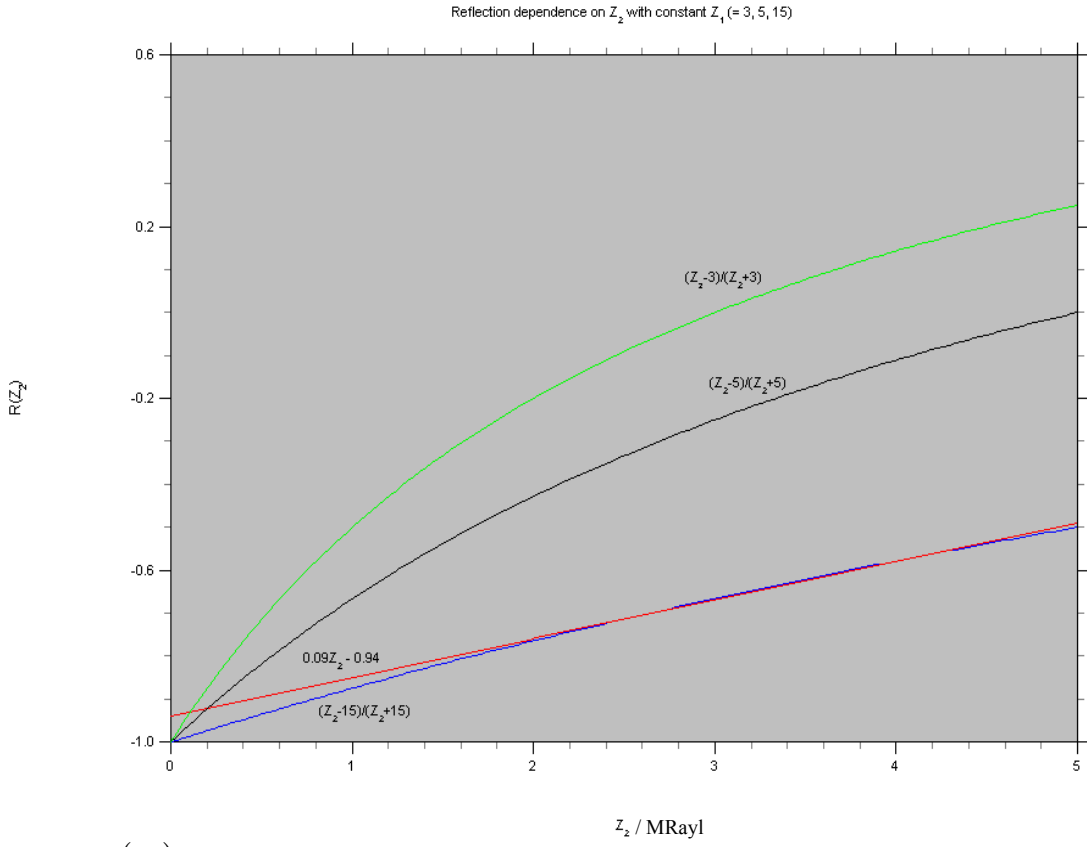

Fig. 30: $R(Z_2)$ for some typical microsystem packaging values of Z_1 and Z_2. Here the values correspond well to adhesives (polymers) under a number of different materials (plastics to glasses) with higher acoustic impedance. The curve for $Z_1 = 15$ MRayl is approximated (red line) with equation (213) in the neighborhood of $Z_2^0 = 3$ MRayl corresponding to adhesive under glass.

(polymers) under a number of different materials (plastics to glasses) with higher acoustic impedance. The actual linear approximation can be derived from the Taylor series of $R_{12}(Z_2)$ at Z_2^0 to the first order which is:

$$R_{12}(Z_2) \approx \frac{2Z_1}{\left(Z_1 + Z_2^0\right)^2} Z_2 + R_{12}\left(Z_2^0\right) - \frac{2Z_1 Z_2^0}{\left(Z_1 + Z_2^0\right)^2} \tag{213}$$

Proceeding from equation (212) to find Z_x we have:

$$g(Z_x) = \frac{\partial g}{\partial Z_2} Z_x + k = \frac{\Delta g}{\Delta Z_2} Z_x + k = \frac{g(Z_b) - g(Z_a)}{Z_b - Z_a} Z_x + k \tag{214}$$

To find *k* we can use that:

$$g(Z_x) = g(Z_b) \tag{215}$$

$$\Updownarrow$$

$$Z_x = Z_b \tag{216}$$

Inserting this in equation (214) above we get:

$$k = g(Z_b) - Z_b \frac{g(Z_b) - g(Z_a)}{Z_b - Z_a} \tag{217}$$

Again inserting in equation (214) we get the expression for Z_x:

$$g(Z_x) = \frac{g(Z_b) - g(Z_a)}{Z_b - Z_a} Z_x + g(Z_b) - Z_b \frac{g(Z_b) - g(Z_a)}{Z_b - Z_a} \tag{218}$$

$$\Updownarrow$$

$$Z_x = Z_b + (g(Z_x) - g(Z_b)) \frac{Z_b - Z_a}{g(Z_b) - g(Z_a)} \tag{219}$$

Case 2:
The acoustic impedance Z_1 of the top material is known. Only one reference acoustic impedance Z_a is known. Then the calculation of the unknown Z_x is based on the linear dependence of *g* on R_{12} i.e.:

$$g(R) = \alpha R + k \tag{220}$$

Then we have:

$$g(0) = \alpha \cdot 0 + k = 0 \tag{221}$$

$$\Updownarrow$$

$$k = 0 \tag{222}$$

so that:

$$g(Z_2) = \alpha \frac{Z_2 - Z_1}{Z_1 + Z_2} \tag{223}$$

Then from the known Z_a we can find α :

$$\alpha = g(Z_a)\frac{Z_1 + Z_a}{Z_a - Z_1} \tag{224}$$

This leads to:

$$Z_x = Z_1 \frac{\frac{\alpha}{g(Z_x)} + 1}{\frac{\alpha}{g(Z_x)} - 1}$$

$$= Z_1 \frac{g(Z_a)(Z_a + Z_1) + g(Z_x)(Z_a - Z_1)}{g(Z_a)(Z_a + Z_1) - g(Z_x)(Z_a - Z_1)} \tag{225}$$

3.7 References

1. J. Crank, The Mathematics of Diffusion, Second Edition, Oxford University Press, 1975, ISBN: 0 19 853411 6.

2. J. Comyn, Editor, Polymer permeability, Chapman & Hall, 1985, ISBN 0 412 53820 2.

3. J. Crank, G. S. Park, Diffusion in polymers, Academic Press, London and New York, 1968.

4. H. S. Carslaw and J. C. Jaeger, Conduction of Heat in Solids, Second Edition, Oxford University Press, 1959, ISBN: 0 19 853368 3.

5. http://en.wikipedia.org/wiki/Laplace_transform

6. http://virtual.cvut.cz/dynlabmodules/ihtml/dynlabmodules/syscontrol/node145.html

7. http://www.stanford.edu/~boyd/ee102/qualitative.pdf

8. http://fourier.eng.hmc.edu/e102/lectures/Laplace_Transform/node17.html

9. Chi-Hung Shen and George S. Springer, Moisture Absorption and Desorption of Composite Materials, Journal of Composite Materials, Vol. 10 (January 1976).

10. Ulf W. Gedde, Polymer Physics, Chapman and Hall, 1995, ISBN: 0 412 62640 3.

11. Ulrich Eisele, Introduction to Polymer Physics, Springer-Verlag Berlin Heidelberg, 1990, ISBN 3-540-50777-9.

12. D. Stroehle, On the penetration of gases and water vapour into packages with cavities and on maximum allowable leakrates, 15th Annual Proceedings, Reliability Physiscs Symposium, (1977), pp. 101-106.

13. http://en.wikipedia.org/wiki/Kelvin_equation

14. Niels Tas, Tonny Sonnenberg, Henri Jansen, Rob Legtenberg and Miko Elwenspoek, Stiction in surface micromachining, Journal of Micromechanical Microengineering, No. 6 (1996), pp. 385-397.

15. J. G. Powles, On the validity of the Kelvin equation, J. Phys. A: Math. Gen. No. 18 (1985), pp. 1551-1560.

16. B. Bhushan, Editor, Springer Handbook of Nanotechnology, Springer 2004, ISBN: 3-540-01218-4.

17. http://en.wikipedia.org/wiki/Young-Laplace_Equation

18. Theodore Frankel, The geometry of physics, An introduction, Second edition, Cambridge University Press, 2004, ISBN: 0 521 53927 7.

19. Jean-Louis Barrat, Basic Concepts for Simple and Complex Liquids, Oxford University Press, 2003, ISBN: 0 521 78953 2.

20. K. R. Trethewey and J. Chamberlain, Corrosion for Science and Engineering, Longman Group Limited, 1995, ISBN: 0-582-238692.

21. Vivekanand Saikumar and Ralph J. Jacodine, Time Lag and Permeation in Multilayer Polymer Coatings, IEEE Transactions on components, hybrids, and manufacturing technology, Vol. 16, No. 5, August 1993.

22. Hal Greenhouse, Hermeticity of Electronic Packages, William Andrew Publishing / Noyes Publications 2000, ISBN: 0-8155-1435-2.

23. Michal Tencer, Moisture Ingress into Nonhermetic Enclosures and Packages. A Quasi-Steady State Model for Diffusion and Attenuation of Ambient Humidity Variations, 44th Proceedings of Electronic Components and Technology Conference, (1994).

24. http://www.leakdetection-technology.com/page_6/page_6.htm

25. A. Christou, Moisture diffusion through hybrid-circuit encapsulants, Electronic Packaging and Production, April, (1979).

26. http://www.efunda.com/formulae/solid_mechanics/mat_mechanics/elastic_constants_G_K.cfm#bulkmod

27. http://chsfpc5.chem.ncsu.edu/~franzen/CH795N/dft_modules/polymer_module/crystalline/elastic_constants.htm

28. http://www.answers.com/topic/bulk-modulus-of-elasticity

29. http://en.wikipedia.org/wiki/Bulk_modulus

30. R. D. Adams, J. Comyn and W. C. Wake, Structural Adhesive Joints in Engineering, Second Edition, Chapman & Hall, London, Weinheim, New York, Tokyo, Melbourne, Madras, ISBN: 0-412-70920-1, (1997).

31. PerkinElmer DSC7 Pyris Kinetics Software Guide.

32. Ranjit K. Roy, A primer on the Taguchi method, SME, Society of Manufacturing Engineers, Dearborn, Michigan, ISBN: 0-87263-468-X, (1990).

33. Ranjit K. Roy, Design of experiments using the Taguchi approach, 16 steps to Product and Process Improvement, John Wiley & Sons, Inc., New York, Chichester, Weinheim, Brisbane, Singapore, Toronto, ISBN: 0-471-36101-1, (2001).

34. Douglas C. Montgomery, Design and Analysis of Experiments, 5th edition, John Wiley & Sons, Inc., New York, Chichester, Weinheim, Brisbane, Toronto, Singapore, ISBN: 0-471-31649-0, (2001).

35. Mark J. Anderson, Patrick J. Whitcomb, DOE simplified, Practical Tools for Effective Experimentation, Productivity, Inc., ISBN: 1-56327-225-3, (2000).

36. James J. Licari, Dale W. Swanson, Adhesives Technology for Electronic Applications, Materials, Processes, Reliability, Materials and Processes for Electronic Applications Series, William Andrew Publishing, Norwich, NY, U.S.A., ISBN: 0-8155-1513-8, (2005).

37. A. Pizzi, K. L. Mittal, Editors, Handbook of Adhesive Technology, Second Edition, Revised and Expanded, Marcel Dekker, Inc., New York, Basel, ISBN: 0-8247-0986-1, (2003).

38. Alphonsus V. Pocius, Adhesion and Adhesives Technology, An introduction, 2nd Edition, Hanser Publishers, Munich, Hanser Gardner Publications, Cincinnati, ISBN: 3-446-21731, (2002).

39. Limhåndbogen, Casco Nobel A/S, ISBN: 91-630-1005-4, (1992).

40. D. M. Brewis, D. Briggs, Editors, Industrial Adhesion Problems, Wiley-Interscience, December 1985, ISBN: 978-0471840053.

41. F. M. Fowkes, (1964), Ind. Eng. Chem., 56(12), 40.

42. http://en.wikipedia.org/wiki/Surface_tension

43. http://www.kruss.info/index.php?content=http%3A//www.kruss.info/techniques/contact_angle_e_2.html

44. Andrew Presley, Elementary Differential Geometry, Springer-Verlag London Limited, 2006.

45. http://www.cvl.iis.u-tokyo.ac.jp/class2006/G-11-differential-geometry06.ppt

46. http://academia.hixie.ch/bath/ultrasound/home.html

47. Marcelo Alonso, Edward J. Finn, Fundamental University Physics, Second Edition, Volume II, Fields and Waves, Addison-Wesley Publishing Company, Inc., 1983, ISBN: 0-201-00077-6.

48. David K. Cheng, Fundamentals of Engineering Electromagnetics, Addison-Wesley Publishing Company, Inc., 1993, ISBN: 0-201-60071-4.

49. http://www.sengpielaudio.com/Calculations03.htm

50. Fred S. Roberts, Barry Tesman, Applied Combinatorics, 2nd Edition, Pearson Education, Inc., 2005, ISBN: 0-13-079603-4.

51. D. A. Porter, K. E. Easterling, Phase Transformations in Metals and Alloys, Van Nostrand Reinhold Co. Ltd., 1988, ISBN 0-442-30440-4.

52. http://hyperphysics.phy-astr.gsu.edu/Hbase/quantum/disbol.html#c2

53. http://phoenix.liu.edu/~nmatsuna/PHS702/statmech/lect3/stat.mech.3.html

4 Conclusions and outlook

In this thesis focus has been on the performed work in relation to how the adhesion of protective polymer adhesives and encapsulations can be characterized theoretically and practically and optimized regarding intrinsic properties, the surroundings and their interaction. The main conclusion is that the interaction makes a system design approach to development of reliable microsystem packaging mandatory.

For the two specific adhesion reliability areas studied the following can be concluded:

Polymers, metal / ceramic -polymer composites

In-diffusion of water to corrosional critical areas in microsystems should be considered the most important single factor influencing microsystem reliability. Polymer adhesive and coating bond strength and mechanical properties depend a lot on the humidity exposure no matter the polymer type. Further water may lead to corrosion etc.

Therefore, with water present it is of utmost importance to evaluate what reliability / life time can be expected for each polymer. This involves carefully determining polymer water diffusivities D, solubilities C or S (equilibrium water uptake), and means of reducing the exposure of or transport through the adhesive / coating and other microsytem elements.

It is possible by mathematical modeling to find a general expression for the water concentration distribution inside e.g. 5 cm · 5 cm · 0.1 cm polymer slabs as a function of time no matter the initial distribution. Considering the mass of water uptake at different times M_t until equilibrium M_∞ by water immersion / 100 % RH exposure it is then possible to determine diffusivities by fitting experimental $\frac{M_t}{M_\infty}$ data to the corresponding analytical expression. Thus, diffusivities have been satisfactorily determined in the specific case where, after drying periods, zero initial water concentration throughout the slabs has been assumed. Using a found diffusivity and solubility for an epoxy (Epotek U300-1) the mathematical expression for the concentration distribution (equation (77), chapter 3) has been confirmed by direct simulation on the non-steady state diffusion equation.

In these calculations D has been assumed constant i.e. water concentration independent. However, it is to be expected that due to water – water interactions, strain increase etc. as the concentration increase D will decrease. D (constant) can be determined by fitting of all, early or late $\frac{M_t}{M_\infty}$ data to the theoretical expression valid at all times. Because of the concentration dependence some discrepancy in the found D's are to be expected. In the early stages of in-diffusion a simple mathematical expression for $\frac{M_t}{M_\infty}$ can be found from the semi-infinite diffusion model. From this D can also be found by fitting of corresponding experimental data. A reasonable early stage in-diffusion limit of less than 5 % "overlap" of water in-diffused from the two large slab surfaces is found to

correspond to $\frac{M_t}{M_\infty} < 0.48$. D can be determined from late $\frac{M_t}{M_\infty}$ data by fitting to a late time limit of the mathematical expression valid at all times.

In case adhesive or coating delamination and stress are no problems corrosion is often the most serious problem. In this case the most important parameters from which the life time can be evaluated are the water flux and solubility. Concerning water flux it may be important for some applications to consider when the steady state diffusion which depends on the diffusivity and barrier thickness sets in. This is because the adhesives and coatings are very thin in microsystems and it can be shown that at steady state the flux is high. Note that high water flux also leads to faster adhesive / coating bond deterioration by e.g. hydrolysis. A number of simple equations have been found from which it is possible to judge when steady state diffusion sets in. For adhesives and coatings barriers are often at least 100 µm thick. This means that for point of care microsystems the non-steady state calculations are the most relevant. For other applications with barrier thicknesses of the same order which should last for years, steady state diffusion calculations apply. Considering a certain corrosion failure mechanism it has been shown for a specific water differential pressure sensor with mm thick barrier (Epotek U300-1 epoxy) to an Al bond pad that a life time of 6.5 to 19.5 years are to be expected at RT. However, it has also been demonstrated that this life time can be reduced more than two orders of magnitude at elevated temperatures. Practical mass spectrometer water flux studies on similar test samples show as expected a lower water flux for epoxy (Epotek H77) than for silicone (DC Q3-6611) with varying temperature. In both cases the flux temperature dependence follows an Arrhenius behavior as also expected. From the Arrhenius plots, assuming that nothing but the water diffusivity change when the temperature is changed, it is possible to determine the steady state activation energies for water diffusion. For the silicone DC Q3-661 and the epoxy Epotek H77 they have been found to be 0.4 eV and 0.8 eV respectively. The activation energy 0.8 eV for water diffusion in Epotek H77 is quite high compared with other polymers. Part of the explanation is probably that this adhesive is highly filled with ceramic Al_2O_3 particles the main purpose of which is to lower the CTE to minimize thermal stresses upon heat cure. The less water penetrable particles also delay the polymer in-diffusion by making the diffusion path longer. However, some fluoro polymers exhibit significantly higher activation energies (2 eV) for water diffusion. It should also be mentioned that in these measurements diffusion in the bulk and along the interfaces were not separated. It was planned but never carried out to do that by measurements on adhesive joints with different thicknesses which keep the interface areas constant while more or less adhesive bulk material is exposed. By linear extrapolation of the leak dependency on adhesive thickness to zero thickness it should be possible to find the diffusivity along the interfaces which might be significantly different from that in the bulk adhesive. Furthermore, as the adhesive / bond begins to deteriorate because of the water presence / flux the diffusivity along the interfaces might also change differently from the way in the bulk adhesive. Epoxies are usually harder than silicones and except for the offset influence due to the consequent thermal stress coupling upon heat cure, Epotek H77 was the only adhesive considered performing well enough, but only for a limited temperature range concerning water tightness.

Since polymers are attractive to use in microsystems for many reasons but have the drawback of high water diffusivities a number of ways has been identified to reduce or delay the amount of water that arrives at critical places. They are all based on delay / diversion by introduction of phase barriers and moisture traps. For instance soft coatings are often attractive because they do not introduce high stresses. However, their water diffusivities are often high due to open structure etc. In that case it has been demonstrated that this problem can be reduced by applying a thin delay layer of a less water penetrable polymer (10 μm Parylene C on top of Macromelt). The most effective diversion phase barrier is air. The idea of using structured polymer surfaces for water capture and diversion by capillary condensation and subsequent diffusion is new. For e.g. square (bottom and side walls) cavities the most effective capture geometries are those with low concave edge angle α and wetting angle θ. Largest amounts are captured at RH very close to 100 %.

Stress which is strongly dependent on water in-diffusion is a very important factor influencing microsystem reliability. Thus, it may lead to adhesive / coating delamination, unstable offsets, accelerated corrosion etc. It can be minimized by controlling the water content in the polymers, use of e.g. DSC, DOE and polymers with the glass transition temperature T_g outside the application temperature interval.
Due to mechanical changes at T_g it is generally recommended to choose adhesives with T_g outside the application temperature interval. If silicone is chosen it will typically be best if T_g is below the application temperature interval. Though, in this case it is not critical that T_g is below the application temperature interval because the adhesive is soft and is not changing much regarding this property on passage of T_g. If an epoxy is chosen it may be important that T_g is high enough that it is never passed in the application. Otherwise it might soften significantly, loose strength and / or bonding and significant stress coupling changes may be observed. If the adhesive is not getting too soft on heating above T_g, it may sometimes be observed that the passage results in higher bond strength. This is due to the fact that thermal stress disappears completely or partly when the adhesive soften and / or the temperature approach the cure temperature.

Surface and adhesive / coating preparation can enhance bond strength and lifetime of the bonds between them significantly. The positive effect of surface preparation has been demonstrated clearly by titanium surface cleaning and priming experiments using the silicone DC Q3-6611. There is around 400 % difference in bond strength between the best and worst cleaning / priming procedure. For the best procedure the bond strength exceeds the adhesive cohesive strength of about 4 N/mm^2.
The strongest and most durable bonds are of the covalent chemical type. However, Van der Wall's adsorption bonds are also strong and durable.
From the thermodynamic adhesion theory it can be shown that the work of adhesion (bond strength) in dry and wet environment is at maximum when the ratio of the dispersive and polar contributions to the adhesive surface tension is equal to the ratio of the dispersive and polar contributions to the substrate surface tension. Also, from the adsorption theory it is clear that a large substrate to adhesive / coating surface tension ratio is an indication that good adhesion can be achieved because this ensures good

surface wetting / contact. The above mentioned surface preparation experiments seem to confirm both these results from the adsorption theory.

Using polymers for microsystem protection by coating, it has been shown and explained theoretically that how well the coat surface follow the topology of the microsystem and therefore how thin the coat can be, largely depend on the uncured polymer surface tension. Besides being important for proper microsystem protection, the conformity also ensures good adhesion on structured surfaces by the inherent better mechanical grip.
Surface tension turns out to be a driving force away from conformal coating i.e. the polymer surface tension should preferably be as low as possible. However, it can also be too low and / or the microsystem is too big since the degree of conformity of coatings to structured surfaces can be shown to be determined by the balance between the surface tensions and gravity forces etc.
On a surface the liquid surface free energy G or area A will be at the minimum corresponding to the situation of forces acting on the liquid. The liquid will move away from convex corners and edges to concave corners and edges. The freer the liquid is the smaller A is and the less the mean curvature H will vary from place to place. This behavior has proven very useful in the precise control of adhesive distribution in microsystem assembly.
Conformal layers of polymer coatings containing metal flakes can by applied on microsystems and effectively protect them against EMI.

Failure analysis
Special equipment and analysis methods are needed for studying microsystem materials reliability.
To judge the reliability of microsystems incorporating polymer water barriers it is as stated above important to find the water diffusion constants by carefully solving the diffusion equation corresponding to adequate test samples. It is further possible to make mass spectrometer leak rate measurements to see how much water actually penetrates to critical areas in situations close to the reality.
SAM is a powerful non-destructive materials characterization and failure analysis tool for microsystems. The feasible determination in SAM of the sound pulse reflection coefficient R, the number N of equal sound pulse reflection sequences in theoretical A-scan amplitudes and the acoustic impedances Z, is of high importance in analyzing adhesion of adhesives and coatings.
The amplitude sign in A-scans is determined by the sign of R at bond interfaces and directly reveals adhesive / coating bond integrity to substrates.
In case there are many thin (say below 50 μm) layers interpretation of the A-scans gets complicated by overlapping amplitudes of different phases and it may be difficult to detect adhesive / coating delamination. The calculation of N may facilitate the interpretation of the A-scans in such cases.
In both these cases it is of cause of paramount importance to use the expression for R which has been demonstrated to be correct.
Determination of Z for the adhesive / coating may reveal if the material is fully cured or uniformly distributed which are a prerequisites for optimal adhesion. It may also reveal stresses which may lead to bond failure.

Based on the thesis the outlook for the subject is:

Outlook

Looking ahead with the appearance of continued miniaturization to NEMS sensors scales are reduced from 1-100 μm to 1-100 nm making packaging issues like system design and the kind of analyses reported in this thesis and new to come even more crucial for their reliability. The delay of scientific attention seems not to be repeated for this next generation of sensors where packaging is already having a scientific reputation.

In the years to come some of the most important packaging activities will be in the areas of Wafer Level Packaging (WLP), System In Package (SIP), lead free electrical interconnect, optical interconnection, and nano-packaging.

In the future polymer adhesives and coating materials as assembly and protective barrier materials are expected to play a less important role in nano-packaging close to e.g. nano-sensing elements due to the lack of sufficient tightness. Metals are probably going to be used here instead. They can be applied very accurately by vacuum techniques like PVD or FIB's. However, it is anticipated that polymer adhesives and coating materials as assembly and protective barrier materials will still be widely used due to the necessary nano-micro integration, perhaps even more than now.

5 APPENDIX – THESIS PUBLICATIONS

Paper 1

R. de Reus, C. Christensen, S. Weichel, S. Bouwstra, J. Janting, G. Friis Eriksen, K. Dyrbye, T. Romedahl Brown, J.P. Krog, O. Søndergård Jensen, P. Gravesen

Reliability of industrial packaging for microsystems

Microelectronics Reliability 38 (1998) 1251-1260

PERGAMON

Microelectronics Reliability 38 (1998) 1251–1260

MICROELECTRONICS RELIABILITY

Reliability of industrial packaging for microsystems

R. de Reus [a,1], C. Christensen [a], S. Weichel [a], S. Bouwstra [a], J. Janting [b], G. Friis Eriksen [b], K. Dyrbye [b], T. Romedahl Brown [b], J.P. Krog [c], O. Søndergård Jensen [c], and P. Gravesen [c]

[a] *Mikroelektronik Centret, DTU bldg. 345-east, DK-2800 Lyngby, Denmark*

[b] *Grundfos A/S, DK-8850 Bjerringbro, Denmark*

[c] *Danfoss A/S, DK-6430 Nordborg, Denmark*

Abstract

Packaging concepts for silicon-based micromachined sensors exposed to harsh environments are explored. By exposing the sensors directly to the media and applying protection at the wafer level the packaging and assembly will be simplified as compared to conventional methods of fabrication.

Protective coatings of amorphous silicon carbide and tantalum oxide are suitable candidates with etch rates below 0.1 Å/h in aqueous solutions with pH 11 at temperatures up to 140 °C. Si–Ta–N films exhibit etch rates around 1 Å/h. Parylene C coatings did not etch but peeled off after extended exposure times at elevated temperatures. The best diamond-like carbon films we tested did not etch, but delaminated due to local penetration of the etchants.

Several glue types were investigated for chip mounting of the sensors. Hard epoxies, such as Epo-tek H77, on the one hand exhibit high bond strength and least degradation and leakage, but on the other hand introduce large sensor output drift with temperature changes. Softening of the Epo-tek H77 was observed at 70 °C.

An industrially attractive thin-film anodic silicon-to-silicon wafer bonding process was developed. Glass layers are deposited at 20 nm/s (1.2 μm/min) by electron-beam evaporation and bond strengths in excess of 25 N/mm^2 are obtained for bonding temperatures higher than 300 °C.

Through-hole electrical feedthroughs with a minimum line width of 20 μm and a density of 250 wires per cm were obtained by applying electro-depositable photo-resist. Hermetically sealed feedthroughs were obtained using glass frits, which withstand pressures of 4000 bar.

1 Introduction

Due to the large diversity in micromachined sensor applications, to date no generic packaging concepts exist. In many occasions chip packaging is not an integral part of the chip design. With a few exceptions, packaging is bulky and performed at chip level, usually resulting in complicated and labor-intensive assembly [1].

Conventional packaging of silicon sensors for aggressive media applications involve stainless steel housings, silicone oil filling, and steel membrane seals to avoid direct exposure of the sensor to the environment. By exposing the sensors directly to the media the packaging volume and assembly costs may be reduced considerably. Such an approach requires adapted sensor designs, wafer-level protective coatings, and reliable chip mount techniques and materials.

This paper reviews the work of an industrial collaboration toward reliable packaging concepts for silicon sensors exposed to harsh environments.

[1] e-mail: reus@mic.dtu.dk

0026-2714/98/$ – see front matter.
PII: S0026-2714(98)00149-8

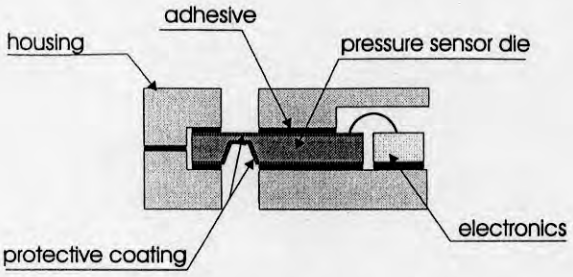

Fig. 1. Cross-sectional drawing of a differential pressure sensor directly exposed to the media. The sensor chip is coated at both sides and mounted in a housing using adhesives.

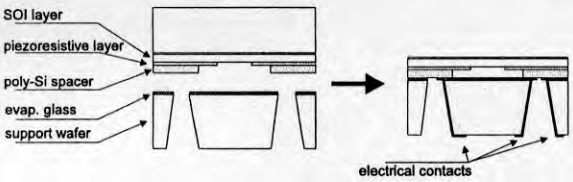

Fig. 2. Flat-surface absolute pressure sensor concept. Poly-silicon piezoresistors and spacers are deposited on an SOI-wafer and anodically bonded to a support wafer. After KOH-etching the SOI device layer forms the membrane and a flat surface is obtained. Electrical contacts are accessible through the holes in the support wafer.

2 Sensor and packaging concepts

Several approaches to packaging of silicon sensors for harsh environments are under investigation. The most straightforward method is shown in Fig. 1. Based on a conventional piezoresistive differential pressure sensor, only small alterations to the pressure sensor design itself are required. The bond pads are all positioned at one end of the sensor die. This creates free surface area for adhesive mounting of the chip in a metal housing and facilitates hybrid integration with integrated circuitry. The sensor is exposed directly to the environment via holes in the housing and must therefore be protected with a coating at both sides prior to chip mounting. Packaging induced stress, penetration of the media through the adhesive and the lack of availability of a suitable coating material are key obstacles for a successful industrialisation of this concept.

Because poor step coverage of the thin (less than 1 μm) protective coating turns out to be a critical issue, the second concept aims at creating a flat-surface sensor. We reported on such a pressure sensor type earlier [2]. Here we present a new

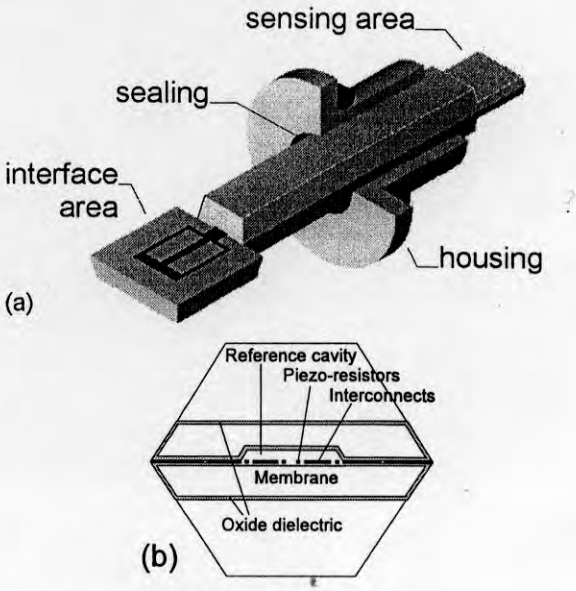

Fig. 3. Drawing of the 'needle sensor' concept (a). The interface area is separated from the medium by a hermetic sealing to the housing. The width of the sensor is typically 1 mm. (b) Cross-sectional drawing of the sensing area showing the bonded wafers, membrane, reference cavity, and integrated interconnects.

type of absolute pressure sensor (single-sided, see Fig. 2). A piezoresistive layer and poly-Si spacers are deposited onto an SOI-wafer and patterned. The spacer layer contains electrical interconnects and is anodically bonded to a support wafer. Access to the poly-Si contacts is provided via contact holes in the support wafer. The substrate-Si of the SOI wafer is then removed by wet chemical etching, leaving the SOI device layer as membrane. The buried oxide serves as etch stop layer and yields a smooth surface suitable for protective coatings which otherwise would suffer poor step coverage. Further advantages of this sensor design are that the active sensing areas are at the backside of the membrane and that electrical contacts are provided at the backside of the sensor. To minimize the chip area and to maintain a rigid support a single contact hole with multiple electrical feedthroughs is preferred. A further challenge is the wafer bonding process to poly-Si. An elaborate paper on the fabrication and characterization of this sensor will be published elsewhere [3].

The innovative 'needle sensor' concept is presented in Fig. 3. This very small sensor (lateral dimensions of the sensor head are 1×1 mm^2) integrates the packaging concept and electrical

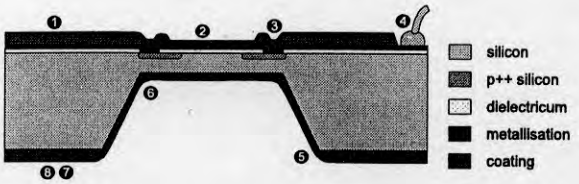

Fig. 4. Requirements for protective coatings. A cross section of a typical piezoresistive pressure sensor is shown. Several critical properties for the coating are identified. Refer to the text for an explanation of the running numbers.

feedthroughs in the device. As in the concept mentioned above, the electrical active parts of the sensor are 'inside' the sensor at the backside of the membrane. Specific challenges to produce this sensor are wafer bonding, a conformal sensor coating of the three-dimensional structure and hermetic sealing between sensor and housing.

In the following section we report on the materials and processes required to accomplish the packaging concepts mentioned above.

3 Materials

3.1 Protective coatings

Protective coatings applied at wafer-level reduce requirements on packaging and assembly. Applying protective coatings as a solution to the sensor concept shown in Fig. 1 requires a number of properties for the coating. In Fig. 4 a number of requirements is identified:

(1) Corrosion resistance: the maximum allowable thickness of the coating and minimum required lifetime sets the upper limit of the etch rate in the media of interest.
(2) Low residual stress and small thickness: to limit the reduction of sensitivity due to stiffness changes in the membrane. Also, a high tensile stress may result in cracking of the coating. Furthermore, the adhesion of the coating, sensor performance, and electrical properties of interconnects may be affected by high stress levels.
(3) Step coverage: poor coverage over interconnects and contact windows are sites where degradation of the sensor will initiate.
(4) Patternable: in many cases it is desired to pattern the protective coating for access to bond pads. Patterning in a batch process, such as wet etching, is preferred.
(5) Coverage of sharp corners: a conformal coating is required.
(6) Coverage of deep cavities: a conformal coating is required down to the bottom of the cavity.
(7) Pinhole density: usually no pinholes are allowed in the exposed area of the sensor. Etchants will penetrate the coating and degrade electrically active components or underetch, eventually resulting in an undesired lift-off of the coating. In case the pinholes are due to particulate contamination, the pinholes may be eliminated by growing thicker films.
(8) Electrical properties: a dielectric film is required to insulate electrical components on the sensor from electrically conducting media.

Furthermore, good adhesion and good diffusion barrier properties are desired. Although the above requirements all are essential, corrosion resistance (1) and low pinhole density (7) may be most important, since these properties cannot be circumvented by alternate sensor designs or materials combinations.

Protection against acidic environments usually is not a problem and conventional materials from semiconductor industry can be used to encapsulate, a.o., metal lines on silicon substrates, which do not etch in, e.g. hydrofluoric acid [4].

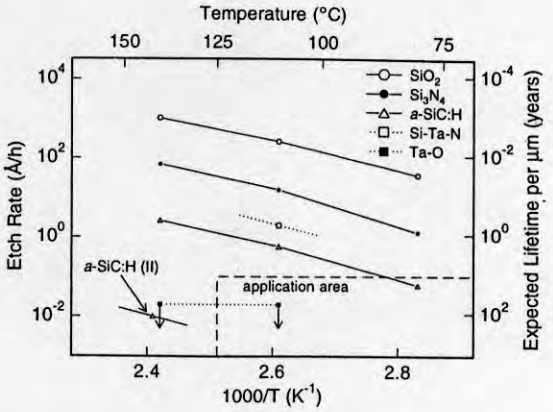

Fig. 5. Etch rates of several coating materials in alkaline solutions. Data points connected with solid line pH 11, dotted line pH 13. The application window is marked. For Ta–O only an upper limit of the etch rate is given (indicated by arrows) since no detectable loss occurred after 3 months of exposure.

Alkaline environments form a greater challenge. The specifications for our sensor applications are a minimum lifetime of ten years for maximum film thickness of one micron in alkaline solutions with pH 11 and temperatures up to 125 °C. Other media of interest include refrigerants, lubricants, and hydraulic oils containing additives. The application window is indicated in Fig. 5, which also shows that conventional passivation layers such as silicon dioxide (SiO_2) and silicon nitride (Si_3N_4) do not fulfill our requirements (this work and [4]).

Grain boundaries are expected to be weak points for corrosion resistance, very similar to diffusion barrier performance [5]. Supported by recent investigations [6] we believe that amorphous materials, although metastable, are excellent candidates for corrosion resistant coatings.

Unless stated otherwise, etch rates in the following were determined by measuring film thickness using variable angle scanning ellipsometry (VASE) before and after exposure to the alkaline solutions. To be able to measure etch rates as low as 0.1 Å/h (≈ 0.1 μm/year) exposure times of several months are required.

The best diffusion barrier known from literature is probably amorphous silicon tantalum nitride (a-$Si_xTa_yN_{1-x-y}$) with $x = 0.14$ and $y = 0.36$ [7], combining the inertness of interstitial compounds with an effective blocking of grain boundary diffusion through its amorphicity. This alloy has also been demonstrated as a micromechanical construction material [8]. We investigated reactively co-sputtered a-$Si_xTa_yN_{1-x-y}$ using a Si and a Ta source in an Ar/N_2 ambient. The etch rate of a-$Si_xTa_yN_{1-x-y}$ in a KOH solution (pH 13) at 110 °C was strongly composition dependent and best results of 2 Å/h were obtained for a composition of $x \approx 0.17$ and $y \approx 0.33$, which is close to the composition of the above-mentioned diffusion barrier.

We recently reported [9] on our investigations of amorphous tantalum oxide (a-Ta_xO_{1-x}) with a composition close to that of stoichiometric tantalum pentoxide (Ta_2O_5). The a-Ta_xO_{1-x} films ($x \approx 0.29$) were deposited by DC-reactive sputtering from a Ta target in an Ar/O_2 plasma. Films with a thickness of 500 nm exhibited fewer than 3 pinholes per cm^2. The a-Ta_xO_{1-x} crystallized into Ta_2O_5 upon annealing in O_2 at temperatures higher than 550 °C. Whereas the crystallized films were released from the silicon substrate after only a few days of exposure to a pH 13 solution at 140 °C during accelerated testing, no change in thickness of the a-Ta_xO_{1-x} was observed after exposure to the same solution for 3 months, yielding etch rates lower than 0.02 Å/h (see Fig. 5).

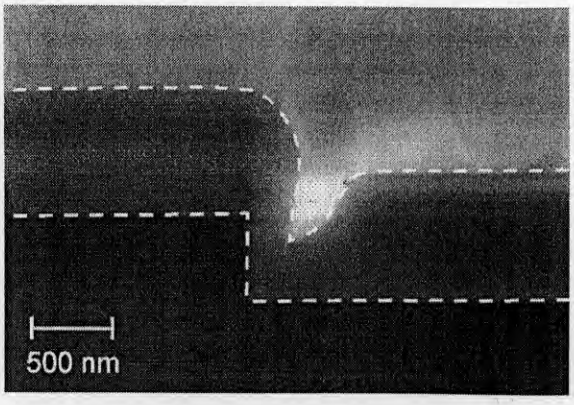

Fig. 6. Cross-sectional scanning electron micrograph showing step coverage of reactively sputtered a-Ta_xO_{1-x} ($T_{dep} = 200$ °C) on an etched Si substrate. The dashed white lines indicate the profile of the a-Ta_xO_{1-x} film.

Although the coverage of sharp corners and deep cavities anisotropically etched in Si(100) is good, the coating is not conformal, as typical for a sputtering deposition process. Such a non-conformal profile is shown in Fig. 6. For this particular case the angle between the substrate surface normal and the Ta target was 45°. If better conformity is required, a metal-organic chemical vapor deposition process may be the solution.

Another important feature of the a-Ta_xO_{1-x} films is that the residual stress can be controlled by annealing. As can be seen in Fig. 7, the compressive stress of 200 MPa of samples deposited at RT can be eliminated by annealing 30 min in oxygen at temperatures slightly higher than 400 °C. This temperature is below the crystallization temperature of the amorphous oxide, thus maintaining the excellent etching and adhesion properties of the film. Other advantageous properties of a-Ta_xO_{1-x} include the possibility of patterning the film by etching in concentrated hydrofluoric acid solutions, a high dielectric strength in excess of 3×10^6 V/cm, as well as biocompatibility.

Hydrogenated amorphous silicon carbide (a-SiC:H), obtained from third parties through a commercially available plasma-enhanced chemical vapour deposition (PECVD) process [10] appears to be an excellent coating as well. Initial

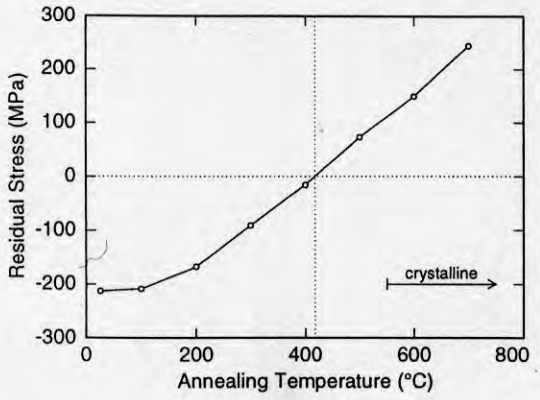

Fig. 7. Residual thin-film stress for a-Ta_xO_{1-x} films (T_{dep} = 20 °C) on Si(100) after post-annealing in 1 bar O_2 for 30 min at the temperatures indicated. After annealing at temperatures slightly above 400 °C stress-free films are obtained, whereas crystallization of a-Ta_xO_{1-x} into Ta_2O_5 first occurs above 550 °C.

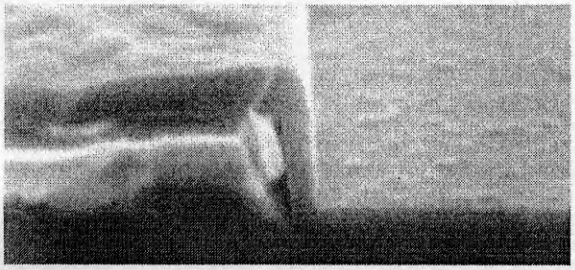

Fig. 8. Cross-sectional scanning electron micrograph showing perfect step coverage of a-SiC:H over a poly-Si interconnect on a Si substrate. The a-SiC:H is 0.2 μm thick and was deposited by PECVD.

measurements [4] showed that the etch rates in pH 11 at 75 °C were sufficiently low (see also Fig. 5). By modifying the PECVD process we were able to reduce the etch rate by more than two orders of magnitude. An etch rate of 0.01 Å/h at 140 °C was determined. The modified material is indicated in Fig. 5 as a-SiC:H(II).

The excellent conformal coating properties of the a-SiC:H PECVD process are depicted in Fig. 8, which shows a cross section of a-SiC:H over a poly-Si interconnect line. Details on this work will be published elsewhere [11].

A (large) number of diamond-like carbon (DLC) films was obtained from several vendors. Although the best DLC films did not etch detectably in pH 11 solutions at 140 °C, we observed, without exception, that the alkaline solution penetrates the film locally. The result is that the DLC

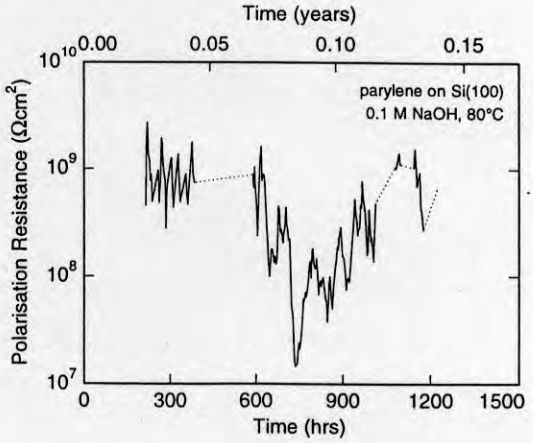

Fig. 9. Polarisation resistance of parylene C on Si(100) as a function of exposure time to a 0.1 M NaOH solution at 80 °C. A polarisation resistance higher than 10^9 Ωcm^2 usually indicates 'no etching'.

films peel off from the silicon or oxidized silicon substrates within a couple of days.

Parylene C is well-known for its passivation behavior. An *in situ* determination of the etch rate of dielectric films was performed by electrochemical measurements similar to those presented by the Motorola group [12]. The ion flux through the coating relates directly to the polarisation resistance. A polarisation resistance higher than 10^9Ωcm^2 represents totally inert films.

A typical polarisation resistance measurement of a parylene C coating in a 0.1 M NaOH solution at 80 °C is shown in Fig. 9. Although variations in the measurements occur, the resistance recovers to its initial value of about 10^9 Ωcm, confirming the inertness of the parylene C films.

We observed no degradation of 4 μm thick parylene C films on Si after exposure to a 0.1 M NaOH solution at RT for three months. Similar films exposed to the same solution at 80 °C seem not to etch either, but after maximum three months the coating delaminates, most likely due to penetration of moisture at the interface. Similar undesired lift-off behavior was observed for polyimides. No etching was observed and the typical exposure time to failure is less than one week.

3.2 *Glue: chip mounting of differential pressure sensors*

We determined the properties of a number of glues and tested the suitability of the most promis-

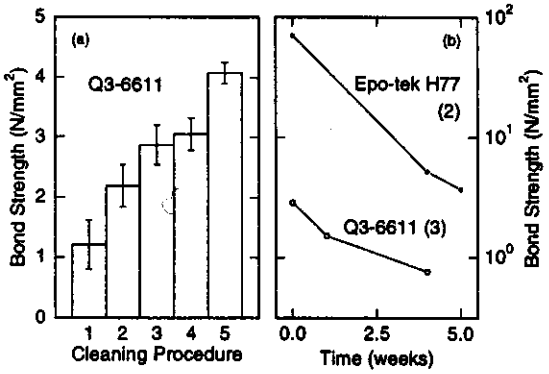

Fig. 10. (a) Bond strength (average of 10 measurements) of Q3-6611 glue directly after gluing for various surface cleaning procedures (see text). Note that the variation in bond strength becomes smaller with increasing strength. (b) Bond strength for Q3-6611 (cleaning procedure 3) and Epo-tek H77 (procedure 2) after exposure to a pH 11 solution at 95 °C as a function of exposure time.

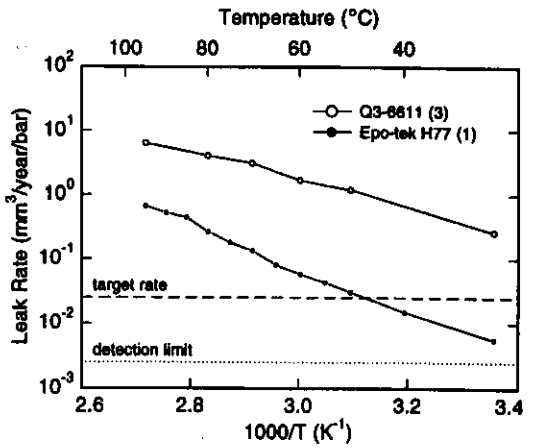

Fig. 11. Leak rates of Q3-6611 silicone glue and Epo-tek H77 epoxy. The Epo-tek H77 was exposed to a pH 11 solution at RT for 18 months prior to the measurements. The dashed line indicates an acceptable leak rate and the dotted line is the detection limit. Cleaning procedures are indicated in brackets.

ing types for chip mounting with the first concept presented in section 2 in mind (Fig. 1). The following glues were selected: Epo-tek H77 epoxy glue (Epoxy Technology Inc.), DM1110HT thermoplastic glue (DieMat), Semicosil 989 silicone glue (Wacker), and Q3-6611 silicone glue (Dow Corning).

Burst pressure tests were performed to determine the bond strength of various glues. $3 \times 4\,mm^2$ dies were glued onto a metal substrate over a hole with a diameter of 2 mm. Pressure was then applied through the hole until the dies were released from the substrate. The influence of the surface cleaning procedure on the bond strength of the Q3-6611 glue is shown in Fig. 10(a). The following cleaning procedures correspond to the numbers in Fig. 10(a):

(1) 2-propanol
(2) soap and 2-propanol
(3) primer
(4) soap, 2-propanol, and primer
(5) soap, 2-propanol, primer, and bake at 150 °C.

From Fig. 10(a) it can be seen that the standard primer for Q3-6611 (treatment 3) is highly effective and the bond strength is only slightly enhanced by soap and propanol cleaning prior to the priming treatment (4). A soap treatment prior to 2-propanol cleaning (2) strongly enhances the effect of 2-propanol cleaning only (1). However, additional baking (5) for several hours at the recommended curing temperature (150 °C) of the Q3-6611 glue yields the highest bond strengths (> 4 N/mm^2). It is also noted that the variation in the bond strength is smaller for higher bond strengths.

Fig. 10(b) shows the degradation of the bond strength for Q3-6611 and Epo-tek H77 due to exposure to a pH 11 solution at 95 °C. The bond strength of the Q3-6611 silicone glue (cleaning procedure 3) is strongly reduced after a few weeks of exposure. Also the bond strength of the Epo-tek H77 (cleaning procedure 2) is reduced. After five weeks of exposure the bond strength has fallen from more than 70 N/mm^2 to less than 4 N/mm^2. The desired bond strength is of course dependent on the bond area and the application, but a minimum value of 4 N/mm^2 is usually required.

Moisture which penetrates the adhesive bond will eventually deteriorate the electrical circuitry in the sensor housing by corrosion. To ensure a sensor system lifetime of 10 years, a maximum leak rate of 2.5×10^{-2} $mm^3/year/bar$ is allowed. A highly sensitive test-rig was built in which the leak rate of heavy water is measured by quadrapole mass spectrometry with a detection limit of 2.5×10^{-3} $mm^3/year/bar$.

Chips ($5 \times 7.5\,mm^2$) were glued on a substrate with a hole (2 mm in diameter). The leak rate of Q3-6611, measured directly after gluing using preparation method 3, is higher than the acceptance level for all temperatures ranging from RT to

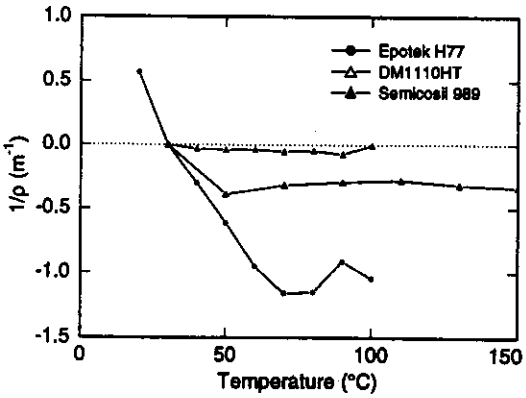

Fig. 12. Curvature $1/\rho$ of mounted Si chips on Al_2O_3 thick film substrates. The measurement at 30 °C is taken as reference. Glue types are indicated.

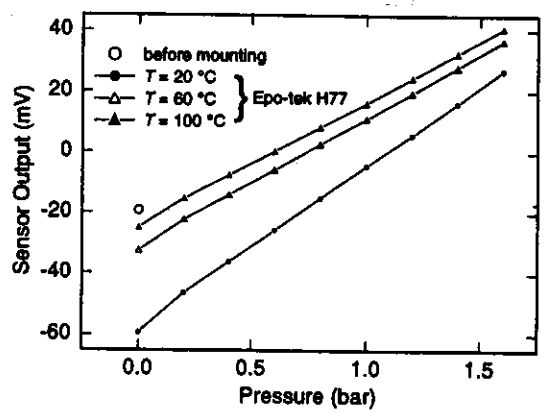

Fig. 13. Output of a piezoresistive pressure sensor before and after mounting using Epo-tek H77 (5 V bias applied). Gluing of the sensor introduces a large offset. We observe an offset drift with temperature change. The drift is strongly reduced for $T > 70$ °C, when the glue softens.

95 °C (see Fig. 11). The leak rate of water through Epo-tek H77 (cleaning procedure 1) is lower than the detection limit of our system. However, after exposure to a pH 11 solution at RT for 18 months, the leak rate of the Epo-tek H77 is above the detection limit but below the target rate for temperatures up to 50 °C (see Fig. 11). Improvements are required to fulfill our specifications.

Chip curvature measurements were performed using an optical surface profiler. Changes in the curvature are related to stress induced by the die attach. A typical situation, where a 350 μm thick silicon chip was glued onto a thick-film Al_2O_3 substrate, was investigated. The curvature, $1/\rho$, was determined from curvature difference measurements with the data collected at 30 °C as reference. In Fig. 12 the results are shown for three types of glue. A negative sign of $1/\rho$ corresponds to compressive stress. The soft silicone glue Semicosil 989 does not introduce considerable bending when the temperature is raised. The DM1110HT thermoplast is slightly harder and introduces additional chip bending for temperatures up to 50 °C, where the glue softens. The hard epoxy, Epo-tek H77, influences the chip curvature most with a change in $1/\rho$ of -1.75 m^{-1} between RT and 70 °C. Above this temperature $1/\rho$ does not change significantly due to softening of the glue.

Not shown is the effect of humidity and moisture absorption in Epo-tek H77. Thin-film stress was measured by wafer curvature difference measurements of a 100 μm thick Epo-tek H77 layer on a silicon wafer. Absolute values of 8 MPa and 2 MPa (tensile stress) were measured for dry (annealed) samples and samples exposed to ambient for one week, respectively. The relaxation time of the moisture absorption process is a few days and the measurements are reversible in the temperature range RT–150 °C.

The influence of chip mounting using Epo-tek H77 glue on pressure sensor performance is shown in Fig. 13. The sensor system was as shown in Fig. 1. Before mounting a sensor offset of −20 mV (using a 5 V bias) was measured at RT (open circle). After mounting the offset changes to −60 mV (closed circles). An offset drift with temperature change is observed. The temperature drift is strongly reduced for temperatures above 70 °C. Below this temperature a small change in sensitivity occurs as well, as can be seen by the change in slope of the data collected at 20 °C and 60 °C, respectively. These observations are in agreement with the curvature measurements above, where we observed softening of the glue around 70 °C.

3.3 *Thin-film anodic wafer bonding*

Wafer bonding processes reduce the need for chip-scale handling and are used to actually form devices (such as the sensor shown in Fig. 2) as well as for back-end processing to encapsulate devices. Anodic bonding is an attractive method due to its relatively low required temperatures (< 450 °C) and silicon-to-glass bonding is frequently

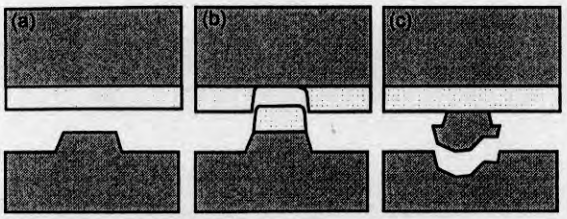

Fig. 14. Typical fracture behaviour of thin-film anodically bonded wafers. A structured wafer is bonded to a glass coated wafer (a) and then subjected to pull test. Fracture occurs either in the glass (b) or the silicon structure (c). Fracture at the bond interface is not observed.

applied (see e.g. Refs. [13] and [14]). Compared with silicon-to-glass bonding major advantages of silicon-to-silicon wafer bonding using thin films are (1) the elimination of differences in thermal expansion between the two wafers and (2) strongly enhanced functionality and the formation of truly 3-dimensional structures by joining highly micromachined and processed wafers.

The glass layers required for thin-film wafer bonding are usually deposited by sputtering [15]. We developed a bonding process for silicon to silicon using evaporated glass layers [16,17]. The deposition rates of the evaporated glass are approximately 20 nm/s (1.2 μm/min), which is three orders of magnitude higher than for sputter-deposited glass. This is in favor of industrial applications, since glass thicknesses of several microns are required for a reliable bonding process.

The typical fracture behaviour of anodically bonded structures using the evaporated glass is shown in Fig. 14. A cross section of a structured and a glass-coated wafer before bonding is shown in Fig. 14(a). After bonding and pull testing it is observed that fracture either occurs in the glass (Fig. 14b) or in the micromachined silicon structure (Fig. 14c). Fracture at the bond interface occurs rarely.

The bond strengths of the thin-film anodic bonding were determined by pull testing after bonding at various temperatures (see Fig. 15). Each data point is averaged over more than 50 samples from several bond experiments, resulting in a typical variation of 5 N/mm^2. We were not able to achieve bonding below 200 °C. From 200 °C to 300 °C the bond strength linearly increases to a value of approximately 25 N/mm^2 and saturates at higher bonding temperatures. Above 225 °C the bond yield is better than 90%.

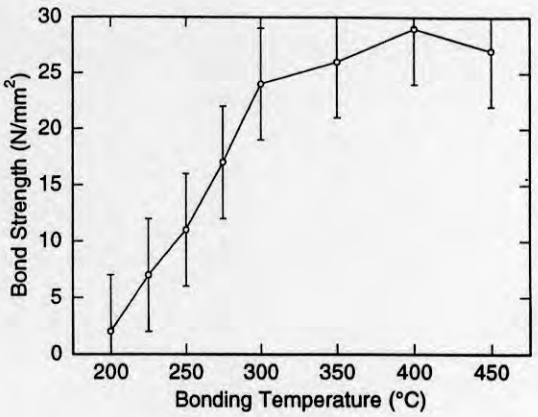

Fig. 15. Bond strength of the thin-film anodic bond as a function of bonding temperature. Bonding is achieved above 200 °C and the bond strength saturates around 300 °C. Each point is averaged over more than 50 samples from several bonding experiments. The typical standard deviation is 5 N/mm^2.

Further, we have shown [18] that not only residual stress in the glass layer, but also small temperature gradients during bonding on the order of a few degrees centigrade strongly influence the curvature of the bonded structures.

3.4 *Feedthroughs*

To obtain the hermetic seals required for mounting of the needle sensor (see Fig. 3) we used glass frits which were customized to match the thermal expansion of silicon. Temperatures of 650 °C were required to obtain hermetic seals. This temperature is much higher than the eutectic temperature of the glass frit and is incompatible with most metallization schemes. The mounted sensors withstood burst pressure tests up to 4000 bar. Furthermore, we subjected the mounted sensors to thermal shock test. After 30 000 cycles from −40 to 120 °C no leakage was observed at RT.

A novel interconnection technique compatible with standard semiconductor processes was developed [19,20]. The technique uses electrodeposited photoresist (Eagle 2100ED by Shipley Europe Ltd.) and provides high vertical wiring densities for wafer through-hole interconnects and into deep cavities. An example of the through-hole interconnects is shown in Fig. 16. The size of the holes in the 350 μm thick Si(100) wafer is 1 × 1 mm^2. The wires consist of Ti/Au with

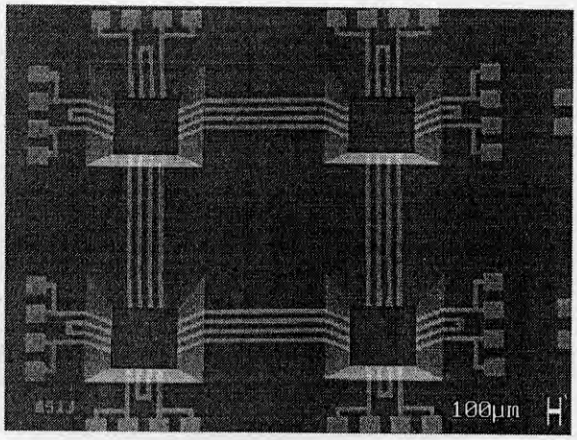

Fig. 16. Multiple vertical electrical feedthroughs. The size of the holes is 1 × 1 mm^2. The line width of the Ti/Au (20 nm/400 nm) wires is 50 μm.

thicknesses of 20 nm/400 nm and are 50μm wide. Reliable through-hole electrical feedthroughs were obtained for line widths down to 20 μm and a density of 250 wires per cm.

4 Conclusions and perspectives

Three concepts for micromachined silicon-based sensors exposed to harsh media are presented and their required technologies were investigated.

Innovative materials are required since conventional chemical resistant layers such as Si_3N_4 do not offer sufficient protection against highly alkaline environments. The protective coatings *a*-Ta_xO_{1-x} and *a*-SiC:H fulfill the requirements for corrosion resistance of 1 μm per 10 years in a pH 11 solution at 125 °C with etch rates around 10^{-2} Å/h. *a*-$Si_xTa_yN_{1-x-y}$, an excellent amorphous diffusion barrier in metallization schemes, exhibits etch rates of approximately 2 Å/h in a narrow composition range around $x = 0.17$ and $y = 0.33$. DLC films apparently do not etch, but delaminate due to local penetration (through pinholes) of the etchant. Delamination after exposure to the media for several hours to days, is the typical failure mechanism we observed for crystalline Ta_2O_5 and a number of polymer coatings, including parylene C.

Several types of glue and their suitability as die attach were investigated. The bond strength of Q3-6611 silicone glue can be improved by extended curing procedures. Bond strengths of Q3-6611 and Epo-tek H77 epoxy are strongly reduced after exposure to pH 11 solutions at 95 °C for several weeks. Leak rates of Q3-6611 are on the order of 1 mm^3/year/bar. Leak rates of Epo-tek H77 are below the detection limit of 2.5×10^{-3} mm^3/year/bar directly after gluing and increased after exposure to a pH 11 solution at RT for 18 months. The target leak rate of 2.5×10^{-2} mm^3/year/bar was obtained below 50 °C. The Epo-tek H77 softens around 70 °C, which is also the temperature above which sensor offset drift is strongly reduced. Glass frits were successfully applied to hermetic sealing of the needle sensor.

Furthermore, we developed a thin-film anodic wafer bonding process using evaporated glass with high deposition rates (20 nm/s) and bond strength (> 25 N/mm^2) for bonding temperatures above 300 °C. Through-hole electrical feedthroughs were obtained using electro-depositable photoresist. Wire densities of 250 wires per cm and line widths down to 20 μm were obtained.

It is expected that a combination of technologies presented in this paper leads to generic total packaging solutions for sensors exposed directly to harsh environments.

Acknowledgements

The authors greatly acknowledge Prof. Dr. K. Najafi (Mikroelektronik Centret, on leave from the University of Michigan, Ann Arbor, U.S.A.) for his critical reading of the manuscript. P.E. Andersen (Grundfos A/S) is thanked for the many helpful discussions. Technical support was provided by P.N. Egginton and F. Jensen (Mikroelektronik Centret), and P. Brandt (Danfoss A/S). M. Lindahl, J. Kuhmann (Mikroelektronik Centret), P. Kersten (present address: Photo Print Electronic GmbH, Schopfheim, Germany) and S. Henke (present address: Angewandte Display-Technologie GmbH, Stuttgart, Germany) participated at an early stage of the project. We would like to thank Dr. S. Gasser and Prof. Dr. M.-A. Nicolet (Caltech, Pasadena, U.S.A.) and Dr. W. Olthuis (MESA Institute, Technical University of Twente, The Netherlands) for providing us with the first Si–Ta–N and Ta–O test samples, respectively. This work was supported by the 'Materials for Advanced Micromechanical Packaging' program, under the Materials Development Program supported by the Danish Agency for

Trade and Industry, The Danish Natural Science Research Foundation, and the Danish Technical Science Research Foundation.

References

[1] Dyrbye K, Brown TR, and Friis Eriksen G. Packaging of physical sensors for aggresive media applications. J. Micromech. Microeng. 6 (1996) 187–192. Invited paper at Micromechanics Europe 1995 (September 1995, Copenhagen, Denmark).

[2] Jensen OS and Gravesen P. A new piezoresistive pressure transducer principle with improvements in media compatibility. J. Micromech. Microeng. 6 (1996) 105–107.

[3] Friis Eriksen G, Dyrbye K, Weichel S, and de Reus R. An SOI-based flat surface pressure sensor. In preparation.

[4] Eriksen GF and Dyrbye K. Protective coatings in harsh environments. J. Micromech. Microeng. 6 (1996) 55–57.

[5] de Reus R. Thin-film diffusion barriers. In: Westbrook JH and Fleischer RL (eds), *Intermetallic Compounds—Principles and Practice*, vol 2: Practice, chap 29, pp 603–635. John Wiley & Sons Ltd., Chicester, UK, 1994.

[6] Andersen P. Protection of micromechanical pressure sensors with metallic glasses. Ph.d. thesis, University of Aarhus, Århus, Denmark, 1998.

[7] Kolawa E, Chen JS, Reid JS, Pokela PJ, and Nicolet MA. Tantalum-based diffusion barriers in Si/Cu VLSI metallizations. J. Appl. Phys. 70 (1991) 1369–1373.

[8] Linder C, Dommann A, Staufert G, and Nicolet MA. Amorphous metals as new materials for transducer applications. In: Puers R (ed), *Proceedings of Eurosensors X, the 10th European Conference on Solid-State Transducers*, pp 473–476. Leuven, Begium, September 1996.

[9] Christensen C, de Reus R, and Bouwstra S. Tantalum oxide thin films as protective coatings for sensors. In: *MME'98 Workshop Digest*, pp 248–251. SINTEF, Ulvik in Hardanger, Norway, June 1998. Also submitted to J. Micromech. Microeng.

[10] Klumpp A, Schaber U, Offereins H, Kühl K, and Sandmeier H. Amorphous silicon carbide and its application in silicon micromachining. Sensors and Act. A 41–42 (1994) 310–316.

[11] Friis Eriksen G, Dyrbye K, and Romedahl Brown T. Silicon carbide protective coatings for sensors in alkaline solutions. In preparation.

[12] Bitko G, Monk D, Maudie T, Stanerson D, Wertz J, Matkin J, and Petrovic S. Analytical techniques for examining reliability and failure mechanisms of barrier coating encapsulated silicon pressure sensors exposed to harsh media. In: Chau K and Roop R (eds), *Micromachined devices and components II*, vol 2882 of *Proc. SPIE*, pp 248–258, 1996.

[13] Esashi M. Encapsulated micromechanical sensors. Microsystem Technol. 1 (1994) 2–9.

[14] Dokmeci M, Von Arx J, and Najafi K. Accelerated testing of anodically bonded glass-silicon packages in salt water. In: *1997 International Conference on Solid-State Sensors and Actuators (Transducers '97)*, vol 1, pp 283–286. IEEE Electron Devices Society, June 1997. Chicago, Illinois, U.S.A.

[15] Hanneborg A, Nese M, and Øhlckers P. Silicon-to-silicon anodic bonding with a borosilicate glass layer. J. Micromech. Microeng. 1 (1991) 139–144.

[16] de Reus R and Lindahl M. Si-to-Si wafer bonding using evaporated glass. In: *1997 International Conference on Solid-State Sensors and Actuators (Transducers '97)*, vol 1, pp 661–664. IEEE Electron Devices Society, June 1997. Chicago, Illinois, U.S.A.

[17] Weichel S, de Reus R, and Lindahl M. Silicon-to-silicon wafer bonding using evaporated glass. Sensors and Act. A (1998). In press.

[18] Weichel S, de Reus R, and Bouwstra S. Residual stress in thin-film anodic bonding. In: *MME'98 Workshop Digest*, pp 47–50. SINTEF, Ulvik in Hardanger, Norway, June 1998. Also submitted to J. Micromech. Microeng.

[19] Christensen C, Kersten P, Henke S, and Bouwstra S. Wafer through-hole interconnections with high vertical wiring densities. IEEE Trans. Components Packag. Manufacturing Technol. A 19 (1996) 516–522.

[20] Kersten P, Bouwstra S, and Petersen J. Photolithography on micromachined 3D surfaces using electro-deposited photoresist. Sensors and Act. A 51 (1995) 51–54.

Paper 2

J. Janting, J. Branebjerg, P. Rombach

Conformal Coatings for 3D Multichip Microsystem Encapsulation

Proceedings of the 14. European Conference on Solid-State Transducers August 27-30, 2000, Copenhagen, Denmark, pp. 275-278

Conformal Coatings for 3D Multichip Microsystem Encapsulation

Jakob Janting[1], Jens Branebjerg[1], Pirmin Rombach[2]
[1]DELTA Danish Electronics, Light & Acoustics, Venlighedsvej 4, DK-2970 Hoersholm, Denmark
[2]Microtronic A/S, CAT/DTU, Building 347, DK-2800 Lyngby, Denmark
e-mail: microsystems@delta.dk, http://www.delta.dk

Summary. *Materials and methods for low cost minimum volume protective encapsulation of microsystems have been investigated. Focus has been on a 3D conformal multilayer coating of silicon microphones. Materials with different properties, e.g. insulating and conductive, can be applied and combined as multilayers around the sharp edges of single crystalline silicon giving a protection which can not be matched by a single material. A 50 µm thick insulating layer with volume resistivity above 10^{16} Wcm with a 150 µm thick conductive layer on top is reported to have an EMI damping higher than 55 dB in the 50 MHz to 1 GHz frequency range.*

Keywords: protection, encapsulation, coating, conformal, electromagnetic interference (EMI)

Introduction

Protective encapsulation is often the final step in microsystems manufacturing. The encapsulation makes up most of the volume and much of the price. Therefore, in order to avoid that small and cheap components are getting bulky and expensive, there is a broad interest in materials and processes making it possible to make encapsulations, which are so thin (< 0.25 mm) that they can be termed coatings.

Many microsystems e.g. sensors are fragile and exposed to chemically, physically and electromagnetically hostile environments. Reducing the amount of encapsulation material makes the right choice of materials and methods even more crucial for the lifetime, performance, and cost of the system. In many cases traditional encapsulation materials like glass-filled epoxies and injection / transfer-moulding techniques can not be used due to the implied high pressures and temperatures.

The motivation for this work has been to protect a fragile 3x3x2 mm^3 silicon microphone three dimensionally with a low cost minimum volume coating. Related work has been going on the last 25 years, mainly with focus on how to protect components and conductors on PCB's and in recent years the silicon in microsystems [1-3] in two dimensions with coatings.

Demands

The demands are high for the microphone coating and can be expressed by the following characteristics:

- EMI E-field shielding (> 50 dB)
- Electrical insulation (> 10^{12} Ωcm)
- Pinhole free
- Applicability below total thickness of 0.2 mm
- Materials compatibility
- Chemical / physical durability

Developed coating concept and critical issue

EMI shielding can only be accomplished with conductive materials. Therefore, the first two demands implies a 2-layered coating, the top layer being conductive and the bottom layer insulating to avoid short circuiting (Fig. 1). In this way materials compatibility

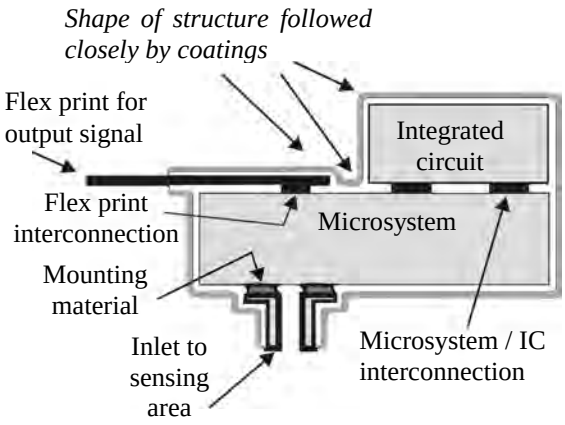

Fig. 1: Coating concept used for the microphone.

becomes a critical issue since materials with very different properties e.g. Thermal Coefficient of Expansion (TCE) may be combined. The required thicknesses and the fragility of the microphone make it critical to achieve pinhole free conformal coverage around the sharp edges on single crystalline silicon edges with gentle techniques.

Results

Selected materials have been tested regarding applicability, volume resistivity, tightness, thickness, conformity, and E-field EMI shielding, to identify the best (Table 1, 2).

Choice of materials

The investigated materials are low viscosity and low surface tension polymers, metal filled polymers and plating solutions.

ISBN 87-89935-50-0

Table 1: Measured first layer materials properties.

Layer configuration	Volume resistivity (10^{16} Ωcm)	Tight	Conformity (Thickness variation / %)
Teflon® AF 1600		Yes	70
Loctite 394	4 ± 2	Not at corners and edges	
TSR 144	6 ± 5	No	

Table 2: Measured damping of different layer configurations.

Layer combination	Thickness (µm)	E-field damping 50 MHz - 1GHz (dB)
Cho-Shield 2052	150	55
Teflon® AF 1600	50	
Leitsilber 200	98	Total: 70 - 90
Cho-Shield 2052	23	
Teflon® AF 1600	80	
Leitsilber 200	36-83	40 - 55
Teflon® AF 1600	50-65	Two samples same damping within 5
Leitsilber 200	30-54	Total: 45 - 70
Teflon® AF 1600	60-66	Three samples
Leitsilber 200	68-104	same damping
Teflon® AF 1600	46-65	within 15
Copper	11	Total: 55 - 65
Leitsilber 200	63	
Teflon® AF 1600	50	
Copper	9	Total: 45 - 55
Leitsilber 200	29	
Teflon® AF 1600	62	
Copper	8	
Leitsilber 200	86	
Teflon® AF 1600	52	

One successful combination of materials is 2 wt.% Teflon® AF 1600 from DuPont dissolved in Fluorinert™ FC 75 from 3M as bottom layer and on top of that Cho-Shield 2052 from Chomerics. Teflon® AF 1600 is an amorphous copolymer of 4,5-difluoro-2,2-bis(trifluoromethyl)-1,3-dioxole and PTFE. The solvent is perfluoro 2-butyltetrahydrofurane. This material was chosen primarily due to its very low surface tension which makes it possible to wet the sharp single crystalline silicon edges. Cho-Shield 2052 is a one component acrylic polymer filled with silver plated copper flakes of max. 40 µm diameter. This material was chosen because of its claimed low electrical resistivity (25-50 Ω/ at 2 mils thickness) and good EMI shielding properties (75 dB in the 20 MHz to 2 GHz frequency range) together with its ease of application.

Other investigated materials have been TSR 144 from TOSHIBA and Loctite 394 from LOCTITE for the first layer and plated / not plated Leitsilber 200 from Degussa-Hüls, ORMECON L5000 from Ormecon Chemie and ConQuest XP 1000 from DSM. TSR 144 is a silicone and Loctite 394 is an acrylate / urethane mixture. Leitsilber 200 consists of small silver particles in a mixture containing acetone and ethoxy propanole. After application acetone and ethoxy propanole evaporates leaving a surface with exposed silver particles. The surface is then easily plated galvanically. This has been done with Cu in saturated $CuSO_4$ solution. The resistivity of Leitsilber 200 is sufficiently low (0.02-0.04 Ω/) for the material to be used as EMI-shield without a plated layer on top. This has not been the case for the intrinsically conductive polymers ORMECON L5000 and ConQuest XP 1000, which are polyaniline and polypyrrole based respectively. These materials were therefore not investigated further.

Choice of processes

All investigated materials can be applied gently by either dipping or spraying and are processed at room temperature. Advantages and disadvantages of these application techniques have been identified to be:

Dipping
- ☺ Simple process
- ☹ Only low viscosity materials can be used
- ☹ Only very low surface tension materials can be used

Spraying
- ☺ Controlled amount of applied material
- ☺ Some poorly wetting (high surface tension) materials can be applied
- ☹ Only low viscosity materials can be applied
- ☹ Shadowing

Teflon® AF 1600 can be applied either by dipping or by spraying. In these investigations it was applied by dipping. Cho-Shield 2052 and Leitsilber 200 can only be applied uniformly on Teflon® AF 1600 by spraying.

Volume resistivity

The insulating properties of first layer coatings have been determined by standard film resistivity measurements in a Keithley 6105 resistivity adapter. Volume resistivities exceeding 10^{16} Ωcm has been measured (Table 1).

Tightness
Pinholes in the insulating layer have been detected by using coated silicon chips (1 cm x 1 cm x 0.5 mm) with a conductor attached with conductive glue, by measuring the resistance through the layer using as contact media either a drop of DI water placed on the surface or a glass of DI water in which most of the chip was dipped. Typical values have been 10^6-10^{10} Ω if the coating was not pinhole free. Values above 10^{12} Ω indicate a pinhole free coating.

Thickness and conformity
In order to determine the conformity and thickness of the coatings microphone demonstrators were moulded in epoxy and cross sections made for microscopy inspection (Fig. 2).

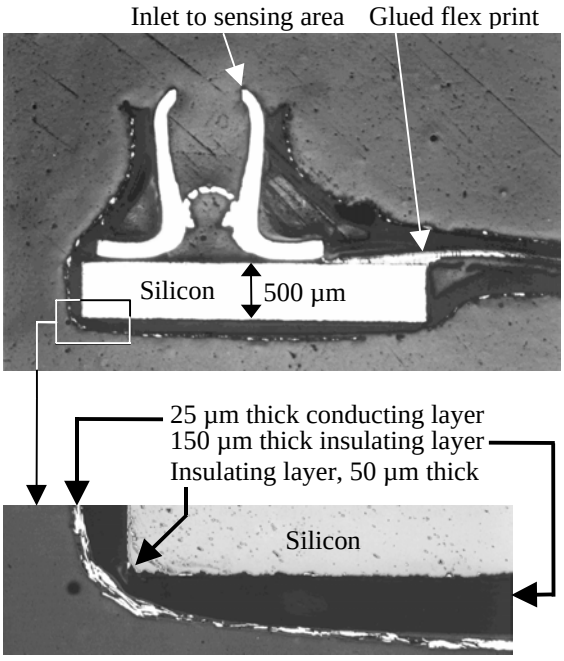

Fig. 2: Cross section of encapsulated microphone demonstrator (top). Close up of coverage at the sharp single crystalline silicon edge (bottom). The insulating layer is Teflon® AF 1600 applied by dipping and the conductive layer is Cho-Shield 2052 applied by hand held spraying.

For the found successful materials combination the total coating thickness is close to 0.2 mm on silicon and the coverage is complete with less than 70% thickness variation.

EMI shielding
The shielding properties were determined on coated antennas of the same size as the microphone according to the Nordtest standard NT ELEC 030 developed at DELTA. The EMI E-field shielding of a 150 µm Cho-Shield 2052 layer on top of 50 µm Teflon® AF 1600 is above 55 dB in the frequency range 50 MHz to 1 GHz (Table 2 and Fig. 3).

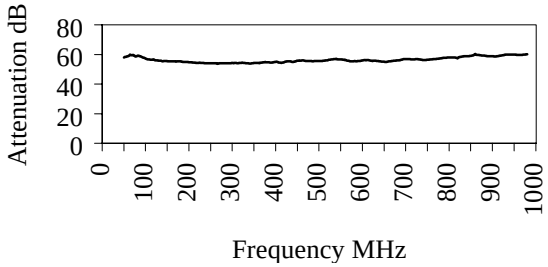

Fig. 3: EMI damping measurement.

The damping of other layer combinations have been investigated (Table 2), and recent measurements show that 70 dB - 90 dB damping is possible by applying one layer of Leitsilber 200 on top of the Teflon® AF + Cho-Shield 2052 layers.

Discussion

The volume resistivity of Teflon® AF 1600 has not been determined, but it is expected to be of the same order as that for PTFE, $\rho_{PTFE} > 10^{18}$ Ωcm because of the chemical resemblance.

Complete coverage of single crystalline silicon sharp edges with the first layer has been the most critical problem to solve. The reason is that the coating material tends to minimise its surface free energy by reducing the surface area to a minimum [4]. At an edge, following the surface contour one unit of length u perpendicular and along the edge changes the coating surface area relatively to the flat regions by $(\pm t/R)u^2$, where t is the coating thickness and R the substrate radius of curvature (Fig. 4). Plus (+) is for convex and minus (-) for concave surfaces.

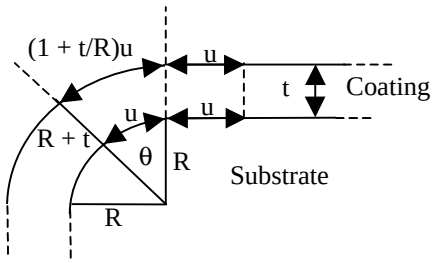

Fig. 4: Geometrical argument for coating surface area per unit substrate length u perpendicular and along a convex edge. The area projected from substrate to coating surface is u^2 in flat regions and $u^2(R + t)\theta = u^2(R + t)/R = (1 + t/R)u^2$ on the curved edge. The area difference is $(t/R)u^2$.

On spherical surfaces (corners) the corresponding area difference is: $A_u((R \pm t)^2\theta - R^2\theta) = A_u(R^2 + t^2 \pm 2tR - R^2)/R^2 = A_u(\pm 2t/R + (t/R)^2)$, where A_u is a unit area. Therefore at corners and edges, changing its thickness by not following the surface contour in three and two dimensions respectively, the coating can save surface free energy. The coating will be thin (fig. 2) in convex regions, which may result in uncov-

ered areas, and thick in concave regions. That is, material will move to concave regions if possible making the coating thick here. Around the inlet in Fig. 2 the coating thickness is therefore >500 µm and another design and optimised application by spraying instead of dipping have to be considered. Using coatings with very low surface tension minimises the energy, which can be saved in these regions and therefore the layer is more conformal. Even with Teflon® AF 1600 at least 5 separate dips were necessary to achieve a complete coverage. Note that the tightness is probably worse than determined here since the contact to silicon through pinholes is dependent on how well the water wets the polymer. This effect might make especially the Teflon® AF 1600 coating coverage seem much more complete than it really is due to its very low critical surface tension $\gamma_{c(\text{Teflon AF 1600})}$ = 15,7 mN/m, which is even lower than that for pure PTFE, $\gamma_{c(\text{PTFE})}$ = 18 mN/m.

Due to the general first layer covering difficulties more complicated and expensive vacuum techniques for deposition of polymers have also been considered. Parylene which is poly(chloro-p-xylylene) is the material which would probably be the best to satisfy the demands [2]. Here monomers of the material condense at the surfaces at low pressure and polymerisation follows. This implies that sharp edges, bond wires etc. can be covered more conformable.

Because of the low critical surface tension of Teflon® AF 1600 difficulties were encountered when attempts were made to coat the Teflon® AF 1600 layer with Cho-Shield 2052 or Leitsilber 200 by dipping or spraying. Though, a uniform coverage can be achieved by spraying because the speed of application can be adjusted for the droplets to cure / dry sufficiently fast upon impact. In this way the retraction of the material because of poor wetting is avoided. The low surface tension of Teflon® AF 1600 is an advantage in case there are still pinholes, since it may prevent the conducting polymer to get in electrical contact with the silicon.

Repetitions of the layer structure, insulator - conductor, have been investigated because the most effective E-field damping takes place at the interface between these layers by reflection. Due to the achieved layer thickness variations the E-field damping efficiency of different layer combinations can not be compared directly. Plated layers were investigated because they have a denser and therefore more tight distribution of conductive crystallites. Galvanic Cu layers were used to explore the effect of a plated layer in an easy way. Electroless plated Ni is preferred since the resulting layer is amorphous and therefore more tight and chemically durable. Besides it is both conductive and ferromagnetic, which means that H-fields are also damped. The drawback for electroless Ni is the instability of the plating solutions.

There has been focused on the initial 5 demands but Teflon® AF 1600 is also a material with very high chemical / physical durability. The chemical inertness and bad adherence of fluorocarbons is due to the strong F bond to the carbon backbone: C-F: 427 KJ/mol. For comparison other similar bond strengths are C-H: 414 KJ/mol, C-C: 335 KJ/mol, C-Cl: 322 KJ/mol. The polymer part of Cho-Shield 2052 however, is an acrylate, which might hydrolyse critically if exposed to a high humidity level for a prolonged period.

Adhesion has not been considered a problem since the coatings are held in place by the 3D structure of the microphone. If necessary perfluorosilanes like 1H,1H,2H,2H-perfluorodecyltriethoxysilane can e.g. be used to enhance the adhesion of Teflon® AF 1600 to silicon.

The materials and methods can easily be used in production. Commercial production equipment for dipping and spraying application exists. Teflon® AF 1600 is the most expensive material investigated, but with a loss of 50% in production the cost per microphone is still below 0.15 €.

Conclusion

Production friendly new materials and methods of applying and combining them have been found for 3D low cost and minimum volume encapsulation of a silicon microphone. The materials and methods comply with the demands and related critical issues.

Generally the concept applies where minimum volume protection against chemical attack, physical attack, fluid penetration and EMI is needed [5]. The choice of materials and methods of application depend on object of encapsulation.

Acknowledgement

This work has been part of projects financially supported by the Danish Agency for Trade and Industry and HISTACK Esprit project No. 25345.

References

[1] Jiali Wu, Randy T. Pike, C. P. Wong. Interface-Adhesion-Enhanced Bi-layer Conformal Coating for Avionics Application. *1999 International Symposium on Advanced Packaging Materials*, 302-310.

[2] C-SHIELD Parylene allows major weight saving for EM shielding of microelectronics. Jan Noordegraaf and Harry Hull. PEP'97, The first IEEE International Symposium on Polymeric Electronics Packaging, 189-196.

[3] R. de Reus, C. Christensen, S. Weichel, S. Bouwstra, J. Janting, G. Friis Eriksen, K. Dyrbye, T. Romedahl Brown, J. P. Krog, O. Søndergård Jensen, and P. Gravesen. Reliability of industrial packaging for microsystems. *Microelectronics Reliability* **38** (1998) 1251-1260.

[4] T. Bieker, S. Dietrich. Wetting of curved surfaces. *Physica A* **252** (1998) 85-137.

[5] DELTA. Encapsulation for a three dimensional microsystem. Patent pending PA199901428.

Paper 3

M. Müllenborn, P. Rombach, U. Klein, K. Rasmussen, J.F. Kuhmann, M. Heschel, S. Bouwstra, M. Amskov, J. Janting, A. Hoogerwerf

Stacked Silicon Microphones

Proceedings of the 14. European Conference on Solid-State Transducers August 27-30, 2000, Copenhagen, Denmark, pp. 209-212

Stacked Silicon Microphones

M. Müllenborn[1], P. Rombach[1], U. Klein[1], K. Rasmussen[1], J. F. Kuhmann[2], M. Heschel[2], S. Bouwstra[2], M. Amskov[3], J. Janting[3], A. Hoogerwerf[4]
[1]Microtronic A/S, CAT/DTU, Building 347, DK-2800 Lyngby, Denmark
[2]MIC/DTU, Building 345 East, DK-2800 Lyngby, Denmark
[3]DELTA, Venlighedsvej 4, DK-2970 Hørsholm, Denmark
[4]CSEM, Jaquet-Droz 1, CH-2007 Neuchâtel, Switzerland
e-mail: mm@cat.dtu.dk http://www.microtronic.org

Summary. *This paper presents results on the first silicon microphones that are completely batch-packaged and integrated with signal conditioning circuitry in a chip stack. The chip stack is designed to be directly mountable into a system, such as a hearing instrument, without further single-chip handling or wire bonding. The devices are fully encapsulated and provided with a well-determined interface to the environment. The integrated microphones operate at a bias of 1.5 V and are expected to reach a sensitivity of 5 mV/Pa, an equivalent input noise of 24 dBA SPL, and a power consumption of about 50 µW in the near future, thereby living up to the tight specifications of microphones for hearing instruments. Other potential applications include mobile phones, headsets, and wearable computers, in which space is constrained.*

Keywords: microphone, acoustic transducers, stacking, packaging

Introduction

Silicon microphones have a large potential to be the next high-volume MEMS application as mentioned by several key players in industry. However, high-quality microphones are delicate mechanical systems and their fabrication requires accurate control of mechanical parameters and a good encapsulation.

Many excellent designs have been presented [1-4]. Recently, specifications have been reached in terms of technical performance [5, 6]. The important issue now is to develop an applicable, robust, compact and economic packaging concept.

Silicon microphone stacking concept

The concept for a stacked silicon microphone has been one of the two focal points of the European ESPRIT-funded project HISTACK [7]. It is based on connecting a transducer chip to an integrated circuit chip by direct wafer-to-wafer and chip-to-wafer bonding, forming a batch-packaged, completely encapsulated smart transducer (Fig. 1). The concept allows also for combining different optimized technologies for transducer and circuit, improving the cost/performance ratio further. The individual technologies for stacking, including feedthroughs and bonding, have been published a.o.

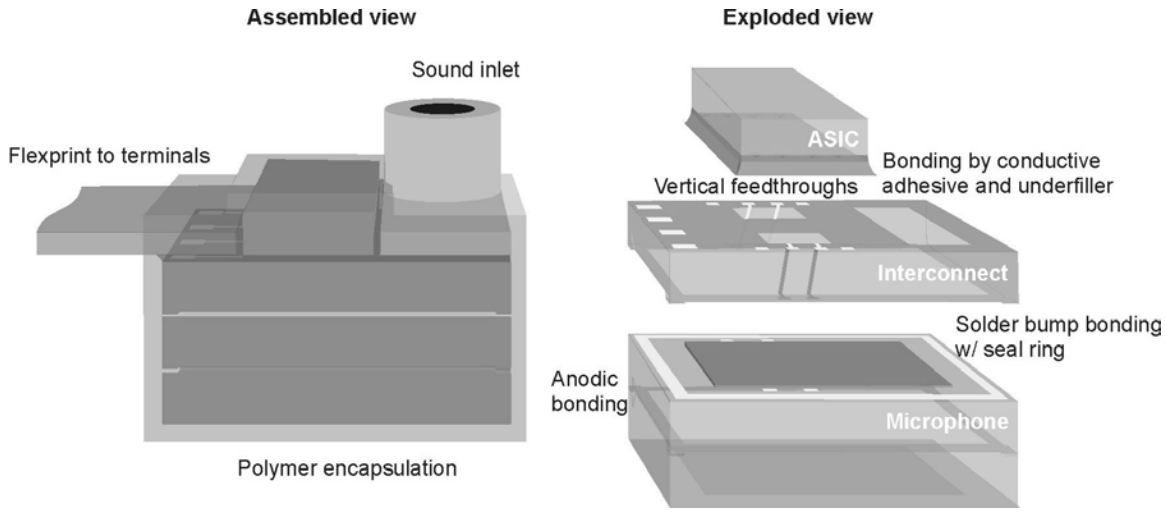

Fig. 1: Stacking concept for a batch-packaged silicon microphone.

ISBN 87-89935-50-0

at Eurosensors XIII [8]. In this paper we present the first stacked microphones.

Transducer performance

The transducer part applies capacitive readout with an external bias of 1.5 V. The membrane stress has been reduced to 50 MPa by using stress-compensated multilayers of silicon nitride and polysilicon, resulting in a sensitivity of typically 4 mV/Pa without amplification and an equivalent input noise of 24 dBA SPL. The air gap, membrane, and backplate are dimensioned as described earlier [5] with a highly perforated backplate to reduce squeeze-film damping and with ventilation holes in the membrane.

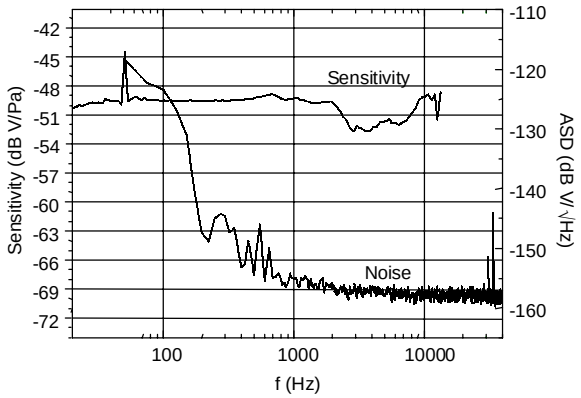

Fig. 2: Measured sensitivity and noise spectra.

All measurements are done on wafer level using an artificial mouth and a characterized and modeled buffer amplifier. The back volume is infinite for these measurements. Typical sensitivity and noise spectra using this setup are shown in Fig. 2. Besides a 50 Hz peak and ripples in the high frequency range due to reflections in the artificial mouth, the frequency response is flat, as expected.

Table 1 lists the sensitivity and equivalent input noise including the buffer amplifier. Figs. 3 and 4 show pictures of the transducer element.

Table 1: Sensitivity and noise measured on wafer level before stacking.

Membrane Size (mm^2)	Sensitivity (mV/Pa)	Eq. Input noise (dBA SPL)
1.00	1.03	32.0
2.25	2.62	27.0
4.00	5.07	24.5

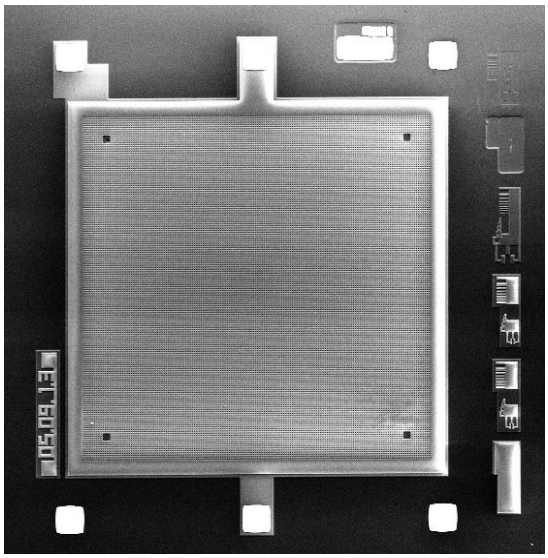

Fig. 3: Scanning electron micrograph of the microphone transducer element (backplate and membrane with contact pads). The four dark squares in the corners are areas with larger openings in the backplate (close-up in Fig. 4).

Fig. 4: Scanning electron micrograph of a ventilation hole in the membrane, exposed in a larger opening in the perforated backplate.

Stacking process flow and its influence on the transducer performance

The characterized transducer wafers have been bonded to backchamber wafers by thin-film anodic bonding (level 1) [9]. All stacked substrates are silicon substrates in order to minimize the thermally induced stresses. The anodic bonding does not affect the microphone performance. However, half of the bonding trials have failed, probably due to the surfaces being contaminated from processing and measuring of the wafers. Alternatively, backchambers can be attached at a later stage by gluing.

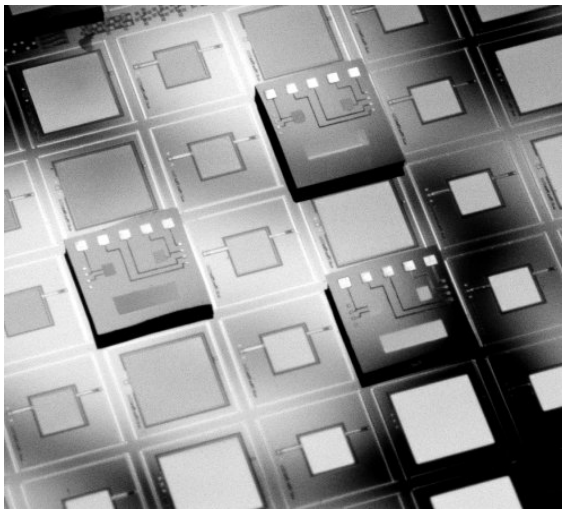

Fig. 5: Microphone wafer with solder bump bonded interconnect dies on top and without a backchamber wafer. The microphone membranes are transparent and the seal ring is visible. The interconnect dies contain the sound inlet and two openings for feedtroughs. The terminals are visible on the top surface of the interconnect dies.

In the next step, interconnect dies are bonded to the transducer side by fluxless chip-to-wafer solder bump bonding (level 2) with an implemented seal ring [8] (Fig. 5). The bonding sequence includes prebonding with a moderate force and heating to form the solder joint. The heating procedure can be applied several times without degradation. Measurements after this step did not indicate any degradation to the microphone performance. About 60 % of all dies were bonded successfully in the lab experiment. Also the insulation resistance and conductivity of feedthrough lines were sufficiently high at lab conditions. The stability during temperature and humidity cycling has still to be tested.

After level-2 bonding, the stacked wafers are diced from the front side, covering the openings of the interconnect dies by a compliant UV-sensitive blue tape. Wafers without backchambers have been diced similarly with another blue-tape film on the backside with no visible effect on the mechanical structure of the microphones. However, the characterization revealed that the seal ring was only partly bonded for a large number of dies. Water that entered through the seal ring during dicing caused the microphones to collapse and contaminated the surface with dicing particles. Underfiller has been successfully used to fill the gaps in the seal ring and keep water and particles outside.

In the next step, ASIC dies are flip-chip mounted onto the stack using conductive adhesive on gold studs and underfiller for sealing and mechanical strength. Two types of circuits have been designed and characterized, one with a buffer amplifier and one with a Σ/Δ converter for a digital microphone.

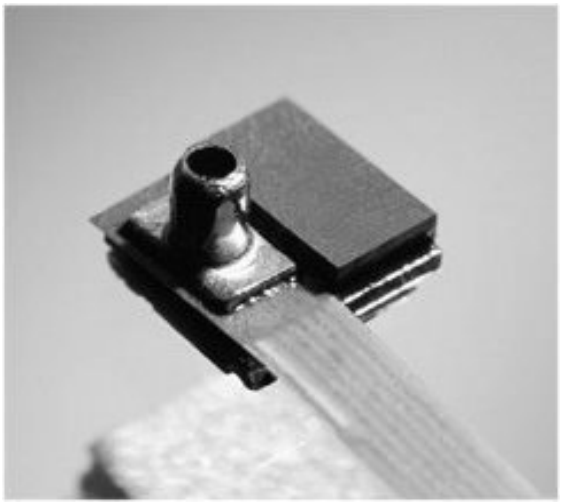

Fig. 6: Silicon microphone assembly before the final polymer coating. Flex-print and sound inlet are flip-chip mounted onto the stack.

After separation of the stacked dies, a flexprint connector and a snout are flip-chip mounted onto the stack (Fig. 6) before encapsulation by spray coating with a conductive polymer for electromagnetic shielding and mechanical protection.

Due to the difficulty of handling devices with larger membranes (and thin frames), stacks have only been made using transducers with 1x1 mm^2 membranes, which do not yet live up to hearing instrument standards. However, it is expected that using specialized and improved tools for die handling will solve this problem.

Conclusion

Wafer and die stacking has a high potential for being a cost-effective packaging technology for microsystems with delicate structures. Wafer-to-wafer feedthroughs play an important role for more flexible and compact constructions. The further development has to include improvements of the electroplating and bonding processes as well as the handling of larger membrane structures.

Acknowledgement

This work was partly funded through the European ESPRIT project *High-Performance Interconnect and Stacking* (HISTACK) No. 25345.

References

[1] P. R. Scheeper, A. G. H van der Donk, W. Olthuis, P. Bergveld, Sensors Actuators A 44 pp 1 1994.

[2] J. Bay, O. Hansen, S. Bouwstra, J. Micromechanics Microengineering., 9 pp 30 1999.
[3] A. Torkkeli, H. Sipola, H. Seppä, J. Saarilahti, O. Rusanen, J. Hietanen, Eurosensors XIII 1999.
[4] P.-C. Hsu, C. H. Mastrangelo, K. D. Wise, MEMS '98, pp 580-585.
[5] P. Rombach, M. Müllenborn, U. Klein, R. Frehoff, Forum Acusticum 1999.
[6] A. Dehé, R. Aigner, T. Bever, K.-G. Oppemann, E. Pettenpaul, S. Schmitt, H.-J. Timme, Forum Acusticum 1999.
[7] http://www.histack.cat.dtu.dk
[8] J. F. Kuhmann, M. Heschel, S. Bouwstra, F. Baleras, C. Massit, Eurosensors XIII 1999.
[9] S. Weichel, R. de Reus, M. Lindahl, Sensors Actuators A 70 pp 179-184 1998.

Paper 4

J. Janting, J. Branebjerg, P. Rombach

Conformal coatings for 3D multichip microsystem encapsulation

Sensors and Actuators A 92 (2001) 229-234

ELSEVIER

Sensors and Actuators A 92 (2001) 229–234

SENSORS AND ACTUATORS A PHYSICAL

www.elsevier.com/locate/sna

Conformal coatings for 3D multichip microsystem encapsulation

Jakob Janting[a,*], Jens Branebjerg[a], Pirmin Rombach[b,1]

[a]*DELTA Danish Electronics, Light and Acoustics, Venlighedsvej 4, DK-2970 Hoersholm, Denmark*
[b]*Microtronic A/S, CAT/DTU, Building 347, DK-2800 Lyngby, Denmark*

Accepted 7 December 2000

Abstract

Materials and methods for low cost minimum volume protective encapsulation of microsystems have been investigated. The focus has been on a 3D conformal multilayer coating of silicon microphones. Materials with different properties, e.g. insulating and conductive, can be applied and combined as multilayers around the sharp edges of single crystalline silicon giving a protection which can not be matched by a single material. A 50 μm thick insulating layer with volume resistivity above 10^{16} Ωcm with a 150 μm thick conductive layer on top is reported to have an EMI E-field damping higher than 55 dB in the 50 MHz–1 GHz frequency range. © 2001 Elsevier Science B.V. All rights reserved.

Keywords: Protection; Encapsulation; Coating; Conformal; Electromagnetic interference (EMI)

1. Introduction

Protective encapsulation is often the final step in microsystems manufacturing. The encapsulation makes up most of the volume and much of the price. Therefore, in order to avoid that small and cheap components are getting bulky and expensive, there is a broad interest in materials and processes making it possible to make encapsulations, which are so thin (<0.25 mm) that they can be termed coatings.

Many microsystems, e.g. sensors are fragile and exposed to chemically, physically and electromagnetically hostile environments. Reducing the amount of encapsulation material makes the right choice of materials and methods even more crucial for the lifetime, performance, and cost of the system. In many cases, traditional encapsulation materials like glass-filled epoxies and injection/transfer-moulding techniques can not be used due to the implied high pressures and temperatures.

The motivation for this work has been to protect a fragile 3 mm × 3 mm × 2 mm silicon microphone three-dimensionally with a low cost minimum volume coating. Related work has been going on the last 25 years, mainly with focus on how to protect components and conductors on PCB's [1–10] and in recent years the silicon in microsystems [11–13] in two dimensions with coatings.

2. Demands

The demands are high for the microphone coating and can be expressed by the following characteristics:

- EMI *E*-field shielding (>50 dB);
- electrical insulation (>10^{12} Ωcm);
- applicability below total thickness of 200 μm;
- multichip microsystem compatibility;
- chemical/physical durability.

3. Developed coating concept and critical issues

EMI shielding can only be accomplished with conductive materials. Therefore, the first two demands implies a two-layered coating, the top layer being conductive and the bottom layer insulating to avoid short circuiting (Fig. 1). The required thicknesses and the fragility of the microphone make it critical to achieve pinhole free conformal coverage around the sharp edges on single crystalline silicon with gentle techniques. Both during application and afterwards the encapsulation should be chemically and physically protective and not aggressive. In this way, materials compatibility becomes a critical issue since materials with very

* Corresponding author. Tel.: +45-45-86-7722; fax: +45-45-86-5898.
E-mail addresses: jaj@delta.dk (J. Janting), jab@delta.dk (J. Branebjerg), p.rombach@cat.dtu.dk (P. Rombach).

[1] URL: http://www.delta.dk

PII: S0924-4247(01)00567-2

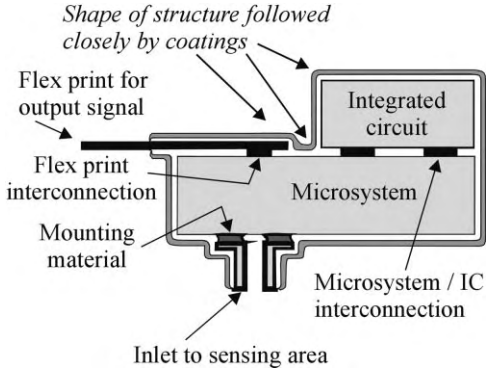

Fig. 1. Coating concept used for the microphone.

different properties, e.g. coefficient of thermal expansion (CTE) may be combined.

4. Results

Selected materials have been tested regarding applicability, volume resistivity, tightness, thickness, conformity, and *E*-field EMI shielding, to identify the best (Tables 1 and 2).

4.1. Choice of materials

The investigated materials are low viscosity and low surface tension polymers, metal-filled polymers and plating solutions. One successful combination of materials is 2 wt.% Teflon® AF 1600 from DuPont dissolved in Fluorinert™ FC 75 from 3M as bottom layer and on top of that Cho-Shield 2052 from Chomerics. Teflon® AF 1600 is an amorphous copolymer of 4,5-difluoro-2,2-bis(trifluoromethyl)-1,3-dioxole and PTFE. The solvent is perfluoro 2-butyltetrahydrofurane. This material was chosen primarily due to its very low surface tension which makes it possible to wet the sharp single crystalline silicon edges. Cho-Shield 2052 is a one component acrylic polymer filled with silver plated copper flakes of maximum 40 μm diameter. This material was chosen because of its claimed low electrical resistivity (25–50 Ω/□ at 50 μm thickness) and good EMI shielding properties (60–80 dB in the 20 MHz–10 GHz frequency range) together with its ease of application.

Other investigated materials have been TSR 144 from TOSHIBA and Loctite 394 from LOCTITE for the first layer and plated/not plated Leitsilber 200 from Demetron, ORMECON L5000 from Ormecon Chemie GmbH and ConQuest XP 1000 from DSM for the second layer. TSR 144 is a silicone and Loctite 394 is an acrylate/urethane mixture. Leitsilber 200 consists of small silver particles in cellulose nitrate dissolved in acetone and ethoxy propanole. After application, acetone and ethoxy propanole evaporates leaving a cellulose nitrate lacquer surface with exposed silver particles. The surface is then easily plated galvanically. This has been done with Cu in saturated $CuSO_4$ and water solution. The resistivity of Leitsilber 200 is sufficiently low (0.004–0.008 Ω/□ at 50 μm thickness) for the material to be used as EMI E-field shield without a plated layer on top. This has not been the case for the intrinsically conductive polymers ORMECON L5000 and ConQuest XP 1000, which are polyaniline and polypyrrole-based, respectively. These materials were therefore not investigated further.

Table 2
Measured damping of different layer configurations

Layer combination	Thickness (μm)	Total *E*-field damping, 50 MHz–1 GHz (dB)
Cho-Shield 2052	150	
Teflon® AF 1600	50	
		55
Leitsilber 200	98	
Cho-Shield 2052	23	
Teflon® AF 1600	80	
		70–90
Leitsilber 200	36–83	
Teflon® AF 1600	50–65	
		40–55[a]
Leitsilber 200	30–54	
Teflon® AF 1600	60–66	
Leitsilber 200	68–104	
Teflon® AF 1600	46–65	
		45–70[b]
Copper	11	
Leitsilber 200	63	
Teflon® AF 1600	50	
		55–65
Copper	9	
Leitsilber 200	29	
Teflon® AF 1600	62	
Copper	8	
Leitsilber 200	86	
Teflon® AF 1600	52	
		45–55

[a] Two samples, each with damping varying within 5 dB.
[b] Three samples, each with damping varying within 15 dB.

Table 1
Measured first layer materials properties

Inner layer material	Volume resistivity (10^{16} Ωcm)	Pinhole density	Conformity (thickness variation (%))
Teflon® AF 1600	High	Low	70
Loctite 394	4 ± 2	Problems at corners	
TSR 144	6 ± 5	High	

Table 3
Advantages and disadvantages for dipping and spraying application techniques

Method	Advantages	Disadvantages
Dipping	Simple process	Only low viscosity materials can be used Only very low surface tension materials can be used
Spraying	Controlled amount of material Some poorly wetting (high surface tension) materials can be applied	Only low viscosity materials can be applied Shadowing

4.2. Choice of processes

All investigated materials can be applied gently by either dipping or spraying and are processed at room temperature. Advantages and disadvantages of these application techniques have been identified (Table 3). Teflon® AF 1600 can be applied either by dipping or by spraying. In these investigations, it was applied by dipping. Cho-Shield 2052 and Leitsilber 200 can only be applied uniformly on Teflon® AF 1600 by spraying.

4.3. Volume resistivity

The insulating properties of first layer coatings have been determined by standard film resistivity measurements in a Keithley 6105 resistivity adapter. Volume resistivities exceeding 10^{16} Ωcm has been measured (Table 1).

4.4. Tightness

Pinholes in the insulating layer have been detected on coated silicon chips (1 cm × 1 cm × 0.5 mm) with a conductor attached with conductive glue. The resistance through the layer has been measured using as contact media either a drop of DI water placed on the surface or a glass of DI water in which most of the chip was dipped. Typical values have been 10^6–10^{10} Ω if the coating was not pinhole free. Values above 10^{12} Ω indicate a pinhole free coating.

4.5. Thickness and conformity

In order to determine the conformity and thickness of the coatings, microphone demonstrators were moulded in epoxy and cross-sections made for microscopy inspection (Fig. 2). For the found successful materials combination, the total coating thickness is close to 0.2 mm on silicon and the coverage is complete with less than 70% thickness variation.

4.6. EMI shielding

The shielding properties were determined on coated antennas of the same size as the microphone according to the Nordtest standard NT ELEC 030 developed at DELTA (Fig. 3). The antennas have been made by bending the inner wire stretching out from a coaxial cable into a loop and filling the loop with SnPb solder to achieve a ball which is easy to coat. The conducting layers have all been applied so that they are in electrical contact with the metal surface of the coaxial cable. The EMI *E*-field shielding of a 150 μm Cho-Shield 2052 layer on top of 50 μm Teflon® AF 1600 is above 55 dB in the frequency range 50 MHz–1 GHz (Table 2 and Figs. 4 and 5).

The damping of other layer combinations have been investigated (Table 2), and recent measurements show that 70–90 dB damping is possible by applying one layer of Leitsilber 200 on top of the Teflon® AF + Cho-Shield 2052 layers where the total thickness is 201 μm.

5. Discussion

The volume resistivity of Teflon® AF 1600 has not been determined, but it is expected to be of the same order as that for PTFE, $\rho_{PTFE} > 10^{18}$ Ωcm because of the chemical resemblance.

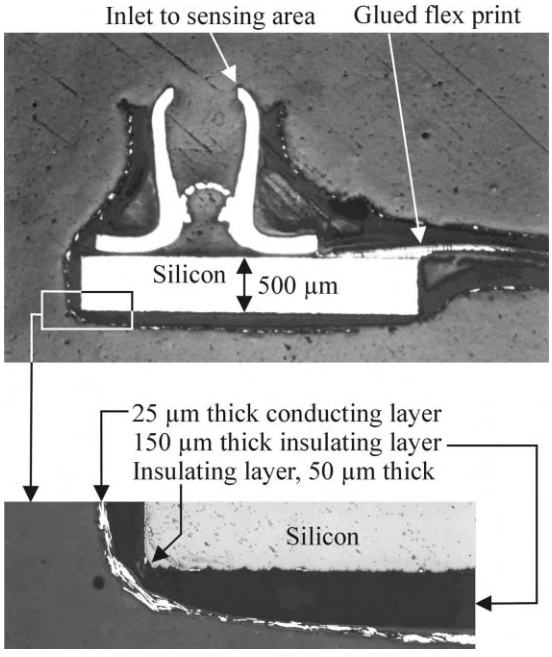

Fig. 2. Cross section of encapsulated microphone demonstrator (top). Close up of coverage at the sharp single crystalline silicon edge (bottom). The insulating layer is Teflon® AF 1600 applied by dipping and the conductive layer is Cho-Shield 2052 applied by hand held spraying.

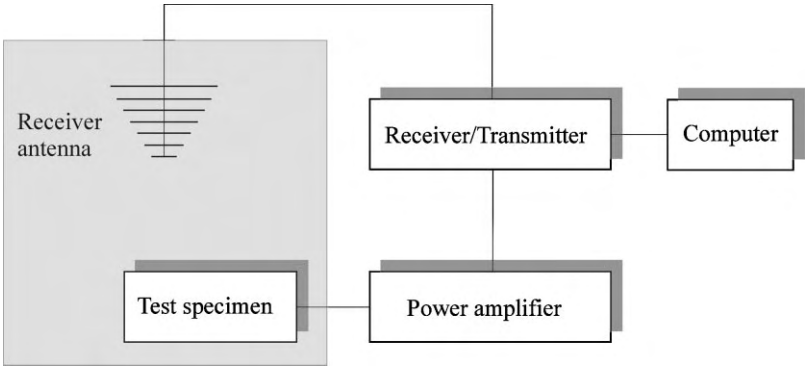

Fig. 3. Experimental set-up for antenna EMI *E*-field damping measurements.

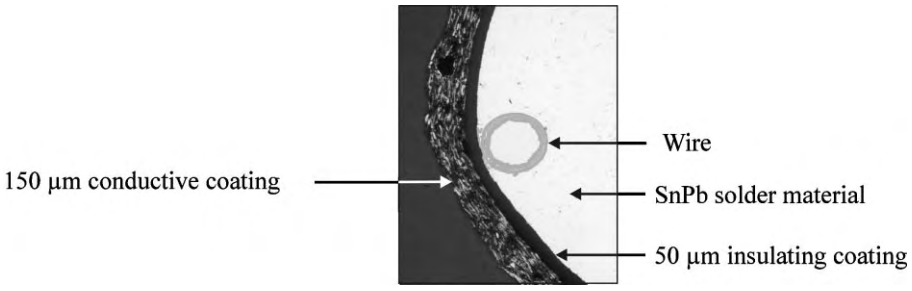

Fig. 4. Cross-section of coated antenna. The insulating layer is Teflon® AF 1600 and the conductive layer is Cho-Shield 2052.

Complete coverage of single crystalline silicon sharp edges with the first layer has been the most critical problem to solve. The reason is that the coating material tends to minimise its free energy by reducing the surface area to a minimum [14,15]. Generally, the free energy G of a system containing an interface of area A and free energy γ per unit area is $G = G_{\text{Bulk}} + A\gamma$, where G_{Bulk} is the free energy of the system assuming that all material in the system has the properties of the bulk. For instance, a free falling cube of liquid changes its shape to a sphere because this shape represents minimum surface and thereby minimum free energy. The saved surface free energy is $(1 - A_{\text{Sphere}}/A_{\text{Cube}})100\% = (1 - 0.5(4\pi/3)^{1/3})100\% = 19.4\%)$. When liquid is placed on solids, the exposed liquid surface is also minimised at equilibrium. Provided sufficient wetting coatings can be applied with a constant thickness on flat substrates. However, on areas with curvature maintaining a certain thickness from flat areas, more or less of a coating material would have to be exposed surface depending on the sign of the curvature. This can be explained geometrically by considering a coating with thickness t on a flat area and an edge with radius of curvature R (Fig. 6). At the edge, following the substrate contour one unit of length u perpendicular and along the edge changes the coating surface area relatively to the flat regions by $(\pm t/R)u^2$. Plus (+) is for convex and minus (−) for concave surfaces. The corresponding difference between a unit area A_u

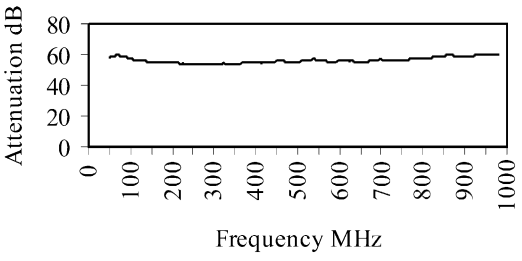

Fig. 5. EMI damping measurement.

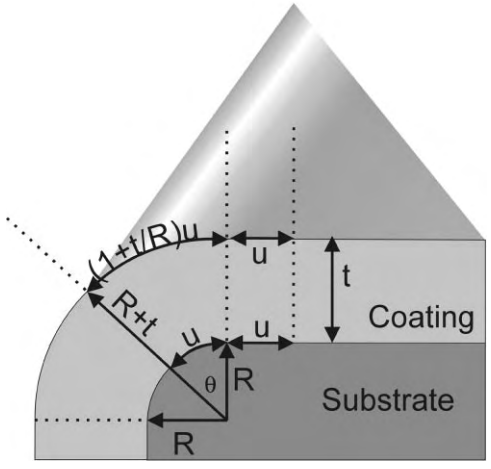

Fig. 6. Geometrical argument for coating surface area per unit substrate length u, perpendicular and along a convex edge. The area projected from substrate to coating surface is u^2 in flat regions and $u^2(R+t)\theta = u^2(R+t)/R = (1+t/R)u^2$ on the curved edge. The area difference is $(t/R)u^2$.

projected to the coating surface from spherical substrate surfaces (corners) and from flat surfaces is: $A_u((R \pm t)^2\theta - R^2\theta) = A_u(R^2 + t^2 \pm 2tR - R^2)/R^2 = A_u(\pm 2t/R + (t/R)^2)$. Therefore, at corners and edges, changing its thickness by not following the surface contour in three and two-dimensions, respectively, the coating can save surface free energy. The coating will be thin (Fig. 2) in convex regions, which may result in uncovered areas, and thick in concave regions. That is, material will move to concave regions if possible making the coating thick here. Around the inlet in Fig. 2, the coating thickness is therefore >500 μm and other optimised designs and application by spraying instead of dipping are currently investigated by using coating behaviour simulations and statistical methods. Note, that a liquid surface with free energy γ (mJ/m^2) exerts a surface tension of γ (mN/m). The surface tension can be regarded as a driving force away from conformal coverage. That is using coatings with very low surface tension minimises the energy, which can be saved in these regions and therefore they are more conformal. Even with Teflon® AF 1600 at least five separate dips were necessary to achieve a complete coverage. The tightness is probably worse than determined here since the contact to silicon through pinholes is dependent on how well the water wets the polymer. This effect might make especially the Teflon® AF 1600 coating coverage seem much more complete than it really is due to its very low critical surface tension $\gamma_{c(\text{Teflon AF 1600})} = 15.7$ mN/m, which is even lower than that for pure PTFE, $\gamma_{c(\text{PTFE})} = 18$ mN/m. The low surface tension of Teflon® AF 1600 is an advantage regarding electrical insulation in case there are still pinholes, since it may prevent the conducting layer to get in electrical contact with the silicon.

Only low viscosity and very low surface tension materials can be used for dipping application because otherwise the material will tend to form a big drop on the microsystem and the single crystalline silicon edges and corners will not be covered as accounted for above. This is also the case for spraying although with relatively high viscosity and surface tension materials thinner and more uniform layers can be applied. Further, with spraying surfaces difficult to wet can be coated since the speed of application can be adjusted for the droplets to cure/dry sufficiently fast upon impact with the surface thereby avoiding the retraction of a continuous wet coating toward minimum surface free energy. In this way, despite its low critical surface tension, Teflon® AF 1600 can be coated uniformly with Cho-Shield 2052 or Leitsilber 200.

Due to the general first layer covering difficulties, more complicated and expensive vacuum techniques for deposition of polymers have also been considered. Parylene which is poly(chloro-*p*-xylylene) is the material which would probably be the best to satisfy the demands [1,2]. Here, monomers of the material condense at the surfaces at low pressure and polymerisation follows. This implies that sharp edges, bond wires, etc. can be covered more conformable.

Repetitions of the layer structure, insulator–conductor, have been investigated because the most effective *E*-field damping takes place at the interface between these layers by reflection. Due to the achieved layer thickness variations the *E*-field damping efficiency of different layer combinations can not be compared directly. Though, it was expected that the multilayer-coated antennas would be shielded best. The explanation why this is not seen might be that the conductive layers are short-circuited. Plated layers were investigated because they have a denser and therefore more tight distribution of conductive crystallites. Galvanic Cu layers were used to explore the effect of a plated layer in an easy way. Electroless plated Ni is preferred since the resulting layer is amorphous and therefore more tight and chemically durable. Besides it is both conductive and ferromagnetic, which means that *H*-fields are also damped. The drawback for electroless Ni is the instability of the plating solutions.

There has been focused on the initial four demands but Teflon® AF 1600 is also a material with very high chemical/physical durability. The chemical inertness and bad adherence of fluorocarbons is due to the strong F bond to the carbon backbone C–F: 427 KJ/mol. For comparison other similar bond strengths are C–H: 414 KJ/mol, C–C: 335 KJ/mol, C–Cl: 322 KJ/mol [16]. The polymer part of Cho-Shield 2052 however, is an acrylate, which might hydrolyse critically if exposed to a high acidic or alkaline humidity level for a prolonged period.

Adhesion has not been considered a problem in these investigations since the coatings are held in place by the 3D structure of the microphone. If necessary cleaning, activation and priming by cold plasma treatment is preferred to enhance adhesion, since the processes involved are clean and dry. For instance O_2 plasma cleaning and/or activation treatment often increase the surface tension and reactivity of especially polymers thereby also increasing the adhesion of applied polymeric coatings [17]. Perfluorosilanes like 1H,1H,2H,2H-perfluorodecyltriethoxysilane can, e.g. be used to enhance the adhesion of Teflon® AF 1600 to silicon.

The materials and methods can easily be used in production. Commercial production equipment for dipping and spraying application exists. Teflon® AF 1600 is the most expensive material investigated, but with a loss, 50% in production of the cost per microphone is still below 0.15 €.

6. Conclusion

Production friendly new materials and methods of applying and combining them have been found for 3D low cost and minimum volume encapsulation of a silicon microphone. The materials and methods comply with the demands and related critical issues.

Generally the concept applies where minimum volume protection against chemical attack, physical attack, fluid penetration and EMI is needed [18]. The choice of materials and methods of application depend on object of encapsulation.

Acknowledgements

This work has been part of projects financially supported by the Danish Agency for Trade and Industry and HISTACK Esprit project No. 25345.

References

[1] J. Noordegraaf, H. Hull, C-SHIELD Parylene allows major weight saving for EM shielding of microelectronics, PEP'97, in: Proceedings of the first IEEE International Symposium on Polymeric Electronics Packaging, pp. 189–196.
[2] J. Wu, R.T. Pike, C.P. Wong, Interface–adhesion–enhanced bi-layer conformal coating for avionics application, in: Proceedings of the IEEE 1999 International Symposium on Advanced Packaging Materials, pp. 302–310.
[3] T. Mäkelä, S. Pienimaa, T. Taka, S. Jussila, H. Isotalo, Thin polyaniline films in EMI shielding, Synth. Met. 85 (1997) 1335–1336.
[4] S. Pienimaa, T. Taka, H. Isotalo, S. Jussila, O. Salmela, H. Stubb, Method and arrangement for electromagnetically shielding and electronic means, European patent application EPA1781085.
[5] L.M. Higgins, Shielded Electronic Component Assembly and Method for Making the Same, US Patent no. 5639989.
[6] J. Lynn Davis, J. Kevin Arledge, Thin film metallization of three-dimensional substrates, Proceedings of the 44th Conference on Electronic Components & Technology, 1–4 May 1994. IEEE 1994, 359–361.
[7] B.Q. Le, E. Nhan, R.H. Maurer, A.L. Lew, J.R. Lander, S.J. Lehtonen, Evaluation of die coating materials for chip-on-board technology insertion in spaceborne applications, in: Proceedings of the IEEE 1997 International Conference on Multichip Modules, pp. 142–147.
[8] B. Miquel, T. Karlinski, Encapsulation/Moulding, Advanced Packaging, May 1998, pp. 44–51.
[9] M.J. Loboda, R.C. Camilletti, L.A. Goodman, L.K. White, H.L. Pinch, J. Shaw, V.K. Patel, C.P. Wu, G.M. Adema, Chip scale packaging with high reliability for MCM applications, in: Proceedings of the ICEMCM '96, pp. 257–262.
[10] P. Clot, MCM-L packaging: technology for die and SMD components under the same overcoating, DVS Berichte 173 (1996) 95–98.
[11] R. de Reus, C. Christensen, S. Weichel, S. Bouwstra, J. Janting, G. Friis Eriksen, K. Dyrbye, T. Romedahl Brown, J.P. Krog, O. Søndergård Jensen, P. Gravesen, Reliability of industrial packaging for microsystems, Microelectronics Reliability 38 (1998) 1251–1260.
[12] G.F. Eriksen, K. Dyrbye, Protective coatings in harsh environments, J. Micromech. Microeng. 6 (1996) 55–57.
[13] K. Dyrbye, T. Romedahl Brown, G.F. Eriksen, Packaging of physical sensors for aggressive media applications, J. Micromech. Microeng. 6 (1996) 187–192.
[14] T. Bieker, S. Dietrich, Wetting of curved surfaces, Physica A 252 (1998) 85–137.
[15] S. Dietrich, Wetting Phenomena, Phase Transistions and Critical Phenomena, Vol. 12, Academic Press, London, 1988, pp. 164–167.
[16] E.S. Gould, Mechanism and Structure in Organic Chemistry, Holt, Reinhardt and Winston, Inc., 1959, p. 37.
[17] J. Palmers, Surface Modification Using Low-Pressure Plasma Technology, Medical Device and Diagnostic Industry, January 2000, p. 96.
[18] DELTA, Encapsulation for a three-dimensional microsystem, Patent application PCT/DK00/00559.

Biographies

Jakob Janting received his MSc degree in materials science from the University Aarhus in Denmark 1991. Here he was employed as a researcher affiliated to the Tribology department from 1991 to 1994 in an EU project where he was working on micro focus X-ray stress measurements. In 1994, he joined the Department for Sensors at Grundfos Research in Denmark where he worked in a national project on materials for advanced micromechanical packaging together with Danfoss A/S and the Microelectronics Center (MIC). Since 1998 he has been employed at DELTA, the department for microsystems, where focus of his work is on polymer microsystem encapsulation.

Jens Branebjerg received his Bachelor degree in electronic engineering in 1981. He was employed as R&D engineer at Radiometer A/S in Copenhagen from 1982 to 1988 developing electrochemical medical sensors. From 1989 to 1997 he worked as R&D engineer at Danfoss A/S, Denmark. He got his PhD degree in 1991 in microtechnology from MIC, DTU, Denmark. From 1991 to 1997 he was project manager for a research project on microchemical analysis systems. Since 1997 he has worked as project manager at DELTA with the responsibility of development and supply of microsystem services in the areas of packaging, testing and reliability. He is currently managing the microsystem group of 10 people.

Pirmin Rombach received the MSc in Electronics Engineering from the Technical University of Karlsruhe in 1989. The PhD in Electronics Engineering, he received from the Technical University of Darmstadt in 1995, for his work on a micromachined torque sensor at the Solid State Electronics Laboratories, where he was working as a research assistant. In 1996 he joined the research group of Microtronic in Roskilde, Denmark. The focus of his research is modeling and process development for micromachined microphones and loudspeakers but also backend processing aspects for microsystems.

Paper 5

M. Müllenborn, P. Rombach, U. Klein, K. Rasmussen, J.F. Kuhmann, M. Heschel, M. Amskov Gravad, J. Janting, J. Branebjerg, A. Hoogerwerf , S. Bouwstra

Chip-size-packaged silicon microphones

Sensors and Actuators A 92 (2001) 23-29

ELSEVIER

Sensors and Actuators A 92 (2001) 23–29

SENSORS AND ACTUATORS A PHYSICAL

www.elsevier.com/locate/sna

Chip-size-packaged silicon microphones

M. Müllenborn[a,*,1], P. Rombach[a], U. Klein[a], K. Rasmussen[a], J.F. Kuhmann[b], M. Heschel[b], M. Amskov Gravad[c], J. Janting[c], J. Branebjerg[c], A.C. Hoogerwerf[d], S. Bouwstra[e]

[a]*Microtronic A/S, CAT/DTU, Building 347, DK-2800 Lyngby, Denmark*
[b]*MIC/DTU, Building 345 East, DK-2800 Lyngby, Denmark*
[c]*DELTA, Venlighedsvej 4, DK-2970 Hørsholm, Denmark*
[d]*CSEM, Jaquet-Droz 1, CH-2007 Neuchâtel, Switzerland*
[e]*Microcosm Technologies BV, Keizersgracht 316, NL-1016 EZ Amsterdam, The Netherlands*

Accepted 5 December 2000

Abstract

The first results of silicon microphones that are completely batch-packaged and integrated with signal conditioning circuitry in a chip stack are discussed. The chip stack is designed to be directly mounted into a system, such as a hearing instrument, without further single-chip handling or wire bonding. The devices are fully encapsulated and provided with a well-determined interface to the environment. The integrated microphones operate at a bias of 1.5 V and are expected to reach a sensitivity of 5 mV/Pa, an A-weighted equivalent input noise of 24 dB sound pressure level, and a power consumption of about 50 μW in the near future, thereby living up to the tight specifications of microphones for hearing instruments. Other potential applications include mobile phones, headsets, and wearable computers, in which space is constrained.

Keywords: Microphone; Acoustic transducers; Stacking; Packaging

1. Introduction

Silicon microphones have a large potential to be the next high-volume MEMS application as mentioned by several key players in industry. However, high-quality microphones are delicate mechanical systems and their fabrication requires accurate control of mechanical parameters and a good encapsulation.

Many excellent designs have been presented [1–4]. Recently, specifications have been reached in terms of technical performance [5,6]. The important issue now is to develop an applicable, robust, compact and economic packaging concept.

2. Silicon microphone stacking concept

The concept for a stacked silicon microphone has been one of the two focal points of the European ESPRIT-funded project HISTACK [7]. It is based on connecting a transducer chip to an integrated circuit chip by direct wafer-to-wafer and chip-to-wafer bonding, forming a batch-packaged, completely encapsulated smart transducer (Fig. 1). The concept allows also for combining different optimized technologies for transducer and circuit, improving the cost/performance ratio further. The individual technologies for stacking, including feed-throughs and bonding, have been published, e.g. at Eurosensors XIII and XIV [8,9]. Here, the influence of the stacking technology on the transducer performance is discussed using first results of functional stacked microphones.

3. Transducer performance

The transducer part makes use of capacitive readout with an external bias of 1.5 V. The membrane stress has been reduced to 50 MPa by using stress-compensated multilayers of silicon nitride and polysilicon, resulting in a sensitivity of typically 4 mV/Pa without amplification and an A-weighted equivalent input noise of 24 dBA SPL (sound pressure level) [10]. The air gap, membrane, and back plate are dimensioned

* Corresponding author. Tel.: +45-4525-6426; fax: +45-4525-6419.
E-mail address: mm@cat.dtu.dk (M. Müllenborn).
[1] URL: http://www.microtronic.org.

0924-4247/01/$ – see front matter
PII: S0924-4247(01)00535-0

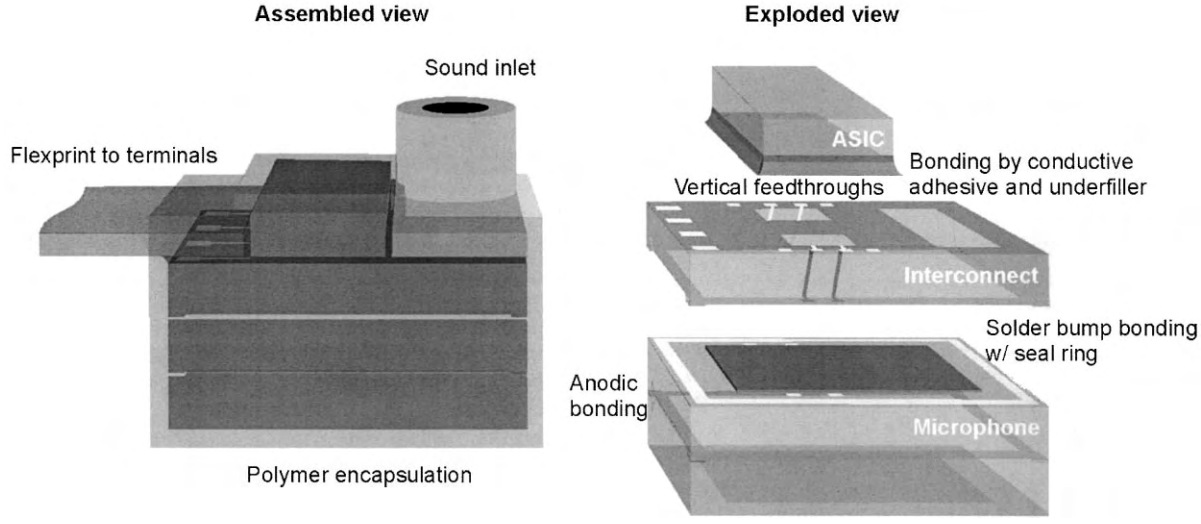

Fig. 1. Stacking concept for a batch-packaged silicon microphone.

as described earlier [5] with a highly perforated back plate to reduce squeeze-film damping and with ventilation holes in the membrane. The transducer is in the last step released and coated with a Teflon-like monolayer, which prevents condensation of water and stiction of the membrane.

The transducer measurements are done on wafer level using an artificial mouth and a characterized and modeled buffer amplifier. The back volume is infinite for these measurements. Typical sensitivity and noise spectra using this setup are shown in Fig. 2. Besides a 50 Hz peak, ripples in the high frequency range due to reflections in the artificial mouth, and a slight increase towards higher frequencies due to the tail of the membrane resonance, the frequency response is flat, as expected. The exact sensitivity response depends on the design of the back plate as well as the stress-level selected for the membrane. A spread of sensitivities is observed and is attributed to inhomogeneous deposition and etching characteristics over the wafer. Since these first transducers have been processed in a research lab, it is expected that this spread can be reduced significantly in a more reproducible environment. The noise floor is very low with spikes in the lower frequency range due to the acoustic environmental noise during the measurement.

Table 1 lists the sensitivity and the A-weighted equivalent input noise including the buffer amplifier for various membrane sizes. Figs. 3 and 4 show pictures of the transducer element.

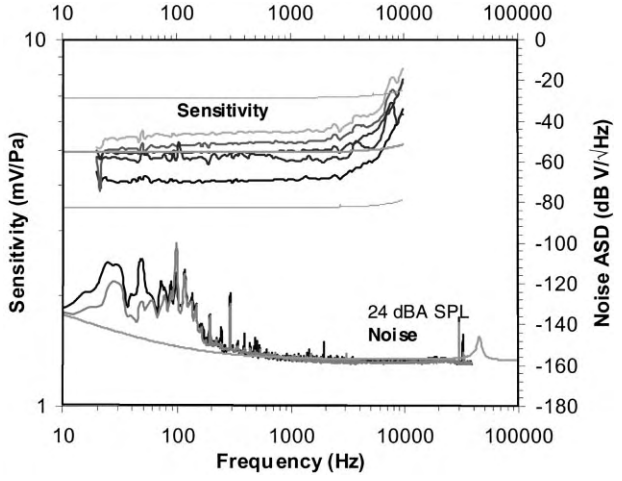

Fig. 2. Measured sensitivity and noise spectra of microphones with a 2 mm × 2 mm membrane, at a bias of 1.5 V. The smooth lines are simulated curves of the sensitivity including ±3 dB lines and noise.

4. Stacking process flow and its influence on the transducer performance

The characterized transducer wafers have been bonded to back chamber wafers by thin-film anodic bonding (level 1) [11]. All stacked substrates are silicon substrates in order to minimize the thermally induced stresses. The anodic bonding does not affect the microphone performance. However, half of the bonding trials have failed, probably due to the surfaces being contaminated from processing and measuring of the wafers. Alternatively, back chambers have been attached at a later stage by gluing.

In the next step, interconnect dies have been bonded to the transducer side by flux less chip-to-wafer solder bump

Table 1
Sensitivity and noise measured on wafer level before stacking.

Membrane size (mm^2)	Sensitivity (mV/Pa)	Equivalent input noise (dBA SPL)
1.00	1.03	32.0
2.25	2.62	27.0
4.00	5.07	24.5

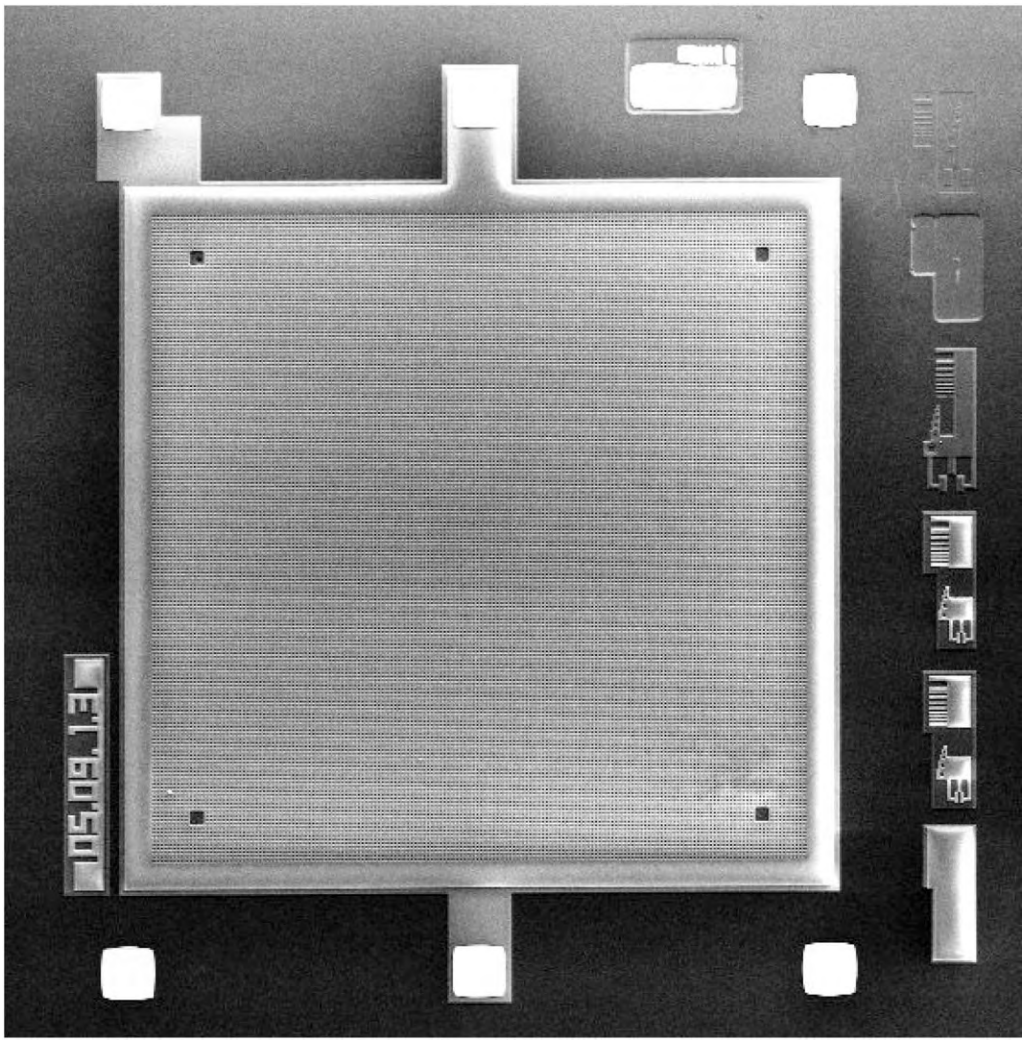

Fig. 3. Scanning electron micrograph of the microphone transducer element (back plate and membrane with contact pads). The four dark squares in the corners are areas with larger openings in the back plate (close-up in Fig. 4).

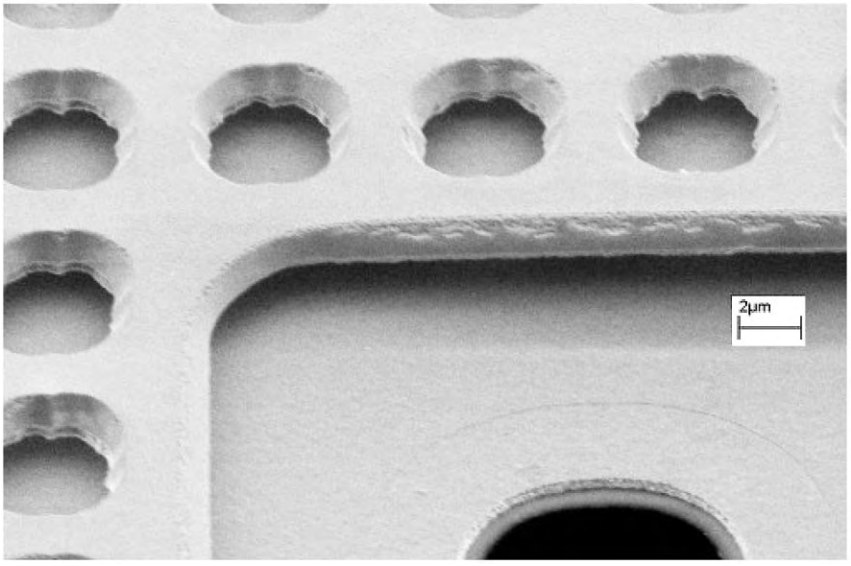

Fig. 4. Scanning electron micrograph of a ventilation hole in the membrane, exposed in a larger opening in the perforated back plate.

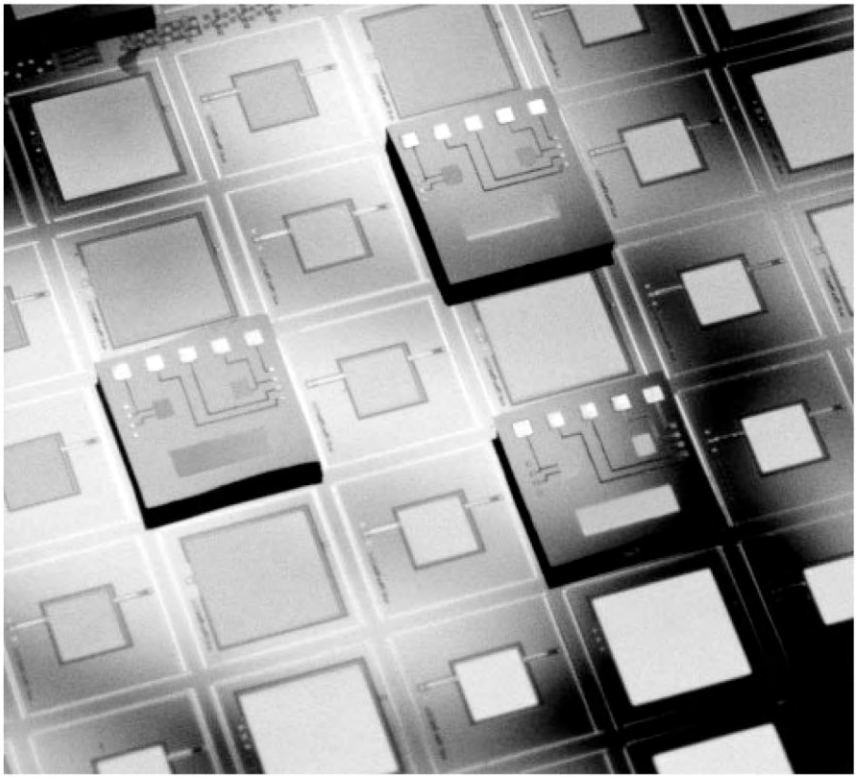

Fig. 5. Microphone wafer with interconnect dies, which are solder bump bonded, without a back chamber wafer. The microphone membranes are transparent and the seal ring is visible. The interconnect dies contain the sound inlet and two openings for feedthroughs. The terminals are visible on the top surface of the interconnect dies.

bonding (level 2) with an implemented seal ring [8] (Fig. 5). The bonding sequence includes prebonding with a moderate force and heating to form the solder joint. The heating procedure can be applied several times without degradation. Measurements after this step did not indicate any degradation to the microphone performance. About 60% of all dies were bonded successfully in the lab experiment. Also the insulation resistance and conductivity of feedthrough lines were sufficiently high at lab conditions. The stability during temperature and humidity cycling has still to be tested.

Although first tests on dummy structures indicated a tight seal, the interconnect dies could not be bonded to microphone wafers with a watertight sealing ring. This is probably due to the wedge error caused by the topography of the backside of the interconnect dies. For first functional devices, underfiller has been applied around the seal ring for additional sealing.

After level-2 bonding, the stacked wafers are diced from the front side, covering the openings of the interconnect dies by a compliant UV-sensitive blue tape. Wafers without back chambers have been diced similarly with another blue-tape film on the backside with no visible effect on the mechanical structure of the microphones.

In the next step, ASIC dies are flip-chip mounted onto the stack using conductive adhesive on gold studs and underfiller for sealing and mechanical strength. Two types of circuits have been designed and characterized, one with a buffer amplifier and one with a Σ/Δ converter for a digital microphone.

Completely stacked functional devices have been achieved demonstrating the feasibility of this concept (Fig. 6). However, improvements have to be done for the solder bump bonding and flip-chip processes. Fig. 7 shows the acoustical performance of a device after each process step. While no degradation can be seen after solder bump bonding, the complete stack has not the intended sensitivity of 20 dB above the wafer-level measurement, which is expected due to the ASIC amplification. This can be related to a bad electrical connection either at the solder bump or at the flip-chip level. Other devices have shown an acceptable performance after complete stacking.

After separation of the stacked dies, a flexprint connector and a snout are flip-chip mounted onto the stack before encapsulation by spray coating with a conductive polymer for electromagnetic shielding and mechanical protection.

Due to the difficulty of handling devices with larger membranes (and thin frames), stacks have only been made using transducers with 1 mm $\times$ 1 mm membranes, which do not yet live up to hearing instrument standards. However, it is expected that using specialized and improved tools for die handling will solve this problem.

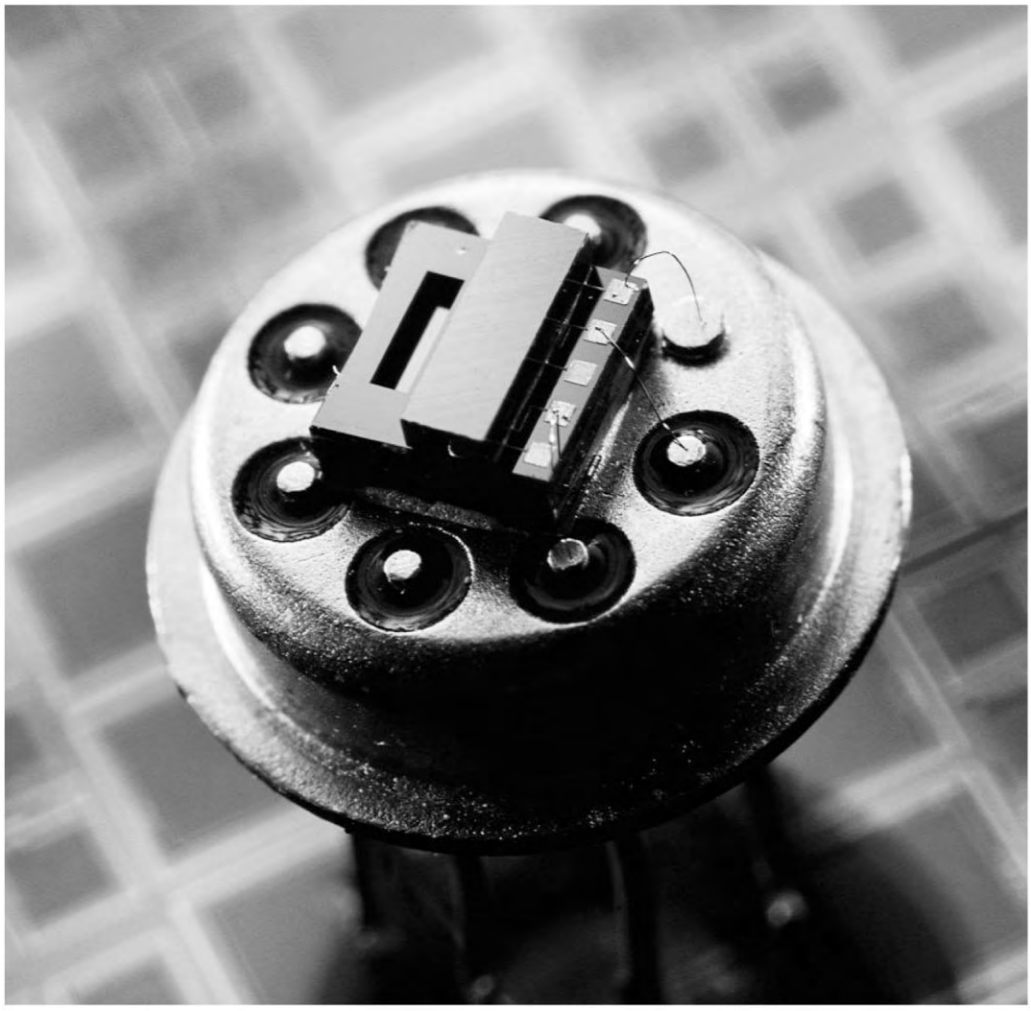

Fig. 6. Complete silicon microphone stack mounted in a TO5 housing for testing. Further processing includes the polymer coating and flip-chip mounting of a flexible printed circuit board and a sound inlet.

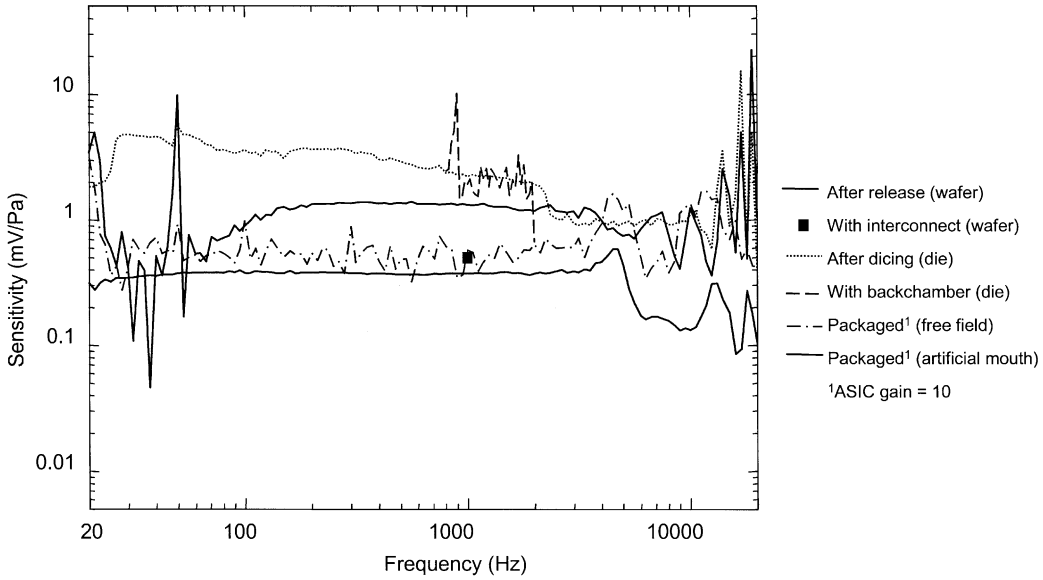

Fig. 7. Sensitivity of a microphone unit before and after each bonding step. The sensitivity at 1 kHz is at the wafer-level around 1 mV/Pa and about the same after stacking, although the integrated circuit should provide an amplification of 20 dB.

5. Conclusion

Wafer and die stacking has a high potential for being a cost-effective packaging technology for microsystems with delicate structures. Wafer-to-wafer feedthroughs play an important role for more flexible and compact constructions. The further development has to include improvements of the electroplating and bonding processes as well as the handling of larger membrane structures.

Acknowledgements

This work was partly funded through the European ESPRIT project High-Performance Interconnect and Stacking (HISTACK) No. 25345.

References

[1] P.R. Scheeper, A.G.H. van der Donk, W. Olthuis, P. Bergveld, A Review of Silicon Microphones, Sens. Actuators A 44 (1994) 1–6.
[2] J. Bay, O. Hansen, S. Bouwstra, Micromachined Double Backplate Differential Capacitive Microphone, J. Micromech. Microeng. 9 (1999) 30–35.
[3] A. Torkkeli, H. Sipola, H. Seppä, J. Saarilahti, O. Rusanen, J. Hietanen, Capacitive Microphone with Low-stress Polysilicon Membrane and High-stress Polysilicon Backplate, Eurosensors XIII, The Hague, The Netherlands, 12–15 September 1999.
[4] P.-C. Hsu, C.H. Mastrangelo, K.D. Wise, A High Sensitivity Polysilicon Diaphragm Condenser Microphone, MEMS'98, pp. 580–585.
[5] P. Rombach, M. Müllenborn, U. Klein, R. Frehoff, A Low-Voltage Silicon Condenser Microphone for Hearing Instrument Applications, Forum Acusticum, Berlin, Germany, 14–19 March 1999.
[6] A. Dehé, R. Aigner, T. Bever, K.-G. Oppemann, E. Pettenpaul, S. Schmitt, H.-J. Timme, Silicon Micromachined Microphone Chip at Siemens, Forum Acusticum, Berlin, Germany, 14–19 March 1999.
[7] http://www.histack.cat.dtu.dk; Public Final Report of HISTACK, European Commission, November 2000.
[8] J. F. Kuhmann, M. Heschel, S. Bouwstra, F. Baleras, C. Massit, Through Wafer Interconnects and Flip-Chip Bonding: A Toolbox for Advanced Hybrid Technologies for MEMS, Eurosensors XIII, The Hague, The Netherlands, 12–15 September 1999.
[9] S. Weichel, R. de Reus, M. Lindahl, Silicon-to-Silicon Wafer Bonding Using Evaporated Glass, Sens Actuators A 70 (1998) 179–184.
[10] L.L. Beranek, Acoustics, American Institute of Physics, New York, 1954, p. 372.
[11] M. Müllenborn, P. Rombach, U. Klein, K. Rasmussen, J.F. Kuhmann, M. Heschel, S. Bouwstra, M. Amskov, J. Janting, J. Branebjerg, A. Hoogerwerf, Stacked Silicon Microphones, Eurosensors XIV, Copenhagen, Denmark, 27 30 August 2000, pp. 119–120.

Biographies

M. Müllenborn received his MSc degree in Physics from the University of Münster, Germany, in 1990 and his PhD degree in Materials Science & Engineering from the University of California at Los Angeles, USA, in 1993. His research projects focused on the optical characterization of III/V materials at the Siemens research labs in Munich (now Infineon) and on the investigation of heterostructure interfaces at UCLA. From 1993 to 1996, he was employed at the Microelectronics Center of the Technical University of Denmark as a research assistant professor, working on high-resolution laser micromachining and nanoscale direct writing. He joined Microtronic A/S, Denmark, in 1996 where he worked on the development of a microtechnology-based microphone for hearing instrument applications. He is project manager of the ESPRIT-funded project HISTACK and manager of the Microsystems Group at Microtronic.

P. Rombach received his MSc in Electronics Engineering from the Technical University of Karlsruhe in 1989. He received his PhD in Electronics Engineering, from the Technical University of Darmstadt in 1995, for his work on a micromachined torque sensor at the Solid State Electronics Laboratories, where he was working as a research assistant. In 1996, he joined the research group of Microtronic in Roskilde, Denmark. The focus of his research is modeling and process development for micromachined microphones and loudspeakers but also back end processing aspects for microsystems.

U. Klein received his Dipl -Ing and Dr -Ing degrees in Electronics Engineering from the Technical University (TU) Braunschweig, Germany, in 1986 and 1990, respectively. In 1987, he joined the Institute of High-Frequency Engineering, TU Braunschweig, working on superconducting electronics. Between 1990 and 1993 he was a Guest Researcher at the Electrotechnical Laboratory, Japan, where he developed Josephson voltage standards. He then worked in academic research on both low and high-temperature superconductor technology for magnetic sensor and electronic devices at the University of Birmingham, England, the University of Strathclyde, Scotland, and the Technical University of Denmark. During 1996 he visited the Department of Materials and Production Engineering, University of Naples, Italy, as a consultant for the design of a SQUID NDE system. Since he joined Microtronic A/S, Denmark, in 1997 as Microsystems Design Engineer, he has been developing microelectromechanical devices for the hearing instrument industry, particularly silicon microphones. Dr. Klein is a member of the IEEE and the IoP.

K. Rasmussen received his MS in Electrical Engineering from the Technical University of Denmark in 1996. From 1996, he was working as a Research Assistant at the Microelectronics Center of the Technical University of Denmark on silicon wafer bonding. In 1999, he joined the research group of Microtronic in Roskilde, Denmark. The focus of his work is process development for micromachined microphones.

J.F. Kuhmann studied Materials Science at the Technical University of Berlin. His PhD work at Heinrich-Hertz-Institut, Berlin focused on packaging of photonic components. Since July, 1996 he is with MIC, Denmark, where he works on packaging for MEMS. In 1999, he was appointed as an Associate Professor.

M. Heschel received his Masters degree in Electrical Engineering from the Technical University of Chemnitz, Germany, in 1995. He joined the Microelectronics Center at the Technical University of Denmark in 1994 and received his PhD degree in Electrical Engineering in 1999 from the same university. His research work focused on advanced stacking technologies for MEMS applications and electrical wafer frontside to backside interconnects. Since 1999, he has been working as an assistant professor at the Microelectronics Center on hybrid integration technologies for photonics telecommunication systems.

M. Amskov Gravad finished her MSc (Titled: Thermooptical Phase Modulation in Glass Waveguides) at Mikroelektronik Centret in 1995. In 1996, she started at DELTA and has worked on several microsystems projects. Her main area at DELTA is advanced packaging.

J. Janting received his MSc degree in Materials Science from the University Aarhus Denmark in 1991. Here he was employed as a researcher affiliated to the Tribology Department from 1991 to 1994 in an

EU project where he was working on micro focus X-ray stress measurements. In 1994, he joined the Department for Sensors at Grundfos Research in Denmark where he worked in a national project on materials for advanced micromechanical packaging together with Danfoss A/S and the Microelectronics Center (MIC). Since 1998, he has been employed at DELTA, the department for microsystems, where focus of his work is on polymer microsystem encapsulation.

J. Branebjerg received his Bachelor degree in Electronic Engineering in 1981. He was employed as R&D Engineer at Radiometer A/S in Copenhagen from 1982 to 1988 developing electrochemical medical sensors. From 1989 to 1997, he worked as R&D engineer at Danfoss A/S, Denmark. He got his PhD degree in microtechnology from MIC, DTU, Denmark in 1991. From 1991 to 1997 he was project manager for a research project on microchemical analysis systems. Since 1997, he has worked as project manager at DELTA with the responsibility of development and supply of microsystems services in the areas of packaging, testing and reliability. He is currently managing the microsystems group of 10 people.

A.C. Hoogerwerf received his Masters Degree with honors from Delft University of Technology, where he graduated on a Thesis: ''Classification of Measurement Principles''. He temporarily worked at Philips Central Research Labs, Eindhoven, before starting his PhD studies at the University of Michigan, Ann Arbor, MI. As a part of his PhD studies he developed a three-dimensional neural recording probe assembly, constructed of silicon micro-machined components. The three-dimensional probe has been used successfully to record in vivo neural signals. The PhD degree was conferred upon him in 1992, for a Thesis titled: ''A Three-Dimensional Neural Recording Array''. He then joined Ascom Microelectronics, Bevaix, Switzerland, where he worked on the development of piezoresistive silicon accelerometers and pressure sensors. The development included the design of the sensors and the modification of the fabrication processes intended to improve yields. In 1994, he joined the CSEM, where he has been responsible for the creation of a CAD department. This includes the purchase of the necessary hardware as well as the specialized software necessary for microsystems development and production. In 1996, he took over the responsibility for the Mechanical Microsystems department. In this function, he is responsible for the development of microsystems for acceleration, absolute and differential pressure measurements, as well as silicon microphone technology.

S. Bouwstra received his MSc in Mechanical Engineering in March 1984 from the University of Twente, The Netherlands. In April 1984 he joined the Micromechanics research group at the University of Twente as an Associate Researcher, where he was active in public-private collaboration projects with Oce Copiers BV and ASM International BV, respectively. He received his Doctorate degree in March 1990 based on his thesis entitled ''Resonating Microbridge Mass Flow Sensor''. After this he was awarded a Research Fellowship of the Royal Dutch Academy of Sciences, with which he collaborated with the Center for Integrated Sensors and Circuits of the University of Michigan, USA. In November 1992 he was appointed Associate Professor at Mikroelektronik Centret at the Technical University of Denmark, where he has been responsible for the Micro-Electro-Mechanical Systems research and education programme. Since January 2000 he has joined the private company Microcosm Technologies BV in The Netherlands, the European technical office of Microcosm Technologies Inc., where he is responsible for the company's Technical Services in Europe.

Paper 6

J. Janting, J. Branebjerg, P. Rombach

Encapsulation for a three-dimensional microsystem

Patent application PCT/DK00/00559

(12) INTERNATIONAL APPLICATION PUBLISHED UNDER THE PATENT COOPERATION TREATY (PCT)

(19) World Intellectual Property Organization
International Bureau

(43) International Publication Date
12 April 2001 (12.04.2001)

PCT

(10) International Publication Number
WO 01/26136 A2

(51) International Patent Classification[7]: H01L

(21) International Application Number: PCT/DK00/00559

(22) International Filing Date: 5 October 2000 (05.10.2000)

(25) Filing Language: English

(26) Publication Language: English

(30) Priority Data:
PA 1999 01428 5 October 1999 (05.10.1999) DK

(71) Applicant *(for all designated States except US)*: **DELTA DANISH ELECTRONICS, LIGHT & ACOUSTICS** [DK/DK]; Venlighedsvej 4, DK-2970 Hørsholm (DK).

(72) Inventors; and

(75) Inventors/Applicants *(for US only)*: **JANTING, Jacob** [DK/DK]; Slangerupgade 27 B, 1. tv., DK-3400 Hillerød (DK). **BRANEBJERG, Jens, Anders** [DK/DK]; Stumpedyssevej 9, DK-2970 Hørsholm (DK). **ROMBACH, Pirmin** [DE/DK]; Christian X's Allé 92, DK-2800 Lyngby (DK).

(74) Agent: **PLOUGMANN, VINGTOFT & PARTNERS A/S**; Sankt Annæ Plads 11, P.O. Box 3007, DK-1021 Copenhagen K (DK).

(81) Designated States *(national)*: AE, AG, AL, AM, AT, AT (utility model), AU, AZ, BA, BB, BG, BR, BY, BZ, CA, CH, CN, CR, CU, CZ, CZ (utility model), DE, DE (utility model), DK, DK (utility model), DM, DZ, EE, EE (utility model), ES, FI, FI (utility model), GB, GD, GE, GH, GM, HR, HU, ID, IL, IN, IS, JP, KE, KG, KP, KR, KR (utility model), KZ, LC, LK, LR, LS, LT, LU, LV, MA, MD, MG, MK, MN, MW, MX, MZ, NO, NZ, PL, PT, RO, RU, SD, SE, SG, SI, SK, SK (utility model), SL, TJ, TM, TR, TT, TZ, UA, UG, US, UZ, VN, YU, ZA, ZW.

[Continued on next page]

(54) Title: ENCAPSULATION FOR A THREE-DIMENSIONAL MICROSYSTEM

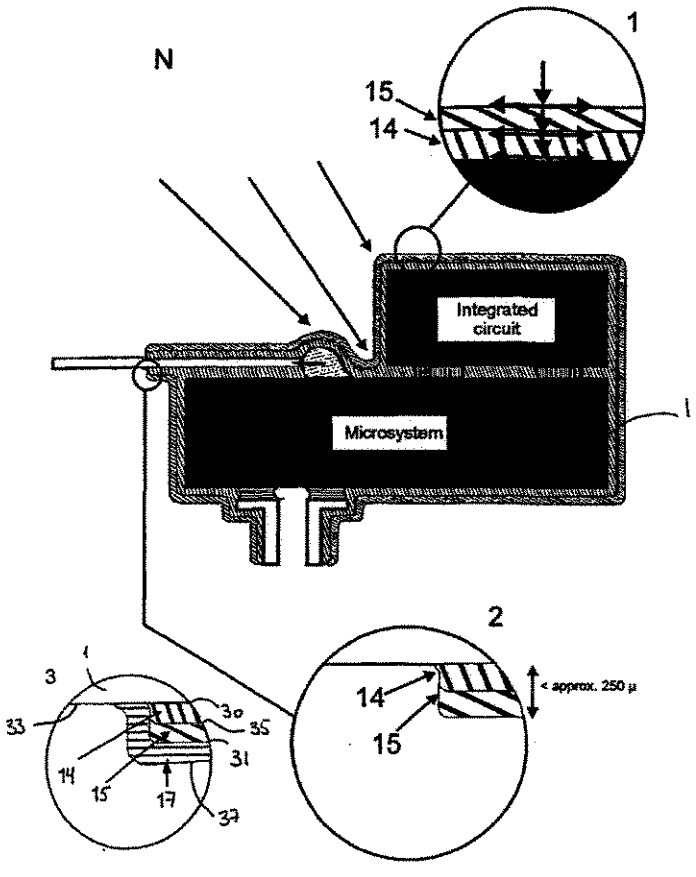

(57) Abstract: The present invention relates to an encapsulation for a microsystem. The microsystems may comprise a sensor, transducer, actuator, MEMS or other three-dimensional microsystems. The encapsulation may serve as a protection against environments such as, chemical attack, physical attack, fluid penetration and Electro Magnetic Interference. The choice of materials of the encapsulation depends on the object of encapsulation. The actual encapsulation may be applied by providing a first layer of a first material onto at least part of an outer surface of the microsystem, providing a second layer of a second material onto the first layer.

WO 01/26136 A2

(84) **Designated States** *(regional)*: ARIPO patent (GH, GM, KE, LS, MW, MZ, SD, SL, SZ, TZ, UG, ZW), Eurasian patent (AM, AZ, BY, KG, KZ, MD, RU, TJ, TM), European patent (AT, BE, CH, CY, DE, DK, ES, FI, FR, GB, GR, IE, IT, LU, MC, NL, PT, SE), OAPI patent (BF, BJ, CF, CG, CI, CM, GA, GN, GW, ML, MR, NE, SN, TD, TG).

Published:

— *Without international search report and to be republished upon receipt of that report.*

For two-letter codes and other abbreviations, refer to the "Guidance Notes on Codes and Abbreviations" appearing at the beginning of each regular issue of the PCT Gazette.

ENCAPSULATION FOR A THREE-DIMENSIONAL MICROSYSTEM

FIELD OF THE INVENTION

The present invention relates to an encapsulation of a three-dimensional microsystem wherein the encapsulation comprises one or more layers with essentially constant thickness.

BACKGROUND OF THE INVENTION

Protective encapsulation is the final step in microsystem manufacturing. In most cases the encapsulation make up the main part of the microsystem volume and most of the price. This is the background for the interest in reducing the amount of encapsulation material used. To achieve a significant reduction in the amount of materials used, the right choice of materials and processing methods is crucial for the lifetime, performance, and cost of the system.

Lifetime and performance are strongly connected with the fact that many systems are exposed to chemically, physically and electro-magnetically hostile environments. Microelectronics is e.g. very sensitive to corrosion due to water encapsulated on the device or water penetrating the encapsulating material. Therefore, a lot of effort is put into avoiding the encapsulation of water and using protective tight materials and seals/and/or bondings between silicon, metals, polymers, and ceramics.

Packaging concepts for silicon based micro mechanical sensors exposed to harsh environments are disclosed in "Reliability of industrial packaging for microsystems" by de Reus et al., Microelectronics Reliability 38 (1998) 1251-1260. Two-dimensional protective properties of coatings of silicon carbide, Si-Ta-N, Parylene C, and diamond-like carbon are described and, further, different glue types for sensor chip mounting have been investigated for leakage, degradation, and influence on sensor performance.

A lot of related work has been going on during the last 25 years, but the focus of this work has not been on three-dimensional Chip Scale Packaging (CSP), but on how to protect two-dimensional components and conductors on Printed Circuit Boards (PCBs) and later microsystems with coatings.

A bi-layer protective coating system for Micro Electro Mechanical Systems (MEMS) is described in "Interface-Adhesion-Enhanced Bi-layer Conformal Coating for Avionics Application" by Wu et al., 1999 International Symposium on Advanced Packaging Materials p. 302-310. The bi-layer structure is selected because of property limitations of a single material. The first layer is mainly applied to planarize the MEMS surface. A second functionality of the first layer is to form a durable dielectric insulation, stress relief, and shock/vibration absorber. The second layer forms a barrier.

In "C-SHIELD Parylene allows major weight saving for EM shielding of microelectronics" by Noordegraaf et al., PEP'97, The first IEEE International Symposium on Polymeric Electronics Packaging, 189-196, a two-dimensional conformal bi-layer coating system for microelectronics protection is described. The first layer serves primarily as an electrical insulation / chemical barrier whereas the top layer serves as Electro-Magnetic Interference (EMI) protection.

Finish Patent application FI 956226 describes a method for coating electronics conformally with polyanilline for EMI shielding of electronics, with emphasis on PCB's.

US 5,639,989 discloses two-dimensional multilayer conformal EMI coatings for PCB protection. The first layer is an insulating layer whereas the others are shielding layers tuned to a specific shielding application.

US 4,977,297 and US 4,982,056 disclose an electronic circuitry having on at least one of its exposed surfaces a protective coating of Teflon® AF 1600.

SUMMARY OF THE INVENTION

It is an object of the present invention to provide a three-dimensional Chip Scale Packaging (CSP) that minimises the overall volume of an encapsulated microsystem.

It is a further object of the present invention to provide an encapsulation protecting the microsystem against environmental influences such as chemical attack, physical attack, fluid penetration, electromagnetic interference (EMI), etc., separately or in various combinations.

It is still a further object of the present invention to provide an encapsulation that protects the environment against the microsystem such as against leakage of chemicals from the microsystem to the environment.

The above-mentioned and other objects are complied with by providing in a first aspect an encapsulation for a three-dimensional microsystem having an outer surface, said encapsulation covering at least a part of the outer surface of the microsystem, the encapsulation comprising

- a first layer of a first material, said first layer defining a first interface region with the outer surface of the three-dimensional microsystem,

- a second layer of a second material having an outer surface, said second layer being held by the first layer and defining a second interface region with said first layer,

wherein the shortest distance between the first and second interface regions is essentially constant, and wherein the shortest distance between the first interface region and the outer surface of the second layer is essentially constant and between 5 μm and 500 μm.

In the present context, the shortest distance is measured in a direction substantially perpendicular to the outer surface of the outermost layer. The shortest distance between the first interface region and the outer surface of the second layer should, thus, be understood as the distance between the first interface region and the outer surface of the second layer in a direction substantially perpendicular to the outer surface of the microsystem.

The encapsulation may further comprise a third layer of a third material being held by the second layer and defining a third interface region with said second layer, the shortest distance between the first interface region and the outer surface of the third layer, thus, being determined as the distance between the first interface region and the outer surface of the third layer in a direction being substantially perpendicular to the outer surface of the third layer.

In a preferred embodiment the shortest distance between the first interface region and the second interface region may be between 5 μm and 250 μm, such as between 10 μm and 250 μm, such as less than 250 μm, such as less than 200 μm, such as less than 150 μm, such as less than 100 μm, such as less than 75 μm, such as less than 50 μm, or even such as less than 20 μm, such as less than 15 μm, or such as less than 10 μm, such as approximately 5 μm.

The shortest distance between the first interface region and the outer surface of the second layer may be essentially constant and between 5 μm and 500 μm, such as between 10 μm and 500 μm, such as less than 500 μm, such as less than 400 μm, such as less than 300 μm, preferably less than 250 μm, such as less than 200 μm, such as less than 125 μm, such as less than 100 μm, such as less than 50 μm, or even such as less than 20 μm, such as less than 15 μm, or such as approximately 10 μm.

In the present context the term microsystem should be understood as a micromechanical transducer, sensor or multi-chip system. The microsystem may be a pure mechanical system or it may be a combination of a mechanical and an

electrical system e.g. an accelerometer. Such systems may be adapted for measuring the flow of a fluid, static or dynamic air pressure, temperature, acceleration, velocity, etc.

The three-dimensional microsystem may be a miniature component, which has at least one transducer function that converts electric or optical energy to or from energy in another domain, such as a mechanical, magnetic, chemical, and/or biological domain, or the at least one transducer function may convert energy between electric and optical energy and/or vice versa. The transducer functions may be used for sensing, actuation or energy converting purposes. Several transducer functions may be combined in one system, and also signal-conditioning functions may form part of the system.

Typically, three-dimensional microsystems are micromechanical sensors like pressure and flow sensors, accelerometers, or chemical or biochemical sensors or sensor systems. A three-dimensional microsystem may further be electro-optical components and integrated optical systems, which contains several optical functions. Other examples are actuators such as miniaturised valves, pumps and/or relays. In more complex three-dimensional microsystems such as MEMS (micro electromechanical systems), micro-fluidic systems or chemical/biochemical microsystems, several actuator and/or sensing functions may be combined to a miniature system often integrated with electric or optic signal conditioning functions.

In a second aspect, the present invention relates to an encapsulation for a three-dimensional microsystem having an outer surface, said encapsulation covering at least a part of the outer surface of the microsystem, and the encapsulation comprises

- a layer comprising a plurality of materials, said layer defining a first interface region with the outer surface of the three-dimensional microsystem and having an outer surface, wherein the material composition of the layer, in a region between the first interface region and the outer surface of the layer and along a direction

defined as the shortest distance between the first interface region and the outer surface, varies as a function of a distance from the first interface region.

Hereby, one layer of material may be adapted to shield the microsystem effectively against different environmental effects so that different parts of the one layer of material shield against different environmental effects according to the composition of the layer.

The plurality of materials may for example comprise a polymer, and the polymer may comprise a filler. The filler may comprise a material selected from the group consisting of ceramics and metals. A ceramic filler may reduce the thermal coefficient of expansion (TCE) of the material so as to for example approach the low TCE of silicon, and further enhance the thermal conductivity of the material. A metallic filler may for example enhance the conductivity of the material.

Preferably, the shortest distance between the first interface region and the outer surface may be essentially constant and the shortest distance may be between 5 μm and 500 μm, the shortest distance may thus be larger than 5 μm, such as larger than 10 μm, or even larger that 15 μm, such as larger than 20 μm, and the shortest distance may at the same time be less than 500 μm, such as less than 400 μm, such as less than 300 μm, such as less than 250 μm, preferably less than 250 μm, such as less than 200 μm, such as less than 125 μm, such as less than 100 μm, or even less than 50 μm, such as less than 25 μm.

Hereby, a minimum of encapsulation material may be used, thus reducing the cost of the microsystem packaging, and, further, the overall size of the microsystem is not remarkably increased.

In a third aspect, the present invention relates to an encapsulation for a three-dimensional microsystem having an outer surface, said encapsulation covering at least a part of the outer surface of the microsystem, the encapsulation comprising

- a first layer of a first material, said first layer defining a first interface region with the outer surface of the three-dimensional microsystem,

- a second layer of a second material, said second layer being held by the first layer and defining a second interface region with said first layer, and

- a third layer of a third material having an outer surface, said third layer being held by the second layer and defining a third interface region with said second layer.

The first layer may comprise a non-conducting material, the second layer may comprise a first conducting material and the third layer may comprise a second conducting material. The second layer may further comprise a seed layer so as to increase adhesion of the third layer.

In a fourth aspect, the present invention relates to a method for encapsulating a three dimensional microsystem having an outer surface, said method comprising the steps of

- providing a first layer of a first material onto at least part of the outer surface of the microsystem,

- providing a second layer of a second material onto the first layer, and

- rotating the three dimensional microsystem around at least a first and a second rotation axis while providing at least one of the first and second layers, said at least first and second rotation axis intersecting the three dimensional microsystem, and wherein the first axis is different from the second axis.

In a fifth aspect, the present invention relates to a method for encapsulating a three dimensional microsystem having an outer surface, said method comprising the steps of

- providing a layer onto at least part of the outer surface of the microsystem, said layer comprising a plurality of materials,

- rotating the three dimensional microsystem around at least a first and a second rotation axis while providing the layer and varying the material composition of the provided layer as a function of time, wherein the at least first and second rotation axis intersects the three dimensional microsystem, and wherein the first axis is different from the second axis.

In a sixth aspect, the present invention relates to a method for encapsulating a three dimensional microsystem having an outer surface, said method comprising the steps of

- providing means for providing a first and a second layer onto at least part of the outer surface of the microsystem,

- providing the first layer of a first material onto at least part of the outer surface of the microsystem,

- providing the second layer of a second material onto the first layer, and

- rotating, while providing the first and second layer, the three dimensional microsystem and the means for providing the first and second layer relative to each other, the rotation being performed around at least a first and a second axis, wherein the first axis is different from the second axis.

In a seventh aspect, the present invention relates to a method for encapsulating a three dimensional microsystem having an outer surface, said method comprising the steps of

- providing means for providing a layer onto at least part of the outer surface of the microsystem, said layer comprising a plurality of materials,

- providing the layer onto at least part of the outer surface of the microsystem,

- rotating, while providing the layer, the three dimensional microsystem and the means for providing the layer relative to each other around at least a first and a second axis, wherein the first axis is different from the second axis.

Regarding the fourth, fifth sixth and seventh aspects, the at least first and second axis may be substantially perpendicular to each other.

The materials to be used for the encapsulation of the microsystem may be carefully chosen to make sure that optimum protection of the microsystem is achieved. For example, each of the layers of the encapsulation or each part of the one layer of material having a varying material composition may possess different material properties and different material characteristics, and thereby each layer or each part of the one layer may have a specific function. The combination of the materials may furthermore provide synergy effects, i. e for example one layer acting as seed layer for another layer, etc., whereby the overall properties of the encapsulation may be improved.

Furthermore, for the encapsulation to be able to withstand harsh environment a certain thickness of the encapsulation material is needed both because a tight film without pinholes is needed and because, other things being equal, longer time is needed to etch through a thicker film.

At least one of the layers of the protective encapsulation may comprise a conductive material to shield E-fields. Pure metals having high conductivity values, for example Ag having a conductivity of 62×10^6 S/m and Ni having a conductivity value of 14×10^6 S/m may be used as conductive material. Furthermore, alloys having high conductivity values may be used, for example Heusler alloy (61Cu26Mn13Al) having a conductivity value of 14×10^6 S/m or Supermalloy (79Ni16Fe5Mo) having a conductivity value of 1.7×10^6 S/m may be used.

Furthermore, in order to shield for H-fields at least one of the layers may comprise a material with a relative magnetic permeability between 100 and 1000, for example such as larger than 100, such as larger than 200, such as larger than 300, such as larger than 500, such as larger than 750, such as larger than 1000, or the relative magnetic permeability may even be larger than 1000. Some pure metals have a high relative permeability (μ), for example Fe having a relative permeability of 1000 and Ni having a relative permeability of 250. Furthermore, alloys may be used, such as Heusler alloy having a relative permeability of 800, such as Supermalloy having a relative permeability of 100000, etc. Ni containing materials have the further advantage that the durability against chemical attacks is relatively high.

It is envisaged that any metal or alloy having a high conductivity value and/or a high relative permeability may be used.

Another layer may comprise a non-conductive material. Typically, the non-conducting layer is the layer closest to the microsystem. The layer may be for example a Teflon® layer, a hydrocarbon containing layer, a parylene layer, etc. The layer may be a thin layer such as a layer having a thickness between 5 μm and 50 μm, such as a layer having a thickness below 50 μm, such as below 25 μm, preferably such as below 20 μm, such as below 10 μm, or even more preferred approximately 5 μm. Typically, the microsystem comprises silicon chips, the silicon chips having very sharp edges and/or corners. It may by conventional coating materials and techniques be difficult to coat these sharp edges and/or corners. By choosing a material having a low viscosity and/or a low surface tension, these edges and/or corners may be coated, for example by applying a dip coating process, for applying the first layer. Hereby, the corners and edges are softened so that application of additional conformal layers are facilitated even with processes not suitable for covering of sharp corners and edges.

Furthermore, hydrocarbons like the GURONIC®, a group of materials from Paul Jordan, Electrotechnische Fabrik GmbH & Co., may be applied by e.g. a dipping

technique. The GURONIC® materials are soft and water-repellent and therefore suitable for the first layer of material to absorb shock and vibrations, and furthermore the materials are suitable for the outer protective layer because of their water-repellent characteristics.

Still further, parylene materials poly(chloro-p-xylylene) may be a group of polymers suitable for protective coating of microsystems and microelectronics in general. During a vacuum process, the dimer is evaporated to form a monomer and the monomer condenses on the sample where it polymerizes. The process may be undertaken at room temperature, and the thickness of the parylene layers are typically between 5 μm and 25 μm, for example such as less than 25 μm, such as less than 15 μm, preferably such as less than 10 μm, for example such as about 5 μm. The parylene layer may be substantially pinhole free, and is furthermore a very tight and durable material in itself.

In addition, in order to prevent water penetrating the encapsulation, at least one of the layers may comprise a material having a water permeability between 10^{-19} g/cm·s·torr and 10^{-9} g/cm·s·torr, such as below 10^{-9} g/cm·s·torr, such as less than 10^{-11} g/cm·s·torr, such as less than 10^{-13} g/cm·s·torr, preferably less than 10^{-15} g/cm·s·torr, such as less than 10^{-17} g/cm·s·torr, such as below 10^{-19} g/cm·s·torr. Materials like e.g. plated metals like Ni and Au and furthermore electroless Ni are tight encapsulation materials because they are amorphous and therefore grain boundary water diffusion will limited.

The encapsulation may comprise a variety of materials e.g.: semiconductors, ceramics, oxides, metals, polymers, hydrocarbons, and silicones.

The encapsulation may further comprise at least one layer that protects the microsystem against light.

The microsystem may be completely encapsulated with at least one layer of material. Alternatively, the encapsulation may have one or more openings each of

said one or more openings extending from an outermost surface of the encapsulation to the outer surface of the microsystem.

The above-mentioned openings may be adapted for different applications. Some of the one or more openings may be adapted for passing fluids to and from the microsystem. Some of the one or more openings may alternatively or additionally be adapted for transmitting electrical signals to and from the microsystem. Finally, some of the one or more openings may be adapted for transmitting pressure, such as an air pressure or a liquid pressure, to the microsystem.

Each layer of the encapsulation or each of the materials of the encapsulation may be designed for a specific use, i.e. to protect the microsystem against penetrating water, shielding the microsystem against EMI E-fields, and/or against magnetic H-fields, etc. Furthermore, more layers may be used, such as 4, 5, 6 and 7 layers, and even up to 10 and 15 layers may be used, and further each layer may comprise for example a first and a second material, the materials being distributed in a sandwich structure, comprising up to 10, 20 or as many as 50 or even up to 100 alternating structures. Repetitions of the layer structures may be more effective than single layers of materials for example for EMI E-field shielding since the most effective E-field damping takes place at the interface between these layers by reflection.

Traditionally, polymer chip encapsulation is performed with quarts filled epoxies by injection/transfer moulding at pressures and temperatures too high for direct contact with the microsystems of concern. The minimum thickness of the material is due to the processing methods limited to around 0.25 mm. Alternatively, more gentle encapsulation processes, such as spraying and/or dipping may be applied. By spraying the encapsulation material onto the microsystem, several advantages may be obtained.

For example, by spraying encapsulation material onto the microsystem, the amount of applied material may be controlled. Furthermore, even badly adhering materials may be applied. The materials to be sprayed onto the microsystem

should preferably have a relatively low viscosity to enable spraying of the materials. Alternatively, the materials may be diluted so as to obtain a material having a viscosity suitable for spraying. The viscosity suitable for spraying depend upon the spaying equipment used, but, typically, a viscosity suitable for spaying may be less than 5 Pascal·second, such as less than 1 Pascal·second, for example such as approximately 0,7 Pascal·second.

To avoid shadowing effects, the microsystem and/or the spray nozzle may be kept in specific positions so as to avoid the shadowing effects, and for example avoid keeping the spray nozzle and the microsystem in stationary positions.

Another example of a process suitable for encapsulation of microsystems is a dipping process, the dipping process being a fairly simple process, and again the materials to be used should preferably have a relatively low viscosity or the materials should be diluted so as to obtain a material having a relatively low viscosity.

Both the spraying process and the dipping process may be used at ambient pressures and temperatures.

By using a dipping process the applied amount is controlled primarily by the surface tension of the selected materials which may result in a coating having an uneven thickness, i.e. a coating being thinnest at the corners of the structures, thus, lowering the reproducibility of the process. To obtain a more conformal coating, the microsystem with the newly applied material may be spinned so as to ensure a proper distribution of the material.

Furthermore, to avoid the thinning effect at the very steep corners, an alternative design of the corners may be used. The very sharp corners and edges may e.g. be softened by applying a step structure so that each corner comprises one or more steps, i.e. two or more corners.

By using a spraying process the applied amount of material is more easily controlled, and by paying attention to the shadowing problem, i.e. the problem that some parts of the system may not be exposed to the applied material due to shadowing by the system itself, the process may be well controlled. It is furthermore important to control the creation of drops on the surface of the microsystem to be spray coated.

To spray coat a first layer of for example Teflon® may be a difficult task due to the poor wetting of the first Teflon® layer. However, by adapting the application speed of the material, the droplets may be allowed to cure and/or dry sufficiently fast upon impact with the surface. In this way retraction of the material because of poor wetting is avoided. Thus, by choosing the application speed for the specific application, coating of the Teflon® layer may be accomplished.

To obtain a well controlled process, the microsystem may be rotated around one or more axes whereby excess material may be removed and/or forced to move to uncovered or badly covered areas e.g. corners, edges, and surfaces difficult to wet. Alternatively, the spray nozzle may be rotated around the microsystem or the microsystem may rotate around one or more axes while the spray nozzle rotates around the microsystem during deposition. In this way by automatically rotating both the microsystem and the spray nozzle during deposition the shadowing effect may be significantly reduced during the spraying process and an improved reproducibility may be obtained.

Since the thickness of the coatings may be down to a few tenth of a mm, particles in the environment during processing may cause for example pinholes and other severe problems for the quality of the coating to occur in the encapsulation, and therefore, the processes are preferably undertaken in clean room environments.

In order to obtain a smooth conformal coating, it is preferred to use materials having a low viscosity and/or a low surface tension, or, alternatively, materials that

may be diluted and/or dissolved so as to lower the viscosity and/or the surface tension of the materials.

Another process for applying polymer materials to form an encapsulation of the microsystem may be fluidised bed coating. In this process air is blown through powder of the material to make the powder behave like a liquid. The powder particles then melt on the surface of the immersed preheated sample. The material may be applied in thickness' from 0.1 mm and up.

When metallizing a non-conductive surface, a number of application techniques may be applied, for example galvanic plating, electroless plating, spraying, dipping, Physical Vapour Deposition (PVD), Low Temperature Arc Vapour Deposition (LTAVD), Chemical Vapour Deposition (CVD), etc. In some cases the purpose of the deposited conductive layer (seed layer) is to make it possible to galvanically plate afterwards and/or to get a better adhesion of the plated material. Some of the techniques are directional (e.g. spray, PVD) so that shadowing may occur due to the way the material is supplied during deposition. Rotation of the sample and/or the source of material supply may be able to at least reduce problem.

The materials relevant for application of a conductive layer on three-dimensional microsystems are numerous, the materials may be certain polymers (e.g. polyaniline), polymers containing fillers, the fillers comprising conductive particles, semiconducting materials, certain ceramics, such as for example TiN deposited by ECRPCVD (Electron Cyclotron Resonance Plasma Chemical Vapour Deposition) and/or metals. Amorphous continuos layers achieved by using electroless plating are preferred because they may be tight, i.e. substantially pinhole free and are generally more durable towards chemical attacks.

A chemical attack on the microsystems may for example be mainly due to encapsulated water or water penetrating the encapsulation of the microsystem. Hereby, mainly the microsystem is affected whereas the encapsulation material may not be severely affected. The microsystem may also be exposed to harsh

media attacking both the encapsulation materials and the microsystem underneath. In many sensor microsystems, it is therefore advantageously that the encapsulation materials themselves are highly durable towards chemical attacks. There are several material factors that generally increase resistance to humidity, some of those are:

1) Low water transmission and equilibrium absorption
2) Low ionic content
3) Low hydrolysis
4) Low plasticization by water
5) Low polar content
6) Good adhesion to fillers
7) Low moisture absorption by fillers
8) Low change on exposure to heat and contaminants
9) Low internal stress

It is, thus, important that there are no means in the material that absorbs the water, and further, if water should be absorbed by the encapsulation materials, it is important that the water is not transported to the first interface region by means of, for example, ions in the encapsulation material. It is furthermore advantageous that the encapsulation material has a good adhesion to fillers that may be contained in the encapsulation material so as not to allow water to migrate in boundary surfaces of bad adhesion between the encapsulating material and the fillers.

Physical attacks such as shock and wear may also often be considered very important. The factors that increase the resistance of the encapsulation materials and the resistance of the microsystems are in these cases their softness, hardness and ductility, respectively. The E-field EMI shielding becomes more and more important and shielding may be accomplished by use of conductive materials. Highly conductive materials are good shields against E-fields, and in many cases the material may preferably also have a high magnetic permeability to shield H-fields effectively.

Furthermore, other than the intrinsic properties of the materials may be evaluated when the materials are to be used for encapsulation of microsystems. Also to be considered when choosing the optimum material is the amount of material to be used, the interaction between the material and the microsystem, and further how the material may be applied. That is, also the following factors should be considered when talking about factors enhancing resistance to water:

10) Large amount encapsulation material
11) Low stress coupling
12) Good adhesion
13) Low chemical / physical change of protected system by water

If the material, for example, has a high stress coupling, it would be likely that cracks would occur when the microsystem and the encapsulation are affected by the environments so that water would be able to migrate through the encapsulation material to the outer surface of microsystem, so, therefore, a low stress coupling may be preferred.

The microsystem encapsulation materials properties may preferably fulfil a number of criteria, either each material as such or the combination of the materials. The encapsulation should be chemically durable, have a bulk water and/or gas tightness, and have an interface water tightness. Furthermore, the encapsulation material(s) and the microsystem materials should be compatible, for example with regard to thermal expansion, stress couplings, etc. Still further, the encapsulation material(s) should preferably form a conformal and thin coverage of the microsystem, and still preferably be applicable by a gentle application method.

The chemical durability and bulk water tightness are even more important when encapsulating microsystems, such as multichip microsystems, than when encapsulating traditional ICs with polymers, for example by applying a globtop, since the coatings according to the present invention are much thinner - of the order of a few tenths of a mm, see above. These factors represent severe

constraints on the range of materials that may be used. In many cases traditional encapsulation materials like quartz/glass-filled epoxies and injection/transfer moulding techniques are not suitable due to the implied high pressures and temperatures during processing. Choosing a very chemically inert material results often in a material having a less good adhesion which again may result in a poor water tightness. Generally, polymers are less water tight than materials like glasses and metals, see Figure 6. On the other hand polymers, such as fluorocarbons, may be more chemically durable than most pure metals, alloys and ceramics. The drawback for fluorocarbons may be that they, due to their very low surface tension and strong C-F bonds, in many cases adhere badly to most materials.

The surface tension is an important parameter since it has a great influence on whether it is possible to make a conformal and thin (between 5 μm and 500 μm, such as between 10 μm and 500 μm) coverage of the multichip microsystem with avoidance of entrapped air. The adaptation of the coverage to the shape of the microsystem is a very critical issue, since microsystems often are made of single crystalline silicon that results in very sharp corners which may be difficult to cover.

Preferably, the encapsulation material(s) should also be chemically and physically compatible with the other materials of the microsystem, not e.g. dissolving any of the materials nor introducing too much stress, etc. Typically, the microsystem comprises Silicon and/or other semiconductor materials, ceramics, polymers, such as polyimides, epoxies, silicones, etc, and metals.

Polymers in the microsystems may be difficult to wet due to their low surface energy and they may be the materials most chemically sensitive e.g. toward solvents in the coating materials. Therefore, polymers represent the biggest challenge concerning chemical compatibility. Polymers may typically be used for encapsulation and underfilling, support of interconnections, such as flex prints, flexible silicon, and other attachments, etc. The larger the exposed polymer area relative to easily wettable areas, the more difficult it may be to cover that area with

a small amount of material and at the same time avoid air entrapment. Typically, the largest areas are represented by polymer encapsulated ICs and insulating materials on interconnections.

Typically, the encapsulation materials suitable for encapsulating electronics are not so tight that it is ensured that the performance will not be affected more or less severely by chemicals penetrating through the encapsulation during the service time of interest. There are no general leak rate limits to ensure proper performance within lifetimes of interest since the allowable leak rate depends on the penetrating chemical and on the exact system considered. Furthermore, it is difficult to correlate between leak rates of different chemicals. Often when interested in the leak rate of water the measurement is made on helium.

Polymers, even when modified by fillers, etc., have a relatively poor water tightness and a high Coefficient of Thermal Expansion (CTE) compared to the silicon in the microsystem . making them less suitable for microelectronics encapsulation purposes. However, due to their low price and ease of handling polymers are very attractive.

It is often impossible to find one encapsulation material which sufficiently protects for all of the above-mentioned areas at the same time. It is therefore preferred to combine different materials having different material properties so that the encapsulation of the microsystem comprises one or more layers of material.

In the case where water tightness is a problem, adhesion may be promoted by using a suitable encapsulation material, such as an encapsulation material comprising silane with organic / inorganic chemical coupling groups and/or by roughening, activating, priming and/or cleaning of the adhesion surface by e.g. plasma treatment, such as cold oxygen plasma treatment, etc so as to increase the surface tension and reactivity of especially polymers thereby also increasing the adhesion of applied polymeric coatings. Furthermore, sealing of the surface by for example applying an epoxy material at the critical areas may be used.

Example of layer structures and processes to fulfil the demands in the previously described are presented in the following. As described the sensitivity of the microsystems and the choice of materials strongly affects the application methods that can be used.

BRIEF DESCRIPTION OF THE DRAWING

Figure 1 shows examples of devices that may be encapsulated according to the present invention,

Figure 2 shows further examples of devices that may be encapsulated according to the present invention,

In Figure 3 two embodiments, L, M, wherein an microsystem as well as an integrated circuit (IC) are encapsulated according to the present invention,

Figure 4 shows details of the coatings of an encapsulated device,

Figure 5 illustrates an embodiment, O, with air entrapped within the encapsulation and an embodiment, P, with underfilling and attachment material,

Figure 6 shows an embodiment having flexible silicon interconnections

In Figure 7 the permeability for various materials such as silicon and glasses are shown,

Figure 8 shows the variation in thickness of the encapsulation depending on how the encapsulation is performed,

Figure 9 illustrates an example of how the encapsulation can be applied, and

Figure 10 shows the variation in a graded composition of a layer in an encapsulated microsystem.

DETAILED DESCRIPTION OF THE DRAWING

In Figure 1 and Figure 2 examples of devices that may be encapsulated are shown. The device to be encapsulated may have the microelectronics integrated with the sensor or the sensor may have the microelectronics included as a separate part. Examples of both cases are shown in Figure 1 A-H. The microelectronics and the sensor may be interconnected via for example bonding wires as shown in device I.

The microsystem may thus comprise several elements, each element having a functionality, such as the microsystem 1, the microelectronics 6, the one or more openings 2, one or more interconnecting and/or carrying chips or parts.

Thus, the device to be encapsulated may be an microsystem for measuring:

- Absolute / relative pressure, sound pressure such as A, E,
- Differential pressure / flow (fluid) / chemical composition such as B, F,
- Light (flow / chemical composition etc.) such as C, G,
- Acceleration (D, H, I).

In Figure 1, the microsystem/transducers 1 have one or more windows or openings 2 (tube 20, transparent material 21, sensing material (not shown)) through which the surroundings have an effect on the microsystem 1, 3 is the window mounting material, 4 is a signal in/out wire, 5 are electrical interconnections (solderings, conductive adhesives, flip-chips, etc.), 6 is an ASIC or other microelectronic component, 7 is a supporting substrate, leadframe etc., 8 is a bondpad and 9 is a bondwire.

In many cases the measurement is performed through a certain port in the microsystem. In Figure 1 (A, B, E and F) a little tube 2 leads the pressure (from e.g. gas, liquid, sound) or material to/past a sensing area on the microsystem. In C and G an optical window of e.g. glass is connected with the microsystem. The

optical window may further be connected to e.g. tubes leading a substance to be analysed past the window. The tube or window material and therefore the mounting material as well as the mounting method may vary, and the tube may even be an integrated part of the microsystem.

Figure 1 (D and H) illustrate the cases where a port is not required e.g. when measuring acceleration. Other microsystems may be similar to these figures e.g. relays, switches etc.

In all of the figures the output signal from either an Application Specific Integrated Circuit (ASIC) or integrated microelectronics is transferred through soldered wires, though it could just as well be a soldered and/or glued flex prints, bond wires, one or more optical fibres, etc. The devices I, J and K, in Figure 2 illustrate various connections, such as a bond wire 9, a flex print 10, a soldering/gluing 11, an optical fibre 12, and a fibre interconnection 13.

Figure 3 shows two embodiments (L and M) of an encapsulated multichip microsystem. In a first embodiment, L, an encapsulated device like E in Figure 1 has been coated with a first conducting layer 14. The conducting layer serves as an EMI shield while at the same time enhancing the physical durability of the microsystem. The layer has been applied by spraying.

In the embodiment, M, the outer plated metal layer 15 is e.g. a Fe-containing layer having a high conductivity and a high magnetic permeability, and is applied on top of the first Teflon® layer 14. The outer layer serves as an EMI E-field and H-field shield while at the same time enhancing the overall water tightness and chemical and physical durability of the encapsulation by several orders of magnitude. The polymer underneath primarily serves as a highly insulating, stress and shock absorbing layer between the EMI shielding layer 15 and the electrically conducting parts on the surface of the microsystem and the integrated circuit. The actual composition and application of the two layers are described in the following case 1.

In a third embodiment, N in Figure 4, an encapsulation like in case 2 is illustrated. Figure 4 shows how the two layers follow the shape of the microsystem closely. In the close up 1) of the two layers the arrows illustrate how e.g. chemicals and water may penetrate the encapsulation. At openings of the layer, as shown in the close up 2), it appears that e.g. water or chemicals may easily enter especially when adhesion is bad. This can be avoided by providing the encapsulation with a sealing as shown in the close up 3) where the black area represents the sealing at the opening of the coatings e.g. where a flex print made of polyimide comes out. In case the bottom layer is Teflon® and the top layer is metal there will be a bad adhesion between polyimide and Teflon® and between Teflon® and metal. By applying e.g. epoxy over the exposed open interfaces the amount of water capable of entering will be limited significantly since epoxies adheres much better to polyimide than Teflon® and very well to metals. Depending on the exact situation the sealing can cover the complete three-dimensional multichip microsystems as a coating. This may be relevant when the metal layer is less resistant to corrosion and needs to be protected.

A first interface region 30 is thus formed between an outer surface 33 of the microsystem 1and the first layer 14 of a first material and a second interface region 35 is formed between the first layer of material 14 and the second layer of material 15. Furthermore, a third interface region 31 is formed between the second 15 and third 17 layer of material. The outermost surface 37 of the encapsulation material is thus the outer surface of the third layer of encapsulation material 17

In O in Figure 5, an example of air 40 entrapped due to the lack of coating material 14 in the space between the IC and the microsystem and the microsystem and the flex print is shown. Instead of having the material 14 to fill out the gaps, a specific underfill material might have been used to avoid the entrapped air. Having air gaps in the encapsulation material may e.g. lead to development of delamination and cracks in the encapsulation if e.g. the ambient pressure changes. In a fourth embodiment, P in Figure 5, underfilling 42 is used, and it is seen that underfill material 42 and attachment material 44 are not highly exposed to the coating 14,

15. At positions where they are in contact it is crucial that the materials are compatible.

In Fig. 6 an embodiment is shown wherein different parts 50, 51, 52, 53 of the microsystem are mechanically interconnected via flexible silicon parts 54. By applying electrically conductive material 55 on the flexible silicon parts, also electrically interconnection is achieved. The different parts 50-53 of the microsystem may be flip-chip bonded to the substrate, the flip-chip bumps 60 being the interconnection between the different parts 50-53 and the silicon substrate. To achieve microsystems having a small a volume as possible, the different components/elements of the microsystem may be mounted on an interconnection substrate with regions which may be bended. By having a single substrate carrying the different components/elements of the microsystem and at the same time interconnecting the different parts, optimal compatibility between the materials of the structure and minimal size is achieved.

Figure 7 shows the time for the interior of a package to reach 50% of exterior humidity depending on the thickness of the material as well as the permeability of the material. From the figure it appears that materials such as silicones and epoxies are less tight to water than e.g. glasses and metals. Furthermore, it appears that the thickness of the material also influence on the time for interior of the package to reach the 50% humidity, i.e. a thicker material is a better protection towards water than a thinner material.

In Figure 8, the thickness of an encapsulated single crystalline silicon chip 81 is shown. A dipping process has been used for application of the encapsulation 80 in Figure 8a. From the figure, it appears that the coating is thinner at the corners and the edges 83 than at the rest of the sides of the chip. In Figure 8b the encapsulation has been applied by e.g. rotating the silicon chip 81 during coating. It appears that by rotating the chip the thickness of the encapsulation 80 is more uniform.

A way to obtain this is illustrated in Figure 9, where an microsystem is rotated around a first 90 and a second 91 axis while providing the material by providing means, such as a spray nozzle, 20. A temporary lid 93 is provided so as to ensure that the opening 2 is not encapsulated.

To be able to predict the behaviour of the materials on a specific microsystem, simulations may be performed to, dependant of the material properties of the encapsulation materials and the structure of the microsystem, predict the distribution of the materials. Preferably, the public domain software 'Surface Evolver' is used.

Instead of encapsulating the microsystem with a plurality of layers, a single layer with a graded composition of two or more materials or phases may be applied. In Figure 10 an example of how the composition of the two components varies as a function of the distance to the surface of the microsystem i.e. from a first interface region to an outer surface of the encapsulation. The materials within the encapsulation layer may be multiphase materials (composites) such as blends of immiscible polymers or polymers with fillers. When blends of immiscible polymers are used the relative amount of each component could be varied e.g. by a suitable mixing apparatus e.g. a spraying equipment.

For polymers with fillers (e.g. ceramic and metal powder) the fillers normally distribute randomly in the matrix material. However, due to gravity the fillers may gather near one of the surfaces of the polymer so that the layer becomes graded.

In case the coating is thin and therefore not graded in composition it can be made so by applying more of the matrix component. Also reacting materials like e.g. multi chemical component systems such as 2 component epoxy may be used. The relative amount and / or chemical structure of the reacting components are varied e.g. by suitable mixing equipment before e.g. spraying. A way to do this could be by using spray nozzles for two component mixing from the company "Spraying Systems Co" together with standard flow meters and pressure gauges for control and monitoring of the supplied amount of each component.

Below a number of cases with different combinations of layers are shown, wherein the layers are applied by e.g. one or more of the application techniques described earlier. All the selected examples illustrate situations where first an insulating layer is applied and thereafter a conducting layer.

Case 1

Example of a two layer structure. The first layer is a highly insulating and chemically durable Teflon® layer. The second layer is conductive and serves primarily as an EMI shielding layer. The second layer is also an example of a layer with a graded composition.

1. layer.

5 times dipping in 5 wt% Teflon® AF 1600 (4,5-difluoro-2,2-bis(trifluoromethyl)-1,3-dioxole with tetrafluoroethylene) dissolved in fluorinert FC 75 (perfluoro(2-butyltetrahydrofuran)) with drying at room temperature for at least 1 hour between each dip. The Teflon® AF 1600 is from DuPont and is preferable dissolved by applying ultrasound for at least 2 hours after mixing. It can be dissolved up to 10 wt% at room temperature. To ensure that all the fluorinert FC 75 has evaporated the coating may be baked following the recipe recommended by DuPont: i.e. 5-10 min. at 50 °C, 5-10 min. at 110 °C, 5 min. at 165 °C. After that 10-15 min. at 330 °C ensures optimum uniformity of coating thickness and adhesion. To further enhance adhesion of Teflon® AF 1600 to silicon perfluorosilanes like 1H, 1H, 2H, 2H-perfluorodecyltriethoxysilane can be used..

Resulting layer thickness on single crystalline silicon chips is around 150 µm at flat surfaces and 50 µm at sharp corners.

2. layer.

Spraying with Chomerics 2052, which is an acrylate loaded with silver plated Cu particles having a diameter of maximum 40 µm.

A thin layer of about 25 µm is applied. The layer is dried for at least 2 hours at room temperature. This layer will give a minimum E-field attenuation of 30 dB in the frequency range 30 MHz - 1 GHz. Applying a second layer after drying of the first layer results in a total Chomerics 2052 thickness of approx. 150 µm which provides E-field attenuation of minimum 55 dB in the frequency range 30 MHz - 1 GHz.

Case 2

This is an example of a 3 layer structure where the second layer acts as a seed and/or adhesion layer for the final plated layer, 3. layer.

1. layer.
A Teflon ® layer as in case 1.

2. layer.
Spraying with Demetron leitsilber 200, nitrocellulose dissolved in ethoxypropanole and acetone and loaded with Ag particles. After application, the ethoxypropanole and acetone evaporates leaving the silver particles locked at the surface in the nitrocellulose and thus exposed to the surroundings and suitable for plating.

3. layer.
Plated Cu, Ni, Cu....Ni, Au
Plated µ-metal, Au

Case 3

This is an example of a three layer structure where the second layer acts as a seed and/or adhesion layer as described earlier for the last plated layer. Electrical contact to the seed layer is accomplished by having an opening in e.g. the flex print close to the microsystem.

1. layer.

A Teflon® layer as in case 1

2. layer.

Spraying with conducting polymers ORMECON L5006, polyaniline in an acrylic binder system.

3. layer

Plated layer as in case 2

Case 4

1. layer

A Teflon® layer as in case 1

2. layer.

Spraying with conducting polymers ORMECON L5000, polyaniline in a polyamide binder system.

3. layer

A plated layer as in case 2

Case 5-8

The 1. layer of any of the above cases have a UV curable Loctite 394, a two component urethane / acrylate mixture, applied by spraying.

CLAIMS

1. An encapsulation for a three-dimensional microsystem having an outer surface, said encapsulation covering at least part of the outer surface, the encapsulation comprising

- a first layer of a first material, said first layer defining a first interface region with the outer surface of the three-dimensional microsystem,

- a second layer of a second material having an outer surface, said second layer being held by the first layer and defining a second interface region with said first layer,

wherein the shortest distance between the first and second interface regions is essentially constant, and wherein the shortest distance between the first interface region and the outer surface of the second layer is essentially constant and between 5 μm and 500 μm.

2. An encapsulation according to claim 1, further comprising a third layer of a third material being held by the second layer and defining a third interface region with said second layer.

3. An encapsulation according to any of the preceding claims, wherein at least one of the layers comprises a conductive material.

4. An encapsulation according to any of the preceding claims, wherein at least one of the layers comprises a non-conductive material.

5. An encapsulation according to any of the preceding claims, wherein at least one of the layers comprises a material with a relative magnetic permeability between 100 and 1000.

6. An encapsulation according to any of the preceding claims, wherein at least one of the layers comprises a material with a relative magnetic permeability larger than 1000.

7. An encapsulation according to any of the preceding claims, wherein at least one of the layers comprises a material having a water permeability between 10^{-9} g/cm·s·torr and 10^{-19} g/cm·s·torr.

8. An encapsulation according to any of the preceding claims, wherein one of the layers comprises a material selected from the group consisting of semiconductors, ceramics, metals, polymers, hydrocarbons.

9. An encapsulation according to claim 8, wherein one of the layers comprises a mixture of materials selected from the group consisting of semiconductors, ceramics, metals, polymers, hydrocarbons.

10. An encapsulation according to any of the preceding claims, wherein the shortest distance between the first interface region and the second interface region is between 5μm and 250 μm.

11. An encapsulation according to any of the preceding claims, wherein the shortest distance between the first interface region and the outer surface of the second layer is essentially constant and between 10 μm and 500 μm.

12. An encapsulation according to any of the preceding claims, wherein the microsystem is completely encapsulated with at least one layer of material.

13. An encapsulation according to any of the claims 1-11, said encapsulation having one or more openings each of said one or more openings extending form an outermost surface of the encapsulation to the outer surface of the microsystem.

14. An encapsulation according to claim 13, wherein a part of the one or more openings are adapted for passing fluids to and from the microsystem.

15. An encapsulation according to claim 13, wherein a part of the one or more openings are adapted for transmitting electrical signals to and from the microsystem.

16. An encapsulation according to claim 15, wherein a part of the one or more openings are adapted for transmitting air pressure to the microsystem.

17. An encapsulation for a three-dimensional microsystem having an outer surface, said encapsulation covering at least part of the outer surface, the encapsultion comprising

- a layer comprising a plurality of materials, said layer defining an interface region with the outer surface of the three-dimensional microsystem and having an outer surface, wherein the material composition of the layer, in a region between the interface region and the outer surface of the layer and along a direction defined as the shortest distance between the interface region and the outer surface, varies as a function of a distance from the interface region.

18. An encapsulation according to claim 17, wherein the plurality of materials comprise a polymer.

19. An encapsulation according to claim 18, wherein the polymer comprises a filler.

20. An encapsulation according to claim 19, wherein the filler comprises a material selected from the group consisting of ceramics and metals.

21. An encapsulation according to any of claims 17-20, wherein the shortest distance between the interface region and the outer surface is essentially constant and between 5 μm and 500 μm.

22. A method for encapsulating a three dimensional microsystem having an outer surface, said method comprising the steps of

- providing a first layer of a first material onto at least part of the outer surface of the microsystem,

- providing a second layer of a second material onto the first layer, and

- rotating the three dimensional microsystem around a at least a first and a second rotation axis while providing at least one of the first and second layers, said at least first and second rotation axis intersecting the three dimensional microsystem, and wherein the first axis is different from the second axis.

23. A method according to claim 22, wherein the at least first and second axes are substantially perpendicular to each other.

24. A method for encapsulating a three dimensional microsystem having an outer surface, said method comprising the steps of

- providing a layer onto at least part of the outer surface of the microsystem, said layer comprising a plurality of materials,

- rotating the three dimensional microsystem around at least a first and a second rotation axis while providing the layer and varying the material composition of the provided layer as a function of time, wherein the at least first and second rotation axis intersects the three dimensional microsystem, and wherein the first axis is different from the second axis.

25. A method according to claim 24, wherein the at least first and second axes are substantially perpendicular to each other.

26. A method for encapsulating a three dimensional microsystem having an outer surface, said method comprising the steps of

- providing means for providing a first and a second layer onto at least part of the outer surface of the microsystem,

- providing the first layer of a first material onto at least part of the outer surface of the microsystem,

- providing the second layer of a second material onto the first layer, and

- rotating, while providing the first and second layer, the three dimensional microsystem and the means for providing the first and second layer relative to each other, the rotation being performed around at least a first and a second axis, wherein the first axis is different from the second axis.

27. A method according to claim 26, wherein the at least first and second axes are substantially perpendicular to each other.

28. A method for encapsulating a three dimensional microsystem having an outer surface, said method comprising the steps of

- providing means for providing a layer onto at least part of the outer surface of the microsystem, said layer comprising a plurality of materials,

- providing the layer onto at least part of the outer surface of the microsystem,

- rotating, while providing the layer, the three dimensional microsystem and the means for providing the layer relative to each other around at least a first and a second axis, wherein the first axis is different from the second axis.

29. A method according to claim 28, wherein the at least first and second axes are substantially perpendicular to each other.

30. An encapsulation for a three-dimensional microsystem having an outer surface, said encapsulation comprising for a part of the outer surface of the microsystem

- a first layer of a first material, said first layer defining a first interface region with the outer surface of the three-dimensional microsystem,

- a second layer of a second material, said second layer being held by the first layer and defining a second interface region with said first layer, and

- a third layer of a third material having an outer surface, said third layer being held by the second layer and defining a third interface region with said second layer.

31. An encapsulation according to claim 30, wherein the first layer comprises a non-conducting material, the second layer comprises a first conducting material and wherein the third layer comprises a second conducting material.

32. An encapsulation according to claim 31, wherein the second layer comprises a seed layer.

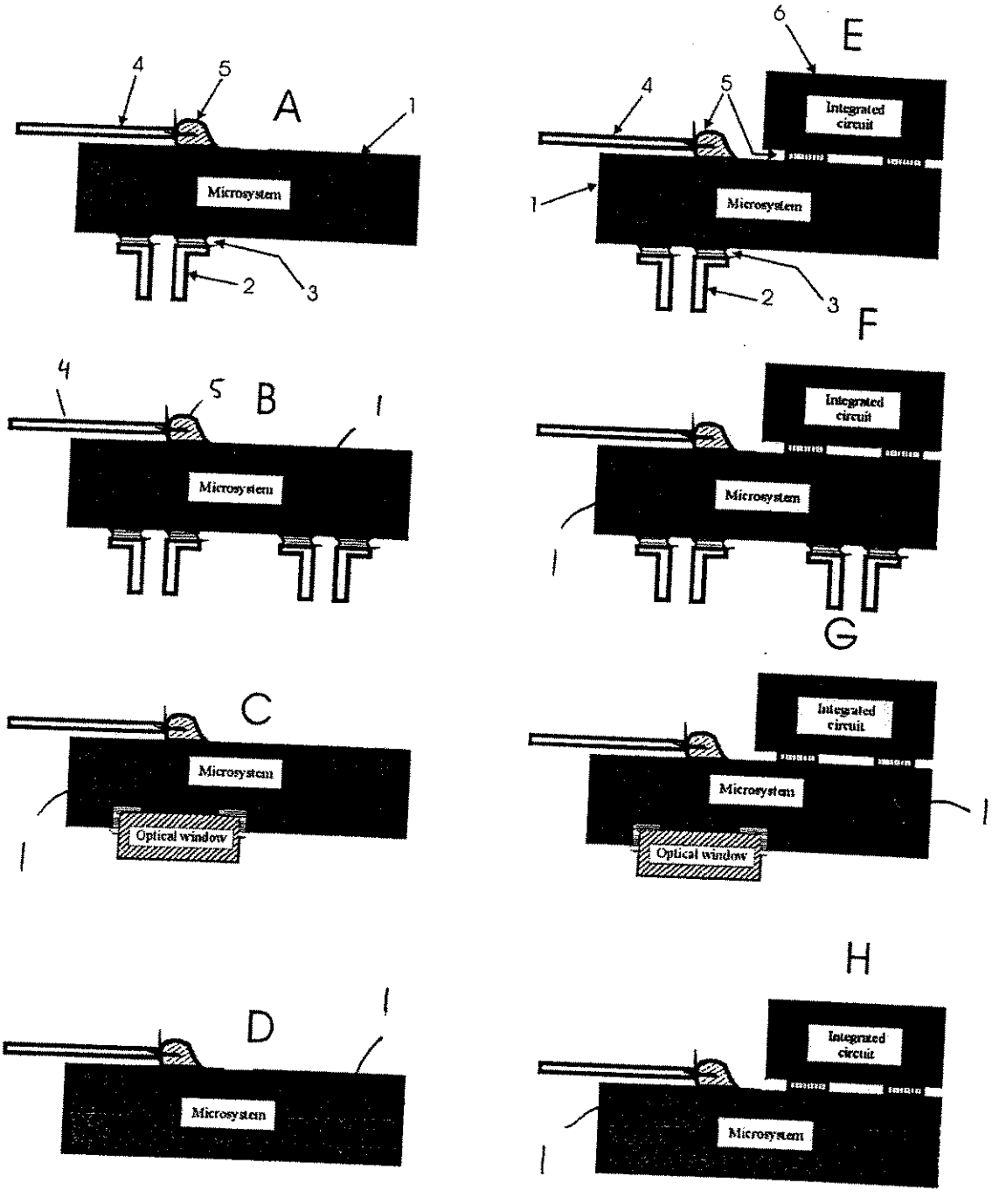
A
4
5
1
Microsystem
2
3
B
4
5
1
Microsystem
C
Microsystem
Optical window
1
D
1
Microsystem
E
6
4
5
Integrated circuit
1
Microsystem
2
3
F
Integrated circuit
Microsystem
1
G
Integrated circuit
Microsystem
Optical window
1
H
Integrated circuit
Microsystem
1

Fig. 1

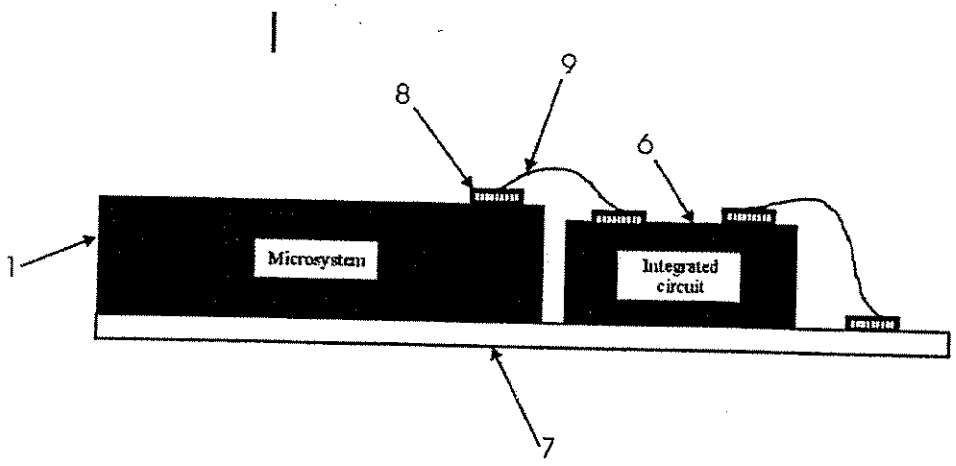
I
9
8
6
1
Microsystem
Integrated circuit
7

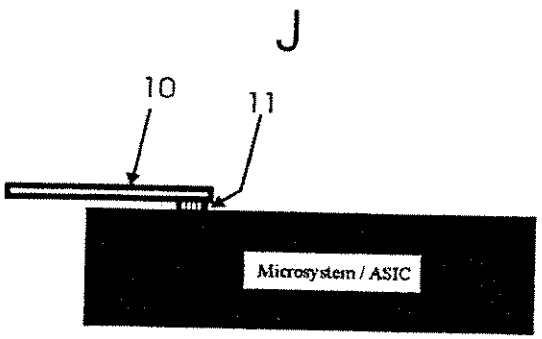
J
10
11
Microsystem / ASIC

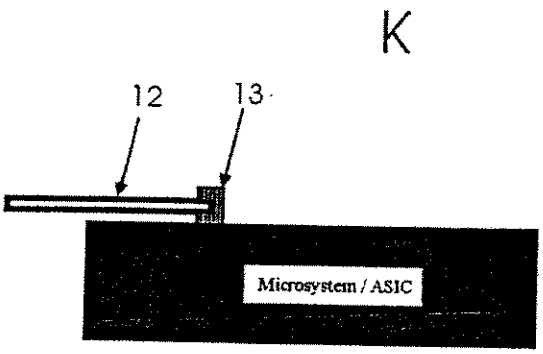
K
12
13
Microsystem / ASIC

Fig. 2

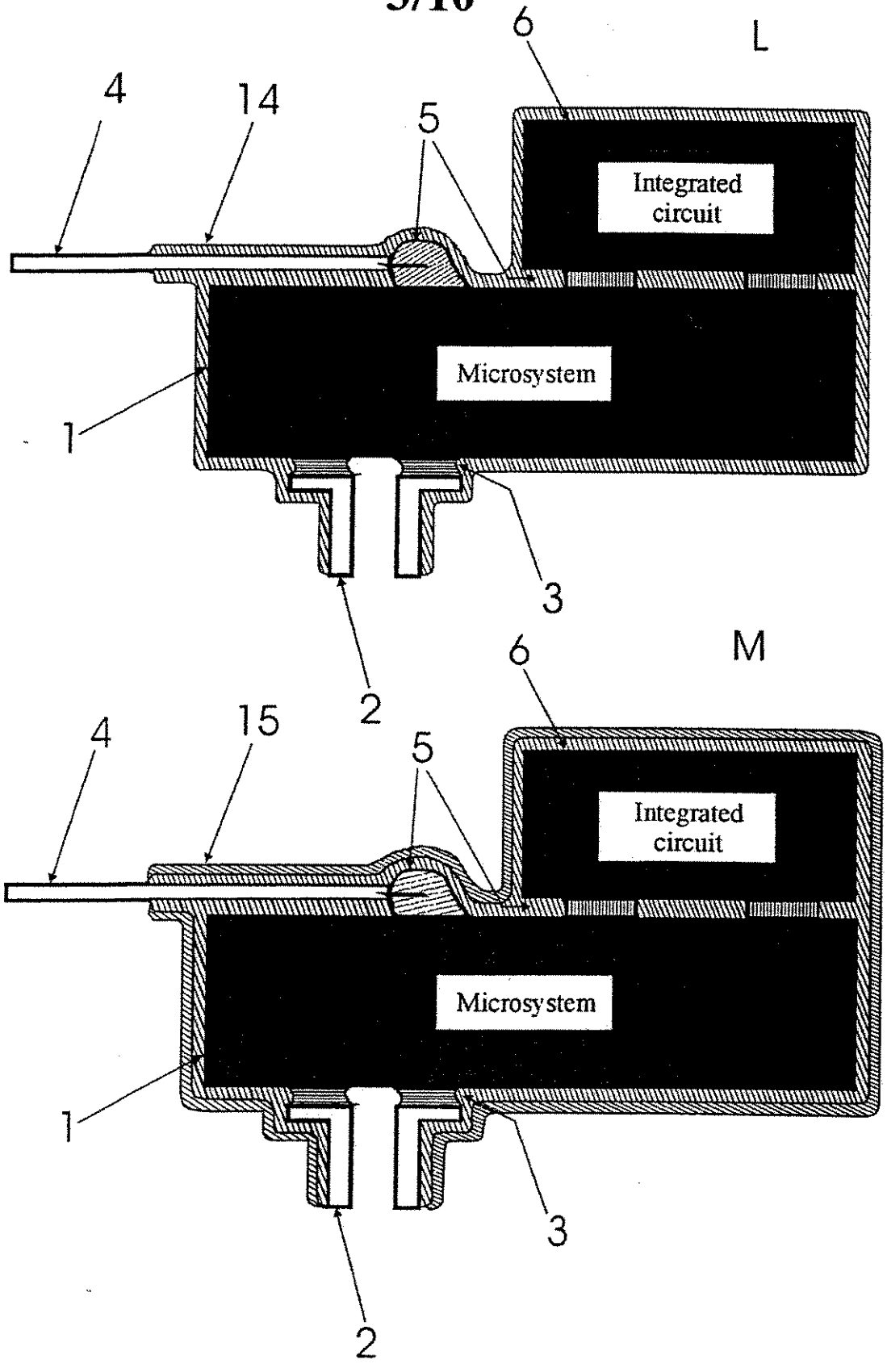
L
6
4
14
5
Integrated circuit
Microsystem
1
3
2
M
6
4
15
5
Integrated circuit
Microsystem
1
3
2

Fig. 3

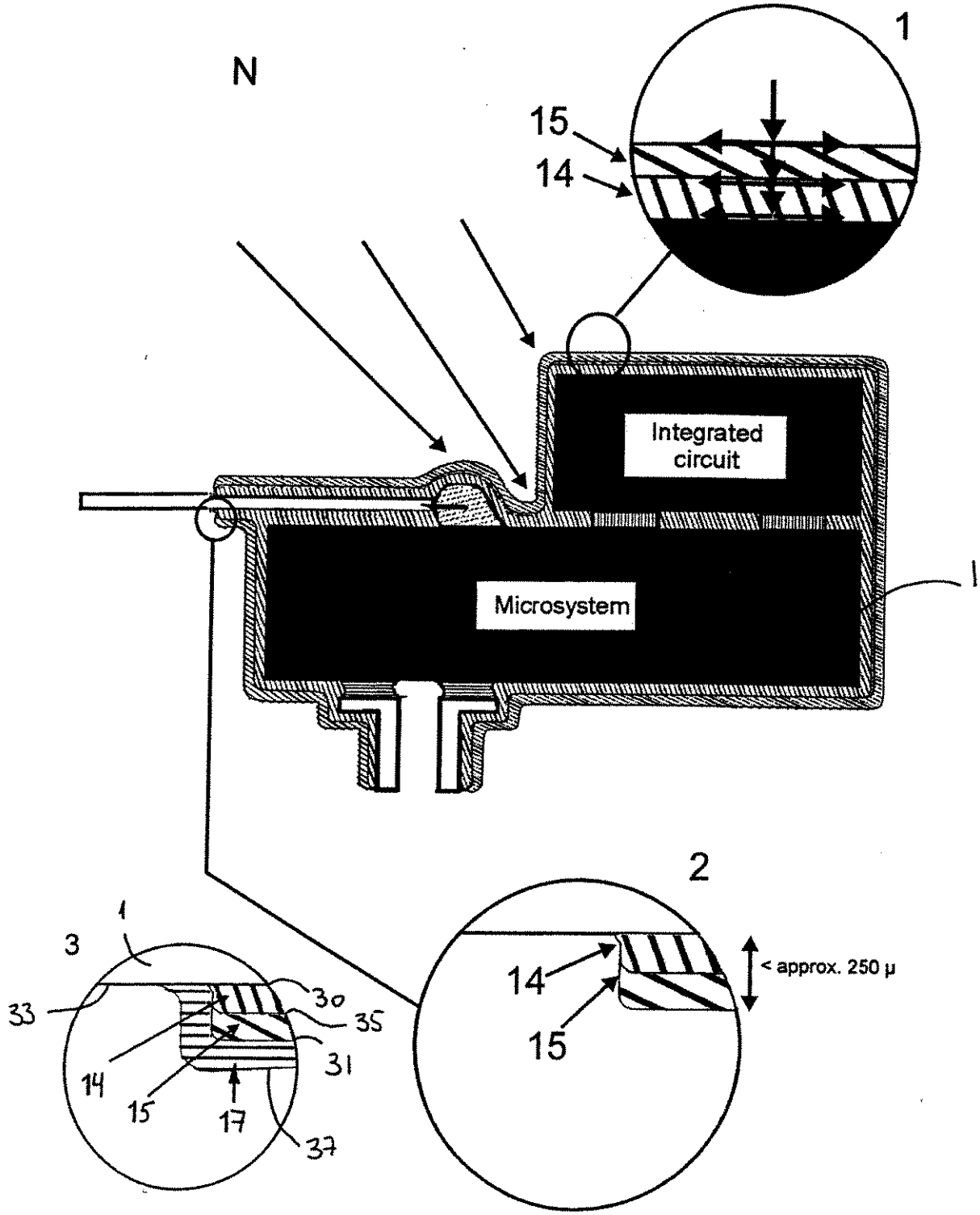
N
1
15
14
Integrated circuit
Microsystem
I
2
< approx. 250 µ
14
15
3
1
33
30
35
31
14
15
17
37

Fig. 4

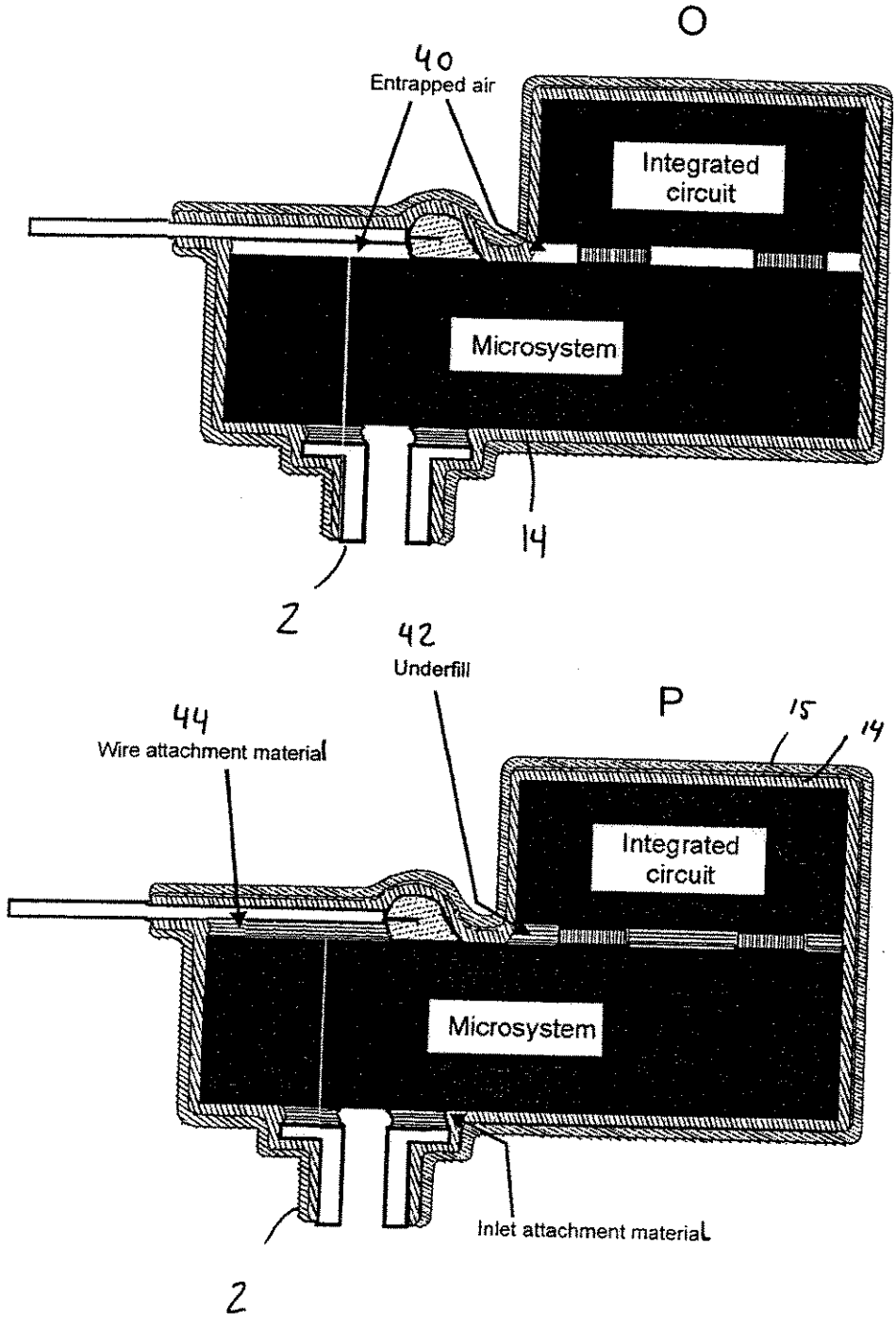
O
40
Entrapped air
Integrated circuit
Microsystem
14
2
42
Underfill
P
44
Wire attachment material
15
14
Integrated circuit
Microsystem
Inlet attachment material
2

Fig. 5

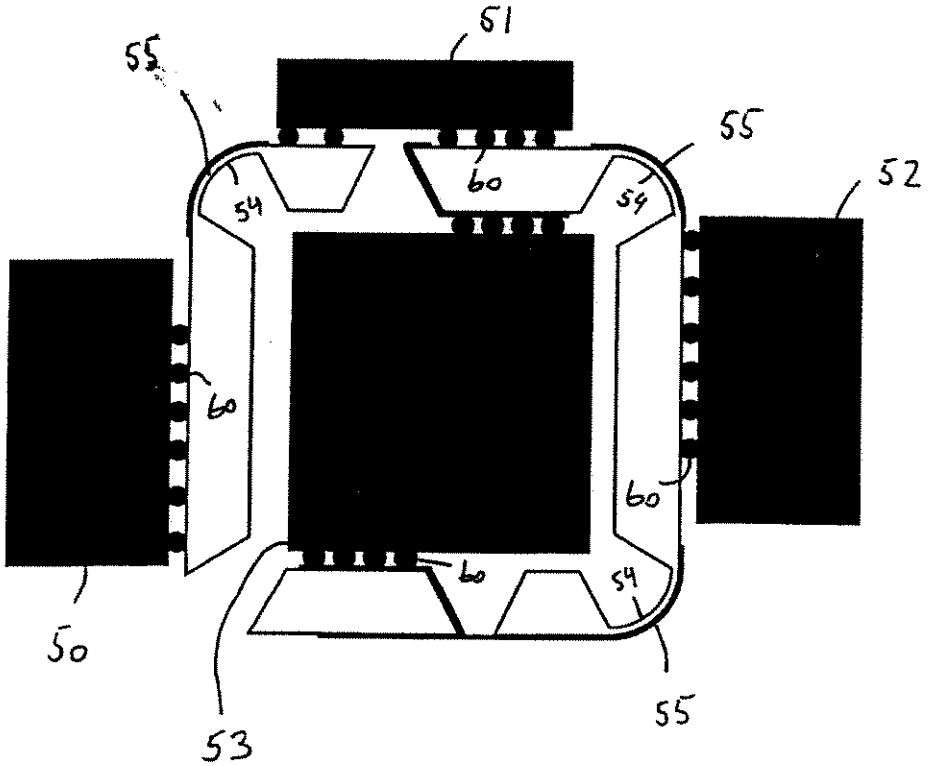

Fig. 6

7/10

Q

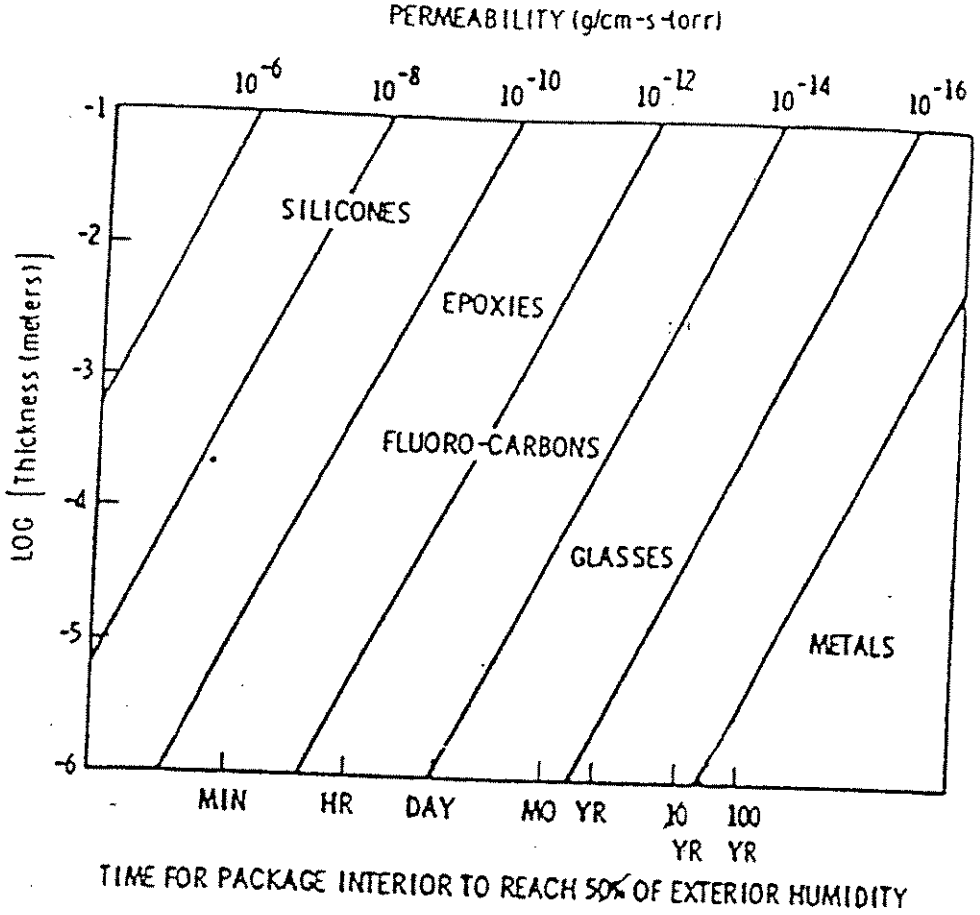
PERMEABILITY (g/cm-s-torr)
10^{-6}
10^{-8}
10^{-10}
10^{-12}
10^{-14}
10^{-16}
LOG (Thickness (meters))
-1
-2
-3
-4
-5
-6
SILICONES
EPOXIES
FLUORO-CARBONS
GLASSES
METALS
MIN
HR
DAY
MO
YR
10 YR
100 YR
TIME FOR PACKAGE INTERIOR TO REACH 50% OF EXTERIOR HUMIDITY

Fig. 7

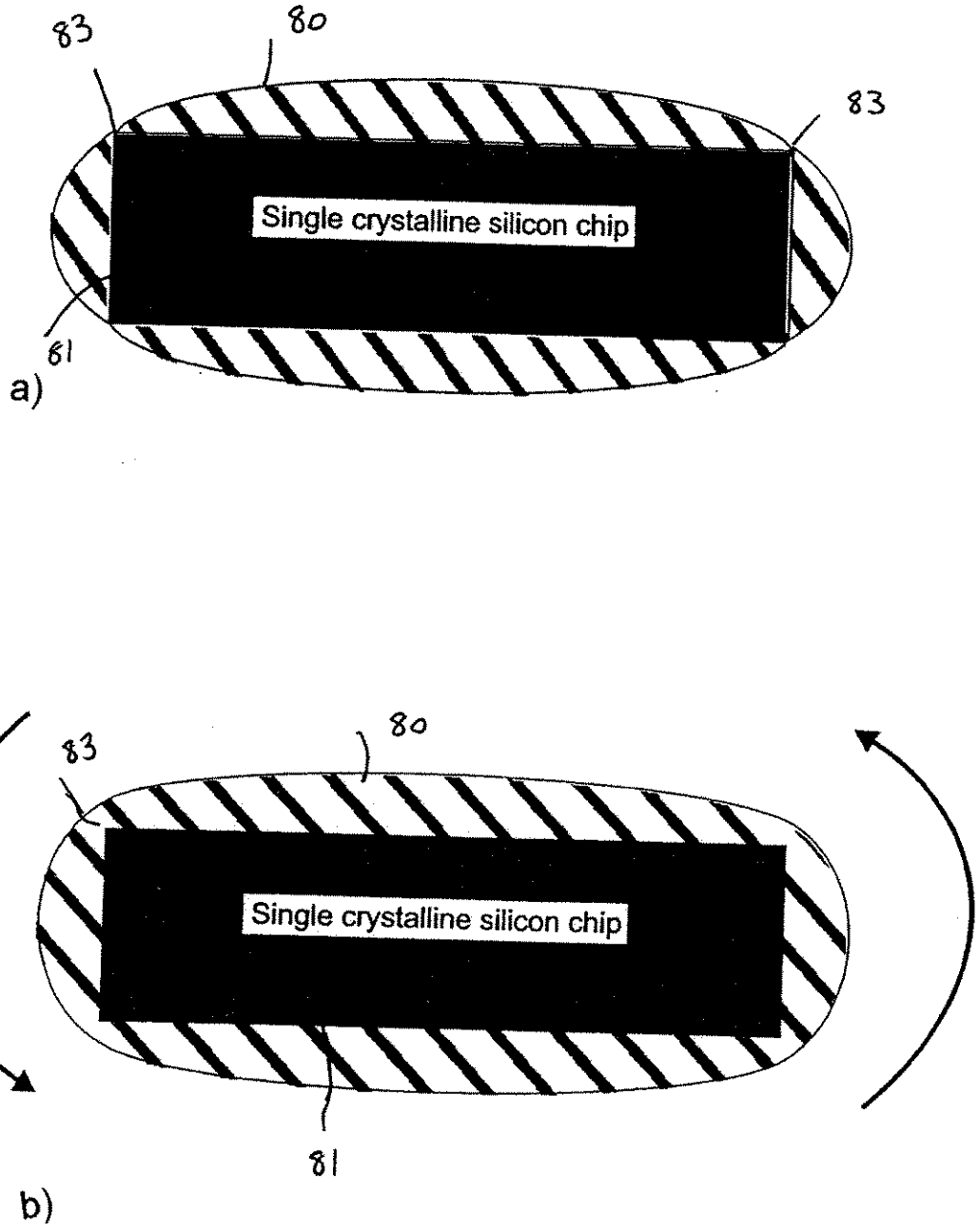
83
80
83
Single crystalline silicon chip
81
a)
83
80
Single crystalline silicon chip
81
b)

Fig. 8

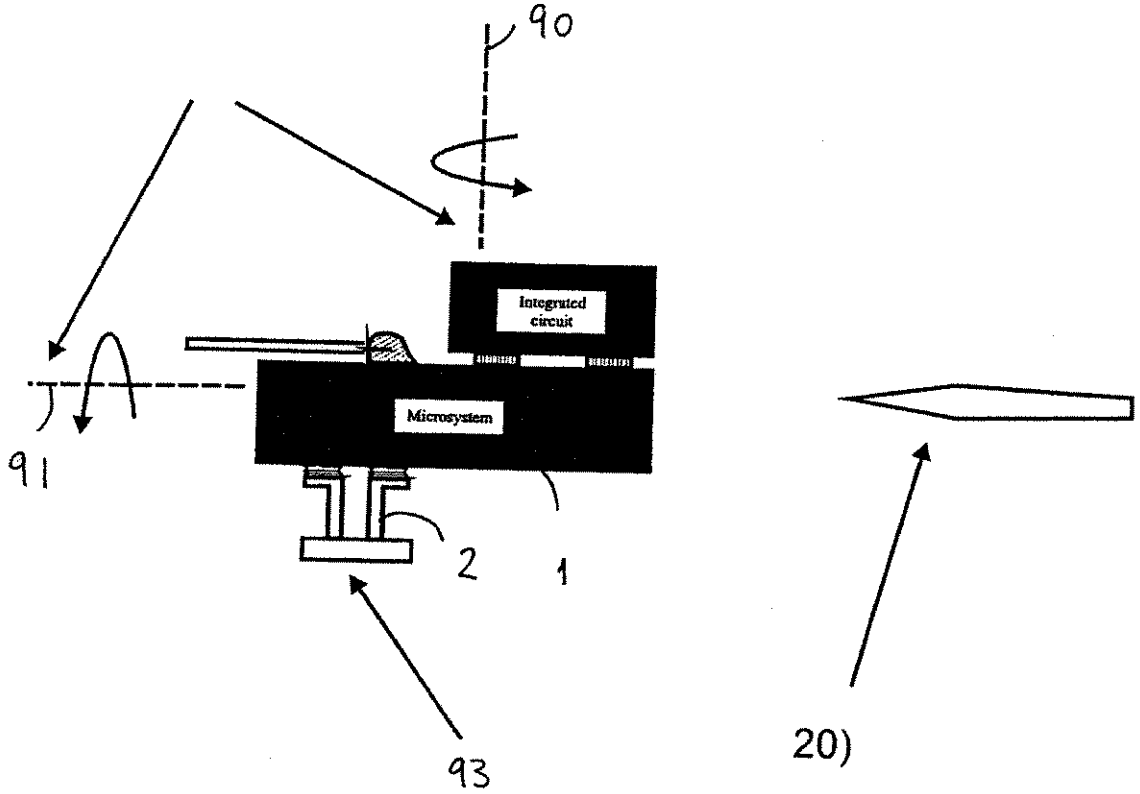

Fig. 9

10/10

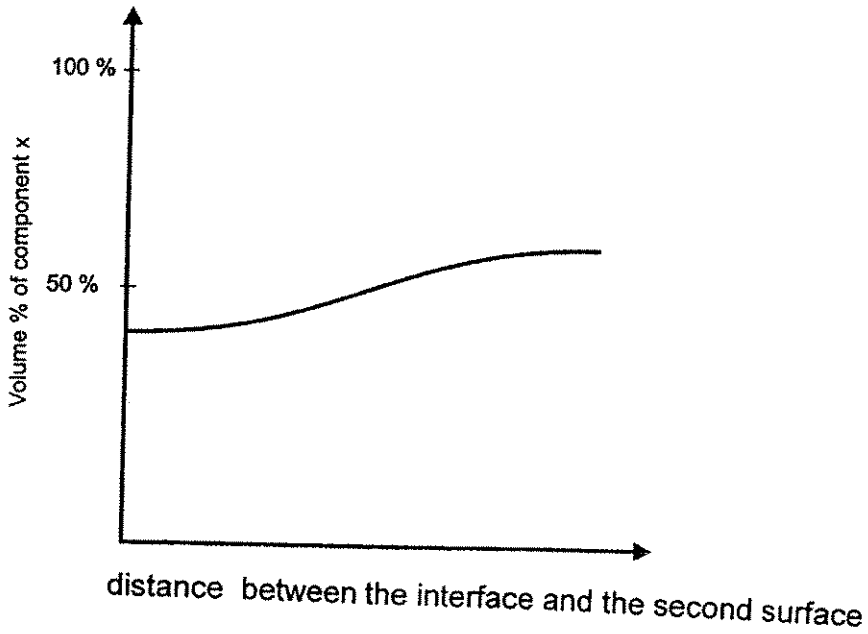
100 %
50 %
Volume % of component x
distance between the interface and the second surface

Fig. 10

Paper 7

Jakob Janting, Dirch Hjorth Petersen, Christoffer Greisen

Simulated SAM A-scans on multilayer MEMS components

Proceedings of 13th European Symposium on Reliability of Electronic Devices, Failure Physics and Analysis, ESREF 2002, pp. 1811-1814

PERGAMON

Microelectronics Reliability 42 (2002) 1811–1814

MICROELECTRONICS RELIABILITY

www.elsevier.com/locate/microrel

Simulated SAM A-scans on multilayer MEMS components

Jakob Janting[a], Dirch Hjorth Petersen[b], Christoffer Greisen[c]

[a]*DELTA Danish Electronics, Light & Acoustics, Venlighedsvej 4, DK-2970 Hoersholm, Denmark*
e-mail: jaj@delta.dk, Fax: +45 72 19 40 01,URL: http://www.delta.dk
[b]*MIC, Building 345, DK-2800 Lyngby, Denmark*
[c]*Danfoss A/S, CAT/DTU, Building 347, DK-2800 Lyngby, Denmark*

Abstract

A spreadsheet program for simulation of Scanning Acoustic Microscopy (SAM) A-scans on multilayer structures has been developed. Using this program, structure variations in samples can be analysed better. Further samples can be prepared to get optimal signal for enhanced failure and materials analysis. Input values for the sample materials are acoustic impedance, speed of sound, and thickness. The simulation is based on calculations of reflection, transmission coefficients, and number N of waves received by the transducer at the same time by reflection at the same interfaces in different order. The calculation of N, the program interface, and simulated A-scans on MEMS test structures for a pressure sensor are presented.

1. Introduction

SAM is a Non Destructive Testing (NDT) method for micro inspection which functions like a sonar, though using much higher frequencies, MHz – GHz. Ultrasound is transmitted through a liquid medium, typically water, to the component and its interior where it is reflected by stiffness changes.

SAM can be considered as a supplement to other NDT methods like X-ray inspection. The contrast in X-ray inspection relies on absorption due to differences in the atomic mass. Bubbles, cracks etc. in polymers are for instance not easy to observe with X-rays, though they are easy to see with sound.

In SAM resolution and penetration depth depends on frequency, focus position, stiffness and stiffness changes in the materials. High frequency gives high resolution but low penetration. For best results plane and smooth surfaces are required. With 200 MHz a lateral resolution of 8 μm in the interface between bonded silicon and glass has been achieved.

Results are most often presented as C-scan pictures, which are 2D pictures of the sound reflected from a certain depth range corresponding to a certain echo time delay where a gate is placed. The gate is positioned in the A-scan 1D picture, which shows the echoes from all depths at a certain place. Pulses and echoes are transmitted and received by the same transducer, which is scanned over the surface of the sample.

SAM has been used for several years as a microelectronics failure analysis tool though often with poor understanding of the A-scan and C-scan pictures This is especially the case when the components consist of layers very close to each other and where phase inversions take place.

MEMS most often contain stacks of several very thin layers. The motivation for this work has therefore been to gain better understanding of SAM A-scans on MEMS multilayer structures.

0026-2714/02/$ - see front matter
PII: S0026-2714(02)00236-6

2. Results

All calculations have been made in an excel spreadsheet. SAM measurements were made on KSI Winsam 200 equipment.

2.1 Spreadsheet calculations

When a sound wave impinges the interface between two materials with acoustic impedances Z_1 and Z_2 the reflected amplitude A_R is given by [1, 2]:

$$A_R = A_0 R = A_0 \frac{Z_2 - Z_1}{Z_1 + Z_2} \tag{1}$$

where A_0 is the amplitude of the incoming wave and R is the reflection coefficient (Fig. 1). Correspondingly the amplitude A_T of the transmitted wave is [1, 2]:

$$A_T = A_0 T = A_0 \frac{2Z_2}{Z_1 + Z_2} \tag{2}$$

where T is the transmission coefficient. Using these formulas wave propagation in layered media can be described with the quadratic layer matrix formalism [2].

For given sets of reflections we calculate first the number N of possible reflection orders in each. The

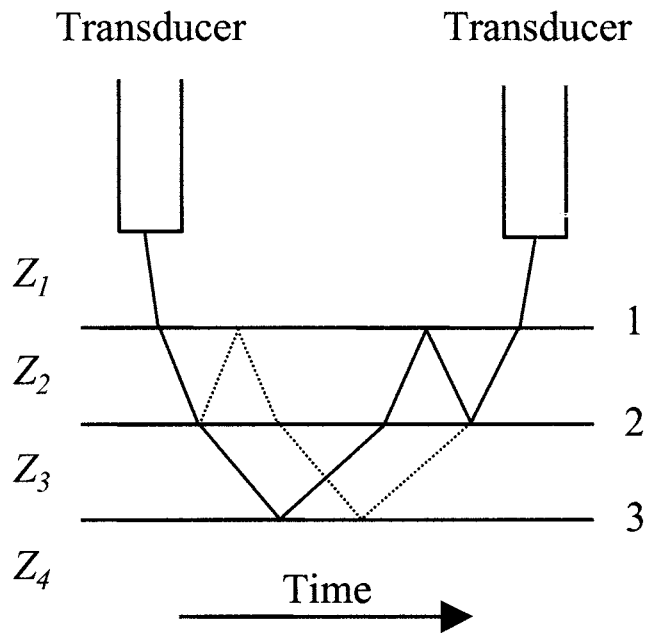

Fig. 1. Illustration of two waves which are equal because they are reflected at the same interfaces only in different order (3-1-2, 2-1-3). They are therefore received at the transducer at the same time.

calculations are based on maximum 4 or 9 impedance transitions with up to 8 or 2 reflections back ($k = 8$ or $k = 2$) towards the transducer respectively (Fig. 1). Then from (1), (2) and N the received amplitudes according to (3) together with the corresponding delay times are calculated.

$$A = A_0 \cdot N \cdot T_{total} \cdot R_{total} \tag{3}$$

T_{total} and R_{total} are the products of all involved transmission and reflection coefficients. Due to limited available data the sound attenuation in each layer is not yet included in the calculations, however, the program is prepared for this.

For the calculation of N the impedance transitions are grouped and ordered as follows:

$$M = \{m_1, m_2, ..m_i, ..m_k\} \quad V = \{v_1, v_2, ..v_j, ..v_{k-1}\}$$

$$m_i \geq m_{i+1} \quad \wedge \quad v_j \geq v_{j+1}$$

where m_i is a number of an impedance transition reflecting the sound towards the transducer and v_j is a number of an impedance transition reflecting the sound away from the transducer. Then in case of n impedance transitions we have the following number of up / down reflection combinations:

$$N(M,V) = \frac{(k - a_k) \cdot (k - 1 - a_{k-1}) \cdot ... \cdot (1 - a_1)}{A_2! \cdot A_3! \cdot A_4! \cdot ... \cdot A_n!} \cdot$$

$$\frac{(k - 1 - p_1) \cdot (k - 2 - p_2) \cdot ... \cdot (1 - p_{k-1})}{P_1! \cdot P_2! \cdot P_3! \cdot ... \cdot P_{n-1}!} \tag{4}$$

where: a_i is the number of elements in V which are greater than or equal to m_i, $i \in \{1, 2, ..,k\}$. p_j is the number of elements in M less than or equal to $v_j, j \in \{1, 2, .., k-1\}$. A and P with subscripts denote the number of elements equal to the subscript values in M and V respectively. The important part here is to realise from the numerators that when a wave is reflected up at some impedance transition it could not be combined / followed by a reflection down by the same transition or some deeper down transition and vice versa.

As an example the series of reflections 4-2-4-1-3-1-3-1-2-1-2 where $k = 6$ takes place in $N(M,V) = 180$ different orders. All these waves are received at the

same time.

The spreadsheet input values are the materials acoustic impedances, the speed of sound in the materials, and the layer thicknesses (Fig. 2).

2.2 A-scans on fusion bonded wafers

Bonded silicon wafers with test cavities for an absolute pressure sensor have been investigated with SAM (Fig. 3). The cavities are used to test the leakage through the bond interface into the cavity [3]. Over the cavities and down the layers are Si (350 μm) / cavity (2 μm) / Si (500 μm) / SiN (0.1 μm).

Simulations show that in order to get a scan of the interface with a minimum of overlapping waves out of phase the bonded wafers should be inspected from the Si side (Fig. 4). Then the reflected waves all have the same sign and are well separated because the time between them is 83 ns. Though, by comparing the real scan from the Si side (Fig. 5) with the simulations it is evident that this looks more like the one expected when scanning from the SiN side (Figs. 2 and 4).

3. Discussion

Spectra much like the one from the SiN side are achieved no matter the thin layer material and position at the exterior or next to the cavities and channels. Therefore we suggest that the thin boron diffused bond layer is acoustically different from bulk silicon, which was not expected from the start. This is supported by the observation that stresses built up in such layers, which might change the longitudinal acoustic impedance Z of silicon significantly through:

$$Z = \sqrt{\frac{\rho\, E(1-\nu)}{(1+\nu)\cdot(1-2\nu)}} \tag{5}$$

where E is Youngs modulus, ν is Poissons ratio, and ρ is density. I.e. we have the layers: Si (350 μm) / approx. 2 μm B diffused Si / cavity (2 μm) / Si (500 μm) / SiN (0.1 μm). Apart from the time position differences due to differences in Si thickness before the cavity the real scan from the Si side resembles the A-scan simulation of inspection from the SiN side quite well because waves of opposite amplitude sign seem to overlap more or less. Note that only two signals from the interface are clearly seen, i.e. the first and second time reflections from cavities / channels at around 83 ns, 166 ns and 118 ns, 237 ns in the real scan from the Si side (Figs. 4 and 5) and in the simulation of inspection from the SiN side (Figs. 2 and 4) respectively. The rest of the signals essentially die because waves with opposite phase are added. Already from the second time echoes this begins to happen e.g.

Material	Impedance, Mrayl	Sound speed	Thickness, μm
Water	1,482	X	X
SiN	34,38	10743	0,1
Si	20,04	8433	500
Cavity	0,0001	0,0001	2
Si	20,04	X	X

Interval	Time, ns	A, %
min.	0	0
max.	1000	25

Transition	from	to	R(total)	Time, ns	R	T(down)	T(up)	T(total)
1	Water	SiN	91,7%	0	92%	192%	8%	16%
2	SiN	Si	-4,2%	0	-26%	74%	126%	93%
3	Si	Cavity	-14,7%	118	-100%	0%	200%	0%
4	Cavity	Si	0,0%	1000	100%	200%	0%	0%

Reflections	Wave intensity	Time, ns	N
1	N/A	0	1
2	-4,2%	0	1
212	-1,0%	0	1
21212	-0,2%	0	1
2121212	-0,1%	0	1
212121212	0,0%	0	1
21212121212	0,0%	0	1
2121212121212	0,0%	0	1
212121212121212	0,0%	0	1
3	-14,7%	118	1
312	-7,1%	118	2
31212	-2,6%	118	3
3121212	-0,8%	118	4
312121212	-0,3%	118	5
31212121212	-0,1%	118	6
3121212121212	0,0%	118	7
312121212121212	0,0%	118	8
313	-12,6%	237	1
31312	-9,1%	237	3
3131212	-4,4%	237	6
313121212	-1,8%	237	10
31312121212	-0,6%	237	15
313121212121212	-0,2%	237	21
31312121212121212	-0,1%	237	28
31313	-10,7%	355	1

Fig. 2. Spreadsheet user interface.

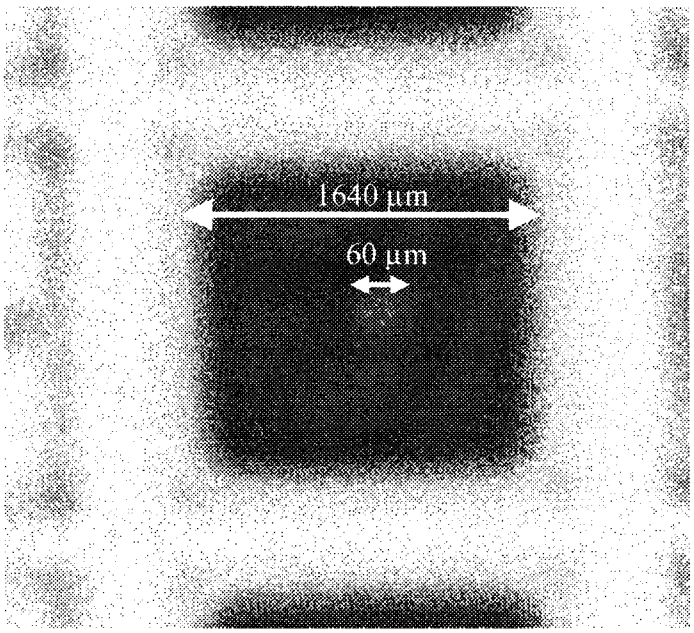

Fig. 3. 110 MHz C-scan SAM picture of interface between two bonded Si wafers with cavities and channels in bottom wafer. Dark areas are bonded. The bright area in centre of the dark square corresponds to the cavity.

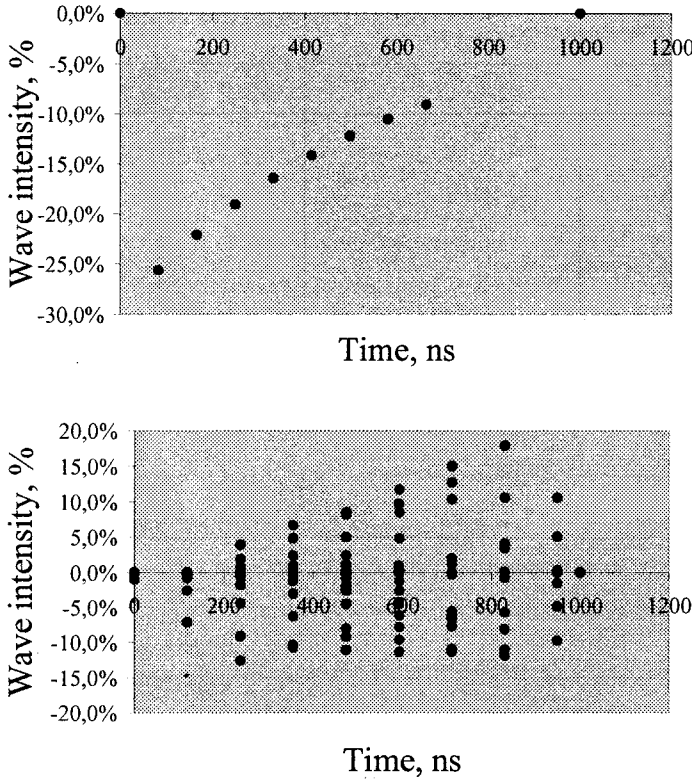

Fig. 4. Simulated amplitudes of A-scans on bonded wafers with cavities. Each dot shows amplitude and time for a back reflected wave. Top: Inspection from Si side. Bottom: Inspection from SiN side, for more details see Fig. 2. Note that in this case many waves are received at the transducer at the same times.

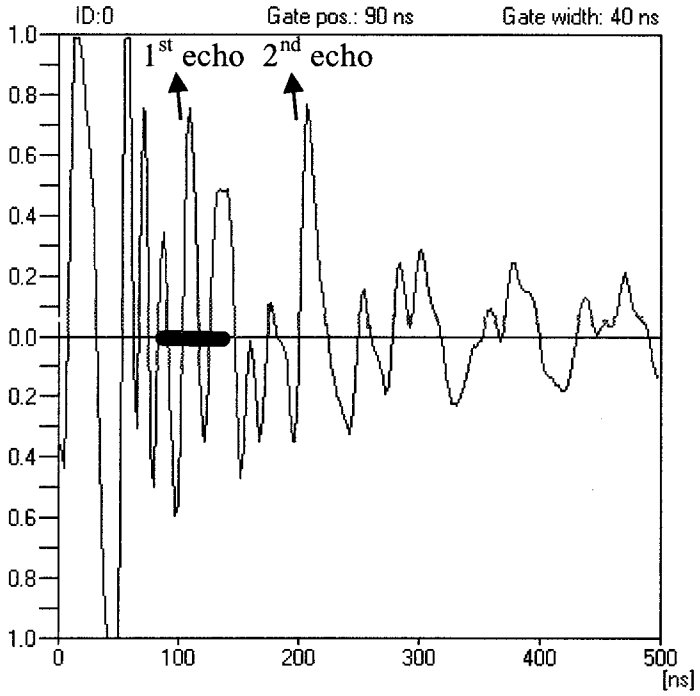

Fig. 5. 110 MHz SAM A-scan on Si (350 μm) / approx. 2 μm B diffused Si / cavity (2 μm) / Si (500 μm) / SiN (0.1 μm) from Si side. Note that surface trigger is in the front of the wave reflected at the top surface. First and second reverberation from the cavity starting at 83 ns and 166 ns respectively are observed (arrows). The gate indicated by a black bar is a filter which is here open for the first signal.

by addition of 3-1-3-.. and 3-2-3-.. reflections in the case of inspection from the SiN side. Even though the second time reflection from the cavity has passed two times through the silicon material, the amplitude is high because of the high N values.

4. Conclusion

A calculation method and spreadsheet program for simulation of SAM A-scans on multilayer structures have been developed. The useful information which the simulations provide has been demonstrated on fusion bonded wafers containing MEMS pressure sensor test cavities in the interface. It was found that an extra layer than expected on the wafer without etched cavities / channels has influence on the A-scans. Presumably this layer is a B diffused bond layer.

Generally it has been shown that structure variations in samples can be simulated and therefore analysed better. Failures or variations in MEMS structures can be analysed by investigating the effect of introducing them in the A-scan simulations and comparing with real A-scans.

Acknowledgement

This work has been part of the collaboration on development of microsystems (SUM) project between two Danish institutes DELTA, the Microelectronics Centre (MIC), and three Danish companies Capres A/S, Danfoss A/S and Grundfos A/S. The project is financially supported by the Danish Agency for Trade and Industry.

References

[1] B. A. Auld, Acoustic fields and waves in solids, Vol 1, Robert E. Krieger Publishing Company, Inc., Malabar, Florida, 1990, pp. 129-130.
[2] http://sepwww.stanford.edu/sep/prof/fgdp/toc.html
[3] K. Birkelund, M. Sørensen, S. Chiriaev, P. Gravesen and P. B. Rasmussen, High pressure sensor based on fusion bonding, abstract 1482 in: Proc. of the 6th. Int. Symp. on Semiconductor Wafer Bonding: Science, Technology and Applications, The Electrochem. Soc., San Francisco (2001).

Paper 8

Jakob Janting, Dirch Hjorth Petersen, Bjarke Schønwandt

Scanning Acoustic Microscopy Study of Flip-Chip Underfill Cure Degree

Proceedings of Materials Week conference, München, Germany,
30. sep. – 2. oct. 2002

Scanning Acoustic Microscopy Study of Flip-Chip Underfill Cure Degree

J. Janting[a], D. H. Petersen[b], B. V. Schonwandt[a]
[a]DELTA Danish Electronics, Light & Acoustics, Denmark
[b]The Microelectronics Centre (MIC), Denmark

1 Introduction

The motivation for this work has been to gain a fast and reliable Compression UnderFill (CUF) based flip-chip interconnection process for MEMS components. In this process electrical contact between bumps and pads is established mechanically by the high curing shrinkage of the underfill, figure 1.

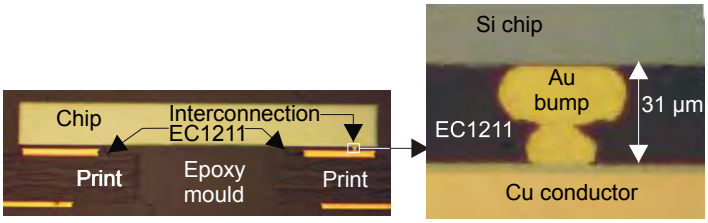

Figure 1: Cross section through bump – pad electrical interconnection between flip-chipped MEMS pressure sensor chip and print.

Although the studied CUF material EC1211 has been cure characterised by Differential Scanning Calorimetry (DSC), the actual temperature environments experienced by the underfill in the flip-chip process might be much different from expected. When trying to run the process as fast as possible it might therefore be that the CUF is not uniformly cured. Using DSC for evaluation is tedious and destructive because samples of the CUF will have to be taken out for the analysis. A better alternative is Scanning Acoustic Microscopy (SAM). Here detection of cure degree relies on the big mechanical (stiffness E) differences between cured and uncured material and the great advantages are that the inspection is 2D and non-destructive.

Acoustic microscopy has many applications, SAM especially in the microelectronics industry to detect failures e.g. cracks, bubbles, delaminations in chip encapsulations, solderings, gluings etc. Generally SAM is a Non Destructive Testing (NDT) method for microinspection which functions like a sonar, though using much higher frequencies, MHz – GHz. Ultrasound is transmitted through a liquid medium, typically water, to the component and its interior where it is reflected and transmitted at an interface between two materials 1 and 2 with amplitudes $A(R)_{12}$, $A(T)_{12}$ because of the changes in acoustic impedance according to [1]:

$$A(R)_{12} = A_0 R_{12} = A_0 \frac{Z_2 - Z_1}{Z_1 + Z_2} \qquad (1)$$

$$A(T)_{12} = A_0 T_{12} = A_0 \frac{2Z_2}{Z_1 + Z_2} \qquad (2)$$

where A_0 is the incoming wave amplitude, R_{12} and T_{12} are the reflection and transmission coefficients respectively, Z_1 and Z_2 are the acoustic impedances of materials 1 and 2 respectively, figures 2, 3.

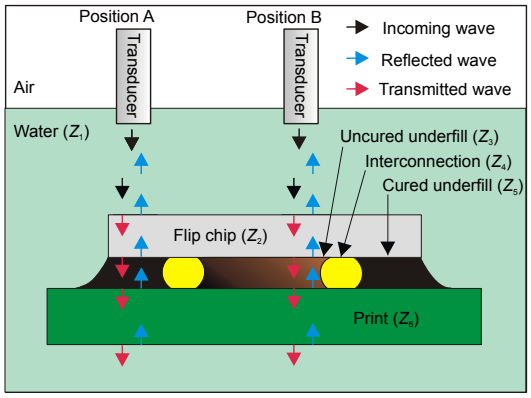

Figure 2: Illustration of SAM study on flip-chip with cured / uncured underfill.

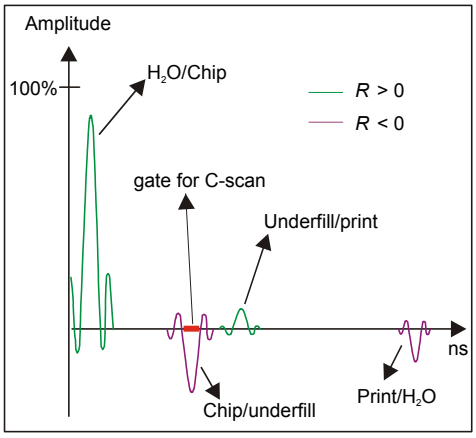

Figure 3: A-scan on flip-chip in figure 1. Reflected sound at chip / underfill varies according to cure degree.

The acoustic impedance is expressed by [2]:

$$Z = \rho V_L = \rho \sqrt{\frac{B(1-\nu)}{\rho(1+\nu)\cdot(1-2\nu)}} = \sqrt{\frac{\rho B(1-\nu)}{(1+\nu)\cdot(1-2\nu)}} \approx \sqrt{\frac{\rho E(1-\nu)}{(1+\nu)\cdot(1-2\nu)}} \approx \sqrt{\rho E} \qquad (3)$$

where V_L is the longitudinal wave velocity, B is the bulk modulus, E is Young's modulus, ρ is the density, and ν is Poisson's ratio. Both E and ρ will increase by curing and therefore $Z_{\text{cured}} > Z_{\text{uncured}}$.

SAM can be considered as a supplement to other NDT methods like X-ray inspection. The contrast in X-ray inspection relies on absorption due to differences in the atomic mass. Bubbles, cracks etc. in polymers are for instance not easy to see with X-rays, though they are easy to see with sound.

Results are most often presented as C-scans, which are 2D pictures of the sound reflected from a certain depth range corresponding to a certain echo time delay where a gate is placed in a sample, figure 3. Pulses and echoes are transmitted and received by the same transducer, which is scanned over the surface of the sample.

In SAM resolution and penetration depth depends on frequency (focal spot size), focus position, stiffness and stiffness changes in the materials. High frequency gives high resolution but low penetration depth and vice versa. Lateral and depth resolution is expressed by equations 4 and 5 below respectively.

$$\Delta_{lateral} = 1.22\lambda_{material} \frac{F}{D} \qquad (4)$$

$$\Delta_{depth} = 2.44\lambda_{material}\left(\frac{F}{D}\right)^2 \quad (5)$$

where $\lambda_{material}$ is the wavelength in the study material, F is the focal length and Δ is the transducer aperture diameter.

The detection limit of delaminations or other gaps (air or vacuum) is below 0.1 µm since even such narrow defects have been demonstrated to reflect all the sound [3]. For best results plane and smooth surfaces are required. Using 200 MHz and the KSI WINSAM 200 instrument of this study a lateral resolution of 8 µm in the interface between bonded silicon and glass has been achieved.

2 Results

Two approaches for determining the degree of CUF curing degree have been studied. First it was attempted to determine the cure degree from differences in sound speed. This requires knowledge about the CUF thickness and reflection time delay between the top and bottom interfaces. The method turns out not to be feasible for typical CUF thicknesses (30 µm – 70 µm) because of too low depth resolution. Even with thick bond lines and therefore well separated reflections from top and bottom interfaces it is difficult to determine the speed with sufficient accuracy because the waves do not have the same form and the places on the waves to measure from / to are not well defined. Though, using C-scan grey tone values good results can be achieved.

2.1 Acoustic impedance calculations from C-scan grey tone values

The advantage of this approach compared to the speed of sound method is that only the degree of reflection at the same depth between different materials e.g. cured / uncured CUF is measured. Depending on the situation, with reference to figure 4, two different calculations can be used to find the acoustic impedance of a material under another:

- The acoustic impedance Z_1 of the top material is unknown.

Calculation of Z_x is based on the approximation that R_{12} has a linear dependence on Z_2. Then Z_x is given by:

$$Z_x = Z_b + (g_x - g_b)\frac{Z_b - Z_a}{g_b - g_a} \quad (6)$$

I.e. to determine Z_x two reference acoustic impedances Z_a, Z_b for materials under the top material are needed. Their grey tone values and that for the studied material x are measured in the C-scan picture.

- The acoustic impedance Z_1 of the top material is known

Calculation of Z_x is based on the linear dependence of g_x on R. Then Z_x is given by:

$$Z_x = Z_1 \frac{g_a(Z_a + Z_1) + g_x(Z_a - Z_1)}{g_a(Z_a + Z_1) - g_x(Z_a - Z_1)} \quad (7)$$

I.e. to determine Z_x in this case only one reference acoustic impedance Z_a for a material underneath the top material is needed. Again the corresponding grey tone value g_a and that for the studied material g_x is found in the C-scan picture.

Normally underfill materials contain a silica filler to lower the Coefficient of Thermal Expansion (CTE). In an attempt to evaluate the uniformity of the filler in cured underfill the above equation 7 has previously been derived in a slightly different form [4].

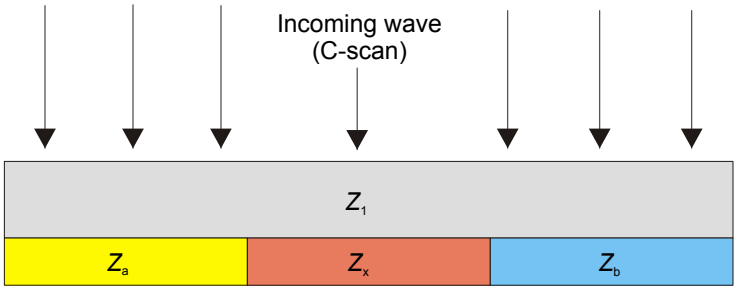

Figure 4: Illustration of the variables in equations 6 and 7.

2.2 Test 1: Determination of acoustic impedance of isopropanole

To test the methods of determining acoustic impedances isopropanole, air, water, and adhesive were placed between two microscope slides (glass) with the purpose of determining the acoustic impedance of isopropanole, fig 5. Isopropanole and air were entrapped in small aluminum pans meant for DSC measurements.

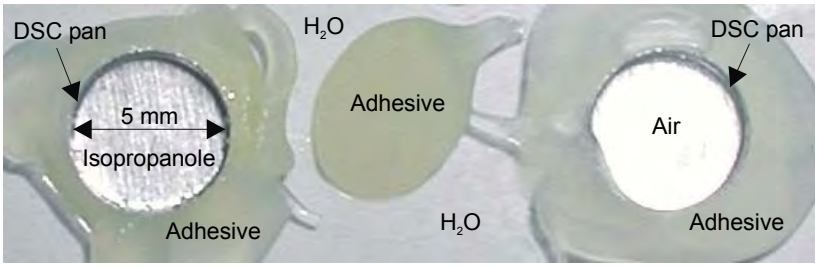

Figure 5: Isopropanole, air, water, and adhesive between two microscope slides.

The sample was placed in the water filled SAM inspection vessel and a gate for the C-scan covering the whole reflected wave from the bottom interface of the microscope slide was placed, figure 6. The C-scan was performed and grey tone values determined with KSI WINSAM 200 software, figure 7.

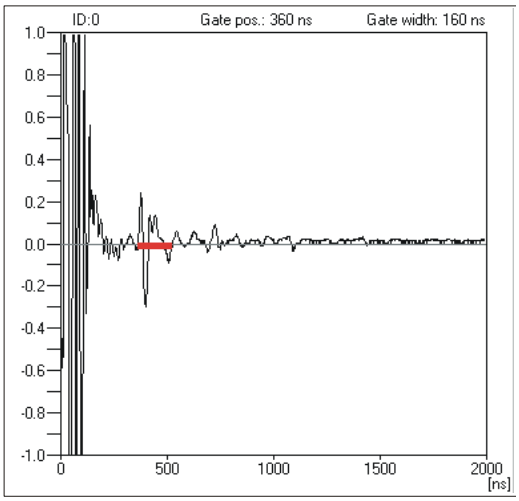

Figure 6: 110 MHz A-scan in centre of figure 5 sample (adhesive under microscope slide).

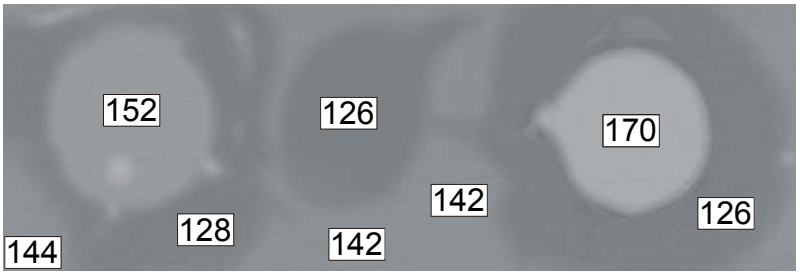

Figure 7: 110 MHz C-scan. Grey tone values for isopropanole, air, water, and adhesive.

The grey tone and the reference acoustic impedance values used for the calculations are shown in table 1. The results derived by use of equation 6 and 7 show satisfactory agreement with the tabulated *Z* value for isopropanole, table 2.

Table 1: Determined grey tone values and reference acoustic impedances.

Reference acoustic impedances / MRayl			Grey tone values (0 => 256)		
Z_1(glass)	Z_a(H_2O)	Z_b(air)	g_a(H_2O)	g_b(air)	g_x(isopropanole)
15	1.48	0.0004	142	170	152

Table 2: Acoustic impedance of isopropanole.

Z_x(isopropanole) / MRayl		
Equation 6	Equation 7	Table
0.95	0.97	0.92

2.3 Test 2: Test on flip-chip with CUF

Cured / uncured epoxy EC1211 CUF material between a 2 cm x 2 cm x 0.35 mm test flip-chip with approximately 30 µm bumps and a Printed Circuit Board (PCB) were studied, figure 8. The narrow gate around the middle of CUF material in the figure 9 A-scan results in a clear picture of the bump positions, figure 10. To get the grey tone values a gate is placed which covers the whole

reflected wave at the chip / CUF / PCB interfaces, figure 9. The resulting C-scan picture with grey tone values is shown in figure 11.

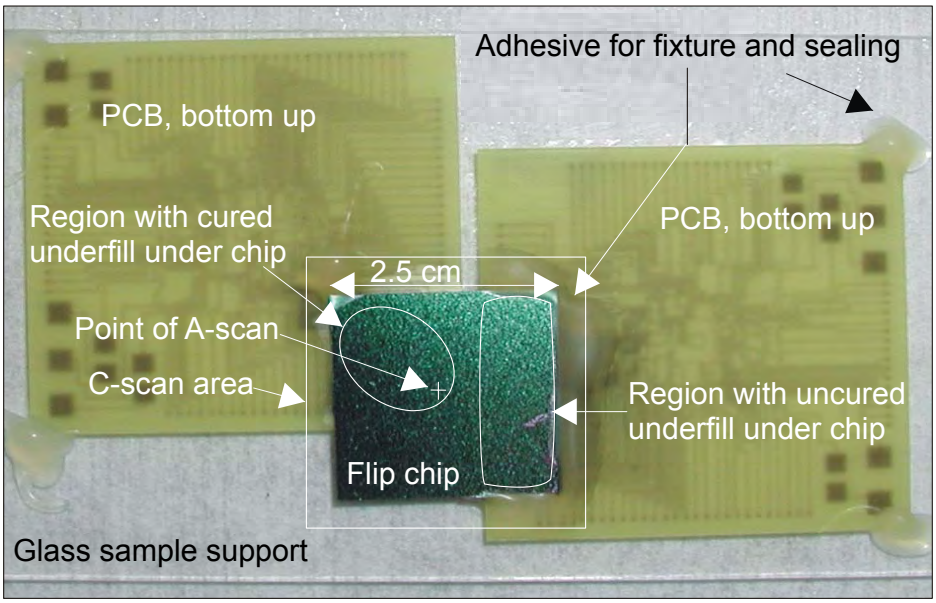

Figure 8: Test flip-chip with 30 µm bump height on PCB's with cured / uncured EC1211 CUF material. During investigation water is under the chip in the bottom left corner.

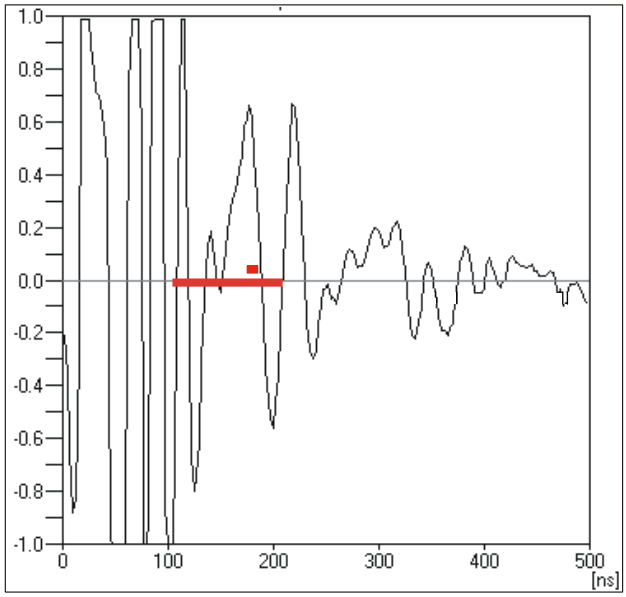

Figure 9: 50 MHz A-scan on flip-chip in figure 8 (white cross)..

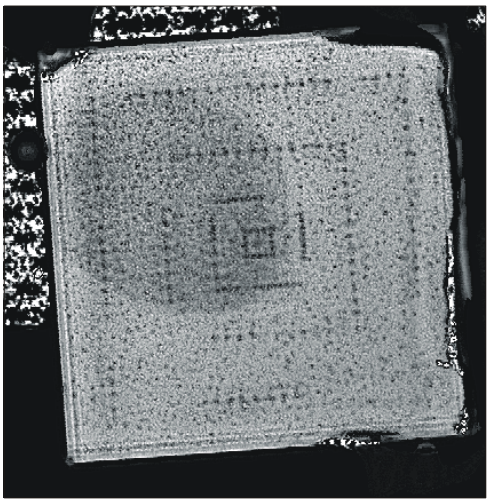

Figure 10: 50 MHz C-scan corresponding to narrow gate in A-scan shown in figure 9.

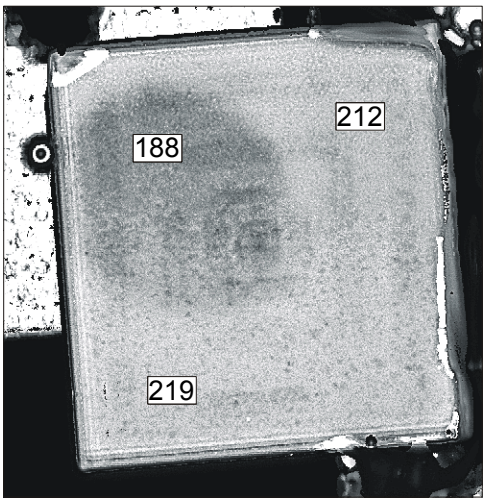

Figure 11: 50 MHz C-scan corresponding to broad gate in A-scan. Numbers indicate grey tone values.

The grey tone and reference acoustic impedance values used for the calculations are shown in table 3. The results derived by use of equation 7 show satisfactory agreements with the tabulated Z value for typical cured epoxy, table 4.

Table 3: Determined grey tone values and reference acoustic impedances.

Reference acoustic impedances / MRayl		Grey tone values (0 => 256)		
Z_1(silicon)	$Z_a(H_2O)$	$g_a(H_2O)$	g_x(EC1211 cured)	g_x(EC1211 uncured)
20	1.48	219	188	212

Table 4: EC1211 and typical epoxy acoustic impedances.

EC1211 acoustic impedances / MRayl		
Equation 7		Table (typical epoxy)
Z_x(cured)	Z_x(uncured)	Z(cured)
3.0	1.8	3 - 4

4 Discussion

The speed sound in the [111] direction of single crystalline silicon is 8.4 µm/ns. I.e. sound travels forth and back in the 350 µm flip-chip within 83 ns. The broad gate for grey tone determination starts about 20 ns later. The surface which is detected automatically at some level which might be quite low can be the explanation for this. Further the explanation might be the roughness of the unpolished top side of the chip. The speed of sound in cured epoxy is around 3 µm/ns. The wave length at 50 MHz is 60 µm. With a bump height of 30 µm the reflections from the chip / EC1211 and EC1211 / print interfaces with a time delay of around 20 ns cannot be resolved according to (5). Though, this interference from the EC1211 / print interface reflection is not critical since the two materials are acoustically well matched, which means that most of the sound is transmitted (see figure 3). This is also evidenced by the fact that A-scan wave forms in the flip-chip test case, figure

9 resembles the A-scan wave form in the isopropanole test case where the thickness of the adhesive is 2 mm.

On curing EC1211 the acoustic impedance changes about 1 MRayl unit / 20 grey tone values. By measuring at different places the uncertainty was estimated to be approximately 2 grey tone values corresponding to 0.1 MRayl.

5 Conclusion

It has been demonstrated that SAM can be used to determine acoustic impedances of materials in layered structures. Two equations have been verified. The usability of one equation depending on knowledge about the top layer acoustic impedance and only one other acoustic impedance of a material in the same depth as the analysed one has been demonstrated on a CUF flip chip with 30 μm bump height. A clear difference between cured / uncured CUF can be observed.

6 Acknowledgement

The work is part of the collaboration on development of microsystems (SUM) project between two Danish institutes DELTA, the Microelectronics Centre (MIC), and three Danish companies Capres A/S, Danfoss A/S and Grundfos A/S. The project is financially supported by the Danish Agency for Trade and Industry.

7 References

[1] B. A. Auld, in *Acoustic fields and waves in solids, 2, 37-38*, John Wiley & Sons, **1973**.
[2] S. P. Timoshenko and J. N. Goodier, in *Theory of Elasticity*, 492-493, McGrawHill, **1970**
[3] Tom Adams, in: *Advanced materials and processes*, **September 2000**, p. 38-40.
[4] S. Canumalla and M. G. Oravecz, In situ Elastic Property Characterization of Flip-Chip Underfills, in: *International Symposion on Advanced Packaging Materials*, **1998**, p. 106-110.

Paper 9

Jakob Janting, Uffe Bennov, Anders Black

Correlation between MEMS Adhesive cure Degree and acoustic Impedance determined with Differential Scanning Calorimetry and Scanning Acoustic Microscopy

Proceedings of Workshop on MEMS Sensor Packaging, March 20th and 21th 2003, ISBN87-89935-46-2

Correlation between MEMS Adhesive cure Degree and acoustic Impedance determined with Differential Scanning Calorimetry and Scanning Acoustic Microscopy

Jakob Janting[a], Uffe Bennov[b], Anders Black[b]

[a]*DELTA Danish Electronics, Light & Acoustics, Venlighedsvej 4, DK-2970 Hoersholm, Denmark*
e-mail: jaj@delta.dk, Fax: +45 72 19 40 01, URL: http://www.delta.dk
[b]*MIC, Building 345, DK-2800 Lyngby, Denmark*

1. Introduction

The motivation for this work has been to gain a fast, reliable and quantitative adhesive cure QA method for MEMS and microelectronics. In earlier studies the feasibility and advantages of using Scanning Acoustic Microscopy (SAM) in order to area detect whether Compression UnderFill (CUF) is cured or not cured at all have been demonstrated [1, 2]. The method relies on comparison of adhesive acoustic impedances Z_x calculated from C-SAM grey values g_x by using equation (1) which is based on the assumption that g_x varies linearly with the reflection coefficient R.

$$Z_x = Z_1 \frac{g_a(Z_a + Z_1) + g_x(Z_a - Z_1)}{g_a(Z_a + Z_1) - g_x(Z_a - Z_1)} \tag{1}$$

In (1) Z_1 is the acoustic impedance of the top material, Z_a, g_a are acoustic impedance and grey tone respectively for some reference material, typically water, underneath the top material.

Here it is demonstrated that the method can be used to determine not only whether an adhesive is cured or not cured at all, but also to determine cure degrees in between these limits.

2. Results

The two component EpoTek T7110 epoxy adhesive was studied. The reaction kinetics was analysed using Differential Scanning Calorimetry (DSC). A single chip with adhesive underneath was used to avoid sample to sample variations. I.e. adhesive between the four corners of flip chip with 30 μm bump height and four PCB corners was cured at different times at 100 °C. Slightly different gate positions and widths were used to explore the reproducibility in determining $Z_{adhesive}$ by C-SAM, figs. 1-3.

3. Discussion

The grey tone depends on the reflected amplitude with polarity (2):

$$A(R)_{12} = A_0 R_{12} = A_0 \frac{Z_2 - Z_1}{Z_1 + Z_2} \tag{2}$$

where A_0 is the incoming wave amplitude, R_{12} is the reflection coefficient corresponding to the interface between materials 1 and 2, Z_1 and Z_2 are the acoustic impedances of materials 1 and 2 respectively. R is not very sensitive to changes in Z_2, as can be seen from (3) inserting typical values (e.g. $Z_{1\,=\,water}$ = 1.48 MRayl, $Z_{2\,=\,microelectronics}$ = 20 Mrayl) though for many applications sensitive enough as also shown by these experiments.

$$\frac{\Delta R}{R} = \frac{2Z_1 Z_2}{Z_2^2 - Z_1^2} \cdot \frac{\Delta Z_2}{Z_2} \tag{3}$$

Using grey tones directly to determine reaction degree is not feasible due to the small relative changes. Acoustic impedances here changes approx. 30 % from 68 % reacted to 100 % reacted adhesive. The method is quite sensitive to the SAM gate adjustment, i.e. when the gate is changed the grey tones change and therefore also the determined acoustic impedances change. However, the grey tone relative values do not change. They can therefore be used as a quick gate-insensitive detection of more or less reacted areas. For quantitative evaluations a reference is needed and the grey tone values should be converted to acoustic impedances.

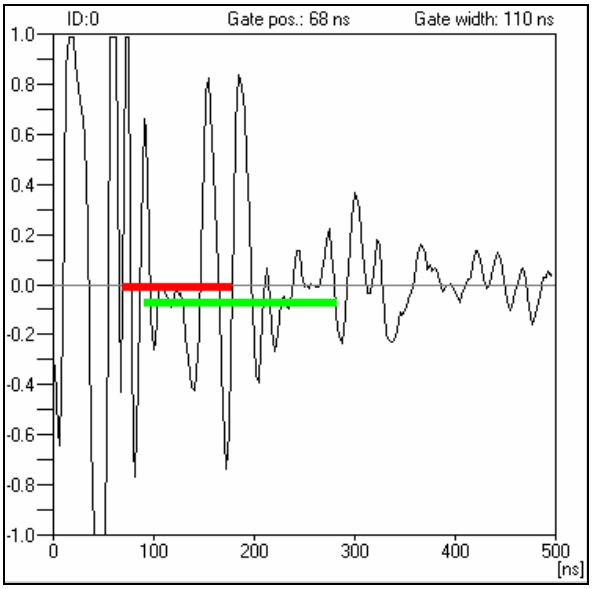

Fig. 1. A-scan in the centre of fig. 2. The top bar is the gate for the reflected signal from the chip / adhesive interface. In another *Z* determination the gate position was e.g. 85 ns and the width 98 ns.

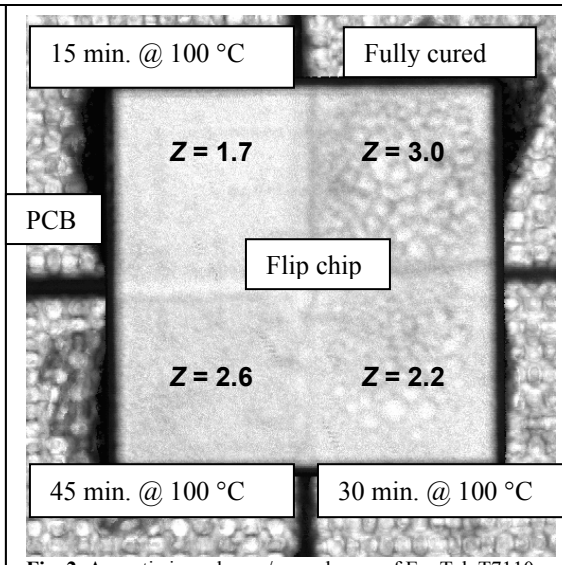

Fig. 2. Acoustic impedance / cure degree of EpoTek T7110 adhesive between flip chip (2.5 cm x 2.5 cm, 30 µm bump height) and PCB (4 pieces, bottom up) determined from SAM grey values. Corresponding A-scan is shown in fig. 1.

4. Conclusion

Generally, it has been shown that a linear correlation between acoustic impedance and adhesive reaction degree can be established. To determine the reaction degree from acoustic impedance a known reference and careful adjustment of the SAM gate is required.

Independent of a reference and precise SAM gate adjustment grey tones can be used as a quick qualitative comparison of more or less reacted areas.

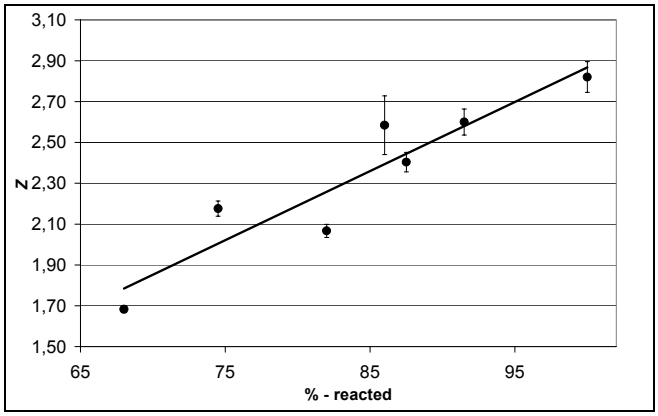

Fig. 3. Average acoustic impedance of EpoTek T7110 adhesive as a function of the reaction degree. *Z* = (0.0339 MRayl/%reacted) % reacted - 0.5183 MRayl, R = 0.93. The reaction degree was determined by DSC kinetic analysis.

5. Acknowledgement

This work has been part of the collaboration on development of microsystems (SUM) project between two Danish institutes DELTA, the Microelectronics Centre (MIC), and four Danish companies Capres A/S, SonionMEMS A/S, Danfoss A/S and Grundfos A/S. The project is financially supported by the Danish Agency for Trade and Industry.

6. References

[1] Jakob Janting, Dirch Hjorth Petersen, Scanning Acoustic Microscopy Investigation of Adhesive cure Degree, In these proceedings.

[2] J. Janting, D. H. Petersen, B. V. Schönwandt, Scanning Acoustic Microscopy Study of Flip-Chip Underfill Cure Degree, in proceedings of Materials Week 2002, Munich

Paper 10

Jakob Janting, Elisabeth Kjærside Storm

Water Uptake of Polymeric Packaging Materials

Proceedings of Workshop on MEMS Sensor Packaging, March 20th and 21th 2003, ISBN87-89935-46-2

Water Uptake of Polymeric Packaging Materials

Jakob Janting, Elisabeth Kjærside Storm

DELTA Danish Electronics, Light & Acoustics, Venlighedsvej 4, DK-2970 Hoersholm, Denmark
e-mail: jaj@delta.dk, Fax: +45 72 19 40 01, URL: http://www.delta.dk

1. Introduction

MEMS and microelectronics are very sensitive to water. Ingress of less than 10^{-4} μL water to bond pads in packages is often critical due to galvanic corrosion. Polymeric materials are widely used for MEMS and microelectronics packaging, but they are not water tight (fig. 1).

The general motivation for this work has been to identify optimal polymeric materials and methods for water protective encapsulation of MEMS and microelectronics.

Studies have been made on Compression UnderFill (CUF) for flip chip electrical interconnection of a MEMS pressure sensor and a two-layer combination of materials to glob-top protect a needle shaped MEMS absolute pressure sensor.

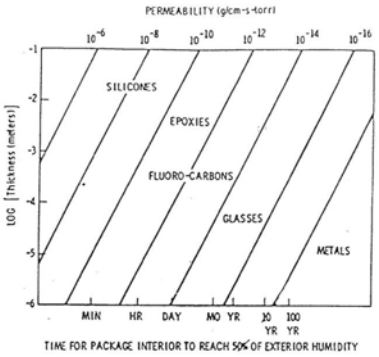

Fig. 1. Tightness of different packaging materials [1].

2. Diffusion theory

Based on Fick's second law of diffusion the amount of water diffusing into a thin square piece of polymer from both sides can be calculated to be [2]:

$$G = \frac{M_t}{M_E} = 1 - \frac{8}{\pi^2}\sum_{n=0}^{\infty}\frac{\exp\left\{-(2n+1)^2\pi^2\frac{Dt}{L^2}\right\}}{(2n+1)^2} \tag{1}$$

where M_t, M_E are the masses of in-diffused water at time t and at equilibrium respectively, D is the diffusion constant, and L is the thickness of the polymer piece. From this equation D can be found.

The flux F of water into a package can then be determined from (2)

$$F = \frac{DS}{d} = PS \tag{2}$$

where S is the water solubility, d is the polymer package thickness, and P is the polymer permeability.

2. Results

2.1 Fit function to determine D

To find D a suitable (r^2 = 1.00) fit function G' to G was found:

$$G' = 1 - 0{,}877\exp\left\{-9{,}18\left[\frac{Dt}{L^2}\right]^{0{,}931}\right\} \tag{3}$$

By fitting this function to the M_t/M_E experimental data D is determined.

2.2 CUF water uptake

Figs. 2 and 3 show measurements on an epoxy based CUF. In one MEMS pressure sensor application where water is supposed to be in direct contact with the CUF d is less than 1 mm. From fig. 3 it is seen that this distance is far too short considering the critical limit of 10^{-4} μL.

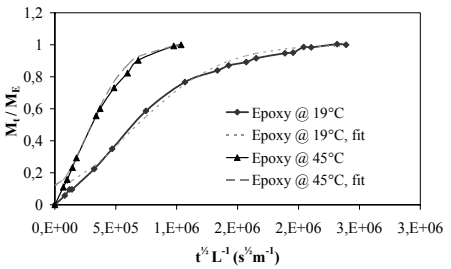

Fig. 2. Sorption curves for epoxy CUF at different temperatures. The sample studied at 19 ºC is 1 mm thick. The sample studied at 45 ºC is 0.85 mm thick. Fitting (3) to the data gives: $D(19\ ºC) = 7 \cdot 10^{-14}$ m^2/s, $D(45\ ºC) = 5 \cdot 10^{-13}$ m^2/s.

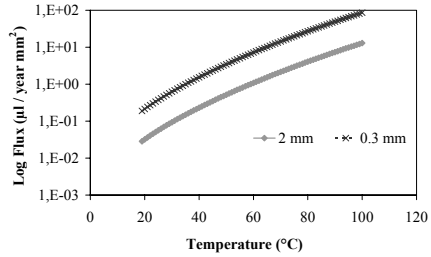

Fig. 3. Flux of water through epoxy CUF of different thickness as function of temperature. Calculations based on fig. 2 data.

2.3 Water uptake of a polymeric bi-layer protective encapsulation for a MEMS absolute pressure sensor

Currently sorption measurements are being performed on a MacroMelt material coated with parylene C (fig. 4). Later measurements on the naked MacroMelt will show the effect of the coating.

4. Discussion

Due to the pre-exponential in the fit function (5) this M_t/M_E estimate is not accurate at short times. If the solubility and therefore M_E are known M_t/M_E can be plotted for short times as a function of $t^{½}L^{-1}$ and $D = \pi h^2/16$ where h is the slope.

Note that by water immersion at 45 ºC the 0.85 mm thick CUF sample is saturated after approx. 8 days. At 19 ºC and 1 mm thickness it is saturated after 25 days. I.e. already after these times throughout the polymer the maximum amount of water which can be in contact with e.g. conductors at any time is achieved.

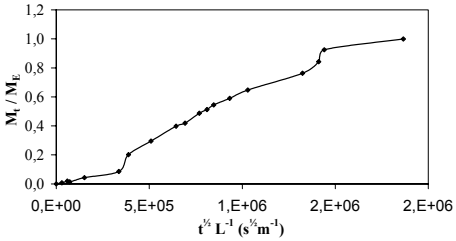

Fig. 4. Sorption curve at 19 ºC for a MacroMelt material coated with 10 µm parylene C. Total sample thickness is approx. 2 mm. Here M_E is not the real equilibrium mass but only the latest measured since saturation has not yet been reached.

Fragile MEMS components can be moulded with thermoplastic materials like the soft polyamide based MacroMelts which are processed at low temperatures and pressures. However, they are not a suitable choice for water protection due to high P. This problem can be reduced by coating with e.g. 10 µm parylene C which has lower P. In this way the good properties of both materials can be combined. Further simulations show that such a coating barrier will have no influence on the pressure measurements.

4. Conclusion

Generally, the water flux at different temperatures through polymeric encapsulation materials for MEMS and microelectronics can be measured. Design with e.g. materials combinations is important to reduce water attack.

For typical flip chip dimensions the amount of water passing through the studied epoxy CUF in direct water contact by far exceeds the critical 10^{-4} µL within typical required lifetimes.

This is also the case for the studied encapsulation materials separately and in combination. Though, by combining the materials in a layered structure improvement can be achieved.

5. Acknowledgement

This work has been part of the collaboration on development of microsystems (SUM) project between two Danish institutes DELTA, the Microelectronics Centre (MIC), and four Danish companies Capres A/S, SonionMEMS A/S, Danfoss A/S and Grundfos A/S. The project is financially supported by the Danish Agency for Trade and Industry.

6. References

[1] Hermiticity of polymeric lid sealants. R. K. Traeger. Proc. 25th Electronic Components Conf. p 361.
[2] The Mathematics of Diffusion. J. Crank (1975), Oxford University Press, Oxford.

Paper 11

Jakob Janting, Dirch Hjorth Petersen

Scanning Acoustic Microscopy Investigation of Adhesive Cure Degree

Proceedings of Workshop on MEMS Sensor Packaging, March 20th and 21th 2003, ISBN87-89935-46-2

Scanning Acoustic Microscopy Investigation of Adhesive Cure Degree

Jakob Janting[a], Dirch Hjorth Petersen[b]

[a]*DELTA Danish Electronics, Light & Acoustics, Venlighedsvej 4, DK-2970 Hoersholm, Denmark*
e-mail: jaj@delta.dk, Fax: +45 72 19 40 01,URL: http://www.delta.dk
[b]*MIC, Building 345, DK-2800 Lyngby, Denmark*

1. Introduction

The motivation for this work has been to gain a fast and reliable Compression UnderFill (CUF) based flip-chip interconnection process for MEMS components. In this process electrical contact between bumps and pads is established mechanically by the high curing shrinkage of the underfill (fig. 1).

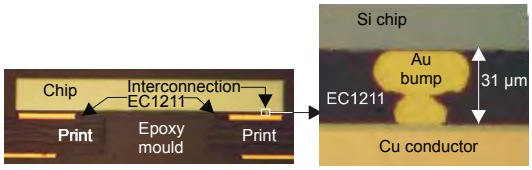

Fig. 1. Cross section through bump – pad electrical interconnection between flip-chipped MEMS pressure sensor chip and print.

Although the studied CUF material EC1211 has been cure characterised by Differential Scanning Calorimetry (DSC), the actual temperature environments experienced by the underfill in the flip-chip process might be much different than expected. When trying to run the process as fast as possible it could be that the CUF is not uniformly cured. Using DSC for evaluation is tedious and destructive because samples of the CUF will have to be taken out for the analysis. A better alternative is Scanning Acoustic Microscopy (SAM). Here detection of cure degree relies on the big mechanical (stiffness *E*) differences between cured and uncured material and the great advantages are that the inspection is 2D and non-destructive.

2. Results

Two approaches for determining the degree of CUF curing degree have been studied. First it was attempted to determine the cure degree from differences in sound speed. This requires knowledge about the CUF thickness and reflection time delay between the top and bottom interfaces. The method turns out not to be feasible for typical CUF thicknesses (30 µm – 70 µm) because of too low depth resolution. Even with thick bond lines and therefore well separated reflections from top and bottom interfaces it is difficult to determine the speed with sufficient accuracy because the waves do not have the same form and the points on the waves to measure from / to are not well defined. Though, using C-scan grey tone values good results can be achieved.

2.1 Acoustic impedance calculations from C-scan grey tone values

The advantage of this approach compared to the speed of sound method is that only the degree of reflection at the same depth between different materials e.g. cured / uncured CUF is measured. Depending on the situation two different calculations can be used to determine the acoustic impedance of a material placed under another:

- The acoustic impedance Z_1 of the top material is unknown.

Calculation of Z_x is based on the approximation that R_{12} has a linear dependence on Z_2. Then Z_x is given by:

$$Z_x = Z_b + (g_x - g_b)\frac{Z_b - Z_a}{g_b - g_a} \qquad (1)$$

i.e. to determine Z_x two reference acoustic impedances Z_a, Z_b for materials placed under the top material are needed. Their grey tone values and the value for the studied material x are measured in the C-scan picture.

- The acoustic impedance Z_1 of the top material is known

Calculation of Z_x is based on the linear dependence of g_x on R. Then Z_x is given by:

$$Z_x = Z_1 \frac{g_a(Z_a + Z_1) + g_x(Z_a - Z_1)}{g_a(Z_a + Z_1) - g_x(Z_a - Z_1)} \quad (2)$$

i.e. to determine Z_x in this case only one reference acoustic impedance Z_a for a material placed under the top material is needed. Again the corresponding grey tone value g_a and the value for the studied material g_x is found in the C-scan picture.

2.1 Test 1: Determination of acoustic impedance of isopropanole

To test the methods of determining acoustic impedances isopropanole, air, water, and adhesive were placed between two microscope slides (glass) with the purpose of determining the acoustic impedance of isopropanole. Isopropanole and air were entrapped in small aluminum pans used for DSC measurements.

Table 1. Acoustic impedance of isopropanole.

Z_x(isopropanole) / MRayl		
Equation 1	Equation 2	Table
0.95	0.97	0.92

The sample was put in the SAM inspection vessel. The vessel was filled with water and a gate was placed for a C-scan covering the whole reflected wave from the bottom interface of the microscope slide. The C-scan was performed and grey tone values determined with KSI WINSAM 200 software. The acoustic impedance as determined from (1) and (2) are shown in table 1. Good agreement with tabulated values is found in both cases.

2.2 Test 2: Flip chip with CUF

Cured / uncured epoxy EC1211 CUF material between a 2 cm x 2 cm x 0.35 mm test flip-chip with approximately 30 µm bumps and a Printed Circuit Board (PCB) were studied. Again to get the grey tone values a gate is placed covering the whole reflected wave at the chip / CUF / PCB interfaces. The acoustic impedances are shown in table 2. Good agreement is observed between the determined acoustic impedance and tabulated typical values for epoxy.

Table 2. EC1211 and typical epoxy acoustic impedances.

EC1211 acoustic impedances / MRayl		
Equation 2		Table (typical epoxy)
Z_x(cured)	Z_x(uncured)	Z(cured)
3.0	1.8	3 - 4

3. Discussion

The speed sound in the [111] direction of single crystalline silicon is 8.4 µm/ns. i.e. sound travels forth and back in the 350 µm flip-chip within 83 ns. The broad gate for grey tone determination starts about 20 ns later. Low pre-determined threshold level for surface detection can be the explanation for this. Further the explanation might be the roughness of the unpolished top side of the chip. The speed of sound in cured epoxy is around 3 µm/ns. The wave length at 50 MHz is 60 µm. With a bump height of 30 µm the reflections from the chip / EC1211 and EC1211 / print interfaces with a time delay of around 20 ns cannot be resolved. Though, this interference from the EC1211 / print interface reflection is not critical as the two materials are acoustically well matched, which means that most of the sound is transmitted. This is also evidenced by the fact that A-scan wave forms in the flip-chip test case resembles the A-scan wave form in the isopropanole test case where the thickness of the adhesive is 2 mm.

4. Conclusion

It has been demonstrated that SAM can be used to determine acoustic impedances of materials in layered structures. Two equations have been verified. The usability of one equation depending on knowledge about the top layer acoustic impedance and only one other acoustic impedance of a material in the same depth as the analysed one has been demonstrated on a CUF flip chip with 30 µm bump height. A clear difference between cured / uncured CUF can be observed.

5. Acknowledgement

This work has been part of the collaboration on development of microsystems (SUM) project between two Danish institutes DELTA, the Microelectronics Centre (MIC), and four Danish companies Capres A/S, SonionMEMS A/S, Danfoss A/S and Grundfos A/S. The project is financially supported by the Danish Agency for Trade and Industry.

Paper 12

Qingshan Yao, Jens Branebjerg, Jakob Janting

FEM Simulation of Influence of Protective Encapsulation on MEMS Pressure Sensor

Proceedings of Workshop on MEMS Sensor Packaging, March 20th and 21th 2003, ISBN87-89935-46-2

FEM Simulation of Influence of Protective Encapsulation on MEMS Pressure Sensor

Qingshan Yao[a], Jens Branebjerg[b], Jakob Janting[c]

[a]*SensoAsian Industrial Consulting, Hostrupsvej 6a, DK-3400, Hilleroed, Denmark*
e-mail: sensoasian@hotmail.com, Fax: +45 45 93 72 88
[b]*DELTA Danish Electronics, Light & Acoustics, Venlighedsvej 4, DK-2970 Hoersholm, Denmark*
e-mail: jab@delta.dk, Fax: +45 72 19 40 01, URL: http://www.delta.dk
[c]*DELTA Danish Electronics, Light & Acoustics, Venlighedsvej 4, DK-2970 Hoersholm, Denmark*
e-mail: jaj@delta.dk, Fax: +45 72 19 40 01, URL: http://www.delta.dk

ABSTRACT

The objective of the work is to evaluate the feasibility of packaging a MEMS silicon pressure sensor by using either a polymer encapsulation or a combination of a polymer encapsulation and a metallic protection Membrane (fig. 1). The potential application of the protected sensor is for harsh environments. Several steps of simulation are carried out:

1) Comparisons of the sensitivities are made among the non-encapsulated silicon sensor, the polymer encapsulated and polymer with metal encapsulated sensor. This is for evaluating whether the encapsulating materials reduce the pressure sensitivity compared to the conventionally exposed sensor.

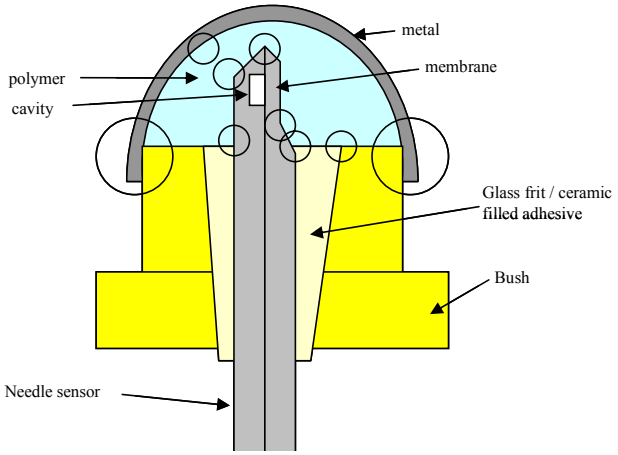

Fig.1: Encapsulated Danfoss pressure sensor with indication of stress zones to investigate.

2) Stress concentration calculations are performed to investigate if the encapsulation could lead to increased stress concentration in the silicon structure. The reliability of the adhesion of the metallic encapsulating membrane is assessed by investigating whether the metallic membrane / coating will peel off when applying the maximum pressure, which is 4000 bar leading to high shear stress between the metallic membrane and the polymer encapsulation material.

3) Thermal calculations are made to evaluate the influence of the environment on the packaged sensor.

Sensitivity related conclusion remarks:

- The polymer and the metallic encapsulation would not lead to a significant reduction of the sensitivity of the silicon sensor.
- Metallic encapsulation has a negligible influence on the sensitivity compared to the polymer-encapsulated design without the metal protection membrane.

Stress concentration related conclusion remarks:

- The coating leads to larger stresses on the interface between the two silicon parts of the sensor die.
- The coating leads to larger stresses in the junction region between the silicon sensor die and the mounting material.
- Whether the stress concentration on the interface between the metallic membrane and the polymer lead to a reliability risk depends on the adhesion of the membrane.
- The polymer encapsulation leads to much larger vertical displacement of the silicon sensor, which might harm the reliability of the mounting of the sensor die to the substrate.

Thermal related conclusion remarks:

- For the currently selected polymer encapsulation material with a thermal expansion coefficient of $5 \cdot 10^{-5}$, the temperature-induced deformation has significant influence on the sensitivity. A temperature change of 15 °C will give a signal as a pressure of 40 bars.

Acknowledgement

This work has been part of the collaboration on development of microsystems (SUM) project between two Danish institutes DELTA, the Microelectronics Centre (MIC), and four Danish companies Capres A/S, SonionMEMS A/S, Danfoss A/S and Grundfos A/S. The project is financially supported by the Danish Agency for Trade and Industry.

Paper 13

Jakob Janting, Dirch Hjorth Petersen, Christoffer Greisen

Simulated SAM A-scans on multilayer MEMS components

Proceedings of Workshop on MEMS Sensor Packaging, March 20th and 21th 2003, ISBN87-89935-46-2

Simulated SAM A-scans on multilayer MEMS components

Jakob Janting[a], Dirch Hjorth Petersen[b], Christoffer Greisen[c]

[a]*DELTA Danish Electronics, Light & Acoustics, Venlighedsvej 4, DK-2970 Hoersholm, Denmark*
e-mail: jaj@delta.dk, Fax: +45 72 19 40 01,URL: http://www.delta.dk
[b]*MIC, Building 345, DK-2800 Lyngby, Denmark*
[c]Danfoss A/S, CAT/DTU, Building 347, DK-2800 Lyngby, Denmark

1. Introduction

SAM has been used for several years as a microelectronics failure analysis tool though often with poor understanding of the A-scan and C-scan pictures. This is especially the case when the components consist of layers very close to each other and where phase inversions take place.

Most often MEMS contain stacks of many very thin layers. The motivation for this work has therefore been to gain better understanding of SAM A-scans on MEMS multilayer structures by simulation.

2. Results

All calculations have been made in an excel spreadsheet. SAM measurements were made on KSI Winsam 200 equipment.

2.1 Spreadsheet calculations

For given sets of reflections we calculate for each first the number N of possible reflection orders. The calculations are based on maximum 4 or 9 impedance transitions with up to 8 or 2 reflections back towards the transducer respectively (Fig. 1). Then the received amplitudes with polarity according to (1) together with the corresponding delay times are calculated.

$$A = A_0 \cdot N \cdot T_{total} \cdot R_{total} \tag{1}$$

T_{total} and R_{total} are the products of all involved transmission and reflection coefficients. Due to limited available data the sound attenuation in each layer is not yet included in the calculations, however, the program is prepared for this. The spreadsheet input values are the materials acoustic impedances, the speed of sound in the materials, and the layer thicknesses.

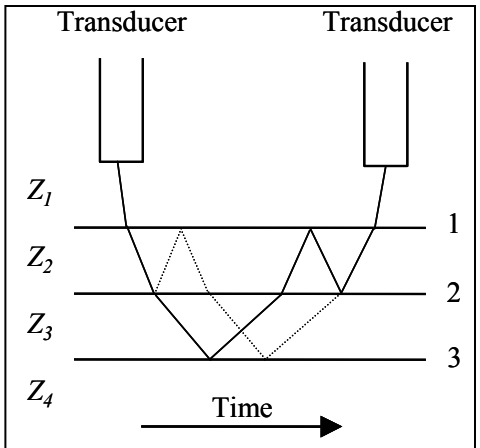

Fig. 1. Illustration of two waves which are equal because they are reflected at the same interfaces only in different order (3-1-2, 2-1-3). They are therefore received at the transducer at the same time.

2.2 A-scans on fusion bonded wafers

Bonded silicon wafers with test cavities for an absolute pressure sensor have been investigated with SAM. The cavities are used to test the leakage through the bond interface into the cavity [1]. Over the cavities and down the layers are Si (350 µm) / cavity (2 µm) / Si (500 µm) / SiN (0.1 µm).

Simulations show that in order to get a scan of the interface with a minimum of overlapping waves out of phase the bonded wafers should be inspected from the Si side (Fig. 2). Then all the reflected waves have the same sign and are well separated because the time between them is 83 ns. Though, by comparing the real scan from the Si side (Fig. 3) with the simulations it is evident that this looks more like the one expected when scanning from the SiN side (Figs. 2 and 3).

3. Discussion

Spectra much like the one from the SiN side are achieved no matter the thin layer material and position at the exterior or next to the cavities and channels. Therefore we suggest that the thin boron diffused bond layer is acoustically different from bulk silicon, which was not expected from the start. This is supported by

the observation that stresses built-up in such layers, which might change the longitudinal acoustic impedance of silicon significantly. I.e. we have the layers: Si (350 µm) / approx. 2 µm B diffused Si / cavity (2 µm) / Si (500 µm) / SiN (0.1 µm).

Apart from the time position differences due to differences in Si thickness before the cavity, the real scan from the Si side resembles the A-scan simulation of inspection from the SiN side quite well because waves of opposite amplitude sign seem to overlap more or less. Note that only two signals from the interface are clearly seen, i.e. the first and second time reflections from cavities / channels at around 83 ns, 166 ns and 118 ns, 237 ns in the real scan from the Si side (Figs. 2 and 3) and in the simulation of inspection from the SiN side (Fig. 2) respectively. The rest of the signals essentially die because waves with opposite phase are added. Already from the second time echoes this begins to happen e.g. by addition of 3-1-3-.. and 3-2-3-.. reflections in the case of inspection from the SiN side. Even though the second time reflection from the cavity has passed two times through the silicon material, the amplitude is high because of the high *N* value.

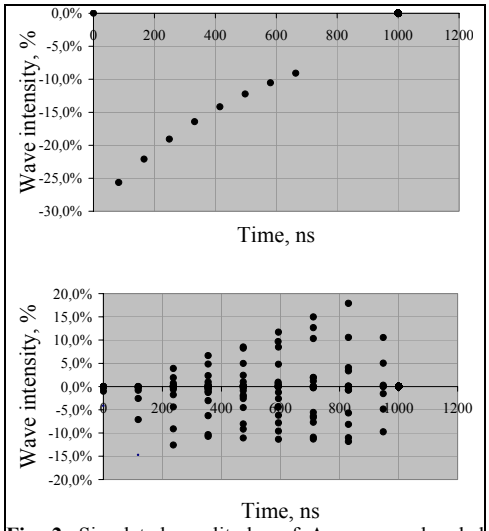

Fig. 2. Simulated amplitudes of A-scans on bonded wafers with cavities. Each dot shows amplitude and time for a back reflected wave. Top: Inspection from Si side. Bottom: Inspection from SiN side. Note that in this case many waves are received at the transducer at the same times.

4. Conclusion

A calculation method and spreadsheet program for simulation of SAM A-scans on multilayer structures have been developed. The useful information, which the simulations provide, has been demonstrated on fusion bonded wafers containing MEMS pressure sensor test cavities in the interface. Unexpectedly it was found that an extra layer on the wafer without etched cavities / channels has influence on the A-scans. Presumably this layer is a B diffused bond layer.

Generally, it has been shown that structure variations in samples can be simulated and therefore analysed better. Failures or variations in MEMS structures can be analysed by investigating the effect of introducing them in the A-scan simulations and comparing them with real A-scans.

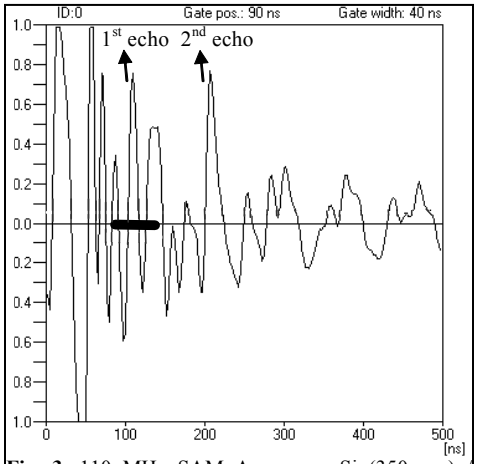

Fig. 3. 110 MHz SAM A-scan on Si (350 µm) / approx. 2 µm B diffused Si / cavity (2 µm) / Si (500 µm) / SiN (0.1 µm) from Si side. Note that surface trigger is in the front of the wave reflected at the top surface. First and second reverberations from the cavity starting at 83 ns and 166 ns respectively are observed (arrows). The gate indicated by a black bar is a filter which is here open for the first signal.

5. Acknowledgement

This work has been part of the collaboration on development of microsystems (SUM) project between two Danish institutes DELTA, the Microelectronics Centre (MIC), and four Danish companies Capres A/S, SonionMEMS A/S, Danfoss A/S and Grundfos A/S. The project is financially supported by the Danish Agency for Trade and Industry.

6. References

[1] K. Birkelund, M. Sørensen, S. Chiriaev, P. Gravesen and P. B. Rasmussen, High pressure sensor based on fusion bonding, abstract 1482 in: Proc. of the 6th. Int. Symp. on Semiconductor Wafer Bonding: Science, Technology and Applications, The Electrochem. Soc., San Francisco (2001).

Paper 14

Jakob Janting

Scanning Acoustic Microscopy for Quality Assurance of MEMS Sensors

Proceedings of Sensor 2003, 11th International Conference, 13-15 May 2003, Nuremberg

Scanning Acoustic Microscopy for Quality Assurance of MEMS Sensors

Jakob Janting
DELTA Danish Electronics, Light & Acoustics
Venlighedsvej 4, 2970 Hoersholm, Denmark

Abstract

An overview of characteristic Scanning Acoustic Microscopy (SAM) inspection cases with focus on requirements and approaches used for Quality Assurance (QA) of MEMS sensors is given. The cases are divided into three sections.

The feasibility of using high frequency, move of sound focus [1], and a developed A-scan simulation program [2] to further enhance QA on MEMS sensors is discussed. New results on wafer to wafer silicon bonding and adhesive cure degree studies are presented.

1 Introduction

Acoustic microscopy has many applications, SAM especially in the microelectronics industry. Acoustic Microscopy is a Non Destructive Testing (NDT) method for microinspection which functions like a sonar, though using much higher frequencies, MHz – GHz. Pulses of ultrasound is transmitted through a liquid medium, typically water, to the component and its interior where it is reflected and transmitted at interfaces between materials due to their differences in acoustic impedance Z.

2 Basic SAM theory

At the interfaces the reflected $A(R)_{12}$ and transmitted $A(T)_{12}$ amplitudes with polarity are given by [3]:

$$A(R)_{12} = A_0 R_{12} = A_0 \frac{Z_2 - Z_1}{Z_1 + Z_2} \tag{1}$$

$$A(T)_{12} = A_0 T_{12} = A_0 \frac{2Z_2}{Z_1 + Z_2} \tag{2}$$

where A_0 is the incoming wave amplitude, R_{12} and T_{12} are the reflection and transmission coefficients respectively, Z_1 and Z_2 are the acoustic impedances of materials 1 and 2 respectively, figs. 1 and 2.

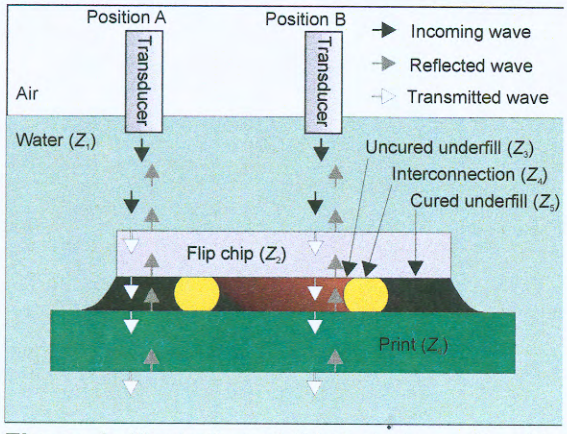

Figure 1: Illustration of SAM study on flip-chip with cured / uncured underfill.

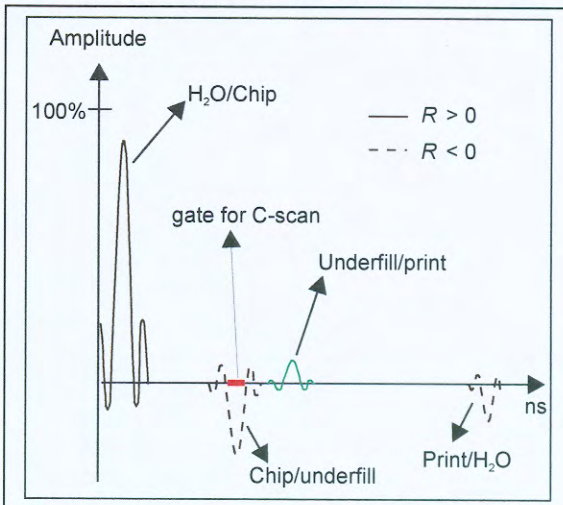

Figure 2: A-scan on flip-chip in figure 1. Reflected sound at chip / underfill varies according to cure degree.

The samples examined in the SAM are considered to be of infinite dimension concerning the description of wave propagation i.e. we have plane waves and the waveform is longitudinal. Then the acoustic impedance is described by [4]:

$$Z = \rho V_L = \rho \sqrt{\frac{B(1-\nu)}{\rho(1+\nu)\cdot(1-2\nu)}} = \sqrt{\frac{\rho B(1-\nu)}{(1+\nu)\cdot(1-2\nu)}} \approx \sqrt{\frac{\rho E(1-\nu)}{(1+\nu)\cdot(1-2\nu)}} \approx \sqrt{\rho E} \qquad (3)$$

where V_L is the longitudinal wave velocity, B is the bulk modulus, E is Young's modulus, ρ is the density, and ν is Poisson's ratio.

3 General SAM requirements

For best results, plane and smooth surfaces are required [1]. If the top surface is not planar the focus will move with respect to the sample during scanning and much of the sound may not be reflected back to the transducer. Further it is an advantage if the top and bottom surfaces are coplanar. Then it will be easier also to ensure that the top and interior surfaces of the component are coplanar with the scanning plane. Problems with planarity and co-planarity are often seen as gradual change in grey tones corner to corner or edge to edge. On rough surfaces the sound is scattered and less reflected sound returns to the transducer and the resolution gets poor.

4 SAM state of the art analysis and qualification

Using acoustic microscopy resolution and penetration depth depends on frequency, focus position, stiffness and stiffness changes in the materials. The choice of transducer therefore depends on the specific situation.

4.1 Analysis

As the sound is transmitted as pulses in SAM it consists of a broad band of frequencies and amplitudes. These are shifted downward on the way to the sample and back because of high attenuation of high frequency components [5]. Generally, high frequency gives high resolution but low penetration depth and vice versa.

SAM wavelengths are high compared to the low pitch of layers and conductors in MEMS sensors, though due to high sensitivity towards changes in Z the thickness detection limit of e.g. narrow delaminations / gaps is below 0.1 µm [6], which is around 1000 times better than the typical wavelength determined depth resolution. I.e. small changes can be detected but usually their in-depth dimension cannot be measured.

High frequencies (2 GHz) and focusing below the surface result in both a high wavelength determined resolution but also a very good detection limit of gaps / cracks perpendicular to the surface due to Rayleigh waves travelling along the surface [7, 8].

Whether focusing below the surface is a suitable method of gaining high resolution at the depth of interest depends on the used transducers and the materials involved. The speed of sound in many MEMS and microelectronics materials is high and above 6000 m/s (e.g. silicon, ceramics). As water is usually the coupling agent the speed of sound here is about 1500 m/s. Then the refractive index is 0.25 which means that the critical angle is 15° and waves incident at angles above this do not excite any longitudinal waves in the solid. As a consequence high resolution transducers with a wide aperture cannot be used effectively.

Using Fourier analysis better resolution has been achieved by filtering out low frequencies in the frequency domain and transforming back to the time domain [9].

Through (1) and (3) materials can be analysed for stiffness variations e.g. whether an adhesive is fully cured everywhere [10, 11].

MEMS A-scan and C-scan pictures are often difficult to analyse because the components consists of layers very close to each other resulting in overlapping reflected waves some of which are with opposite phases. For better A-scan analysis in these cases a spreadsheet simulation program has been developed [2]. The simulations are based on calculations of reflection, transmission coefficients, and the number of waves received by the transducer at the same time by reflection at the same interfaces in different order.

4.2 Qualification

In SAM QA on electronics the commonly used procedure is to make the inspections comply with the standard IPC/JEDEC J-STD-035 "Acoustic Microscopy for Nonhermetic Encapsulated Electronic

Components" [12]. In a number of cases this standard is not directly applicable because of the large diversity of products and failure modes. Therefore efforts are put into describing more product specific QA procedures [13] and to develop new analysis tools [2, 10, 11]. Using for instance the above mentioned A-scan simulation program components can be analysed before the actual scan and prepared to get optimal signal for enhanced failure and materials analysis.

5 General failure examples and new results on MEMS sensor packaging

SAM QA on MEMS and microelectronics components comprises assurance that there are no failures in:

- Interfaces between component parts
- Component materials
- Uniformity of component materials

An example of a MEMS sensor in production where SAM has been a part of the moisture sensitivity classification is a pressure sensor in principle constructed as shown in fig. 3 and 4.

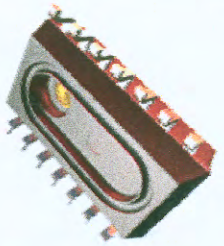

Figure 3: MEMS absolute pressure sensor

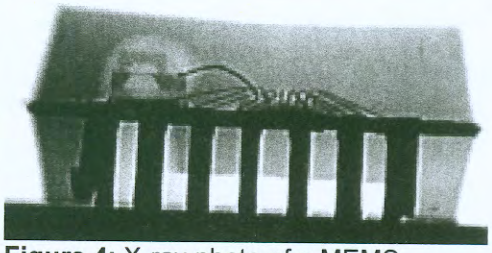

Figure 4: X-ray photo of a MEMS absolute pressure sensor in fig. 3 showing the listed areas interest for SAM inspection.

5.1 Interface failures

The failures of the first type is mainly delaminations e.g. in interfaces between encapsulation material and chip / leadframe, and between chip and adhesive. The term "delamination" here also covers the area of failures where for instance there is no contact or only partly contact between bond wires / bumps and bond pads. A typical example of a delamination between encapsulation material and leadframe is shown in fig. 5.

SAM is also used as a QA method in the MEMS sensor development process. Figs. 6-10 show recent results on how well the quality of test bonding interfaces between silicon wafers for an absolute pressure sensor can be inspected with SAM. Often IR transparency is used to monitor silicon wafer to wafer bond quality, however here SAM is far more sensitive.

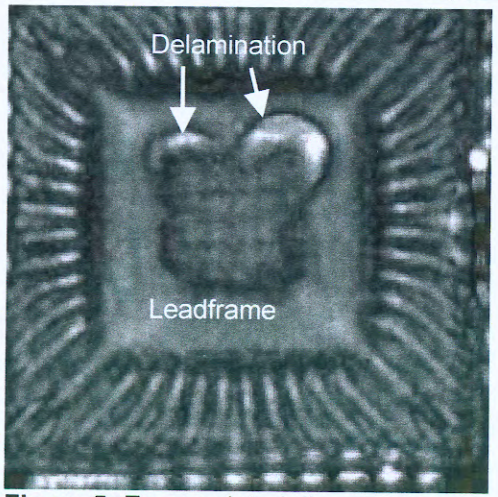

Figure 5: Encapsulated die on leadframe. Delamination between encapsulation material and leadframe.

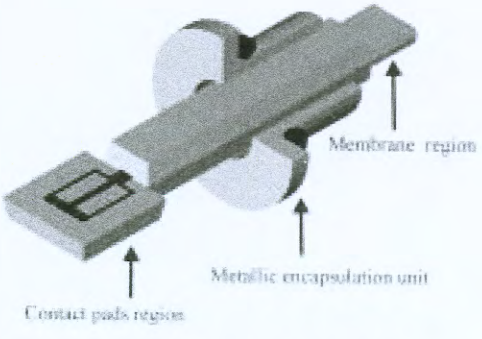

Figure 6: Drawing of Danfoss MEMS absolute pressure sensor. The dimensions are approx. 3 mm x 7 mm x 0.9 mm.

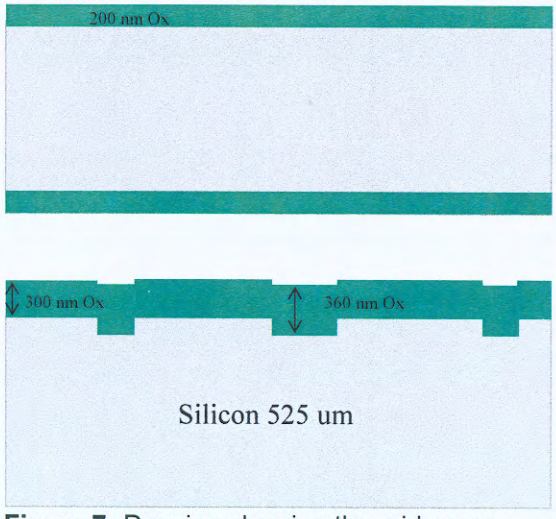

Figure 7: Drawing showing the mid cross-section dimensions of pattern between fusion bonded silicon wafers.

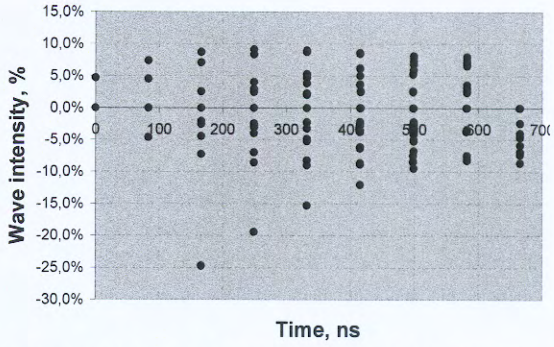

Figure 8: Simulated amplitudes of A-scan on structure between wafers shown in fig. 7. Each dot indicates amplitude, polarity and time for a back reflected wave. The software described in [2] was used.

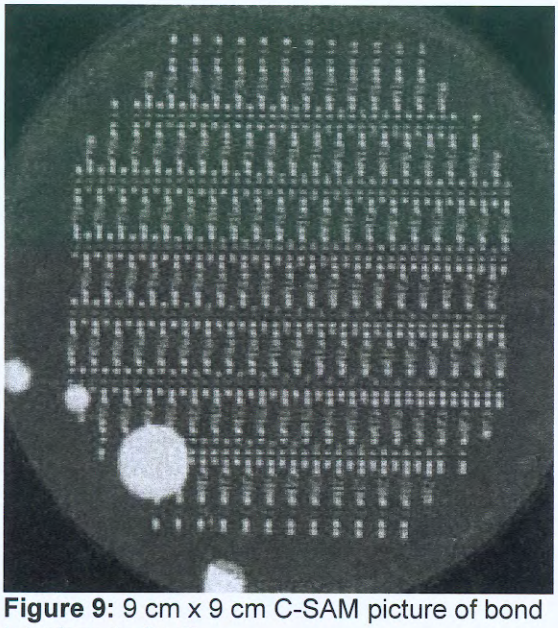

Figure 9: 9 cm x 9 cm C-SAM picture of bond interface in fig. 7.

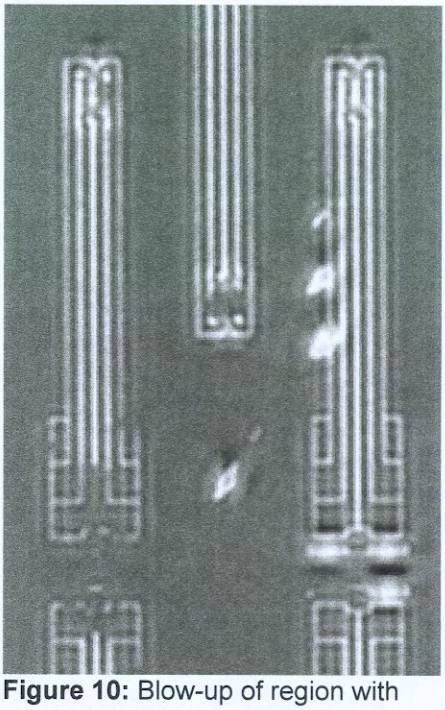

Figure 10: Blow-up of region with small disbonds.

Using IR inspection only the large round disbond can be seen at the bottom left area of fig. 9. Note the very small pattern features detected. Height differences less than 100 nm are detected, see figs. 7, 9 and 10, with frequencies as low as 50 MHz and an unpolished top wafer. Often the surface reflection is masking the much lower intensity reflections from material transitions close to the surface. In these cases the second echo with double time delay can be used. In this case it is also the only echo from the interface which can be used since the other echoes die because of overlapping waves with different polarity, see fig. 8.

Using 400 MHz and the KSI WINSAM 200 instrument at these studies, MEMS test cavities with a lateral pitch of 8 µm in the interface between bonded silicon and glass have also been clearly resolved by scanning through the silicon wafer isotropically etched down to approx. 50 µm thickness.

5.2 Failures inside component materials

Failures of the second type are e.g. cracks and bubbles in the encapsulation, adhesive and soldering. Bubbles in the encapsulation originate from the moulding process and often they contain air / moisture. In later soldering processes this is critical because the air / moisture expansion may result in cracks (popcorning) extending all the way from the exterior to the vulnerable MEMS and microelectronics interior parts. Poor wetting may result in bad or no contact between parts and bubbles either entirely in the solder or perhaps extending from one or both surfaces into the solder like in fig. 11.

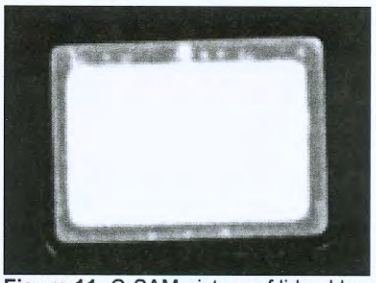

Figure 11: C-SAM picture of lid solder interface of package housing (approx. 8 mm x 4 mm x 3 mm) for MEMS and microelectronics. White areas in soldered rim are without contact between lid and solder.

5.3 Failures in materials uniformity

The third type of failures comprises measurement of variations in adhesive cure degree, adhesive filler distribution etc. by measurement of variations in Z, see figs. 12 and 14.

Methods for determining acoustic impedances in layered structures have previously been developed [10, 11]. The method relies on determination of R from C-SAM grey values. Here it is demonstrated that this can be used to determine not only whether an adhesive used in MEMS sensor applications is cured or not cured at all, but also to determine cure degrees in between these limits, see figs. 12 and 13. R is not very sensitive to changes in Z_2, as can be seen from (4) inserting typical values though for many applications sensitive enough.

$$\frac{\Delta R}{R} = \frac{2Z_1Z_2}{Z_2^2 - Z_1^2} \cdot \frac{\Delta Z_2}{Z_2} \qquad (4)$$

Measurement of adhesive cure degree on whole bond areas non-destructively instead of by use of DSC where samples have to picked out is of broad interest. Our recent study was motivated by a wish to establish a suitable QA method for the flip chip Compression UnderFill (CUF) electrical interconnection of MEMS components with flex print / PCB. In this interconnection method the contact is established mechanically by the shrinkage of the adhesive when it cures in a flip chip machine. When trying to make the process as fast as possible it is important to assure that the adhesive is fully cured.

SAM can also be used for QA of MEMS sensor underfilling e.g. on wafer level. One problem to control in that process is adhesive filler distribution as illustrated in fig. 14, where the underfill is dispensed at the right flip chip and flows under both of them. At the left chip, filler is unevenly distributed. By analysis of acoustic impedances the amount of filler at different places can be determined [11].

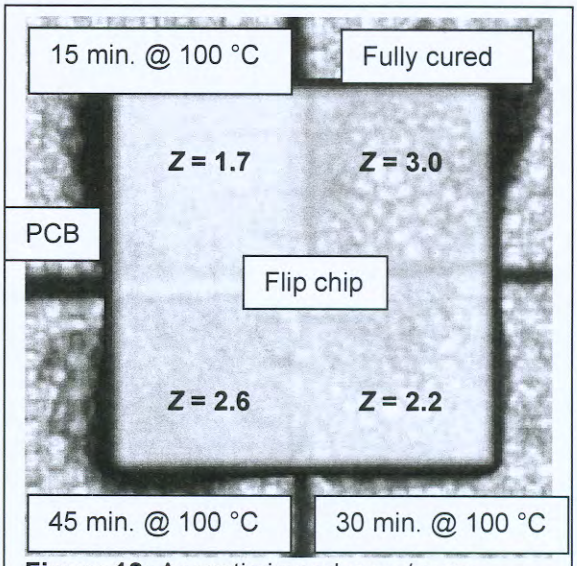

Figure 12: Acoustic impedance / cure degree of EpoTek T7110 adhesive between flip chip (30 µm bump height) and PCB (4 pieces, bottom up) determined from SAM grey values.

6 Conclusion

Generally, established and newly developed SAM QA modes and analysis methods has been listed and exemplified. The trend is toward more application specific standard procedures and development in the analysis methods rather than the equipment.

The feasibility of using SAM as a MEMS sensor QA tool has been exemplified with recent studies and analysis on bonded silicon wafers, a soldered package lid, and adhesive cure degree.

It has been demonstrated that detection of material changes between bonded silicon wafers over distances smaller than 100 nm is possible. The feasibility of using a developed A-scan simulation program to analyse A-scan spectra from MEMS sensor structures containing thin layers has been

illustrated with this sample. Further it has been shown that it is possible to determine the cure degree of a MEMS sensor adhesive with SAM.

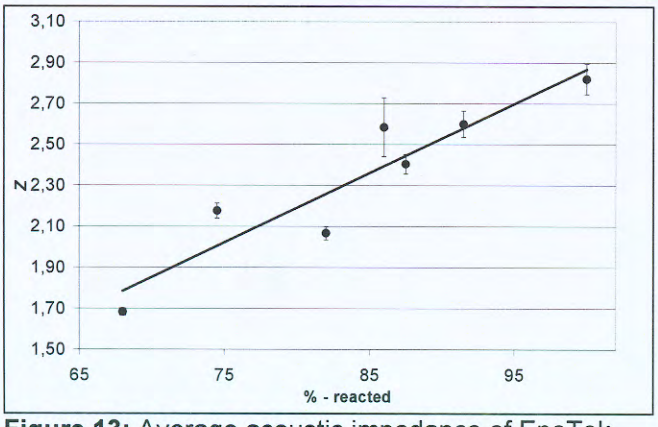

Figure 13: Average acoustic impedance of EpoTek T7110 adhesive as a function of the reaction degree. The reaction degree was determined by kinetic DSC analysis.

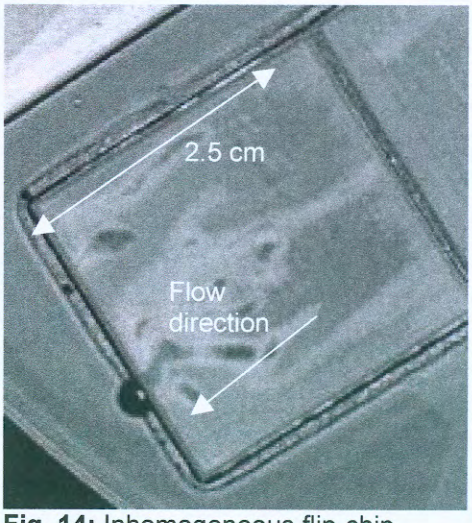

Fig. 14: Inhomogeneous flip-chip underfill flow.

7 Acknowledgement

This work has been performed in the "Packlab" facility of the collaboration on development of microsystems (SUM) project between two Danish institutes DELTA Danish Electronics Light & Acoustics, the Microelectronics Centre (MIC), and four Danish companies Capres A/S, SonionMEMS A/S, Danfoss A/S and Grundfos A/S. The project is financially supported by the Danish Agency for Trade and Industry.

8 References

[1] J. Janting, K. Borggreen, A. Horsewell, F.B. Grumsen, Scanning Acoustic Microscopy Study of the Adherence of Coatings on Gas Turbine Components, Materials Week 2002, October 2002.
[2] Jakob Janting, Dirch Hjorth Petersen, Christoffer Greisen, Simulated SAM A-scans on multilayer MEMS components, Microelectronics Reliability 42 (2002) 1811-1814. [1] B. A. Auld, in Acoustic fields and waves in solids, 2, 37-38, John Wiley & Sons, 1973.
[3] B. A. Auld, in Acoustic fields and waves in solids, 2, 37-38, John Wiley & Sons, 1973.
[4] S. P. Timoshenko and J. N. Goodier, in Theory of Elasticity, 492-493, McGrawHill, 1970
[5] Sridhar Canumalla, Resolution of Broadband Transducers in Acoustic Microscopy of Encapsulated ICs: Transducer selection, IEEE Transactions on Components and Packaging Technology, Vol. 22, No. 4, December 1999, pp 582-592.
[6] Tom Adams, in: Advanced materials and processes, September 2000, p. 38-40.
[7] Andrew Briggs, An introduction to scanning acoustic microscopy, Oxford University Press, Royal Microscopical Society, 1985.
[8] Sridhar Canumalla, Kerry Oren and Pedro Ramirez, Acoustic Microscopy of Tightly Closed Delaminations in Multilayer Ceramic Chip Capacitors, www.acoustech-inc.com.
[9] Janet E. Semmens and Lawrence W. Kessler, Application of Acoustic Frequency Domain Imaging for the Evaluation of Advanced Micro Electronic Packages, Microelectronic Reliability 42 (2002) pp 1735-1740.
[10] J. Janting, D. H. Petersen, and B. V. Schonwandt, Scanning Acoustic Microscopy Study of Flip-Chip Underfill Cure Degree, Materials Week 2002, October 2002.
[11] S. Canumalla and M. G. Oravecz, In situ Elastic Property Characterization of Flip-Chip Underfills, in: International Symposion on Advanced Packaging Materials, 1998, p. 106-110.
[12] www.jedec.org
[13] Aprem Benjamin, Lynn Strauman, and John Goings, Scanning Acoustic Microscopy: Analytical Procedure and Techniques for Metal Ball Grid Array (MBGA) Substrates, www.acoustech-inc.com.

Index

Paper 15

Jakob Janting, Elisabeth Kjærside Storm

Water Uptake of Polymeric MEMS Packaging Materials

Proceedings of MicroSystem Technologies (MST) 2003, p 520-522, ISBN 3-7723-7020-9

Water Uptake of Polymeric MEMS Packaging Materials

M.Sc. Jakob Janting, DELTA Danish Electronics Light and Acoustics, Hoersholm, Denmark
B.Sc. Elisabeth Kjærside Storm, DELTA Danish Electronics Light and Acoustics, Hoersholm, Denmark

1 Introduction

MEMS and microelectronics are very sensitive to water. Ingress of less than 10^{-4} µL water to bond pads in packages is often critical due to galvanic corrosion. Polymeric materials are widely used for MEMS and microelectronics packaging, but they are not water tight.

The general motivation for this work has been to identify optimal polymeric materials and methods for water protective encapsulation of MEMS and microelectronics. Studies have been made on Compression UnderFill (CUF) for flip chip electrical interconnection, fig. 1 and a two-layer combination of materials for glob-top protection of a needle shaped MEMS absolute pressure sensor, fig. 2.

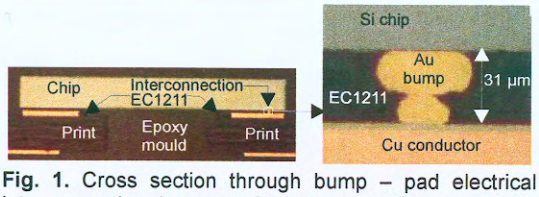

Fig. 1. Cross section through bump – pad electrical interconnection between flip-chipped MEMS pressure sensor chip and print. Here the CUF is EC1211.

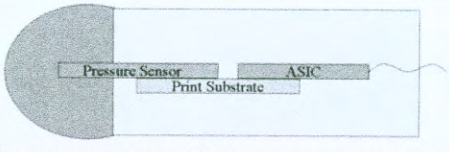

Fig. 2. Sketch of MEMS pressure sensor in stainless steel tube. Sensor chip size is approx. 2 mm x 6 mm. To the left the sensing area is glob top protected.

2 Diffusion theory

Based on Ficks second law of diffusion, the amount of water diffusing into a thin square piece of polymer from both sides can be calculated to be [1]:

$$G = \frac{M_t}{M_E} = 1 - \frac{8}{\pi^2}\sum_{n=0}^{\infty}\frac{\exp\left\{-(2n+1)^2\pi^2\frac{Dt}{L^2}\right\}}{(2n+1)^2} \qquad (1)$$

where M_t and M_E are the masses of in-diffused water at time t and at equilibrium respectively, D is the diffusion constant, and L is the thickness of the polymer piece. From this equation D can be found. The flux F of water into a package can then be determined from $F = DS/d$. = PS, where S is the water solubility, d is the polymer

package thickness, and P is the polymer permeability. D and S both depend on temperature.

3 Results

3.1 Fit function to determine D

To find D a suitable (r^2 = 1,00) fit function G' to G was found:

$$G' = 1 - 0{,}877\exp\left\{-9{,}18\left[\frac{Dt}{L^2}\right]^{0{,}931}\right\} \qquad (2)$$

By fitting this function to the M_t/M_E experimental data D is determined.

3.2 CUF water uptake

Figs. 3 and 4 show measurements on an epoxy CUF. In one pressure sensor application where water is supposed to be in direct contact with the CUF d is less than 1 mm, fig. 1. From fig. 4 it is seen that this distance is far too short considering the critical limit of 10^{-4} μL.

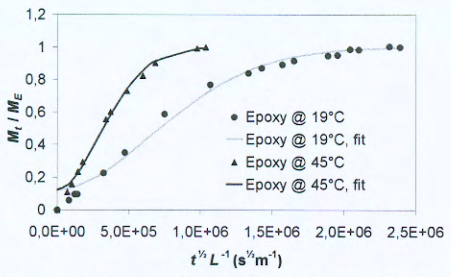

Fig. 3. Sorption curves for epoxy CUF at different temperatures. The sample studied at 19 °C is 1 mm thick. The sample studied at 45 °C is 0,85 mm thick. Fitting (2) to the data gives: D(19 °C) = $7 \cdot 10^{-14}$ m^2/s, D(45 °C) = $5 \cdot 10^{-13}$ m^2/s.

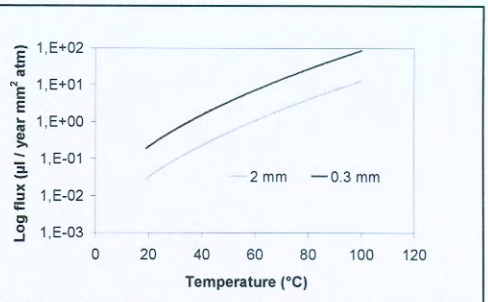

Fig. 4. Flux of water through epoxy CUF of different thickness as function of temperature. Calculations based on fig. 3 data. S is assumed temperature independent i.e. S(19 °C) has been used at all temperatures.

3.3 Water uptake of a polymeric bi-layer for MEMS pressure sensor encapsulation

Fragile MEMS components can be moulded with thermoplastic materials like the soft polyamide based Macromelts which are processed at low temperatures and pressures. But, they are not a suitable choice for water protection due to high P. This problem can be reduced by coating with e.g.10 μm Parylene C which have lower P, fig. 5.

4 Discussion

Due to the pre-exponential in the fit function (2) this M_t/M_E estimate is not accurate at short times. Though, an overall better fit is achieved with this pre-exponential. If the solubility and therefore M_E is known D can instead be calculated from the short times approximation $M_t/M_E = 4(D/\pi)^{1/2}(t^{1/2}/L)$. In the sorption plots we then have $D = \pi h^2/16$, where h is the slope.

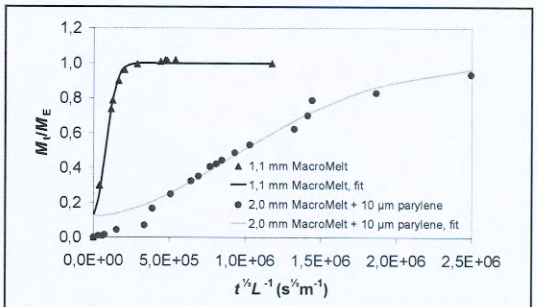

Fig. 5. Sorption curve for a Macromelt material with and without Parylene C coating at 19 °C. Macromelt + Parylene is not yet saturated after 9 months. $D_{Macromelt}(19\ °C) = 5{\cdot}10^{-11}$ m^2/s, $D_{Macromelt+Parylene}(19\ °C) = 5{\cdot}10^{-14}$ m^2/s. Using the 15 first points we have from the linear short times approximation $D_{Macromelt+Parylene}(19\ °C) = 2{\cdot}10^{-14}$ m^2/s.

Note that by water immersion at 45 °C the 0,85 mm thick CUF sample is saturated after approx. 8 days. At 19 °C the 1 mm thick sample is saturated after 2 months. That is to say, already after these times the maximum amount of water, which can be in contact with conductors etc. at any time is achieved throughout the polymer. The worst cases are when a lot more water gets into contact with the electronics due to the saturation transport process or when there is a continuous transport due to e.g. a pressure gradient.

5 Conclusion

Generally, the water flux at different temperatures through polymeric encapsulation materials for MEMS and microelectronics can be measured. Design with e.g. material combinations is important to reduce water attack. For typical flip chip dimensions, the amount of water passing through the studied epoxy CUF in direct water contact by far exceeds the critical 10^{-4} µL within typical required lifetimes. This is also the case for the studied encapsulation materials separately and in combination. However, by combining the materials in a layered structure, improvements can be achieved.

6 Acknowledgement

This work has been part of the collaboration on development of a microsystems project (SUM) between two Danish institutes DELTA, the Microelectronics Centre (MIC), and four Danish companies Capres A/S, SonionMEMS A/S, Danfoss A/S and Grundfos A/S. The project is financially supported by the Danish Agency for Trade and Industry.

7 References

[1] The Mathematics of Diffusion. J. Crank (1975), Oxford University Press, Oxford.

Paper 16

Jakob Janting, Elisabeth K. Storm, and Oliver Geschke

Surface tension driven shaping of adhesive microfluidic channel walls

Proceedings of μTAS, 8th International Conference on Miniaturised Systems for Chemistry and Life Sciences, Malmö, Sweden, 26-30 September, (2004), pp. 378-380

SURFACE TENSION DRIVEN SHAPING OF ADHESIVE MICROFLUIDIC CHANNEL WALLS

Jakob Janting[1], Elisabeth K. Storm[2] and Oliver Geschke[3]

[1]Dept. of microelectronics, DELTA Danish Electronics Light & Acoustics, Venlighedsvej 4, 2970 Hoersholm, Denmark

[2]Oticon A/S, Strandvejen 58, DK-5900 Hellerup, Denmark

[3]Dept. of Micro and Nanotechnology, Technical University of Denmark, Bldg 345 east, DK 2800 Kongens Lyngby, Denmark

Abstract

The feasibility of making microfluidic channels with different wall geometries using adjacent lines of dispensed adhesive between substrates has been studied. Important parameters for the geometry have been identified to be: surface tension (adhesive / substrates), adhesive viscosity / thixotropy, line height and distance, and temperature. Focus of the work has been on predicting the equilibrium geometries with FEM simulations using as input measured adhesive wetting angles, different adhesive line distances and height. The studied substrates are glass microscope slides, PEEK and PMMA. The studied adhesives are DYMAX 9-20318-F, 3070, 9001 version 3.5, and Sylgard 184 PDMS.

Keywords: channels, adhesive wall, shape, simulation, surface tension

1. Introduction

Adhesives are used in packaging of microelectronics, MEMS, and μTAS components for bonding and sealing. In previous μTAS studies e.g. the spread before cure of screen printed UV adhesive for bonding of component parts and sealing of channels have been characterized [1]. Channels with adhesive walls between substrates have also been made by exposure with UV light through a mask [2]. Microfluidic channel flow depends to a large extent on channel geometry. Therefore the motivation for this work has been to study the possibilities of making different channel wall geometries with a new method: Adjacent lines of adhesive between substrates.

2. Theory

The surface tension γ of the adhesive act as a driving force towards an equilibrium situation with minimum free area A because this situation represents minimum adhesive surface free energy $G_{\text{Surface}} = \gamma A$ [3]. Therefore adhesives / coatings on surfaces fill up concave regions, avoid convex, and adapt round shapes [1, 3].

3. Experimental

Adhesive surface tensions have been measured with a CCA-100 tensiometer using the Wilhelmy plate method and a FTA-125 pendant drop equipment. The FTA-125 equipment was also used to measure the wetting angle of sessile drops. The wetting angles were measured on substrates as received and only at one spot and should therefore be considered as rough estimates. The FEM simulations were made with Surface Evolver [4]. To inspect the channel geometries cross sections were made with a Struers Accutom cutting equipment.

4. Results and discussion

In table 1 possible channel wall geometries between different substrates are envisaged by measured wetting angles. Fig. 1 shows channels of different height and wall spacing formed with DYMAX 9-20318-F between glass microscope slides. Fig. 2 is a Surface Evolver FEM simulation example where the used wetting angle (55 °) is that of DYMAX 9-20318-F on PEEK which is also close to that of DYMAX 9-20318-F on glass (51 °). Because of the high viscosity of the material it was

expected that it would be possible to dispense lines with width, height, and pitch of 1 mm, fig 2. This has not yet been achieved. Due to the spreading these lines have so far not been higher than around 150 µm shortly after dispensing and they coalesce already during dispensing. This effect is expected to be even more pronounced for the other adhesives with much lower wetting angles and viscosities. Current studies will show how a high degree of spreading with the risk of line coalesce before assembly can be avoided with a) very low surface tension substrates compared to the adhesive, b) adhesives with even higher higher thixotropic index or viscosity. Presumably the trumpet shapes of the channels, fig 2, can be compensated by placing larger adhesive volumes at the line ends because then the adhesive will need more time for the redistribution into that shape. Confirmation of these predictions is part of ongoing and future work.

Material	Surface tension γ (mN/m)	Wetting angle on glass θ_{Glass} (degrees)	Wetting angle on PMMA θ_{PMMA} (degrees)	Wetting angle on PEEK θ_{PEEK} (degrees)	Viscosity (datasheet) (mPas)	Application comments
DYMAX 9-20318-F	44 (WP) 42 (PD)	51 (SD)	60 (SD)	55 (SD)	50000	Masking
DYMAX 3070	24 (PD)	30 (SD)	14 (SD)	22 (SD)	8500	Plastic adhesive
DYMAX 9001 version 3.5	18 (PD)	39 (SD)	28 (SD)	39 (SD)	20000	Damming adhesive
PDMS Sylgard 184	19 (WP) 18 (PD)	18 (SD)	13 (SD)	25 (SD)	4000	Encapsulant / bonding material

Table 1: Surface tension and wetting angles. Used methods: WP = Wilhelmy plate, SD = Sessile drop, PD = Pendant drop. From the wetting angles of DYMAX 9-20318-F and 3070 Zisman plots yield the following critical surface tensions: γ_{glass} = 13 mN/m, γ_{PMMA} = 23 mN/m, γ_{PEEK} = 20 mN/m.

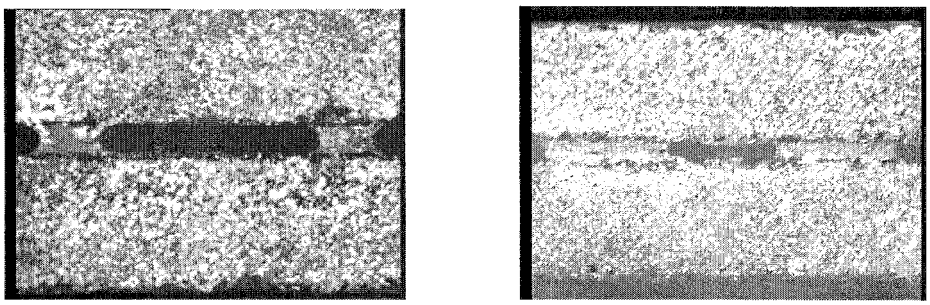

Fig. 1: Cross sections of channels between glass microscope slides and DYMAX 9-20318-F adhesive lines. The channels are in the centre of the pictures. Left: Channel height 150 µm. Right: Channel height 100 µm. Line pitch is 2 mm in both cases. Note the approx. 51 ° wetting angle.

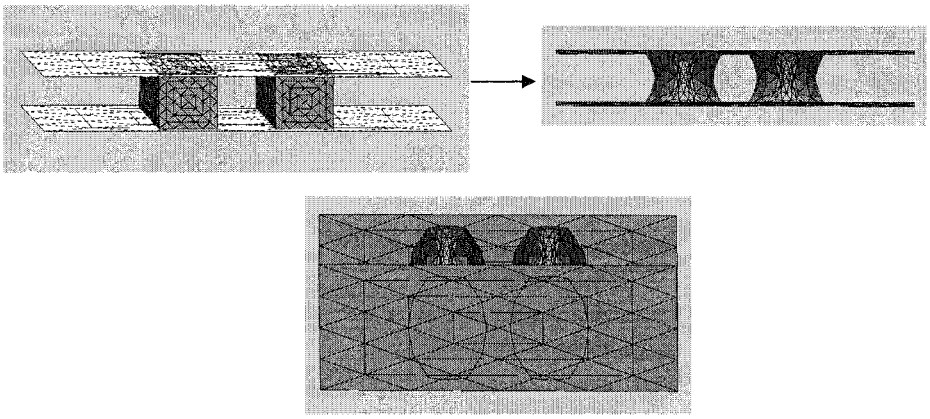

Fig. 2: Simulation of channel formed between two lines of DYMAX 9-20318-F where top and bottom substrate is PEEK. Top: Development from square lines. Here the line height, width and distance are equal. Bottom: Illustration of the double trumpet channel shape.

5. Conclusions

At this stage we can conclude: 1) Among other geometries it is possible to achieve nearly round channels, 2) Due to fast spreading channels are difficult to make from close proximity adhesive lines especially with low viscosity but also low wetting angle adhesives, 3) Due to surface free energy minimization channels will tend to have an inner double trumpet shape.

Acknowledgements

This work has been part of projects financially supported by the Danish Ministry of Science Technology and Innovation.

References

[1] J. Han, S. Lee, A. Puntambekar, S. Murugesan, J-W. Choi, G. Beaucage, C. H. Ahn, *Proceedings of MicroTAS 2003*, pp. 1113-1116.

[2] C. Harrison, J. T. Cabral, C. M. Stafford, A. Karim, and E. J. Amis, *J. micromech. Microeng.*, **14**, pp. 153-158 (2004).

[3] Jakob Janting, Jens Branebjerg, Pirmin Rombach, *Sensors and Actuators* A 92 (2001) 229-234.

[4] http://www.susqu.edu/facstaff/b/brakke/evolver/

Paper 17

Peter Friis, Elisabeth K. Storm, Karsten Hoppe, and Jakob Janting

Adhesive Bonding Methods for Polymer microTAS Components

Proceedings of μTAS, 8th International Conference on Miniaturised Systems for Chemistry and Life Sciences, Malmö, Sweden, 26-30 September, (2004), pp. 354-356

ADHESIVE BONDING METHODS FOR POLYMER microTAS COMPONENTS

Peter Friis[1], Elisabeth K. Storm[2], Karsten Hoppe[1] and Jakob Janting[1]
[1]DELTA Danish Electronics, Light & Acoustics, Venlighedsvej 4, DK-2970 Hørsholm, Denmark
microsystems@delta.dk, http://www.delta.dk
[2]Oticon A/S, Strandvejen 58, DK-5900 Hellerup, Denmark

Abstract

For bonding micro-Total-Analysis-Systems made of polymeric materials, many different approaches exist, each with their advantages and disadvantages. Here, we concentrate on adhesive bonding and propose various methods of applying the adhesive to both structured and unstructured system parts.

Keywords: polymer, microfluidic, bonding, adhesive

1. Introduction

With respect to bonding of micro-TAS structures made of polymeric materials some relevant processes might rely on one of the following methods: thermal bonding, chemical assisted bonding, laser or ultrasonic welding or adhesive bonding. Thermal bonding is simple but requires high temperature processing, chemical bonding tend to clog the channels when working in the micro scale, laser and ultrasonic welding are limited in number of useful material combinations. Adhesive bonding is a rapid and versatile prototyping method which can be employed in various ways [1,2]. Here we focus on different approaches for selectively dispensing the adhesives when joining two polymeric structures.

Ideally, the adhesive should result in a strong, chemical resistant, void-free bond. This can to some extend easily be controlled through a careful selection of the right type of adhesive, however, the real challenge when bonding microfluidic structures is to control the flow and volume of the adhesive. If incorrectly applied, e.g. too close to the channel as in Figure 1A, the adhesive will flow into the channel when the lid is applied. Another scenario, which should be avoided, is where an insufficient amount of adhesive is applied or it is too far from the channel edge, which result in the adhesive flow (during assembly) is stopped before reaching the channel. Consequently, small voids are created alongside the channel, which could cause cross-contamination if reusing the system, see Figure 1B.

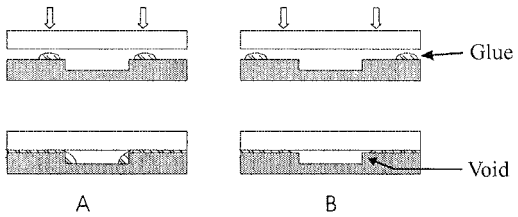

Figure 1. When applying adhesive next to a channel it might end up (A) too close to the edge and flow into the channel or (B) too far form the edge and form voids.

One possible way of categorizing the different adhesive bonding method is presented in Figure 2. The 'Standard' methods include no special structures for controlling the adhesive flow, i.e. have planar surfaces, whereas in each of the 'Advanced' methods some additional structuring is made.

Regarding the 'standard' methods we propose two different approaches. First approach, and the most obvious, is to try and dispense a pattern of adhesive on the substrate next to the channel. The second method uses an underfilling process known from flip-chip bonding. In the present experiment the technique has been adopted with dispensing the adhesive along one side of the component. To avoid adhesive in the channel an UV-curing adhesive is used, which is cured with UV-light as it arrives at the channel edge.

In order to investigate the possibilities for fabricating 'advanced' structures, which could facilitate a less troublesome assembly, we developed four concepts, see Figure 2. In the first method spacers are used to keep the lid a small distance from the channel so room for the adhesive flow is created. In the second method a cavity is made alongside the channel where the adhesive is dispensed before placing the lid. The 'locking' method is similar to the 'cavity' but locking structures are made in the lid to facilitate alignment during assembly. The last principle relies on forming bumps along the channel, which will be dipped in adhesive prior to applying the lid.

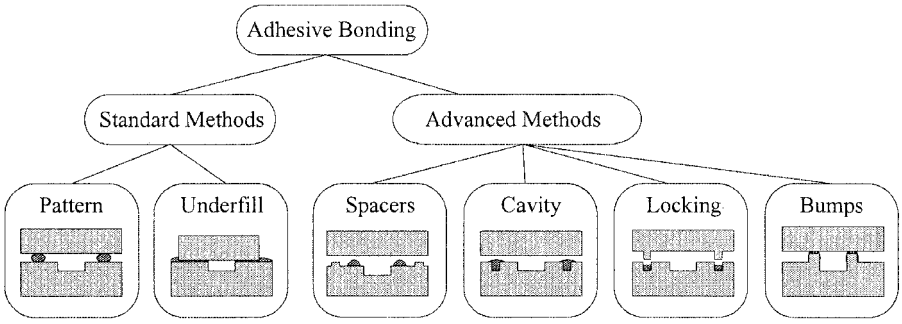

Figure 2. One way of categorizing adhesive bonding methods.

2. Experimental

Although the 'standard' methods, mentioned above, seem attractive because of their simplicity, it proved very difficult to control the flow of adhesive. It is extremely critical to control the position and volume of the dispensed adhesive, especially when going around corners or ends. Additionally, the surface quality is crucial to ensure a consistent and reproducible flow of adhesives. Moreover, we found that the sharpness of the channel edge play in important role in a successful assembly. Figure 3 shows an unsuccessful dispensing of an adhesive (Dymax 3070) using the 'pattern' method. The flow is, to some extend, stopped at the channel edge but due to uneven adhesive dispensing a part of the channel is not sealed correctly and a void is created.

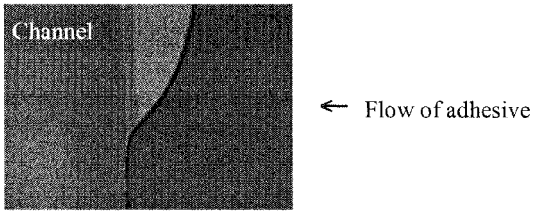

Figure 3. Top view of right side of a channel where the adhesive was not successfully applied.

To have a less critical process where possible dispensing variations will have reduced influence on the bond quality, structured parts might be used. To characterize the 'spacers' method two lines of UV-curing adhesive (Dymax 3070) were dispensed and cured on both sides of a channel 'far' from the edge. In the next step, two lines of sealing adhesive were dispensed close to the edge. These second lines were slightly higher than the spacer-lines (controlled by reducing the dispensing needle velocity), thus, a minor flow of adhesive occurred when the lid was applied. However, due to the presence of the spacers, the adhesive flow was not as pronounced as without the spacers i.e. in the 'pattern' method. It was also observed that minor dispensing irregularities were more easily compensated for as the adhesive had more space to redistribute.

Figure 4 shows a cross-sectional view of a channel formed between a substrate with a channel and a covering lid, with the sealing and spacer adhesive lines marked. It is worth noticing that the right side meniscus of the sealing line has a larger contact angle than the left side. This is expected as the surface tension at the channel edge is larger than the surface tension in between the substrate and lid. This also explains the reasoning behind the expected increased willingness for the adhesive to redistribution without filling the channel.

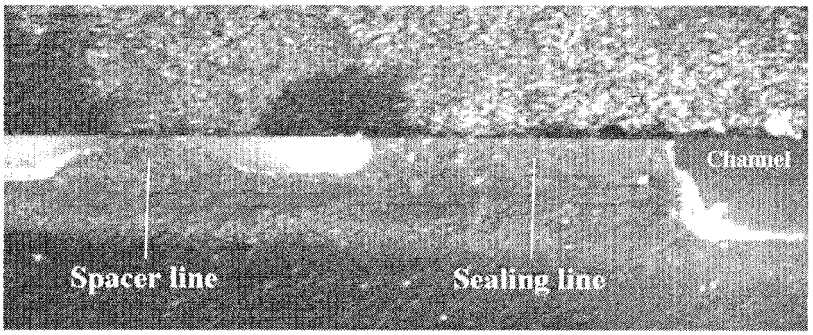

Figure 4. The channel is sealed by first applying and curing the spacer line, then applying the sealing line and finally placing the lid and curing the sealing line. Note that the shape of the spacer line is as dispensed whereas the sealing line has clearly flown.

3. Conclusion and prospects

Preliminary results indicate that assembly processes that rely on the spreading of dispensed adhesive next to a microfluidic channel are difficult to control on unstructured parts. By introducing some sort of spacers to lift the cover glass from the substrate, a better control of the adhesive flow is obtained and the probability of adhesive flowing into the channel is reduced.

Future work includes characterization of the rest of the proposed micromechanical structures for controlling the flow and volume of the dispensed adhesive during bonding as well as determining the bonding strength for each of the methods.

References

[1] C. Harrison, J. T. Cabral, C. M. Stafford, A. Karim, and E. J. Amis, *J. micromech. Microeng.*, **14**, pp. 153-158 (2004).

[2] J. Han, S. Lee, A. Puntambekar, S. Murugesan, J.-W. Choi, G. Beaucage, and C. H. Ahn, *Proc. μTAS '03, Squaw Valley, CA, USA, Oct. 5*-9, pp. 1113-1116 (2003).

Paper 18

J. Janting

Sensor packaging for harsh environments

Encyclopedia of Sensors, Vol. 9, pp. 271-288, Edited by C. A. Grimes, E. C. Dickey, and M. V. Pishko, American Scientific Publishers, 2006, ISBN: 1-58883-065-9

EOS Encyclopedia of SENSORS
www.aspbs.com/eos

Sensor Packaging for Harsh Environments

J. Janting
DELTA Danish Electronics, Light and Acoustics, Venlighedsvej, Hoersholm, Denmark

CONTENTS

1. OVERVIEW

The problem of bringing microsystem sensors to the market originates from one important fundamental difference between microelectronics packaging and microsystem sensor packaging which is that in the latter case often very aggressive surroundings has to have access to a sensing part of the naked chip or almost naked chip through a sensor window (Fig. 1). This implies application specific packaging and test solutions [1–5] which are why microsystem sensor packaging of today and the future is a challenging field. Also due to the often mandatory access hole microsystem failure analysis is considered an area quite different from that of microelectronics. A comprehensive overview of microsystem packaging has been given in [4]. A general overview of microsystem sensor/actuator packaging is given in [5]. Here focus is on the packaging of the sensor chip for harsh environments. About 30 years ago when the first silicon micromechanical sensor and actuator structures were developed the packaging was not really given any attention by the scientific community. However, during the last 10 years this has changed dramatically. With the appearance of continued miniaturization to NEMS sensors scales are reduced from 1–100 μm to 1–100 nm making packaging issues even more critical. The delay of scientific attention seems not to be repeated for this next generation of sensors where packaging is already having a scientific reputation [6–11]. In the years to come some of the most important packaging activities will be in the areas of Wafer Level Packaging (WLP), System In Package (SIP), lead free electrical interconnect, optical interconnection, and nano-packaging [12–14].

The encapsulation part of the microsystem sensor packaging makes up most of the sensor volume and much of the price. Minimization of the encapsulation volume to keep sensors small requires new materials and processes to achieve sufficient protection [1, 2]. Since the size reduction means that the surface to volume ratio is increased, surface physical/chemical properties, e.g., surface tension become much more dominant than bulk properties. This is for instance seen for fluid in small channels [15, 16] and in unwanted adherence between silicon micromechanical parts (stiction) [17]. It is also used for alignment and self-assembly of microstructures [18].

In some cases the encapsulation accounts for 70% of the total cost of the microsystem sensor [5]. Furthermore, wafer level testing requires specialized equipment [3].

In many cases bulky and expensive microsensor protective packages have been reduced to thin films and coatings some of which can be applied at silicon wafer level. One example is pressure sensors where steel membranes and oils for pressure transmission have been substituted with coatings [19, 20]. Another example could be a high performance silicon micromechanical microphone for, e.g., cell phones or hearing aids [21, 22]. This microphone is placed in the ear where the environment is hot and moist. The microphone has to receive sound as physical stimuli requiring access through a hole in the packaging while at the same time being robust or insensitive toward other physical or chemical stimuli like ElectroMagnetic Interference (EMI) and sweat respectively. To meet these demands special coatings and thin films have been used to protect the device.

2. PACKAGING TECHNOLOGIES

Microsystem sensors are miniaturized systems for analysis involving many different disciplines as: Mechanics, fluidics, biology, chemistry, microelectronics, optics, etc. Microsystem sensor packaging comprises (see Fig. 1): (1) Die attach, (2) Interconnection between the micromechanical chip and microelectronics, photonics, RF/wireless, (3) In/out interconnection between the system and the outside world,

ISBN: 1-58883-056-X/$50.00

Encyclopedia of Sensors
Edited by C. A. Grimes, E. C. Dickey, and M. V. Pishko
Volume X: Pages (1–18)

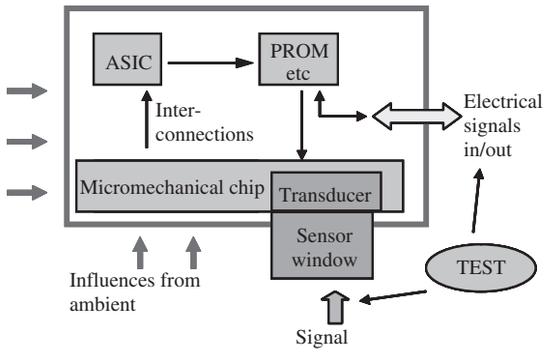

Figure 1. Typical packaged microsystem sensor.

(4) Sensing interconnection (sensor window), (5) Protective encapsulation. These elements are dealt with in this chapter.

In microsystem sensor manufacturing, the packaging is given more and more attention since it represents a large part of the price and volume. The sensor die is often based on a silicon micromechanical transducer. However, during the last decade a lot of work has also been put into microsensors which are not based on the traditional silicon MicroElectroMechanical Systems (MEMS). They are for instance made of polymers or ceramics [23–33]. Some of the technologies and materials involved in microsystem sensor and microelectronics packaging are the same, however, microsystem sensor packaging is severely complicated because it is often directly exposed to the surroundings, which are avoided in microelectronics. The consequence is very high demands on the materials and methods used. Especially the protective encapsulation/housing of the component has to be carefully selected keeping in mind that the whole system should be kept small. Very harsh environments are found in, e.g., the high market potential automotive and oil/gas industries [34–42]. During a Europractice Workshop on "Packaging Issues and Requirements," September 2000, a survey among the participants was conducted. This survey confirmed that up to 60% or more of the production cost is used on the packaging of microsystems. The survey interestingly showed that the participants found that application specific solutions are nearly always needed. Another conclusion was that the development phase of the product is either in-house or subcontracted to a manufacturer. It is very seldom in collaboration with consultants, institutes, etc. In connection with this, it was said that the search for packaging sources is very difficult and therefore the use is limited. This work has been conducted by the Nordic Microsystems Manufacturing Cluster (NORMIC) consortium.

It should be clear that many aspects of microelectronics packaging can be directly transferred to microsystem sensor packaging, although the sensors have some special requirements to fulfil, e.g., sensor die access holes [see Section 31.3(a)]. Examples of the latter are given in Chapter 4. Many sensor packaging solutions e.g., adhesive die attach, wirebond interconnection to standard packages originate from microeletronics.

High microelectronics reliability in harsh environment is important for microssystem sensors even when the sensors themselves are non-standard packaged since microelectronics packaging of a more standard kind will most often have to be close to the sensor. Chapter 2 therefore mainly deals with a description of microelectronics packaging technologies of relevance for microsystem sensor packaging. Due to the variety of existing and coming microsystem sensors it is not possible to specify a generic package. However, it is attempted to ease production of microsystems by modularization [43–45]. Focus is therefore not on giving a full description of the many existing packages but to give an overview of key packaging components of today and the future which when brought together results in the many complete and existing microsensor packaging solutions and more to come.

2.1. Definitions

The purpose of this section is to provide a common understanding of the term packaging with special attention to microsystem sensors. Microsystem, MEMS, and micro machines are the European, American and Japanese terms for the same small sensors and actuators which are typically based on silicon micromechanical structures. Here as in [4] "microsystem" is defined to include microelectronics, photonics, RF/wireless and MEMS. Using this definition the microsystem sensor is not necessarily the MEMS. The focus here is MEMS sensor packaging for harsh environment application.

The word "packaging" covers mounting/assembly of the different parts in a system including electrical, physical, optical, RF/wireless connections and encapsulation. In that way packaging constitutes all the interfacing between the microsystem components (active, passive) and the surroundings: Die attach, mechanical support (substrate, carrier, encapsulation), interconnection, and protective package (encapsulation) including access to the environment.

Microelectronics packaging is traditionally divided into a 4-level hierarchy which also applies for microsystem packaging [4]:

0 Level: Wafer Level Packaging Wafer Level Packaging (WLP) is packaging before the wafer containing several chips is diced out into single chips. This packaging provides interconnection (plated conductors and/or solder balls) and protection (inorganic, organic, metallic film, encapsulation or sealing) of chip/interconnections.

1st Level: Micromechanical Chip and/or Integrated Circuit Level Packaging at this level is based either on single or Multi Chip Modules (MCM). The micromehanical chip and/or Integrated Circuit (IC)/Application Specific Integrated Circuit (ASIC) etc. is bonded (e.g., anodic, glued, soldered) to a supporting and interconnecting carrier/substrate/housing which is typically a leadframe, ceramic substrate, silicon substrate, Printed Circuit Board (PCB) or flex print of some sort. The interconnection between components is established by wirebonding, flip-chip soldering/gluing, or conductive adhesive electrical contact to conductors on the carrier. The techniques are also used in 3D packaging by interconnecting stacked chips which saves space [46–49]. For lateral interconnection by the flip-chip method a carrier with interconnecting conductors is needed. Then the component is protected with an encapsulation. The substrate with interconnecting conductors between the

components or to the outside world may be part of the encapsulation/housing or vice versa. This is e.g., seen in 3D Mould Interconnect Devices (3D MID) [50]. Encapsulations in direct contact with the components are typically low thermal stress glass/quartz filled epoxies. They are applied by techniques as glob topping and injection moulding and combinations thereof. Housings where the components are inside a cavity are typically pre-moulded on a leadframe and made of e.g., ceramic, epoxy, Liquid Crystal Polymer (LCP). Lids are then attached by e.g., gluing, soldering, etc.

2nd Level: System Level or Board Level 1st level packaging on a MCM including both a micromechanical chip, an ASIC and perhaps more components may result in a complete microsystem or MEMS. However, often more signal processing is required which is certainly the case if the 1st level packaging only comprises the micromechanical chip (single chip module). Then we do only have a MEM component and still not a MEMS. The packaging on this level consists of mounting the 1st level package onto some board (typically FR4 PCB or card) to interconnect active and passive components.

3rd Level: Board to Board Interconnection High capacity, multi-functionality and/or flexibility needs may require the possibility to interconnect boards like in PCs where several slots for insertion of different cards exist. This is the 3rd level packaging.

2.2. Die Attach and Sealing

Each step in microsystem packaging has a certain direct purpose and influences on the whole system. The first step in microsensor packaging is to attach the chips (Si with a SiO_2 or SiN surface) diced from a wafer to some sort of support (ceramic, plastic, metal, etc.) which also carries the electrical leads to the next level of packaging. Since this is a large area process performed directly on the chip surface, influences on performance can be very large and sometimes detrimental. Most often the chip is glued, soldered, or directly bonded [51, 52]. Except for the adhesion the major concerns are about secondary influences on the chip like stress, thermal management, and barrier properties.

As with the other parameters good adhesion depends on the choice of bonding material/method and the surfaces. Adhesive materials used for die attach are typically epoxies, cyanate ester, urethanes, silicones, and glass frit [4, 53]. To enhance the adhesion with these materials different physical/chemical roughening cleaning, activation and priming methods are used [54–58]. For adhesives adhesion enhancement is often important because the choice of adhesive material has to comply with secondary influences on the die. For instance epoxies usually have a very good adhesion to most materials but introduce high stresses because of high modulus E and Coefficient of Thermal Expansion (CTE). Then a soft silicone might be a better choice although it does not adhere as well. In this way the whole system and all the materials properties have always to be taken into account. O_2 plasma treatment is often used to physically/chemically roughen, clean and activate microsystem surfaces before bonding with adhesives. Especially polymers which are very hydrophobic can have their surface tension much increased with this treatment which in turn often results in better adhesion. Cleaning with solvents and priming with thin layers, e.g., silanes, metals, etc., which adhere well to both the microsystem surface and the adhesive, are also used. Using solders most often requires deposition of thin metallic (Cr, Ti, Ni, Au, AuSi) adhesion and diffusion barrier layers. Often fluxless eutectic $Au_{20}Sn_{80}$ is the solder used; however, Sn-Pb is also used. Due to environmental demands lead free solders like $SnAg_{3.9}Cu_{0.6}$ are being developed [59–63]. Cleaning can be performed with the same methods as for adhesives, and adhesion is normally very good.

Stress usually originates from CTE mismatch between materials bonded and the bond material. The quite high CTE for adhesives is accommodated to the surrounding materials by adding ceramic and metallic fillers. For precise positioning of the sensors it is very important that these fillers are very regularly shaped and have a very narrow micron size diameter distribution. Careful handling may also be necessary to avoid fillers with sharp corners scratching through thin protective layers on the die. At the glass transition temperature T_g adhesives change their CTE with a factor up to 4 [4]. They must therefore be carefully selected so that T_g is outside the application temperature range. Very stress sensitive sensor dies are not mounted with solders. To isolate extremely stress sensitive sensors (e.g., some pressure sensors) from mounting stresses some sensors are bonded to glass with a CTE close to that of Si before dicing i.e., as a WLP step. To maintain good electrical contact in flip-chip interconnection the chip is adhesive underfilled to distribute stresses so that they are not only located at the contacts. This also has the secondary effect of holding i.e., bonding the chip to the substrate. Thirdly the underfill adhesive protects (encapsulates) the interconnection sites. Underfill adhesives are typically highly ceramic filled (up to approx. 90 wt%) and the CTE is matched to the solder ball interconnects.

Sensors do not produce heat which has to be dissipated; however, this might be the case for the adjacent microelectronics which might influence overall microsystem performance. In that case solders are preferably used for the microelectronics die attachment. If adhesives are used they are filled with metal (e.g., Ag) or ceramic (e.g., Al_2O_3) to conduct heat. An important advantage of flip-chip attachment is that heat can be dissipated easily from the upward face of the chip.

In some instances the attachment also functions as barrier toward harsh environment. Flip-chipping is one example where the underfill protects the interconnections. Then the chemical/physical durability of attachment materials is very important. This means that the material should be as stable as possible toward corrosion and diffusion of chemicals and ions. Unlike polymeric adhesives solders are very tight. On the other hand they often corrode faster.

2.3. Signal Interconnection

The signal interconnections in a microsystem can be electrical or non-electrical (optical, RF/wireless. Ways of creating and carrying the signals, e.g., optically is by use of components as Vertical Cavity Surface Emitting Lasers (VCSELs) and optical waveguides as fibers and planar Arrayed Wave Guides (AWG) respectively. Packaging of optical sensors

and interconnects requires high positioning precision and clean hermetic environment [64–70]. Here only the electrical interconnections will be discussed in detail.

2.3.1. Electrical Interconnections

There is a wide variety of electrical connections within a microsystem. They can roughly be divided into internal and external connections, where the internal connections can vary from the connections between the different parts toward connection to a leadframe or the like.

For the internal electrical connections, wirebonding with Au or Al wire is often used. Another option is flip-chip which can be used for chip stacking. Chip stacking can also be accomplished using a combination of wirebonding and flip-chip interconnection. In some cases microsystem sensors are not planar on the surface and thus traditional flip-chip assembly is impossible. In these cases more creative ways of assembly/electrically connecting the parts must be used. Conductive adhesives are also getting more and more widespread in the electronic industry. An interconnection technology which is less used for interconnection of sensors is Tape Automated Bonding (TAB).

The external electrical connections should provide the user of the microsystem with a reasonable way of being connected to the microsystem sensor. In many "standard" microsystem sensor packages leaded or lead-less types of packages are used. With more custom-designed systems wires or some kind of substrate are extended from the inside of the package and thus provides the connection. Here it is not always possible to distinguish between internal and external electrical connections.

a. Wirebonding Wirebonding with both Au and Al wires has been used by the semiconductor industry for many years, where the technique has proven to be very reliable. There are two different bonding techniques used: wedge-wedge and ball-wedge.

Wedge-wedge bonding can be performed using both Au and Al wires. During the bonding process, heat and ultrasound combined with force are forming the metallurgic bond between the wire and the bond pad on the chip and substrate.

The ball-wedge bonding process can only be performed using Au wire. Again, it is the combination of heat, ultrasound and force that is forming the metallurgic bond between the wire and the bond pads. For both bonding processes the metallization on the chip is typically Al, however, Au can also be used. On the substrates the metallization is most often Au. Au is generally preferred for harsh environment applications.

b. Flip-Chip Flip-chip mounting is one of the more advanced interconnection techniques used in the semiconductor industry and it is becoming more and more popular mostly because of size and thereby cost reduction. Electrical performance is also better because of the short interconnect distance. Flip-chip can be performed in a number of different ways but in general the idea is to flip the chip upside down so that the interconnection is under the chip [71]. Connection is then made using either solder or Au studs usually placed in an area array under the chip. Flip-chipping can be regarded a combined electrical interconnection and die attachment. However, as already mentioned the interconnect/attachment is too weak to sustain CTE mismatch stresses, and chip underfill with CTE matched with the solder balls or Au studs are used to stress stabilize the interconnection/attachment [4, 72]. In the solder technique solder is deposited by, e.g., electroplating onto the chip pads. Then the chip is flipped and soldered to the contact pads on the substrate. In the stud or Stud Ball Bumping (SBB) technique [73–77] the process usually is: Placement of Au wirebond balls or studs on the chip interconnect pads, coining against a flat substrate to ensure same height of the studs, dipping of studs in conductive adhesive, placement on substrate pads, curing of conductive adhesive, underfilling of chip with epoxy, curing of underfill. The advantage of the SBB technique is that no special pad metallization layers like diffusion barriers are needed. Mechanical establishment of contact between Au studs and substrate pads by compression because of underfill shrinkage has also been studied [2].

c. Conductive Adhesives A comprehensive overview of conductive adhesives has been given in [78]. Conductive adhesives are typically highly filled epoxies or tapes. Depending on the amount of filler they are either Isotropic Conductive Adhesives (ICA) or Anisotropic Conductive Adhesives (ACA). The filler is Ag, Ni, Cu, or metal (e.g., Au) coated polymer or glass particles with 3 μm–10 μm diameter [79, 80]. Contact resistance is in the mΩ range. Conductive adhesives are very interesting for microsystems for several reasons. Much of the research in the area of conductive adhesives is motivated by their potential as a substitute for solders containing Pb which has become a burden on the environment. According to, e.g., the European Union (EU) Pb containing solders will not be allowed in electronic equipment from July 2006 [61, 62]. Further, conductive adhesives offer combined electrical interconnection and attach, High Density Interconnection (HDI), low temperature processing, good heat conduction, and limited space and alignment requirements [79, 81].

Besides electrical interconnection ICA's are used as high thermal conductivity, low CTE, die attach materials. ACA's are used, e.g., for the electrical interconnection of Liquid Crystal Displays (LCD's) and flip-chips without the need for underfill [81, 82]. One important drawback of conductive adhesives is that generally they are not as environmentally stable as, e.g., protected wirebond and solder electrical interconnections. Therefore they are less used in sensor packaging for harsh environments.

d. Tape Automated Bonding TAB is less used for microsystem sensor packaging applications. In TAB chips are mounted and interconnected on Cu, Al, steel, or Alloy 42 metallized flexible polymer (polyimide (PI), epoxy-glass, polyester, and Bismaleimide Triazine (BT) resins) tapes before the attachment in a package or on Printed Wiring Board (PWB). The polymer can consist of up to three layers with thickness ranging between 35 μm and 125 μm. The interconnect lines are fabricated by etching the metallization. Free beams of the Cu lines are soldered to both chip and substrate by thermocompression locally on the joints. There is one advantage of TAB compared to wirebonding

and that is that TAB has a lower profile, and one disadvantage when compared to flip-chip is that the interconnection is peripheral.

2.4. Package Components

The package serves as protection of the rest of the system toward the often aggressive environment. Package components can vary in size from a standard ceramic or plastic package with a leadframe, to a thin layer of metal, polymer or a specially designed metal or plastic house. In some microsystem sensors the packaging is more or less integrated in the system [cf. Chip Scale Packaging, (CSP) and System In Package (SIP)]. Examples are special metal layers in order to provide protection where the media can be allowed almost directly onto the surface of the system.

The package is what surrounds the chip and interconnection, except usually for the die attach/underfill. Packages or parts thereof are called encapsulations when in direct contact with the chip, and housings when the chip is contained in a cavity i.e., the package is not in direct contact with the chip.

2.4.1. Transfer Moulding

Transfer moulding is the most common encapsulation technique in the IC packaging industry. Often the material comes in direct contact with the chip, which means that this type of package can be called an encapsulation. In transfer moulding the molten resin, typically silica-filled epoxy, is transferred by pressure from a melting-pot into a mould which is at a temperature above the melting point of the resin. In injection moulding, the mould temperature is below the resin melting point. In injection moulding the temperature and pressure are e.g., 300 °C and 60 bar respectively. Gentler prototype microsystem sensor encapsulations can be made with thermoplastic materials like the polyamide based Macromelts [2] at temperatures around 150 °C and pressures around 5 bar.

An IC or microsystem interconnected (wirebonding) to a leadframe is placed in the mould and the material is transferred. This kind of encapsulation is typically a Dual Inline Package (DIP) with leads on two sides or Quad Flat Package (QFP) with leads on all four sides. The higher temperature in transfer moulding is important for the filling of moulds with high flow length, wall thickness, and to allow for shrinkage compensation. Furthermore, it is very important to avoid bond wire sweeping.

Moulding of other substrates than metallic leadframes (Kovar, Alloy 42) with an IC and/or a sensor is also possible. Printed Wiring Boards (PWB) made of ceramic and plastic can also be moulded with plastic.

2.4.2. Premould

Premould packages are typically made of ceramics, plastics and metals [83]. Ceramics are used for high reliability and high frequency products. The high reliability is due to their hermeticity. In ceramic packages (e.g., CERamic Dual in Line Package, CERDIP and Ceramic Quad Flat Package, Cerquad) the chip or microsystem is mounted in a cavity in a premoulded ceramic base with some connections e.g., a leadframe for in/out signals. On top of the base a ceramic lid is typically mounted with different hermetic glass sealings. The lid can also be made of metal, for instance Kovar and soldered with e.g., $Au_{20}Sn_{80}$. In that case the rim and the ceramic base and lid are first plated with metals. Note that the ceramic material is not in direct contact with the chip or microsystem like in traditional IC epoxy encapsulation. Consequently, these types of packages are often termed "housings." Metal packages are used for microwave multichip modules and hybrid circuits because of their good thermal conduction and electromagnetic shielding. They are typically made of $Cu_{10}W$, $Cu_{15}W$, Silvar™ (Ni-Fe alloy), $Cu_{15}Mo$, Kovar and Alloy 42. Hermetic sealing between base and lid is achieved either by soldering with $Au_{20}Sn_{80}$ or by welding. Hermetic and insulated electrical feedthroughs are achieved with glass or ceramics. Just like the ceramic and metallic packages also plastic houses are made with many different configurations. New high performance (low moisture penetration, low stress and chemical inertness) plastic materials are for instance LCP [50, 84–86]. Packages of all the above mentioned materials can also just consist of moulded sheets or foils with plated or screen printed conductors.

2.4.3. Glob-Top and Coatings

To protect wirebond and TAB interconnection against corrosion and/or wire sweep during moulding typically epoxies filled with fused silica or quartz is dispensed to cover these areas. In less aggressive environments thin conformal coatings are also used. These are for instance vacuum deposited like Parylene C (poly-para-xylylene) [1, 2, 87] applied by Chemical Vapor Deposition (CVD) and perfluorinated polymers like Teflon AF1600 [1] applied by dip or spray methods. Since all polymers are easily penetrated by moisture it is more important (like for many other packaging materials) that these materials have a low solubility of water and other chemicals, that they are chemically resistant and that they do not take up much volume.

2.4.4. Stacked Interconnection Layers

Newer (around 1990) more compact ways of interconnecting chips as compared to e.g., DIP and QFP are by connecting them to different multilayer interconnection structures [4, 66, 88–91]. The layers alternate between conductive layers and insulating layers. These packages are more compact than DIP and QFP because the wirebonding to a leadframe is eliminated and because the conducting layers are interconnected vertically inside (flip-chip) or nearly inside (wirebonding) the chip footprint. The substrates are used in two ways: One way is on single chips, the other on multiple chips.

When used on single chips this is just a more compact way of getting the same chips interconnected with the next level of packaging i.e., the chips are connected through the layered structure to the bottom side. The chip is not interconnected directly to the next level of packaging, usually a PWB, because of too fine pad pitch on the chip (typically 100 μm on the chip and 200 μm on the PWB). In that way the layered structure acts as a necessary space transforming interposer. The interconnect points on the bottom are solder balls arranged in an array. This package is called a

Ball Grid Array (BGA). They are further subdivided according to different substrates as: plastic (PBGA), tape (TBGA), and ceramic (CBGA). For the flexible TBGA all three conventional interconnection methods are used to interconnect the chip to the interposer. The tape or thin film is typically polyimide, epoxy-glass, polyester, and BT resins. The chip in the rigid PBGA and CBGA packages are interconnected to the substrate by wirebonding and flip-chipping respectively. TAB and wirebond interconnections in TBGA and PBGA are protected by over-moulding. The interposer in PBGA packages is FR-4, or BT-epoxy Printed Circuit Boards (PCB). Ceramic interposers in CBGAs are High Temperature Cofired Ceramics (HTCC) and Low Temperature Cofired Ceramics (LTCC) [66, 88–90]. Due to the high sinter temperature of 1550 °C in the HTCC case W, Mo is used as conductors.

When the primary use of the stacked interconnection substrates is to interconnect multiple components on the same substrate these boards are called Multi Chip Modules (MCM). Multi chip packages have also existed before the MCM in form of hybrid circuits. The difference is in the packaging density. A packaged electronic circuit is said to be a MCM when more than half of the substrate area is covered with active devices.

These even more compact packages also come in three types depending on different substrates: Plastic laminate MCM-L, mutilayer ceramic MCM-C, and deposited multilayer thin films MCM-D. The plastic laminates are like for the PBGA package often epoxy-glass based PCB-like substrates. More special resins are polyimide, Teflon®, and PEEK. Special fillers are quartz, Kevlar®, and Aramid® [4]. The ceramic substrates are HTCC and LTCC. MCM-D offers the highest packaging density with feature sizes down to around 10 μm. Here deposition often starts out on a silicon wafer. The insulating dielectric layers consist of polyimides deposited by spin coating and CVD SiO_2 and oxynitrides. The conductors are normally Cu, Al, and Au deposited by Physical Vapor Deposition (PVD). Even denser packaging can be achieved if the active/passive component is embedded in the layered structure [66, 88]. Such packages are called System On Package (SOP) or System In Package (SIP).

2.4.5. Wafer Level Packaging

WLP or 0-level packaging means packaging before the wafer with chips is diced into separate chips for subsequent packaging. The degree of packaging on wafer level varies. Since this is the only packaging type in which the footprint area of a packaged chip on a board equals that of the unpackaged chip the WLP is considered the ultimate packaging. The use is already widespread in the field of microsystem sensor packaging [12–15, 17–22, 52, 92–105]. Except for the size reduction which is nearly always beneficial in itself the motivation for WLP originates from huge economic advantages of packaging and test before dicing. One important disadvantage is that also bad dies will be packaged.

Actually many chips are wafer level packaged with a thin inorganic layer of SiO_2, or Si_3N_4 to protect it chemically against corrosion (environment, moulding, etc.) and physically against scratches (handling). For more than 30 years IBM has also been bumping chips on wafer level for subsequent single chip packaging (flip-chip) [4]. Flip-chip interconnection and underfilling is also done at wafer level [21]. Interconnection in WLP is almost entirely of the area array type; however, recent studies show that even higher integration can be achieved by using flexible silicon structures. Flexible silicon substrates consist of rigid (thick) regions and thin flexible regions [97, 98]. This interconnect type has many advantages compared to other methods: Complete Wafer Scale Integration (WSI) of microsystem sensors and active circuits is possible, CTE match between components, possibility of 3D folding/stacking of interconnected components, no moisture uptake, can be sealed with glass. Current major types of WLP can be categorized as [4]: Redistribution WLP, encapsulated WLP, and flex/tape WLP. The redistribution type is most commonly used. The Al and Cu rerouting conductors are embedded in Benzocyclobutene (BCB) dielectric. The new contact sites are bumped with solder as on flip-chips and BGAs.

Using wafer level processes underfilling of the area array interconnections is not necessary. Instead interconnections can for instance be embedded in a polymer by combined etch, metallization, and polymer re-deposition. In this way flexible interconnections can be made. In encapsulated WLP the entire wafer is sealed with a glass wafer on one or both sides. The glass can either be glued or anodic bonded [52]. The glass can be lapped down to a thickness of e.g., 100 μm if low profile is needed. For some sensors this "packaging" constitutes part of the sensor bulk structure and functionality to such a degree that it becomes increasingly difficult to define packaging in the traditional sense. This situation is very close to complete WSI or System On Chip (SOC) where all functionalities, mechanical as well as electrical, RF, etc. are integrated inside a single chip. In tape/flex WLP a sheet of tape e.g., wsCSP™ is mounted on and interconnected to the wafer. WLP by moulding whole wafers is also a subject to current research [4].

2.4.6. System Integration

The trend toward system integration i.e., WSI is seen on all packaging levels by features getting smaller and by components brought closer to each other, etc. Overall packaging efficiency is increasing and more and more packages fulfill the Chip Scale Package (CSP) criteria that the package footprint area is maximum 20% larger than that of the naked die. This is for instance the case for CBGA, MCM-D, and WLP packages. Packaging efficiency is defined as the ratio of the naked chip footprint area to the area of the system board/substrate on which it is mounted. Packaging efficiencies for some of the mentioned packages are [4]: DIPs around 10%, BGAs at maximum 50%, MCM up to 80%, SOP up to 90%, WLP close to or at 100%. SOP, WSI (WLP or SOC) are packaging areas of intensive research.

2.5. Sensor Die-Environment Interconnection

The drivers for direct, close proximity, partly or no access to sensing elements can be divided up as the economic (minimal size, number of processes), the physical (sensing principle, sensitivity, protection), and the chemical (sensing

principle, sensitivity, protection). What is the primary driver depends on the specific sensing situation.

Micro sensors like motion (accelerometers) and optical sensors do not require access in any form (direct, close proximity, partly) to the environment. Chemical (fluidic, gas) sensors may need direct access and others at least partly access through membranes/filters. The surroundings can have direct access (gas) or by use of a thin protective film barrier/interposer close proximity access (aggressive gasses, liquids) to pressure sensors.

Close proximity access to the sensing area is often not needed for sensing purposes but because of a cost reduction need. The drive to make the microsystem sensor packaging less expensive is very high since it accounts for up to 70% of the total sensor manufacturing cost [5]. The main reason for this high cost is mainly the many processes performed on single dies more or less separately. To avoid this, the packaging has to approach the chip size by going to the wafer level (WLP, SOC). This in turn has the consequence that the packaging has to be very small and extremely durable to withstand the often very harsh environments sufficiently. Many bulky pressure sensors for harsh environment applications are e.g., packaged with steel membranes and silicone oils as pressure transmitting interface to the sensor element instead of close proximity access through a hole in the outer package to a thin film on the sensing area [19, 102–104]. Thehuge economic advantage of the thin film is that it can be applied at wafer level. Furthermore, in many applications it is also important that sensors are small even after packaging.

The physical/chemical access hole to the system can be provided in many ways depending on the sensing situation. One type of access is a simple hole (premould package, glob-top/underfill interconnect protection, lid with hole) into the heart of the microsystem sensor. Transfer moulding with die access holes can be made with special gentle ways of avoiding mould material on the sensing area [106]. In this case the access is an integral part of the encapsulation. Other examples are optical wires [65–69] for e.g., optical sensors, snouts for microphones [21], microhoses/tubes, O-rings, etc. for microliquid handling systems which are mounted/interconnected to the sensor as seen for instance in many Micro Total Analysis Systems (μTAS) [67, 107].

3. PACKAGING STRATEGY

When starting the development of a new microsystem sensor from the elements mentioned above, it is very important to think holistically in terms of system design and of what the system is expected to experience/endure during the projected lifetime i.e., the common design for reliability but also packaging. Examples of different MEMS packaging strategies and designs are given in [17]. All the knowledge (MEM sensor die designers, microelectronics circuit designers, materials scientists, etc.) has to be collected for best performance [108, 109]. Every step in the fabrication of microsystems has a certain purpose but also great influence on what can be done next and in this way often a large influence on final performance. Therefore solutions on each step cannot be freely chosen. It might be as simple as to remember to start fabrication temperatures at the high end. Very costly and well designed MEMS sensors have been fabricated, however, they were never produced because the packaging was not taken into consideration and it turned out they were impossible to package [110, 111]. Another example of the importance of overall design is that some materials problems cannot be solved directly because of limited intrinsic properties. However, by combined materials design the problems can often be solved. Tightness of protective materials is for instance very important in microsystem sensor packaging for harsh environments. Polymers are attractive for many reasons except for their tightness. Actually no material is hermetic (completely tight), but by properly designed combinations of materials/phases sufficient tightness might be reached [2]. This is very important to remember for microsystem sensor packaging.

3.1. Reliability

Reliability issues are far more complex for microsystem sensors than for microelectronics. Common electronics reliability is e.g., reviewed in [112–115]. The reliability of sensors is complicated because they are closely exposed to harsh environments and contain moving parts [17]. Further required service life longer than 10 years is common. For some pressure sensors protected with specially designed thin films for harsh environment applications this means that the allowed corrosion of the film is below one atomic layer per day [103]. Special care in the packaging component materials and process choices for microsystem sensors have already been mentioned in chapter 2.

3.1.1. Failure Modes

The microsystem sensor failures can roughly be divided in two categories: inherent and environmental. Inherent microsystem sensor failures can already occur before the final product service life, but can also be induced/affected by the environment. These failures are specific for microsystem sensors because they occur due to the very nature of the sensor. One inherent failure is where closely separated surfaces come into contact and adhere to each other. This is called stiction [17]. Another example is where the silicon micromechanical parts break during wafer dicing. It could be argued that the latter is actually an environmental failure; however, it has not occurred in the final product environment.

Environmentally induced failures are due to: humidity, thermal cycling, vibration, shock, pressure variations, radiation, etc. separately and in combinations. Combinations usually accelerate failures. The failures may be inevitable due to materials limited intrinsic properties and in that case materials and designs can only be chosen to maximize the time delay to failure. This is for instance the case for hermetic packages for sensors because no package is entirely tight. Here the Mean Time Before Failure (MTBF) may be increased by e.g., designs involving getters [17, 116, 117] and multilayers as already mentioned. In other cases failure is observed because the exposure to these conditions changes the materials properties. T_g for polymers (e.g., epoxy for die attach, moulding, etc.) is for instance lowered when water is absorbed [118]. Then essentially we have a new material and perhaps T_g is now in the application temperature range which in turn means that (above T_g) high stresses are

developed due to higher polymer volume and CTE. This can have detrimental consequences for the measurement and may lead to delamination [115]. These failures are also seen for ICs in microelectronics, however to a much lesser extent. Because of this sharing of problems some solutions from microelectronics can be used for the sensor packaging [17]. However, many sensors need application specific solutions as already mentioned in chapter 1. Humidity failures are linked to the ingress or outgassing of chemicals from environment and package materials respectively, and loss of package hermeticity. These failures are very important for sensors because they initiate many other failures. They are less important for microelectronics. The consequence of these failures may be seen as e.g., damping of moving parts, corrosion, stress, delamination, etc. When combined with other environmental factors like thermal cycling, vibration, shock, pressure variations, then ingress, outgassing, loss of hermeticity and consequent damping of moving parts, corrosion, stress, delamination, etc. are highly accelerated [119]. Damping of moving parts which can also be induced by other means (e.g., stress) is a failure mode which is not observed at all in microelectronics. Thermal cycling induces solder joint and package failures (e.g., popcorning) in microelectronics but is less important in microsystem sensors except when combined with humid environments as mentioned earlier. Vibration, shock, and pressure variations may result in failures observed as mechanical fatigue, breakage and delamination. The latter will be highly accelerated if also moisture is present. In addition the stresses from vibration, shock, and pressure variations will often accelerate corrosion in humid environment. Polymer packaging materials may also be very susceptible toward radiation and embrittle in e.g., sunlight. This may also be accelerated by other environmental factors. The embrittling may result in e.g., increased stress levels which have impact on sensor performance.

3.1.2. Failure Analysis

Failure analysis of microsystems is a scientific discipline in itself. When designing for reliability it is mandatory to analyze what the sensor will experience during production and the rest of its lifetime in use. Then from resulting specifications simulations on the whole sensor performance and accelerated testing can be performed. Simulation and statistics can help making fabrication process and design improvements to minimize e.g., unwanted stresses [4, 120–123] influencing sensor measurement. Stresses are one of the major causes for microsystem sensor drift and failure. One way of improving stress simulations and therefore gain better prediction of potential failure sites is by use of actual measured CTE values instead of not very representative (due to differences in processing, etc.) tabulated values. At best the CTE values are measured with the new OMISTRAIN® [124] equipment where nm movements during temperature cycling of whole component surfaces are mapped. The measurements also give direct information on stress levels. Then combined functional/environmental test with *in situ* electrical measurement can be performed at wafer level on unpackaged, partly packaged or fully packaged sensors with testing equipment also developed recently [3]. Alternatively, it may be done on separate sensors. Then OMISTRAIN® measurements and subsequent simulations may be repeated. Both types of equipment can be used for both microelectronics and microsystem sensors. Among more common instrumental tools to analyze/locate failures are Scanning Electron Microscopy (SEM), Scanning Acoustic Microscopy (SAM) [125], X-rays, electrical probe stations, Focussed Ion Beams (FIB) equipment [126], etc. They are used to detect physical/chemical failures like delamination, cracks bubbles, corrosion and electrical circuit failures.

3.1.3. Microsystem Materials Selection

General overviews of materials for microsystems can be found in [4, 23, 127]. Careful selection of materials is as indicated in previous sections very important for the overall sensor performance and reliability. Sensor performance (access holes, electrical, sensitivity) and minimal size (preferably WLP processing and small hidden pervasive sensors [47, 128]) drive the demand for packaging with high protective capability and applicability without affecting sensor performance negatively. In cases where low cost and small package size is not mandatory materials and design can be chosen more freely and extremely robust sensors can be fabricated.

In Table 1 an overview of selected microsystem packaging materials and methods is given. Some of those which are generally considered most important in microsystem sensor packaging for harsh environment are indicated. Due to the diversity of sensors it is important to stress that whether each material is relevant or not depends on the specific application. These materials and methods have been selected from physical/chemical properties such as high chemical/physical barrier and durability properties, high CTE match capability, low cost processing, etc. which are also important in microelectronics, but are considered even more important for reliable packaging of microsystem sensors.

The major problem to be solved in sensor packaging for harsh environments is to get sufficient access to the sensing area while still providing adequate chip protection. Materials are chosen for different main purposes: Attachment, heat dissipation, conductance (interconnection), insulation, support (boards), protection, and combinations thereof.

However, the materials purposes are all more or less interrelated with each other and the purpose of the final component cf. system design. Table 1 also reflects that generally degrees of freedom in selecting materials for some materials primary purpose is more or less reduced due to some other demands.

a. Electrical Interconnection Materials Often compromises which severely complicate the packaging have to be made. One simple example is that the demand for a hermetic package which has a low CTE and high physical/chemical durability may require that it is made of ceramic sintered at 1550 °C, i.e., only conductors, e.g., leadframes of W, Mo, with high melting point at the cost of electrical conductance can be used. In that way, the relative importance of purposes/properties (conductance vs. melting temperature, etc.) have been altered because of higher purposes, hermeticity, low CTE, durability, etc. Melting temperatures for these metals are $T_m(W) = 3422\,^{\circ}\mathrm{C}$, $T_m(\mathrm{Mo}) =$ 2623, and both have a low CTE of 4.5 ppm which is very

Table 1. Selected microsystem packaging materials. Italic: Important in microsystem sensor packaging for harsh environments.

Primary purpose (process and other characteristics)	Use and materials
Die attach by:	
Gluing (hard to *compliant* attach, *acceptable electrical*/thermal *conductance, and CTE with fillers*).	*Mounting on substrates and inside packages.* Adhesives: *Epoxy, cyano esters*, urethane, *silicone*, *filled with* e.g., Ag, *fused silica, quartz.*
Anodic and frit bonding (Silicon CTE matched attach, and sealing).	*Glass, glass frits, silicon (wafer level sealing, stress isolation).*
Electrical conduction by:	
Wirebond (flexibility/compliancy).	*Interconnect between pads on top of die and substrate.* *Au*, Al.
Flip-chip (compact).	*Microelectronics assembly near sensor die (e.g., ASICs).* Sensor die flip-chip interconnect to substrate. *SnPb soldering*, solder materials without Pb, e.g., $SnAg_{3.9}Cu_{0.6}$ or *Au bumps dipped in Ag filled adhesives (Stud Ball Bumping SBB process).*
Conductive adhesive (low temperature processing, compact, attach, *HDI*, good heat conduction).	*Au, Ag,* Ni, Cu.
TAB (compact).	SnPb soldering, solder materials without Pb, e.g $SnAg_{3.9}Cu_{0.6}$.
Interconnect on substrate/package by:	
Under Bump Metallization (UBM) (adhesion and diffusion barrier).	*Solder ball interconnect, e.g., ASIC flip-chip* Sensor die flip-chip. Al, Cu, Ti, W, TiW, Cu, Mo, Ni, Pt, Pd, Cr.
Pastes (*conductors*, resistors, etc.).	*Hybrid circuits.* *Ag/Pd*, Ru_2O_3 *in matrix of glass, organic fillers and solvents.*
Conductors (high conductance).	Low temperature processed substrates *Au*, Al, Cu.
Leadframes (conductance, high temperature sealing).	*DIP.* *Cu, $Ni_{42}Fe$ (Alloy 42), $Ni_{29}Fe_{53}Co_{17}$(Kovar™) W, Mo (moulded packages).*
Package for protection and chip/interconnection support by:	
Deposition of thin films at wafer and higher levels.	*Physical (mechanical, EMI screening) and chemical protection.* SiO_2, Si_3N_4,*a-CrTa, a-TaO, a-SiC, Cr, Ti, a- Ni.*
Moulding/premoulding (support, barrier, low stress).	*DIP*, QFP: *Polymers: Heat and UV processed phenolic-epoxy filled with quartz, LCP* MCMs, and hybrid circuits with good thermal dissipation and electromagnetic shielding. Metals: $Cu_{10}W$, $Cu_{15}W$, Silvar™ (Ag-Ni-Fe alloy), $Cu_{15}Mo$, Kovar™ and Alloy 42 plated with Au, Ag, Cu. *Ceramics: Al_2O_3.*
Getters (trapping of unwanted chemicals and particles, use of cheaper packages).	*Inside or as part (ceramic) of hermetic (liquids, gasses)* *Silicone–zeolite composites: STAYDRY™ GA2000-2.* *Metals: Zr-Al-Fe, Ti, Th, Pd, Pt.* *Metal-oxides: PdO.* *Zeolites.* *NanoGetter™.* *Al_2O_3(e.g., CERDIP).* *Silicon rich oxides.*
Glob-top (barrier, mechanical protection).	*Protection toward liquids, gasses, light.* *Avoidance of wire sweep in moulding.* *Adhesives: Anhydride-epoxy e.g., filled with ceramics, carbon.*
Underfill (mechanical protection).	*Microelectronics flip-chip.* Sensor flip-chip. *Adhesives:* Anhydride-epoxy, *Cyanate ester e.g., filled with ceramics.*
Coatings (barriers, wear protection).	Microelectrinics components/boards, *sensors* protection against *liquids, gasses, light.* Polymers: Solder masks, *Parylene C, Nova HT, Teflon AF, adhesive type* (epoxy, urethane, *cyano esters,* acrylates, silicone) *Polymer–metal composites: e.g., UV curable acrylates with flakes of Cu plated with Ag.*
Lid mounting (tight, low stress lid attachment).	*Lid: Plastics, ceramics, glass, metal.* *Sealing: Adhesives, glass or assembly by anodic* bonding, welding.
Stacked substrate layers (dense, durable low stress interconnection).	Dense MCM packaging of microelectronics and *microsystem sensors.* *Hybrids: Al_2O_3.* *MCMs:* HTCC, *LTCC*, epoxy filled with glass, Kevlar® and Aramid®, *polyimide* (PI), *bismaleimide triazine (BT), Polytetrafluoroethylene (PTFE or Teflon®), Polyether ether ketone (PEEK).*

close to that of Si and many sealing glasses like borosilicates. Generally, more corrosion stable metals like Au instead of Al in wirebonding and Cu, Ni in conductive adhesive is used where required by the environment. For microsystem sensors in harsh environment flip-chip interconnection is very attractive from the materials point of view due to small amount of interconnect solder/bump material prone to chemical attach. This explains why Sn-Pb solders can still be used in many applications although they are not very corrosion stable.

b. Highly Protective Die Attach, Underfill and Package Materials Most often the basic innermost microsystem materials (Si, GaAs) and to some extent also the interconnection materials are chosen for their electrical properties without regarding their other properties, which have influence on the reliability.

Therefore one of the most important purposes of die attach, underfill and package materials is to protect the sensor/IC and other packaging materials (wirebonds, etc.) both by constituting a physical (mechanical, temperature) robust interface to the surroundings and by keeping away chemicals, particles, and radiation detrimental for the sensor performance due to their change of materials properties.

The chemicals protected against can be both liquids and gasses. Amongst liquids water and its ionic content are the most common problems. The critical ions are usually Na^+, K^+, and Cl^- coming from salt in sweat, sea water, or it is born from the packaging materials. The ions may diffuse around both in the packaging materials and semiconductors and in this way destroy the electrical functionality directly or they may participate in electrolytic corrosion [129]. The water can also corrode the materials directly (hydrolysis) [4] and indirectly by reactions with corrosive end products. The latter occurs e.g., when too much P is in P doped (to lower melt temperature) glass used as a dielectric layer. Water react with P to give H_3PO_4 acid which further corrodes the surrounding materials [130]. Just the presence of water is most often critical, especially for polymers. The polymers swell, modulus E, CTE, T_g and strength are lowered, etc. The resulting failure modes are e.g., delamination, cracks, popcorning, etc. The presence of water can also induce stiction in silicon micromechanical sensors [17].

The gas chemicals are typically H_2O, H_2, NH_3, SO_2, H_2S, etc. originating from the harsh environment surroundings and outgassed from the packaging materials themselves, e.g., from plated metals and polymers (epoxy). They can all affect microsystem sensors performance severely for instance by corrosion and damping (resonators).

Particles from the surroundings and from component processing can be critical because they can interfere with subsequent processing, short circuit, and block the movement of parts in microsystem sensors. Therefore the processing has to take place in a clean room environment all the way to the final component and appropriate cleaning methods have to be employed.

Electromagnetic radiation can cause the electronics (e.g., amplifiers) and sensors (e.g., capacitive MEMS microphones) to malfunction. To achieve ElectroMagnetic Compatibility (EMC) ElectroMagnetic Interference (EMI) is commonly shielded with the use of metal packages (houses)/grids, metal filled polymers [1], glob-top filled with C, and by deposition of magnetic thin films.

Mechanical robustness is provided first by protecting chips so that they can withstand further handling and processing by applying thin protective films (see Table 1). Moulded packages and substrates provide mechanical protection toward the surroundings. Here it is important to note the materials differences in E and toughness.

Generally, heat dissipation from microsystem sensors is not an important issue. However, in special cases as micro hotplate gas sensors where temperatures as high as 500 °C are reached it can be an important issue [131]. A bigger problem is to find packaging solutions which can meet the many high temperature applications within e.g., the automotive and oil/gas industry [34–42].

Ingress of water from the surroundings is often considered to be the biggest problem to solve in microsystem packaging [132–143]. Only 0.1 nL water may be critical due to direct corrosion of narrow Al conductors on chips [133]. No material is actually completely tight toward water. However, their decreasing tightness can be ranked as: Metals, glasses, LCP, Parylene, fluorocarbons, epoxies, silicones. A package is defined as hermetic if the He leak rate is below 10^{-8} $cm^3\ s^{-1}$ [4]. Qualifying leak testing is usually done in accordance with the military standard MIL-STD-883. However, since the diffusivities of He and water in any material differ a lot testing directly with water is often mandatory. Polymers are attractive because of easy and cheap processing. An extensive overview of polymer permeability data is given in [144]. Water uptake (solubility S) and diffusion constants can be determined in accordance the standard SEMI G66–96 [2, 118, 145, 146]. This is done by using the short times approximation of (1)

$$\frac{M_t}{M_E} = 1 - \frac{8}{\pi^2}\sum_{n=0}^{\infty}\frac{\exp\{-(2n+1)^2\pi^2(Dt/L^2)\}}{(2n+1)^2} \tag{1}$$

where M_t is the weight gain of a thin slab of material after exposure for a period of time t, M_E is the weight gain at equilibrium i.e., after saturation, D is the diffusion constant, and L is the slab thickness [147]. M_E depends exponentially on the humidity H as

$$M_E = KH^{\alpha} \tag{2}$$

where K and α are temperature dependent constants [4]. The short time approximation of (1) is

$$\frac{M_t}{M_E} = 4\sqrt{\frac{D}{\pi}}\frac{\sqrt{t}}{L} \tag{3}$$

and given M_E, D can be found from the short times slope h in a plot of M_t/M_E as a function of $t^{1/2}/L$ as

$$D = \frac{\pi h^2}{16} \tag{4}$$

It is then important to note that the flux F of water will be determined by

$$F = \frac{DS}{L} = PS \tag{5}$$

where P is the permeability, i.e., that how much is actually passing critical areas is not only determined by D but also by S [2]. It is also very important to realize that for encapsulations S determines how much water is actually in contact with the critical areas. This means that even though a material may have a high D for water (e.g., silicone) they might be a good choice anyway in some application due to low S. The worst case occurs for instance in pressure sensors where a pressure gradient may cause a continuous flux across critical areas. Another critical situation is when the material has taken up a lot of water at high temperature and the temperature then suddenly falls to a temperature where S (determined from M_E) is significantly lower. Then the material literally begins to sweat. This may cause high stresses followed by delamination, cracks, etc. This is one of the reasons why good adhesion at interfaces is so important. Slower mechanisms are creation of weak boundary layers with high water content and hydrated metal oxides and finally delamination. Interfaces are generally very prone to failure due to stress concentration.

The materials used for die attach, underfill, and packages are: polymers, ceramics, glasses, metals, organic/inorganic/metallic thin films and coatings, and getters (see Table 1).

Polymers are used more and more in microsystems, especially microelectronics because they are becoming higher grade concerning Na^+, Cl^-, K^+. Nowadays the content of these ions is usually only a few ppm for electronic grade polymers. Further, thin film protection (oxides, nitrides) has also made chips sufficiently mechanically/chemically robust for transfer moulding [4]. Generally, the polymers chemical resistance against solvents can be evaluated using the Hansen Solubility Parameters (HSP) [148]. A common polymer mould compound is phenolic epoxy. Better performing polymer packages for microsystem sensors can e.g., be made of LCP [85, 86] or cyano ester adhesive [4, 149]. Both these polymers are highly chemically resistant and water tight. Actually LCP is the tightest polymer known. Also cyano ester adhesive is a very good water barrier in that it actually captures (get) the water by reaction without degradation [4]. They are both very chemically resistant and both come filled with very low CTEs.

Epoxy based polymers are normally used for die attach because of their good adhesion and durability. They are also quite tight compared to many polymers e.g., silicone. Highly filled with quartz the CTE can come as low as 11 ppm. This is not possible with silicones which are also less chemically durable especially toward solvents. However, they are used in sensor applications where completely stress free assembly or encapsulation (silicone gel) is needed. Water flux through silicones can be as low as for epoxies due to low S. Very low stress sensor attach and encapsulation can also be approached by use of UV curable epoxies. This is due to room temperature curing, step curing, and quartz filling [84].

Anhydride epoxies are commonly used for underfill and glob-top base materials, but will not be good enough in the many sensor application where water comes close because these systems give polyester linkages which are prone to hydrolysis [4]. Here cyano ester based adhesive is more promising.

Epoxy is also used for PCBs (FR4) and layered substrates (MCM-L) with different fillers (see Table 1). This is also the case for PI, BT, PTFE, and PEEK all of which are very interesting candidates for microsystem sensor packaging because of low permeability and/or chemical durability.

Ceramic substrates and house packages are typically Al_2O_3, HTCC, and LTCC which are very water tight partly due to their dense structure and because of water getter properties. It is also very tight toward other substances. Besides CTE is very low, chemical durability high, and E is high. These materials are very attractive to microsystem sensor packaging [66, 88–90].

Glasses are basically SiO_2. Differently doped (e.g., with P) glasses can have low melting temperatures making them usable for ceramic and metal package sealing (lid and electrical feed-through in metal packages) and actually also for die attach e.g., silver-filled for thermal conductance. In humid environment it is important that the glass contains no alkalis like Na^+ because they can be released by water corrosion and destroy the microelectronic circuit.

Metal packages are usually chosen to have good thermal conductivity and low CTE. Examples are shown in Table 1 [83]. The metal packages are used as houses for hybrids and MCMs. Together with glass-sealed lids and electrical feed-throughs these packages are hermetic. Metal lids are also soldered or welded. Moisture is often a serious problem when using metallic packages because metals are generally hydophillic [4, 150]. Good adhesion of e.g., adhesives is very often correlated with surface energies/tensions [151]. To achieve good adhesive bonding good spreading is usually a prerequisite. This can be achieved by ensuring a low surface tension of the adhesive compared to that of the substrate. Moisture on metals has the effect of lowering the surface tension [152] and therefore often the adhesion strength.

Organic conformal coatings are often urethane based [4]. They are used mostly for circuit board protection. They have very good protective properties regarding humidity, corrosive environment, and toughness. They can be as protective as hermetically sealed packages. They cure both by heat and UV light. Other organic conformal coatings of greater interest for microsystem sensor protection are the parylenes (poly-para-xylylene) and Teflon AF [1]. This is primarily because they cover bond wires and single crystalline silicon edges and corners highly conformal in layers thinner than 10 μm and because of their high chemical durability. Parylene C is also very tight (comparable to LCP) and is therefore used as barrier [20]. Also of interest for MEMS sensors is thin conformal coatings of polymer-metal composites for EMI shielding [1].

Inorganic/metallic thin (around 1 μm) films are of particular interest for compact chemical and EMI protection [19–22, 102–104]. Some coatings are amorphous to avoid chemical attack and fast diffusion otherwise observed at crystallite boundaries (see Table 1).

Getters are materials that traps unwanted chemicals e.g H_2O moisture, H_2, NH_3, SO_2, H_2S either by adsorption or reaction [17, 116, 117]. Silicon gas compatibility guidelines are described in the SEMI F79–0703 standard. Getters are used inside packages because it is well known that no material can keep out the mentioned chemicals sufficiently for the periods of interest. They consist of sticky polymer capturing particles typically from the processing

and metal and metaloxides (see Table 1). The unwanted gases flow may also be diverted by phase barriers as e.g., air. For moisture this can be very effective since D in e.g., epoxy is around 5×10^{-13} m^2 s^{-1}, and in air it is around 2×10^{-5} m^2 s^{-1} at room temperature. As depicted in Section 3.1.3 high durability packaging can be achieved with high durability packages and smaller demands on sensor performance. However, the performance of the above mentioned hermetic ceramic package (Section a) may e.g., also be achieved in a cheaper way by use of a less tight polymer package with one or more getters inside and Cu as conductor. This is one way of achieving Reliabilty WithOut Hermeticity RWOH. Alternatively very high performance concerning tightness and the often ultimate goal to keep chemicals and particles away from the critical sensor parts may be achieved by use of the ceramic package including getters inside.

c. Sensor Die-Environment Interconnection Materials

In many cases the access hole is part of the package and consequently made of that material. However, often some guide of the media to be sensed on, has to be fixed to the microsystem sensor. For that small commercial or specifically manufactured fittings (plastic, glass, etc.) are used together with adhesives like epoxy and silicone [1, 20, 21, 29, 67, 107]. The fixation has to be completely microsystem sensor compatible regarding the same parameters as the rest of the packaging, i.e., minimum stress, high adhesion, no corrosion, etc.

4. SPECIFIC APPLICATIONS

Below specific microsystem sensor packaging examples are given. They are grouped according to whether they can be considered standard packaging, modified standard packaging, or custom designed packaging. Pressure sensors and accelerometers represent the largest markets. To cover all these types of packages and sensors the examples comprise 3 pressure sensors, 2 accelerometers, and 1 microphone. They are commented regarding application (environment), and how the packaging has been solved concerning electrical interconnection, sensor die–environment interconnection, and protective package. Many examples can be found in the literature e.g., from other areas like biotechnology and telecommunication [153, 154].

4.1. Standard Packaging

This kind of packaging involves conventional packaging technologies from microelectronics. An example is the ADXL202 dual axis accelerometer from analog devices (Fig. 2). This is a house type ceramic DIP. The accelerometer is mounted in a ceramic package cavity and interconnected with Al-wirebonds to the leadframe. No access hole/window is needed for such a sensor. A lid is hermetically sealed to the package cavity.

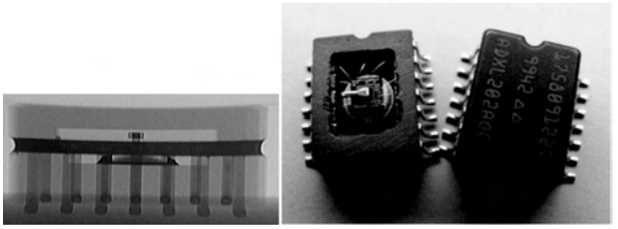

Figure 2. Left: X-ray photo of dual axis accelerometer. The aluminum wirebonds cannot be seen on an X-ray photo. Right: Grinding the ceramic away opens the package.

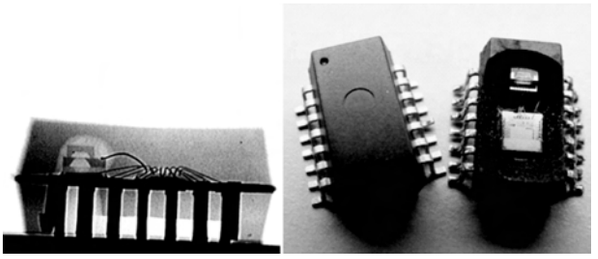

Figure 3. Left: X-ray photo of absolute pressure sensor. Right: Etching with dry HNO_3 exposes the sensor and the chip.

4.2. Modified Standard Packaging

These packages are based on materials and shaping of the package that to a varying degree differs from what is seen in the microelectronics industry in order to meet the requirements of the specific microsystem sensor.

One example is the SP13 tire pressure sensor from SensoNor (see Fig. 3). This is an absolute pressure sensor in a plastic DIP. It should be noted that in this case a glob-top has been placed around the sensor stack in order to minimize the thermal stress and wire sweep from the injection moulding encapsulation. Gold wirebondings are used as electrical connections from both the sensor to the ASIC and from the system to the leadframe which provides the external connection. Note also that the packaging differs from microelectronics packages as it includes glass bonded at wafer level (cf. WLP) on both sides providing minimum stress on the silicon sensor die in the middle, reference pressure cavity on the top side, and part of the pressure access hole/channel to the sensor die. The rest of the hole to the sensor die is in the leadframe and plastic mould material.

Another example is the SLP004D pressure sensor from SensorTechnics (see Fig. 4). It can be used for measuring differential or absolute pressure. This sensor is wirebonded to a leadframe which provides the external connections resulting in a Single Inline Package (SIP). A hole in each Al plate provides physical connection. The hole gives direct access to the chip surface i.e., the component is relatively vulnerable

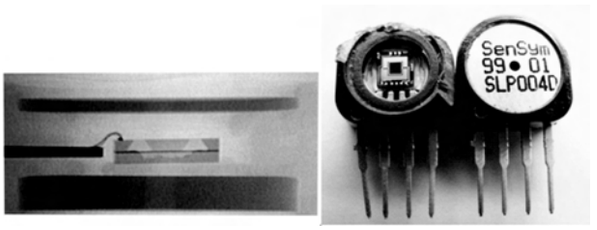

Figure 4. Left: X-ray photo showing wirebonds, sensor unit and the two aluminum plates. Right: The sensor is exposed for inspection by removing one aluminum plate.

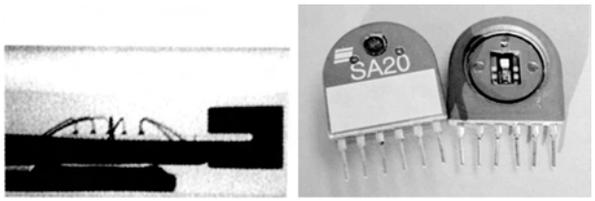

Figure 5. Left: X-ray photo showing the seismic mass and the wirebonds. Right: Grinding exposes the die.

to pollution. The package is a plastic house with Al plates on both front and back.

A third example is the SA20 airbag accelerometer from SensoNor (see Fig. 5). The internal electrical connections are made using gold wirebonding, and the external connections are provided via the pins, in this case a SIP. The house is a welded polyphenylene sulfide (PPS) plastic housing. This is a thermoplastic material with excellent thermal, mechanical and chemical resistance. The sensor does not need a physical connection to the outside, since it measures only the movement of a seismic mass via a piezo resistive bridge. The cavity in the house is filled with silicone oil for the purpose of dynamic damping.

4.3. Custom Designed Packaging

In more complex packages even the interconnections are of a more advanced type. The development of the bare silicon MEM die, is not the main area of work, however, the entire system including the sensor, the interconnection and the package have to be planned together, because they can have multiple functions and constrain each other severely. At this point there is very little to be said about standard packaging. With the example in Figs. 6 and 7 which is a 3 mm · 3 *mm* · 2 mm microphone (dummy) for e.g., hearing

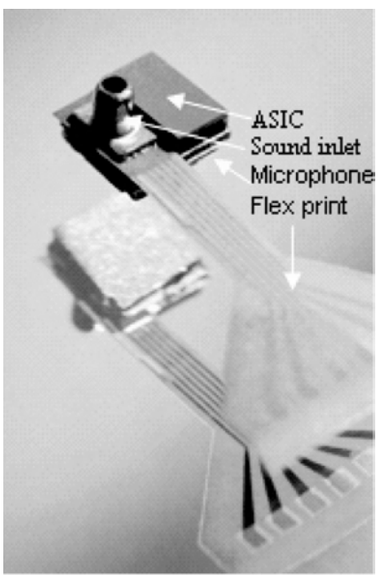

Figure 6. A dummy sample of a silicon micromechanical microphone before encapsulation.

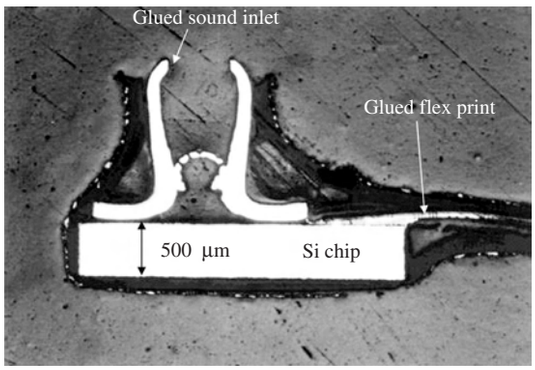

Figure 7. Cross section showing the built-up of the test structure. Two protective encapsulation layers are needed. A conductive top layer for EMI (Electro Magnetic Interference) shielding and an insulating layer beneath to avoid short circuiting anywhere on the microphone. The first layer has been applied by dipping, the second by spraying. Note that it has been possible to cover the sharp corners of the silicon. Here the insulating layer has a thickness of approx. 50 μm. The thickness of the conducting layer is around 25 μm everywhere.

aids, mobile phones, focus is only on the demands for a protecting encapsulation material that practically takes up no space [1]. Other minimum packaging volume methods used have been chip stacking involving: anodic bonding, sealing with fluxless solder bump bonding, and through-hole microphone/ASIC interconnection, together with flip-chip interconnection (ASIC, flex print) and mounting (sound inlet) [21, 22].

Even though they are often the simplest microsystems, pressure sensors are usually placed in very rough environments. As mentioned earlier, keeping the microsystem small and cheap means high demands on the packaging materials and methods. An example is the Grundfos differential pressure sensor (see Fig. 8). Here the sensor has to be able to withstand direct exposure to water under pressure at 125 °C via the holes in the housing for at least 10 years. To solve this problem focus has been on:

1. Materials with high corrosion stability. Especially the thin protective film has to be very corrosion stable. For a sufficiently thin film, which should be able to last for 10 years, no more than one atomic layer may be corroded per day [19, 20, 102–104].

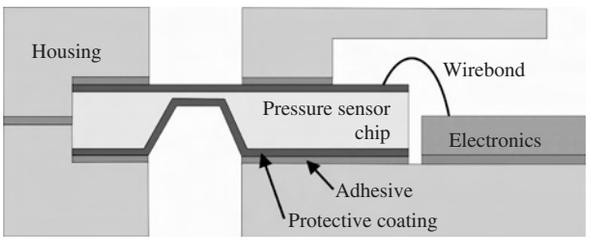

Figure 8. Cross-sectional drawing of a differential pressure sensor. The sensor chip is protected with a coating on both sides and mounted in a housing using adhesive. Through the access holes in the housing and contact with the coating the media gets in close proximity to the pressure sensor chip.

2. Tight and low stress mounting/sealing of die in housing. The tightness depends entirely on the adhesives/O-rings bulk and interface tightness to house/film on the die. The tightness is important since the very corrosion sensitive microelectronics is placed close to the water. The allowed leak rate to ensure low enough corrosion has been estimated to 2.5×10^{-2} mm^3/year/bar [20]. Stress is important because it may couple into the pressure sensing membrane area and thereby disturb the measurement [109, 120]. The stress depends on both the adhesives/O-ring and the house materials CTE. The adhesives/O-rings CTE might change significantly over time.

GLOSSARY

ACA Anisotropic Conductive Adhesive. Adhesive where the amount of electrically conductive filler is adjusted for conduction in only one direction perpendicular to the substrate.

Anodic bonding A joining method where e.g., silicon and borosilicate glass can be bonded making use of heat at around 400 °C and high voltage.

ASIC Application Specific Integrated Circuit.

BCB Benzocyclobutene. A polymer used in microsystem packaging as dielectric material in layered electrical interconnection.

BGA Ball Grid Array. A package where a chip is interconnected to the next level of packaging using a space transforming interposer. An area array of solder balls on the interposer is typically used for interconnection to the next level of packaging.

BT Bismaleimide Triazine. Polymer used as dielectric material in PCB and layered electrical interconnect substrates.

CBGA Ceramic Ball Grid Array. A BGA where the interposer is HTCC or LTCC.

CSP Chip Scale Packaging. A package where the footprint area is maximum 20% larger than that of the naked die.

CTE Coefficient of Thermal Expansion. Indicates how much a material expands as a function of temperature. The symbol is typically μm/m °C.

CVD Chemical Vapor Deposition. A vacuum deposition process where chemical reactions take place both in the gas and on the substrates. Used e.g., to deposit parylene (poly-para-xylylene) as protective coating.

DIP Dual Inline Package. A package with leads on two parallel sides.

EMC ElectroMagnetic Compatibility. Refers to the situation where an electronic component is constructed/protected so that EMI is not a problem.

EMI ElectroMagnetic Interference. Disturbance of electronics by electromagnetic radiation.

FIB Focused Ion Beams. In electronics FIB is used for failure analysis where e.g., conductors are cut or repaired.

Flip-chip An electrical interconnection method where a chip is turned upside down (flipped) to connect contact points typically in an array area on the chip and chip carrier.

Getter In microsystems a material that traps or keep away unwanted chemicals and particles by being reactive or sticky.

HDI High Density Interconnect. Refers to electrical interconnection with a very low pitch.

HSP Hansen Solubility Parameters. Parameters that helps predicting the chemical durability of polymers toward solvents.

HTCC High Temperature Cofired Ceramic. Electrical interconnect substrates consisting of alternating layers of conductors and ceramic as dielectric material. The soft and compliant ceramic layers are cofired/hardened at high temperature (1550 °C).

IC Integrated Circuit.

ICA Isotropic Conductive Adhesive. Electrical conductive adhesive with a high filler content resulting in isotropic conduction.

LCD Liquid Crystal Display. Flat displays based on liquid crystals which change orientation when a voltage is applied across them.

LCP Liquid Crystal Polymer. Thermoplastic polymers with unique structural, physical and chemical properties. Consists of linked rigid and flexible monomers. Rigid molecule segments align in the liquid state during flow and this alignment is maintained when cooling to the solid state. An example of a LCP is Vectra A-950.

0 level packaging See WLP.

1st level packaging Packaging at the micromechanical chip and/or IC level. It comprises chip (micromechanical, IC, ASIC, etc.) mounting (anodic bonding, gluing, soldering) on some support (carrier, housing, substrate e.g., with interconnecting conductors) and interconnection (wirebond, flip-chip soldering/gluing, conductive adhesive).

2nd level packaging Packaging at system level or board level. Packaging on this level consists of mounting the 1st level package onto some board (typically FR4 PCB or card) to interconnect active and passive components.

3rd level packaging Packaging at the board to board interconnection level like in PCs where several slots for insertion of different cards exist.

LTCC Low Temperature Cofired Ceramic. Stacked electrical interconnection layers like HTCC, only the ceramic layers are cofired at low temperatures.

MCM Multi Chip Module. A packaged electronic circuit is a MCM when more than half of the substrate area is covered with active devices. The substrate is typically a layered interconnect substrate like HTCC or LTCC.

MEMS MicroElectroMechanical System. Miniaturized sensors and actuators with micrometer size features. Sensing and actuating is electromechanical. The MEMS comprises a MicroElectroMechanical (MEM) component and some low level packaging e.g., interconnection to a substrate, an ASIC, etc. Normally the MEM is a single crystalline silicon micromechanical structure fabricated by etching methods.

Microsystem MEMS together with microelectronics, photonics, RF/wireless packaged to the 2nd and 3rd level.

Microsystem sensor Miniaturized sensor with micrometer size features for analysis involving disciplines as: Mechanics, fluidics, biology, chemistry, microelectronics, optics, etc.

μTAS Micro Total Analysis Systems. Systems with micrometer size features comprising all necessary components for complete analysis.

MID Mould Interconnect Device. Moulded polymer supporting and interconnecting carrier where the interconnecting conductors are applied e.g., by chemical/galvanic metallization or by hot embossing.

MTBF Mean Time Before Failure.

NEMS NanoElectroMechanical Systems. Electromechanical sensors or actuators with nanometer size features.

Packaging The interfacing between active/passive microsystem components and the surroundings: Attachment, support (substrate, carrier, encapsulation), signal interconnection between components and environment (electrical, optical, chemical/physical, access for sensing/actuation), and protection (encapsulation, housing).

PBGA Plastic Ball Grid Array. A BGA type where the interposer is made of some kind of plastic which is most often FR-4 or BT-epoxy PCB.

PCB Printed Circuit Board. Typically a FR4 board made of epoxy-glass with printed conductors for electrical interconnection.

Popcorning Cracks and delaminations in house and encapsulation type packages because of sudden heating of entrapped moisture in the materials. The sudden heating is e.g., due to wave soldering.

PWB Printed Wiring Board. Boards with conducting lines for interconnection e.g., FR4.

QFP Quad Flat Package. A package with leads on all four sides.

RWOH Reliability WithOut Hermeticity.

SAM Scanning Acoustic Microscopy. SAM is a Non Destructive Testing (NDT) method for microinspection which functions like a sonar, though using much higher frequencies, MHz–GHz. Pulses of ultrasound is transmitted through a liquid medium, typically water, to the component and its interior where it is reflected and transmitted at interfaces between materials due to their differences in acoustic impedance Z. It is used in microsystem failure analysis for detection of e.g., cracks, bubbles, delamination in packages.

SBB Stud Ball Bumps. Bumps which can be used for electrical interconnection in the flip chip process by first dipping them in conductive adhesive.

SEM Scanning Electron Microscopy. A kind of microscope for surface inspection using electrons instead of light giving much higher magnification.

SIP (1) Single Inline Package. A package with leads on one side. (2) System In Package. Packaging where the components are more or less integrated or encapsulated in the packaging, i.e., in layered interconnect substrates. Another word for SIP is System On Package (SOP).

SOC System On Chip. SOC is the ultimate integration level accomplished when a whole functional system is integrated in one monolithic chip.

SOP System On Package. See SIP.

Stiction The unwanted natural adherence between surfaces of MEMS structures that come very close.

TAB Tape Automated Bonding. A low profile chip electrical interconnection method using soldering by thermocompression of free conductors e.g., Cu on the tape to both chip and some package or PWB.

TBGA Tape Ball Grid Array. BGA where the interposer is made of some kind of polymer tape. The tape is typically polyimide, epoxy-glass.

WLP Wafer Level Packaging. Packaging at the wafer level, i.e., before dicing of the wafer into separate components. WLP is also called 0 level packaging.

WSI Wafer Scale Integration. The act of moving the packaging processes to the wafer level.

REFERENCES

1. Jakob Janting, Jens Branebjerg, and Pirmin Rombach, *Sens. Actuat. A* 92, 229–234 (2001).
2. Jakob Janting, "Proceedings of Micro System Technologies (MST) Conference," pp. 520–522. München, October 7–8, 2003.
3. Søren Pihl Rybro, "Proceedings of Micro System Technologies (MST) Conference," pp. 451–455. München, October 7–8, 2003.
4. Rao R. Tummala, McGraw-Hill, 2001.
5. Marc Madou, CRC Press, 1997.
6. Y. C. Lee, Babak Amir Parviz, J. Albert Chiou, and Shaochen Chen, *IEEE Transactions on Advanced Packaging* 26(3), 217–226 (2003).
7. Matthias Werner, Hans-Jörg Fect, and Richard W. Siegel, *MSTNEWS* 3, 4–6 (1999).
8. Matthias Werner, Thomas Köhler, and Werner Grünwald, *MSTNEWS* 3, 4–8 (2001).
9. Ken Snowdon, Calum McNeil, and Jeremy Lakey, *MSTNEWS* 3 (2001).
10. T. I. Kamins and R. Stanley Williams, *MSTNEWS* 3, 34–36 (2001).
11. Volker Türck, and Dieter Bimberg, *MSTNEWS* 3, 17–19 (1999).
12. R. Tummala, *Components, Packaging, and Manufacturing Technology (CPMT) Society Newsletter* 25(4), 1–2 (2002).
13. Mats Robertsson, "Proceedings of The IMAPS Nordic Annual Conference," pp. 2–24. Helsingør, Denmark 2004.
14. Bharat Bhushan, Springer-Verlag, Berlin, Heidelberg, New York, (2004).
15. Achim Wixforth, Jürgen Scriba, and Christoph Gauer, *MSTNEWS* 5, 42–43. (2002).
16. Kwang-Seok Yun, Il-Joo Cho, Jong-Ik Bu, Chang-Jin (CJ) Kim, and Euisik Yoon, *Journal of Microelectromechanical Systems* 11(5), 454–461 (2002).
17. K. Gilleo, "Proc. IMAPS 2000," pp. 598–604. Boston, USA, September 2000.
18. Richard R. A. Syms, Eric M. Yeatman, Victor M. Bright, and George M. Whitesides, *Journal of Microelectromechanical Systems*12(4), 387–417 (2003).
19. Karsten Dyrbye, Tina Romedahl Brown, and Gert Friis Eriksen, *J. Micromech. Microeng.* 6, 187–192 (1996).
20. R. de Reus, C. Christensen, S. Weichel, S. Bouwstra, J. Janting, G. Friis Eriksen, K. Dyrbye, T. Romedahl Brown, J. P. Krog, O. Søndergaard Jensen, and P. Gravesen, *Microelectron. Reliab.* 38, 1251–1260 (1998).
21. M. Müllenborn, P. Rombach, U. Klein, K. Rasmissen, J. F. Kuhmann, M. Heschel, M. Amskov Gravad, J. Janting, J. Branebjerg, A. C. Hoogerwerf, and S. Bouwstra, *Sens. Actuat. A* 92, 23–29 (2001).
22. Christian Wang, "Proceedings of Workshop on MEMS Sensor Packaging," Danish Technical University (DTU), Lyngby, Denmark, March 20 and 21, 2003.
23. "Materials Science of Microelectromechanical Systems (MEMS) Devices," in "the MRS Symposium Proceeding Series,"

(Arthur H. Heuer and S. Joshua Jacobs, Eds.) Vol. 546. Boston, Massachusetts, U.S.A., 1998.
24. Yvette Kaminorz, *MSTNEWS* Special Issue, 4–6 (2003).
25. M. Calleja, J. Tamayo, A. Johansson, P. Rasmussen, L. M. Lechuga, and A. Boisen, *Sens. Lett.* 1(1) (2003).
26. J. Thaysen, A. D. Yalçinkaya, R. K. Vestergaard, S. Jensen, M. W. Mortensen, P. Vettiger, and A. Menon, "Proceedings of MEMS, 2002," pp. 320–323, Las Vegas, January 2002.
27. Mark Denninger, Claus Narholm-Hansen, and Jacques Jonsmann, "Proceedings of Workshop on MEMS Sensor Packaging," Danish Technical University (DTU), Lyngby, Denmark, March 20th and 21th, 2003.
28. F. J. Blanco, M. Agirregabiria, J. Garcia, J. Berganzo, M. Tijero, M. T. Arroyo, J. M. Ruano, I. Aramburu, and Kepa Mayora, *J. Micromech., Microeng.* 14, 1047–1056 (2004).
29. Jakob Janting, Elisabeth K. Storm, and Oliver Geschke, "Proceedings of μTAS, 8th International Conference on Miniaturised Systems for Chemistry and Life Sciences," pp. 378–380. Malmö, Sweden, 26–30 September 2004.
30. Peter Friis, Elisabeth K. Storm, Karsten Hoppe, and Jakob Janting, "Proceedings of mu TAS, 8th International Conference on Miniaturised Systems for Chemistry and Life Sciences," pp. 354–356. Malmö, Sweden, 26–30 September 2004.
31. I-B. Kang, M. Manda, A. Hariz, N. D. Samaan, and M. R. Haskard, "Proc. MICRO 1997," pp. 129–133, Melbourne, Australia.
32. Y. C. Su, L. Lin, *IEEE MEMS-2001 Conf.* Interlaken, Switzerland, 50–53 (2001).
33. Dr. G. Krötz, *MST News* 21/97, (1997).
34. Colin Johnston, *MSTNEWS* 4, 4–5 (2001).
35. Eberhard Kaulfersch, Jürgen Auersperg, Bernd Michel, and Andreas Schubert, *MSTNEWS* 4, 8–9 (2001).
36. K. Gottfried, M. Vogel. R. Hoffmann, C. Kauffmann, St. Guenther, and F. Dieckmann, *MSTNEWS* 4, 10–11 (2001).
37. Emanuele Pace and Mara Bruzzi, *MSTNEWS* 4, 12–13 (2001).
38. Ovidiu Vermesan, Ralph W. Bernstein, and Geir Uri Jensen, *MSTNEWS* 4, 14–15 (2001).
39. Riccardo Groppo, Wolfgang Wondrak, Guenter Lugert, and Thomas Riepl, *MSTNEWS* 4, 16 (2001).
40. U. Kaufmann, J. Hauβelt, and H. Moritz, *MSTNEWS* 4, 35–38 (2001).
41. Martin Nese and Frode Meringdal, *MSTNEWS* 4, 35–40 (2001).
42. Patrick McCluskey and LiangYu Chen, *MSTNEWS* 4, 41–42 (2001).
43. Volker Grosser, Matthias Schuenemann, Herbert Reichl, and Helmut Kergel, *MSTNEWS* 1, 4–8 (2000).
44. Jeroen M. Wissink, *MSTNEWS*, No. 1, 20–22 (2000).
45. Marcel F. Dierselhuis and Gerben W. A. Kolkman, *MSTNEWS*, No. 1, pp. 16–17 (2000).
46. Vern Solberg, "Proceedings of The IMAPS Nordic Annual Conference," pp. 42–48. Helsingør, Denmark, 2004.
47. E. Jan Vardaman and Linda Matthew, "Proceedings of The IMAPS Nordic Annual Conference," pp. 26–29. Helsingør, Denmark, 2004.
48. G. Kelly, J. Alderman, C. Lyden, J. Barrett, and A. Morrissey, "Microsystem packaging in 3D, Proceeding of SPIE 3224," Vol. 142, 1997.
49. V. K. Varadan and V. V. Varadan, "Proc. SPIE," 2722, 156–164 (1996).
50. Ulrike Scholz, Wolfgang Eberhardt, Ulrich Keβler, Heinz Kück, "Proceedings of Micro System Technologies (MST) Conference," pp. 172–179. München, October 7 and 8, 2003.
51. Leo G. Feinstein, in "Electronic Materials Handbook," Vol. 1. pp. 213–223. ASM International, 1989.
52. Elmar Cullmann, "Proceedings of Workshop on MEMS Sensor Packaging," Danish Technical University (DTU), Lyngby, Denmark, March 20th and 21th 2003.
53. Charles H. Small, *EDN 74–82*. July 21 (1988).
54. Barbara Kanegsberg and Edward Kanegsberg, CRC Press, Boca Raton, London, New York, Washington, D.C., 2001.
55. P. Amirfeiz, A. Weinert, and S. Bengtsson, "Proceedings of Eurosensors XIV, The 14th European Conference on Solid-State Transducers," August 27–30, pp. 427–430. Copenhagen, Denmark, 2000.
56. Liyu (Steve) Yang, Joseph B. Bernstein, and Kai Choong Leong, *IEEE Trans. Elec. Pack. Manufact.* 25(2) 91–99 (2002).
57. Shijian Luo, and C. P. Wong, *IEEE Trans. Components Pack. Techn.* 24(1), 43–49, March (2001).
58. Shijian Luo and C. P. Wong, *IEEE Trans. Components Pack. Techn.* 24, 1, 38–42 (2001).
59. Al Hawes and Tom Adams, *Electron. Prod.* (2001).
60. Zhuqing Zhang nd C. P. Wong, *IEEE Trans. Electron. Pack. Manufact.* 25(2), 113–119 (2002).
61. J. Stary and I. Szendiuch, "Proceedings of The IMAPS Nordic Annual Conference," pp. 49–55, Helsingør, Denmark, 2004.
62. Hirokazu Tanaka, Akihiko Saito, Toshiro Nagayama, Hiromi Umeda, "Proceedings of The IMAPS Nordic Annual Conference," pp. 56–67, Helsingør, Denmark, 2004.
63. Minna Arra, David Geiger, Dongkai Shangguan, and Jonas Sjöberg, "Proceedings of The IMAPS Nordic Annual Conference," pp. 68–73, Helsingør, Denmark, 2004.
64. F. Caloz, D. Ernst, P. Rossini, L. Gherardi, L. Grassi, and J. Arnaud, *Microelectron. Reliab.* 42, 1323–1328 (2002).
65. Guenter Schiebel, "Proceedings of The IMAPS Nordic Annual Conference," pp. 216–225, Helsingør, Denmark, 2004.
66. Jaakko Lenkkeri, Tuomo Jaakola, Kari Kautio, and Markku Lahti, "Proceedings of The IMAPS Nordic Annual Conference," pp. 108–114, Helsingør, Denmark 2004.
67. Oliver Geschke, Henning Klank, and Pieter Telleman, Wiley-VCH Verlag GmbH & Co. KGaA, Weinheim, 2004.
68. Jochen Kuhmann, Lior Shiv, Gordon Elger, Andreas Hase, and Matthias Heschel, "Proceedings of Workshop on MEMS Sensor Packaging," Danish Technical University (DTU), Lyngby, Denmark, March 20th and 21th 2003.
69. Magnus Olson, "Proceedings of Workshop on MEMS Sensor Packaging," Danish Technical University (DTU), Lyngby, Denmark, March 20th and 21th 2003.
70. Kim P. Hansen and Hans Ole Nielsen, *DOPS-NYT 1* 20 (2001).
71. Torben Hillingsøe Lisby, "Proceedings of Workshop on MEMS Sensor Packaging," Danish Technical University (DTU), Lyngby, Denmark, March 20th and 21th 2003.
72. P. Fine, B. Cobb, and L. Nguyen, *IEEE Transactions on Components and Packaging Technologies* 23(3), 420–427 (2000).
73. R. Aschenbrenner, A. Ostmann, G. Motulla, K. Becker, E. Zakel and H. Reichl, "IZM Proceedings," Vol. 2, pp. 258–269, 1996.
74. Masahiro Ono, Yoshihiro Tomura, Yoshihiro Bessho, Tsukasa Shiraishi, Kazuo Eda and Toru Ishida, "Proceedings IEMT/IMS," Japan 1997.
75. Richard Estes, Frank Kulesza, "Proceedings of workshop on smart card technologies and applications," pp. 315–323, Berlin, Germany, November 18–20, 1996.
76. Bela Rösner, Johan Liu and Zonghe Lai, "Proceedings of the 46th Electronic Components and Technology Conference (ECTC)," pp. 578–581, May 28–31, Florida, USA, 1996.
77. Alan M. Lyons, G. W. Kammlott, Y.-H. Wong, and G. Adams, "Proceedings of International Conference on Flex Circuits," pp. 1–8, Flexcon'95, Sunnyvale, California, USA, 1995.
78. "Conductive Adhesives for Electronics Packaging" (J. Liu, Ed.). Electrochemical Publications Ltd., London, UK, 1999.
79. H. Kristiansen, T. O. Grønlund, and Johan Liu, "Proceedings of The IMAPS Nordic Annual Conference," pp. 86–91, Helsingør, Denmark, 2004.

80. Liquang Cao, Yanli Wang, Guoliang Chen, and Johan Liu, "Proceedings of The IMAPS Nordic Annual Conference," pp. 92–97, Helsingør, Denmark, 2004.

81. Itsuo Watanabe, N. Nakazawa, Tohru Fujinawa, Motohiro Arifuku, Masaki Fujii, and Yasushi Gotoh, "Proceedings of The IMAPS Nordic Annual Conference," pp. 74–79, Helsingør, Denmark, 2004.

82. Petri Savolainen and IIkka Saarinen, "Proceedings of The IMAPS Nordic Annual Conference," pp. 98–103, Helsingør, Denmark, 2004.

83. R. D. Gerke, Jet Propulsion Laboratory, Pasadena, California, January, 1999.

84. K. K. Baikerikar and A. B. Scranton, *Polymer* 42, 431–441 (2001).

85. Xuefeng Wang, Jonathan Engel, and Chang Liu, *J. Micromech. Microeng.* 13, 628–633 (2003).

86. Liu (Caroline) Chen, Midhat Crnic, Zonghe Lai, and Johan Liu, *IEEE Trans. Electron. Pack. Manufact.* 25, 4 (2002).

87. Jiali Wu, Randy T. Pike, C. P. Wong, Namsoo P. Kim, and Minas H. Tanielian, *IEEE Tans. Adv. Pack.* 23(4), (2000).

88. Jaakko Lenkkeri and Tuomo Jaakola, "Proceedings of Workshop on MEMS Sensor Packaging," Danish Technical University (DTU), Lyngby, Denmark, March 20th and 21th, 2003.

89. H. Kopola, J. Lenkkeri, K. kautio, A. Torkkeli, O. Rusanen, and T. Jaakola, "Proc. of MICRO/MEMS 2001," Adelaide, Australia, December 2001.

90. Torsten Thelemann, Heiko Thust, and Michael Hintz, *Microelectronics International* 19/3, 19–23 (2002).

91. S. Manjula, V. Sundararaman, S. K. Sitaraman, C. P. Wong, J. Wu, and R. T. Pike, "Proceedings of International Symposium on Advanced Packaging Materials. Processes, Proporties and Interfaces," 14–17 March 1999.

92. Harrie Tilmans, Myriam Van de Peer, and Eric Beyne, *MSTNEWS* 1, 9–11 (2000).

93. Heiko Krassow and F. Campabadal, *MSTNEWS* 1, 12–13 (2000).

94. Stéphane Renard and Vincent Gaff, *MSTNEWS* 1, 18–19 (2000).

95. Sonbol Massoud-Ansari, Yafan Zhang, Srinivas Tadigadapa, and Nader Najafi, *MSTNEWS* 3, 8–9 (1999).

96. Frank Niklaus, Peter Enoksson, Edvard Kälvesten, and Göran Stemme, "13th IEEE Int. Conference on MicroElectroMechanical Sytems (MEMS'00)," pp. 247–252, Miyazaci, Japan, January 23–27, 2000.

97. T. Lisby, S. A. Nikles, K. Najafi, O. Hansen, S. Bouwstra, and J. A. Branebjerg, *J. Microelectromechan. Syst.* 13(3), 452–464 (2004).

98. Torben Hillingsøe Lisby, "Proceedings of Workshop on MEMS Sensor Packaging," Danish Technical University (DTU), Lyngby, Denmark, March 20th and 21th 2003.

99. Pirmin Rombach, Matthias Müllenborn, Kurt Rasmissen, Christian Wang, Eddie H. Pedersen, Jörg Rehder, and Thor Viken, "Proceedings of Workshop on MEMS Sensor Packaging," Danish Technical University (DTU), Lyngby, Denmark, March 20th and 21th, 2003.

100. Frank Niklaus, "Proceedings of Workshop on MEMS Sensor Packaging," Danish Technical University (DTU), Lyngby, Denmark, March 20th and 21th 2003.

101. Karsten Dyrbye, "Proceedings of Workshop on MEMS Sensor Packaging," Danish Technical University (DTU), Lyngby, Denmark, March 20th and 21th 2003.

102. Gert F. Eriksen and Karsten Dyrbye, *J. Micromech. Microeng.* 6, 55–57 (1996).

103. Carsten Christensen, Roger de Reus, Per E. Andersen, and Gert Friis Eriksen, "Proceedings of Workshop on MEMS Sensor Packaging," Danish Technical University (DTU), Lyngby, Denmark, March 20th and 21th 2003.

104. Nicholas Pedersen, Per E. Andersen, "Proceedings of Second IEEE International Conference on Sensors," Vol. 1, pp. 320–325, Toronto, Canada, October 22–24, 2003.

105. Heikki Kuisma, "Proceedings of Workshop on MEMS Sensor Packaging," Danish Technical University (DTU), Lyngby, Denmark, March 20th and 21th 2003.

106. Torsten Eggers, H. Dobrinski, I, van Dommelen, O. Lüdtke, A. Nebeling, J. Raben, and D. Wüllner, "Proceedings of Workshop on MEMS Sensor Packaging," Danish Technical University (DTU), Lyngby, Denmark, March 20th and 21th 2003.

107. Ashish V. Pattekar and Mayuresh V. Kothare, *J. Micromech. Microeng.* 13, 337–345 (2003).

108. Way Kuo and V. Rajendra Prasad, *IEEE Trans. Reliab.* 49(2), (2000).

109. Simon Tage Jespersen, MSc Eng. thesis, Research Center MIC, Technical University of Denmark, 10th September 2003.

110. David Forman, *Smaal Times* (10/03) 3(6), 16.

111. Erik Jung, Maik Wiemer, Volker Grosser, Karlheinz Bock, and Jürgen Wolf, *OnBoard Techn.* 36–39 (2002).

112. Finn Jensen, John Wiley & Sons Ltd., 1995.

113. V. Lakshminarayanan, *Test and Measure. Europe* 8(4), 21 (2000).

114. William L. Schultz and Sheldon Gottesfeld, Report, The Harris Semiconductor Corporation, 1994 (http://uk.builder.com).

115. P. Liu, L. Cheng, and Y.-W. Zhang, *Interf. IEEE Trans. Adv. Pack.* 26(1), 1–9 (2003).

116. M. Moraja, M. Amiotti, and G. Longoni, "Proceedings of Micro System Technologies (MST) conference," pp. 195–201, München, October 7–8, 2003.

117. Thierry Corman, Vacuum-Sealed and Gas-Filled Micromachined Devices, Ph.D. thesis, KTH, Stockholm, 1999.

118. R. D. Adams, J. Comyn, and W. C. Wake, Chapman & Hall, 1997.

119. L. T. Nguyen, S. A. Gee, M. R. Johnson, H. E. Grimm, H. Berardi, and R. L. Walberg, *IEEE Trans. Components Pack. Manufact. Techn.* A18, 1, 210–217 (1995).

120. C. Pedersen, S. T. Jespersen, K. W. Jacobsen, J. P. Krog, C. Christensen, and E. V. Thomsen, "Proceedings of Eurosensors XVII—17th European Conference on Solid-State Transducers," pp. 418–421, Guimarães, Portugal, September 21–24, 2003.

121. Zhimin Mo, Helge Kristiansen, and Morten Eliassen, "Proceedings of Workshop on MEMS Sensor Packaging," Danish Technical University (DTU), Lyngby, Denmark, March 20th and 21th 2003.

122. Qingshan Yao, Jens Branebjerg, and Jakob Janting, "Proceedings of Workshop on MEMS Sensor Packaging," Danish Technical University (DTU), Lyngby, Denmark, March 20th and 21th 2003.

123. Douglas C. Montgomery, John Wiley & Sons, Inc., New York, Chichester, Weinheim, Brisbane, Toronto, Singapore, 2001.

124. Liam Kehoe, Vincent Guènebaut, Pat Lynch, Maura O'Sullivan, and Pat Kelly, *European Semiconductor* 2–4 (2003).

125. Jakob Janting, Dirch Hjorth Petersen, and Christoffer Greisen, *Microelectronics Reliability* 42, 1811–1814 (2002).

126. Stefan Lipp and Trevor Dingle, *MSTNEWS* 3, 20–21 (1999).

127. M. G. Pecht and R. Agarwal, CRC Press, 1999.

128. J. Johansson, M. Völker, J. Eliasson, Å. Östmark, P. Lindgren, and J. Delsing, "Proceedings of The IMAPS Nordic Annual Conference," pp. 265–271, Helsingør, Denmark, 2004.

129. H. Koelmans, "IEEE-IRPS Proceedings," pp. 168–171, 1974.

130. W. M. Paulsson and R. W. Kirk, "12th Annual Proc. Rel. Phys." pp. 172–179, 1974.

131. Don L. DeVoe, *IEEE Trans. Components Pack. Tech.* 25(4), 576–583 (2003).

132. Helmut Eckhardt, Jerome J. Cuomo, C. Richard Guarnieri, Vinay Sakhrani, H. Troy Nagle, and Stefan Ufer, "Advancing Microelectronics," pp. 10–11, November/December 2002.

133. D. Stroehle, "15th Annual Proceedings, Reliability Physiscs Symposium," pp. 101–106, 1977.

134. Malcolm L. White, *Proceedings of the IEEE* 57(9), 1610–1615 (1969).

135. Harry A. Schaft, "ARPA/NBS Workshop II, Hermeticity Testing for Integrated Circuits," 1974.
136. A. DerMarderosian and V. Ginot, "16th Ann. Proc., Rel. Phys. Symp.," pp. 179–183 ,April 1978.
137. Michal Tencer, "44th Proceedings of Electronic Components and Technology Conference," 1994.
138. J. Gordon Davy, "IEEE Transactions on Parts, Hybrids, and Packaging," Vol. PHP-11, 3, September 1975.
139. A. Christou, *Electron. Pack. Prod.* (1979).
140. Diane Feliciano-Welpe, "Metals Handbook," Vol. 1. ASM International, Packaging, 1993.
141. Robert W. Thomas, *IEEE Trans. Parts, Hybrids Pack.* PHP-12, 3 (1976).
142. Marjorie Byrnes, Jerry L. Carter, Jerry E. Sergent, and Dennis King, *Solid State Tech.* August (1984).
143. S. A. Tison, *Vacuum* 44(11/12), 1171–1175 (1993).
144. Liesl K. Massey, "Plastics Design Library." William Andrew Publishing, 2003.
145. Chi-Hung Shen and George S. Springer, *J. Composite Mater.* 10, 2–20 (1976).
146. Ken Oota, Hiroshi Iida, and Masumi Saka, *IEEE Trans. Components Pack. Tech.* 25(1), 164–168 (2002).
147. J. Crank, Oxford University Press, Oxford, 1975.
148. Charles M. Hansen, CRC Press, 2000.
149. Irving Y. Chien and My N. Nguyen, *Solid State Tech.* 87–88 (1994).
150. W. E. Swartz Jr., J. H. Linn, J. M. Ammons, M. Kovac, and K. Wilson, "Proc. Reliability Physics Symposium," pp. 52–59, 1983.
151. J. R. Huntsberger, *J. Adhes.* 12(1), 3–12 (1981).
152. M. K. Bernett, *J. Colloid Interf. Sci.* 28(2), 243–249 (1968).
153. Thomas Baal, *MSTNEWS* 1, 5–8 (2004).
154. Marlene Bourne, Ayman el-Fatatry, and Patric Salomon, *MSTNEWS* 4, 5–8 (2003).

Paper 19

J. Janting

Techniques in Scanning Acoustic Microscopy for Enhansed Failure and Material Analysis of Microsystems

MEMS/NEMS Handbook, Techniques and Applications, Vol. 3, pp. 293-309, Edited by Cornelius T. Leondes, Springer, 2006, ISBN: 0-387-24520-0

7

Techniques in Scanning Acoustic Microscopy for Enhanced Failure and Material Analysis of Microsystems

J. Janting

DELTA, Danish Electronics Light & Acoustics, Venlighedsvej 4, 2970 Hoersholm, Denmark

1. INTRODUCTION

Acoustic microscopy is a widely used Non Destructive Testing (NDT) method for micro-inspection. Introductions to ultrasonic NDT in general and acoustic microscopy is given in [1–5] and [6–9] respectively.

In acoustic microscopy pulses of ultrasound is transmitted through a liquid medium which is typically water, to the component and its interior where it is reflected and transmitted at interfaces between materials according to their differences in acoustic impedance *Z*. Common types of acoustic microscopy is C-mode or reflection mode Scanning Acoustic Microscopy (C-SAM) [6–53] and Through-mode Scanning Laser Acoustic Microscopy (SLAM) [25, 38, 54, 55]. Useful information on what microscopy method to use is given in [25].

Acoustic microscopy can be considered as a supplement to other NDT methods like X-ray inspection. The contrast in X-ray inspection relies on absorption due to differences in the atomic mass. Bubbles, cracks etc. in polymers are for instance not easy to observe with X-rays, though they are easy to see with sound due to large differences in *Z*. Often samples are X-ray inspected prior to acoustic microscopy for two reasons: 1) Internal interfaces are located, 2) Detection of structures/features not seen acoustically, e.g. thin Al wirebonds in electronic packages.

Typically the sound is emitted and received by the same transducer in C-SAM. It function like a sonar, though by using much higher frequencies, MHz–GHz. In SLAM the

detector is a scanning laser on the backside of the inspected sample. The SLAM frequencies are also in the MHz–GHz range.

Application areas of C-SAM and SLAM are e.g. in microelectronics [6–41, 53–55], constructions [6–9, 51–54], biology [42–44, 53, 54] and materials characterization [6–8, 37–50, 53, 54]. The primary use is in the microelectronics industry. Microsystems comprise microelectronics, photonics, RF/wireless and MEMS [56]. This chapter gives an overview of C-SAM inspection methods for microsystems with focus on the requirements and approaches used for Quality Assurance (QA) of MEMS. A number of characteristic examples are presented.

2. BASIC C-SAM THEORY

In SAM a transducer emits sound as short pulses and receives the reflected sound. The emitted sound is focused on or inside the sample and the reflected $A(R)_{12}$ and transmitted $A(T)_{12}$ amplitudes with polarity at interfaces are given by [1]:

$$A(R)_{12} = A_0 R_{12} = A_0 \frac{Z_2 - Z_1}{Z_1 + Z_2} \tag{1}$$

$$A(T)_{12} = A_0 T_{12} = A_0 \frac{2Z_2}{Z_1 + Z_2} \tag{2}$$

where A_0 is the incoming wave amplitude, R_{12} and T_{12} are the reflection and transmission coefficients respectively, Z_1 and Z_2 are the acoustic impedances of materials 1 and 2 respectively, see figs. 1 and 2. If the inspected sample can be considered to be of infinite dimension concerning the description of wave propagation, the waves in SAM are plane

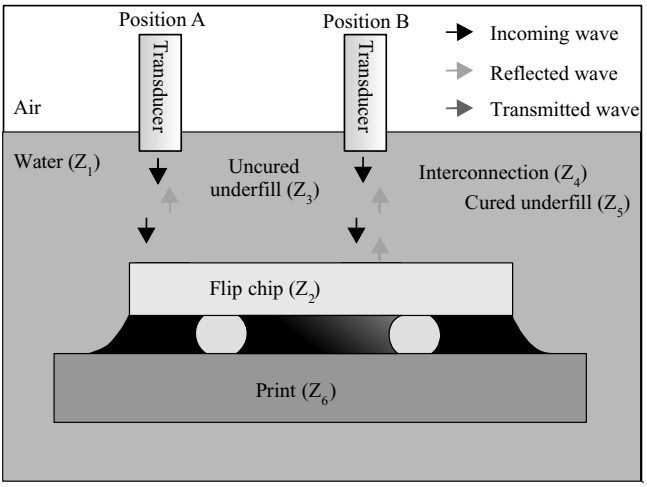

FIGURE 1. Illustration of C-SAM study on flip-chip with cured/uncured or stressed underfill adhesive. Note that the reflections travel time in water is subtracted on the time axis in Fig. 2.

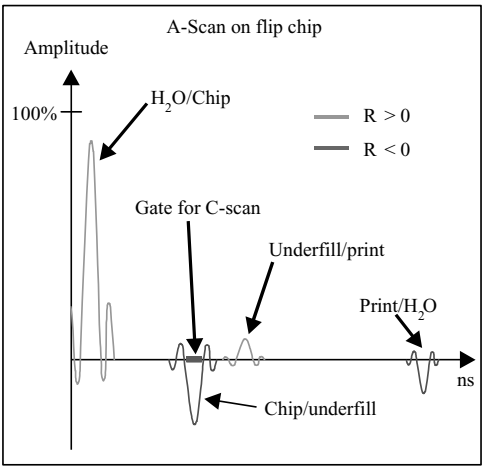

FIGURE 2. A-scan on flip-chip in figure 1. Reflected sound at chip/underfill interface varies according to cure degree or stress.

and longitudinal and the acoustic impedance is given by [57]:

$$Z = \rho V_L = \rho\sqrt{\frac{B(1-\nu)}{\rho(1+\nu)\cdot(1-2\nu)}} = \sqrt{\frac{\rho B(1-\nu)}{(1+\nu)\cdot(1-2\nu)}}$$
$$\approx \sqrt{\frac{\rho E(1-\nu)}{(1+\nu)\cdot(1-2\nu)}} \approx \sqrt{\rho E} \tag{3}$$

where V_{L} is the longitudinal wave velocity, B is the bulk modulus, E is Young's modulus, ρ is the density, and ν is Poisson's ratio.

A graph showing the reflected sound amplitudes with polarity as a function of time delay at a certain point is called an A-scan, fig. 2. A-scans are 1D or point interface depth profiles. In C-SAM a 2D or area C-scan is performed where only reflected sound from a certain depth range is collected corresponding to a gate placed at a certain time interval in the A-scan.

Resolution in SAM depends to a large extent on a combination of the studied samples mechanical materials properties i.e. stiffness and stiffness changes c.f. equations (1)-(3) and the equipment. Important parameters defining or influencing resolution is the focal spot size, focus position, and the resolution of the generated picture. C-SAM is usually confocal acoustic microscopy and the depth of focus is [6]:

$$\Delta Z_{Focus} = \frac{1.28\lambda_{material}}{\sin^2\theta_0} = \frac{1.28v_{material}}{f}\left(\frac{F}{NA}\right)^2 \tag{4}$$

Where $\lambda_{\mathrm{material}}$ is the wavelength of the sound in the material where the focal spot is located, θ_0 is the semi-angle of the lens aperture subtended at the focus, $\sin\theta_0 = NA$ is the lens numerical aperture, v_{material} is the velocity of sound in the material where the focal spot is located, f is the tranducer frequency, F is the focal length. v_{material} values can e.g. be found in [58]. Within the depth of focus the lateral resolution is determined by the focal spot size

by [6]:

$$\Delta X = \frac{\lambda_{material}}{2\sin\theta_0} = \frac{v_{material}}{f}\left(\frac{F}{2NA}\right) \tag{5}$$

Typically the coupling medium between the sound emitting transducer and the studied sample is water. Then ΔX is e.g. 30 μm for $f = 200$ MHz, $F = 8$ mm, $NA = 2$ mm and $v_{\text{water}} = 1500\,\text{ms}^{-1}$. A lateral resolution of 15 nm has been achieved with special equipment [7]. With more common 2 GHz equipment a resolution of 0.7 μm can be reached [7].

The depth or axial resolution is determined by the limit at which reflected wave pulses from different depths are completely separated in the A-scan and is thus given by:

$$\Delta Z = \lambda_{material} \tag{6}$$

3. GENERAL SAM SAMPLE REQUIREMENTS

Best results are achieved when samples with plane i.e. un-curved and smooth surfaces are studied [52]. If the top surface is not planar the focus will move with respect to the sample surface during x-y scanning and much of the sound may not be reflected back to the transducer. However, detection of curvature i.e. warpage as a consequence of stress is also sometimes the purpose of the SAM analysis [14].

It is also an advantage if the top and bottom sample surfaces are coplanar, because this ensures that the top and interior surfaces of the component are coplanar with the scanning plane. Problems with planarity and co-planarity are typically seen as a gradual change in grey tones corner to corner or edge to edge.

On rough surfaces the sound is scattered and less reflected or transmitted sound is received by transducers and the resolution gets poor.

Edge effects may be pronounced in analysis of MEMS with features of sizes comparable to or smaller than that of the focal spot size. In these samples often the waves cannot be considered plane and longitudinal, see section 5.1.

When inspecting the interior of a sample it is an advantage if the liquid sound coupling agent has a Z which is as close as possible to that of the top material, because according to (1) and (2) this ensures more sound transmitted to the depth of interest. For water $Z = 1.482$ MRayl the worst case is when the region of interest is encapsulated with e.g. Au which has a $Z = 63.8$ MRayl far above any liquid. Then most of the sound never reaches the region of interest and the fraction which does will be trapped by multiple reflections within the high Z transitions. This situation is e.g. encountered in some Ball Grid Array (BGA) electronic packages, and the best solution to this problem usually is to remove some or all of the Au. Alternatively, in some very special cases Hg ($Z = 19.6$ MRayl) or Ga ($Z = 17.5$ MRayl) might be used as a coupling agent. Hg and Ga are almost perfect coupling agents for interior inspection of Si ($Z = 19.7$ MRayl) [58].

Analysis with sufficient penetration and resolution inside or under composite materials like Printed Circuit Boards (PCBs) which consist of epoxy and glass filler is also difficult in C-SAM. Like for rough surfaced this is due to scattering of the sound. In this case the sound is scattered on the glass filler. BGAs often include a PCB making them even more difficult to analyse with C-SAM.

4. SAM STATE OF THE ART ANALYSIS AND QUALIFICATION

In acoustic microscopy resolution and penetration depth depends primarily on frequency, focus position, stiffness and stiffness changes in the materials. The choice of transducer therefore depends on the specific situation.

Below the feasibility of using high frequency, move of sound focus and modelling to further enhance QA on MEMS components is discussed. Further new results on wafer to wafer silicon bonding, wafer to glass bonding, and adhesive cure degree studies are presented.

4.1. Analysis

It is important to note that the pulses in SAM consist of a band of frequencies and amplitudes. These are shifted downward on the way to the sample and back because of high attenuation of high frequency components which means that (4) should only be considered a rough estimate of lateral resolution [29, 30, 44]. Using Fourier analysis better resolution has been achieved by filtering out low frequencies in the frequency domain and transforming back to the time domain [10]. Generally, high frequency gives high resolution but low penetration depth and vice versa. Common C-SAM is in the range of 15 MHz–300 MHz and therefore wavelengths are high compared to the low pitch of layers and conductors in MEMS. However, due to high sensitivity towards changes in Z the thickness detection limit of e.g. narrow delaminations/gaps which is wavelength independent is below 100 nm [27], which is far better than the typical wavelength determined depth resolution. That is generally very small changes can be detected but usually their in-depth dimension cannot be measured directly [7, 9, 26–28, 31–35, 49, 50]. This might make conventional SAM equipment useful for future analysis of some NEMS structures. For nm lateral SAM resolution special equipment is required [7]. Research in these areas is important not only because of the NEMS analysis possibilities, but also due to the continued micro-, nanosystem including MEMS/NEMS miniaturization trend towards Wafer Scale Integration (WSI) or System On Chip (SOC) [56].

High frequencies (2 GHz) and focusing below the surface result in both a high wavelength determined resolution but also a very good detection limit of gaps/cracks perpendicular to the surface due to Rayleigh waves travelling along the surface [7, 9, 26, 28, 49, 50]. Whether focusing below the surface is a suitable method of gaining high resolution at the depth of interest depends on the used transducers and the materials involved. When moving the sound focus from the surface of a component to the interior, it is important to note that each transition between layers acts as a lens obeying Snells law of refraction. Thus Snells law determines the necessary transducer movement d_1 to achieve focus on an interior plane at depth d_2. This distance is:

$$d_1 = \frac{V_2 d_2}{V_1} = \frac{d_2}{n} \tag{7}$$

where V_1 is e.g. the velocity of sound in the coupling liquid, V_2 is the velocity of sound in the sample material and n is the refractive index of the fluid and sample material interface. Downward movement of the transducer a distance d_1 results in a sound wave travel time in

the coupling liquid reduced by t_1:

$$t_1 = \frac{2d_1}{V_1} \tag{8}$$

This means that all the reflections in the A-scan come t_1 earlier. Rewriting (7) in terms of time, t_1 can also be found from the sound wave travel time t_2 inside the material:

$$t_1 = \left(\frac{V_2}{V_1}\right)^2 t_2 = \frac{t_2}{n^2} \tag{9}$$

The speed of sound in many electronic materials except polymers is high and above 6000 m/s (e.g. silicon, ceramics). As water is usually the coupling agent the speed of sound here is about 1500 m/s. Then the refractive index is 0.25 which means that the critical angle is 15° and waves incident at angles above this do not excite any longitudinal waves in the solid. As a consequence high resolution transducers with a wide aperture cannot be used effectively [9].

MEMS A-scan and C-scan pictures are often difficult to analyse because the components consists of layers very close to each other resulting in overlapping reflected waves some of which are with opposite phases [33–35]. One approach for better A-scan analysis in these cases is the full wave propagation description [34]. Another is simple spreadsheet simulations based on calculations of reflection, transmission coefficients and the number of waves received by the transducer at the same time by reflection at the same interfaces in different order [35].

Further, through (1) and (3) materials can be analysed for stiffness variations e.g. whether an adhesive is fully cured everywhere [40, 41]. R is not very sensitive to changes in Z_2, as can be seen from (10) inserting typical values though for many applications sensitive enough.

$$\frac{\Delta R}{R} = \frac{2Z_1 Z_2}{Z_2^2 - Z_1^2} \cdot \frac{\Delta Z_2}{Z_2} \tag{10}$$

Depending on the available information Z of an interior material can be found in two different ways [40], fig. 3. One situation is where the acoustic impedance of the top material Z_t is unknown. Then if Z_1 is large compared to Z_2 $A(R)_{12}$ varies approximately linearly with Z_2 and an unknown acoustic impedance Z_x of a material underneath the top material can be determined from two know acoustic impedances Z_a, Z_b of other materials and their

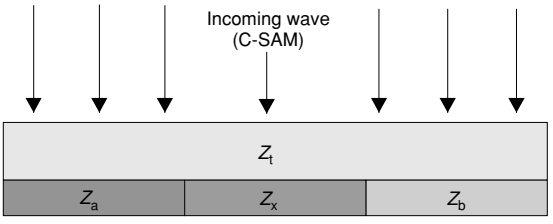

FIGURE 3. Illustration of the variables in equations (11) and (12).

respective grey tone values g_x, g_a, and g_b in the C-SAM picture using (11):

$$Z_x = Z_b + (g_x - g_b)\frac{Z_b - Z_a}{g_b - g_a} \tag{11}$$

Another situation is when Z_t is known. Then because $A(R)_{12}$ varies linearly with R_{12}, Z_x can be determined from only one known acoustic impedance of a material underneath the top material and their respective grey tone values g_x and g_a in the C-SAM picture using (12):

$$Z_x = Z_t \frac{g_a(Z_a + Z_1) + g_x(Z_a - Z_1)}{g_a(Z_a + Z_1) - g_x(Z_a - Z_1)} \tag{12}$$

Since stress σ depend on E through (13):

$$\sigma = \varepsilon E \tag{13}$$

(3), (10) and (11) implies that C-SAM can also be used to measure stress.

Depth resolution can be enhanced to be better than one wavelength in the studied material using special modelling techniques [32].

4.2. Qualification

In SAM QA on electronics the commonly used procedure is to make the inspections comply with the standard IPC/JEDEC J-STD-035 "Acoustic Microscopy for Nonhermetic Encapsulated Electronic Components" [59]. Often this standard is not directly applicable because of the large diversity of products and failure modes. Therefore efforts are put into describing more product specific QA procedures [60] and to develop new analysis tools [10, 32–35, 40, 41]. For instance using the above mentioned A-scan simulation programme components can be analysed before the actual scan and prepared to get optimal signal for enhanced failure and materials analysis.

5. GENERAL FAILURE EXAMPLES AND NEW RESULTS ON MEMS TEST STRUCTURES

A relatively new area of microsystem failure analysis is SAM analysis of MEMS. However, many MEMS materials, manufacturing processes and packaging methods are more or less the same as in microelectronics. SAM QA on MEMS and microelectronics components comprises assurance that there are no failures in [35, 36]: Interfaces between component parts, component materials and uniformity of component materials, see fig. 4.

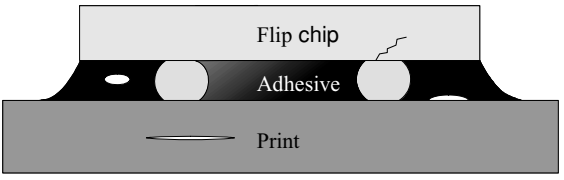

FIGURE 4. Sketch showing the general areas interest for SAM inspection in microsystems. Interface failures: Delamination between adhesive and print and between layers in print. Failures inside component materials: Cracks (in the chip), bubbles (in the adhesive). Failures in materials uniformity: Variation in adhesive cure degree, stress. Note that warpage which is a consequence of stress is not shown.

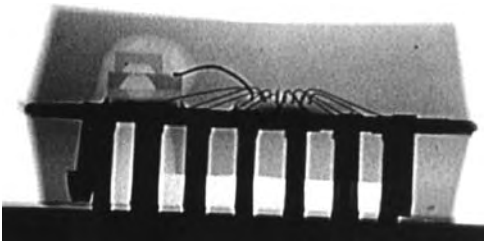

FIGURE 5. X-ray picture of Dual In Line (DIP) packaged MEMS absolute pressure sensor. All the areas of interest mentioned in fig. 4 are also present here. Reprinted from "Encyclopedia of Sensors" Edited by C. A. Grimes, E. C. Dickey and M. V. Pishko, Copyright (2005), with permission from American Scientific Publishers. http://www.aspbs.com/eos.

An example of a MEMS sensor in production where SAM has been a part of the moisture sensitivity classification is a pressure sensor in principle constructed as shown in fig. 5.

5.1. Interface Failures

The failures of the first type is mainly delaminations e.g. in interfaces between encapsulation material and chip/leadframe, and between chip and adhesive [18, 24, 26]. Many microelectronics examples of SAM detection of interface failures can be found in the literature, e.g.: [11–18, 21–24, 26, 36, 37]. The term "delamination" here also covers the area of failures where for instance there is no contact or only partly contact between bond wires/bumps and bond pads. Conversely SAM can also be used to detect unwanted adherence i.e. stiction between mechanical MEMS structures [36]. A typical example of a delamination between encapsulation material and leadframe is shown in fig. 6.

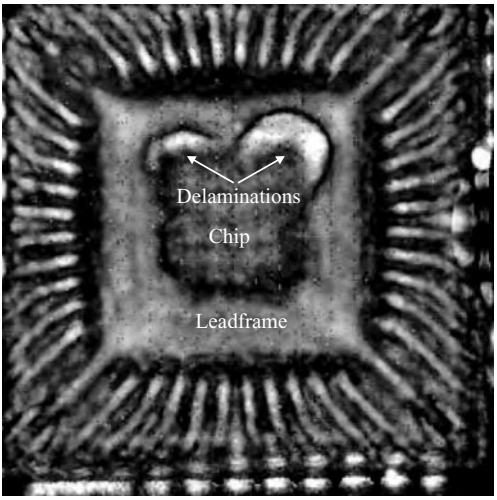

FIGURE 6. Encapsulated die on leadframe. Delamination is C-SAM detected between encapsulation material and leadframe.

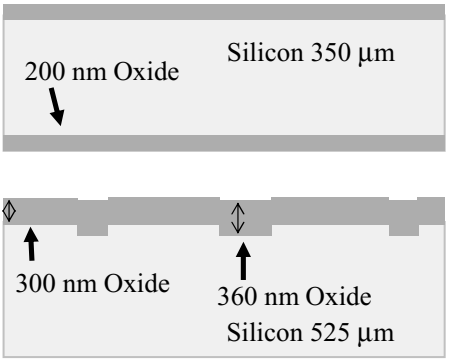

FIGURE 7. Drawing showing the mid cross-section dimensions of test pattern between fusion bonded silicon wafers. The final MEMS absolute pressure sensor dimensions are approx. 3 mm · 7 mm · 0.9 mm.

SAM is also used as a QA method in the MEMS development and manufacturing process. Direct bonding of silicon wafers and anodic bonding of silicon and glass wafers are manufacturing and packaging processes which are specific to MEMS. Figs. 7–11 show recent results on how well the quality of test bonding interfaces between fusion bonded silicon wafers for an absolute pressure sensor can be inspected with SAM. Often IR transparency is used to monitor silicon wafer to wafer bond quality, however here SAM is far more sensitive as illustrated. Using IR inspection only the large round disbond at the bottom left area of fig. 8 can be seen. Note the very narrow and thin pattern features which are also detected with SAM. Height differences less than 100 nm are detected, see figs. 9, 10, with frequencies as low as 50 MHz and with an unpolished top wafer. Often the surface reflection is masking the much lower intensity reflections from material transitions close to the surface, fig. 11. In these cases the second echo with double time delay can be used. In

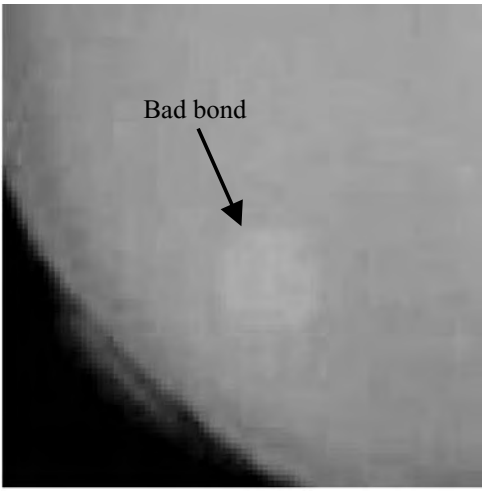

FIGURE 8. IR picture of one quarter of the 4 inch fusion bonded wafer where a disbond is observed.

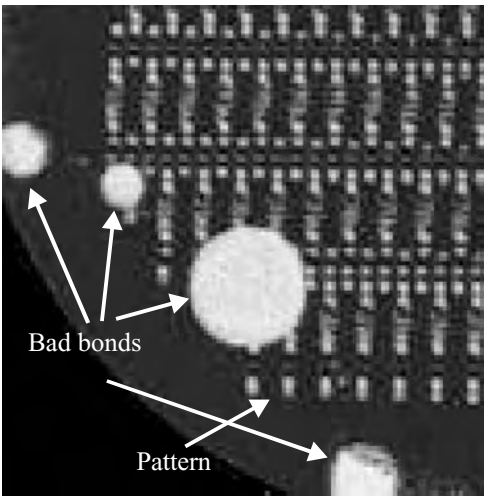

FIGURE 9. C-SAM picture of bond interface in fig. 7. The region is the same as in fig. 8. More disbonds and the pattern can now be seen.

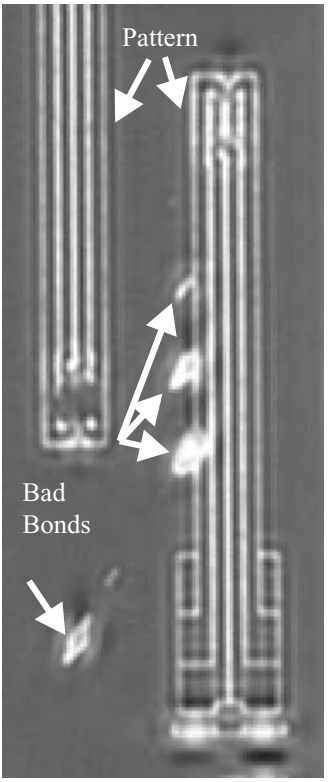

FIGURE 10. Blow-up of region with small disbonds.

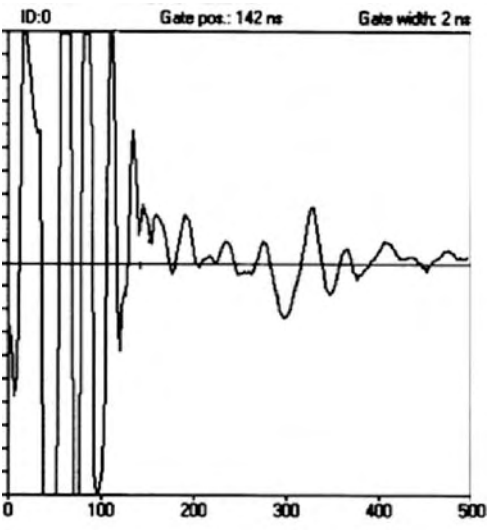

FIGURE 11. A-scan on structure between wafers shown in fig. 7.

this case it is also the only echo from the interface which can be used since the other echoes die because of attenuation and overlapping waves with opposite polarity, see fig. 12.

Fig. 13 is an example of diced MEMS test strips of anodic bonded silicon wafers. A transducer with $f = 110\,\text{MHz}$, $F = 12.7\,\text{mm}$, $NA = 1.5\,\text{mm}$ was used and the coupling liquid was water. The sound was focused on the top strip. Then $\Delta X = 58\,\mu\text{m}$. Clearly badly bonded areas could be detected but also edge/resolution effects was observed i.e. 3 distinct grey zones is seen and the measured width is only $938\,\mu\text{m}$ as compared to the nominal $1000\,\mu\text{m}$.

Using 400 MHz and the KSI WINSAM 200 instrument of these studies, MEMS test cavities with a lateral pitch of $8\,\mu\text{m}$ in the interface between wafers of anodic bonded silicon

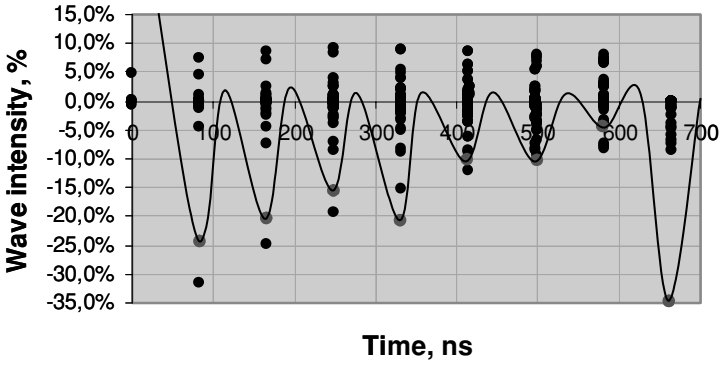

FIGURE 12. Simulated amplitudes of A-scan on structure between wafers shown in fig. 7. Each dot indicates amplitude, polarity and time delay for a back reflected wave. The software described in [35] was used. Attenuation was not included in the simulation.

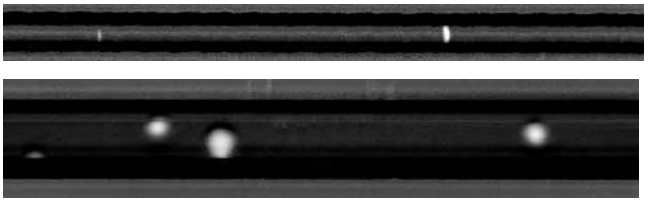

FIGURE 13. C-SAM pictures of interface between anodic bonded silicon strips. Top: Width of strip 500 μm. Bottom: Width of strip 1000 μm.

and glass have also been clearly resolved by scanning through the silicon wafer isotropically etched down to approx. 50 μm thickness, see fig. 14.

Warpage of e.g. electronic components is due to stresses at interfaces which originate from mismatch between materials Coefficient of Thermal Expansion (CTE). Warpage can be pronounced for thin electronic components like Chip Scale Packages (CSP's) [14]. It can be a failure in itself or a source of potential failure i.e. delamination.

5.2. Failures Inside Component Materials

Failures of the second type are e.g. cracks and bubbles in the encapsulation, adhesive and soldering. Also here many microelectronics examples of SAM detection can be found in the literature, e.g. [16, 19, 38]. Bubbles in the encapsulation originate from the moulding process and often they contain air/moisture. In later soldering processes this is critical because the air/moisture expansion may result in cracks (popcorning) extending all the way from the exterior to the vulnerable MEMS and microelectronics interior parts [16]. Poor

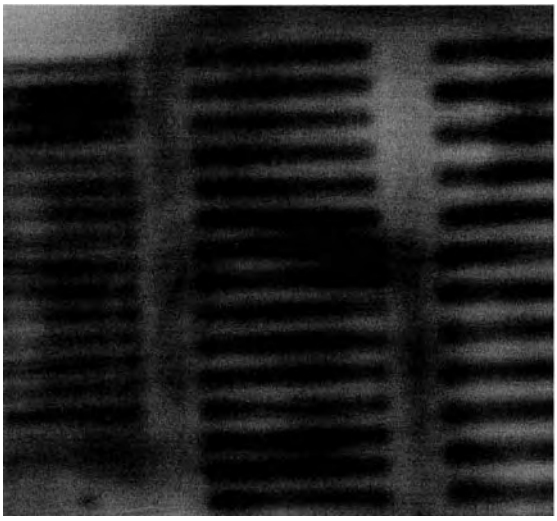

FIGURE 14. C-SAM picture of cavities between a wafer of silicon and wafer of glass anodic bonded.

FIGURE 15. C-SAM picture of lid solder interface of package housing (approx. 8 mm · 4 mm · 3 mm) for MEMS and microelectronics. White areas in soldered rim are without contact between lid and solder.

wetting may result in bad or no contact between parts and bubbles either entirely in the solder or perhaps extending from one or both surfaces into the solder like in fig. 15.

5.3. Failures in Materials Uniformity

The third type of failures comprises measurement of variations in adhesive cure degree, adhesive filler distribution etc. by measurement of variations in Z, see figs. 16 and 17. Methods for determining acoustic impedances in layered structures have been developed, [40, 41]. The method relies on determination of $A(R)_{12}$ from C-SAM grey values, see section 4.1. This can e.g. be used to determine not only whether an adhesive used in MEMS

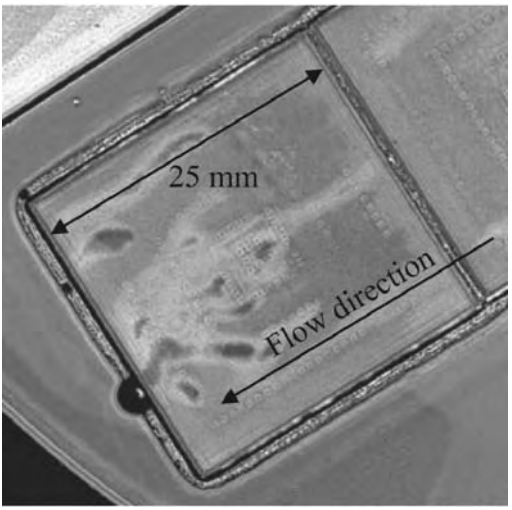

FIGURE 16. Inhomogeneous flip-chip underfill flow.

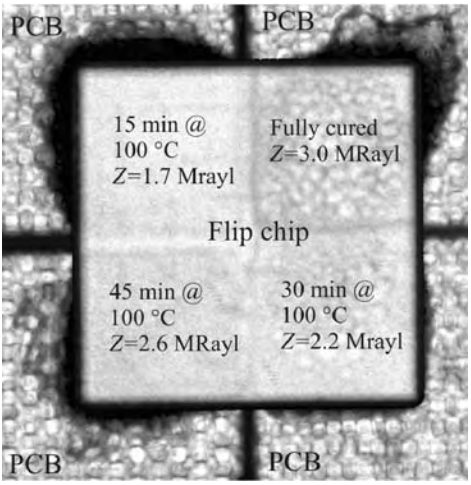

FIGURE 17. Acoustic impedance/cure degree of EpoTek T7110 adhesive between flip chip (30 μm bump height) and PCB (4 pieces, bottom up) determined from C-SAM picture grey values.

applications is cured or not cured at all, but also to determine cure degrees in between these limits, see figs. 17 and 18. Further it can be used to measure stress.

Measurement of adhesive cure degree on whole bond areas non-destructively instead of by use of Differential Scanning Calorimetry (DSC) where samples have to be picked out is of broad interest. Recent studies [40] was motivated by a wish to establish a suitable QA method for the flip chip Compression UnderFill (CUF) electrical interconnection of MEMS components with flex print/PCB, figs. 17, 18. In this interconnection method the

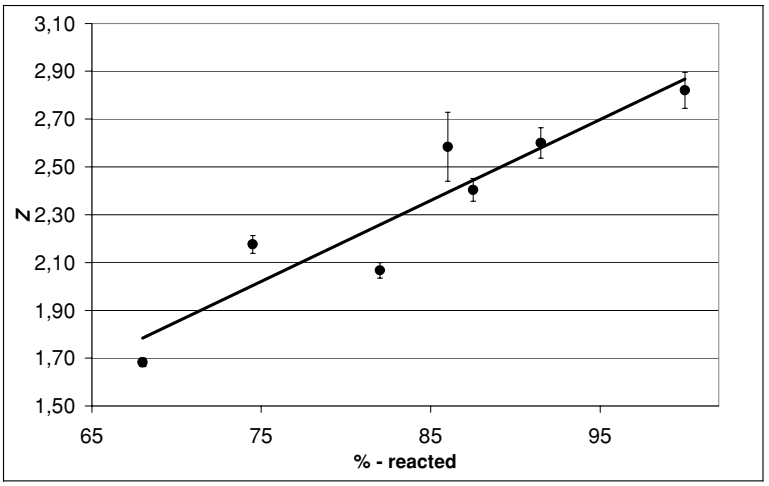

FIGURE 18. Average acoustic impedance (MRayl) of EpoTek T7110 adhesive as a function of reaction degree as determined by DSC kinetic analysis.

contact is established mechanically by the shrinkage of the adhesive while it cures in a flip chip machine. In trying to make the process as fast as possible it is important to assure that the adhesive is fully cured.

When stress due to CTE mismatch do not result in long range movement i.e. warpage the materials have to adjust locally by tension or compression which change their effective physical properties e.g. E and therefore also $A(R)_{12}$ c.f. (1), (3), (10), (11), (12). Therefore if stress variations are large enough they can be detected with SAM.

C-SAM can also be used for QA of MEMS chip underfilling e.g. on wafer level. One problem to control in that process is adhesive filler distribution as illustrated in fig. 16, where the underfill is dispensed at the right flip chip and flows under both of them. At the left chip the filler is unevenly distributed. By analysis of acoustic impedances the amount of filler at different places can be determined [41].

REFERENCES

1. Krautkrämer, J. and Krautkrämer, H., *Ultrasonic Testing of Materials*, 4th Ed., Springer-Verlag Berlin Heidelberg New York, 1990, ISBN:3-540-51231-4.
2. Szilard (Ed.), J., *Ultrasonic Testing, Non-Conventional Testing Techniques*, John Wiley & Sons, Ltd., 1982, ISBN:0-471-27938-2.
3. Fundamentals of Nondestructive Testing, American Society for Metals (ASM) and The American Society for Nondestructive Testing, Lesson 5, Ultrasonic Testing—Fundamentals, 1972.
4. http://www.ndt-ed.org/EducationResources/CommunityCollege/Ultrasonics/cc_ut_index.htm.
5. http://www.ndt-ed.org/index_flash.htm.
6. Kino, G.S., *Acoustic Waves: Devices, Imaging, and Analog Signal Processing*, Prentice-Hall, Inc, 1987, ISBN: 0-13-003047-3-025.
7. Andrew Briggs, Acoustic Microscopy-a Summary, *Rep. Prog. Phys.*, 1992;55:851–909.
8. Kessler, L.W., Acoustic Microscopy. in *ASM International, Metals Handbook*, 9th Ed., Nondestructive Evaluation and Quality Control, 1987, Vol. 17, pp. 465–482.
9. Andrew Briggs, An Introduction to Scanning Acoustic Microscopy, Oxford University Press, Royal Microscopical Society, 1985, ISBN:0-19-856412-0.
10. Janet E. Semmens, and Lawrence W. Kessler, Higher Resolution Acoustic Images Using Frequency Domain Imaging, *Proceedings of the 10th International Symposium on the Physical and Failure Analysis of Integrated Circuits, 2003*, IPFA 2003, pp. 103–107.
11. Martell, S.R., Semmens, J.E., Basterfield, A.J., and Kessler, L.W., Quality Assurance for Multichip Modules with AMI Techniques, 9th European Hybrid Microelectronic Conference Proceedings, 1993, pp. 474–483.
12. Semmens, J.E., Martell, S.R., and Kessler, L.W., Evaluation of Flip Chip Interconnects Using Acoustic Microscopy for Failure Analysis and Process Control Applications, *International Journal of Microcircuits and Electronic Packaging*, 18(4):382–387.
13. Damon Rachell, At the Speed of Sound, *Test*, November 2000:19, 21.
14. Tom Adams, Getting a Slice of the Action, *Electronic Production*, November 2000:21–22.
15. Tom Adams, Beyond the Vanishing Point, *European Semiconductor*, November 2000:53–54.
16. Shook, R.L., Moisture Sensitivity Characterization of Plastic Surface Mount Devices Using Scanning Acoustic Microscopy, *30th Annual Proceedings of International Reliability Physics Symposium (IRPS)*, 1992, pp. 157–168.
17. Moore, T.M., McKenna, R., and Kelsall, S., The Application of Scanning Acoustic Microscopy to Control Moisture/Thermal-Induced Package Defects, *Proceedings of the 16th International Symposium for Testing and Failure Analysis (ISTFA 90)*, 1990, pp. 251–258.
18. Moore, T.M., Kelsall, S.J., and McKenna, R.G., The Importance of Delamination in Plastic Package Moisture Sensitivity Evaluation, *Proceedings of Surface Mount International*, San Jose, California, August 1991, pp. 1231–1238.

19. Fauser, S.N., Miles, B., and Ramirez, C., PBGA Susceptibility to IR Reflow-induced Damage as a Function of Moisture Content, *Proceedings of International Electronics Packaging Conference (IEPS)*, 1994, pp. 573–587.
20. Khang Zhang and Michael Pecht, Effectiveness of Conformal Coatings on a PBGA Subjected to Unbiased High Humidity, High Temperature Tests, *Microelectronics International*, 2000;17(3):16–20.
21. Tom Adams, Early Boost to Yields, *European Semiconductor*, September 2001:45–46.
22. Larry Dues and Tom Adams, Checking for Wafer-to-wafer Bonding Integrity, *Electronics Engineer*, December 1999.
23. John Goings and Jim Stradling, Acoustic Inspection of Bonded and Bumped Wafers, TapTechnology (Ed.) 2: Section 4: *Packaging*, pp. 105–107.
24. Van Doorselaer, K., Moore, T.M., Tiziani, R., and Baelde, W., Evaluation of Methods for Delamination Detection by Acoustic Microscopy in Plastic-Packaged Integrated Circuits, *Proceedings of the 18th International Symposium for Testing & Failure Analysis (ISTFA)*, Los Angeles, California, USA, 17-23 October 1992, pp. 425–431.
25. Baker, K.M., A Practical Method for Characterization and Correlation of Acoustic Microscopes, *Proceedings of the 1993 International Electronics Packaging Conference*, 1993, pp. 836–852.
26. Sridhar Canumalla, Kerry Oren, and Pedro Ramirez, Acoustic Microscopy of Tightly Closed Delaminations in Multilayer Ceramic Chip Capacitors, www.acoustech-inc.com.
27. Tom Adams, in *Advanced Materials and Processes*, September 2000, pp. 38–40.
28. Briggs, G.A.D., Jenkins, P.J., and Hoppe, M., How Fine a Surface Crack can You See in a Scanning Acoustic Microscope? *Journal of Microscopy*, July 1990;159(Part 1):15–32.
29. Sridhar Canumalla, Michael G. Oravecz, and Lawrence W. Kessler, Resolution and Signal Loss in Acoustic Microscopy of Encapsulated IC Packages, *Proceedings of 48th Electronic Components and Technology Conference*, 1998, pp. 962–968.
30. Sridhar Canumalla, Resolution of Broadband Transducers in Acoustic Microscopy of Encapsulated ICs: Transducer Selection, *IEEE Transactions on Components and Packaging Technology*, December 1999;22(4):582–592.
31. Sridhar Canumalla and Lawrence W. Kessler, Characterization of Thin Layers in Microelectronic Packaging Using Acoustic Microscopy, *Proceedings of 4th International Conference on Adhesive Joining and Coating Technology in Electronics Manufacturing*, 2000, pp. 225–231.
32. Sridhar Canumalla and Bryan P. Schackmuth, Metrology of Thin Layers in IC Packages Using an Acoustic Microprobe: Bondline Thickness, *Proceedings of 49th Electronic Components and Technology Conference*, 1999, pp. 602–606.
33. Sridhar Canumalla, Metrology of Adhesive Layers using Acoustic Microscopy, *Proceedings of 3rd International Conference on Adhesive Joining and Coating Technology in Electronics Manufacturing*, 1998, pp. 193–201.
34. Sridhar Canumalla, Critical Issues in Thin Layer Acoustic Image Interpretation and Metrology for Microelectronics, *Proceedings of Electronic Components and Technology Conference*, 2002, pp. 205–218.
35. Jakob Janting, Dirch Hjorth Petersen, and Christoffer Greisen, Simulated SAM A-scans on multilayer MEMS components, *Microelectronics Reliability*, 2002;42:1811–1814.
36. Steven R. Martell, Janet E. Semmens, and Lawrence Kessler, Nondestructive Acoustic Micro Imaging (AMI) Analysis of MEMS Materials, Manufacturing and Packaging, *Proceedings of SPIE—The International Society for Optical Engineering*, 2001, Vol. 4558, pp. 260–267.
37. Andrew Briggs and Oleg Kolosov, Acoustic Microscopy for Imaging and Characterization, MRS Bulletin, *Ultrasonic Nondestructive Techniques for Materials Characterization*, October 1996, Vol. 21, No. 10, pp. 30–35.
38. Semmens, J.E., Martell, S.R., and Kessler, L.W., New Quantitative Acoustic Micro Imaging Methods for Plastic Moulding Compound Characterizations, *Proceedings of the International Intersociety Electronic Packaging Conference—INTERpack'95*, 1995, Vol. 10-1, Part 1 of 2, pp. 493–499.
39. Sridhar Canumalla and Lawrence W. Kessler, Towards a Nondestructive Procedure for Characterization of Molding Compounds, *Proceedings of 35th Annual IEEE International Reliability Physics Symposium*, 1997, pp. 149–155.
40. Janting, J., Petersen, D.H., and Schonwandt, B.V., Scanning Acoustic Microscopy Study of Flip-Chip Underfill Cure Degree, Materials Week 2002, October 2002.
41. Canumalla, S. and Oravecz, M.G., In Situ Elastic Property Characterization of Flip-Chip Underfills, in *International Symposium on Advanced Packaging Materials*, 1998, pp. 106–110.

42. Kundu, T. and Jørgensen, C.S., Measuring Elastic Properties of Bones and Silicon from $V(z)$ Curve Generated by Multiply Reflected Signals, *Ultrasonics*, 2002;39:515–524.
43. Yoshifumi Saijo, Motonao Tanaka, Hiroaki Okawai, Hidehiko Sasaki, Shin-Ichi Nitta, and Floyd Dunn, Ultrasonic Tissue Characterization of Infracted Myocardium by Scanning Acoustic Microscopy, *Ultrasound in Med. & Biol.*, 1997;23(1):77–85.
44. Johnston, R.N., Atalar, A., Heiserman, J., Jipson, V., and Quate, C.F., Acoustic Microscopy: Resolution of Subcelluar Detail, *Proc. Natl. Acad. Sci. USA*, July 1979;76(7):3325–3329.
45. Knauss, D. and Briggs, G.A.D., Subsurface Crack Signals in Time-resolved Acoustic Microscopy, *J. Phys. D: Appl. Phys.*, 1994;27:1976–1983.
46. Knauss, D. and Briggs, G.A.D., The Effect of Anisotropy in Time-resolved Acoustic Microscopy, *J. Phys. D: Appl. Phys.*, 1996;29:1093–1099.
47. Chai, J.-F. and Wu, T.-T., Determination of Surface Wave Velocities in a Prestressed Anisotropic Solid, *NDT&E International*, 1996;29(5):281–292.
48. Ghosh, T., Maslov, K.I., and Kundu, T., A New Method for Measuring Surface Acoustic Wave Speeds by Acoustic Microscopes and Its Applications in Characterizing Laterally Inhomogeneous Materials, *Ultrasonics*, 1997;35:357–366.
49. Warren, P.D., Pecorari, C., Kolosov, O.V., Roberts, S.G., and Briggs, Characterization of Surface Damage Via Surface Acoustic Waves, *Nanotechnology*, 1996;7:295–301.
50. Bozkurt, Yaralioglu, G., Atalar, A., Koymen, H., Krämer, K., Levy, M., Schneider, S.C., and McAvoy, B.R., Characterization and Imaging with Lamb Wave Lens at Gigahertz Frequencies, *Proceeding of IEEE Ultrasonics Symposium*, 1994, Vol. 3, pp. 1417–1420.
51. Zinin, P., Manghnani, M.H., Wang, Y.C., and Livingston, R.A., Detection of Cracks in Concrete Composites Using Acoustic Microscopy, *NDT&E International*, 2000;33:283–287.
52. Janting, J., Borggreen, K., Horsewell, A., and Grumsen, F.B., Scanning Acoustic Microscopy Study of the Adherence of Coatings on Gas Turbine Components, *Materials Week 2002*, October 2002.
53. Martin Hoppe and Jürgen Bereiter-Hahn, Applications of Scanning Acoustic Microscopy—Survey and New Aspects, *IEEE Transactions on Sonics and Ultrasonics*, March 1985;SU-32(2).
54. Manabu Oishi, Nondestructive Evaluation of Materials with the Scanning Laser Acoustic Microscope, *IEEE Electrical Insulation Magazine*, 7(3):25–30.
55. William P. Robbins, Rolf K. Mueller, and Eric Rudd, Thin-Film Characterization Using a Scanning Laser Acoustic Microscope With Surface Acoustic Waves, *IEEE Transactions On Ultrasonics, Ferroelectrics, and Frequency Control*, July 1988;35(4):477–483.
56. Rao R Tummala, *Fundamentals of Microsystems Packaging*, McGraw-Hill, 2001, ISBN:0-07-137169-9.
57. Timoshenko, S.P. and Goodier, J.N., in: *Theory of Elasticity*, McGrawHill, 1970, pp. 492–493.
58. http://www.ondacorp.com/tecref_acoustictable.html.
59. www.jedec.org.
60. Aprem Benjamin, Lynn Strauman, and John Goings, *Scanning Acoustic Microscopy: Analytical Procedure and Techniques for Metal Ball Grid Array (MBGA) Substrates*, http://www.semiconductorfabtech.com/features/tap/articles/edition1/edition1_4.shtml 34.